Earth and Environmental Sciences Library

Ahmed Hassan Ahmed

Mineral Deposits and Occurrences in the Arabian–Nubian Shield

Springer

Earth and Environmental Sciences Library

Earth and Environmental Sciences Library (EESL) is a multidisciplinary book series focusing on innovative approaches and solid reviews to strengthen the role of the Earth and Environmental Sciences communities, while also providing sound guidance for stakeholders, decision-makers, policymakers, international organizations, and NGOs.

Topics of interest include oceanography, the marine environment, atmospheric sciences, hydrology and soil sciences, geophysics and geology, agriculture, environmental pollution, remote sensing, climate change, water resources, and natural resources management. In pursuit of these topics, the Earth Sciences and Environmental Sciences communities are invited to share their knowledge and expertise in the form of edited books, monographs, and conference proceedings.

More information about this series at https://link.springer.com/bookseries/16637

Ahmed Hassan Ahmed

Mineral Deposits and Occurrences in the Arabian–Nubian Shield

Springer

Ahmed Hassan Ahmed
Faculty of Earth Sciences
King Abdulaziz University
Jeddah, Saudi Arabia

Geology Department
Faculty of Science
Helwan University
Cairo, Egypt

ISSN 2730-6674 ISSN 2730-6682 (electronic)
Earth and Environmental Sciences Library
ISBN 978-3-030-96442-9 ISBN 978-3-030-96443-6 (eBook)
https://doi.org/10.1007/978-3-030-96443-6

This Springer imprint is published by the registered company Springer Nature Switzerland AG
The registered company address is: Gewerbestrasse 11, 6330 Cham, Switzerland

For my beloved wife Hoda and children, Sarah, Mahmoud, Hassan, and Yousof.

A special dedication of this book to my former supervisor Prof. Shoji Arai.

For my dearest friend Prof. Moustafa Gharib who passed away before publishing this book.

Preface

There is a general consensus that the different parts of the continental crust merged together in their entirety three times throughout the Earth's history, forming three giant continents, namely "Columbia," "Rodinia," and "Pangaea." In addition to these three giant continents (***Supercontinents***), the process of assemblies had taken place several times during the geologic history, which assembled "some" (but not all) parts of the continental crust and resulted in the formation of large "***Cratons***" and continental blocks in a period of time prior to the formation of the giant "Colombia" supercontinent. These "Supercontinents" and "Cratons" constitute the majority of the ancient Earth's surface and play an important role in Earth's history. The continental "Cratons," also called "proto-continents," are large and stable continental masses that have been stable over a billions of years. Cratonic areas have a thick crust and deep lithospheric roots that reached few hundreds kilometers into the Earth's mantle to make the cratons have long-time stability. The exposed Precambrian crystalline basement and high-grade metamorphic rocks of the cratonic areas are called "***Shields***," whereas the extensive sedimentary cover of these areas is called "***Platforms***." Both shields and platforms of specific continental masses form the cratons. Cratonic areas are economically important where most of the world's diamonds and many other valuable mineral deposits are produced from cratonic areas. Furthermore, these old cratonic masses store a complete record of the long Earth's history, which provide us with great information.

The continental shields are tectonically large stable areas of continental crust exposed on the surface that mainly consisting of igneous and high-grade metamorphic rocks with age more than 570 Ma. The oldest rocks on the Earth are found in the continental shields, where sometimes their age ranges between 2000 and 3500 million years (Ma). All the tectonic events affecting the continental shields have taken place during the Precambrian age, although some of the shields were also affected by weak tectonic events in periods following the Precambrian. The continental shields are exposed at the present time in the form of flat-lying regions, due to the effect of erosion and orogenic movements (e.g., structural movements, mountain building processes), compared with the obvious tectonic activities on the margins and between the continental plates. The shield rocks are commonly overlain by folded belts of

volcano-sedimentary sequences ranging from the degree of greenschist to amphibolite and granulite facies metamorphism. About 50% of the total exposed surface areas of the continental shield built up of gneisses rocks.

The Arabian-Nubian Shield (ANS) is considered as one of the largest surface exposures of the juvenile continental crust belonging to the Precambrian age, which appears on both sides, the eastern and western sides, of the Red Sea. The ANS extends to cover large areas in a number of countries including Saudi Arabia, Yemen, Egypt, Sudan, Eritrea and Ethiopia. The ANS rocks have a wide spectrum of lithology and geological ages ranging from Archean (as those in Yemen) to the lowest Paleozoic, which gives a good opportunity to host various types of mineral deposits. The Nubian part of the ANS (in Egypt, Sudan, Eritrea and Ethiopia) has one of the oldest geological attempts to explore and extract minerals in the world, especially gold, by the ancient Egyptians in 1150 BC. Likewise, mining and extraction of precious and base metals, such as gold, silver, copper, zinc, tin and lead, began in Saudi Arabia at least about 5000 years ago at Mahd Adh Dhahab gold mine (Cradle of Gold). In the last few decades, exploration activities for mineral resources other than hydrocarbons had led to significant discoveries in the countries covered by the ANS. The numerous scientific studies on the geology and mineral deposits of the ANS greatly contribute to understand the origin and tectono-stratigraphic setting of the mineral deposits and occurrences in the shield.

This book gives a detailed review of the mineral deposits and occurrences in the ANS, including their geologic distribution, mineralization styles, economic importance and their geological controls. The objective of this book is to compile the available old and new data on the mineral deposits and occurrences in the ANS. The book will discuss in details the various mineralization styles in the ANS including orthomagmatic mineral deposits associated with mafic-ultramafic rocks (e.g., chromite, Ni–Cu–Co–PGE magmatic sulfides, Fe–Ti oxides, etc.), magmatic-hydrothermal or intrusion-related deposits associated with felsic to intermediate rock types (porphyry, epithermal Au–Ag/sulfide vein-type family, skarn, granite-related pegmatite-REE deposits), orogenic style gold deposits, volcanogenic massive sulfide deposits (VMS) and surficial mineral deposits (chemical-sedimentary, residual, mechanical and supergene enrichment deposits). This book mainly focuses on the geologic distribution and characterization of various types of mineral deposits and occurrences in the countries covered by the ANS, including the Arabian part (Saudi Arabia and Yemen) and the Nubian part (Egypt, Sudan, Eritrea and Ethiopia). This book is prepared with an interest in the geology and metallic mineral resources in the ANS countries for the levels of geoscientists, postgraduate higher educational geoscience students and for general public companies interested in the mineral deposits and resources with an up-to-date geologic distribution, description and economic potentiality of this important part of the World. This book is the result of compilation of numerous scientific works and projects on the mineral deposits and occurrences by the author and many other contributors in the countries covered by the ANS.

As a terminology, and before interring into the different types of mineral deposits and occurrences in the ANS, it is important to address the difference in terminology

between ***mineral occurrence***, ***mineral prospect*** and ***mineral deposit***. The "***mineral occurrence***" is referring to any locality where a useful mineral or material is found. The "***mineral prospect***," on the other hand, is any occurrence that has been developed by underground or by surface techniques or by subsurface drilling to determine the extent of a mineralization. The terms of mineral occurrence and mineral prospect do not have any resource or economic implications. The "***mineral deposit***" is, however, any naturally occurring accumulation/concentration of a valuable commodity or mineral that found in sufficient size and grade (concentration) that has potential for economic development under past, present or future favorable conditions. The economic concentration of metals or any mineral commodity is known as ***ore***. The "***ore deposit***" is thus a well-defined mineral deposit that has been tested and found to be of sufficient size, grade and accessibility to be extracted (i.e., mined) and processed at a profit at a specific time. Ore refers to industrial minerals as well as metals.

The information presented in this book is organized into eight distinct chapters including:

Chapter 1: This chapter focuses on the review of general geology and lithostratigraphy of the shield rocks in the specified countries covered by the ANS.

Chapter 2: This chapter consists of two main divisions: (1) a review on the historical classification of the mineral deposits, with special concern on the genetic classification used in this book and (2) a general review on the distribution of mineral deposits in the Arabian-Nubian Shield (ANS). The latter division of this chapter will briefly summarize the main ore deposits and their distribution as a whole in the ANS, to come to details in terms of their types, rock associations and economic importance in the coming chapters.

Chapter 3: This chapter focuses on the orthomagmatic mineral deposits associated with mafic and ultramafic rocks. It consists of two main parts: (1) an overview on the various types of mafic-ultramafic rocks of different origins, with special concern on the ophiolitic and Alaskan-type concentrically zoned complexes and (2) the distribution of mineral deposits associated with mafic-ultramafic rocks in the countries covered by the Arabian-Nubian Shield (ANS), including chromite deposits, Cu-Ni-Co-PGE magmatic sulfide deposits and Fe–Ti–V magmatic oxide deposits.

Chapter 4: This chapter describes the geologic distribution and economic potentiality of the magmatic-hydrothermal or what so-called intrusion-related deposits in the ANS countries including porphyry Cu–Mo–Au deposits, epithermal Au–Ag/sulfide deposits, skarn deposits and Nb–Ta–Zr–REE-bearing granites and granitic pegmatites.

Chapter 5: This chapter discusses the distribution and economic importance of the first category of hydrothermal mineral deposits, which occur in the orogenic environments and their occurrences and economic potentiality in the ANS countries.

Chapter 6: It reviews the geologic distribution and occurrences of the second category of hydrothermal mineral deposits which occur in the volcano-sedimentary environments, including volcanogenic massive sulfide deposits (VMS) and stratiform-stratabound sedimentary exhalative deposits (SEDEX and VHMS base metal deposits) in the ANS countries.

Chapter 7: This chapter describes the distribution and economic importance of surficial (exogenic) mineral deposits including: chemical-sedimentary deposits (sedimentary iron ores, phosphorite deposits), residual and mechanical deposits (bauxite, Ni-laterite and place deposits) in the ANS countries. As the book is dealing mainly with the mineral deposits and occurrences in the Precambrian shield rocks, so this chapter will be focusing mainly on the Precambrian banded iron formation (BIF) deposits.

Chapter 8: This chapter mainly focuses on the available information about the most important known historical and currently operating mining projects in each country of the ANS, in terms of their history and current progress.

Cairo, Egypt/Jeddah, Saudi Arabia Ahmed Hassan Ahmed

Acknowledgments

I could realize that writing a book is much harder than I thought and more rewarding than I could have ever imagined. Although this period of my life was full of challenges including the world pandemic of COVID-19, which lead to the agony of losing one of my dearest friends, Dr. Moustafa Gharib, none of this would have been possible without encouragement of my wife, family members, and sincere friends.

I would like to express my deep thanks to my former supervisor, Prof. ***Shoji Arai***, from who I learnt a lot and built my scientific experience during my stay in Japan as a Ph.D. student, postdoctoral fellowship, and subsequent scientific collaboration. Many thanks to the external reviewer ***Tucker Barrie*** for his critical scientific review of some book chapters which improve the earlier version.

A very special thanks to my sincere friend ***Nuru Sayed*** who encouraged me to do my best to complete this book and for reviewing an early draft of some book chapters. My sincere friend ***Kamal Ali*** is also indebted for his support and discussion during writing of this book. A special thanks to ***Gregory Zelchenko*** for his critical language editing and proofreading the book chapters. Special thanks to ***Annett Buettner***, ***Jeevitha Shreenath***, ***Sindhu Sundararajan***, and all members of the Springer Publisher for their patient and managing this book to be in its excellent final form.

Finally, so many thanks to all those who have been a part of my getting there, including my mother, brothers, friends, and students, who supported me during my life in general, and during the preparation of this book, in particular.

Contents

1 Geology and Lithostratigraphy of the Arabian–Nubian Shield 1
1.1 Introduction 1
1.2 General Geology of the Arabian–Nubian Shield 5
1.2.1 Ophiolite Complex (Relicts of Oceanic Lithosphere) 8
1.2.2 Relicts of Precambrian Island Arcs 11
1.2.3 Arc-Accretion Related Suture Zones 12
1.2.4 Core (Gneiss Dome) Complexes 15
1.2.5 Sedimentary Basins and Alkaline Granites—(Late Orogenic Features) 17
1.3 Lithostratigraphy of the ANS 19
1.3.1 Lithostratigraphy of the Arabian Shield Rocks in Saudi Arabia 19
1.3.2 Lithostratigraphy of the Arabian Shield Rocks in Yemen 32
1.3.3 Lithostratigraphy of the Nubian Shield Rocks in Egypt 37
1.3.4 Lithostratigraphy of the Nubian Shield Rocks in Sudan 46
1.3.5 Lithostratigraphy of the Nubian Shield Rocks in Eritrea 50
1.3.6 Lithostratigraphy of the Nubian Shield Rocks in Ethiopia 53
References 57

2 Classification and General Distribution of Mineral Deposits in the Arabian–Nubian Shield: A Review 69
2.1 Classifications of Mineral Deposits 69
2.1.1 Introduction 69
2.1.2 Genetic Classification Scheme (Used in This Book) 71
2.2 Mineral Deposits in the Arabian–Nubian Shield: An Overview 79
2.2.1 Afro-Arabian Domain 80
2.2.2 Eastern Domain 85
2.2.3 Southern Domain 85
2.2.4 Western Domain 86
References 86

3 Magmatic (Orthomagmatic) Deposits (Ore Deposits Associated with Mafic–Ultramafic Complexes) 89
3.1 Introduction 90
3.2 Types of Mafic–Ultramafic Rocks 91
3.2.1 Ophiolitic Mafic-Ultramafic Complexes 91
3.2.2 Layered Mafic-Ultramafic Complexes 92
3.2.3 Alaskan-Type Concentrically Zoned Mafic-Ultramafic Complexes 92
3.3 Magmatic Mineral Deposits in Saudi Arabia 93
3.3.1 Chromitite–PGE Deposits in Ophiolitic Mafic–Ultramafic Complexes 95
3.3.2 Magmatic Cu–Ni–PGE Sulfides and Fe–Ti Oxides Mineralization 109
3.4 Magmatic Mineral Deposits in Yemen 116
3.4.1 The Suwar-Wadi Qutabah Ni–Cu–Co–PGE Occurrences 116
3.4.2 The Byhan Cu–Ni–PGE Occurrence 118
3.4.3 Al-Qabyta Occurrence 120
3.4.4 The Qaifa Occurrence 120
3.4.5 The Wadi Mabar Area 121
3.4.6 The Al-Hamurah Cu–Ni Occurrence 121
3.4.7 The Wadi Silbah Occurrence 125
3.4.8 The Mukayras Fe–Ti–P–V Occurrence 125
3.5 Magmatic Mineral Deposits in the Eastern Desert of Egypt 125
3.5.1 Chromitite–PGE Deposits in Ophiolites 126
3.5.2 Non-ophiolitic Cu–Ni–PGE Sulfide Occurrences 134
3.5.3 Non-ophiolitic Fe–Ti Oxide Occurrences 138
3.6 Magmatic Mineral Deposits in Sudan 141
3.6.1 Ingessana Hills Area 144
3.6.2 Qala En Nahal—Umm Saqata Areas 145
3.6.3 The Nuba Mountains 146
3.6.4 The Red Sea Hills Region 147
3.6.5 The Gebel Rahib Occurrences 148
3.6.6 The Southern Sudan Occurrences 149
3.6.7 The Northern Sudan Occurrences 150
3.7 Magmatic Mineral Deposits in Eritrea 150
3.8 Magmatic Mineral Deposits in Ethiopia 151
3.8.1 PGE Mineralization in Western Ethiopia 152
3.8.2 Southern Ethiopian Ni–Co–Cu Mineralization 156
3.8.3 Chromitite-Fe–Ti Mineralization in Western and Southern Ethiopia 158
References 159

4 Magmatic—Hydrothermal Deposits (Intrusion-Related Deposits) 167
4.1 Introduction 168
4.2 Magmatic-Hydrothermal Deposits in Saudi Arabia 169
4.2.1 Porphyry Cu–Mo–Au Mineralization 169
4.2.2 Epithermal Au–Ag Vein-Type Mineralization 172
4.2.3 Greisen-Related Mineralization 178
4.2.4 Granite-Related Mineralization 184
4.3 Magmatic-Hydrothermal Deposits in Yemen 186
4.3.1 Skarn-Related Sn–W Mineralization 187
4.3.2 Granite-Related Radioactive and REE Mineralization 188
4.4 Magmatic-Hydrothermal Deposits in Eastern Desert of Egypt 189
4.4.1 Porphyry Cu–Au Mineralization 190
4.4.2 Skarn-Related Mineralization 199
4.4.3 Epithermal Vein-Type Mineralization 203
4.4.4 Granite- and Pegmatite-Related Mineralization 204
4.5 Magmatic-Hydrothermal Deposits in Sudan 222
4.5.1 Porphyry Cu–Au Deposits 223
4.5.2 Granite-Related Mineralization 226
4.6 Magmatic-Hydrothermal Deposits in Eritrea 228
4.7 Magmatic-Hydrothermal Deposits in Ethiopia 228
4.7.1 Rare-Metals Granitic Pegmatites 229
4.7.2 Beryllium (Emerald) Mineralization 233
References 237

5 Hydrothermal Mineral Deposits in Orogenic Environments 245
5.1 Introduction 245
5.2 Orogenic Mineral Deposits in Saudi Arabia 247
5.2.1 Orogenic Au Deposits 247
5.2.2 Iron Oxide–Copper–Gold Deposits 263
5.3 Orogenic Gold Deposits in Yemen 264
5.4 Orogenic Mineral Deposits in the Eastern Desert of Egypt 268
5.4.1 Allaqi–Sol Hamed Block 269
5.4.2 Um Samiuki–Abu Dahr Block 275
5.4.3 East Nugrus Block 276
5.4.4 Mubarak–Hamash Block 277
5.4.5 Meatiq–Sibai Block 283
5.5 Orogenic Deposits in Sudan 293
5.6 Orogenic Deposits in Eritrea 304
5.7 Orogenic Deposits in Ethiopia 307
References 316

6 Hydrothermal Mineral Deposits in Volcano–Sedimentary Environments 323
6.1 Introduction 323
6.2 Volcano–Sedimentary Mineral Deposits in Saudi Arabia 327
6.2.1 Volcanogenic–Massive Sulfide Deposits 327
6.3 Volcano–Sedimentary Mineral Deposits in Yemen 340
6.3.1 Jabali Mississippi Valley–Type Zn–Pb–Ag Deposit 348
6.4 Volcano–Sedimentary Mineral Deposits in the Eastern Desert of Egypt 352
6.4.1 Introduction 352
6.4.2 The Hamama West Prospect (Abu Marawat Mineral District) 354
6.4.3 The Um Samiuki Mineral District 359
6.4.4 The Derhib–Abu Gurdi Mineral District 362
6.5 Volcano–Sedimentary Mineral Deposits in Sudan 367
6.5.1 Oxidized Surface Zones (Gossans) 371
6.5.2 Hypogene Cu–Zn–Au–Ag Volcanogenic Massive Sulfide Deposits 371
6.6 Volcano–Sedimentary Mineral Deposits in Eritrea 378
6.6.1 Bisha Volcanogenic Massive Sulfide District 379
6.6.2 Asmara Volcanogenic Massive Sulfide District 390
6.7 Volcano–Sedimentary Mineral Deposits in Ethiopia 397
References 406

7 Sedimentary/Surficial Mineral Deposits 411
7.1 Introduction 411
7.2 Banded-Iron Formations in Saudi Arabia 415
7.3 Banded-Iron Formations in Yemen 421
7.4 Banded-Iron Formation in the Eastern Desert of Egypt 422
7.4.1 Um Anab Banded Iron Formation 425
7.4.2 Abu Marawat Banded Iron Formation 426
7.4.3 The Gebel Semna Banded Iron Formation 430
7.4.4 Wadi Kareim Banded Iron Formation 431
7.4.5 Wadi El Dabbah Banded Iron Formation 433
7.4.6 Um Shaddad Banded Iron Formation 436
7.4.7 Um Ghamis Banded Iron Formation 438
7.4.8 Gebel El Hadid Banded Iron Formation 439
7.4.9 The Um Nar Banded Iron Formation 441
References 443

8 Mining History of the Arabian–Nubian Shield 447
8.1 Introduction 448
8.2 Mining History in the Shield Rocks of Saudi Arabia 449
8.2.1 Introduction 449
8.2.2 Mahd Adh Dhahab Old and New Gold Mines 452
8.3 Mining History in the Shield Rocks of Yemen 462

8.4 Mining History in the Shield Rocks of Egypt 467
8.4.1 Introduction 467
8.4.2 Mining During the Pharaonic Civilizations (3100–332 BCE) 468
8.4.3 Mining During the Hellenic and Roman Civilizations (332 BCE–641 CE) 477
8.4.4 Mining from the Arab Conquest (641 CE) Until the French Campaign (1798 CE) 482
8.4.5 Gold as an Example for Mining History in Egypt 482
8.5 Mining History in the Shield Rocks of Sudan 493
8.5.1 Introduction 493
8.5.2 Gold as an Example of Mining History in Sudan 496
8.5.3 Hassaï Project as an Operating Gold-Copper Mine in Sudan 498
8.6 Mining History in the Shield Rocks of Eritrea 502
8.6.1 Introduction 502
8.6.2 Mining Districts in Eritrea 503
8.6.3 Bisha Copper-Zinc-Gold Project as an Example of Operating Mine in Eritrea 507
8.7 Mining History in the Shield Rocks of Ethiopia 511
8.7.1 Introduction 511
8.7.2 Gold Mining in Ethiopia 513
8.7.3 Tantalum Mining in Ethiopia 517
References 520

Chapter 1
Geology and Lithostratigraphy of the Arabian–Nubian Shield

Contents

1.1 Introduction 1
1.2 General Geology of the Arabian–Nubian Shield 5
1.2.1 Ophiolite Complex (Relicts of Oceanic Lithosphere) 8
1.2.2 Relicts of Precambrian Island Arcs 11
1.2.3 Arc-Accretion Related Suture Zones 12
1.2.4 Core (Gneiss Dome) Complexes 15
1.2.5 Sedimentary Basins and Alkaline Granites—(Late Orogenic Features) 17
1.3 Lithostratigraphy of the ANS 19
1.3.1 Lithostratigraphy of the Arabian Shield Rocks in Saudi Arabia 19
1.3.2 Lithostratigraphy of the Arabian Shield Rocks in Yemen 32
1.3.3 Lithostratigraphy of the Nubian Shield Rocks in Egypt 37
1.3.4 Lithostratigraphy of the Nubian Shield Rocks in Sudan 46
1.3.5 Lithostratigraphy of the Nubian Shield Rocks in Eritrea 50
1.3.6 Lithostratigraphy of the Nubian Shield Rocks in Ethiopia 53
References 57

1.1 Introduction

The "*Supercontinents*" constitute the majority of the ancient Earth's surface and play an important role in Earth's history (Meert 2012). Supercontinent defined as a large, solid, homogeneous massif of the Earth's crust, which contains nearly all the continental crust of the planet. It is believed that the largest part of the continental crust formed in the period of 3,200–2,500 million years (Ma) and its fragments are included in all the modern continents (Lubnina and Slabunov 2011). There are several attempts made by many researchers to reconstruct continents, large continental masses, and cratons, to provide a primary information for understanding what has been happened in the past during the Earth's history. This information includes ancient paleogeography, paleoclimatology, paleobiology, earth tectonics,

A. Hassan Ahmed, *Mineral Deposits and Occurrences in the Arabian–Nubian Shield*,
Earth and Environmental Sciences Library,
https://doi.org/10.1007/978-3-030-96443-6_1

mantle dynamics, and important knowledge on the origin of regional metallogenesis (e.g., Bleeker 2003; Rogers and Santosh 2003; Evans and Pisarevsky 2009; Vérard 2019a, b; Vérard 2021). According to the "continental drift" theory of Wegener (1912), the current continents resulted from breakup, fragmentation, and drifting of what so-called as "Pangaea" supercontinent, some 200 Ma ago. Studying the origins of the orogenic belts proved that "Pangaea" was not the only giant continent during Earth's history spanning more than 4.6 billion years. It was preceded by at least twice assemblies of the entire continents, one of them is in the Paleo-Mesoproterozoic called "Columbia", and this supercontinent was formed about 1,800 Ma ago, and began to separate, fracture, and rifting since 1,500 Ma ago. The second possible assembly of the continents supposed to be at the end of the "Mesoproterozoic" era, where the continental masses merged to form "Rodinia" supercontinent, which was existed during the period between 1,100 and 700 Ma ago.

It is believed, therefore that, in the very distant past, our planet, the Earth, had only one supercontinent, where the Earth was very different from what we are seeing today. There is a consensus that the different parts of the continental crust merged in their entirety at least three times throughout the Earth's history, forming three giant supercontinents, namely: "Columbia", "Rodinia", and "Pangaea". In addition to these three supercontinents, the process of assemblies had taken place several times during the geologic history, which assembled some (but not all) parts of the continental crust and resulted in the formation of large "cratons" and continental blocks in a period of time prior to the formation of the "Colombia" supercontinent, such as: Ur (~3,000 Ma), Arctica (~2,500 Ma), and Atlantica (~2,000 Ma).

"*Craton*", also called "proto-continent", on the other hand, is a large and stable continental mass that has been stable for many hundreds of millions of years. The exposed Precambrian crystalline basement and high-grade metamorphic rocks of the cratonic areas are called "*Shields*", whereas the extensive sedimentary cover over these areas called "*Platforms*". Both shields and platforms of specific continental masses form the cratons. Cratonic areas have a thick crust and deep lithospheric roots that reach a few hundred kilometers into the Earth's mantle to make the cratons have long-lasting stability. Cratonic areas are economically important as the source for most of the world's diamonds and many other valuable mineral deposits. Furthermore, they retain a record of the early Earth history. The term "*cratonization*" is used to describe the process by which cratons formed. There are, at least, three hypotheses of cratonization processes that interpret the formation of cratons (Petit 2010): (1) rising plumes and accumulation of deep molten materials that lead to increase the thickness of surface crust, (2) under-plating processes by successive subducting plates of oceanic lithosphere, and (3) island arc or continental fragment accretion at the craton margins that add surface area and ultimately thicken the craton. The lithology of Archean cratons includes ancient gneissic complexes, greenstone belts, granulite gneiss zones, intracratonic sedimentary basins, and less common mobile belts (Baranov and Bobrov 2018).

The continental *shields* are tectonically large stable areas of continental crust exposed on the surface that mainly consist of igneous and high-grade metamorphic rocks with ages of greater than 570 Ma. In some places, the age of shield rocks range

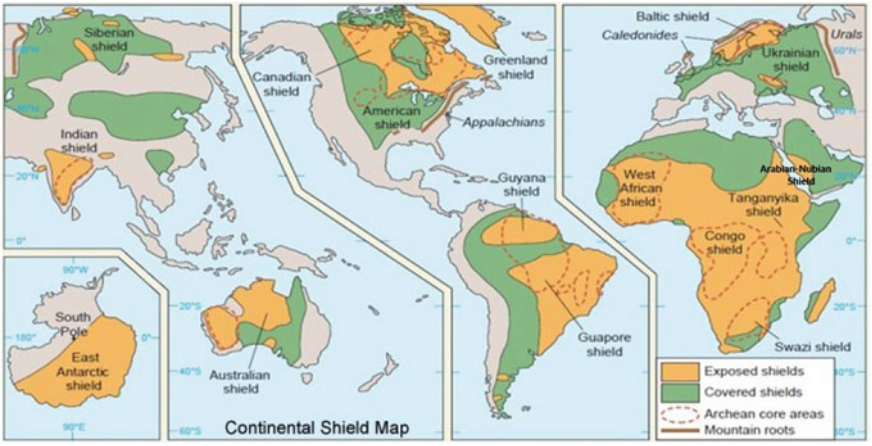

Fig. 1.1 Simplified map of the Earth's continental shields. Areas encircled by broken red lines represent the continental crust of early Precambrian age, while the heavy brown solid lines show mountain roots of later orogenies

between 2,000 and 3,500 Ma; the oldest rocks on the Earth are found in the continental shields. Tectonic events affecting the continental shields have taken place during the Precambrian age, although some of the shields were also affected by weak tectonic events in periods following the Precambrian. The continental shields exposed at the present time in the form of flat-lying regions, due to the effect of erosion and orogenic movements (e.g., structural movements, mountain building processes), compared with the obvious tectonic activities on the margins and between the continental plates. Locally, shield rocks are overlain by folded belts of volcano-sedimentary sequences with greenschist to amphibolite and granulite facies metamorphism (Fig. 1.1). About 50% of the total exposed surface areas of the continental shield built up of gneissose rocks. Almost all the cratonic areas of major continents have exposed Precambrian continental shields; Fig. 1.1 shows the main continental shields in all the present-day continents.

The *Arabian–Nubian Shield* (ANS) is considered as one of the largest surface exposures of Precambrian juvenile continental crust, and is present on both sides of the Red Sea (Figs. 1.1 and 1.2). The ANS extends to cover large areas in a number of countries, including: Saudi Arabia, Yemen, Egypt, Sudan, Eritrea, and Ethiopia; it is also present to a lesser degree in Jordan, Kenya and Somaliland. In the Nubian part of the ANS (in Egypt, Sudan, Eritrea, and Ethiopia), there is abundant archeological evidence for ancient mineral exploration and extraction, especially for gold, with records dating back to 1150 BC in Egypt. Likewise, mining and extraction of precious and base metals, such as gold, silver, copper, zinc, tin and lead, began in Saudi Arabia at least 5,000 years ago at Mahd Ad Dhahab gold mine ("Cradle of Gold"). The ANS rocks have a wide spectrum of lithology, with ages ranging from Archean (as those in Yemen) to the Early Paleozoic, and a wide spectrum of mineral deposit types. In the last few decades, exploration activities for mineral resources

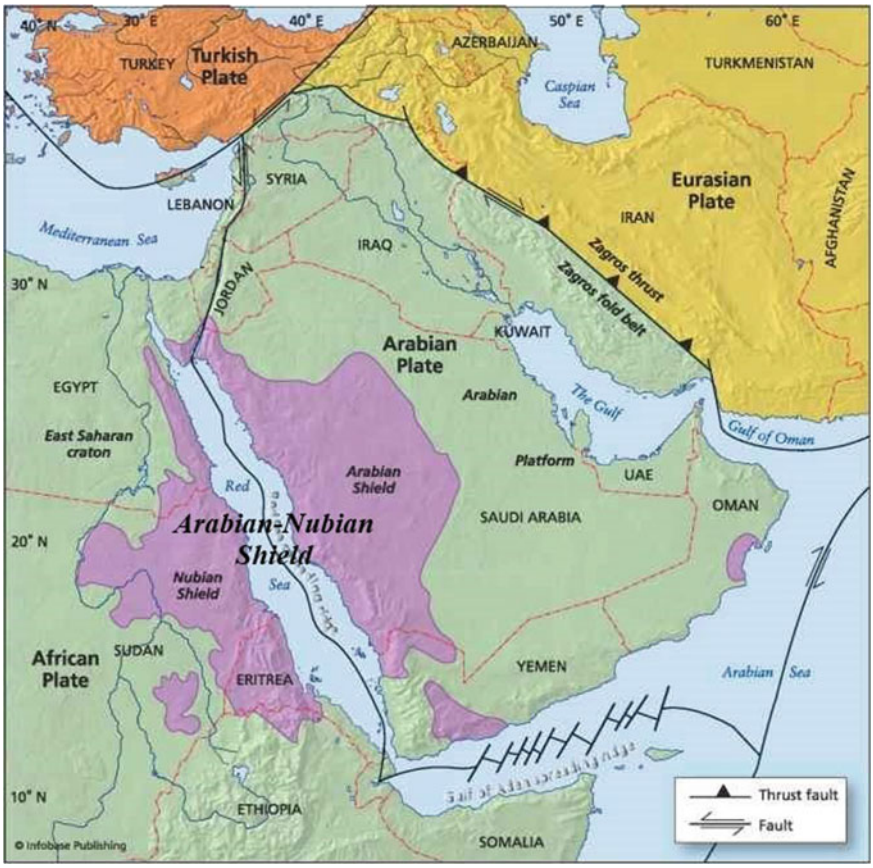

Fig. 1.2 Simple map showing the position of the Arabian–Nubian Shield in relation to the surrounding regions and tectonic plates. To the west, it borders the Saharan Metacraton

other than hydrocarbons had led to significant discoveries in the countries covered by the ANS. The ANS is exceptionally much younger than other continental shields which are mostly evolved during the Neoproterozoic age.

The ANS extends about 3,500 km from north to south, and about 1,500 km from east to west, underlying a total area of about 2.7×10^6 km^2 (Fig. 1.2) (Johnson and Woldehaimanot 2003). The geologic terranes of the ANS show complex nature, where their amalgamation ages range from 780 to 550 Ma, with post-amalgamation events (Johnson and Woldehaimanot 2003; Stern and Johnson 2010; Johnson et al. 2011; Cox et al. 2012; Fritz et al. 2013), as part of the Rodinia-Gondwana supercontinent cycle. The ANS was sandwiched between colliding continental blocks of eastern and western Gondwana during Neoproterozoic times. The ANS represents the northern half of the great collision zone called the East African Orogeny (EAO), which formed near the end of Neoproterozoic time when East and West Gondwana

merged to form the "Gondwana" supercontinent. The EAO is apart from the global Pan-African orogeny that extends southward to the Mozambique Belt. The amalgamation of Gondwana coincided with the breakup of Rodinia, and the closure of the Mozambique Ocean at about 870 Ma. The growth of ANS continuedfor the next 300 Ma and included accretion of island arcs and terrane suturing at about 780 Ma, with final assembly by 550 Ma (Johnson and Woldehaimanot 2003).

In the following parts of this chapter, more details about the geology, lithostratigraphy, and mineralization of the ANS in the above-mentioned countries will be reviewed.

1.2 General Geology of the Arabian–Nubian Shield

This part aims to present an overview of the general geological features of the Arabian–Nubian Shield (ANS) as published in the literature. The ANS is considered as one of the largest surface exposures of the Precambrian juvenile continental crust; it is exposed on both sides of the Red Sea and represents remnants of the basement rocks that formed during the Neoproterozoic age (Patchett and Chase 2002). The oldest geological map (Fig. 1.3) in the world—known as the Turin Papyrus—which located in the Italian Turin Museum—has painted by ancient Egyptian for a gold mine in the Egyptian Eastern Desert in 1150 BC (during the reign of Ramses IV). The map shows multiple colors that indicate different rock units in the region, in addition to the different mining methods and works in the gold mine and extraction

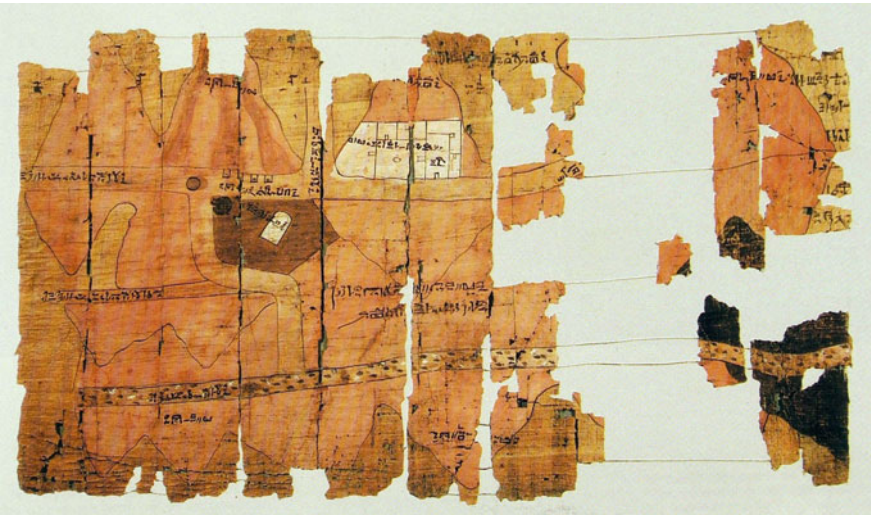

Fig. 1.3 A multiple colors photo of the Turin Papyrus, an oldest geological map in the world, for a gold mine in the Egyptian Eastern Desert that was prepared at about 1150 BC

of ornamental stones from quarries in the region. Likewise, mining and extraction of precious and industrial minerals, such as gold, silver, copper, zinc, tin and lead, began in Saudi Arabia at least 5,000 years ago. The Mahd Ad Dhahab "Cradle of Gold" mine is considered as one of the oldest gold mines in the ANS, and its history dated back to the time of the Prophet Solomon, peace be upon him.

The ANS is composed of gneisses and granitoid rocks with various types of volcanic and sedimentary rocks (Fig. 1.4) affected by different degrees of metamorphism (metavolcanics and metasedimentary rocks). The ANS represents a protracted accretion of juvenile arc terranes with anomalously high rate of magmatic addition within the Mozambique Ocean (Patchett and Chase 2002; Johnson and Woldehaimanot 2003; Stoeser and Frost 2006). Until Tertiary time, the ANS was blanketed by a thick Paleozoic sequence, however rifting the Red Sea accompanied by regional uplift and exposed the Neoproterozoic crystalline basement of the ANS on its flanks. Abundant Neoproterozoic ophiolites (ca. 870–690 Ma) in the ANS are consistent with a convergent margin setting (Berhe 1990; Stern et al. 2004). The evolutionary history of the ANS is intimately linked with Neoproterozoic supercontinent cycles (Stern and Johnson 2010) and the northern sector of the EAO underwent a series of orogenic events bracketed by the fragmentation of Rodinia (ca. 879 Ma) and the assembly of Gondwana (ca. 550 Ma) (Stern et al. 1994; Johnson and Woldehaimanot 2003; Jacobs and Thomas 2004; Li et al. 2008; Stern and Johnson 2010; Yeshanew et al. 2017).

The exposed rocks of the ANS are composed mostly of volcanic and related immature sedimentary rocks, which are metamorphosed in greenschist-facies conditions, and granodioritic intrusions of "I-type" that formed during the Tonian-Cryogenian to Ediacaran and earliest Cambrian ages (Fig. 1.4). The earlier stage (~250 Ma in duration), corresponds to an accretionary tectonic episodes that dominated by the formation of volcanic-arc assemblages, and then accretion of multiple arcs to form proto-continental crust (Stern and Johnson 2019). They are juvenile rocks that added to the ancient crust from the mantle as it is indicated by their isotopic compositions (Stern 2002), which are sometimes referred to as the western arc or oceanic terranes of the ANS (Stoeser and Frost 2006). The later stage (~50 Ma in duration) was very active including continental collision, orogenic collapse, escape tectonics and possible lithospheric delamination. The rocks formed during this stage include slightly metamorphosed volcanic and sedimentary rocks and widely distributed granitoids (Fig. 1.4).

Uplift and stabilization of the ANS at the end of Ediacaran period are possibly resulted from the lithospheric delamination accompanied with the regional compression and collision between crustal blocks of the eastern and western Gondwana (Avigad and Gvirtzman 2009; Abu-Alam et al. 2011; Powell et al. 2014). The exposures of the Nubian Shield rocks to the west of the Red Sea extend about 500 km inland in Sudan, from the Red Sea coast to the Saharan metacraton (Fig. 1.2), a region of mainly pre-Neoproterozoic crust that was extensively reworked during the Neoproterozoic age (Abdelsalam et al. 2002). The exposures of the Nubian Shield rocks are narrow (less than 100 km) in the northern part of the Eastern Desert of

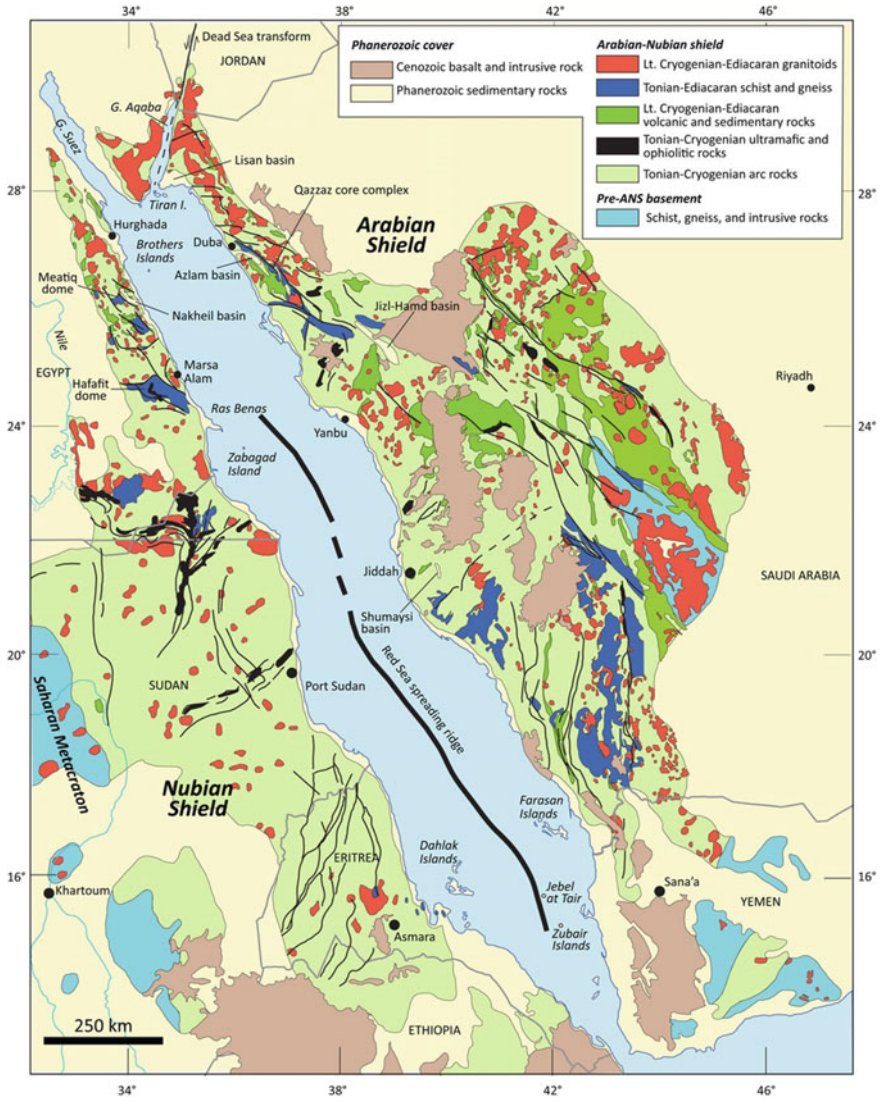

Fig. 1.4 Simplified geological map showing the different rock units of the Arabian–Nubian Shield (from Stern and Johnson 2019)

Egypt (Fig. 1.4). During the Tonian-Cryogenian periods, the volcanic-arc assemblages constitute tectono-stratigraphic terranes, which namely as the Eastern Desert, Gebeit, Haya and Tokar terranes in Egypt, Sudan, and Eritrea, respectively, and called as the Midyan, Hijaz, and Jiddah terranes in Saudi Arabia (Fig. 1.4). The Eastern Desert Terrane of Egypt correlates with the Midyan, the Gebeit terrane in Sudan correlates with the Hijaz, the Haya terrane correlates with the Jiddah, and the Tokar

terrane correlates with the Asir, which it is evident that these terranes were once continuous and now bisected by the Red Sea (Stern and Johnson 2019).

Before discussing the geological sequence of the ANS, a summary of principal rock units is given, to be followed by detailed descriptions of the lithostratigraphic units in the countries covered by the ANS.

1.2.1 Ophiolite Complex (Relicts of Oceanic Lithosphere)

In general, the ophiolite sequences or the ophiolitic rocks are originally belonging to the oceanic crust and the upper part of the Earth's mantle (oceanic lithosphere). These ophiolite complexes appeared on the Earth's surface as a result of the tectonic uplift. The term "ophiolite" used for the first time in 1813 by the French scientist "Alexandre Brongniart", who called it on the group of green rocks in the Alps, which includes serpentine and diabase. In 1927, the scientist "Steinmann" made a modification of this terminology, so it refers to both the serpentine rocks, the pillow lava, and the chert, which are found in the Alps. This term remained little used in other regions until late in the 1950s and early 1960s, where the researchers noted the big similarity between these sequences and other rocks that form at the mid-ocean ridges as a result of the seafloor spreading. The issue of this resemblance is resolved when Ian Graham Gass and his research team in 1968 noted the presence of sheeted dike complexes in Troodos ophiolite in Cyprus, which proved later that these sheeted dike complexes were formed by a similar way to the ocean-floor spreading. Since that date, it becomes universally accepted that the ophiolite sequences are part of the oceanic crust that was obducted on the Earth's surface. The importance of the ophiolite sequences is attributed to their existence as mountain belts as those in the Alps and Himalaya Mountains, where its existence demonstrates on the closing of the ocean basins, the occurrence of subduction processes and the existence of Suture zones. Such a conclusion has become one of the milestones in understanding the theory of plate tectonics, which in turn becomes a general framework to understand the tectonic settings of the different cratons, shields, and terranes.

Due to the scientific and economic importance of the ophiolite sequences, an international conference hold in the city of Penrose, under the auspices of the American Geological Society, called the "GSA Penrose Conference on Ophiolites". The aim of this conference was to come up with specific concepts and scientific controls on the use of the term "ophiolite". The conference participants recommended that this term should be used to refer to "a specific grouping of mafic-ultramafic rocks, and not to refer to a lithological or a specific rock unit". In the complete sequence of ophiolite, according to the concept approved by the Pinros conference, the types of rocks found in this sequence are arranged from top to bottom as follows:

(1) *Pelagic sediments*: They are alluvial and clayey deposits with a small percentage of cherts (flint) and limestone intercalated with each other in the

ocean floor as a successive sequence deposited during the formation of the oceanic crust.

(2) *Basaltic pillow lava*: It shows characteristic features that indicate a direct contact with seawater in the ocean floor.
(3) *Sheeted dike complex*: It is almost vertical basaltic dikes, parallel to each other, and is considered to be the feeder of the overlying basaltic pillow lava.
(4) *Gabbroic complex*: It consists mainly of gabbroic rocks of cumulus texture, which built up of either layered or isotropic gabbros, or both.
(5) *Ultramafic rocks*: It consists of different parts of harzburgite, lherzolite, and subordinate dunite and chromitite, which are characterized by a metamorphic tectonic fabric that is metamorphosed to various extents into serpentinites.

The ANS contains numerous remnants of the ancient oceanic lithosphere (ophiolite sequence), which represent the oldest rock units, either as complete sequence with all rock units mentioned above, or sometimes the sequence is not fully represented due to the absence of one, or more, of these rock units. This oceanic crust represented by the presence of ophiolite complexes in many countries covered by the ANS (Fig. 1.5). For example, a complete ophiolite sequence can be found in many parts of the Eastern Desert of Egypt, in Sudan and in Saudi Arabia. The estimated age of ophiolite complexes in the ANS (e.g., Stern et al. 2004; Johnson et al. 2004) ranges from 870 to 740 Ma. The origin of ANS ophiolites is still a matter of debate. Some researchers believe that the ANS ophiolites are formed in a mid-ocean ridge (MOR) environment, while others are believed to be formed in the back-/fore-arc basin environments, or they initially formed in the MOR setting then substantially modified in the subduction zone setting (Bentor 1985; Pallister et al. 1988; Ahmed et al. 2001, 2012; Ahmed 2013; Ahmed and Habtoor 2015).

Ophiolite complexes and ophiolitic rocks are widely distributed in the ANS belts, and considered as one of the most important fragments of juvenile oceanic crust during the late Precambrian. Ophiolite covers wide areas in the ANS up to about 3000 km^2, extending from the far north of the Arabian Shield to the Mount Rahib in Sudan, and from the west of the Egyptian Eastern Desert to the Mount Al-Awja in Saudi Arabia in the east (Fig. 1.5). If we accept that the ophiolites are remnants of the oceanic crust, the ANS should considered as one of the main components that contain large parts of this oceanic crust. Rittmann (1958) was the first one to describe serpentinite rocks as parts of the ophiolite complexes of the Nubian Shield in the Egyptian Eastern Desert. This important description was ignored until the coming of (Bakor et al. 1976; Garson and Shalaby 1976; Neary et al. 1976) and using the term "ophiolite" in some areas of the ANS according to the description mentioned in the Pinros Ophiolite Conference. These works were followed by a lot of scientific research that applied the idea of plate tectonics in the formation of ophiolite complexes as remnants of oceanic crust of the ANS (e.g., Frisch and Al-Shanti 1977; Gass 1977). In a later period, a large number of petrological, geochemical, and structural studies continued in several places of ophiolite and ophiolitic rocks in the ANS during the eighties and nineties of the twentieth century. Among the most prominent of these studies are the following: Dixon (1979), El Sharkawy and

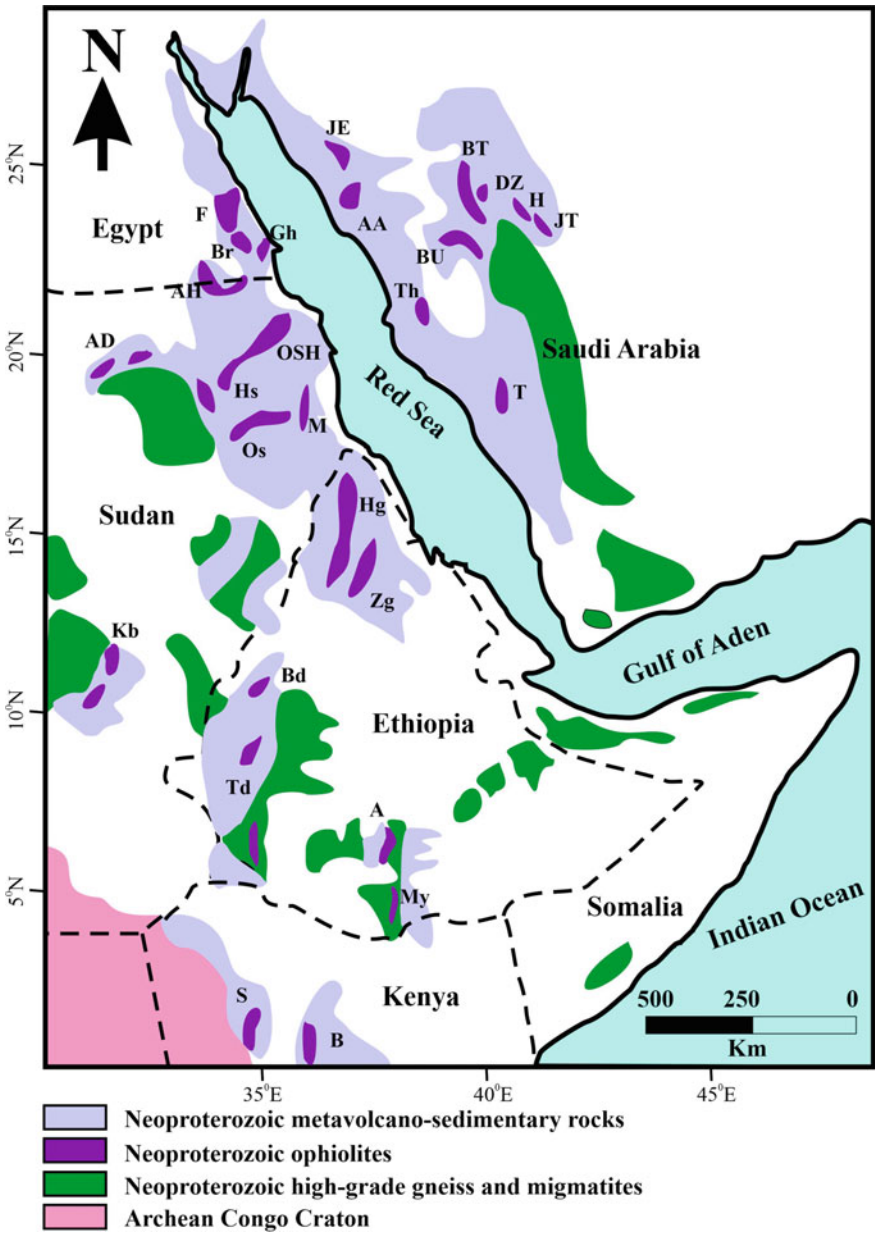

Fig. 1.5 Distribution map of the Arabian–Nubian Shield ophiolites (modified after Abdelsalam and Stern 1996). Abbreviation characters of the best studied ophiolites are: Saudi Arabia (H = Halaban, JT = Jebel Tays; JU = Jebel Uwayjah; JE = Jebel Ess; AA = Al'Ays (Wask); BT = Bi'r Tuluhah; A = Arjah; DZ = Darb Zubaydah; BU = Bi'r Umq; Th = Thurwah; JN = Jebel Nabitah; T = Tathlith). Egypt: (F = Fawkhir; Br = Barramiya; Gh = Ghadir; AH = Allaqi-Heiani; G = Gerf). Sudan (OSH = Onib-Sol Hamed; Hs = Hamisana; AD = Atmur-Delgo; K = Keraf; R = Rahib; M = Meritri; Os = Oshib; Kb = Kabus (Nuba Mts); I = Ingessana; Kk = Kurmuk). Eritrea (Hg = Hagar Terrane). Ethiopia (Zg = Zager Belt; DT = Daro Tekli Belt; Bd = Baruda; TD = Tulu Dimtu; Y = Yubdo; A = Adola; My = Moyale. Kenya: S = Sekerr, B = Baragoi)

El Bayoumi (1979), Nasseef et al. (1980, 1984), Hassan and Hashad (1990), Quick (1990), Stern et al. (1990). Then the interest to study the ophiolite rocks in the ANS decreased from the early nineties until the beginning of the twenty-first century, after which the interest is revived again by some researchers interested in the economic importance of these rocks. Among of them are: Ahmed et al. (2001), Johnson et al. (2004), Stern et al. (2004), Azer and Khalil (2005), Ahmed (2007), Azer and Stern (2007), Ahmed and Hariri (2008), Abd El-Rahman et al. (2009), Ahmed (2013), Ahmed et al. (2012), Ahmed and Habtoor (2015), Gahlan et al. (2015), Ahmed and Surour (2016), Habtoor et al. (2017), and many others up to date.

For simplicity, the ANS is divided into two halves: the northern half and the southern half. The northern half of the ANS includes the ophiolite complexes north of the Bi'r Umq-Nakasib Suture, which extends to the northeast direction, and includes ophiolite complexes in northwest Sudan, such as Oshib (OSH) and Meritri (M) ophiolites, passing through the Red Sea, and continuing in the Arabian Shield in Saudi Arabia to include the Thurwah (Th) and Bi'r Umq (BU) ophiolite complexes that extending in east/west direction (Fig. 1.5). The ophiolite of this part of the ANS are relatively well preserved, which display almost all the characteristics of typical ophiolite sequence, indicating that these complexes are not affected by the strong structures striking in the north/south direction, which prevailed at the end of the collision stage between "East Gondwana" and "West Gondwana". Similarly, there are many ophiolite complexes in the northern part of the ANS affected by strike-slip faults and shear zones in the north/west direction, and these structures belonging to the Najd fault system (Sultan et al. 1988). Regarding to the southern part of the ANS (south of the Bi'r Umq-Nakasin suture), it is difficult to determine the identity and features of the ophiolite complexes, as this part was strongly affected by compressional tectonics that occurred in the late Neoproterozoic, and modified or obliterated many of the original ophiolite features (Abdelsalam and Stern 1996). In spite of this, it is possible to judge, but with some caution, that some of these rock associations might be belong to the mafic-ultramafic rocks of the ophiolite complex, using some of the resistant minerals such as chromite (e.g., Sofiya et al. 2017).

1.2.2 Relicts of Precambrian Island Arcs

There are many rock types belonging to the ancient oceanic island arcs that are widely distributed in the ANS such as tonalites, gabbros, basalts, andesites, and metavolcanic rocks, which have geochemical properties similar to those of the oceanic island arcs, such as those in the Eastern Desert of Egypt (El Gaby et al. 1984; Bentor 1985; El Din et al. 1991; Rashwan 1991). Sequences of the gabbro-diorite rocks have also been identified in the plutonic complexes of the ancient oceanic island arcs, as in the Um Naggat complex in the central part of the Eastern Desert of Egypt (Mohamed and Hassanen 1996), as well as many of the remnants of amphibolite rocks that bear the characteristics of the parent rock of the islands arcs.

The age of the island arc rocks in the Eastern Desert of Egypt was estimated to be around 900 and 700 Ma, and the oldest island arc rocks in Saudi Arabia are between 850 and 900 Ma (Blasband 2006). They are tholeiitic andesite rocks that represent an early stage of the young immature island arcs, as has been mentioned in a lot of scientific research (e.g., Jackson 1986; Brown et al. 1989; Blasband 2006). At the end, the thickening and melting of the immature island arc rocks lead to the formation of mature island arcs, which are characterized by the presence of rocks with calc-alkaline affinity.

Most of the low- and high-K_2O contents of tonalite, trondhjemites and andesite rocks are thought to have formed in this stage of the development of the ANS, which ranges in age from 825 to 730 Ma (Jackson 1986; Brown et al. 1989). In addition, many rocks belonging to the oceanic island arcs are believed to have formed in the Mozambique ocean, just as in the case of ophiolitic rocks (Abdelsalam and Stern 1996). There is strong evidence for the process of accretion (assembly) of the oceanic island arcs in many parts of the ANS. For example, there are several deformed linear belts of ophiolite complexes in parts of the shield, which are interpreted as suture zones separating between the island arcs.

1.2.3 Arc-Accretion Related Suture Zones

There are numerous linear belts of deformed ophiolitic rocks throughout the ANS (Fig. 1.6), which are interpreted as suture zones related to the accretion of the island arcs (e.g., Ries et al. 1983; Vail 1985; Abdelsalam and Stern 1996). The Yanbu-Onib-Sol Hamed-Gerf-Allaqi-Heiani (YOSHGAH), is a composite structure (suture) trends east/west to northeast/southwest across southern Egypt and northern Sudan, and irregularly trends northeast/southwest across the northwestern Saudi Arabia (Stern et al. 1990). The length of western part of the YOSHGAH suture zone in Egypt and Sudan is about 400 km as fold and thrust ophiolite-decorated belts. This part of the YOSHGAH suture zone is composed of imbricate thrust sheets and slices of ophiolitic rocks, such as serpentinite, amphibolite, metagabbro and metabasalt, as well as island arc components of metavolcanic and metasedimentary rocks (Stern and Johnson 2019). Radiometric dating of ophiolitic rocks has yielded ages of about 730 Ma, whereas the accretion between the Gebeit terrane in Sudan and the Eastern Desert terranes in Egypt, and emplacement of the ophiolitic nappes occurred between 730 and 709 Ma (Ali et al. 2010b).

The Yanbu and Bi'r Umq suture zones represent examples of the ophiolitic linear belts that extend in the northeast/southwest trending in the Arabian Shield of Saudi Arabia (Fig. 1.6). These sutures separate slightly deformed domains that are distinguished from each other based on different petrological, geochemical and age characteristics. Accordingly, the Arabian Shield terranes in Saudi Arabia that named Asir, Midyan, Afif, Ar Rayn and Hijaz, are interpreted as accreted terranes, which separated by the linear belts of ophiolitic sutures (Vail 1985; Stoeser 1986). A few reliable age constraints are available for these northeast/southwest sutures; for example, the

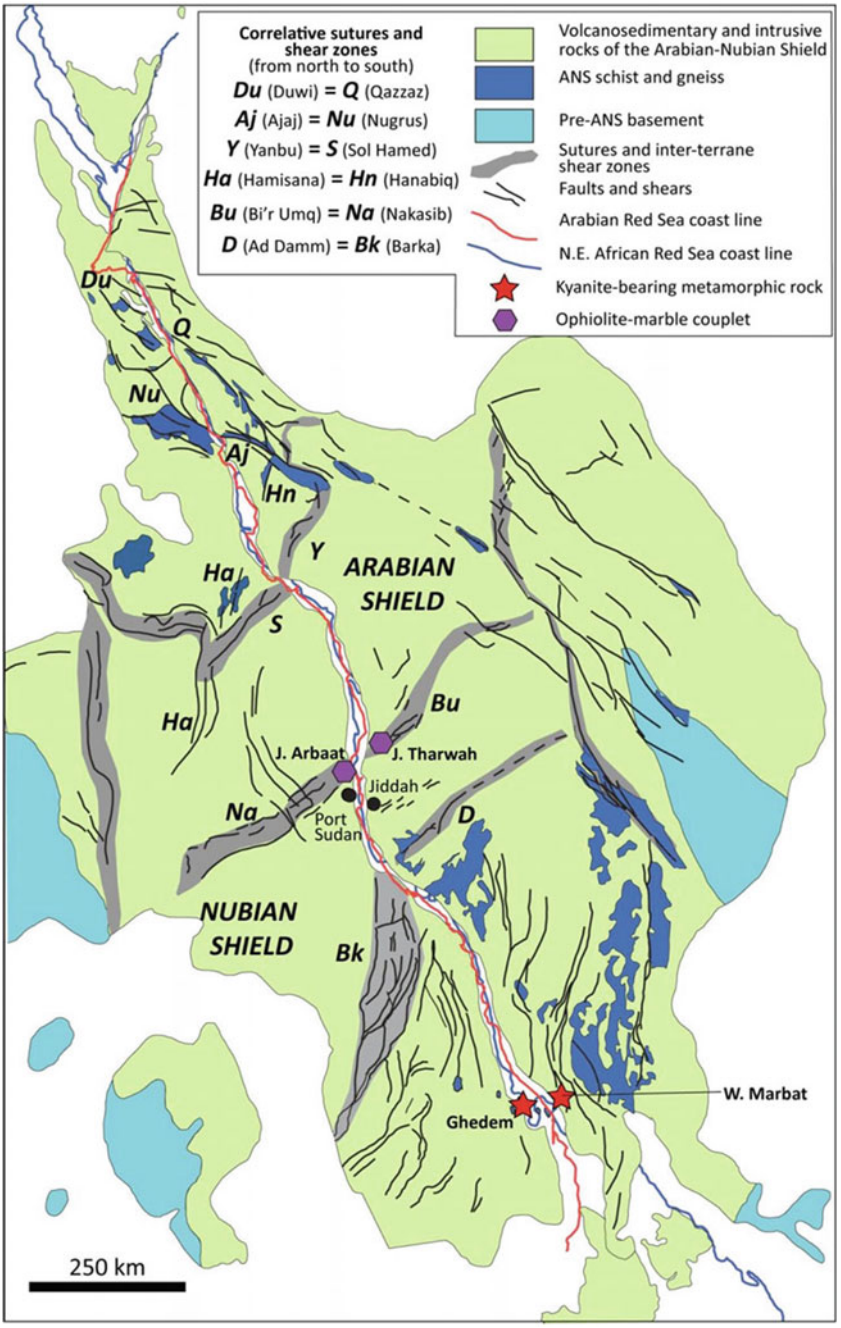

Fig. 1.6 Names of major structures (suture and shear zones) shown on the reconfiguration of the pre-Red Sea rifting in the ANS. This shows a near coastline to coastline closure based on the alignment of major structures in the ANS basement (from Stern and Johnson 2019)

Bi'r Umq suture zone was dated at about 780–760 Ma (Johnson et al. 2002). The deformation along the Yanbu Suture zone, on the other hand, is estimated at about 740–700 Ma (Stoeser and Camp 1985). The western part of suture zone in Egypt and Sudan extends to the shield/coastal plain boundary, whereas the Yanbu suture stops about 50 km before the contact with the Red Sea basin due to its interruption by granite intrusions (Fig. 1.6).

Another important suture zone is the Bi'r Umq-Nakasib suture zone, which extends from N to E across the ANS as a linear belt of juvenile ophiolite complex and metavolcanic, metasedimentary and intrusive rocks. It is one of the best-exposed Neoproterozoic suture zone in the world. It formed by amalgamation between the Jiddah-Haya and Hijaz-Gebeit terranes in Saudi Arabia and Sudan (Fig. 1.6) and extends about 5–65 km wide and over 600 km long. The ophiolitic rocks, volcanic rocks, and pre- and syn-tectonic plutonic rocks along this suture have radiometric ages of about 870–830 Ma, with the suturing taken place at about 780–760 Ma (Hargrove 2006).

Another prominent suture zone in the ANS is the Ad Damm-Barka shear zone (Fig. 1.6). This feature has subvertical shearing and folding at the contact between the Jiddah-Haya and Asir-Tokar terranes The Barka shear zone dips to the west between 45° and 80°, which is as much as 40 km wide, while the Ad Damm shear zone is a subvertical fault zone of about 2–4 km wide and extending in NE direction of more than 350 km long from the Red Sea coastal plain (Fig. 1.6). The Ad Damm-Barka shear zone characterized by greenschist- to amphibolite-facies phyllite and schist rocks developed from volcanic and volcaniclastic rocks as well as mylonitic gneiss developed from granitic rocks dated back to about 620 Ma in the Numan Complex (Hamimi et al. 2014; Stern and Johnson 2019). The Ad Damm-Barka shear zone contains very few ophiolite exposures, and its tectonic significance is uncertain. It may be a cryptic suture, or a young dextral strike-slip shear zone superimposed on an earlier suture (Stern and Johnson 2019).

The Hamisana shear zone, which extends in the north/south direction, also contains ophiolitic remnants (Abdelsalam and Stern 1996). It is a dextral strike-slip movement dated back to about 640–600 Ma, and displaced the Onib-Sol Hamid Suture (Fig. 1.6) (Abdelsalam et al. 2003). In addition, the N-S trending Keraf Suture in Sudan separated between the continental Bayuda Terrane and the juvenile Gebeit Terrane and may thus be a relict of an active continental margin (Abdelsalam and Stern 1996; Küster and Liégeois 2001; Blasband 2006). The north/south trending Keraf and Atmur-Delgo sutures in Sudan display evidence for closure of the ocean that is represented by the ophiolitic rocks of these sutures at about 700 Ma (Abdelsalam et al. 2003). Furthermore, the north/south trending shear zones in Eritrea, which formed as a result of arc-accretion, display high pressure metamorphism (De Souza Filho and Drury 1998; Beyth et al. 2003). These collisional and metamorphic events ended before 650 Ma (De Souza Filho and Drury 1998). Generally, the north/south trending sutures occasionally postdated the NE-SW trending ophiolitic sutures throughout the ANS.

Another large northwest/southeast trending Najd Shear Zone in Saudi Arabia and the Oko Shear Zone in Sudan, represent important structural features in the ANS

(e.g., Fleck et al. 1980; Stern 1985; Dixon et al. 1987). These shear zones crosscut the northeast/southwest and north/south trending structures in the ANS (Stern 1985; Dixon et al. 1987). The Najd shear zone, one of the largest northwest/southeast strike-slip zones, started its activity around 680 Ma during arc-accretion and collision events (Stern 1985; Johnson and Kattan 1999). The activity of Najd shear zone continued until 600 Ma or even later (Abdelsalam and Stern 1996; Johnson and Kattan 1999; Blasband 2006). Furthermore, calc-alkaline rocks such as granodiorites, tonalites and andesites represent igneous relicts of subduction-related magmatism in the ANS that often associated with arc-accretion (Brown et al. 1989; Wilson 1989). The I-type granitoids in the ANS were generally interpreted to result from melting of an amphibolitic crust (e.g., Jarrar et al. 2003; Küster and Liégeois 2001). These I-type granitoid rocks in the ANS are approximately 760–650 Ma (e.g., Jarrar et al. 2003; Küster and Liégeois 2001).

1.2.4 Core (Gneiss Dome) Complexes

A number of gneissic dome (core) complexes are described in the Nubian part of the ANS, especially in the Eastern Desert of Egypt, which dated back to the Precambrian age, named as Meatiq, Hafafit, Gebel El Sibai, El Shalul and Wadi Kid gneissic domes (Fig. 1.7). These gneissic domes have similar petrological and structural characteristics; they are sharing their rock units that represented by the lower- and upper-crustal units. The lower crustal units contain deformed rocks of tonalite, diorite, granodiorite, meatsedimentary rocks, metavolcanic rocks, and meta-ophiolitic schists. The upper crustal units contain folded and thrusted island-arc volcanics, in addition to island-arc related sedimentary sequences and ophiolites that show low-grade metamorphism (Fritz et al. 1996; Bregar et al. 2002).

The *Meatiq dome*, one of the most studied gneissic domes in the ANS, consists of gneiss and amphibolite-schists as a lower-crustal unit, and ophiolitic mélanges, low-grade island-arc related rocks and other volcano-sedimentary rocks as an upper-crustal unit (Loizenbauer et al. 2001). The lower- and upper-crustal units are separated by a deformed cataclasite rock (Habib et al. 1985). The high-temperature, low-pressure metamorphism of the Meatiq dome complex took place during the final stages of formation, when the Meatiq Dome complex got its domal structure (Loizenbauer et al. 2001). The shear zone of the Meatiq Dome is dated at about 590 Ma. The doming of the Meatiq complexes is accompanied by late anorogenic granites (Greiling et al. 1994).

Other gneissic domes are present in Saudi Arabia (Okrusch and Jamal-Allil 1979; Schmidt et al. 1980; Brown et al. 1989) but they have not been studied in detail. In the Taif area, Hijaz, Saudi Arabia, Nasseef and Gass (1977) described gneissic rock complexes concordantly overlying an amphibolite-grade schist. The Abha Complex, another gneissic complex, SW Saudi Arabia, consists of a core of sillimanite-bearing gneisses overlain by biotite schist (Okrusch and Jamal-Allil 1979). The biotite schist of the Abha core complex overlain by low-grade volcanic rocks (Okrush and

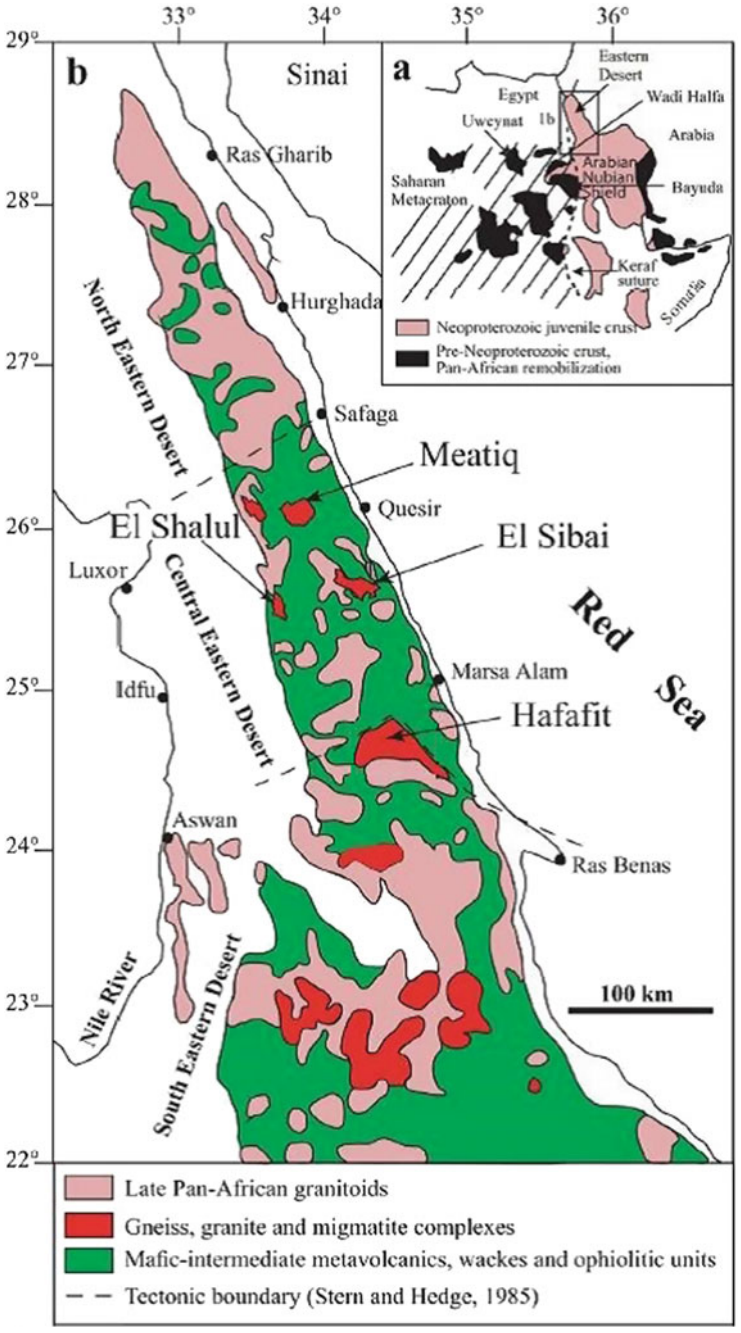

Fig. 1.7 Simplified geological map of the Nubian Shield rocks in the Eastern Desert of Egypt, showing the gneiss core complexes, granitoids, and arc assemblages. The basement subdivisions of the Eastern Dessert of Egypt is also shown. Inset map shows the reconstructed of the ANS (modified from Ali et al. 2015)

Jamal-Allil 1979). The sillimanite-bearing gneisses of this complex are indicative of high-temperature, low-pressure conditions. The Al Qarah Dome complex, is a third core complex in southern Najd of Saudi Arabia, consists of gneissic tonalites and granodiorite rock associations that overlain by schist rocks (Schmidt et al. 1980).

1.2.5 Sedimentary Basins and Alkaline Granites—(Late Orogenic Features)

There are number of late orogenic features that characterize the final development stage of the ANS, such as the sedimentary basins and alkaline granites. These geological units were formed simultaneously with, or slightly younger than, the low-angle shear zones that affected the gneissic dome complexes in the ANS (Blasband 2006; Johnson et al. 2011). The arc assemblages of the ANS comprise juvenile suites of tholeiitic and calc-alkaline volcanic rocks, large number of volcaniclastic sedimentary basins, and voluminous epizonal granitic intrusions. There are many sedimentary and volcano-sedimentary basins (Fig. 1.8) that unconformably overlain the older arc sequences in the ANS. These basins developed on new crust created by the amalgamation and suturing of the ANS arcs. The Neoproterozoic sedimentary basins of the ANS are important geologic features, where they record important evolution stages of the juvenile crust worldwide. They are scientifically important as they have recorded the geology and evolution of the East African Orogeny, as well as the Ediacaran time scale and the final timing of assembly of the Gondwana supercontinent (Johnson et al. 2011, 2013).

These volcano-sedimentary basins are widely distributed in the Arabian Shield, but limited to the northern part of the Nubian Shield (Fig. 1.8), with only one locality described in Sudan (Johnson et al. 2013). This distribution may be due to differential erosion during Cretaceous tectonics, or it may reflect Neogene uplift related to the Afar hotspot and separation of the African and Arabian plates. A prominent feature of these basins is the basal unconformities of a direct depositional contact with the underlying basement of the amalgamated arc systems and terranes (Johnson et al. 2013). The assemblages of these volcano-sedimentary basins are Cryogenian to Ediacaran age, ranging from about 785 Ma (Hali Group) to about 560 Ma (Jibalah and Saramuj Groups) (Fig. 1.8; Johnson et al. 2013). They vary in size from as much as 72,000 km^2 to small, isolated basins of about 200 km^2, and they count about 18% of the shield's total surface area (Johnson and Kattan 2012). The largest reported sedimentary basin in the ANS is located in the northeastern part of the Arabian Shield, which filled by the Murdama group and Afif and Hibshi formations (Fig. 1.8). Smaller sedimentary basins are filled by the Atura formation in the far southern Arabian Shield, the Amaki formation in the south-central Nubian Shield, and the Hammamat Group-Dokhan Volcanics of Egyptian Eastern Desert, and Jibalah group in the northern ANS (Fig. 1.8).

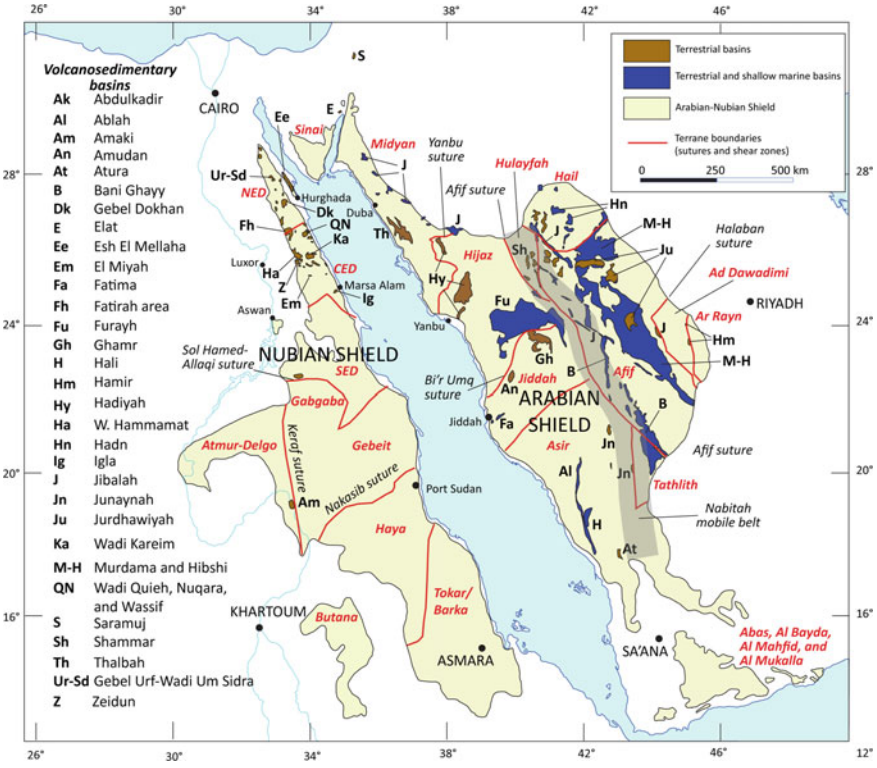

Fig. 1.8 Volcano-sedimentary basins in the ANS unconformably overlain the older arc rocks and amalgamated terranes (red italics) of the basement complex (taken from Johnson et al. 2013)

Depositional units within these volcano-sedimentary basins are largely volcanic and/or volcano-clastic rocks, containing basalt, andesite, rhyolite flows, agglomerates, ignimbrites, and tuffs (Johnson et al. 2013). Other basins are dominantly filled by sedimentary rocks such as sandstone, siltstone, and limestone. Some of these basins are terrestrial, whereas others are formed in terrestrial to shallow marine environments. The rock units of these volcano-sedimentary basins are deformed to some extent. Their sedimentary structures (i.e. bedding planes) are slightly to vertically dipping, strongly folded, and commonly show pervasive cleavage and lineations. These basins are internally disrupted by brittle faults, where in places, basins affected by shear zones forming mylonite rocks. The volcano-sedimentary rocks of these basins are mostly weak to moderately metamorphosed, but in some places, ductile shear zones may reach amphibolite facies metamorphism. Furthermore, at the contact with the granitoid intrusions these rocks may form hornfelsic zones (Johnson et al. 2013).

More details about the lithology and petrogenesis of these volcano-sedimentary basins is given in (Grothaus et al. 1979; Johnson and Kattan 2012; Johnson et al. 2011, 2013).

Late orogenic alkaline granite intrusions are widely distributed in the ANS, which are mostly undeformed alkaline granites that cut lower-crustal sequences of the ANS. These alkaline granite intrusions range in age from 620 to 530 Ma (e.g., Schmidt et al. 1980; Habib et al. 1985; El Din et al. 1991; Greiling et al. 1994). Geochemical studies revealed that these granitoids are generally A-type granites derived from mantle source magmas (Kessel et al. 1998; Moghazi 2003).

Precambrian dyke swarms are present in some parts of the Eastern Desert of Egypt, their direction extended from northeast to southwest, and they have a bimodal mafic and felsic composition, and records a geological age between 620 and 550 Ma (Stern et al. 1984). Also, in the Median and Al-Awijah regions, in the northwest and central Saudi Arabia, there are mafic to intermediate and acidic Precambrian dykes, extending to the northwest-southwest direction. Research studies that conducted by a number of researchers (e.g., Kessel et al. 1998; Jarrar et al. 2003) revealed that these dykes of late mafic to acidic composition formed from magma derived from the mantle, largely similar to the composition of the A-type granites mentioned before. The ANS also contains undeformed basaltic and rhyolitic rocks overlain the lower and upper metamorphic sequences. These rocks, in Egypt, are also called the Dukhan volcanics, got its name from the Gebel El Dokhan in the Eastern Desert of Egypt, which is also derived from a mantle source magma (Moghazi 2003).

1.3 Lithostratigraphy of the ANS

Before starting to describe the rock types in the countries covered by the ANS, it should be noted here that, the rocks of the ANS belong to the Neoproterozoic, which is generally classified from the youngest to the oldest as follows. (1) The Ediacaran period (630–542 Ma), (2) the Cryogenian period (850–630 Ma), and (3) the Tonian period (1000–850 Ma).

Following is a summary of the most important rock units of the ANS in each of the ANS countries, starting with the Arabian Shield rocks (Saudi Arabia and Yemen), and then review the Nubian Shield rocks (Egypt, Sudan, Eritrea and Ethiopia).

1.3.1 Lithostratigraphy of the Arabian Shield Rocks in Saudi Arabia

(A) ***Introduction***

The largest exposure of the Arabian Shield is located in Saudi Arabia, where its width in the middle part reached about 700 km, while its width in the northern part ranges between 50 and 100 km, and in the south, reached about 200 km. The Arabian Shield covers a small area in Jordan, where it contains Neoproterozoic volcanic, sedimentary, and plutonic rocks mostly similar to those in northwest Saudi Arabia (Jarrar

et al. 2003). Thus, the discussion here will focus only on the lithology of the Arabian Shield in Saudi Arabia and Yemen. The shield rocks in Yemen include Archean gneisses as well as Neoproterozoic arc rocks (Windley et al. 1996; Whitehouse et al. 2001). Before opening of the Gulf of Aden and the Red Sea, these rocks continued into the Horn of Africa and Northeast Africa, linking the Arabian Shield with the Nubian Shield and other parts of the African Plate.

In general, the geology of the Kingdom of Saudi Arabia (KSA) is predominantly divided into two main units: (1) the Precambrian igneous/metamorphic basement complex (about one third of the KSA), which is called the shield rocks in the west, and (2) the Phanerozoic sedimentary cover (about two thirds of the KSA total area) in the east (Fig. 1.9). A narrow band of Cenozoic strata also found along the Red Sea coast. Saudi Arabia is one of the best exposed Neoproterozoic areas in the world. The NW-SE trending Najd fault system deformed and metamorphosed the volcano-sedimentary rocks through the Najd event, which also affected rock types of the whole region in the form of fragile and ductile tectonic structures, creating channels for hydrothermal fluids and grabens that filled later by Cambro-Silurian sediments. Consequently, the whole region was covered by the Tethys transgression

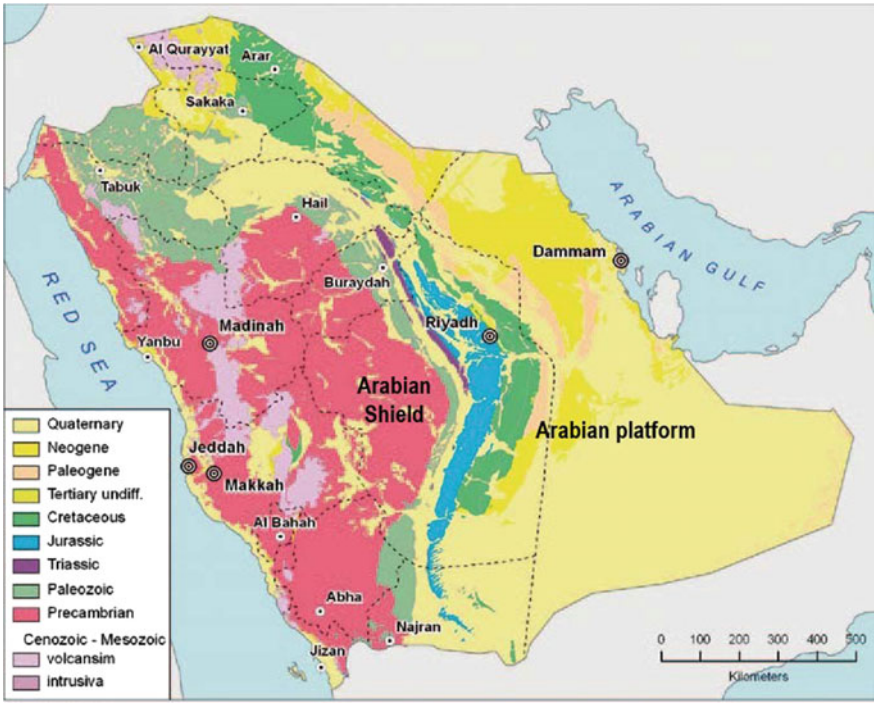

Fig. 1.9 Simplified geologic map of the Kingdom of Saudi Arabia showing the shield rocks in the west and the sedimentary cover in the east of the country (*Source* Maps of Geological Survey of Saudi Arabia)

event, and shallow marine conditions prevailed during most of the Phanerozoic era, when a thick pile of sediments (platform) covered the whole region (Fig. 1.9). The covering platform sedimentation is the source of oil that has produced the wealth of the country. The Tertiary and Quaternary periods have been characterized by alternating hot humid and arid climates. Ancient lakes dried up, generating evaporites, and playa deposits. The opening of the Red Sea during the Miocene has generated basic volcanism along both sides of the Red Sea graben.

About two thirds of the rocks exposed in the Arabian Shield are volcanic, volcaniclastic, sedimentary, and plutonic rocks that make up belts of deformed and metamorphosed rocks identified as magmatic arcs. These arcs are juvenile additions to the crust, constituting the bulk of material present in the Arabian Shield terranes. The amalgamation of these arcs created a neo-craton where post-amalgamation basins and late- to posttectonic plutons were subsequently deposited and intruded (Johnson and Kattan 2012). The amalgamation of these arcs is fundamental to the formation of the Arabian Shield. The Arabian Shield is divided into a number of lithostratigraphic terranes, but the number of these terranes and where to draw their boundaries is debated and has changed with time. The most recent terrane divisions with estimated ages are shown in Fig. 1.10 (Johnson and Kattan 2012). The terrane-forming rocks are folded, metamorphosed and formed a newly amalgamated basement into which late- to posttectonic plutons were intruded, and on which younger sedimentary and volcanic basins were deposited. Terranes in the Arabian Shield are mostly consisting of volcanic, volcaniclastic, and intrusive assemblages that formed as arcs above subduction zones in the Mozambique Ocean. These spatially and temporally distinct terranes are juxtaposed during the subsequent cratonization of the Arabian Shield. The overlying layered rocks and late- to posttectonic intrusions are superimposed on these terranes. The later geologic events and epicratonic volcanic and sedimentary rocks occasionally obscure terrane boundaries. These geologic terranes are further subdivided into provinces, which appear to form distinct stratigraphic and/or structural packages. Although, in general, these provinces were not as well defined as terranes, it was recognized that some of the provinces might themselves be shown to represent distinct terranes (Abd-Allah et al., 2014).

(B) ***Tectonostratigraphic Terranes***

The "*terrane*", as a tectonostratigraphic term, is a "fault-bounded package of rocks of regional extent characterized by a geologic history which differs from that of neighboring terranes" (Howell et al. 1985) (Fig. 1.10). In the Arabian Shield, differences in geologic history can be established by differences in age, crustal origin (whether juvenile or older reworked material), tectonic setting, and timing of metamorphism and deformation (Johnson and Kattan 2012). In most cases, however, these differences are based on reconnaissance geologic mapping and therefore terrane boundaries in the shield are still largely uncertain. Terranes that contain rock assemblages of different ages and origins, or rock assemblages internally divided into structural belts or domains, are referred to as "composite terranes". For example, the Afif terrane (Fig. 1.10), is comprised of the Khida sub-terrane (1800–1650 Ma), along with pre-Siham metavolcanic rocks (~850 Ma), the Nuqrah (~840 Ma), Siham (750–685 Ma)

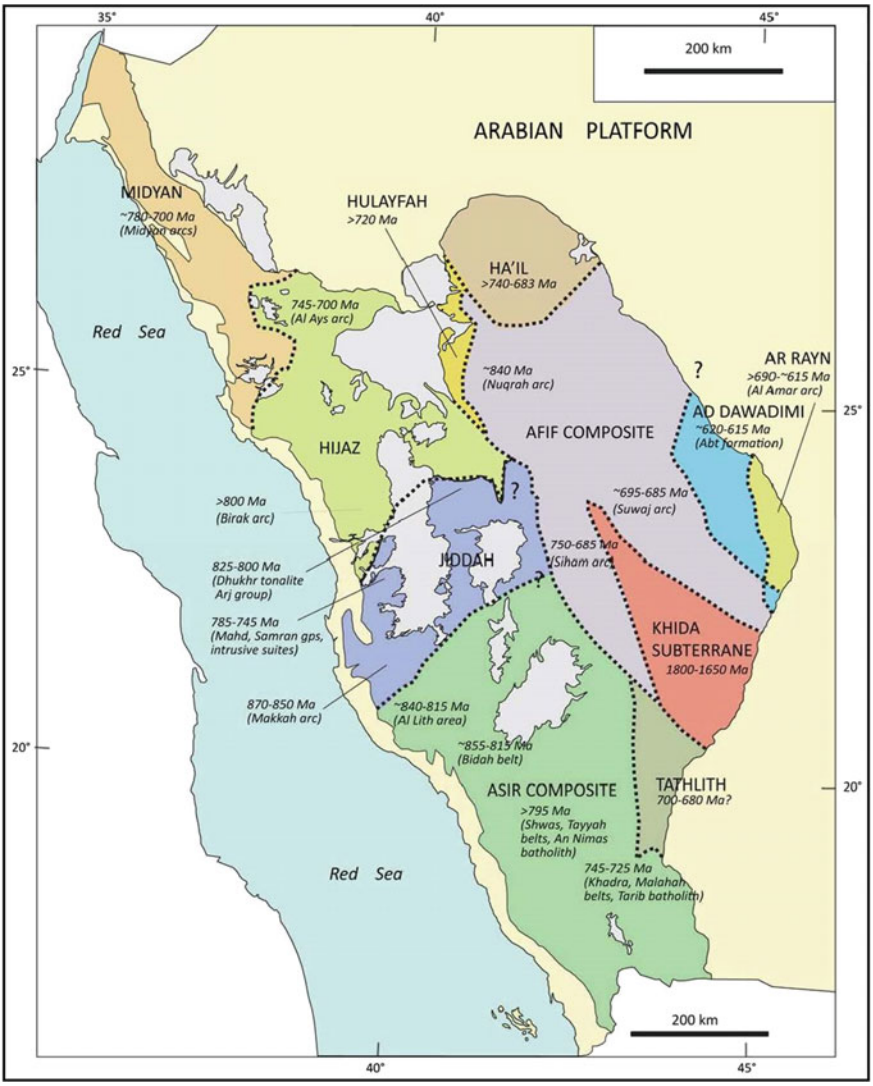

Fig. 1.10 The most recent terrane divisions and types of the Arabian Shield with estimated ages (after Johnson and Kattan 2012)

and the Suwaj arcs (695–685 Ma) (Johnson and Kattan 2012). The Asir terrane is also likely to be a composite terrane, but further work is required to determine this with confidence. Younger layered rocks in any given terrane include sedimentary and volcanic successions deposited in "post-amalgamation" basins on deformed and metamorphosed arc rocks that had undergone an episode of terrane amalgamation.

Terranes in the Arabian Shield are bounded by shear zones, which either represent sutures between the terranes or later transform or trans-current faults. Suture zones

are the sites where terranes converge. They reflect the original positions of the downgoing slab, which in most cases, contain preserved fragments of oceanic crust or ophiolite. Such shear zones may have formed during a process of oblique subduction (transpression) or as a later deformation event superimposed on a suture or displacing terranes. The convergence and joining the terranes together is termed as "amalgamation" process, while the addition of a terrane or terranes to a continental margin is called "accretion" (Howell et al. 1985). Thus, the terranes of Asir, Jiddah, and Hijaz (and correlative terranes in the Nubian Shield) subsequently amalgamated with the Afif terrane, then with the Ad Dawadimi and Ar Rayn terranes, and eventually all the amalgamated terranes of the ANS accreted with the Saharan Metacraton (Johnson and Kattan 2012). The Precambrian rocks in the Arabian Shield of Saudi Arabia can be classified based on the geologic studies conducted on the whole shield areas into two types (Stoeser 1986; Al-Shanti 1993): (1) *Precambrian volcano-sedimentary rocks*, and (2) *Precambrian plutonic rocks*. The Arabian Shield consists of almost equal proportions of layered rocks (sedimentary, volcanic and volcaniclastic varieties) and plutonic rocks (granodiorite, tonalite, diorite and granites) (Fig. 1.11, Johnson and Kattan 2012). Following is a brief description of these geologic terranes and their Precambrian layered and plutonic rocks in Saudi Arabia.

Based on the geochronological data, stratigraphy, and structures, the Arabian Shield can be subdivided into eight tectonostratigraphic terranes (Fig. 1.10), these terranes were referred to as plates or microplates (Viland 1986). Volcano-sedimentary and intrusive rocks in all terranes are poly-deformed and commonly metamorphosed to greenschist or lower amphibolite facies. Geologic terranes of the Arabian Shield are separated by zones of intense deformation (sutures), many of which are marked by lenses and slivers of serpentinites. Ages of suturing are indirectly dated by crystallization ages of syntectonic intrusions along the sutures, ages of overlapping sedimentary sequences, and posttectonic intrusions. Based on the Sr- (Fleck et al. 1980) and Pb-isotopic data (Stacey et al. 1980; Stacey and Stoeser 1983a, b), terranes in the western portion of the Arabian Shield (Midyan, Hijaz, Jiddah, and Asir) are interpreted to have formed in a juvenile oceanic environment (i.e., ensimatic), whereas those in the eastern portion (Afif, Ha'il, Ad Dawadimi, and Ar Rayn) were derived from mixed oceanic and evolved continental sources. The following short descriptions of these tectonostratigraphic terranes begin with the western ensimatic-derived terranes, presented in order from north to south, then followed by the eastern mixed oceanic-continental ones (Fig. 1.10).

Midyan Terrane: It is located in the extreme northwestern part of the Arabian Shield (Fig. 1.10). Midyan terrane consists of two deformed units, the Zaam group and the Bayda and Hegaf groups. The former is a volcano-sedimentary sequence and chemical sedimentary rocks possibly formed between 800 and 725 Ma (Stoeser and Camp 1985; Nehlig et al. 2002; Stoeser and Frost 2006; Johnson and Kattan 2012). Coeval rocks in the Nubian Shield of the Eastern Desert of Egypt and in Sinai were coterminous with the Midyan terrane prior to the onset of the Red Sea rifting at ~25 Ma (Bosworth 2015), and formed a continuous block of Neoproterozoic crust in the African Plate referred to as the Midyan-Eastern Desert-Sinai composite terrane (Kozdroj et al. 2017). The Midyan-Eastern Desert-Sinai composite terrane

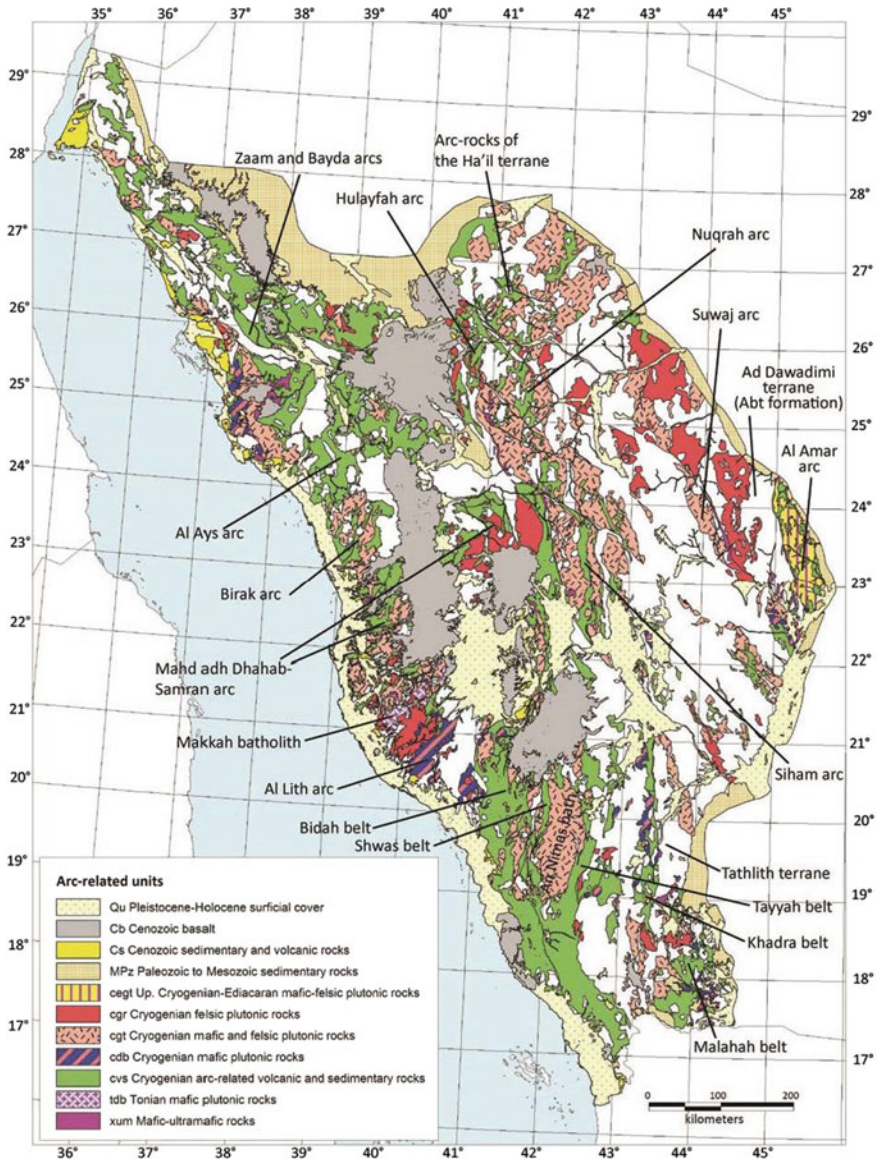

Fig. 1.11 Geologic map of the Arabian Shield rocks containing the Cryogenian to Ediacaran terrane-forming, arc-related assemblages, and structural belts in Saudi Arabia (after Johnson and Kattan 2012)

comprises accreted volcanic arcs, obducted ophiolite complexes, a large range of syn-arc tonalite-trondhjemite-granodiorite (TTG) intrusions, late- to posttectonic granites, and volcanic and sedimentary rocks deposited in Ediacaran post-amalgamation and fault-related pull-apart basins (Johnson and Kattan 2012; Kozdroj et al. 2017). The layered sedimentary series of Median terrane comprise banded-iron formation, pyritic and graphitic shale, black chert, and carbonaceous limestone. The Bayda and Hegaf volcano-sedimentary groups consist of an island-arc assemblage of low-K basaltic, andesitic, and intercalated rhyolitic volcanic and volcaniclastic rocks and epiclastic sedimentary rocks. Dated intrusions into these two groups indicated that they are older than 710 Ma (e.g., Ali et al. 2010a, b). The Midyan terrane is separated from the Hijaz Terrane to the south by the Yanbu suture zone along which ophiolitic rocks scattered, separating the Midyan terrane from the Hijaz terrane to the south. The Yanbu-Allaqi suture have been dated at 780–740 Ma indicating that the rocks along Yanbu suture are juvenile, composed of material newly separated from the mantle (Ali et al. 2010a, b; Kozdroj et al. 2017).

Hijaz Terrane: The Hijaz terrane is separated from the Midyan terrane to the north by the Yanbu suture which consists of large fault-bounded lenses of mafic and ultramafic rocks (the Gebel Al Wask-Gebel Ess ophiolite), which are discontinuously exposed and partially covered by Cenozoic flood basalt. The terrane comprises two volcanic arcs (the Birak and Al'Ays groups), Farri marginal basin, and two overlying volcano-sedimentary units (the Hadiyah and Furayh groups). The Birak group (thought to be older than 807 Ma, Johnson et al. 1987) contains abundant low-K to tholeiitic pillow basalt, tuff, and volcaniclastic rocks. Ophiolite within the Bi'r Umq suture to the south probably belongs to the Birak group. The Al'Ays group ranges from a forearc succession in the west to an eastern volcanic-arc facies of low- to high-K volcanic mafic rocks, rhyolite, and welded tuff. About 6 km-thick assemblage of conglomerate, marble, rhyolite tuff, andesite, and basalt, along with diorite, tonalite, and granodiorite intrusions comprise an enigmatic assemblage at the northern end of the Hulayfah-Ad Dafinah-Ruwah suture. The Farri marginal basin crops out on the northwestern margin of the terrane as a strongly deformed accretion prism (Camp 1984). It consists of highly metamorphosed volcanosedimantary rocks associated with dismembered ophiolitic assemblages. It is intruded by a suite of tonalite (Jar tonalite) dated at 796 ± 23 Ma (U-Pb zircon; Kemp et al. 1980) and 743 ± 10 Ma (U-Pb zircon; Ledru and Auge 1984). The ophiolitic rocks yielded U-Pb and Sm-Nd ages of 780–740 Ma (Claesson et al. 1984), 882 ± 12 Ma (Kemp et al. 1980) or 776 ± 9 Ma (Ledru and Auge 1984). The Al 'Ays volcanic complex with an approximate age of 735–705 Ma (Kemp et al. 1980) occupies the greater part of the Hijaz terrane. The Al'Ays group is predominantly sedimentary in the west and mainly volcanic in the east (Kemp 1981), interpreted to represent fore-arc and volcanic-arc assemblages, respectively (Camp 1984). To the south, the Bi'r Umq suture is separating the Hijaz terrane from the Jiddah terrane (Fig. 1.10); it is the oldest known suture in the Arabian shield at 780–760 Ma (Kemp et al. 1980; Claesson et al. 1984; Ledru and Auge 1984; Johnson et al. 2004, 2013).

Jiddah Terrane: It is a composite terrane comprising a Tonian arc (870–850 Ma) in the south, represented by deeply eroded plutonic rocks of the Makkah batholith

and flanking amphibolite-grade volcanic strata, and early to middle Cryogenian arc rocks (825–745 Ma) in the north, represented by the Arj, Mahd, and Samran groups and intrusive TTG suites (Hargrove 2006; Johnson et al. 2013). The Jiddah terrane is dominated by northeasterly structural trends (Fig. 1.10), and consists of two main supracrustal group rocks of: (1) Samran and Mahd group rocks of volcanic, volcaniclastic, and sedimentary strata (810–780 Ma), and (2) Ghamr group rocks of a sequence of basalt, andesite, dacite, rhyolite, epiclastic sandstone, and polymictic conglomerate (less than 760 Ma) that unconformably overlying the earlier groups (Hargrove 2006; Johnson et al. 2013). Ophiolite complexes suggestive of mixed mid-ocean-ridge and island-arc environments have been dated at 828–838 Ma. The terrane is joined to the Asir terrane to the south along the undated Ad Damm fault zone (Fig. 1.10).

Asir Terrane: It is one of the largest and most strongly deformed terranes in the Arabian Shield. Island-arc volcanic and related intrusive rocks in the western part of the Asir terrane (850–790 Ma) comprise the oldest rock assemblage (Johnson et al. 2001). The eastern part of the Asir terrane is underlain by younger groups of volcanic rocks (785–680 Ma) and a narrow north-trending belt of orthogneiss of variable composition. The Asir terrane consists of metamorphosed volcanic, sedimentary, and plutonic rocks deformed by isoclinal, north-trending folds and ductile shear zones. The terrane includes both older and younger island-arcs assemblages. The older assemblage is dominated by intercalated low-K tholeiitic basalt and graywacke (Baish, Bahah and Jeddah groups). These rocks are intruded by dioritic to tonalitic plutonic rocks dated from 950 to 800 Ma (e.g., Fleck et al. 1980; Johnson et al. 2001). In the southwestern part of the terrane, the older assemblage is underlain by, and intercalated with, pelitic and quartzo-feldspathic clastic metasedimentary rocks of Sabya formation that was interpreted to be derived from the African craton to the west. Elongate post-tectonic basins are filled with sedimentary rocks ranging in age from <664 to <638 Ma (Johnson et al. 2001). The Asir terrane is characterized by shear zones (e.g., Nabitah fault zone) whose histories and tectonic significance are poorly understood. Some may have originated as sutures but many also portray evidence of post-amalgamation movement so that their true tectonic significance is unclear. The brittle-ductile dextral Ad Damm shear zone, possibly representing a cryptic suture, separates the Asir terrane from the Jiddah terrane to the northwest. The Asir terrane joins the Afif terrane to the northeast along the Ruwah fault zone (Fig. 1.10).

Afif Terrane: It is composite in age and provenance; composed of four sub-terranes comprising Khida, an Archean to Paleoproterozoic continental microplate, and four Neoproterozoic volcanic arcs (Siham, Nuqrah, and Suwaj) (Fig. 1.10). Isolated exposures of poly-deformed, high-grade metamorphosed volcanics, schist and gneiss define the Khida sub-terrane, considered to be old continental crust now fragmented by extensive intrusions of Neoproterozoic granite. Upper greenschist Siham group volcanic and sedimentary rocks unconformably overlain on the Khida sub-terrane characterize the Siham sub-terrane and possibly represent a continental-margin volcanic arc. Agar (1985) and Stacey and Agar (1985) have indicated that the Siham group rocks represent an Andean type continental-margin volcanic arc

(named the Siham arc) formed between 750 and 695 Ma above east-dipping subduction zone beneath the western continental margin of the Afif terrane represented by the Khida sub-terrane. The arc-related mafic and intermediate intrusions of gabbro, diorite, tonalite, granodiorite and monzogranite of calc-alkaline composition, which belong to the Naim complex and Jiddah suite, were emplaced between 750 and 705 Ma (Agar 1985, 1986; Stacey and Agar 1985; Johnson and Kattan 1999). The Nuqrah sub-terrane consists of island-arc volcanic and sedimentary rocks of the Nuqrah formation (839 and 821 Ma), which were widely intruded by mafic to intermediate plutons (Calvez et al. 1983). Mafic and ultramafic complexes, interpreted as remnant ophiolite and dated at 823 and 847 Ma, occur as roof pendants and as lenses distributed along the Hulayfah-Ad Dafinah-Ruwah suture zone. The Suwaj sub-terrane is an assemblage of strongly deformed felsic intrusions with lesser basalt and dacite, and large amounts of dioritic to granodioritic intrusive rocks tentatively dated at 745–667 Ma (Johnson and Kattan 1999). The Afif terrane converged with, and truncated, terranes to the west along the Hulayfah-Ad Dafinah-Ruwah suture at about 680 Ma. The terrane is in contact with others farther east along the Halaban-Zarghat fault zone (Fig. 1.10).

Ad Dawadimi Terrane: The Afif terrane is bounded to the east by the Ad Dawadimi terrane; they are separated by the Halaban suture, which in turn, decorated by 695–675 Ma Halaban ophiolite (Johnson et al. 2013). It is evidenced from the deep-water sedimentation in the Ad Dawadimi terrane that the margin was active into the Ediacaran age, until after ~620 Ma, and metamorphosed and deformed of its sedimentary rocks at about 620 Ma (Cox et al. 2012; Johnson et al. 2013). The Ad Dawadimi terrane is a distinctly homogeneous crustal unit that dominated by metasedimentary rocks (sandstone and siltstone) of the Abt formation. Mafic and ultramafic rocks, which interpreted to be remnant of ophiolites, are exposed as linear belts along the margins and within the Ad Dawadimi terrane. The original depositional environment of the Abt sedimentary rocks is uncertain; possibilities include the margin of the Afif terrane (to the west), the margin of the Ar Rayn terrane (to the east), or a completely independent tectonostratigraphic unit. The ophiolites were emplaced about 680 Ma, thereby establishing the age of the unnamed suture separating the Ad Dawadimi from the Afif terrane to the west.

Ar Rayn Terrane: It is dominated by tholeiitic to calc-alkalic andesite and rhyolitic volcanic and volcaniclastic rocks of the Al Amar group. The Al Amar group has a bimodal character, which is probably formed in a mature island arc; it has not been directly dated but indirect evidence indicates it was deposited prior to 690 Ma (Johnson et al. 2001). Three distinct suites of mafic to intermediate plutonic rocks, ranging in age from 616 to 689 Ma, complete the Ar Rayn assemblage. The 670 to 640 Ma of Al Amar fault zone (suture) separates the Ar Rayn terrane from the Ad Dawadimi metasedimentary terrane to the west.

Ha'il Terrane: Ha'il terrane which discontinuously exposed rocks in the north-eastern part of the shield was treated by some geologist as part of the Afif terrane. Features supporting the interpretation that it is a separate terrane include: (i) the distinctive northeast structural trend that is different in orientation to trends in adjacent areas; and (ii) the presence of shear zones and magmatic boundaries that separate

the terrane from other parts of the shield (Johnson et al. 1987). It consist of strongly deformed volcanic and sedimentary rocks intruded by mafic to intermediate plutonic rocks considered to be roughly coeval with the supracrustal rocks (Johnson et al. 1987). Granodiorite intrusions have been dated at 740 Ma, which establishing a minimum age for the layered assemblage (Johnson et al. 1987, 2001).

(C) ***Layered Volcano-sedimentary Shield Rocks***

The ***Precambrian layered volcano-sedimentary shield rocks*** of the Arabian Shield were divided into three successive tectonic cycles, each of which has its distinct characteristic types of layered volcano-sedimentary and intrusive rocks. Based on the types of layered rocks and plutonic intrusions, the tectonic successive cycles are classified from older to younger into: (1) lower-layered rocks (ancient Neoproterozoic cycle), (2) middle-layered rocks (middle Neoproterozoic cycle), and (3) upper-layered rocks (newest Neoproterozoic cycle).

(1) *The ancient Neoproterozoic cycle*, also called lower-layered rocks, includes both the Aqiq orogeny and/or the Tuluhah orogeny. This tectonic cycle is approximately covered the period older than 800 Ma. The oldest units in this cycle represented by the ophiolitic ultramafic rocks, which are widely distributed along almost all suture zones between the terranes. The most complete, but fragmented, ophiolite is located at Gebel Ess; the largest exposures are around Gebel Rayyan (El-Wask) within the Al'Ays region northwest of Yanbu. The longest outcrop of ophiolitic ultramafic and related rocks follows the Nabitah fault zone from the Yemen border northward to the Najd fault zone at lat 21°N, where it is offset 120 km left laterally along the Najd fault zone to the northwest (in various fragments). The most northwestern outcrop being located to the Tuluhah tectonic belt, north of lat 25° 30′ N. The easternmost ophiolitic zone is along the Al Amar-Idsas fault near the eastern edge of the shield (Fig. 1.11). The volcanic rocks related to the lower-layered group are dominated by tholeiitic affinity; they are represented by basaltic rocks and their derivatives (such as those of the *Bish and Al-Bahah groups*), which are more than 800 Ma old. These rocks are scattered in the western part of the Arabian Shield (Fig. 1.11). It is conformable with these volcanic rocks of an oceanic origin, sediments with abundant detrital components, which believed to be derived from the nearby continental cratons, especially the African Craton, or derived from the continental terrane separated from it, such as the Afif terrane.

(2) *The middle Neoproterozoic cycle*, also called the middle-layered rocks, includes both the Yafih Orogeny and/or Ar Ragabah Orogeny. This tectonic cycle approximately covered the period from 800 to 700 *Ma*. The majority of rocks that belong to this group is dominated by calc-silicate volcanic rocks in which the intermediate rock compositions predominate, which are found in many areas in the Arabian Shield. The *Jiddah group* rocks are the best example of these middle-layered rocks. The Jiddah group consists of a lower volcanic

formation named as "Qirshah formation", and an upper clastic, predominately immature arkosic and volcaniclastic wacke named as "Khutnah formation". The Qirshah formation consists mainly of andesitic pyroclastic and flow rocks and includes dacite breccia, ignimbrite, marble, and some pillow basalt, suggesting a marginal marine origin. Much of the sedimentary and volcanoclastic schist of the Jiddah group is graphitic and includes beds of chert and minor basalt, which resembling the upper Bahah froup.

(3) *The newest Neoproterozoic cycle*, also called the upper-layered rocks, includes both the Bishah orogeny and/or Rimmah orogeny, which approximately covered the period 700–560 *Ma.* The rocks of this group are dominated by the calc-silicate and alkaline volcanics, in which acidic rocks predominate, which are also found in many parts of the Arabian Shield. The *Ablah group* rocks are the best examples of this newest Neoproterozoic tectonic cycle. The Ablah group rest non-conformably on Jiddah group metavolcanic and plutonic rocks. The Ablah group is subdivided into three formations: (1) Rafa formation represents the basal polymict conglomerate-wacke-marble series that metamorphosed to greenschist, (2) Jerub formation represents the middle unit composed essentially of calc-alkaline flows but including rhyolite, quartz latite, some basaltic extrusives with pillow structure, marble, and pyroclastic rocks, and (3) Thurat formation represents the younger beds making up the original Ablah formation. Andesite flows and feeder dikes are present in the midsection (in the Jerub formation). Some of the coarser grained sedimentary rocks contain fluorite, seemingly epigenetic and coeval with the Ablah fluorite pipe. The basal conglomerates of Ablah group contain boulders of the Jiddah group rocks as well as some rocks from the older Bish-Bahah groups. The *Fatimah group* is remarkably similar to the Ablah group; it rests non-conformably on the granodiorite of Mecca and includes red and green immature clastics, stromatolitic limestone, tuffaceous sediments, andesite and basalt flows. The age of the Ablah-Fatimah groups may fall somewhere within the timespan between 816 ± 3 Ma (Kemp et al. 1982) for the Mahd adh Dhahab area and 763 ± 55 Ma for the Bagarah gneiss dome of the Ablah belt (Fleck et al. 1980).

The *Halaban group* (Brown and Jackson 1979) covers large areas in the eastern and northern parts of the shield. The outcrops extend in folded and faulted belts for at least 800 km in a north or northwesterly direction and extend laterally as much as 40 km in the type locality. The predominantly calc-alkalic rocks and uppermost beds that contains rhyolitic flows, ignimbrite, and tuffaceous sedimentary rocks, are all, of a typical island-arc assemblage. These rock assemblages of the Halaban group in the southeastern part of the Arabian Shield is comparable to the Hulayfah Group in the northeastern part of the shield. The *Murdama group* consists of a succession of slate, phyllite, quartzite, graywacke, and conglomerate in a traverse across the north end of the Murdama Mountain. Based on the lithologic similarity, thickness, degree of metamorphism, and an apparent stratigraphic position above rocks considered the Murdama group to be comparable with the Halaban group.

The *Shammar group* considered as the youngest Precambrian layered rocks in the Arabian Shield (Brown and Jackson 1979), which composed of alkalic and peralkalic acidic volcanic rocks (Shammar rhyolite) and associated gently folded sedimentary beds. The sedimentary beds and flows originally mapped above and interbedded with the upper Shammar rhyolite were later separated and recognized as a distinct unit above an unconformity (Delfour 1967), which named as *Jubaylah group*. They are the youngest rocks involved in the layered succession of the Arabian Shield. Delfour (1967) divided the Jubaylah group informally at the type locality east of Harrat Khaybar into three units: a basal conglomerate; andesite, basalt, and welded silicic tuff; and a cherty limestone containing stromatolitic structures. After several attempts to date the Jubaylah group using K-Ar method of dating, Binda (1981) concludes that the Jubaylah group is probably uppermost Vendian (600–570 Ma).

(D) ***Intrusive Plutonic Shield Rocks***

The intrusive plutonic shield rocks of Saudi Arabia are subdivided into an older, pre-tectonic dioritic suite; and a younger, syn-tectonic and post-tectonic (mostly granitic) suite, which includes an early, layered gabbroic phase (Fig. 1.11). The Precambrian plutonic granitoid rocks comprise about 17% of the total area of the Arabian Shield in Saudi Arabia, and are concentrated mainly in the northeast, central, and southwest regions of the shield (Greenwood and Brown 1973; Stoeser 1986). The late major tectonism associated with granite emplacement was most intense in the eastern and northeastern parts of the shield, and resulted in a greater abundance of granitic plutons in the northeast. In the central part of the shield, in a belt about 200 km wide including the major Najd fault zones, late orogeny was intense and the erosion level is moderately shallow, so that many late granitic plutons are exposed with few cogenetic rhyolitic rocks of the Shammar Group. The southern part of the shield is deeply eroded and was less deformed during the late major orogeny, so that this region has the smallest area of granitic plutons and only have rare exposures of Shammar volcanic rocks. In addition to the plutonic granitic and dioritic suites, a mafic-ultramafic suite of plutonic rocks is also present and characterized by serpentinite in association with ultramafic, gabbroic, basaltic, and diabasic rocks. The mafic-ultramafic suite is confined mostly to narrow belts in large fault zones, is independent of the dioritic-suite rocks, and makes up less than 1 percent of the Precambrian plutonic rocks of the Arabian Shield in the Kingdom of Saudi Arabia. The mafic-ultramafic suite is described earlier in this chapter as ophiolite complexes that are rarely complete at any locality and that most probably represent tectonic remnants of oceanic crust of a Neoproterozoic age.

In general, the Precambrian plutonic rocks of the dioritic and granitic suites are petrographically classified into standard rock types, where "granitic" refers to leucocratic plutonic rocks containing more than 5% modal K-feldspar and more than 20% modal quartz. The Precambrian plutonic rocks of Saudi Arabia are further classified as pre-tectonic, syn-tectonic, and posttectonic in reference to a Culminant Orogeny (dated to about 650 $\pm$ 25 Ma), during which most of the rocks of the early crust were intensely tectonized during the cratonization of the Arabian Shield (dated at

about 675–560 Ma). The *dioritic rock suite* consists of, in decreasing order of abundance: diorite, quartz diorite, tonalite, trondhjemite, and gabbro. These rocks were emplaced between about 1,000 and 700 Ma ago (Greenwood et al. 1976; Fleck et al. 1980; Johnson et al. 2001, 2004; Johnson and Kattan 2012) and, together with their volcanic equivalent rocks of the andesite assemblage, constitute the primary crust that represents most of the early (pre-cratonization) crust of the shield. Rocks of the dioritic suite are pre-tectonic in reference to the Culminant Orogeny.

The *granitic rock suite* consists of, in decreasing order of abundance: granodiorite, granite, alkali-feldspar granite, and peraluminous-peralkalic granite, as well as gabbro. The granitic rock suites are widely exposed throughout the Arabian Shield of Saudi Arabia and are most abundant in the northeastern half of the shield (Fig. 1.11). Many of the Precambrian granitic rocks in the shield are slightly to strongly deformed and partly metamorphosed, which are classified as syn-tectonic (intruded during the Culminant orogeny). Other granitic rocks were intruded in a post-tectonic setting (from after the Culminant orogeny to the end of the Precambrian). Granitic rocks commonly produce contact metamorphic aureoles in the adjacent wall rocks. Most of the syn-tectonic granitic rocks commonly form large batholiths of granodioritic composition, which are commonly associated with the large gneiss domes of tonalitic and trondhjemitic orthogneiss. The post-tectonic granite (monzogranite and syenogranite) was intruded as large and irregularly shaped plutons. With increasing depth of erosion, circular granitic plutons were subsequently emplaced at later time, about 600 Ma. Many of these plutons have ring structure where they intruded a preexisting structure. These post-tectonic circular granitic intrusions are prominently associated with mafic intrusions (e.g., gabbros), which are leucocratic in composition and sparsely distributed throughout the shield (Fig. 1.11). These circular and, sometimes layered, gabbroic rocks are most probably intruded in later time, since they are mostly non-metarnorphosed, and in few places they show crosscut relationship with the late granite intrusions. The youngest granitic rocks of the Precambrian shield are those with granite to alkali-feldspar granite composition, which form small plutons or stocks in or adjacent to the Najd fault zone. These small plutons are readily considered as slightly younger than the most of the Najd faulting events where they cut the strongly sheared rocks alongside the fault zone, and commonly form small circular stocks, less than several kilometers in diameter. These younger granitic intrusions are also considered to be intruded during the Najd faulting event where these small plutons are greatly elongated in the fault zone and they highly flow foliated and sheared.

In addition, many late Cryogenian-Ediacaran mafic, felsic, and composite mafic-felsic dikes are widespread in the Arabian Shield, which cover large areas between the Najd faults system (Moore 1979; Genna et al. 2002). They are similarly abundant in the northern part of the Nubian Shield in Sinai and Jordan, where they have been thoroughly studied (Stern et al. 1984; Jarrar 2001; Jarrar et al. 1992, 2004; Ibrahim and McCourt 1995). Such dikes considered as a clear evidence of extension during the final stages of shield development (Stern et al. 1984; Stern 1985; Genna et al. 2002). They considered as post-tectonic event, where they crosscut most other Precambrian rocks and structures and represent some of the youngest Neoproterozoic rocks in any

given area. Dated dikes on the Arabian Shield include lamprophyre dikes that cross-cut the Ajjaj shear zone in the Midyan terrane (573 ± 6 Ma U-Pb zircon age; Kennedy et al. 2010), dikes between 575 ± 6 Ma and 545 ± 13 Ma in the northern Midyan terrane in Jordan (Jarrar 2001), and a dike that intrudes the Jibalah group in the north-central part of the Arabian Shield (577 ± 5 Ma U-Pb zircon age; Kusky and Matsah 2003). These posttectonic dikes occur in linear or curved swarms varying from a few centimeters to meters in thickness and from several meters to several tens of kilometers in length (Genna et al. 2002). The dikes are mostly subvertical, commonly rhyolitic, but also include basalt and andesite, where the bimodal swarms commonly contain andesite and rhyolite dikes that display intrusive relationships indicative of synchronous emplacement of mafic and felsic magmas (Stern et al. 1984). The orientations of these dikes are strong evidence of broad northerly extension in the northern ANS during the Ediacaran period.

1.3.2 Lithostratigraphy of the Arabian Shield Rocks in Yemen

The geology of Yemen, as a whole, is related to the regional geology of the Arabian Peninsula (Fig. 1.12), in which the Precambrian basement complex is a part of the Arabian Shield within a larger geologic framework of the ANS. The geology of Yemen is extending from the Precambrian basement rocks to the recent sediments. It includes metamorphic rocks that formed during Archean-Proterozoic time, transected by Jurassic rift system related to the break-up of the supercontinent of Gondwanaland, and a Tertiary to recent geological history determined by the propagating Indian Ocean Ridge, which triggered the opening of the Gulf of Aden-Red Sea rift (Menzies et al. 1994; Windley et al. 1996).

The Precambrian basement rocks of Yemen occupy a key location (about 105,000 km^2) in the Pan-African orogeny of Gondwana (Whitehouse et al. 2001; Heikal et al. 2013), where they form the southern extension of the Arabian Shield (Fig. 1.12). Basement rocks of Yemen include a large variety of intensely folded, faulted and eroded rocks of Paleoproterozoic to Neoproterozoic age (Windley et al. 1996). They are found throughout western Yemen from the northwest around Sa'dah to as far away as Ras Sharwayn (Fig. 1.13). The Precambrian basement rocks are located between the collage of lower grade (mainly island arc) terranes of ANS to the west and higher grade (mainly gneissic) terranes of the Mozambique belt to the south, extending to Somalia, Ethiopia and East Africa (Heikal et al. 2013).

The basement rocks of Yemen are subdivided into two main geographic categories (Windley et al. 1996; Heikal et al. 2013): the southeastern exposures and the northwestern ones. Six Precambrian terranes have been identified in the basement complex of Yemen (Fig. 1.14), which include Paleoproterozoic to Neoproterozoic gneissic terranes and Pan-African island arc terranes and suture zones (Bosworth et al. 2005). These are namely, Abas and Al Mahfid gneissic terranes, and Al Bayda and Al Mukalla island arc terranes, in the southeastern exposure (Windley et al. 1996). These four terranes represent the most complicated and deformed rocks in

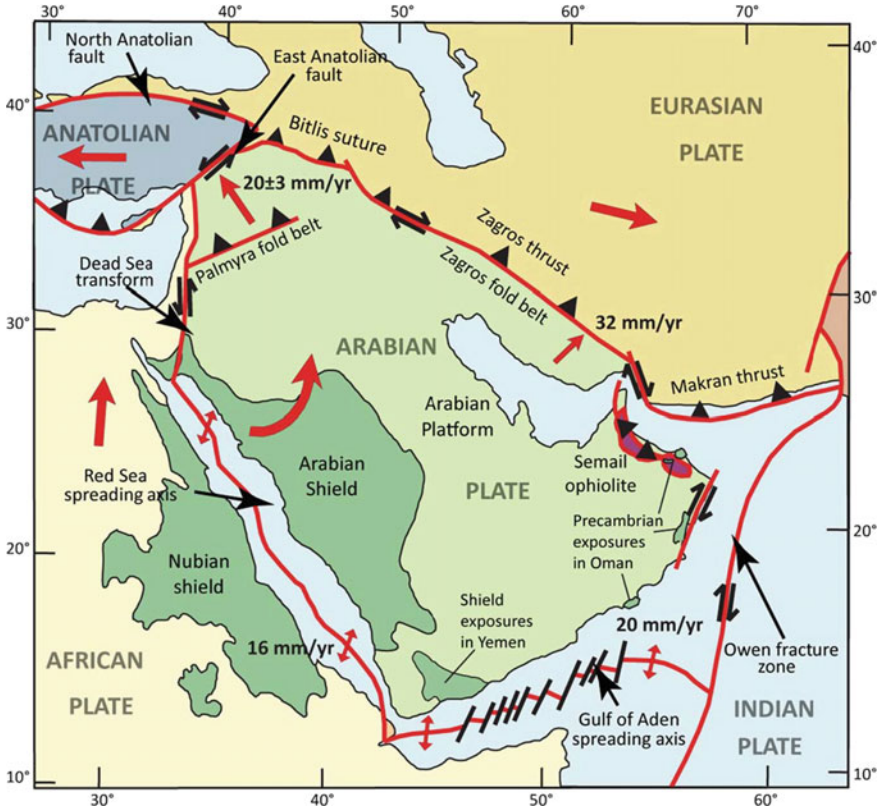

Fig. 1.12 Tectonic setting of the ANS showing the basement exposure in Yemen. The rate of drift and boundaries of Arabian and African plates are also shown (after Stern and Johnson 2010)

terms of their lithology and structural implications, than the Asir and Afif terranes in the northwestern exposure, which they are different in lithology and age. The Asir and Afif terranes of Saudi Arabia (Stoeser and Camp 1985) are also recognizable in northwest Yemen (Fig. 1.14). Therefore, the basement rocks of Yemen combine between the arc collage of the Arabian Shield and the gneissic Mozambique belt of East Africa. These Precambrian terranes were accreted together during the Pan-African orogeny. On the other hand, four provinces within the Yemen basement complex were identified based on their lithologic and structural features and developments (As-Saruri and Wiefel 1998; Albaroot et al. 2016). These provinces are bounded by major faults or sutures (Fig. 1.14), that could be correlated with the Saudi Arabia and Somalia on the basis of geological description, geometric constrains and isotopic and geochronological data (Whitehouse et al. 2001).

Starting from the northwestern exposures, following are brief descriptions of the main Precambrian terranes in Yemen.

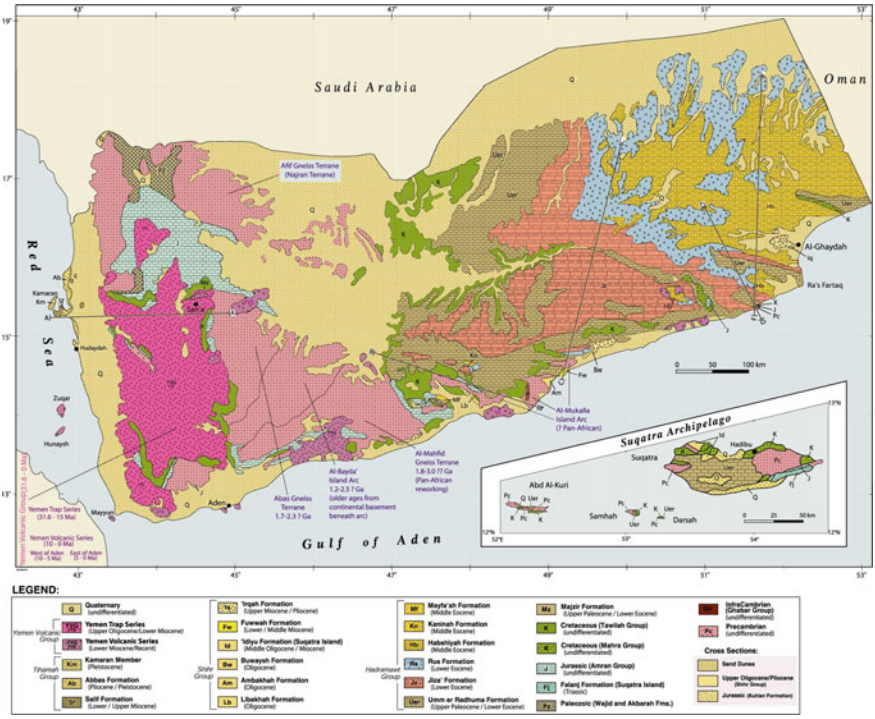

Fig. 1.13 Simplified geologic map of Yemen showing the different rock units including the basement complex

The *Asir terrane* is consisting mainly of gneissic rocks with amphibolite-facies metamorphism, and arc-type volcanics. These gneissic rocks alternating with greenschist-grade supracrustal belts. The isotopic data is not available for Asir terrane in Yemeni side, but it has been dated to about 840–740 Ma in Saudi Arabia (Whitehouse et al. 2001). The *Hajjah group* highly metamorphosed sedimentary and volcanic rocks are a prominent component of the Asir terrane in Yemen basement. Hajjah group divided into two distinct formations, the lower member named Ain Ali formation, and Mawr formation that represents the upper most rock unit (Heikal et al. 2013). The lower member, Ain Ali formation, consists mainly of low-grade metasedimentary rocks, including pelitic schist, marble, and quartzite, which possesses a structural contact with the upper Mawr formation. The upper member, Mawr formaton, is characterized by strong foliation trending northeast and northwest of the mafic metavolcanics, amphibolites, and hornfelsic rocks. The rock associations of the Asir terrane are also found in Sa'dah and Marib areas (Abas terrane) forming island arc rock assemblages of metavolcanics (metabasalts, metaandesites, metadacites, and metatuffs), and metasedimentary rocks (graphite schist, hornblende schist, biotite–muscovite schist, metagreywacke, and marble) indicating their calcareous, siliceous, and pelitic origin (Heikal et al. 2013).

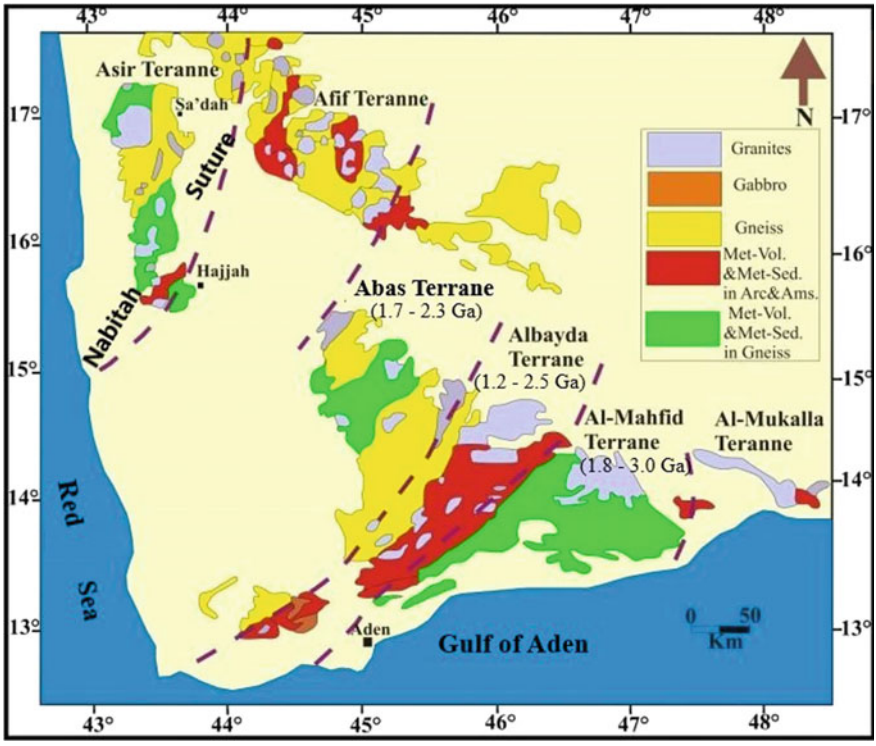

Fig. 1.14 Distribution of the basement rocks in Yemen showing the different terranes with the estimated ages of each terrane (after Windley et al. 1996; Whitehouse et al. 2001)

The *Afif terrane* represents the southwestern extension of the same terrane in Saudi Arabia, which consists of in Yemen a monotonous orthogneiss of unknown age intercalated with arc-type pillow basalts, andesites, and rhyolites. The gneisses and lavas being intruded by undated post-tectonic granitic to gabbroic plutons. The Afif terrane was tentatively interpreted as a Pan-African Andean-type continental margin as the arc has a continental basement (Windley et al. 1996).

The *Abas terrane* is an essential part of the Precambrian continental crust of southeast Arabian Shield of Yemen (Fig. 1.14). The Abas terrane composed of two components: amphibolite facies orthogneisses and metamorphosed supracrustal rocks (Whitehouse et al. 1998; Windley et al. 1996; Albaroot et al. 2016). The Abas gneisses are typically homogeneous, as hornblende-biotite orthogneisses, and some of which are extensively migmatized. Two largely different groups of age were defined for the Abas terrane rocks, a younger age of about 790–730 Ma, and a very old age dated back to 2,700–1,300 Ma (As-Saruri et al. 2013). One of major metamorphic belts belongs to the Abas terrane known as the Rada Group of supracrustal rocks, containing rhyolite, biotite schist, chlorite schist, amphibolite, metatuff, metaarkose and marble. These supracrustal rocks are intruded by numerous discordant

intermediate to mafic dykes. Both the Abas and Al-Mahfid terranes record a major 760 Ma event, which generated orthogneisses in the Abas terrane and granitic sheets in the Al-Mahfid terrane (Whitehouse et al. 1998).

The *Al Bayda terrane* (island arc terrane) is an essential part of the southeastern exposure that dated back to 2,500–1,200 Ma (Windley et al. 1996). The Al Bayda terrane consists mainly of supracrustal rocks of island-arc signature such as rhyolites, andesites, basalts, tuffs and granitic intrusions. Ophiolitic sequences occur at both the eastern and western margins of the Al Bayda terrane, and it is prominently intruded by post-tectonic granitic plutons. The Al Bayda arc rocks are also intruded by undeformed younger rhyolite dikes, as well as intrusive rocks of granodiorite, diorite, gabbros, and late tectonic granites, along the eastern margins (Al-Khirbash et al. 2001). The Al Bayda terrane was interpreted as a juvenile Pan-African island arc sutured to adjacent older gneiss terranes (Windley et al. 1996). Other fragmented groups of Precambrian rocks (Fig. 1.14) such as Fahman, Al Aswad, Hatib groups and Gharish supergroup are mostly belong to the Al Bayda terrane (As-Saruri and Wiefel 2012). The lack of bimodality in volcanic rocks and the lack of terrigeneous sedimentary deposits, coupled with the presence of ophiolites and arc-type volcanic rocks, argue against the rift origin of the Al Bayda terrane, or its formation on top of continental basement (Windley et al. 1996).

The *Al-Mahfid terrane* forms a large area in the southeastern corner of the Yemen basement complex (Fig. 1.14), which mainly comprises of granite-gneiss assemblage, consisting of belts of high-grade gneiss, amphibolites, gneissic granites, as well as low-grade ophiolitic fragments of gabbros, basalts and marbles. Al-Mahfid gneiss is dated back to 2,900–2,550 Ma (Ba-Bttat 1991; Whitehouse et al. 2001), which constitutes supracrustal rocks of late Archean to late Proterozoic ortho- and paragneisses and migmatites and amphibolites, banded metataxite migmatites, anatectic granites, and mylonites. The highly deformed and migmatized supracrustal gneisses are metamorphosed under upper amphibolite facies conditions and are variably migmatized. The less deformed (younger) supracrustal belt is up to 1 km thick, and consists of unmigmatized rhyolites, basaltic andesites, marbles, and thin conglomerates, which have beenmetamorphosed under greenschist facies conditions (Windley et al. 1996). Similar rock associations are also found in Lawdar and Shabwa, where they are exposed as northeast/southwest refolded and faulted sheets. The previously known Aden Metamorophic group is partly included in the Al-Mahfid terrane. The Ahwar supergroup, which comprises highly metamorphosed gneisses of Neoarchean to Neoproterozoic age (3,030–1,200 Ma), is also assigned to the Al-Mahfid terrane (Windley et al. 1996; As-Saruri and Wiefel 2012; Heikal et al. 2013).

The *Al-Mukalla terrane* forms the most southeastern exposure of the basement complex of Yemen (Fig. 1.14), and is comprised ofisland arc tuffs, rhyolites, basalts, volcanic breccia that undergo greenschist-facies metamorphism. There is no confirmed age dating for Al-Mukalla terrane, but probably, by close geologic affinity with the Al-Bayda arc, is a Pan-African island arc age (Windley et al. 1996). The Al-Mukalla Proterozoic basement is located in the southeast edge of the Al-Mukalla horst, in the linking zone between the Marib-Shabwa-Hajar basin

and the Al-Mukalla-Sayut basin (Le Garzic et al. 2011). The basement rocks of Al-Mukalla terrane are cut by homogeneous hornblende granodiorite plutons, which in turn, are cut by a major mafic dike swarms metamorphosed under greenschist-facies conditions.

1.3.3 Lithostratigraphy of the Nubian Shield Rocks in Egypt

Igneous and metamorphic rocks of Egypt, which occasionally named as "basement complex", are well exposed in the northwestern flank of the Red Sea and along the border with Sudan (Fig. 1.15). Although most of the Egyptian subsurface area (about 90%) occupied by basement complex, only a small fraction (about 10%) of this basement is exposed on the surface. The basement complex of Egypt is generally considered to be Precambrian; however, in some locatins, younger igneous and metamorphic rocks are present as well. The Precambrian basement of Egypt is exposed mainly in three places: (1) in southern Sinai, (2) in the Eastern Desert, and (3) in the southernmost Western Desert (Fig. 1.15). The basement complex in the Western Desert of Egypt is mostly Archean in age and not related to the Nubian Shield rocks. They mainly exposed in the most southwestern corner, along the triple-point borders between Libya, Egypt and Sudan, which called in the literature as the "Uweinat-Kamil inlier" (Fig. 1.15). The lithology of these basement rocks in the southern Western Desert of Egypt are dominated by migmatites, gneisses, post-tectonic granites, dikes, and sills.

As this part is concerning with the Nubian Shield rocks, which are mainly concentrated in the Eastern Desert and Sinai, the basement rocks in the Western Desert of Egypt will not discussed here. The exposures in the Eastern Desert can be further subdivided into three smaller sectors: *North Eastern Desert (NED)*, *Central Eastern Desert (CED)*, and *South Eastern Desert (SED)* (Fig. 1.15). Seeking for simplicity, the description of these Precambrian basement rocks will be dealt with in the same arrangement mentioned above as follow (Sinai, NED, CED and SED).

(A) ***Sinai Peninsula***

Sinai peninsula is covering about 60,000 km^2, which counts around 6% of the Egypt's total area. It is located between the Mediterranean Sea to the north and the Red Sea to the south, forming a land link between Africa and Asia (Fig. 1.16a). Sinai peninsula is characterized by a significant variation from the geological point of view, where the Precambrian basement rocks form the southern part of the peninsula bounded by the Gulf of Suez and Gulf of Aqaba (Fig. 1.16a). The central part of Sinai peninsula, on the other hand, occupied mainly by Mesozoic to Tertiary sedimentary rocks. During the Tertiary opening of the Red Sea, volcanism in the western and central Sinai resulted in the formation of many basaltic volcanic rocks, which are mostly doleritic sills, plugs and flows.

The Precambrian basement exposures of Sinai occupy about 10,000 km^2 in the southernmost part of the peninsula, which are composed mainly of granites (~80%),

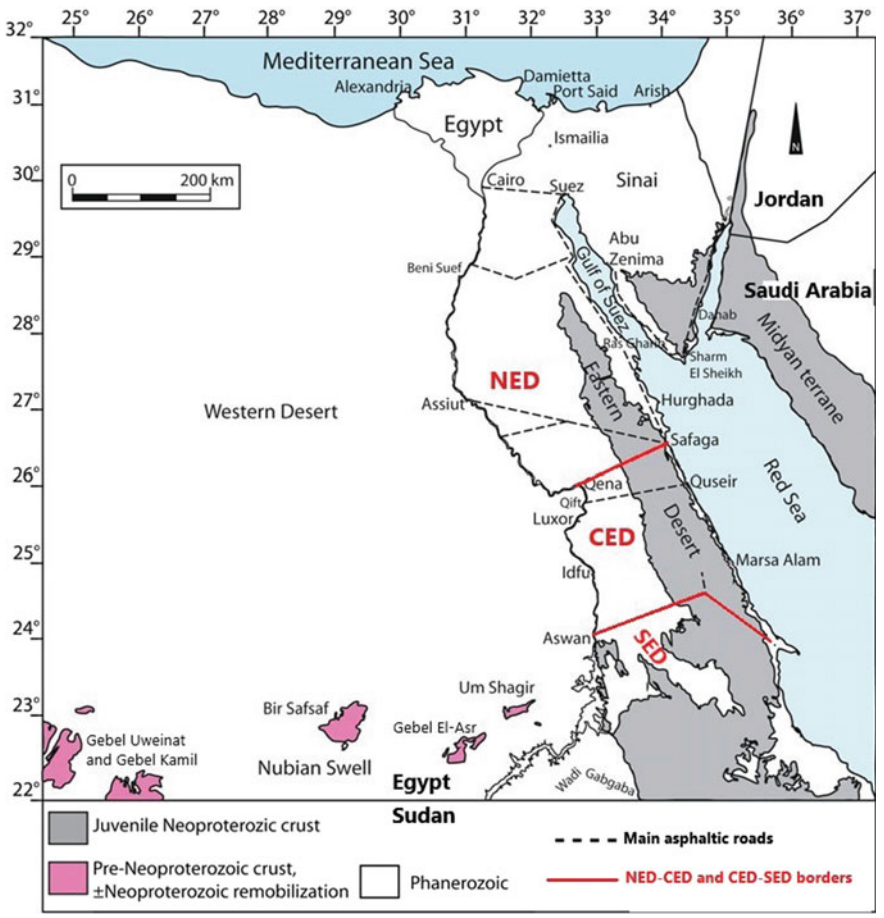

Fig. 1.15 Simplified geologic map of Egypt showing the Precambrian basement exposures and the division borders of the Eastern Desert (after Stern and Ali 2020). NED = North Eastern Desert, CED = Central Eastern Desert, SED = South Eastern Desert

volcanics (~20%) and sedimentary cover (Stern and Hedge 1985). The Exposed basement rocks in Sinai can be further subdivided into three groups, from oldest to youngest: (1) metamorphic complexes; (2) calc-alkaline granitoids; and (3) within-plate granitoids (Stern and Ali 2020). Ediacaran granitoid rocks are much more predominate over the Cryogenian, Tonian, and Stenian metamorphic rock complexes. The metamorphic complexes and granitoid rocks of the Sinai basement are all cross cut by Ediacaran dykes. The metamorphic rocks exposed in four localities are named as: (1) the Taba complex in the northeast, (2) the Kid complex in the southeast, (3) the Sa'al complex in the center, and (4) the Feiran-Solaf complex in the west (Fig. 1.16b). The following is a brief descriptive summary of these rocks.

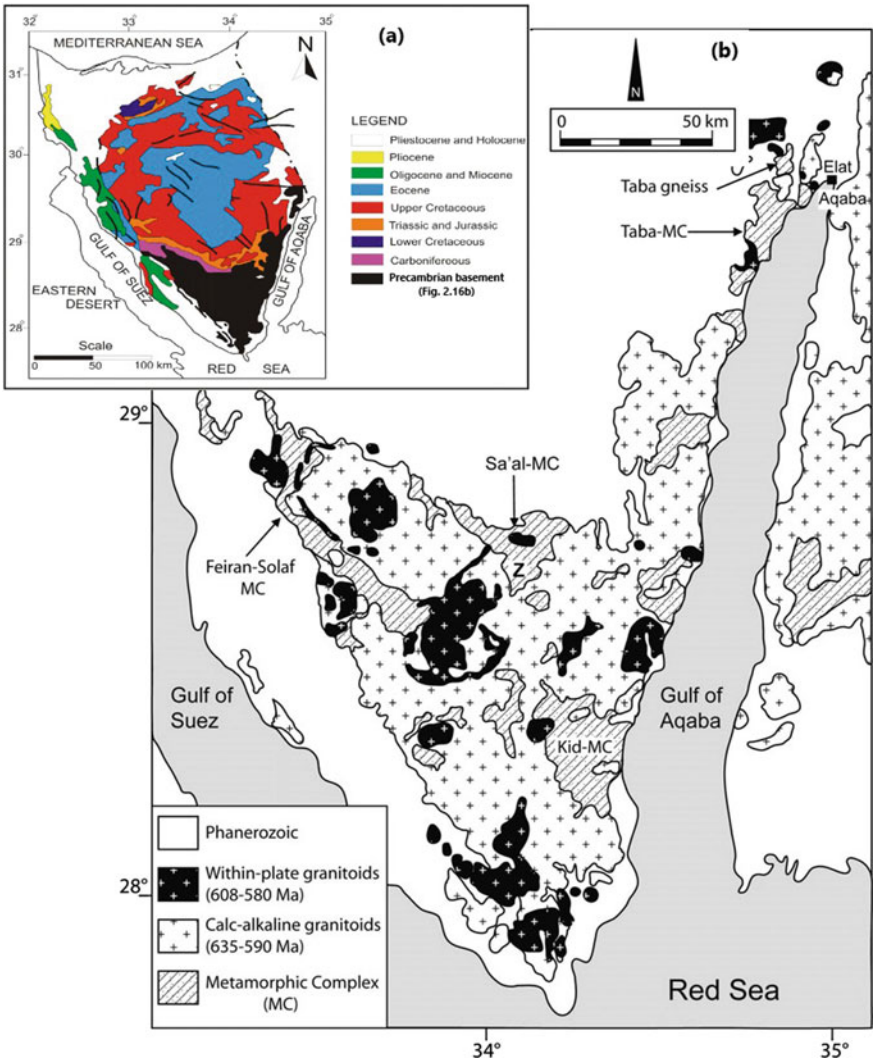

Fig. 1.16 Simplified geological map of Sinai (**a**), showing distribution of the main Precambrian rocks in the southern Sinai (**b**) (modified after Stern and Ali 2020)

The *Taba complex* lies in the extreme northeastern part of the Sinai basement; it extends for about 20 km along the northernmost western margin of the Gulf of Aqaba (Fig. 1.16b). Taba metamorphic complex composed of metapelites, metagabbros-metadiorites, orthogneisses and migmatites of Tonian–Cryogenian age (760–850 Ma) (Abu El-Enen et al. 2004). The *Kid complex* is occupying about 600 km^2 in the southernmost Sinai (Fig. 1.16b), consisting of a volcano-sedimentary succession with island-arc affinity, where the degree of metamorphism increases towards the

central and northern parts of the complex (e.g., Abu El-Enen and Okrusch 2007). These metamorphic volcano-sedimentary rocks of the Kid complex dated back to about 615–605 Ma (Moghazi et al. 2012). The *Sa'al complex* is located in the center of the Sinai Precambrian basement exposures (Fig. 1.16b); it is exceptionally old (1,120–950 Ma) comparing to the other metamorphic complexes of Sinai (Beeri-Shlevin et al. 2012). There are numerous intrusions dividing and isolating parts of the Sa'al volcano-sedimentary exposures from each other. The *Feiran-Solaf complex* is covering a larger area (~100 km^2) than the other metamorphic complexes, in the northwestern part of the Sinai basement complex (Fig. 1.16b). It is a medium- to high-grade terrane consisting of ortho- and para-gneisses, migmatized gneiss, metapelitic and metapsammitic schist and calc-silicate rocks (El-Shafei and Kusky 2003). The Feiran-Solaf complex has yielded a wide range of U-Pb zircon ages, from about 1,000 to <600 Ma, which reveal a succession of magmatic and metamorphic events (Abu El-Enen and Whitehouse 2013). The Feiran-Solaf metamorphic rocks were experienced peak metamorphism at about 700–750 °C and 7–8 kbar, and subsequent isothermal decompression to about 4–5 kbar (Abu-Alam and Stüwe 2009).

The Precambrian calc-alkaline and within-plate granitoids occupying about 80% of the total basement complex of the Sinai Peninsula, which display a wide compositional range from mafic to felsic plutons. Precambrian granitoids of the Sinai Peninsula are mostly related to the Ediacaran magmatism, with ages from 635 to 580 Ma. However, granitoids with relatively older ages (pre-Ediacaran at 782 ± 7 to 844 ± 4 Ma) are also recorded (Stern and Manton 1987; Bea et al. 2009). The Sinai granitoids are probably originated from mafic lower crust, which are mostly similar to the lower crustal granitoids identified beneath the western Saudi Arabia (Stern and Johnson 2010).

(B) ***North Eastern Desert (NED)***

The NED covers the smallest area (~10,000 km^2) among the other two subdivisons of the Eastern Desert of Egypt; it lies north of the Qena-Safaga road (Fig. 1.17). The exposed Precambrian basement of NED is dominated by Ediacaran igneous rocks and associated sedimentary rocks (Stern and Ali 2020); consisting of about 75% granite and gneiss, and the rest 25% are volcanics and sedimentary rocks (Stern and Hedge 1985). The Precambrian geology of the NED is quite similar to those in the Sinai Peninsula, but different from those in the CED and SED of Egypt. The majority of NED basement rocks are much younger than those in the CED and SED, where the Ediacaran igneous rocks are predominant in the former, and Cryogenian and Tonian igneous rocks are predominat in the CED and SED divisions (Stern and Hedge 1985). Furthermore, except in few places, the ophiolitic rocks and gneisses are almost absent in the NED. The absence of Najd deformation features on the NED basement rocks is another evidence for the younger age compared with the CED and SED ones (Stern and Ali 2020). The common abundance of Dokhan volcanics (dated at 592–630 Ma) (Fig. 1.17) is another evidence for the Ediacaran-dominated magmatic activity in the NED (Stern and Hedge 1985; Wilde and Youssef 2000; Breitkreuz et al. 2010). Despite of the predominant of Ediacaran igneous rocks in the NED, there are some recent attempts to document a pre-Ediacaran crust of Cryogenian-Tonian basement

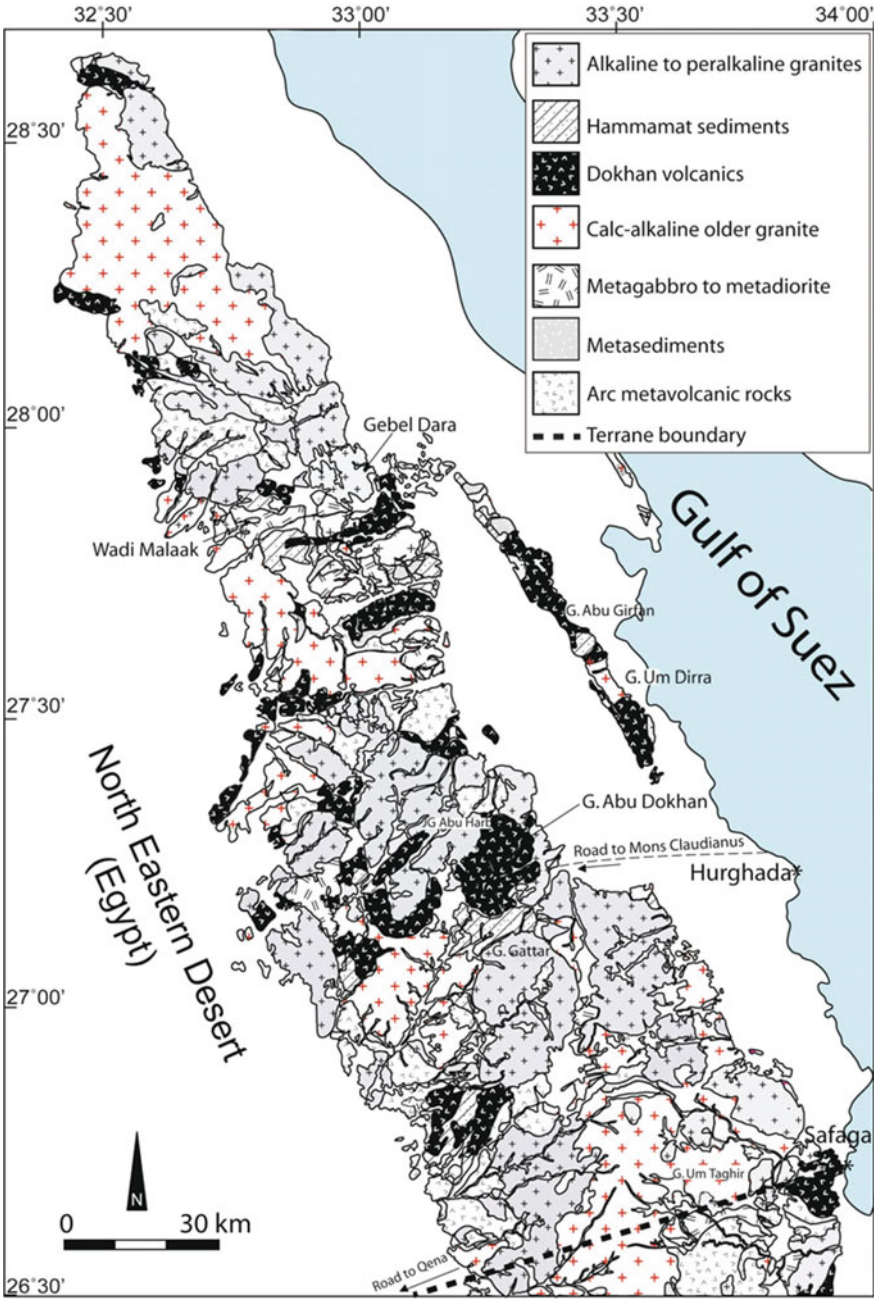

Fig. 1.17 Simplified geologic map of the North Eastern Desert (NED) of Egypt showing the Precambrian basement rocks (after Stern and Ali 2020)

rocks in the NED portion (e.g., Moussa et al. 2008; Bühler et al. 2014; Eliwa et al. 2014; Abd El-Rahman et al. 2017).

(C) ***Central Eastern Desert (CED)***

The CED of Egypt is the best-known part of the three Eastern Desert subdivisions, being the best-preserved oldest (Tonian–Cryogenian) rock types of Egypt. The CED also preserves the Ediacaran deformation features (Najd-Fault System), volcanism (Dokhan volcanics) and sedimentation (Hammamat sedimentary rocks), all of which are associated with intense igneous activity (Stern and Ali 2020). The CED lies to the north of an irregular boundary, ~24° 30′ N, where the SED begins (Fig. 1.18), to the south boundary of the NED (Stern 2018; Stern and Ali 2020). The CED basement

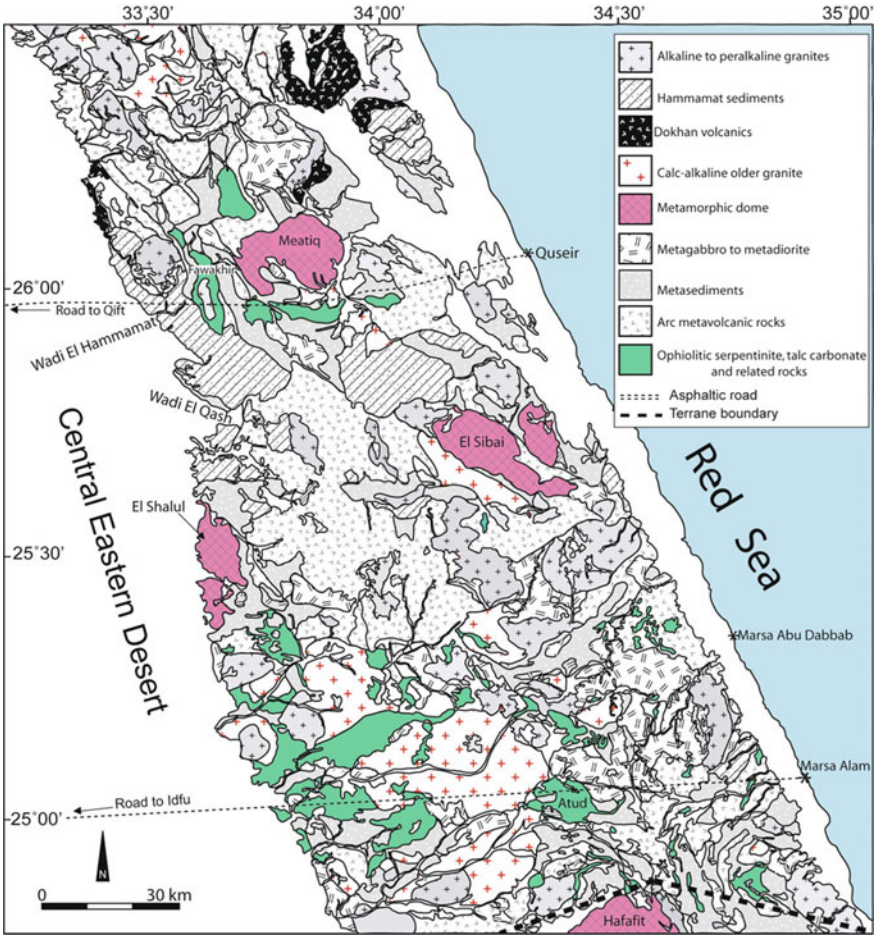

Fig. 1.18 Simplified geologic map of the Central Eastern Desert (CED) of Egypt showing the distribution of the Neoproterozoic shield basement rocks (after Stern and Ali 2020)

exposures cover large area from the Eastern Desert of Egypt (Fig. 1.18), about 20,000 km^2, of which ~55% sedimentary rocks and volcanics, ~40% granite and gneiss, and about 5% ophiolitic serpentinites and related rocks (Stern and Hedge 1985). The CED division received much attention and scientific studies compared with the other Eastern Desert subdivisions because it is accessible by two asphaltic roads, have relatively subdued relief, and because it has the most gold mineralization in Egypt.

The infrastructure rocks, which also named as Tier 1, or high-grade metamorphic rocks, or core complex (El Gaby et al. 1984; Greiling et al. 1994) are exposed in several places in the CED and SED, including the Meatiq, Abu Had, El Shalul, and El Sibai domes as well as the Migif-Hafafit and Beitan domes (Figs. 1.18 and 1.19). These high-grade metamorphic rocks (granitic gneiss and amphibolites) of these core complexes have been dated at 744–630 Ma (Andresen et al. 2009; Ali et al. 2015; Abu El-Enen et al. 2016). The infrastructure rocks consist of upper amphibolite-facies quartzo-feldspathic (granitic) gneisses and amphibolites. On the other hand, the suprastructure rocks, which are also named as Tier 2, or low-grade metamorphic rocks of the CED comprise an oceanic assemblage characterized by a wide range of ophiolitic rocks and arc volcanics, along with volcaniclastic wackes,

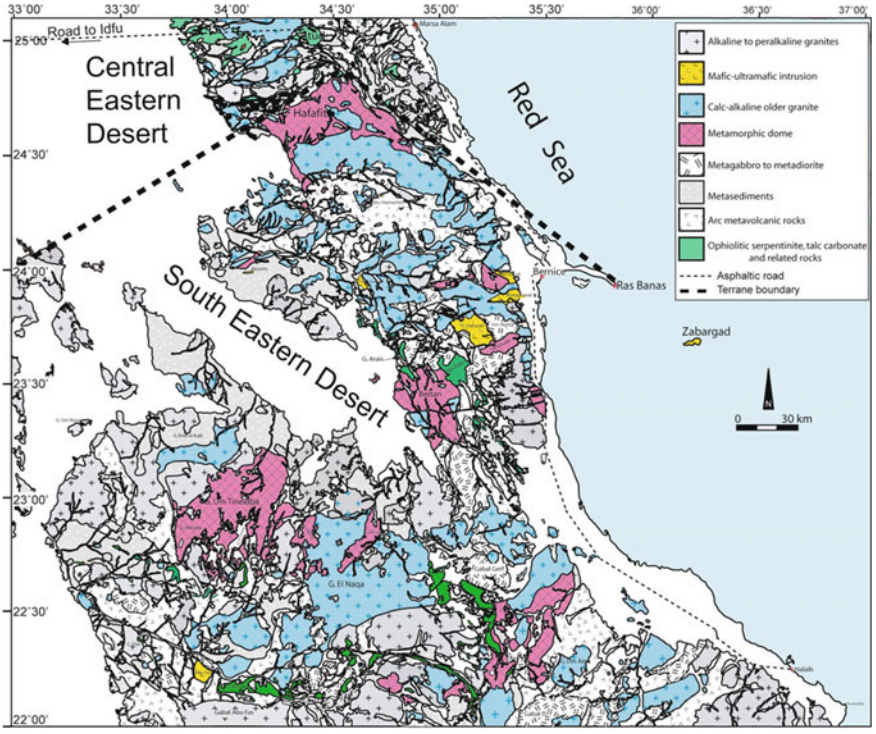

Fig. 1.19 Simplified geologic map of the Southern Eastern Desert (SED) of Egypt showing the distribution of the Neoproterozoic shield basement rocks (after Stern and Ali 2020)

banded iron formation, and diamictite. These suprastructure rocks were dated at 790–640 Ma (Ali et al. 2009). The contact between infrastructure and suprastructure rock units is commonly an intrusive contact, but in some cases, it is marked by high strain mylonitic zones (Stern 2018). The suprastructure or ensimatic (oceanic) assemblages of the CED comprises one of the oldest rock units (ophiolitic rocks) in the Eastern Desert of Egypt, with about 750 Ma (Andresen et al. 2009; Ali et al. 2009). These rock assemblages were intensely intruded by Cryogenian I-type granites and Ediacaran I- and A-type granites and are further disrupted by several Ediacaran magmatic-metamorphic core complexes of the infrastructure rocks (Fig. 1.18). The suprastructure sequences of CED are locally overlain by Ediacaran (~600 Ma) sedimentary basins of the Hammamat Group.

One of characteristic features of the CED Precambrian basement of Egypt is the common abundance of ophiolite complexes, which form the base of the suprastructure rocks (Fig. 1.18). There are numerous localities of ophiolite complexes in the CED and SED, which are mostly disrupted and carbonated to various extents. The relatively complete sequences represented by peridotites, gabbros, and pillow basalts are broadly exposed along the Qena-Quseir road near Fawakhir and at Wadi Ghadir areas (Abd El-Rahman et al. 2009; Abdel-Karim and Ahmed 2010; Farahat 2010; El Bahariya 2018). Two CED ophiolites have U-Pb zircon ages of 745 ± 23 Ma and 736.5 ± 1.2 Ma (Andresen et al. 2009). Petrological studies of CED ophiolitic serpentinized ultramafic rocks show that, the protoliths of these mantle rocks were highly depleted harzburgites and dunites that contain medium- to large-scale chromitite pods, which have been interpreted as forming in a mid-ocean ridge environment, then substantially modified in supra-subduction zone settings (fore-arc and/or back-arc environments) (Ahmed et al. 2001; Azer and Stern 2007; Khalil and Azer 2007; Ahmed 2013).

The ophiolitic rocks overlain by thick sequences of greenschist-facies Hammamt molasse sedimentary rocks and associated wackes and volcanoclastic rocks. Hammamat sedimentary rocks occupy a significant proportion of the CED basement outcrops, which are dominated by immature volcanoclastic sedimentary rocks such as greywacke, siltstone and shale, and sometimes are interbedded with lava flows. The best exposures of the Hammamat sediments (type locality) found in Wadi Hammamat area of the CED, where they un-conformably overlie the older rock units and consist of unmetamorphosed thick sequences (4000–7500 m thick) of unsorted conglomerates, sandstones, and siltstones. The Hammamat sedimentary basins are filled with coarse clastic sedimentary rocks that were largely eroded from the Dokhan volcanics in the highlands of NED, carried by one or more rivers southward and deposited in terrestrial basins that are now best preserved in the northern CED. Less abundant granitic intrusions of Ediacaran age cut the older rocks of the CED (Fig. 1.18). The I-type granites are predominant in the Early Ediacaran age, whereas the A-type granites are more common in the Late Ediacaran age of the CED (Stern and Ali 2020).

(D) *Southern Eastern Desert (SED)*

Although the Precambrian basement rocks in the SED cover a larger area (~30,000 km^2) than those in the CED, NED and Sinai, they are less studied due to their remote locations hard accessibility. The geologic boundary between SED and CED is mostly tectonic boundary, while the southern boundary of the SED is marked by the Nubian portion of the Yanbu-Sol Hamed-Onib-Gerf-Allaqi-Heiani (YOSHGAH) suture zone (Stern et al. 1990). The northern part of the SED basement exposures are dominated by gneiss, migmatite, and granitic rocks of the Migif-Hafafit region, one of the best exposed metamorphic domal structures of the infrastructure in the Eastern Desert of Egypt. The Migif-Hafafit metamorphic gneiss separated from the southernmost CED part by a broad mylonitic shear zone, which named as Nugrus thrust zone. There are numbers of large and separated, but poorly studied, metamorphosed dome complexes in the SED; mostly to the south of Migif-Hafafit dome such as Beitan and Gebel Um Tineidba domes (Fig. 1.19). The age of some of these gneissic metagabbros-meta-tonalite dome complexes (~675 to 700 Ma) (Kröner et al. 1994), and their Nd-Sr isotopic compositions indicating their juvenile crustal origin (Liégeois and Stern 2010). Neoproterozoic granitic bodies and metavolcanic rocks (also named Shadli metavolcanics) cover large areas throughout the SED basement complex, which are mostly found to the south of Migif-Hafafit dome (Fig. 1.19). The Shadli metavolcanics extend about 25 km in the E-W direction, and have an age of about 711 ± 24 Ma (Stern et al. 1990). In many places in the SED, the metavolcanic belt is occasionally associated with polymetallic massive Zn-Cu-Pb-Ag sulfides deposits, which are most probably of hydrothermal origin in a submarine environment.

To the south from the Shadli metavolcanics until the southernmost part of the SED, at the YOSHGAH suture zone, there are several localities of mafic-ultramafic complexes of different origins. Some of these mafic-ultramafic complexes are ophiolitic in origin, but some others are Alaskan-type, or concentrically-zoned complexes (Helmy and El Mahallawi 2003; Helmy 2004; Ahmed et al. 2008; Ahmed 2013; Helmy et al. 2014; Abdel-Karim et al. 2016; Khedr and Arai 2016, 2017). The ophiolitic mafic-ultramafic complexes are distributed mainly in the central and southernmost parts of the SED (Fig. 2.19), where several localities have been studied such as Abu Dahr, Abu Siayil, Arays, Belamhandeit, Umm Thagar and Gerf-Allaqi-Heiani areas (Ahmed 2013; Azer et al. 2013; Khedr and Arai 2013; Gahlan et al. 2015; Abdel-Karim et al. 2016, 2021). The Gerf ophiolitic complex in the southernmost part of the SED represents the largest ophiolitic complex in Egypt (~1 to 5 km wide and about 17 km long), consisting of pillow basaltic lavas, sheeted dykes, layered and isotropic gabbros and ophiolitic mélange. All of these previous studies on the SED ophiolite concluded that these ophiolite complexes were formed in a fore-arc supra-subduction zone environment. The ophiolite of SED was dated back to 741 ± 42 Ma (Kröner et al. 1992). In the central part of the SED basement, there are several mafic-ultramafic Alaska-type (concentrically-zoned) and layered intrusion complexes (Fig. 1.19) aligned approximately E-W around 24° N (Helmy and El Mahallawi 2003; Helmy et al. 2014; Khedr and Arai 2016; Azer et al. 2017). From W to E these are: (1) Gabbro Akarem, (2) Genina Gharbia, (3) Abu Hamamid, (4)

Dahanib, (5) El Motaghairat, and Zabargad island in the Red Sea (Fig. 2.19). All of these Alaskan-type intrusions have more or less similar lithological characteristics including dunite core, then hornblende lherzolite, olivine–plagioclase hornblendite, and plagioclase hornblendite. Most of these mafic-ultramafic intrusions in the SED basement found to be associated with potentially economic Cu-Ni-PGE deposits, such as those in the Gabbro Akarem and Genina Gharbia complexes (Helmy 2004). There is no confirmed geochronological data for these Alaskan-type and layered mafic-ultramafic intrusions in the SED.

1.3.4 Lithostratigraphy of the Nubian Shield Rocks in Sudan

Sudan is mostly underlain by the Precambrian basement rocks, particularly in its southwest, center and northeast parts (Fig. 1.20). The Precambrian basement complexes of Sudan were exclusively reworked during the Neoproterozoic Pan-African tectono-thermal event (Schlüter 2006). The large parts in the north of Sudan are mostly covered by continental clastic sedimentary sequences of the predominantly Mesozoic Nubian cycle (known as Nubian Sandstone), whereas in the south, Tertiary to Quaternary unconsolidated superficial sediments predominate. Some exposures of Tertiary and younger basalts are exposed in the border zone with Ethiopia (Fig. 1.20).

The Precambrian basement complex of Sudan covers large portions of the total area, up to about 50%, where the metamorphic, igneous, volcanic and sedimentary rocks are predominant. The basement complex in most parts of the country, except for the northwestern part, are Neoproterozoic in age (Fig. 1.20). Geologically, there are two different parts in the Precambrian basement of Sudan: Arabian–Nubian Shield rocks in the east, and the layered volcano-sedimentary rocks in the west. The principal difference between these two parts is the isotopic signature, where the former rocks are uniformly magmatic, and the later rocks are highly metamorphosed volcano-sedimentary rocks (Stern et al. 1994). Generally, there is no significant difference in radiometric ages between the two Precambrian rocks. However, a boundary can be drawn between the ensimatic (oceanic) crust in the east and ensialic (continental) crust in the west, based on the isotopic and metamorphic discriminants. Therefore, the Precambrian basement complex of Sudan includes reworked foreland ensialic inliers that reactivated during the Pan-African tectono-thermal magmatism of the Arabian–Nubian ensimatic crust. The Sudanese Precambrian basement is forming what so-called: the Nuba Mountains, the Darfur Block and the Bayuda and Nubian Deserts (Schlüter 2006) (Fig. 1.21). In the Nubian Desert area, in northeastern Sudan, high-grade granitoid gneisses with minor high-grade metasedimentary rocks were migmatized and intensively intruded by voluminous late Pan-African granitoids. Small gneisses and metasedimentary rocks with amphibolite-facies metamorphism also occur within the lower-grade volcanic ophiolite assemblages (Atmur-Delgo suture) of the Red Sea Hills of the Sudan (Fig. 1.21). The metasedimentary belts that scattered between the East Saharan Craton and the Red Sea fold and thrust

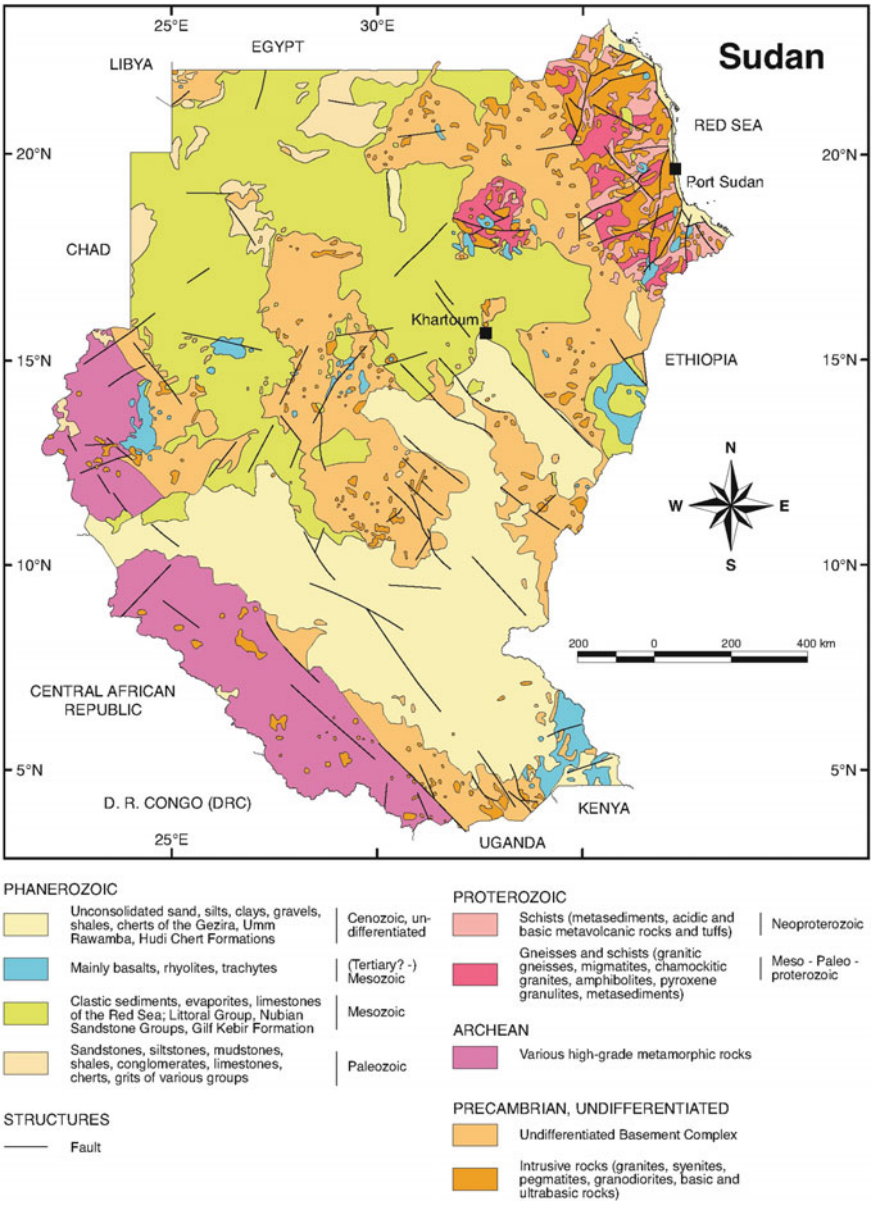

Fig. 1.20 Geological map of Sudan showing the distribution of shield rocks among other geological units (after Schlüter 2006)

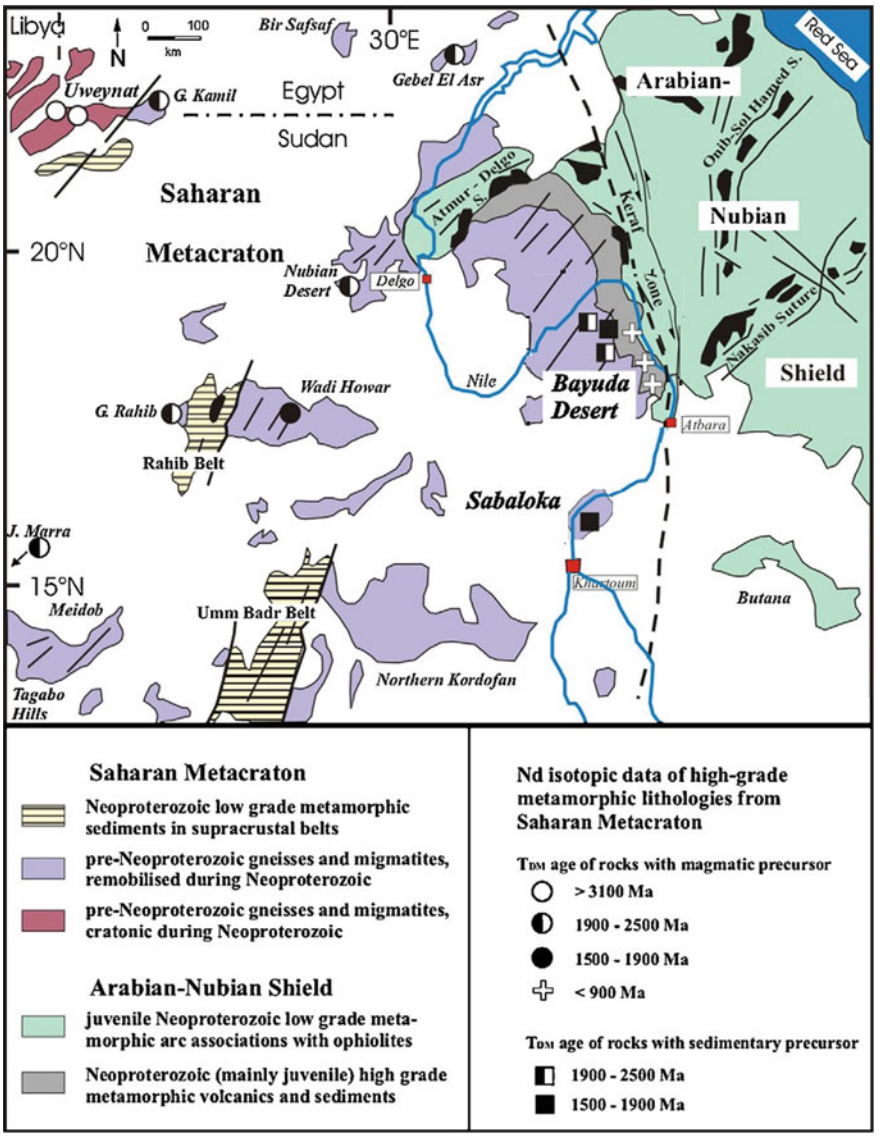

Fig. 1.21 Simplified geologic map of Precambrian basement complex divisions of Sudan (modified from Küster et al. 2008)

belt assumed to represent a zone of early rifting, which developed along the eastern margin of the East Saharan Craton during the initiation of the Neoproterozoic Ocean. The Gebel Rahib Belt, in central northwestern Sudan (Fig. 1.21), contains a complex deformed mafic and ultramafic igneous rocks and a thick sequence of metasedimentary rocks that interpreted as a Red Sea-type Pan-African rift basin (Schlüter

2006). The post-orogenic granitoids in the Gebel Rahib belt have the minimum age of 570 Ma for its deformation and low-grade metamorphism. There is also an ophiolite assemblage that comprising ultramafic rocks, podiform chromitites, layered and isotropic gabbros, pyroxenites, sheeted dykes, pillow lavas and sedimentary chert, which furnish the evidence of newly formed oceanic crust in the Gebel Rahib rift. The existence of such ophiolitic rocks in Gebel Rahib belt in the central northwestern Sudan implies that a juvenile Pan-African crust was generated in the Nubian Shield outside the Red Sea Hills.

The North Kordofan Belt, central Sudan (Fig. 1.21), is similar, in its depositional and structural settings, to the Gebel Rahib Belt, except for the absence of ophiolite complex. A tourmaline-bearing granite in the North Kordofan Belt has been dated at about 590 Ma. The late Pan-African shear zones, which are sealed by mica-bearing pegmatites, have yielded ages of about 560 Ma (Stern et al. 1994; Schlüter 2006). The low-grade metasedimentary Darfour Belt, in western central Sudan, is structurally overlying basement gneisses in the southeastern Darfour block, which may also be equivalent to those in the North Kordofan and Gebel Rahib metasedimentary rocks. Intrusive granitoids in the Darfour Block are dated back to about 570–590 Ma (Stern et al. 1994; Schlüter 2006). In the eastern Nuba Mountains (Fig. 1.21), a belt of low-grade volcano-sedimentary rocks is exposed striking NE-SW to NNE-SSW direction, which contains fragments of highly dismembered ophiolites and mafic to acidic plutons. These arc ophiolitic assemblages were metamorphosed at about 700 Ma, with posttectonic magmatism terminated at about 550 Ma (Stern et al. 1994; Schlüter 2006). The Pan-African rocks occur also as two different tectonostratigraphic units in the Bayuda Desert in northern central Sudan (Fig. 1.21). One of them located in the eastern part, along the River Nile, which occurs as a narrow strip of low-grade metasedimentary rocks, metavolcanics and granitoids. There are two stages of granitoid intrusions, the oldest one dated back to about 898 Ma, and the youngest one at about 678 Ma. These are followed by anorogenic within-plate magmatism that yielded an age of about 549 Ma (Stern et al. 1994; Schlüter 2006).

The basement complex rocks in Sudan are classified into five main groups (Stern et al. 1994): (1) the highly foliated gneissic rocks in the south and west; (2) the metamorphosed mafic volcanic sequence; (3) the sequence of metamorphic sediments and metamorphic felsic volcanics; (4) syntectonic granodiorite intrusions, which cross-cut all the previous three groups; and (5) Post-tectonic alkali granites. Following is a brief description of the layered and intrusion rocks of the Nubian Shield in Sudan, which are predominant mainly in the Red Sea Hills.

Old Gneisses: Gneiss rocks are the oldest rock units in Sudan, and are widely distributed in the south and west of the country; most of them are feldspathic quartz gneiss, which is accompanied by migmatite and some amphibolite rocks. These rocks are believed to belong to the upper Proterozoic age.

Kashabib group: This group is un-conformably overlain the gneiss group and it consists mainly of sequences of meta-sedimentary rocks metamorphosed into the amphibolite facies. This includes quartzite and schist rocks and layers of gray marble, along with the amphibolite rocks. Such kind of rocks are widely distributed in the

Bayuda Desert, west of the Nile River, and in the southern and northern Red Sea Hills, which belonging to the Late Proterozoic age.

Naferdeeb group: This group overlain the Kashabib group, and it is believed to belong to the Late Proterozoic era. It consists of andesite and basaltic volcanic rocks and their detrital derivatives, such as tuffs, agglomerates, graywacke and some carbonate layers. This group of rocks display a greenschist metamorphic facies, and the degree of deformation is less than those in the lower Kashabib group. All of the above-mentioned layered groups of rocks (old gneiss group, Kashabic group and Naferdeeb group) are intruded by granitic batholiths that consisting of adamellite, diorite, granodiorite, and granite. These granitoid intrusions are usually heterogeneous, elongated in shape and containing enclaves from the older rocks.

Homogar and Awat group: This group of rocks is un-conformably overlain the former layered rocks and the heterogeneous granitic intrusions, which is also, belong to the upper Proterozoic era. It consists of intermediate and acidic volcanic rocks, such as rhyolite, dacite and andesite, as well as their volcanic derivatives of tuffs, agglomerates, and few layers of claystone, phyllite, graywacke and conglomerates. This group of rocks is not affected by metamorphism, but at the same time, it is affected by a low degree of deformation and folding. The layered rocks of this group, and the previous groups, are intensively penetrated by alkali granite and syenite intrusions, which takes the oval and circular shapes, in addition to a group of igneous dykes.

1.3.5 Lithostratigraphy of the Nubian Shield Rocks in Eritrea

Eritrea is located in the far north of the "Neoproterozoic East African Orogen", and it represents one of the corners of the far south of the Arabian–Nubian Shield. Although Eritrea covers a small area, it consists of different rock units, which can be classified into three main groups (Fig. 1.22): (1) Precambrian igneous and metamorphic rocks, (2) Mesozoic sedimentary rocks, and (3) Tertiary to Quaternary volcanic and sedimentary rocks. Eritrea is thus, mainly underlain by Neoproterozoic terranes un-conformably overlain by Tertiary to Quaternary volcanic and sedimentary rocks. The sedimentary rocks of marine Mesozoic to Recent ages are mainly exposed in the coastal area of Eritrea along the Red Sea (Fig. 1.22).

Precambrian Shield rocks occupy a large area of Eritrea; being covered about 60% of the total area of this small country. Basement rocks of Eritrea contain many rock units ranging from high-grade metamorphic gneiss dated back to the Archean age, to volcano-sedimentary rocks of medium- to low-grade metamorphism that belonging to the Neoproterozoic age, to the pre-, syn- and post-tectonic granitoid intrusions that are also belonging to the Neoproterozoic age. All the Precambrian rocks of Eritrea are suggested to be formed in the Pan-African orogeny. Until recently, the bloody tribal conflicts, as well as conflicts with neighboring countries, prevented real geological studies on Eritrea where most of the geological classifications and studies

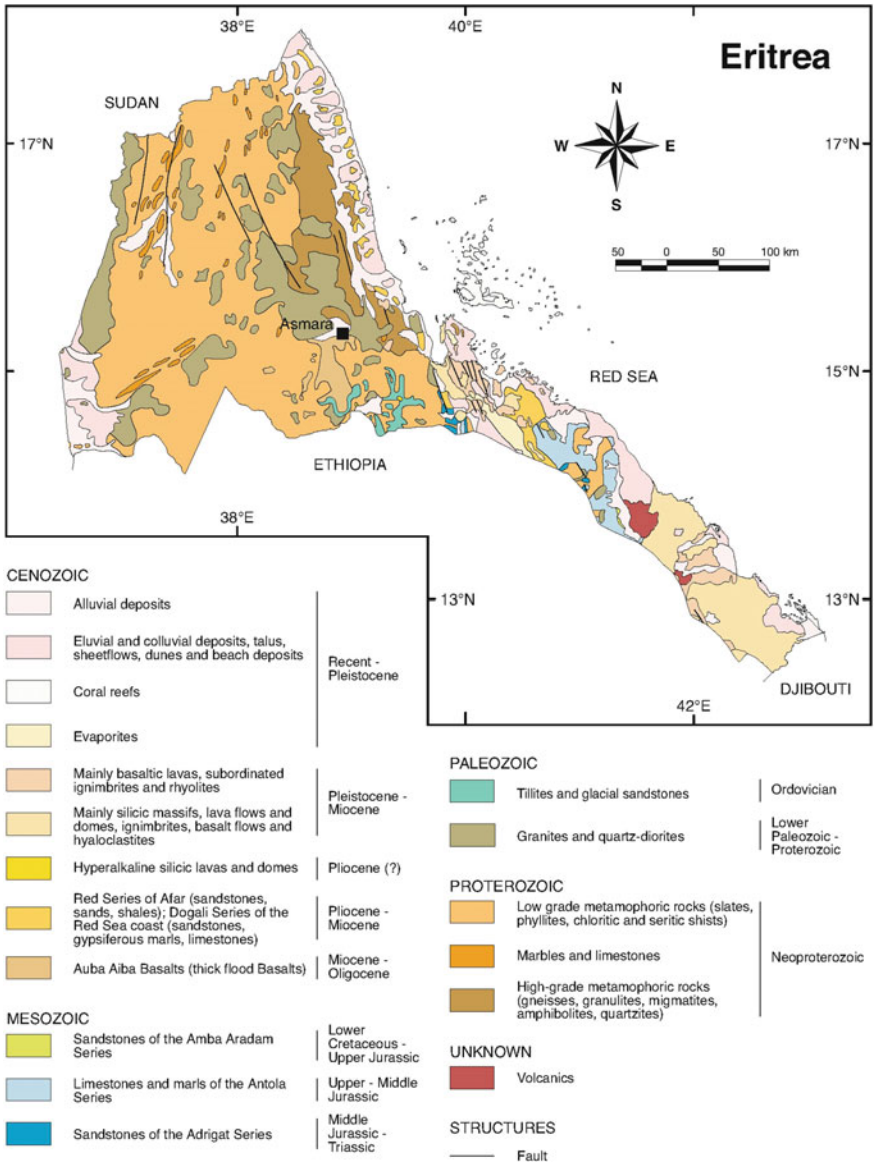

Fig. 1.22 Simplified geologic map of Eritrea showing the distribution of shield rocks among other geological units (after Schlüter 2006)

were based mainly on the use of aerial and satellite images, without verifying the geological situation on the ground (Drury and Berhe 1993). After that, extensive field studies have been conducted (Drury and De Souza Filho 1998) through which the Nubian Shield rocks can be classified into four main terranes or blocks, separated by tectonic boundaries. The major part of the Precambrian rocks of Eritrea consists of Neoproterozoic (ca. 870–670 Ma) continental-marginal and juvenile intra-oceanic magmatic-arc rocks. These terranes arranged from west to east as follows (Barrie et al. 2007): Barka Terrane (to the west), Hagar Terrane (northwest), Nakfa Terrane (to the center) and Arag Terrane (to the east) (Fig. 1.23). The southeastern part (the Denakil segment) and the northeastern part of the country, consists of Cenozoic volcanic and sedimentary rocks (Figs. 1.22 and 1.23). Following is a brief geological description of these geologic shield terranes of Eritrea.

Western Segment (Barka Terrane): The western segment of the Barka terrane developed in the northwestern part of Eritrea underlies the Barka lowlands (Fig. 1.23). It comprises ortho-gneisses (amphibolites) that metamorphosed under the upper amphibolite facies to hornblende-granulite facies conditions. In addition, there are amphibolite-facies pelitic schist containing kyanite and staurolite, quartzites and

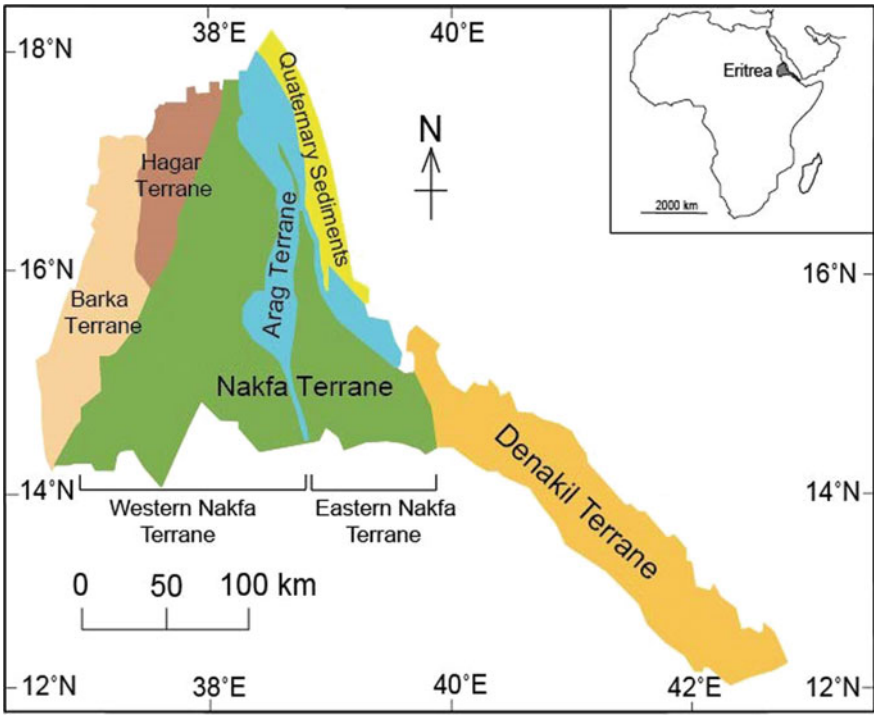

Fig. 1.23 Index map of Eritrea showing the geologic terrane divisions (modified after Barrie et al. 2007)

marble units. All of these rocks are cut by felsic dyke swarms striking in the east/west direction.

Central Segment (Hagar Terrane): The central segment, referred to as the "Hagar terrain", extends from the Barka river up to the Adobha Abiy valley in the east (Fig. 1.23). This terrane comprises several large elliptical bodies of various tectonic units that are dominantly composed of oceanic and accretionary wedge materials of ophiolitic origin. Layered sequences of chlorite schist are occasionally observed, interlayered with epidote and chlorite metabasalts, thin and discontinuous marbles, and manganiferrous and ferruginous cherts. This terrane is very famous for various types of mineral deposits related to the ophiolitic mafic-ultramafic rocks such as chromite, platinum-group elements, nickel, gold, and copper mineralization.

Eastern Segment (Nakfa-Arag Terrane): The eastern segment, referred to as the "Nakfa terrane", is the largest of the four terranes in Eritrea. It is bounded by the Adobha Abiy valley in the west and by the Red Sea escarpment to the east (Fig. 1.23). It consists of calc-alkaline volcanic and volcanoclastic rocks that conformably overlain by a metasedimentary sequence of chlorite schist, grits, polymict conglomerates, pelitic sericite schist and carbonates (Teklay et al. 2001; Barrie et al. 2007). These layered metavolcanic and metasedimentary rocks are intruded by variably deformed plutonic to hypabyssal calc-alkaline granites. The sequence as a whole is crosscut in places by post-kinematic granites and gabbros, which are also transected by several narrow shear zones sub-parallel to the regional strike. The western Nakfa terrane, near Bisha mine, comprises basin and range style topography with intrusive rocks and a flat valley floor underline by volcanic and sedimentary rocks. The Nakfa terrane is considered to be a relict of island arc assemblage. Several volcanogenic massive sulfides (VMS), base-metal deposits and gold ores occur in this tectonic unit (Barrie et al. 2007). The Arag terrane (Fig. 1.23) is bounded to the east by several late Tertiary rocks, which consists of granitoid and metasedimentary rocks.

Southern Segment (Denakil Terrane): The southern segment, referred to as the Denakil terrane (Fig. 1.23), is composed of metamorphic rocks, which may be grouped into three formations; (1) migmatitic hornblende biotite gneissic, (2) phyllitic formation consisting of schist, conglomeratic phyllites, crystalline limestones, and graphitic schist, and (3) a post-tectonic granitoids (Barrie et al. 2007).

1.3.6 Lithostratigraphy of the Nubian Shield Rocks in Ethiopia

Ethiopia located at the northern tip of the continental part of the East African Rift System. The main rock types of Ethiopia as shown on the geologic and geographic maps of Ethiopia (Figs. 1.24 and 1.25) are classified into the following types: (1) Basement complex that contains Precambrian metamorphic rocks and associated

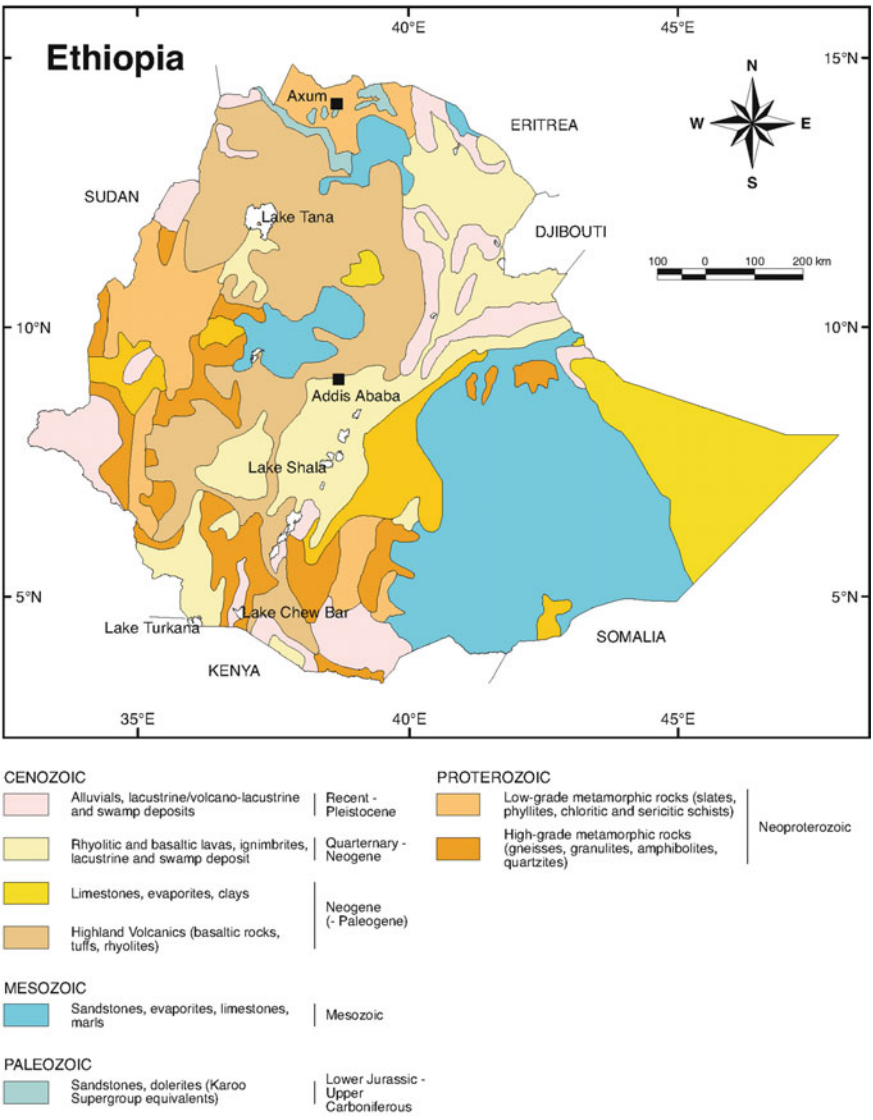

Fig. 1.24 Simplified geologic map of Ethiopia, showing the distribution of shield rocks among other geological rock units (after Schlüter 2006)

syn- to post-tectonic intrusions (23% of total surface); (2) late-Paleozoic to Mesozoic marine and continental sediments (25% of total surface); (3) Cenozoic mafic and felsic volcanics (34% of total surface); and (4) volcano-sedimentary and volcanoclastic rocks, associated with the Cenozoic volcanics, including Early and Late Tertiary and Quaternary sedimentary rocks and sediments (18% of total surface)

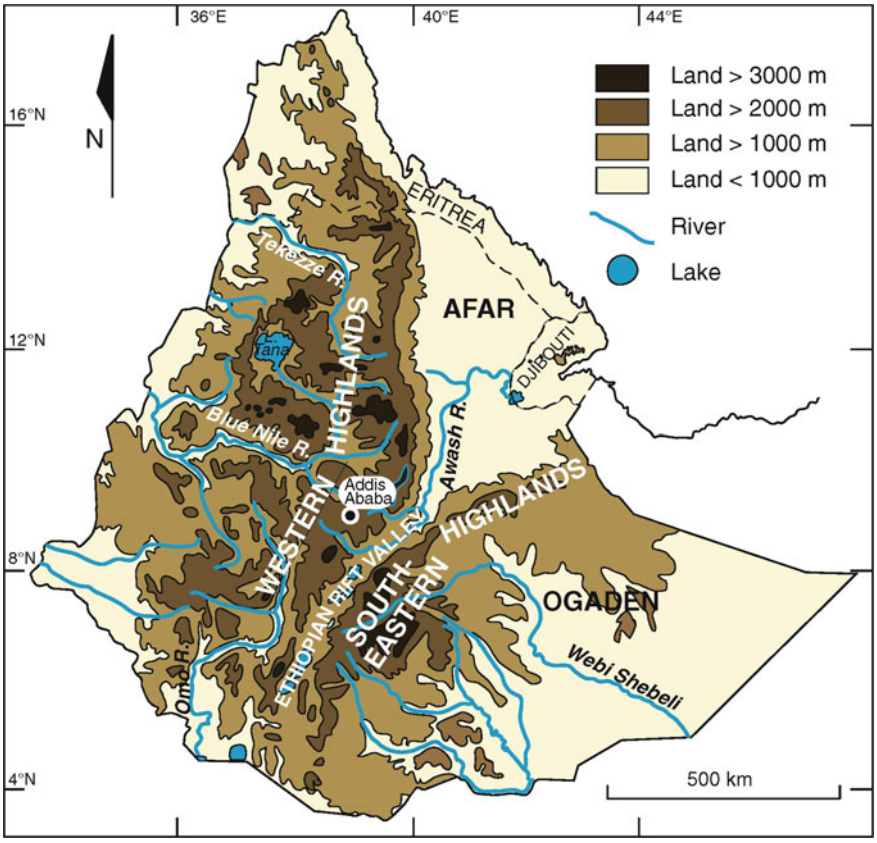

Fig. 1.25 Simplified map showing the Ethiopia's main topographic regions (after Williams 2016)

(Tadesse et al. 2003). The Precambrian basement rocks are covering large area in the northern and western Ethiopia, and smaller areas in the south and east of the country (Fig. 1.24). Thick piles of Cenozoic volcanic rocks related to the East African Rift System cover most of the highland regions of western Ethiopia. Mesozoic and Cenozoic sediments occupy the eastern part of the country, and the rift valley is mainly covered with relatively young lacustrine sediments and volcanics (Fig. 1.25) (Tadesse et al. 2003; Williams 2016).

The geology of shield rocks in Ethiopia is still poorly known. The Precambrian rocks of Ethiopia contain wide varieties of sedimentary, volcanic and intrusive rocks, which suffered from varying degrees of deformation and metamorphism. The Precambrian exposures in Ethiopia lying at the interface between the gneissic terranes of the Mozambique Belt to the south, and the Arabian–Nubian Shield complex of Sudan, Egypt and Saudi Arabia to the north. A generalized tectonostratigraphic classification of Precambrian rocks in Ethiopia suggests the existence

of three major complexes: (1) Lower Archean complex, (2) Middle Paleo- to Meso-proterozoic complex, and (3) Upper Neoproterozoic complex. However, most of the Precambrian rocks (granite-gneiss, volcano-sedimentary and ophiolitic suites) of Ethiopia have apparently been belonging to the Pan-African orogeny of a Neoproterozoic age (Ayalew et al. 1990; Gichile 1992; Teklay et al. 1998; Gerra 2000). The Archean or pre-Neoproterozoic rocks of the Lower Complex could be a part of the pre-Neoproterozoic continental crustal fragments, or possibly reworked and remobilized components (e.g., Teklay et al. 1998). These rocks are mainly exposed (Fig. 1.24) in northern (Tigray), western (Wollega), southern (Sidamo) and eastern (Harar) parts of the country (Tadesse et al. 2003).

The basement rocks in the south and west of Ethiopia (mainly granitic and gneissic rocks) are strongly metamorphosed than those in the north. Following is a brief geological description of these Precambrian complexes of Ethiopia.

Lower Complex: The Lower complex of Ethiopian basement is considered as the oldest rock unit, which consists mainly of high-grade gneisses and migmatites with subordinate quartz–feldspathic gneisses, schist and amphibolites. The estimated age of this lower complex (about 2500 Ma) is considered as an Archean age.

Middle Complex: The Middle complex represented by platform-type psammitic and pelitic metasedimentary rocks with subordinate amounts of marbles and schist. The rocks of this complex exposed in the north, north-east, west, and parts of the south of Ethiopia (Fig. 1.24), where it is known as the "Wadera group" in the Sidamo province, and the "Boye series" in the Hararge province. The Middle complex in the Sidamo and Hararge provinces is composed mainly from pelitic metasedimentary rocks such as biotite/muscovite schist, meta-arkose and quartzite, with subordinate amounts of marble, calc-silicates rocks and amphibole schist. In the western part of Ethiopia, these rocks are found intercalated with the amphibole schist and amphibolite, which are believed to be derived from the mafic volcanic rocks.

Upper Complex: The Upper complex includes a thick sequence of low-grade metamorphosed island-arc and ophiolitic assemblages. This complex consists of several rock types that are less metamorphosed, which represent the Neoproterozoic age. It is represented by the following sequence, which ranges in age from the oldest to the youngest, and from the south to the north: ophiolitic rocks, meta-andesitic volcanics and their associated meta-sediments, detrital sediments and little carbonates. The Neoproterozoic rocks of this Upper complex can be classified into eight groups and rock formations (from oldest to youngest) as follows:

(1) *Adola group*: It consists of amphibolite rocks of continental volcanic origin, which are found conformable with graphitic and chloritic phyllites and graphitic quartzite.
(2) *Mormora group*: It consists of graphitic phyllite rocks that conformable with carbonate schist, sandstone and few layers of marble and conglomerates.
(3) *Tsaliet group*: This group consists of meta-volcanics derived from basalt, andesite, dacite and rhyolite, where andesite is abundant with its detrital derivatives from graywacke, conglomerates, agglomerates and slate. This group of

rocks were intruded by various bodies of diorite, granodiorite and granite, which recorded a geologic age between 800 and 700 Ma.

(4) *Tambien group*: This group of rocks is abundant in northern Ethiopia, and is mainly composed of slates and graphitic clayey rocks that conformable with limestone, which sometimes-containing algal fossils. This group is found intercalated with the underlying Tsaliet group.

(5) *Ultramafic group*: The mafia-ultramafic rocks are found in the form of spaced, disconnected bodies parallel to the boundary between the oldest rock units (Archean basement complex) and the overlying younger Neoproterozoic rocks. These types of rocks are well exposed in the areas of Yubdo and Kenticha Hills.

(6) *Didikama formation*: The rocks of this formation are exposed in the northern part of Ethiopia. It is composed of white and light dolomitic rocks conformable with gray and black slate, which un-conformably separated from the earlier groups by basal conglomeratic contact.

(7) *Shiraro formation*: This formation is also found in the northern part of Ethiopia and consists of layers of sandstone, with laminated conglomerates containing abundant pebbles of slate, granite and phyllite. The degree of deformation and folding in the rocks of this formation are less than those in the underlying groups, which indicates an unconformity surface between it and the older rocks in the sequence.

(8) *Mathos formation*: It is considered as the youngest rock unit of the Nubian Shield rocks in Ethiopia. It is mainly exposed in the northern part of the country, and it is formed from calcareous rocks, such as limestone, dolomite and dolomitic limestone.

References

Abd El-Rahman Y, Polat A, Dilek Y, Fryer BJ, El-Sharkawy M, Sakran S (2009) Geochemistry and tectonic evolution of the Neoproterozoic Wadi Ghadir ophiolite, Eastern Desert, Egypt. Lithos 113:158–178

Abd El-Rahman Y, Seifert T, Gutzmer J, Said A, Hofmann M, Gärtner A, Linnemann U (2017) The south Um Mongol Cu-Mo-Au prospect in the Eastern Desert of Egypt: from a mid-Cryogenian continental arc to Ediacaran post-collisional appinite-high Ba-Sr monzogranite. Ore Geol Rev 80:250–266

Abd-Allah A, Ahmed AH, El-Fakharani A, El-Sawy EK, Ali KA (2014) Fatima suture: a new amalgamation zone in the western Arabian Shield, Saudi Arabia. Precambr Res 249:57–78

Abdel-Karim A-AM, Ahmed Z (2010) Possible origin of the ophiolites of Eastern Desert, Egypt, from geochemical perspectives. Arab J Sci Eng 35:115–143

Abdel-Karim AAM, Ali S, Helmy HA, El-Shafei SA (2016) A fore-arc setting of the Gerf ophiolite, Eastern Desert, Egypt: evidence from mineral chemistry and geochemistry of ultramafites. Lithos 263:52–65

Abdel-Karim AAM, El-Shafei SA, Azer MK (2021) The Neoproterozoic ophiolitic ultramafic rocks in Eastern Desert of Egypt: implications for petrogenesis and metasomatic processes. Int Geol Rev 63:208–232

Abdelsalam MG, Abdeen MM, Dowaidar HM, Stern RJ, Abdel Ghaffar AA (2003) Structural evolution of the Neoproterozoic Western Allaqi-Heiani suture, southeastern Egypt. Precambr Res 124:87–104

Abdelsalam MG, Liégeois JP, Stern RJ (2002) The Saharan metacraton. J Afr Earth Sc 34:119–136

Abdelsalam MG, Stern RJ (1996) Sutures and shear zones in the Arabian–Nubian Shield. J Afr Earth Sc 23:289–310

Abu El-Enen M, Okrusch M (2007) The texture and composition of tourmaline in metasedimentary rocks of the Sinai, Egypt: implications for the tectono-metamorphic evolution of the Pan-African basement. Mineral Mag 71:17–40

Abu El-Enen M, Whitehouse MJ (2013) The Feiran-Solaf metamorphic complex, Sinai, Egypt: geochronological and geochemical constraints on its evolution. Precambr Res 239:106–125

Abu El-Enen M, Will TM, Okrusch M (2004) P-T evolution of the Pan-African Taba metamorphic belt, Sinai, Egypt: constraints from metapelitic mineral assemblages. J Afr Earth Sc 38:59–78

Abu-Alam T, Stüwe K, Kadi K (2011) Pan-African exhumation mechanisms. Geophysical Reseach Abstracts, EGU General Assembly 13, EGU2011-10307-1

Abu-Alam TS, Stüwe K (2009) Exhumation during oblique transpression: the Feiran-Solaf region, Egypt. J Metamorph Geol 27:439–459

Agar RA (1985) Stratigraphy and palaeography of the Siham group: direct evidence for a Neoproterozoic continental microplate and active continental margin in the Saudi Arabian Shield. J Geol Soc 142:1205–1220

Agar RA (1986) The Bani Ghavy Group; sedimentation and volcanism in pull-apart grabens of the Najd strike-slip orogen, Saudi Arabian shield. Precambr Res 31:259–274

Ahmed AH (2007) Diversity of platinum-group minerals in podiform chromitites of the late Proterozoic ophiolite, Eastern Desert, Egypt: genetic implications. Ore Geol Rev 32:1–19

Ahmed AH (2013) Highly depleted harzburgite-dunite-chromitite complexes from the Neoproterozoic ophiolite, south Eastern Desert, Egypt: a possible recycled upper mantle lithosphere. Precambr Res 233:173–192

Ahmed AH, Arai S, Attia AK (2001) Petrological characteristics of the Pan African podiform chromitites and associated peridotites of the Proterozoic ophiolite complexes, Egypt. Mineral Depos 36:72–84

Ahmed AH, Habtoor A (2015) Heterogeneously depleted Precambrian lithosphere deduced from mantle peridotites and associated chromitite deposits of Al'Ays ophiolite, Northwestern Arabian Shield, Saudi Arabia. Ore Geol Rev 67:279–296

Ahmed AH, Harbi HM, Habtoor AM (2012) Compositional variations and tectonic settings of podiform chromitites and associated ultramafic rocks of the Neoproterozoic ophiolite at Wadi Al Hwanet, northwestern Saudi Arabia. J Asian Earth Sci 56:118–134

Ahmed AH, Helmy HM, Arai S, Yoshikawa M (2008) Magmatic unmixing in spinel from late Precambrian concentrically-zoned mafic–ultramafic intrusions, Eastern Desert, Egypt. Lithos 104:85–98

Ahmed AH, Surour AA (2016) Fluid-related modifications of Cr-spinel and olivine from ophiolitic peridotites by contact metamorphism of granitic intrusions in the Ablah area, Saudi Arabia. J Asian Earth Sci 122:58–79

Ahmed Z, Harriri MM (2008) Neoproterozoic ophiolites as developed in Saudi Arabia and their oceanic and pericontinental domains. Arab J Sci Eng 33:17–54

Al Shanti AMS (1993) Geology of the Arabian Shield. Scientific Publishing Center, King Abdulaziz University, Jeddah, Saudi Arabia (in Arabic)

Albaroot M, Ahmad AHM, Al-Areeq N, Sultan M (2016) Tectonostratigraphy of Yemen and geological evolution: a new prospective. Int J New Technol Res (IJNTR) 2:19–33

Ali KA, Stern RJ, Manton WI, Kimura J-I, Whitehouse M, Mukherjee SK, Johnson PR, Griffin WR (2010a) Geochemical, U-Pb zircon and Nd isotopic investigations of the Ghawjah Metavolcanics of Northwestern Saudi Arabia: the ~750 Ma Crust-Forming Event correlated across the Red Sea. Lithos 120:379–392

Ali KA, Azer MK, Gahlan HA, Wilde SA, Samuel MD, Stern RJ (2010b) Age of formation and emplacement of Neoproterozoic ophiolites and related rocks along the Allaqi Suture, south Eastern Desert, Egypt. Gondwana Res 18:583–595

Ali KA, Kröner A, Hegner E, Wong J, Li S-Q, Gahlan HA, El Ela FF (2015) U-Pb zircon geochronology and Hf–Nd isotopic systematics of Wadi Beitan granitoid gneisses, South Eastern Desert, Egypt. Gondwana Res 27:811–824

Ali KA, Stern RJ, Manton WI, Kimura J-I, Khamis HA (2009) Geochemistry, Nd isotopes, and U-Pb SHRIMP zircon dating of Neoproterozoic volcanic rocks from the Central Eastern Desert of Egypt: new insights into the ~750 Ma crust-forming event. Precambr Res 171:1–22

Al-Khirbash S, Takla M, Abdelwaheed M, Sakran S (2001) Tectonic evolution of the southeast Precambrian basement complex, Yemen. Faculty Sci Bull sana'a Univ 14:67–83

Andresen A, Abu El-Rus MA, Myhre PI, Boghdady GY, Corfu F (2009) U-Pb TIMS age constraints on the evolution of the Neoproterozoic Meatiq Gneiss Dome, Eastern Desert of Egypt. Int J Earth Sci 98:481–497

As-Saruri MA, Sorkhabi R, Baraba R (2013) Sedimentary basins of Yemen: their tectonic development and lithostratigraphic cover. Front Earth Sci 5:361–373

As-Saruri MA, Wiefel H (2012) The lithostratigraphic subdivision of the Proterozoic basement rocks of the Mudiyah-Mukalla area, Yemen. Arab J Geosci 5:1127–1150

As-Saruri ML, Wiefel H (1998) The lithological–structural provinces of the basement in the central region of southwestern Arabian Peninsula. Z Geol Wiss 26:731–741

Avigad D, Gvirtzman Z (2009) Late Neoproterozoic rise and fall of the northern Arabian–Nubian Shield: the role of lithospheric mantle delamination and subsequent thermal subsidence. Tectonophysics 477:217–228

Ayalew T, Bell K, Moore JM, Parish RR (1990) U-Pb and Rb–Sr geochemistry of the western Ethiopian Shield. Geol Soc Am Bull 102:1309–1316

Azer M, Stern RJ (2007) Neoproterozoic serpentinites in the Eastern Desert, Egypt: fragments of fore-arc mantle. J Geol 115:457–472

Azer MK, Gahlan HA, Asimow PD, Al-Kahtany K (2017) The Late Neoproterozoic Dahanib Mafic-ultramafic intrusion, south-eastern desert, Egypt: is it an Alaskan-type or layered intrusion? Am J Sci 317:91–940

Azer MK, Khalil AES (2005) Petrological and mineralogical studies of Pan-African serpentinites at Bir Al-Edeid area, central Eastern Desert, Egypt. J Afr Earth Sci 43:525–536

Azer MK, Samuel MD, Ali KA, Gahlan HA, Stern RJ, Ren M, Moussa HE (2013) Neoproterozoic ophiolitic peridotites along the Allaqi-Heiani Suture, South Eastern Desert, Egypt. Mineral Petrol 107:829–848

Ba-Bttat MAO (1991) Geology, petrochemistry and tectonics of the Lowdar-Mudiah Area, Abyan Province, Yemen Republic (Ph.D. Thesis). Leicester, United Kingdom, Leicester University, p 178

Bakor AR, Gass IG, Neary C (1976) Jabal Al Wask, NW Saudi Arabia: an Eocambrian back-arc ophiolite. Earth Planet Sci Lett 30:1–9

Baranov AA, Bobrov AM (2018) Crustal structure and properties of Archean cratons of Gondwanaland: similarity and difference. Russ Geol Geophys 59:512–524

Barrie CT, Nielsen FW, Aussant CH (2007) The Bisha volcanic-associated massive sulfide deposit, western Nakfa terrane, Eritrea. Econ Geol 102:717–738

Be'eri-Shlevin Y, Eyal M, Eyal Y, Whitehouse MJ, Litvinovsky B (2012) The Sa'al volcano-sedimentary complex (Sinai, Egypt): a latest Mesoproterozoic volcanic arc in the northern Arabian Nubian Shield. Geology 40:403–406

Bea F, Abu-Anbar M, Montero P, Peres P, Talavera C (2009) The ~844 Ma Moneiga quartz-diorites of the Sinai, Egypt: evidence for Andean-type arc or rift-related magmatism in the Arabian–Nubian Shield? Precambr Res 175:161–168

Bentor YK (1985) The custal evolution of the Arabo-Nubian massif with special reference to the Sinai Peninsula. Precambr Res 28:1–74

Berhe SM (1990) Ophiolites in Northeast and East Africa: implications for Proterozoic crustal growth. J Geol Soc London 147:41–57

Beyth M, Avigad D, Wetzel H-U, Matthews A, Berhe SM (2003) Crustal exhumation and indications for Snowball Earth in the East African Orogen, N Ethiopia and east Eritrea. Precambr Res 123:187–201

Binda PL (1981) The Precambrian-Cambrian boundary in the Arabian Shield: a review. Bull Faculty Earth Sci King Abdulaziz Univ 4:107–120

Blasband BB (2006) Neoproterozoic Tectonics of the Arabian–Nubian Shield: Utrecht University, Utrecht, Netherlands, p 256

Bleeker W (2003) The Late Archean record: a puzzle in Ca. 35 pieces. Lithos 71:99–134

Bosworth W (2015) Geological evolution of the Red Sea: Historical background, review, and synthesis. In: Rasul NMA, Stewart ICF (eds) The Red Sea, The formation, morphology, oceanography and environment of a young ocean basin: Springer Earth System Sciences. Springer, Berlin, pp 45–78

Bosworth W, Huchon P, McClay K (2005) The Red Sea and Gulf of Aden Basins. J Afr Earth Sc 43:334–378

Bregar M, Bauernhofer A, Pelz K, Kloetzli U, Fritz H, Neumayr P (2002) A late Neoproterozoic magmatic core complex in the Eastern Desert of Egypt: emplacement of granitoids in a wrench-tectonic setting. Precambr Res 118:59–82

Breitkreuz C, Eliwa H, Khalaf I, El Gameel K, Bühler B, Sergeev S, Larionov A (2010) Neoproterozoic SHRIMP U-Pb zircon ages of silica-rich Dokhan Volcanics in the northeastern Desert, Egypt. Precambrian Res 182:163–174

Brown GF, Jackson RO (1979) An overview of the geology of western Arabia. In: Tahoun SA (ed) Evolution and mineralization of the Arabian–Nubian Shield: King Abdulaziz University, Institute of Applied Geology Bulletin 3, vol 1. Pergamon Press Ltd., Oxford, New York, pp 3–10

Brown GF, Schmidit DL, Huffman ACJR (1989) Geology of the Arabian Peninsula; shield area of Western Saudi Arabia. USGS Professional Papers, 560-A.

Bühler B, Breitkreuz C, Pfänder JA, Hofmann M, Becker S, Linnemann U, Eliwa HA (2014) New insights into the accretion of the Arabian–Nubian Shield: depositional setting, composition and geochronology of a mid-Cryogenian arc succession (North Eastern Desert, Egypt). Precambr Res 243:149–167

Calvez JY, Alsac C, Delfour J, Kemp J, Pellaton C (1983) Geologic evolution of western, central, and eastern parts of the northern Precambrian Shield, Kingdom of Saudi Arabia. Saudi Arabian Deputy Ministry for Mineral Resources Open-File Report BRGM-OF-03-17, 57 p

Camp VE (1984) Island arcs and their role in the evolution of the western Arabian Shield. Geol Soc Am Bull 95:913–921

Claesson S, Pallister JS, Tatsumoto M (1984) Samarium-neodymium data on two late Proterozoic ophiolites of Saudi Arabia and implications for crustal and mantle evolution. Contrib Miner Petrol 85:244–252

Cox GM, Lewis CJ, Collins AS, Halverson GP, Jourdan F, Foden J (2012) Ediacaran terrane accretion within the Arabian–Nubian Shield. Gondwana Res 21:341–352

De Souza Filho CR, Drury SA (1998) A Neoproterozoic supra-subduction terrane in northern Eritrea, NE Africa. J Geol Soc 155:551–566

Delfour J (1967) Report on the mineral resources and geology of the Hulayfah-Musayna'ah region (sheet 78, zone 1 north): Bureau des Recherches Geologiques et Minieres (BRGM), Open File Report, JED-66, 138 p, scale 1:100,000.

Dixon TH (1979) The evolution of continental crust in the Late Precambrian Egyptian Shield. PhD Thesis, Univ California, San Diego

Dixon TH, Stern RJ, Husseini IM (1987) Control of Red Sea rift geometry by Precambrian structures. Tectonics 6:551–571

Drury SA, Berhe SM (1993) Accretion tectonics in northern Eritrea revealed by remotely sensed imagery. Geol Mag 130:177–190

Drury SA, De Souza Filho CR (1998) Neoproterozoic terrane assemblages in Eritrea: review and prospects. J Afr Earth Sc 27:331–348

El Bahariya GA (2018) Classification of the Neoproterozoic ophiolites of the Central Eastern Desert, Egypt based on field geological characteristics and mode of occurrence. Arab J Geosci 11:313. https://doi.org/10.1007/s12517-018-3677-1

El Din GMK, Khudeir AA, Greiling RO (1991) Tectonic evolution of a Pan-African gneiss culmination, Gabal El Sibai area, Central Eastern Desert, Egypt. Zentralblattfuer Geologie Und Palaeontologie, Teil I 11:2637–2640

El Gaby S, El Nady O, Khudeir AA (1984) Tectonic evolution of the basement complex in the Central Eastern Desert of Egypt. Geol Rundsch 73:1019–1036

El-Enen MA, Abu-Alam TS, Whitehouse MJ, Ali KA, Okrusch M (2016) P-T path and timing of crustal thickening during amalgamation of East and West Gondwana: a case study from the Hafafit Metamorphic Complex, Eastern Desert of Egypt. Lithos 263:213–238

Eliwa HA, Breitkreuz C, Murata M, Khalaf IM, Bühler B, Itaya T, Takahashi T, Hirahara Y, Miyazaki T, Kimura J-I, Shibata T, Koshi Y, Kato Y, Ozawa H, Daas MA, El Gameel KH (2014) SIMS zircon U-Pb and mica K-Ar geochronology, and Sr–Nd isotope geochemistry of the north Eastern Desert, Egypt. Gondwana Res 25:1570–1598

El-Shafei MK, Kusky TM (2003) Structural and tectonic evolution of the Neoproterozoic Feiran-Solaf metamorphic belt, Sinai Peninsula: implications for the closure of the Mozambique Ocean. Precambr Res 123:269–293

El-Sharkawi MA, El-Bayoumi RM (1979) The ophiolites of Wadi Ghadir area, Eastern Desert, Egypt. In: 5th Conference on African Geology, Cairo. Annuls of Geological Survey of Egypt, vol 9, pp 125–135

Evans DAD, Pisarevsk SA (2009) Plate tectonic on early Earth? Weighing the paleomagnetic evidence. Geol Soc Am Spec Pap 440:249–263

Farahat ES (2010) Neoproterozoic arc–back-arc system in the Central Eastern Desert of Egypt: evidence from supra-subduction zone ophiolites. Lithos 120:293–308

Fleck RJ, Greenwood WR, Hadley DG, Anderson RE, Schmidt DL (1980) Rubidium-Strontium geochronology and plate-tectonic evolution of the southern part of the Arabian Shield. USGS Professional Paper 1131, 38 p

Frisch W, Al-Shanti A (1977) Ophiolite belts and the collision of island arcs in the Arabian Shield. Tectonophysics 43:293–306

Fritz H, Wallbrecher E, Khudeir AA, Abu El Ela F, Dallmeyer DR (1996) Formation of Neoproterozoic metamorphic core complexes during oblique convergence (Eastern Desert, Egypt). J Afr Earth Sc 23:311–329

Fritz H, Abdelsalam M, Ali KA, Bingen B, Collins AS, Fowler AR (2013) Orogen styles in the East African Orogen: a review of the Neoproterozoic to Cambrian tectonic evolution. J Afr Earth Sc 86:65–106

Gahlan HA, Azer MK, Khalil AES (2015) The Neoproterozoic Abu Dahr ophiolite, South Eastern Desert, Egypt: petrological characteristics and tectonomagmatic evolution. Mineral Petrol 109:611–630

Garson MS, Shalaby TM (1976) Precambrian-Lower Paleozoic plate tectonics and metallogenesis in the Red Sea region. In: Said R (ed) The geology of Egypt. Special Paper in Geological Association of Canada, vol 14, pp 573–596

Gass IG (1977) The evolution of the Pan African crystalline basement in NE Africa and Arabia. J Geol Soc London 134:129–138

Genna A, Nehlig P, Le Goff E, Guerrot C, Shanti M (2002) Proterozoic tectonism of the Arabian shield. Precambr Res 117:21–40

Gerra S (2000) A short introduction to the geology of Ethiopia. Chronique De La Recherche Minière 540:3–10

Gichile S (1992) Granulites in the Precambrian basement of southern Ethiopia: geochemistry, P-T conditions of metamorphism and tectonic setting. J Afr Earth Sc 15:251–263

Greenwood WR, Brown GF (1973) Petrology and chemical analysis of selected plutonic rocks from the Arabian Shield, Kingdom of Saudi Arabia: Saudi Arabian Directorate General of Mineral Resources Bulletin 9, 9 p

Greenwood WR, Hadley DG, Anderson RE, Fleck RJ, Schmidt DL (1976) Late Proterozoic cratonization in southwestern Saudi Arabia. Philos Trans R Soc Lond 280:517–527

Greiling RO, Abdeen MM, Dardir AA, El-Akhal H, El-Ramly MF, Kamal El-Din GM, Osman AF, Rashwan AA, Rice AHN, Sadek MF (1994) A structural synthesis of the Proterozoic Arabian–Nubian Shield in Egypt. Geologische Rundshau 83:484–501

Grothaus B, Eppler D, Ehrlich R (1979) Depositional environment and structural implications of the Hammamat Formation. Ann Geol Surv Egypt 9:564–590

Habib ME, Ahmed AA, El Nady OM (1985) Tectonic evolution of the Meatiq infrastructure, Central Eastern Desert, Egypt. Tectonics 4:613–627

Habtoor AM, Ahmed AH, Akizawa N, Harbi H, Arai S (2017) Chemical homogeneity of high-Cr chromitites as indicator for widespread invasion of boninitic melt in mantle peridotite of Bir Tuluha ophiolite, Northern Arabian Shield, Saudi Arabia. Ore Geol Rev 90:243–259

Hamimi Z, El-Sawy EK, El-Fakharani A, Matsah M, Shujoon A, El-Shafei MK (2014) Neoproterozoic structural evolution of the NE-trending Ad-Damm Shear Zone, Arabian Shield, Saudi Arabia. J Afr Earth Sc 99:51–63

Hargrove US (2006) Crustal evolution of the Neoproterozoic Bi'r Umq suture zone, Kingdom of Saudi Arabia: Geochronological, isotopic, and geochemical constraints (Unpublished Ph.D. dissertation). Richardson, University of Texas, 359 p

Hassan MA, Hashad AH (1990) Precambrian of Egypt. In: Said R (ed) The geology of Egypt. Balkema, Rotterdam, pp 201–245

Heikal MTS, Al-Khirbash SA, Hassan AM, Al-Kotbah AM, Al-Selwi KM (2013) Lithostratigraphy, deformation history, and tectonic evolution of the basement rocks, Republic of Yemen: an Overview. Arab J Geosci. https://doi.org/10.1007/s12517-013-0951-0

Helmy HM (2004) Cu-Ni-PGE mineralization in the Genina Gharbia mafic-ultramafic intrusion, Eastern Desert, Egypt. Can Mineral 42:351–370

Helmy HM, Abd El-Rahman YM, Yoshikawa M, Shibata T, Arai S, Tamura A, Kagami H (2014) Petrology and Sm-Nd dating of the Genina Gharbia Alaskan-type complex (Egypt): insights into deep levels of Neoproterozoic island arcs. Lithos 198–199:263–280

Helmy HM, El Mahallawi MM (2003) Gabbro Akarem mafic-ultramafic complex, Eastern Desert, Egypt: a Late Precambrian analogues of Alaskan-type complexes. Mineral Petrol 77:85–108

Howell DG, Jones DL, Schermer ER (1985) Tectonostratigraphic terranes of the Circum-Pacific region, in Howell DG, ed., Tectonostratigraphic terranes of the Circum-Pacific region: Circum-Pacific Council for Energy and Mineral Resources Earth Sciences Series, vol 3, pp 3–30

Ibrahim KM, McCourt WJ (1995) Neoproterozoic granitic magmatism and tectonic evolution of the northern Arabian shield: evidence from southwest Jordan. J Afr Earth Sc 20:103–118

Jackson NJ (1986) Petrogenesis and evolution of Arabian felsic plutonic rocks. J Afr Earth Sc 4:47–59

Jacobs J, Thomas RJ (2004) Himalayan-type indenter-escape tectonics model for the southern part of the late Neoproterozoic-early Paleozoic East African-Antarctic orogen. Geology 32:721–724

Jarrar G (2001) The youngest Neoproterozoic mafic dyke suite in the Arabian shield: mildly alkaline dolerites from south Jordan–theirgeochemistry and petrogenesis. Geol Mag 138:309–323

Jarrar G, Saffarini G, Baumann A, Wachendorf H (2004) Origin, age and petrogenesis of Neoproterozoic composite dikes from the Arabian–Nubian Shield, SW Jordan. Geol J 39:157–178

Jarrar G, Stern RJ, Saffarini G, Al-Zubi H (2003) Late- and post-orogenic Neoproterozoic intrusions of Jordan: implications for crustal growth in the northernmost segment of the East African Orogen. Precambr Res 123:295–320

Jarrar G, Wachendorf H, Saffarini G (1992) A late Proterozoic bimodal volcanic/subvolcanic suite from Wadi Araba, Southwest Jordan. Precambr Res 56:51–72

Johnson PR, Abdelsalam M, Stern RJ (2002) The Bir Umq-Nakasib shear zone: Geology and structure of a Neoproterozoic suture in the northeastern East African Orogen, Saudi Arabia and Sudan: Saudi Geological Survey Technical Report SGS-TR-2002-1

Johnson PR, Andersen A, Collins AS, Fowler AR, Fritz H, Ghebreab W, Kusky T, Stern RJ (2011) Late Cryogenian-Ediacaran history of the Arabian–Nubian Shield: a review of depositional, plutonic, structural, and tectonic events in the closing stages of the northern East African Orogen. J Afr Earth Sc 61:167–232

Johnson PR, Halverson GP, Kusky TM, Stern RJ, Pease V (2013) Volcanosedimentary basins in the Arabian–Nubian Shield: Markers of repeated exhumation and denudation in a Neoproterozoic accretionary orogen. Geosciences 3:389–445

Johnson PR, Kattan F (1999) The timing and kinematics of a suturing event in the northeastern part of the Arabian Shield, Kingdom of Saudi Arabia. Open File Report USGS-OF-99-3. Saudi Arabian Deputy Ministry for Mineral Resources.

Johnson PR, Kattan FH (2012) The Geology of the Arabian Shield. Saudi Geological Survey, p 466

Johnson PR, Woldehaimanot B (2003) Development of the Arabian–Nubian Shield: perspectives on accretion and deformation in the northern East African orogeny and the assembly of Gondwana. In: Yoshida M, Windley BF, Dasgupta S (eds) Proterozoic East Gondwana: Supercontinent Assembly and Breakup. Geological Society, London, Special Publications, vol 206, pp 289–325

Johnson PR, Kattan FH, Wooden JL (2001) Implications of SHRIMP and microstructural data on the age and kinematics of shearing in the Asir Terrane, southern Arabian Shield, Saudi Arabia. Gondwana Res 4:172–173

Johnson PR, Kattan FH, Al-Saleh AM (2004) Neoproterozoic ophiolites in the Arabian Shield: field relations and structure. In: Kusky TM (ed) Precambrian ophiolites and related rocks. Elsevier, Amsterdam, pp 129–162

Johnson PR, Scheibner E, Smith AE (1987) Basement fragments, accreted tectonostratigraphic terranes, and overlap sequences: elements in the tectonic evolution of the Arabian Shield. In: Kroner A (ed) Proterozoic lithospheric evolution. American Geophysical Union Geodynamics Series, vol 17, pp 235–257

Kemp J (1981) Geologic map of the Wadi al 'Ays quadrangle, sheet 25 C, Kingdom of Saudi Arabia: Saudi Arabian Deputy Ministry for Mineral Resources Geologic Map GM-53, p 39

Kemp J, Pellaton C, Calvez JY (1980) Geochronological investigations and geological history in the Precambrian of northwestern Saudi Arabia. Saudi Arabian Deputy Ministry for Mineral Resources Open-File Report, BRGGM-OF-01-1

Kemp J, Yves G, Jean-Pierre P (1982) Geologic map of the Mahd adh Dhahab quadrangle, sheet 23E, Kingdom of Saudi Arabia: Saudi Arabian Deputy Ministry for Mineral Resources Geologic Map GM-64 A, scale 1:250,000, with text, 39 p

Kennedy A, Kozdroj W, Kattan FH, Kodzroj MZ, Johnson PR (2010) SHRIMP geochronology in the Arabian Shield (Midyan terrane, Afif terrane, Ad Dawadimi terrane) and Nubian Shield (Central Eastern Desert): Part IV Data acquisition 2008: Saudi Geological Survey Open-File Report SGS-OF-2010-10, 101 p

Kessel R, Stein M, Navon O (1998) Petrogenesis of late Neoproterozoic dikes in the northern Arabian–Nubian Shield: implications for the Origin of A-type granites. Precambr Res 92:195–213

Khalil AES, Azer MK (2007) Supra-subduction affinity in the Neoproterozoic serpentinites in the Eastern Desert, Egypt: evidence from mineral composition. J Afr Earth Sc 49:136–152

Khedr MZ, Arai S (2013) Origin of Neoproterozoic ophiolitic peridotites in south Eastern Desert, Egypt, constrained from primary mantle mineral chemistry. Mineral Petrol 107:807–828

Khedr MZ, Arai S (2016) Chemical variations of mineral inclusions in Neoproterozoic high-Cr chromitites from Egypt: evidence of fluids during chromitite genesis. Lithos 240–243:309–326

Khedr MZ, Arai S (2017) Peridotite-chromitite complexes in the Eastern Desert of Egypt: insight into Neoproterozoic sub-arc mantle processes. Gondwana Res 52:59–79

Kozdrój W, Kennedy AK, Johnson PR, Ziółkowska-Kozdrój M, Kadi K (2017) Geochronology in the southern Midyan terrane: a review of constraints on the timing of magmatic pulses and

tectonic evolution in a northwestern part of the Arabian Shield. Int Geol Rev. https://doi.org/10.1080/00206814.2017.1385425

Kröner A, Krüger J, Rashwan AAA (1994) Age and tectonic setting of granitoid gneisses in the Eastern Desert of Egypt and south-west Sinai. Geol Rundsch 83:502–513

Kröner A, Todt W, Hussein IM, Mansour IM, Mansour M, Rashwan AA (1992) Dating of late Proterozoic ophiolites in Egypt and the Sudan using the single grain zircon evaporation technique. Precambr Res 59:15–32

Kusky TM, Matsah MI (2003) Neoproterozoic dextral faulting on the Najd fault system, Saudi Arabia, preceded sinistral faulting and escape tectonics related to closure of the Mozambique Ocean. In: Yoshida M, Windley BF, Dasgupta S (eds) Proterozoic East Gondwana: supercontinent assembly and breakup. Geological Society, London, Special Publications, vol 206, pp 327–361

Küster D, Liégeois JP (2001) Sr, Nd isotopes and geochemistry of the Bayuda Desert high-grade metamorphic basement (Sudan): an early Pan-African oceanic convergent margin, not the edge of the East Saharan ghost craton? Precambr Res 109:1–23

Küster D, Liégeois J-P, Matukov D, Sergeev S, Lucassen F (2008) Zircon geochronology and Sr, Nd, Pb isotope geochemistry of granitoids from Bayuda Desert and Sabaloka (Sudan): evidence for a Bayudian event (920–900 Ma) preceding the Pan-African orogenic cycle (860–590 Ma) at the eastern boundary of the Saharan Metacraton. Precambr Res 164:16–39

Le Garzic E, de L'Hamaide T, Diraison M, Géraud Y, Sausse J, de Urreiztieta M, Hauville B, Champanhet J-M (2011) Scaling and geometric properties of extensional fracture systems in the Proterozoic basement of Yemen. Tectonic interpretation and fluid flow implications. J Struct Geol 33:519–536

Ledru P, Auge T (1984) The Al Ays ophiolitic complex; petrology and structural evolution. BRGM-OF-04-15. Saudi Arabia Deputy Ministry for Mineral Resources

Li ZX, Bogdanova SV, Collins AS, Davidson A, De Waele B, Ernst RE, Fitzsimons ICW, Fuck RA, Gladkochub DP, Jacobs J, Karlstrom KE, Lu S, Natapov LM, Pease V, Pisarevsky SA, Thrane K, Vernikovsky V (2008) Assembly, configuration, and break-up history of Rodinia: a synthesis. Precambr Res 160:179–210

Liégeois J-P, Stern RJ (2010) Sr-Nd isotopes and geochemistry of granite-gneiss complexes from the Meatiq and Hafafit domes, Eastern Desert, Egypt: no evidence for pre-Neoproterozoic crust. J Afr Earth Sc 57:31–40

Loizenbauer J, Wallbrecher E, Fritz H, Neumayr P, Khudeir AA, Kloetzli U (2001) Structural geology, single zircon ages and fluid inclusion studies of the Meatiq metamorphic core complex: Implications for Neoproterozoic tectonics in the Eastern Desert of Egypt. Precambr Res 110:357–383

Lubnina NV, Slabunov AI (2011) Reconstruction of the Kenorland Supercontinent in the Neoarchean based on paleomagnetic and geological data. Mosc Univ Geol Bull 66:242–249

Meert JG (2012) What's in a name? The Columbia (Paleopangaea/Nuna) supercontinent. Gondwana Res 21:987–993

Menzies M, Al Kadasi M, Al Khirbash S, Al Subbary A, Baker J, Blakey S, Bosence D, Davison I, Dar, C, Owen L, McClay K, Nicholls G, Yelland A, Watchorn F (1994) Geology of the Republic of Yemen. In: McCombe DA, Fernette GL, Alawi AJ (eds) Geology and Mineral Resources of Yemen. Geological Survey and Mineral Exploration Board, Yemen Mineral Sector Project Technical Report, pp 21–48

Moghazi AM (2003) Geochemistry and petrogenesis of a high-K calcalkaline Dokhan volcanic suite, South Safaga area, Egypt: the role of late Neoproterozoic crustal extension. Precambr Res 125:161–178

Moghazi A-KM, Ali KA, Wilde SA, Zhou Q, Andersen T, Andresen A, Abu El-Enen MM, Stern RJ (2012) Geochemistry, geochronology, and Sr-Nd isotopes of the Late Neoproterozoic Wadi Kid volcano-sedimentary rocks, southern Sinai, Egypt: implications for tectonic setting and crustal evolution. Lithos 154:147–165

Mohamed FH, Hassanen MA (1996) Geochemical evolution of arc-related mafic plutonism in the Umm Naggat District, Eastern Desert of Egypt. J Afr Earth Sc 22:269–283

Moore JM (1979) Tectonics of the Najd Transcurrent Fault System, Saudi Arabia. J Geol Soc London 136:441–454
Moussa EMM, Stern RJ, Manton WI, Ali KA (2008) SHRIMP zircon dating and Sm/Nd isotopic investigations of Neoproterozoic granitoids, Eastern Desert, Egypt. Precambrian Res 160:341–356
Nasseef AO, Bakor AR, Hashad AH (1980) Petrography of possible ophiolitic rocks along the Qift-Quseir, Eastern Desert, Egypt. IAG Bull Jeddah 3:157–168
Nasseef AO, Gass IG (1977) Granitic and metamorphic rocks from the Taif area, western Saudi Arabia. Geol Soc Am Bull 88:1721–1730
Nasseef MO, Macdonald R, Gass IG (1984) The Jebel Thurwah upper proterozoic ophiolite complex, western Saudi Arabia. J Geol Soc London 141:537–546
Neary CR, Gass IG, Cavanagh HBI (1976) Granitic association of northeastern Sudan. Bull Geol Soc Am 87:1501–1512
Nehlig P, Genna A, Asfirane F, Dubreuil N, Guerrot C, Eberlé JM, Kluyver HM, Lasserre JL, Le Goff E, Nicol N, Salpeteur N, Shanti M, Thiéblemont D, Truffert C (2002) A review of the Pan-African evolution of the Arabian Shield. GeoArabia 7:103–124
Okrusch M, Jamal-Allil SH (1979) Studies in the Abha Crystalline Complex, Asir, Saudi-Arabia. Neues Jahrbuch Für Mineralogie Abhandlun-Gen 135:148–179
Pallister JS, Stacey JS, Fischer LB, Premo WR (1988) Precambrian ophiolites of Arabia: geologic settings, U-Pb geochronology, Pb-isotopes characteristics, and implications for continental accretion. Precambr Res 38:1–54
Patchett PJ, Chase CG (2002) Role of transform continental margins in major crustal growth episodes. Geology 30:39–42
Petit C (2010) "Continental hearts—science news". Science news. Soc Sci Public 178:22–26
Powell JH, Abed AM, Le Nindre Y-M (2014) Cambrian stratigraphy of Jordan. GeoArabia 19:81–134
Quick JE (1990) Geology and origin of late Proterozoic Darb Zubaydah ophiolite, Kingdom of Saudi Arabia. Geol Soc Am Bull 102:1007–1020
Rashwan AA (1991) Petrography, geochemistry and petrogenesis of the Migif-Hafifit at Hafifit Mine area, Egypt. Scientifc series of the International Bureau/Forschungszentrum Jülich GmbH 5
Ries AC, Shackleton RM, Graham RH, Fitches WR (1983) Pan-African structures, ophiolites and melanges in the Eastern Desert of Egypt: a traverse at 26 N. J Geol Soc London 140:75–95
Rittmann A (1958) Geosynclinal volcanism, ophiolites, and Barramiya rocks. Egypt J Geol 2:61–66
Rogers JJW, Santosh M (2003) Supercontinents in Earth History. Gondwana Res 6:357–368
Schlüter T (2006) Geological Atlas of Africa. With notes on stratigraphy, tectonics, economic geology, geohazards and geosites of each country. ISBN 10 3-540-29144-x. Springer Berlin Heidelberg, New York, p 256
Schmidt DL, Hadley DG, Stoeser DB (1980) Late Proterozoic crustal history of the Arabian Shield, Southern Najd Province, Kingdom of Saudi Arabia. Institute of Applied Geology, King Abdulaziz University (Jeddah), Bulletin, vol 3, pp 41–58
Sofiya A, Ishiwatari A, Hirano N, Tsujimori T (2017) Relict chromian spinels in Tulu Dimtu serpentinites and listvenite, Western Ethiopia: implications for the timing of listvenite formation. Int Geol Rev 59:1621–1631
Stacey JS, Agar RA (1985) U-Pb isotopic evidence for the accretion of a continental microplate in the Zalm region of the Saudi Arabian Shield. J Geol Soc London 142:1189–1203
Stacey JS, Doe BR, Roberts RJ, Delevaux MH, Gramlich JW (1980) Lead isotope study of mineralization in the Saudi Arabian shield. Contrib Mineral Petrol 74:175–188
Stacey JS, Stoeser DB (1983a) Distribution of oceanic and continental leads in the Arabian–Nubian Shield. Contrib Miner Petrol 54:91–105
Stacey JS, Stoeser DB (1983b) Distribution of oceanic and continental leads in the Arabian–Nubian Shield. Contrib Miner Petrol 84:91–105

Stern RJ (1985) The Najd fault system, Saudi Arabia and Egypt: a late Precambrian rift-related transform system? Tectonics 4:497–511
Stern RJ (2002) Crustal evolution in the East African Orogen: a neodymium isotopic perspective. J Afr Earth Sc 34:109–117
Stern RJ (2018) Neoproterozoic formation and evolution of Eastern Desert Continental Crust—the importance of the infrastructure-superstructure transition. J Afr Earth Sc 18:15–27
Stern RJ, Ali KA (2020) Crustal Evolution of the Egyptian Precambrian Rocks. In: Hamimi et al (eds) The Geology of Egypt, regional geology reviews. Springer Nature Switzerland AG 2020, pp 131–151
Stern RJ, Gottfried D, Hedge CE (1984) Late Precambrian rifting and crustal evolution in the Northeastern Desert of Egypt. Geology 12:168–172
Stern RJ, Hedge CE (1985) Geochronologic constraints on late Precambrian crustal evolution in the Eastern Desert of Egypt. Am J Sci 285:97–127
Stern RJ, Johnson PR (2010) Continental lithosphere of the Arabian plate: a geologic, petrologic, and geophysical synthesis. Earth-Sci Rev 101:29–67
Stern RJ, Johnson PR, Kröner A, Yibas B (2004) Neoproterozoic ophiolites of the Arabian–Nubian Shield. In: Kusky T (ed) Precambrian ophiolites and related rocks. Elsevier, Amsterdam, pp 95–128
Stern RJ, Johnson PR (2019) Constraining the Opening of the Red Sea: evidence from the Neoproterozoic Margins and Cenozoic Magmatism for a Volcanic Rifted Margin. In: Rasul NMA, Stewart ICF (eds) Geological setting, palaeoenvironment and archaeology of the Red Sea, pp 53–79. https://doi.org/10.1007/978-3-319-99408-6_4
Stern RJ, Kroner A, Reischmann T, Bender R, Dawoud AS (1994) Precambrian basement around Wadi Halfa: a new perspective on the evolution of the Central Saharan Ghost craton. Geol Rundsch 93:564–577
Stern RJ, Manton WI (1987) Age of Feiran basement rocks, Sinai: implications for late Precambrian evolution in the northern Arabian–Nubian Shield. J Geol Soc London 144:569–575
Stern RJ, Nielsen KC, Best E, Sultan M, Arvidson RE, Kroner A (1990) Orientation of late Precambrian sutures in the Arabian Nubian shield. Geology 18:1103–1106
Stoeser DB (1986) Distribution and tectonic setting of plutonic rocks of the Arabian Shield. J Afr Earth Sc 4:21–46
Stoeser DB, Camp VE (1985) Pan-African microplate accretion of the Arabian Shield. Geol Soc Am Bull 96:817–826
Stoeser DB, Frost CD (2006) Nd, Pb, Sr, and O isotopic characterization of Saudi Arabian Shield terranes. Chem Geol 226:163–188
Sultan M, Arvidson RE, Duncan IJ, Stern RJ, El Kaliouby B (1988) Extension of the Najd shear system from Saudi Arabia to the Central Eastern Desert of Egypt based on integrated field and Landsat observations. Tectonics 7:1291–1306
Tadesse S, Milesi J-P, Deschamps Y (2003) Geology and mineral potential of Ethiopia: a note on geology and mineral map of Ethiopia. J Afr Earth Sc 36:273–313
Teklay M, Kröner A, Mezger K (2001) Geochemistry, geochronology and isotope geology of Nakfa intrusive rocks, northern Eritrea: products of a tectonically thickened Neoproterozoic arc crust. J Afr Earth Sc 33:283–301
Teklay M, Kröner A, Metzger K, Oberhänsli R (1998) Geochemistry Pb–Pb single zircon ages and Nd–Sr isotope composition of Precambrian rocks from southern and eastern Ethiopia: implications for crustal evolution in East Africa. J Afr Earth Sc 26:207–227
Vail JR (1985) Pan-African (Late Precambrian) tectonic terrains and the reconstruction of the Arabian–Nubian Shield. Geology 13:839–842
Vérard C (2019a) Panalesis: towards global synthetic palaeogeographies using integration and coupling of manifold models. Geol Mag 156:320–330
Vérard C (2019b) Plate tectonic modelling: review and perspectives. Geol Mag 156:208–241
Vérard C (2021) 888–444 Ma global plate tectonic reconstruction with emphasis on the formation of Gondwana. Front Earth Sci 9:666153

Viland JC (1986) Assessment for gold in the Zalim area, central Arabian shield: Review of BRGM work: Saudi Arabian Deputy Ministry for Mineral Resources Open-File Report BRGM-OF-06-11

Whitehouse MJ, Stoeser DB, Stacey JS (2001) The Khida Terrane-Geochronological and isotopic evidence for Paleoproterozoic and Archean crust in the eastern Arabian shield of Saudi Arabia. Gondwana Res 4:200–202

Whitehouse MJ, Windley BF, Ba-Bttat MAO, Fanning CM, Rex DC (1998) Crustal evolution and terrane correlation in the eastern Arabian Shield, Yemen: geochronological constraints. J Geol Soc 155:281–296

Wilde SA, Youssef K (2000) Significance of SHRIMP U-Pb dating of the Imperial Porphyry and associated Dokhan Volcanics, Gabal Dokhan, North Eastern Desert, Egypt. J Afr Earth Sci 31:403–413

Williams FM (2016) Understanding Ethiopia: geology and scenery (geoguide), 1st edn. Springer, 377 p. ISBN-10: 3319021796

Wilson M (1989) Igneous petrogenesis. Unwin Hyman, London, p 446

Windley BF, Whitehouse MJ, Ba-Bttat MAO (1996) Early Precambrian gneiss terranes and Pan-African island arcs in Yemen: crustal accretion of the eastern Arabian Shield. Geology 24:131–134

Yeshanew FG, Pease V, Abdelsalam MG, Whitehouse MJ (2017) Zircon U-Pb ages, $\delta^{18}O$ and whole-rock Nd isotope compositions of the Dire Dawa Precambrian basement, Eastern Ethiopia: implications for the assembly of Gondwana. J Geol Soc London 174:142–156

Chapter 2
Classification and General Distribution of Mineral Deposits in the Arabian–Nubian Shield: A Review

Contents

2.1 Classifications of Mineral Deposits 69
2.1.1 Introduction 69
2.1.2 Genetic Classification Scheme (Used in This Book) 71
2.2 Mineral Deposits in the Arabian–Nubian Shield: An Overview 79
2.2.1 Afro-Arabian Domain 80
2.2.2 Eastern Domain 85
2.2.3 Southern Domain 85
2.2.4 Western Domain 86
References 86

2.1 Classifications of Mineral Deposits

2.1.1 Introduction

The geology of mineral deposits, or simply the "economic geology", is the science dealing with the discovery and evaluation of the Earth's mineral resources. One of the main goals of economic geologists is to understand the genesis of mineral deposits within the framework of the Earth's geologic history. Mineral deposits mainly form by physical and chemical changes in the Earth's asthenosphere. They formed in the mantle and crust of the Earth by magmatic, metamorphic, sedimentary, and hydrothermal processes, and can be affected by several factors such as tectonic setting, pressure-temperature conditions, erosion, climate, etc. These physico-chemical processes may concentrate some certain elements into economic concentrations with characteristic mineralogical and chemical compositions. These mineral deposits are also characterized by their color, texture and structure that can be easily recognized from the un-mineralized or poorly mineralized surrounding

A. Hassan Ahmed, *Mineral Deposits and Occurrences in the Arabian–Nubian Shield*,
Earth and Environmental Sciences Library,
https://doi.org/10.1007/978-3-030-96443-6_2

country rocks. The categorization (classification) of mineral deposits is important to simplify dealing with a certain number of types having certain features in common. Any classification scheme of mineral deposits should propose generalizations about the genesis of ore deposits and should be applicable in the field for descriptions of mineral deposits. Thus, the description and characteristics of common mineral deposit types are an integral step in the geology of ore deposits to understand their nature, spatial/temporal distribution and genesis.

There are many historical attempts to classify mineral deposits. Some classification schemes have an economic basis linked to the end use of the metal or mineral, whereas others are based partly or entirely on geologic factors. Since the Middle Ages (the time of Agricola), several classification schemes of mineral deposits have been proposed. Among the earlier attempts, which classified mineral deposits in a modern way, are those proposed by the pioneers Lindberg (1922) and Lindgren (1934). After that, several different approaches have been proposed by many researchers to classify the wide range of mineral deposits, some of them provided a general overview about mineral deposits and ore-forming processes, some others selected only one group of mineral deposit, or select a certain type of ore deposits such as those related to magmatic processes (Whitney and Naldrett 1989), or those related to hydrothermal system and processes (Henley et al 1984; Barnes 1987). In some other cases, scientists can classify mineral deposits based on the metal and treat each commodity separately, for example uranium deposits, coal deposits, base metal deposits and so on (e.g., Diessel 1992; Dill 2010).

Different classification schemes of mineral deposits based mainly on different features of primary attribute for categorization, where the commonly used attributes can be summarized as follow:

(1) Elements or minerals content: Cu, Au, Fe, etc.
(2) Types of host rock: mafic-ultramafic rocks, carbonate-bearing sedimentary rocks, felsic intrusive bodies, etc.
(3) Tectonic settings: back-arc basin, intra-cratonic sedimentary basin, Proterozoic intra-cratonic basins, active/passive continental margin, etc.
(4) Ore forming processes: magmatic processes, sedimentary processes, hydrothermal processes.

There are so many classification schemes for mineral deposits during the twentieth century, based mainly on the types of host rocks and/or the geometry of the deposit and its relation to the host rocks. For example, the mineral deposits in granites are quite distinguished from those in sedimentary rocks; the dike-like deposits are distinguished from those in layered-like ones that conformable with the stratification of the host rock; and the massive ores are distinguished from disseminated ones. In addition, after the discovery of "plate tectonics" theory, at the end of twentieth century, many classification schemes of mineral deposits were proposed based on the tectonic settings. For example, mineral deposits in mid-ocean ridge basins were distinguished from those in the subduction zone (convergent margins) settings or intracratonic settings, and so on. The tectonic setting classification scheme is still used

in general, and particularly when discussing the large-scale distribution of mineral deposits.

2.1.2 Genetic Classification Scheme (Used in This Book)

Newer classification schemes, however, become more popular in categorization of mineral deposits in which the main attributes are the ore-forming processes and types of host rocks (e.g., Meyer 1981; Guilbert and Park 1986; Misra 2000; Einaudi 2000; Robb 2004; Ridley 2013), they widely replaced the older classifications. The newer classification scheme also called "*genetic classification*", which is much easier to use in the field studies where it is primarily based on two-fold criterions: (1) according to the host rocks for mineral deposits related to magmatic rocks, and (2) according to the process of formation for other mineral deposits. The genetic classification is the most desirable scheme, as it has considerable advantages to other classifications. It mainly considered the ore-forming processes and their relation to the host rocks in a specific set of descriptive categories. The common host rocks of mineral deposits are universally classifying into three-fold subdivisions: magmatic (igneous), sedimentary and metamorphic rocks, which are representing the main active processes in the Earth's crust.

Mineral deposit types are similar to rocks in terms of their genesis, they can easily attributed to either magmatic (igneous) or sedimentary/surficial origin. The magmatic and sedimentary mineral deposits are, in most cases, syngenetic where they formed at the same time and under the same conditions with their host rocks. Although metamorphic processes can modify the original nature of pre-existing mineral deposits and their host rocks, they do not themselves represent fundamental processes in the mineral deposits formation. However, a third category of mineral deposits is considered as an important group that is the hydrothermal deposits. Therefore, the most simple and convenient classification scheme of mineral deposits is a three-fold subdivisions of magmatic, sedimentary/surficial, and hydrothermal categories (Einaudi 2000; Robb 2004). This type of classification "*genetic classification*" will be the basis for the coming chapters of this book.

The magmatic host rocks can be geologically classified into plutonic, hypabyssal (subvolcanic), and extrusive (effusive) rocks, based on their position from the Earth's surface. Based on rock chemistry, especially SiO_2 content and sum of alkalies ($Na_2O + K_2O$), magmatic rocks subdivided into four major classes: the ultramafic rocks (SiO_2 undersaturated), mafic rocks, intermediate rocks and felsic or acidic rocks (SiO_2 saturated). These subdivisions of magmatic rocks are the main host rocks of the magmatic mineral deposits, which will be discussed later in the coming chapter. Sedimentary host rocks are those rocks resulted from the erosion and deposition of chemical, physical and biological weathering products of pre-existing magmatic, metamorphic or sedimentary rocks. The mechanically and chemically disintegrated materials are transported, by various transportation agents (water, wind and glaciers), far away from the source rocks. The transported materials are precipitated and then

undergo lithification through time within the depositional basins. The third type of host rocks is the metamorphic rocks, which could be any of pre-existing rocks, whether igneous or sedimentary rocks that undergo metamorphic processes.

As mentioned above, the ore-forming processes, as one of the basic attributes of the genetic classification scheme, could be magmatic, sedimentary/surficial, and hydrothermal processes (Table 2.1). However, the ore-forming processes are complex, for example, magmatic processes become magmatic-hydrothermal as the igneous intrusion cools, crystallizes and exsolved its water content. On the other hand, the fluid flow resulted from diagenesis and metamorphism of sedimentary

Table 2.1 Genetic classification scheme of mineral deposits used in this book

1. Magmatic deposits: ores formed by direct crystallization and accumulation from a magma *Deposits associated with mafic-ultramafic rocks* • Chromite deposits: (i) stratiform chromite in layered intrusions, and (ii) podiform chromite in ophiolite complexes • Magmatic sulfide deposits (Cu-Ni-Fe-PGE) • Magmatic Fe-Ti oxide deposits • Metals-bearing carbonatites • Diamonds in kimberlites
2. Magmatic-hydrothermal deposits (intrusion-related deposits): concentration of metals during magma formation and subsequent cooling and crystallization *(a) Porphyry (Cu-Mo-Au-W) deposits in granitic intrusions* *(b) Epithermal-vien deposits* *(c) Skarn deposits* *(d) Greisen deposits* *(e) deposits associated with felsic intrusions* • Mineral deposits in granites • REE-bearing pegmatites
3. Hydrothermal deposits*:* ore minerals precipitated from high-temperature aqueous fluids of different origins *(a) Deposits in orogenic environments* • Orogenic gold deposits • Carlin-type gold deposits • Iron oxide-copper-gold (IOCG) deposits *(b) Deposits in volcano-sedimentary environments* • Volcanogenic massive sulfide (VMS) deposits • Sedimentary exhalative (SEDEX) deposits • Mississippi-Valley Type (MVT) deposits • Red-bed copper deposits • Uranium deposits
4. Sedimentary/surficial deposits: concentrations of detrital minerals or precipitates *(a) Deposits related to sedimentation (chemical and clastic deposits)* • *Iron ore deposits (banded iron formation-BIF, and oolitic ironstones)* • *Evaporites, phosphorites, Mn deposits,* etc. • *Placer deposits* *(b) Deposits related to weathering* • *Residual deposits (Al-laterites-bauxite, Ni-laterite)* • *Supergene enrichment deposits*

Modified from Guilbert and Park (1986), Robb (2004), Ridley (2013)

rocks could be a potential agent for mineralization in any rock types. Therefore, the ore-forming processes can cover more than one of the three categories with a considerable overlap between magmatic and hydrothermal processes, from one hand, and between sedimentary and hydrothermal processes, from the other hand.

The broad groups of genetic classification scheme of mineral deposits can be summarized in Table 2.1. The first category, the magmatic deposits, contains many types of important mineral deposits in mafic-ultramafic rocks, while there is only a few less important types in the evolved counterpart of the felsic or acidic rocks. On the other hand, there are many mineral deposits hosted by granitic rocks, where the ore minerals are indirectly precipitating from aqueous fluids and not directly from the granitic magma itself. This type of ores is categorized under the "magmatic-hydrothermal" deposits. The type of ore minerals in the former process, the magmatic deposits, is directly linked to the composition of the host rock, while those in the latter process, the magmatic-hydrothermal deposits, are linked to the fluids and source magma compositions. For example, in the mafic-ultramafic rocks, the Ni, Cr and PGE deposits are predominant, which are strongly partitioning into the early-crystallized minerals (e.g., olivine pyroxenes and chromite).

Some specific metals, such as Cr for example, are restricted to a specific type of ore-forming process, which mined from the magmatic chromite deposits that concentrated during the crystallization of mafic-ultramafic magmas. Although hydrothermal chromite is recently proposed to be formed by hydrothermal process (Arai and Akizawa 2014; Arai et al 2020), until now a real economically important hydrothermal chromite ore (chromitite) is unknown. On the other hand, ore minerals in acidic rocks, by contrast, are composed of elements that partition into the evolved magmatic liquids. Some of these minerals are present in late crystallizing phases such as cassiterite (Sn ore) and wolframite (W ore), while some others exsolved into the water-rich fluids that separates from the silicate liquid. These metal-charged aqueous fluids will be a potential source of rare metals, which could be precipitated in the last magmatic stage in the form of hydrothermal ore bodies or in pegmatite rocks. Pegmatites are one of the important sources of economic rare metals such as Li, Be and other REE. Furthermore, the main aluminum ore is bauxite, which forms in hot and humid climates as a lateritic soil, but few amount (~2% of the world production) of Al metal can also be extracted from the magmatic nepheline syenite rock. Thus, most metals occur in mineral deposits of diverse origins.

The approach is applying the knowledge of geological processes and types of host rock, including the behavior of major and trace elements during melt crystallization, the stability of mineral phases in hydrothermal aqueous solutions, and the role of surficial conditions to concentrate and redistribute valuable metals, all of which aim to better understanding how the ore deposits are formed. The boundary between the magmatic and hydrothermal deposits is not sharp, where there is an overlap between the pure magmatic processes and the pure hydrothermal processes, which called here as "magmatic-hydrothermal" deposits that involving the concentration of metals during igneous processes or magma formation and subsequent cooling and crystallization.

Following is a brief description of the different groups of ore-forming processes of the genetic classification scheme (Table 2.1), which used as the base of the current book structure in the coming chapters.

(1) ***Magmatic Deposits*** (Chap. 3)

Magmatic mineral deposits (also known as *"orthomagmatic"*), are syngenetic deposits located within igneous rocks in which ore minerals directly crystallized from a melt. A large number of different mineral deposits are typically hosted in igneous rocks. Both mafic-ultramafic and felsic rocks are important host to mineral deposits, which are ranging from chromite deposits that crystallized by mafic magma fractionation to tin deposits related to an evolved felsic magma and hosted within certain types of granitic rocks. This magmatic ore-forming process is directly linked to the magma cooling and solidification. The mineral deposits related to this process will be discussed in Chap. 3. The magmatic system involves four distinguishable ore-forming processes (Ridley 2013), each of which have a specific mineral deposit type:

(i) ***Magmatic accumulation and concentration*** (e.g., chromite deposits). Under specific conditions, both chromite and/or magnetite concentrated directly from mafic magmas as layers and pods in the mafic-ultramafic rocks of layered and ophiolitic complexes.

(ii) ***Separation of immiscible liquids*** (e.g., magmatic sulfide deposits, and Fe-Ti-P oxide deposits). The chalcophile and siderophile elements (e.g., Cu, Ni, Fe, PGE) tend to be compatible and retained within sulfide melt than in silicate melt, which thus be concentrated mainly within the immiscible sulfide melt. The Fe-Ti-P oxide deposits of magnetite-ilmenite-apatite ores in some anorthosite intrusions are also formed by the melt-melt immiscibility.

(iii) ***Very low degrees of partial melting of mantle rocks*** (e.g., metals-bearing carbonatites and alkaline rocks). Metals-bearing carbonatite and alkaline rocks are formed by the strong partitioning of incompatible elements within the small-fraction partial melts in the mantle.

(iv) ***Crystallization at a great depth*** (e.g., diamond-bearing kimberlites). A special case of these mineral deposits is the diamond-bearing kimberlites and lamproite, which generated from a magma below the graphite–diamond transition depth in the mantle.

(2) ***Magmatic-Hydrothermal Deposits (Intrusion-related deposits)*** (Chap. 4)

Magmatic-hydrothermal mineral deposits are those deposits in which the aqueous solutions were directly derived from the magma. The transition between magmatic and hydrothermal processes plays an important role in the formation of a wide variety of mineral deposits, particularly in the near surface environments where silicate melts and fluids are spatially and genetically linked. This type of mineral deposits has not segregated directly from the crystallizing magma but they formed from the hydrothermal activity associated with igneous bodies that emplaced at high levels in the Earth's crust. This category of mineral deposits in the ANS will be described

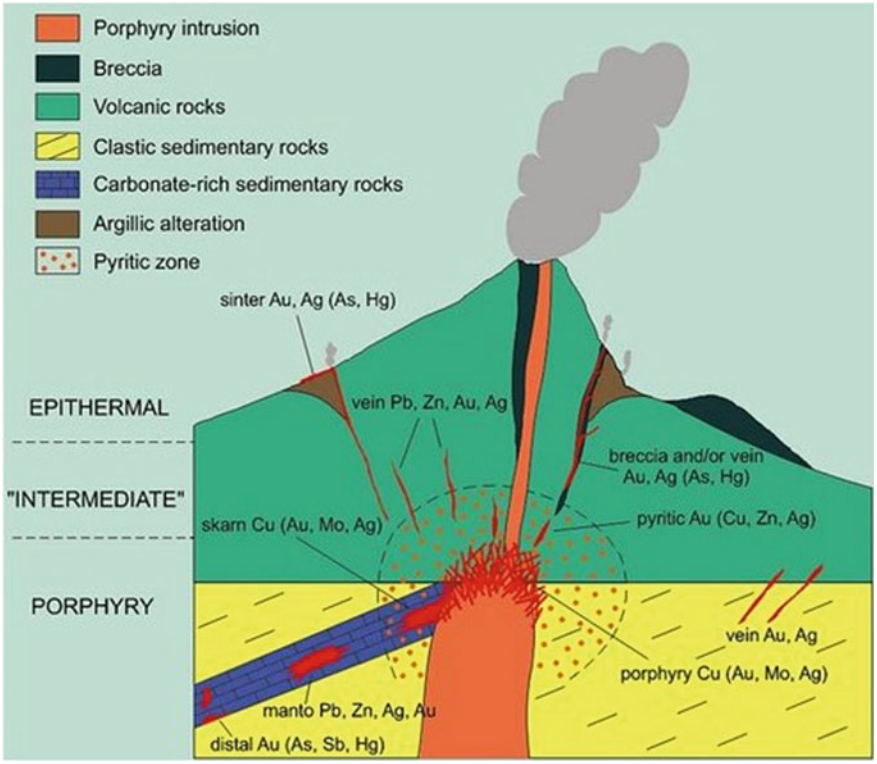

Fig. 2.1 Schematic diagram of a porphyry system (porphyry, skarn, and vein-type deposits) in the root zone of an andesitic stratovolcano (Kirkham and Sinclair 1995)

in Chap. 4. Examples for these mineral deposits represented by the following types (Table 2.1, Fig. 2.1):

(i) ***Porphyry deposits***: refers to very large-tonnage, but low-grade disseminated deposits associated with intermediate to felsic porphyritic granitic stocks that have emplaced into shallow crustal levels (Fig. 2.1). Porphyry deposits are the main producer of Cu (porphyry Cu deposits), or Cu with Au or Mo (porphyry Cu-Mo-Au deposits), and more rarely of Mo or of Sn-W-Ag deposits.

(ii) ***Polymetallic epithermal vein-type deposits***: refers to swarms of veins related to small intermediate to felsic intrusions, being extending over several kilometers from the intrusions that show spatial zonation of metal contents. Epithermal vein deposits are near-surface deposits that formed at relatively low temperatures and shallow depths around volcanic centers and geothermal fields (Fig. 2.1). They are a source of various metals including of Au, Ag and Cu. They can be subdivided into: (a) *High-sulfidation epithermal deposits*, which are close to the heat source (volcanic centers) and are hosted in intensely altered rocks, and (b) *Low-sulfidation epithermal deposits*, which are located at

the distal side from the volcanic centers; they show different ore and alteration mineralogy.

(iii) ***Polymetallic skarn deposits***: refer to metasomatic replacement of carbonate rocks (limestone and dolomite) by high-temperature calc-silicate mineral assemblages during contact and/or regional metamorphism. Skarn deposits typically produced by contact metamorphism and metasomatism of granitic intrusions into carbonate rocks. They include a wide variety of mineral deposits rich in W, Sn, Mo, Cu, Fe, Pb–Zn, and Au metals (Fig. 2.1).

(iv) ***Greisen-related deposits***: refers to mineral deposits predominantly rich in Sn and W, in addition to Mo, F, Li and B in greisenised (metasomatically altered) quartz–muscovite granite at the top of felsic intrusions, or in quartz veins in and adjacent to altered granites.

(v) ***Pegmatite-related deposits***: The cooling and crystallization of fluid-rich peralkaline granitic magma may result in the formation of pegmatites, which are important source for a suite of rare elements (e.g., Ta, Nb, Li, and Be) that tend to be concentrated in the residual volatile-rich melt. Rare-element pegmatites can be classified into two sub-types: LCT (Li-, Cs- and Ta-rich) and, NYF (Nb-, Y- and F-rich) types.

(3) ***Hydrothermal Deposits*** (Chaps. 5 and 6)

Hydrothermal mineral deposits are those not directly linked to the magmatic activity. This category of mineral deposits in the ANS will be discussed in Chaps. 5 and 6 of this book. The mineralizing fluids of hydrothermal deposits derived from sources other than magmatic solutions include those formed from metamorphic dehydration reactions (orogenic environment), from the expulsion of pore fluids during compaction of sediment (connate water), from meteoric waters, and seawater. These hydrothermal deposits can be subdivided into two main parts: (1) *Hydrothermal deposits of orogenic environments* (metamorphic hydrothermal fluids) (Table 2.1 and Fig. 2.2), which represented by: (i) orogenic gold deposits, (ii) Carlin-type gold deposits, and (iii) Iron oxide-copper-gold (IOCG) deposits. This part will be discussed in Chap. 5. (2) *Hydrothermal deposits of volcano-sedimentary environments*, which represented by various deposit types including (Table 2.1): (i) volcanogenic massive sulfide (VMS) deposits, (ii) Mississippi Valley-type (MVT) deposits, (iii) sedimentary exhalative (SEDEX) deposits, (iv) red-bed copper deposits, and (v) uranium deposits. This part of hydrothermal deposits will be discussed in Chap. 6.

In the first part (*hydrothermal deposits of orogenic environments*), there are three important types of hydrothermal gold and gold-copper deposits, which form during the regional metamorphism/tectonism in the host geological terranes, these represented by (Table 2.1 and Fig. 2.2):

(i) ***Orogenic gold deposits***: also known as, "lode" Au deposits, "quartz-vein" Au deposits, "Au-only" deposits or "mesothermal" Au deposits. These deposits

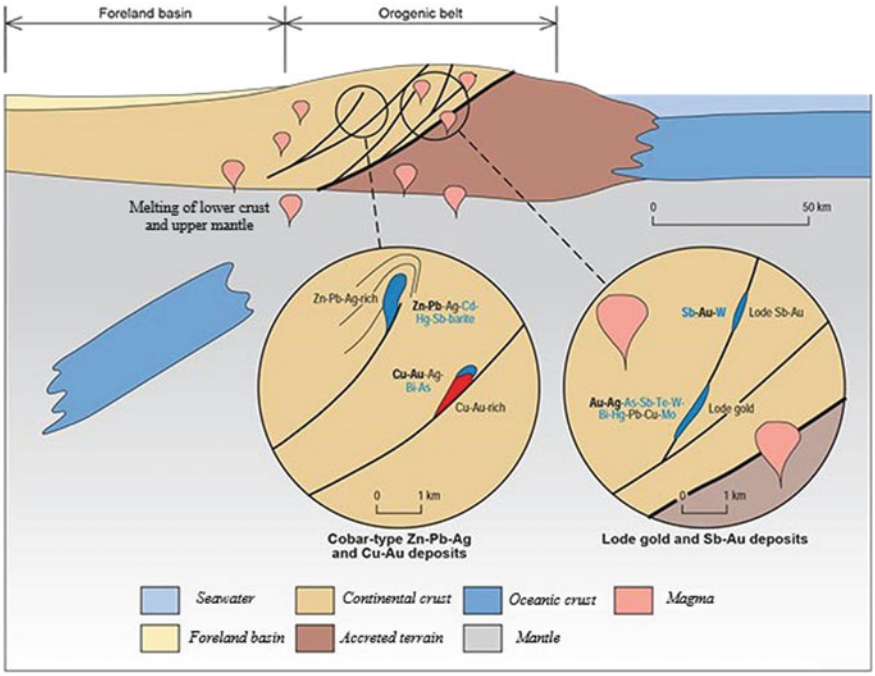

Fig. 2.2 Schematic diagram of the orogenic mineral system illustrating the relative location of deposits types, and the distribution of critical and other metals within and around these deposit types (*Source* Geoscience Australia)

existed as vein and replacement Au deposits in metamorphic and intrusive igneous rocks; they are mostly formed during the periods of regional metamorphism.

(ii) ***Carlin-type gold deposits***: also known as, "sediment-hosted" gold deposits and "disseminated" gold deposits, based on the host-rocks and the nature of the ore. They found as replacement ore bodies in metasomatically-altered impure carbonate and calcareous siliciclastic sedimentary rocks.

(iii) ***Iron oxide–copper–gold (IOCG) deposits***: the major Fe-bearing minerals in this type of ores is iron oxides (magnetite and/or hematite) rather than iron sulfides. This deposit type is an important source for copper and gold, but also many of them are producing other metals (U, Ag, LREEs) as by- and co-products.

The second part of hydrothermal deposits (*Hydrothermal deposits of volcano-sedimentary environments*) can be subdivided into five types of hydrothermal deposits existed in volcano-sedimentary basins; these are (Table 2.1):

(i) ***Volcanogenic massive sulfide (VMS) deposits***: also named as "volcanic-hosted massive sulfide" (VHMS) deposits, mainly found as stratabound and sometimes stratiform bodies of hydrothermal massive sulfide ores that formed

at, or just below, the sea floor near active magmatic centers in a relatively deep marine environment. The VMS deposits are polymetallic, containing variable metal sulfides such as Cu, Zn and Pb, in addition to Au and Ag; where the host rocks are submarine volcanic rocks, or sometimes deep-sea sedimentary rocks intercalated with volcanic rocks.

(ii) ***Sedimentary exhalative (SEDEX) deposits***: occur as stratiform or stratabound Pb-Zn sulfide deposits hosted in sedimentary rock of early Proterozoic to Mesozoic age, with silver (Ag) and minor Cu as significant co-products. Barite can also be accumulated nearby the SEDEX deposits.

(iii) ***Mississippi-Valley Type (MVT) deposits***: occur as epigenetic Pb-Zn sulfide deposits in solidified carbonate rocks, which contain a few percent, up to about 10 wt%, with equal grades of Pb and Zn metals. The MVT deposits contain some other metals as by-products include one or more of Ag, Ge, Cd, Cu, barite and fluorite.

(iv) ***Red-bed copper deposits***: occur as large, laterally extensive, stratabound Cu deposits, with Co and minor amounts of Ni, Ag, Zn, Pb and U as important by-products. This deposit type provide about 30% of the Cu world's supply. The host rock of this deposit type is largely red-bed sandstones overlying black shales of shallow-marine or lacustrine origin. It is thus distinct from those of MVT and SEDEX deposits.

(v) ***Uranium deposits***: uranium resources are mostly formed by leaching and syn-diagenetic migration of low-temperature waters through sedimentary basins, especially in the high-permeability sandstones in intracontinental basins. All sedimentary U deposits are of epigenetic, fine-grained precipitates of U^{+4} oxide and silicate minerals in pore space or as replacement products of earlier minerals. All these U deposits resulted from leaching of U from rocks in the host basin, then transport by basinal waters and precipitation in the form of U ore bodies.

(4) ***Sedimentary/Surficial Deposits*** (Chap. 7)

Surficial or external systems refer to all processes taken place on or near the Earth's surface by chemical and physical phenomena and led to the concentration of surficial mineral deposits within the regolith, lakes, and/or shallow marine environments. Two major ore-forming processes are taking place in the formation of sedimentary/surficial deposits (Table 2.1): (1) deposition by sedimentary processes (e.g., sedimentary iron ores, phosphorites, evaporites, Mn nodules, and placer deposits), and (2) deposition related to weathering (e.g., Al-laterite or bauxite, Ni-laterite, and supergene enrichment deposits).

Except for the sedimentary-banded iron formations (BIF), all of the sedimentary/surficial mineral deposits (Table 2.1) in the ANS are of Phanerozoic in age (<541 ± 10 Ma). Thus, as the target of this book is to deal with the ANS rocks of Proterozoic age (Tonian to Ediacaran age, >541 Ma); Chap. 7 of the sedimentary/surficial mineral deposits in the ANS will only discuss the distribution and occurrence of the Precambrian BIF deposits. Other younger sedimentary/surficial mineral deposits of

the ANS (e.g., oolitic ironstones, phosphorites, bauxites, placer deposits, etc.) might be only listed in the countries covered by the ANS without further details.

Following are brief descriptions of the sedimentary/surficial processes responsible for the formation of external mineral deposits.

(1) ***Deposition by sedimentary processes***: Mineral deposits formed by sedimentary processes are those resulted from either mineral precipitation from surface waters, or as a result of mechanical accumulation of ore minerals during processes of erosion, transportation and deposition. There are a number of different mineral deposits that are formed through chemical processes in sedimentary environments including (Table 2.1): (i) Sedimentary iron ores (banded iron formation-BIF and oolitic ironstones), which are the major world source of iron. (ii) Phosphorite deposits—composed mainly of apatite minerals (~40 to 90% modal apatite). (iii) Evaporates—marine and non-marine (lakes) evaporites formed by evaporation and concentration of dissolved ions in seawaters (e.g., common salt, potash, Mg-Ca carbonates and sulfates), and (iv) manganese deposits—manganese nodules on ocean floors composed dominantly of fine-grained manganese oxide minerals with high concentrations of adsorbed metals (e.g., Mn, Ni and Cu). The second type of mineral deposits formed by mechanical accumulation and sorting in a present-day sedimentary environment called "*placer deposits*". A special type of these deposits is the "*palaeoplacer*" deposits, which are in some cases deformed and metamorphosed, that formed in a sedimentary unit and then has been buried. Placer environments typically contain black sand (a mixture of iron oxides, mostly magnetite with variable amounts of ilmenite and hematite), and valuable industrial mineral components such as monazite, rutile, zircon, chromite, wolframite, and cassiterite.

(2) ***Deposits related to weathering***: Refers to mineral deposits formed at or near the Earth's surface as a result of oxidation and chemical weathering processes, including (Table 2.1): (i) residual deposits produced by in situ weathering of rocks in the regolith profile (e.g., bauxite and Ni-laterite deposits), and (ii) supergene enrichment deposits that formed by chemical and mineralogical modification of the exposed hypogene mineral deposits. The supergene enrichment process is significantly affect both the nature and the economic value of the often low-grade pre-existing mineral deposits such as those in the porphyry deposits.

2.2 Mineral Deposits in the Arabian–Nubian Shield: An Overview

In this part of this chapter, the main types and occurrences of mineral deposits as a whole in the ANS are summarized, to come to details in terms of their types and relation to the different host rocks hereafter in the next five chapters of this book. In the last few decades, many mineral resources, other than oil, have been discovered in

the Precambrian rocks in northeast Africa and Arabia. As discussed in the previous part of this chapter (Table 2.1), the favored classification scheme of mineral deposits used in this book is the genetic classification, which based mainly on the type of host rocks, for the magmatic mineral deposits, and the ore-forming processes for the other deposits. Different types of mineral deposits in the ANS, based on the genetic classification scheme, will be discussed in detail in the next five chapters:

- Chapter 3: Magmatic (orthomagmatic) mineral deposits (ores associated with mafic and ultramafic rocks), including chromite deposits, magmatic-sulfide deposits, Fe-Ti oxide deposits, and metals-bearing carbonatite deposits.
- Chapter 4: Magmatic-hydrothermal deposits (intrusion-related deposits), including porphyry deposits, epithermal vein-type deposits, skarn deposits, greisen-related deposits, and pegmatite-related deposits.
- Chapter 5: Hydrothermal deposits of orogenic environments (metamorphic hydrothermal fluids), including orogenic gold deposits, Carlin-type gold deposits, and iron oxide-copper-gold (IOCG) deposits.
- Chapter 6: Hydrothermal deposits of volcano-sedimentary environments represented by various deposit types including, volcanogenic massive sulfides (VMS) deposits, Mississippi Valley-type (MVT) deposits, sedimentary exhalative (SEDEX) deposits, red-bed copper deposits, and uranium deposits.
- Chapter 7: Sedimentary/surficial deposits, in this chapter the banded-iron formation (BIF) deposit is the only thing discussed in this chapter because it is the only Precambrian sedimentary/surficial mineral deposits in the ANS.

For convenience, and based on the general classification of (Jackson 1987), the Precambrian rocks in northeast Africa and Arabia can be subdivided into four main domains: (1) Afro-Arabian Domain, (2) Eastern Domain, (3) Southern Domain, and (4) Western Domain. Before going to details in the next chapters, following is a general summary of the different types of mineral deposits and their occurrences in the above-mentioned four domains of the northeast Africa and Arabia, especially the Afro-Arabian and Southern Domains; the two domains cover the ANS (Fig. 2.3). Mineral deposits of these domains are categorized into four main categories: (a) deposits in ophiolites and mafic-ultramafic complexes, (b) deposits related to late felsic intrusions, (c) gold deposits, and (d) volcanogenic massive sulfide deposits.

2.2.1 Afro-Arabian Domain

It includes the parts of the Neoproterozoic juvenile crust of the ANS in both Egypt and Saudi Arabia, in addition to the southern extensions of the Nubian Shield, to the boundaries between Sudan and Ethiopia. Many parts of this region are considered as separate parts of island arcs, or in other words, as a mixture of continental-island arcs bounded by a number of suture zones that contain parts of the ancient oceanic crust. The Afro-Arabian Domain can be divided into four parts: (i) southwestern part of the Arabian Shield, (ii) the middle part of the Arabian–Nubian Shield, (iii) the eastern

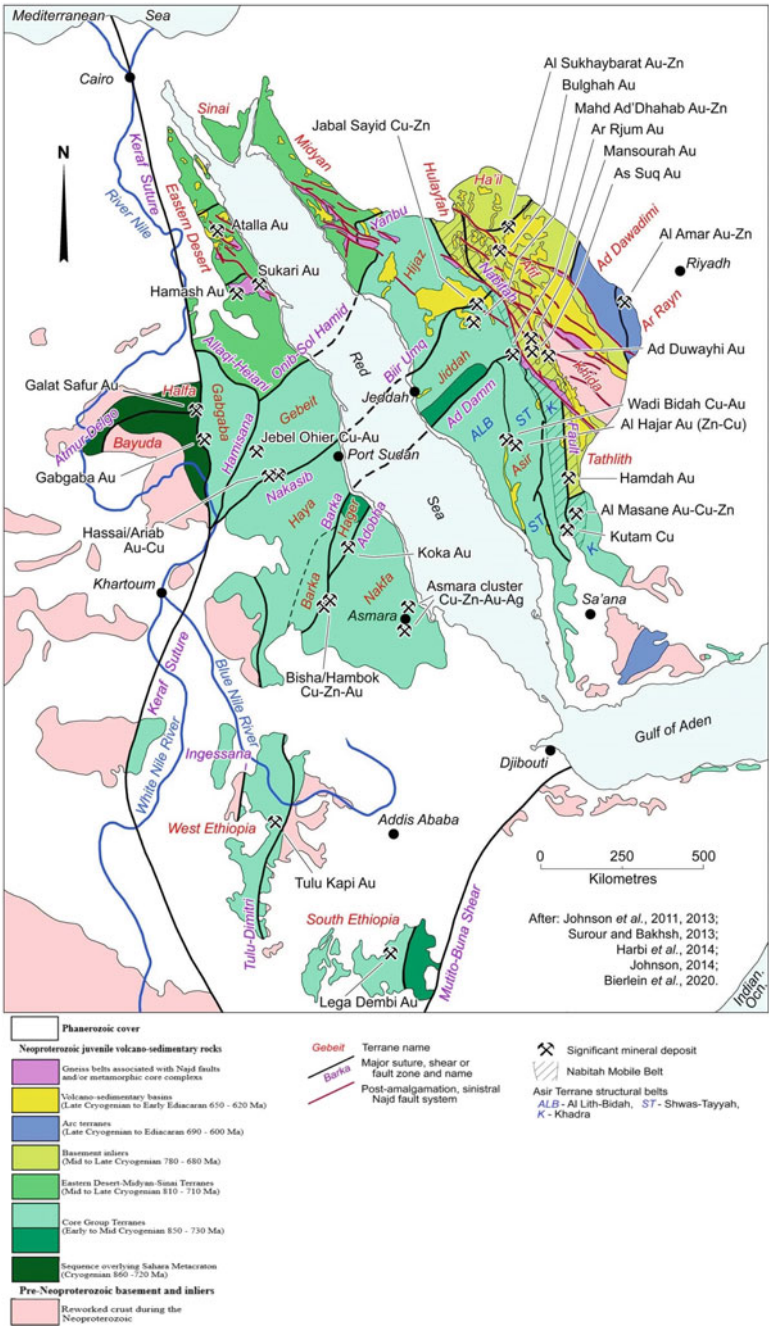

Fig. 2.3 General map showing the geology, structure, tectonic terranes, and mineral deposits of the Arabian–Nubian Shield (*Source* PorterGeo Database)

part of the Arabian Shield, and (iv) the southern part of the Nubian shield. Following is a brief description of the main covering areas and distribution of mineral deposits of these four parts.

(i) ***Southwestern Arabian Shield***: This includes the Asir terrane and the northwestern part of Yemen (Fig. 2.3). This part is characterized by the presence of a belt of mineralization in Wadi Bidah and Wadi Shwas districts extending in an N-S direction (Fig. 2.4). This part consists of bimodal (mafic to felsic) volcanic rocks of older ages (800–900 Ma) to relatively younger ages (700–800 Ma). These volcanic rocks contain highly sheared lensoidal bodies of pyrite-rich massive sulfide deposits enriched in Cu and Zn, with small percentage of Au and Ag. These mineralized ore bodies are hosted mainly by acidic pyroclastic and rhyolite rocks that represent the upper part of thick piles of low-K tholiitic basalts (Binda et al 1993). There are also, particularly in Wadi Shwas, some mineralization in the form of stockworks and veins, with high concentrations of Au in the gossan cover, as well as in some veins and sheared rock lenses that rich in hematite and jasper in Wadi Bidah (Fig. 2.4). There is also, in a zone extending to the south in Wadi Yiba of the Ablah area, some clastic sedimentary rocks containing low-grade Cu ores of little importance. In the nearby areas of Mount Ishmas and Wadi Tathlith, there are some quartz veins with a small content of Au (Fig. 2.4).

(ii) ***Central Arabian–Nubian Shield***: This part from the Afro-Arabian Domain is characterized by the presence of several mineralized clusters of economic importance; including Au-rich massive sulfide ores. This is most probably originated in the time period (800–700 Ma) in which the surrounding sedimentary basins formed behind the Arc/oceanic back-arc basins, which are located precisely along the main suture zones, as in the Gebel Sayid, Samran, Ariab, and Ash Shizm districts (Figs. 2.3 and 2.4). There are also stratabound mineralization associated with large stratavolacanoes of immature island arc tholiites. The mineralization zones found in the upper part of a thick pile of acidic volcanics, often near the rhyolite domes, and they consist of large, but low-grade, lenticular bodies of sulfide-rich deposits containing pyrite, and Cu-Zn-Au-Ag ores, as in Gebel Sayid and Ariab districts. These lenticular sulfide-rich bodies are overlying a group of discordant Cu-rich, pipe-like bodies and stockworks associated with a zone of mafic hydrothermal alteration products such as Mg-Fe-rich chlorite, talc, tremolite-actinolite, and locally chromite, which are showing Au- and Ag-rich tellurides and selenides. Another important mineralization in this part is the Mahd Adh-Dhahab "epithermal vein-type" deposits, which are hosted by rock sequences affected by hydrothermal alteration, of distal felsic pyroclastics and ash fall sheets grading into andesite and uncomformably overlain by volcanic agglomerates, tuffs and breccia. This mineralization in the Mahd Adh Dhahab area takes the same extensions of those in the eastern part of the Arabian Shield in Al Amar and Umm ash-Shalahib districts (Figs. 2.3 and 2.4).

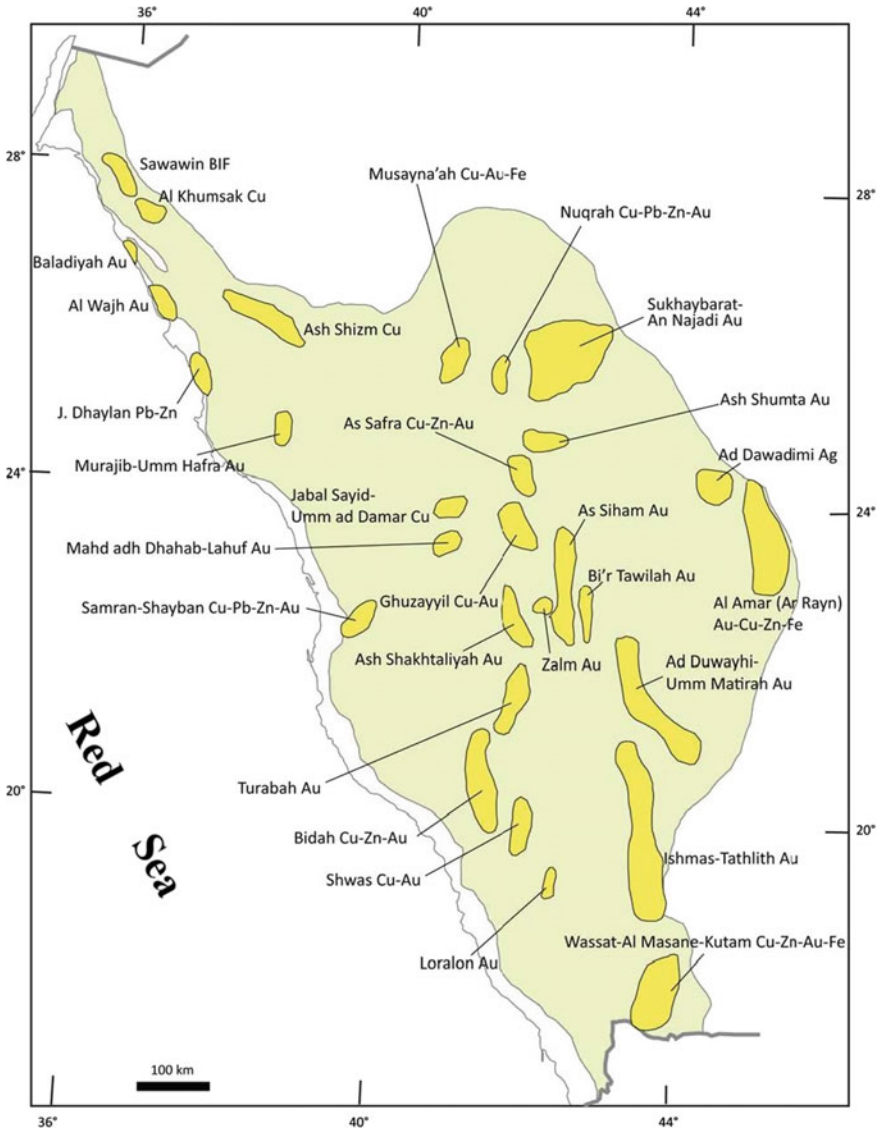

Fig. 2.4 General mineralized districts in the Arabian Shield in Saudi Arabia (after Johnson and Kattan 2012)

(iii) ***Eastern Arabian Shield***: There are several small to medium size mineral deposits in this part, such as the Nuqrah, As Safra, Sha'ib Lamisah, Al Masane, Kutam, and other nearby areas (Figs. 2.3 and 2.4), which are located on the western boundaries of the Afif continental terrane. These mineral deposits are mostly stratiform, rich in Zn with substantial amount of Cu, Pb and

Ag. They also characterized by their enrichment of Cu-Sb-Pb-Ag sulfosalts, as well as Bi-Ag tellurides and sulfides. This mineralization are hosted by andesitic volcanic sequences (changing upward to more acidic agglomerates) that containing pyrite-rich calcareous shales, and dolomitic marble, and covered by a thick pile of black shales and pyroclastics. There are some other stratiform "Ba-Mn-Zn-Ag" mineralization in high-grade metasedimentary rocks, as in the Ash Shaib and Hanash districts, which are very similar to sedimentary exhalative (SEDEX) deposits in the Abu Samar deposits in Sudan (El Samani et al. 1986; Binda et al 1993). In the southeastern part of the Arabian Shield, as well as in some parts of the Sa'da region in Yemen, there are some mineral deposits of Ni-, Co-, and Mo-rich pyrite, similar to those in the Arabian–Nubian shield. Furthermore, the mineralization of Zn, Au and Cu in the Al Amar region is very similar to that in the Mahd Adh Dhahab area, where they are controlled by the extent of the fault zone extending parallel to the Najd faults (Pouit et al 1989). There are also some chromitite deposits as lenses of variable sizes and shapes, and Listwaenite (corbonatized ultramafic rocks) containing low to intermediate concentrations of Au and PGE, which are found in the ophiolite belts in the east, center, and northwest of the Arabian Shield. In addition, there are some mineralization associated with the late felsic intrusions in the western, center, and northeastern parts of the Arabian Shield, which is an important source of many rare and trace elements. This mineralization found in some areas such as those in Gebel Sayid, Gebel Hamra, Mahd Adh Dhahab, and other areas that are characterized by containing high concentrations of Zr, Nb, U, Th, and many other rare and trace elements.

(iv) ***Southern Nubian Shield***: This part covers the Eastern Desert of Egypt, Sudan, Eritrea and Ethiopia, where some small-sized mineralization is found. The best case of this mineralization is those in the Shadli metavolcanics and the Um Samiuki polymetallic deposits in the Eastern Desert of Egypt, which are rich in Zn, Cu, Pb and Ag that are largely similar to the sulfide deposits in the eastern part of the Arabian Shield. In the northwestern part of Eritrea, there are some stratabound Zn and Cu ores hosted in andesite-dominated volcanics, which located in a wide zone of epidote-carbonate alteration, or sometimes hosted in more acidic rocks rich in barite and Pb deposits, along the transition zone with overlying metasedimentary rocks. In the Wollega region of Ethiopia, there are some Cu-Zn mineralization anomalies associated with layers of magnetite-quartzite and barite that scattering throughout the region, as well as the pyrite-rich calcareous shales, but it seems that the polymetallic sulfides are not present in this area. The southern part of the Nubian Shield is characterized by its numerous gold mineralization sites; starting from the North Eastern Desert (NED) of Egypt, as those of Um Mongul, Abu Marawat, through the Central Eastern Desert (CED) of Egypt, as those of El Sid, Um Rus, Barramiya, and Hamash (Fig. 2.3). In addition, there are many areas of gold mineralization along the Red Sea Hills in Sudan, as in the Gebeit Terrane, Abirkatib, and other areas extending northward parallel to the general trend of the Hamisana Shear Zone. In the northwestern part of Eritrea, and the Wollega

area of Ethiopia in the south, there are other gold deposits of significance. Furthermore, as in the Arabian Shield, there are many sites in the Nubian Shield (in the Eastern Desert of Egypt, Eritrea, and Ethiopia) that contain lenses and bodies of chromitite ores in ophiolitic ultramafic rocks, and some other metamorphic minerals, such as asbestos, Ni-rich garnerite, magnesite, some magnetite, and talc. Base-metal sulfides and Fe-Ti oxide deposits are also common in gabbroic rocks that containing high concentrations of PGE in some areas. There are also some mineralizations associated with the late felsic intrusions, such as trace and REE mineralization in some granites in the Eastern Desert of Egypt in the areas of Abu Dabbab, Al-Egleh, Homr Akarem, Zarqat Naam, and other areas.

2.2.2 Eastern Domain

This domain also belongs to the Proterozoic age, and in some cases, it is possible to be related to the Archean age. It is covered the eastern part of the Arabian Shield in Saudi Arabia, as well as the Arabian Gulf and the Zagros mobile belt. This domain connect with the Afro-Arabian domain at the Al Amar suture zone, located in the eastern Saudi Arabia. This is partly covered by the Afro-Arabian Domain in the eastern part of the Arabian Shield in Saudi Arabia, while the remaining parts are beyond the interest of the ANS.

2.2.3 Southern Domain

It represents the northeastern part of the Mozambique Belt, and includes the northern part of Somalia and Yemen, the group of Harar inliers, the Adola Rift Zone in Ethiopia, and the Bur region of Somalia (Fig. 2.3). This domain is composed entirely of old Proterozoic continental crust, which severely reworked in the Neoproterozoic age. The Adola area in southern Ethiopia is characterized by the presence of high-grade Au mineralization, and it contains several mineral deposits of Fe-Cu-Zn sulfides in the old greenstone belt. The Bur region, southeast of Ethiopia, to the northeast of the Mozambique Belt, contains large banded iron formation (BIF) deposits, which are within a geological setting that indicates an older age than the Neoproterozoic. The high-grade gneisses of Bur area also contain a number of uranium mineralization sites, and some other metals. As for the northern block of Somalia and Yemen, it is divided into two parts: (a) the eastern part, which includes the Sa'da and Al-Mukalla belt in Yemen, which represents southeastern extension of the Arabian Shield. This belt contains Au-Cu mineralization and Sn-bearing pegmatite veins associated with younger granitic intrusions. (b) The western part of this block, which includes a volcano-sedimentary belt in western Yemen and northwestern Somalia, contains less mineralization, and follows the southeastern

edges of the ANS. This part, especially in Wollega area, only includes some barite beds and disseminated Cu-skarn deposits associated with magnetite, but lacks any Fe-Au mineralization. The transition zone to the continental gneisses of the Mozambique Belt—in the Wollega region in western Ethiopia—marked by the presence of mafic-ultramafic bodies from the Alaskan-type intrusions. These concentrically-zoned mafic-ultramafic bodies also found in Yemen and northern Somalia, where there are numerous metallic mineralization in a belt of gabbro-syenite-carbonatite rocks containing several mineralization types such as Fe-Ti-V-P-PGE, Ni-Cu-Co, Mo-Bi, Nb-REE-Zr, and Ba-Sr deposits. The northern part of Somalia, as well as the eastern part of Ethiopia, are characterized by the presence of pegmatite veins cutting across the gneissic rocks, which are a source of beryl, and columbite-tantalite in Somalia, and a source of many metallic elements such as REE, Y, Zr, Be, Mo, U and Th, in eastern Ethiopia.

2.2.4 Western Domain

It represents the northern extension of the Mozambique Belt, and includes the ancient continental crust that belongs to the Archean to Middle Proterozoic age in both southwestern Egypt and northern Sudan, which largely concealed under the southern part of the Afro-Arabian domain. This part of the northeast Africa is mostly not related to the ANS areas, where it covers large areas in the East Sahara Craton (ESC) to the east, and Tanzania and Kenya to the south. On the other hand, some parts of the ESC in Sudan and Ethiopia such as Wollega trough, Nuba Mountains, South Kordofan, and Gebel Rahib, contain some mineral deposit occurrences such as BIF, fluorite, U, galena and Au (Fig. 2.3). There are also some belts located in southwestern Sudan having promising Cu-bearing tourmaline deposits. In the Bayuda desert (northeastern Sudan), there are some pegmatite bodies carrying REE-Y-Nb-U-Th, and mica deposits.

As mentioned before, the next chapters will deal with these mineral deposits separately in details, in terms of their types, distribution-occurrence, and the host rocks. The next chapter (Chap. 3) will deal with the magmatic (orthomagmatic) mineral deposits. In all of the coming chapters (Chaps. 3–7), the mineralization in the Arabian Shield (Saudi Arabia, and Yemen) will come first, then followed by the mineralization in the Nubian Shield (Egypt, Sudan, Eritrea, and Ethiopia).

References

Arai A, Miura M, Tamura A, Akizawa N, Ishikawa A (2020) Hydrothermal chromitites from the Oman ophiolite: the role of water in chromitite genesis. Minerals 10:217. https://doi.org/10.3390/min10030217

Arai S, Akizawa N (2014) Precipitation and dissolution of chromite by hydrothermal solutions in the Oman ophiolite: New behavior of Cr and chromite. Am Mineral 99:28–34
Barnes RG (1987) Multi-stage mobilization and remobilization of mineralization in the Broken Hill Block, Australia. Ore Geol Rev 2:247–267
Binda PL, Omenetto P, Warden (1993) Mineral deposits and occurrences in the Precambrian of northeast Africa and Arabia: a review. From geology and mineral resources of Somalia and surrounding regions, 1st Agron. Oltremare, Firenze. Relaz e Monogr 113:429–516
Diessel CFK (1992) Coal-bearing depositional systems. Springer, New York, p 721
Dill HG (2010) The "chessboard" classification scheme of mineral deposits: mineralogy and geology from aluminum to zirconium. Earth Sci Rev 100:1–420
Einaudi M (2000) Mineral resources: assets and liabilities. In: Ernst WG (ed) Earth systems: processes and issues. Cambridge University Press, Cambridge, pp 346–372
El-Samani Y, Touray JC, Pouit G, Guyot G (1986) La Mineralisation en Zn-Cu-Mn-Ba d'Abu Samar et les indicesde la plaine d'Allaikaleib (Sudan): de accumulation metalliferes metamorphisees d'origine exhalative-sedimentaire. Chron Rech Min 483:3–18
Guilbert JM, Park CF (1986) The geology of ore deposits. W.H. Freeman and Co., New York, p 985
Henley RW, Truesdell AH, Barton PB (1984) Fluid-mineral equilibria in hydrothermal systems. Rev Econ Geol 1:1–267
Jackson NJ (1987) Precambriab evolution of northeast Africa and Arabia. 14th Coll. African Geology Tu Berlin, Cifeg publ. 12 (Schandelmeier-Matheis, eds.), pp 19–23
Johnson PR, Kattan FH (2012) The geology of the Arabian Shield. Saudi Geological Survey, p 466
Kirkham RV, Sinclair WD (1995) Porphyry copper, gold, molybdenum, tungsten, tin, silver. In: Eckstrand OR, Sinclair WD, Thorpe RI (eds) Geology of Canadian mineral deposit types; Geology of Canada, no. 8: Geological Survey of Canada, pp 421–446 (also Geological Society of America, The Geology of North America, v. P-1)
Lindberg W (1922) A suggestion for the terminology of certain mineral deposits. Econ Geol 17:292–294
Lindgren W (1934) Mineral deposits. Wiley, New York
Meyer C (1981) Ore-forming processes in geologic history. Economic Geology, 75th Anniversary Volume, 6–41
Misra KC (2000) Understanding mineral deposits. Kluwer Academic Publishers, 845 p
Pouit G, Milesi JP, Sabir H (1989) Cadres geotectoniquedu bouclier Arabo-Nubien. Report BRGM 98 SAU 077 DEX, pp 1–32
Ridley J (2013) Ore deposit geology. Cambridge University Press, ISBN 978-1-107-02222-5
Robb LJ (2004) Introduction to Ore-forming Processes. Blackwell Publ., 416 p
Whitney JA, Naldrett AJ (1989) Ore deposition associated with magmas / volume editors. Reviews in economic geology, 0741-0123; 4:250. Socorro, NM: Society of Economic Geologists

Chapter 3
Magmatic (Orthomagmatic) Deposits (Ore Deposits Associated with Mafic–Ultramafic Complexes)

Contents

3.1 Introduction 90
3.2 Types of Mafic–Ultramafic Rocks 91
3.2.1 Ophiolitic Mafic-Ultramafic Complexes 91
3.2.2 Layered Mafic-Ultramafic Complexes 92
3.2.3 Alaskan-Type Concentrically Zoned Mafic-Ultramafic Complexes 92
3.3 Magmatic Mineral Deposits in Saudi Arabia 93
3.3.1 Chromitite–PGE Deposits in Ophiolitic Mafic–Ultramafic Complexes 95
3.3.2 Magmatic Cu–Ni–PGE Sulfides and Fe–Ti Oxides Mineralization 109
3.4 Magmatic Mineral Deposits in Yemen 116
3.4.1 The Suwar-Wadi Qutabah Ni–Cu–Co–PGE Occurrences 116
3.4.2 The Byhan Cu–Ni–PGE Occurrence 118
3.4.3 Al-Qabyta Occurrence 120
3.4.4 The Qaifa Occurrence 120
3.4.5 The Wadi Mabar Area 121
3.4.6 The Al-Hamurah Cu–Ni Occurrence 121
3.4.7 The Wadi Silbah Occurrence 125
3.4.8 The Mukayras Fe–Ti–P–V Occurrence 125
3.5 Magmatic Mineral Deposits in the Eastern Desert of Egypt 125
3.5.1 Chromitite–PGE Deposits in Ophiolites 126
3.5.2 Non-ophiolitic Cu–Ni–PGE Sulfide Occurrences 134
3.5.3 Non-ophiolitic Fe–Ti Oxide Occurrences 138
3.6 Magmatic Mineral Deposits in Sudan 141
3.6.1 Ingessana Hills Area 144
3.6.2 Qala En Nahal—Umm Saqata Areas 145
3.6.3 The Nuba Mountains 146
3.6.4 The Red Sea Hills Region 147
3.6.5 The Gebel Rahib Occurrences 148
3.6.6 The Southern Sudan Occurrences 149
3.6.7 The Northern Sudan Occurrences 150
3.7 Magmatic Mineral Deposits in Eritrea 150
3.8 Magmatic Mineral Deposits in Ethiopia 151
3.8.1 PGE Mineralization in Western Ethiopia 152
3.8.2 Southern Ethiopian Ni–Co–Cu Mineralization 156
3.8.3 Chromitite-Fe–Ti Mineralization in Western and Southern Ethiopia 158
References 159

A. Hassan Ahmed, *Mineral Deposits and Occurrences in the Arabian–Nubian Shield*,
Earth and Environmental Sciences Library,
https://doi.org/10.1007/978-3-030-96443-6_3

3.1 Introduction

***Magmatic deposits*:** ores formed by direct crystallization and accumulation from a magma

Deposits associated with mafic–ultramafic rocks

- Chromite deposits: (i) stratiform chromite in layered intrusions, and (ii) podiform chromite in ophiolite complexes
- Magmatic sulfides (Cu–Ni–Fe–PGE), and Fe–Ti oxides deposits
- Metals-bearing carbonatites
- Diamonds in kimberlites

This chapter consists of two main divisions: (1) an overview on the various types of mafic–ultramafic rocks of different origins, with special concern on the ophiolitic and Alaskan-type concentrically zoned complexes, and (2) the distribution of mineral deposits associated with mafic–ultramafic rocks in the countries covered by the Arabian–Nubian Shield (ANS). In general, oxide-dominant mineral deposits (chromitite, Fe–Ti oxides), base-metal sulfides (Ni, Cu, Fe), and precious metals (platinum-group elements "PGE–Or, Ir, Ru, Rh, Pt, Pd", and Au) deposits, are commonly associated with mafic–ultramafic igneous rocks. Field and textural observations indicate that these mineral deposits were formed under magmatic conditions, while the carrying melt was essentially liquid and before the total solidification. This class of mineral deposits is thus called magmatic or "orthomagmatic" deposits. The low metal contents of silicate melt segregated to form small volume of metallic deposits by melt saturation in metals, so either a solid, as in the case of chromite, or a liquid, as in the case of sulfide melt, accumulates the metallic ores. Many parameters may affect this process, including the depth of melt formation, tectonic activities, geothermal gradient, fractional crystallization, dynamics of the melt body, fresh melt injection, assimilation of country rocks, liquid immiscibility of ore and silicate melts, and so on (Kerr and Leitch 2005). Due to the higher density of oxide and/or sulfide metals/melts compared to silicate liquids, they accumulate in the floor of magma chamber by gravitational settling, forming a massive and/or net-textured oxide/sulfide deposits. As the system cools, the oxide/sulfide-rich melts may then separate into cumulates (e.g., Fe-rich sulfides) and residual liquids (Cu-rich sulfide melt).

Thus, orthomagmatic deposits may take one of the following forms (see Table 2.1, the magmatic part is shown above).

(a) Ophiolitic chromitite–PGE deposits of Alpine-type ultramafic rocks, and Cu–Ni–PGE seams in reefs of layered mafic intrusions. Gravitational settling is the most important process of this mineral deposit type.
(b) Fe–Ni–Cu-(PGE) mineral deposits hosted by Archean to Mesoproterozoic komatiites and complex subvolcanic mafic–ultramafic intrusions.

(c) Fe–Ti oxides deposits in Mesoproterozoic anorthosite-ferrodiorite complexes. Ilmenite and/or rutile, magnetite or hematite, are the main ore minerals, and apatite and some graphite are the main gangue minerals of the orebody of this type.
(d) Metal-bearing (Fe–P–Nb–Zr or REE-U-F) carbonatite plugs and nephelinite intrusions formed by low-degree partial melting of a mantle source. These types of mineral deposits are potential sources of Cu, REE, Fe, Ti, V, U-Th, and Zr; as well as non-metallic resources such as vermiculite, apatite, fluorite and barite.
(e) Kimberlites: derived from the deep Earth's mantle at more than 140 km depth. They are basically porphyritic, SiO_2-undersaturated, K-rich (1_3 wt% K_2O) peridotites with xenoliths, and xenocrysts of diamond, olivine, Mg-ilmenite and Cr-rich pyrope garnet in a carbonated and serpentinized groundmass with accessory phlogopite, perovskite, Cr-spinel and magnetite.

Except the last category (kimberlites), all the other forms of magmatic mineral deposits can be found in the ANS rocks, which will be discussed in details later in this chapter.

3.2 Types of Mafic–Ultramafic Rocks

Before entering into the details of different mineral deposits associated with mafic–ultramafic rocks in the ANS, it is necessary to be acquainted with the most important types of mafic–ultramafic rocks. The mafic–ultramafic rocks are classified into three main categories: (1) mafic–ultramafic rocks related to ophiolite complexes, (2) mafic–ultramafic rocks related to layered mafic intrusions, and (3) mafic–ultramafic rocks related to the Alaskan-type concentrically zoned complexes. Following is a simplified description of these three types:

3.2.1 Ophiolitic Mafic-Ultramafic Complexes

Ophiolitic mafic-ultramafic complexes represented by the uppermost part of upper mantle and the lower crust, which are separated by what so-called the Moho transition zone (MTZ) that consists of alternations of mafic and ultramafic rocks. The uppermost part of the upper mantle is often made up of harzburgite rocks that resulting from the partial melting of a fertile lithosphere (i.e., lherzolite), and to a little extent, transition dunites caused by increasing partial melting of the harzbergite rocks; the transition dunites found below and above the MTZ. The MTZ overlain by layered gabbros, which consists of intercalations of mafic to ultramafic layers that represent the lower portion of the Earth's crust. Among the most important mineralization types associated with the ophiolitic mafic-ultramafic rocks: the podiform chromitite

deposits, which usually found in the uppermost part of the Earth's upper mantle just below the MTZ; sometimes accompanied by high PGE concentrations. In some cases, Cu–Ni–Co–PGE sulfide mineralization is associated with layered gabbros in the lower part of the oceanic crust, as well as some metamorphic industrial minerals, such as asbestos and talc. Examples of this type of ophiolitic mafic-ultramafic rocks include the Oman and Cyprus ophiolites. Many mafic-ultramafic rocks in the ANS in the Kingdom of Saudi Arabia, Sudan, Egypt and Ethiopia are believed to represent parts of ophiolites, which will be dealt with in details later in this chapter.

3.2.2 Layered Mafic-Ultramafic Complexes

They are typically igneous-layered mafic intrusions (LMI), consisting of sequences of ultramafic rocks such as peridotites and pyroxenites in the lower part, with mafic layers of gabbro, norite, anorthosite, and plagioclase-rich troctolite, in the upper parts. The mafic-ultramafic rocks of LMI represent the most important rocks that are containing startiform chromitite and PGE deposits in the world. The best examples of the LMI include the Bushveld Complex in South Africa, which is a major global source for chromitite and PGE deposits; the Stillwater Complex in the USA, the Muskox Complex in Canada, and the Great Dike in Zimbabwe. These LMI among others worldwide, represent the most economically significant source for many mineral deposits. In the ANS, there are mafic-ultramafic rocks that are believed to belong to the LMI, such as the Wadi Kamal mafic-ultramafic complex in Saudi Arabia.

3.2.3 Alaskan-Type Concentrically Zoned Mafic-Ultramafic Complexes

They are a distinct group of mafic-ultramafic rocks arranged in concentrically zoned form. The most important feature that distinguishes these rocks is that they contain a dunite core (olivine rock), which in most cases contains small chromitite bodies, evolved outward to clinopyroxenite, hornblende- and magnetite-rich peridotites, and then at the end an outer shell of more evolved rocks such as hornblende gabbros and diorite. This type of mafic-ultramafic complex is present in Alaska, Australia, the Urals, Russia; and many other locations. This type of mafic-ultramafic complex is an important source for Ni–Cu–Co–PGE, chromitite, and asbestos deposits. In the ANS, this type of mafic-ultramafic complex is present at: Wadi Kamal, Gebel Taftafan, and other places in Saudi Arabia, and those of gabbro Akarem, the Genena Gharbia, and Abu Hamamed complexes in the Eastern Desert of Egypt, and Yubdo complex in Ethiopia.

3.3 Magmatic Mineral Deposits in Saudi Arabia

The Precambrian mafic–ultramafic rocks in Saudi Arabia are represented mainly by two different categories: (1) ophiolitic complexes along suture zones (Fig. 3.1), and (2) non-ophiolitic complexes (layered/Alaskan-type concentrically zoned mafic–ultramafic intrusions). The ophiolite complexes of Saudi Arabia are dismembered to various extents and have suffered multiple phases of alteration, deformation and

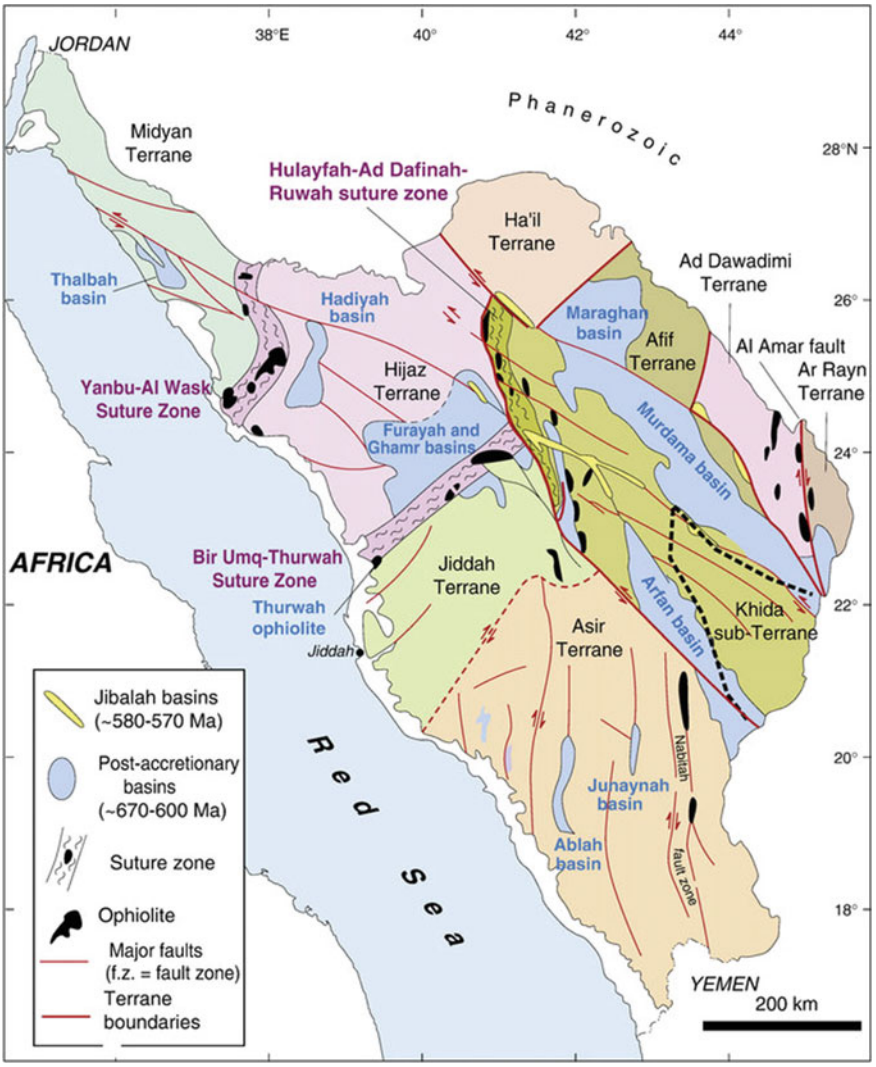

Fig. 3.1 Tectono-stratigraphic map of the Arabian Shield showing the distribution of ophiolite belts and suture zones in western Saudi Arabia (from Nehlig et al. 2002)

greenschist facies metamorphism. They are found along various suture zones in the Arabian Shield (Fig. 3.1), and may contain pods of massive chromitite ore and disseminated Cu–Ni–PGE mineralization in their mafic–ultramafic parts. Some of the most recently studied ophiolitic mafic–ultramafic complexes in Saudi Arabia are those of Wadi Al Hwanet, Al'Ays (Gebel Al Wasq), Gebel Ess, and Bir Tuluhah ophiolites (Ahmed et al. 2012; Ahmed and Habtoor 2015; Habtoor et al. 2017) (Fig. 3.2). The non-ophiolitic layered mafic–ultramafic intrusions represented mainly by the Wadi Kamal complex in the Yanbu suture zone (Fig. 3.2). The concentrically zoned mafic–ultramafic complexes, on the other hand, are a class of intrusions, which are distinct with regard to their tectonic setting, internal structure and petrology. Their classical distinctive geologic and petrographic features are the zonal distribution

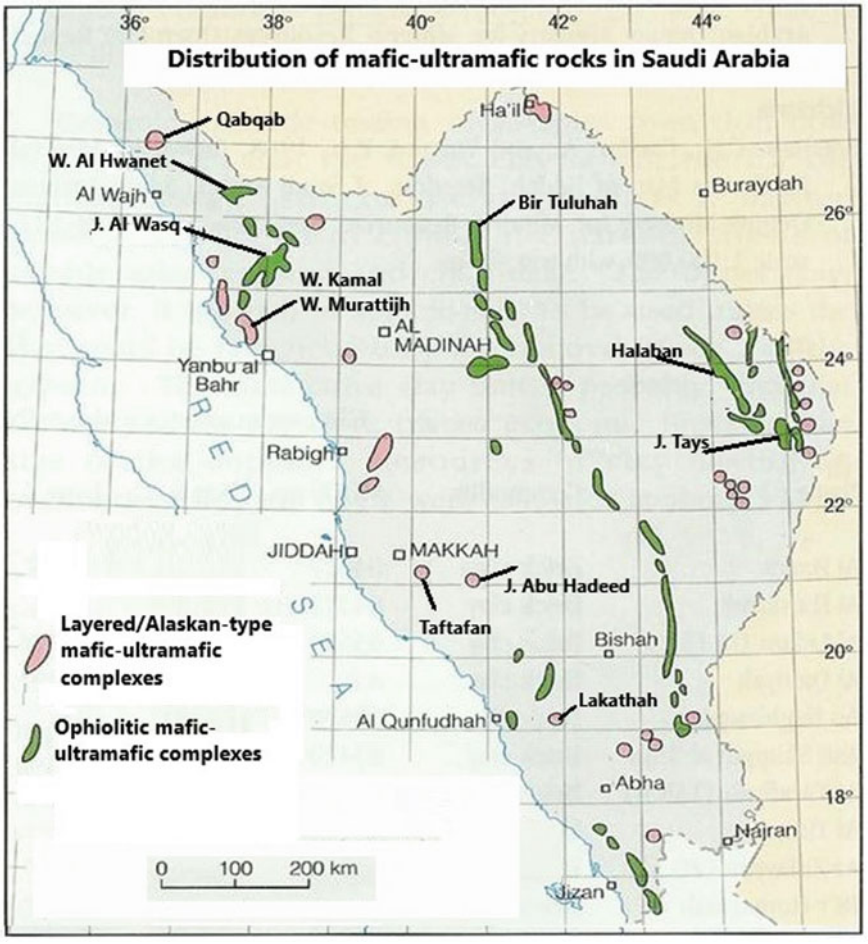

Fig. 3.2 Simplified map of the Arabian Shield showing the distribution of different types of mafic–ultramafic rocks in the Kingdom of Saudi Arabia (modified from Collenette and Grainger 1994)

of mafic and ultramafic rocks with common bodies of dunite core grades outward into wehrlite, clinopyroxenite and marginal gabbroic lithologies. Many localities of layered/Alaskan-type mafic–ultramafic complexes are distributed alongside the suture zones between the different terranes of the Arabian Shield in Saudi Arabia (Fig. 3.2), some of them containing disseminated Cu–Ni–PGE sulfides and Fe–Ti oxides deposits (Harbi 2008; Habtoor et al. 2016).

3.3.1 Chromitite–PGE Deposits in Ophiolitic Mafic–Ultramafic Complexes

In general, chromitite deposits are the only primary source of chromium (Cr) metal. The mineral "chromite", used hereafter as "Cr-spinel", is one of the end-members of the spinel oxide group of minerals. The ideal chemical formula for spinel is AB_2O_4, where "A" site filled by divalent cations (e.g., Mg^{2+}, Fe^{2+}), and "B" site filled by trivalent cations (e.g., Cr^{3+}, Fe^{3+} and Al^{3+}). Less common minor cations are also present in the Cr-spinel structure such as Mn^{2+}, Ti^{4+}, V^{3+}, Ni^{2+}, Co^{2+} and Zn^{2+}. The ore of chromite is occasionally termed as "chromitite" ore. There are two principal economic types of chromitite deposits: (i) "*Stratiform chromitite*" deposits typically located in stable continental shield environments and hosted by layered igneous intrusions such as those of the Bushveld Igneous Complex, South Africa. (ii) "*Podiform chromitite*" deposits typically occur in the upper mantle peridotites and crustal rocks of ophiolites. The ophiolitic (podiform) chromitites are present either as layers at the base of the magmatic cumulates or, more typically, as dykes, disc shaped lenses and pods in upper mantle peridotites (Stowe 1994; Arai and Ahmed 2018). There are numerous examples of podiform chromitites worldwide in various ophiolite complexes of different tectonic settings and ages.

Podiform chromitite deposits include both high-Al and high-Cr varieties with distinctly different geochemical characteristics. High-Al chromitite is formed by low degrees of partial melting via melt-peridotite interaction in nascent spreading centers (mid-oceanic ridge) with higher Ti contents, less Mg–silicate minerals and intermediate Cr# (= Cr/(Cr + Al) atomic ratio) less than 0.7, and relatively poor in platinum-group elements (PGE) contents. The high-Al chromitite deposits are essentially formed in a mature spreading center and are typically hosted in less depleted harzburgites (Zhou 1996; Ahmed and Arai 2002). High-Cr chromitites, on the other hand, are believed to have been formed by high degrees of partial melting via melt-peridotite interaction in island arc environments with low Ti and Mg-rich olivine and orthopyroxene. This type of chromitite deposits have high Cr# (> 0.7) of Cr-spinels, and relatively rich in PGE contents. The high-Cr chromitites are suggested to be formed from a boninitic magma produced by melting above a subduction zone and are typically hosted in highly depleted harzburgites (Zhou et al. 1996; Ahmed and Arai 2002; Ahmed et al. 2001, 2005, 2012; Ahmed and Habtoor 2015).

Chromitite mineralization in Saudi Arabia is restricted to Neoproterozoic ophiolitic mafic–ultramafic rocks of the Arabian Shield (850–700 Ma) (Al-Shanti and El-Mahdy 1988; Ahmed and Harriri 2008). Almost all ophiolitic ultramafic rocks of the Arabian Shield are chromitite-bearing, especially the Gebel Ess–Wadi Al Hwanet (Al' Ays) belt (Chevremont and Johan 1982; Al-Shanti and El-Mahdy 1988; Ahmed et al. 2012). There are numerous known ophiolitic mafic–ultramafic complexes in Saudi Arabia that are containing massive podiform chromitites such as (i) Al'Ays and Gebel Ess in the northwest of the Arabian Shield; (2) Al Qunfudhah in the southwest of the shield; (3) Bi'r Tuluhah, Gebel Hamdaniyah, Gebel Sakhirah and Zalim in the center of the shield; and Ha'il and Gebel Tays in the north and east of the shield, and others throughout the different suture zones of the Arabian Shield (Fig. 3.2). Chromitite deposits in Saudi Arabia found in different forms: (1) massive lenses and lenticular pods with chromite mineral forming more than 80% of the rock. They range in length from 5 cm up to 30 m, and from 5 cm up to 15 m wide. (2) Leopard type, where chromite occurs as discrete grains or aggregates disseminated within gangue serpentine minerals and forms about 40–50% of the rock volume. (3) Nodular and anti-nodular (orbicular) types where aggregates of fine- to medium-grained chromite found as nodules cemented by silicate minerals. (4) Schlieren (banded) type, where chromite grains form thin parallel bands constituting 25–50% of the rock volume. (5) Disseminated type, where chromite occurs as random disseminations in serpentinized host rocks. Following is a brief description of the most famous chromitite-bearing ophiolite complexes in Saudi Arabia (Al'Ays, Wadi Al Hwanet, and Bir Tuluhah ophiolites) in terms of their chromitite chemistry and PGE-PGM contents.

One of the best examples of ophiolite complexes rich in chromitite deposits in Saudi Arabia is the "*Al'Ays ophiolite*" in the northwestern side of the Arabian Shield (Figs. 3.2 and 3.3). About 350 chromitite lenses and irregular pods of different shapes and sizes are discontinuously distributed in the ultramafic mantle rocks of Al'Ays ophiolite (Al-Shanti and El-Mahdy 1988; Prichard et al. 2008; Ahmed and Habtoor 2015). Podiform chromitite deposits of Al'Ays ophiolite are approximately homogeneous that are occurring either as individual lenses of varying sizes, mostly extending few meters long and wide, or as a group of lenses of several meters across. The largest chromitite pod is located in the southern part of Gebel Al Wasq (Jabal Al Wask, in Ahmed and Habtoor 2015) where its dimensions reach up to 30 m across (Fig. 3.4). Chromitite pods have lenticular or pod-like shapes, and sometimes forming layers within the host peridotites. Several chromitite pods of different shapes and sizes are randomly scattering and protruded on the surface, which are mainly concordant to sub-discordant with the host harzburgite foliation. The chromitite lenses are generally massive (~90% Cr-spinel grains) where the Cr-spinel–silicate ratio varies from place to place and sometimes forms rhythmic layering in the chromitite pods. The bulk composition of Al'Ays chromitites shows considerable variation, from high-Cr_2O_3 variety (average 63.45 wt% Cr_2O_3 and 5.37 wt% Al_2O_3) in some places, to intermediate-Cr_2O_3 variety (average 48.95 wt% Cr_2O_3 and 11.66 wt% Al_2O_3) in some other places (Fig. 3.5a) (Ahmed and Habtoor 2015). The average SiO_2 content varies from 1.57 up to 4.39 wt%, depending on the Cr-spinel-silicate ratio in chromitite ores.

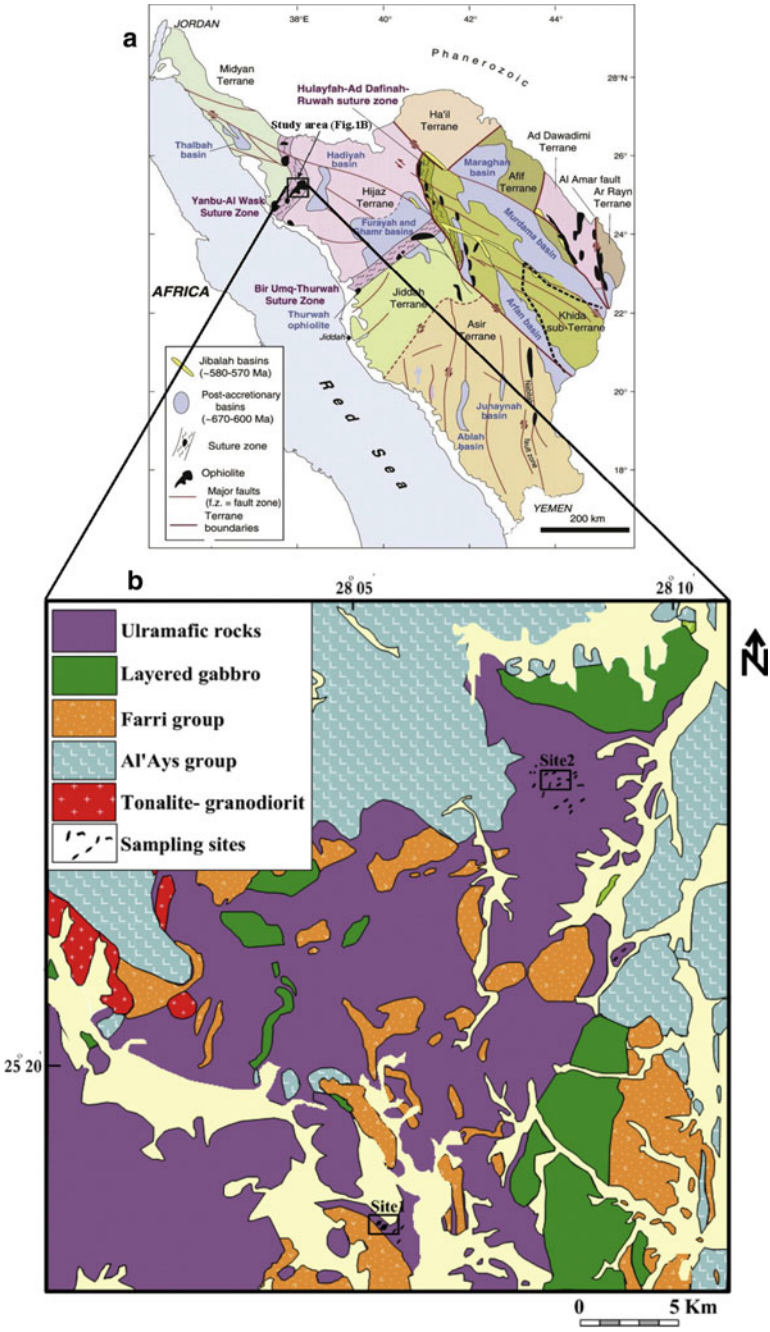

Fig. 3.3 Simplified geological map **b** of Al'Ays ophiolite (modified from Collenette and Grainger 1994). The **a** panel shows the distribution of ophiolite belts and suture zones of the Arabian Shield in Saudi Arabia

Fig. 3.4 The largest chromitite pod protruded within serpentinized harzburgite at the Gebel Al-Wasq of Al'Ays ophiolite, Saudi Arabia

The Al'Ays massive chromitite deposits have high PGE concentrations. Recent studies (Prichard et al. 2008; Ahmed and Habtoor 2015) found very high PGE contents in chromitite deposits and associated peridotites from Al'Ays ophiolite. The concentrations of PGE in chromitites vary considerably from a few ppb to several ppm of total PGE except Rh, which has a maximum value of 840 ppb. Individual values of PGE of 1 ppm or more are reported in many chromitite lenses. The highest values of each PGE obtained are 2570 ppb Pt and 6870 ppb Pd, and other contains 5800 ppb Ru, 840 ppb Rh, 6200 ppb Ir, and 3300 ppb Os (Prichard et al. 2008). The massive podiform chromitites contain higher concentrations of total PGE than the host peridotites. Prichard et al. (2008) recognized three types of PGE mineralization in chromitites in Al'Ays ophiolite that are characterized by the relative proportions of PGE and the shape of their chondrite-normalized profiles. Other characteristics that distinguish these three types include composition of the host chromite, the PGM and their textural position, associated marker elements, and geographic location. Despite the difference in PGE concentrations, all chromitite samples of Al'Ays chromitites are distinctly enriched in the Ir-subgroup (IPGE = Os, Ir, Ru) in preference to the Pd-subgroup (PPGE = Rh, Pt, Pd). The total PGE content in chromitites vary from place to place based on the geochemical composition of the ore. The PGE-rich chromitites display distinctive PGE distribution patterns; being highly enriched in IPGE and strongly depleted in PPGE with very steep negative slopes, mostly similar to those of the PGE-rich chromitites of the Oman ophiolite (Ahmed and Arai 2002) and the ultra-high pressure (UHP) chromitites of the Luobusa ophiolite (Fig. 3.5b) (Zhou et al. 1996). The $(Pd/Ir)_N$ ratio of PGE-rich chromitites ranges from 0.01 to

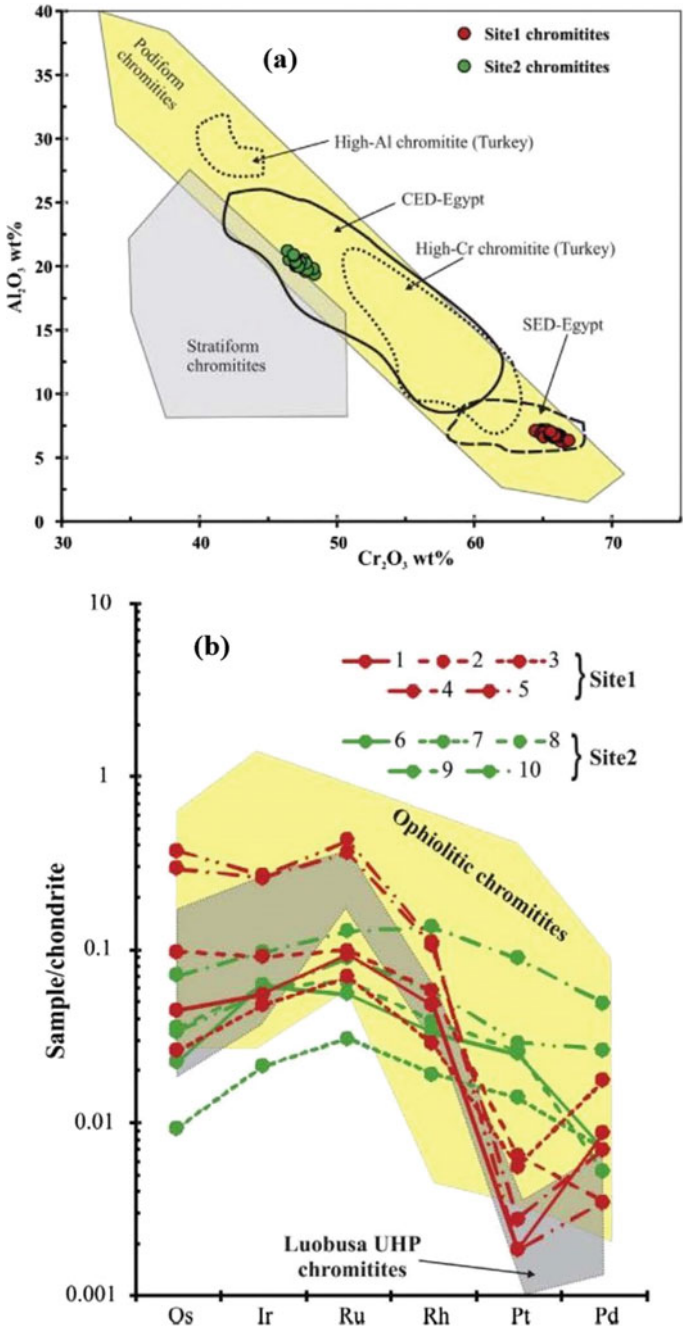

Fig. 3.5 **a** Variation diagram of Al_2O_3 versus Cr_2O_3 wt% of the studied chromitite pods at Gebel Al-Wasq area, Al'Ays ophiolite. **b** Chondrite-normalized PGE patterns of the chromitite deposits of Al'Ays ophiolite, Saudi Arabia. For compositional fields that used for comparison refer to Ahmed and Habtoor (2015), and references therein

0.37, and the ΣIPGE/ΣPPGE ranges from 4 to 24. The PGE-poor chromitites, on the other hand, show slightly negative slope of PGE distribution patterns, where the $(Pd/Ir)_N$ ratio vary from 0.10 to 0.51 and the ΣIPGE/ΣPPGE ranges from 1 to 3 (Fig. 3.5b), almost similar to those of the PGE-poor chromitites of the Oman ophiolite. Numerous grains of platinum-group minerals (PGM) were identified in both types of chromitites mostly are Ir–Os–Ru alloys (Fig. 3.6) (Prichard et al. 2008; Ahmed and Habtoor 2015).

Another chromitite-bearing ophiolitic locality along the same belt (Gebel Ess–Wadi Al Hwanet) is the "*Wadi Al Hwanet ophiolite*" in the most northwestern part of Midyan terrane of the Arabian Shield (Figs. 3.2 and 3.7). There are several chromitite lenses and bodies varying in size from centimeter-scale (micropods) in the transition zone between massive dunites and harzburgites (Figs. 3.7 and 3.8) to larger meter-scale in the host harzburgite. Within harzburgite, the chromitite pods arelarger and have a variety of shapes, including elliptical, dike-like, boudinaged and irregular. Several chromitite pods are randomly scattered on the surface of outcrops, and have concordant to sub-discordant contacts with the host harzburgite foliation (Fig. 3.8). The Wadi Al Hwanet chromitite deposits are similar to those in Al'Ays ophiolite; being display wide compositional variations from high-Cr to high-Al varieties, with PGE-rich in the former and intermediate to PGE-poor in the latter (Ahmed et al. 2012). Petrographic investigations of Wadi Al Hwanet chromitite deposits reveal

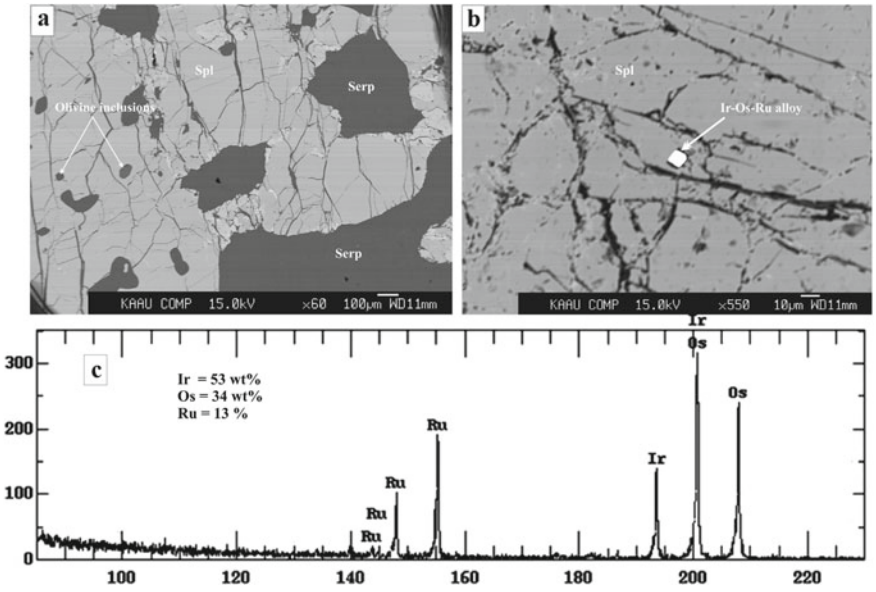

Fig. 3.6 **a** Back-scattered electron (BSE) image of massive chromitite of A'Ays ophiolite with olivine inclusions within Cr-spinel. **b** BSE image of euhedral polygonal Ir–Os–Ru alloy isolated within slightly altered massive chromitite Cr-spinel, reflected light. **c** Semi-quantitative EDX pattern of the Ir–Os–Ru alloy in **b**. For details, refer to Ahmed and Habtoor (2015)

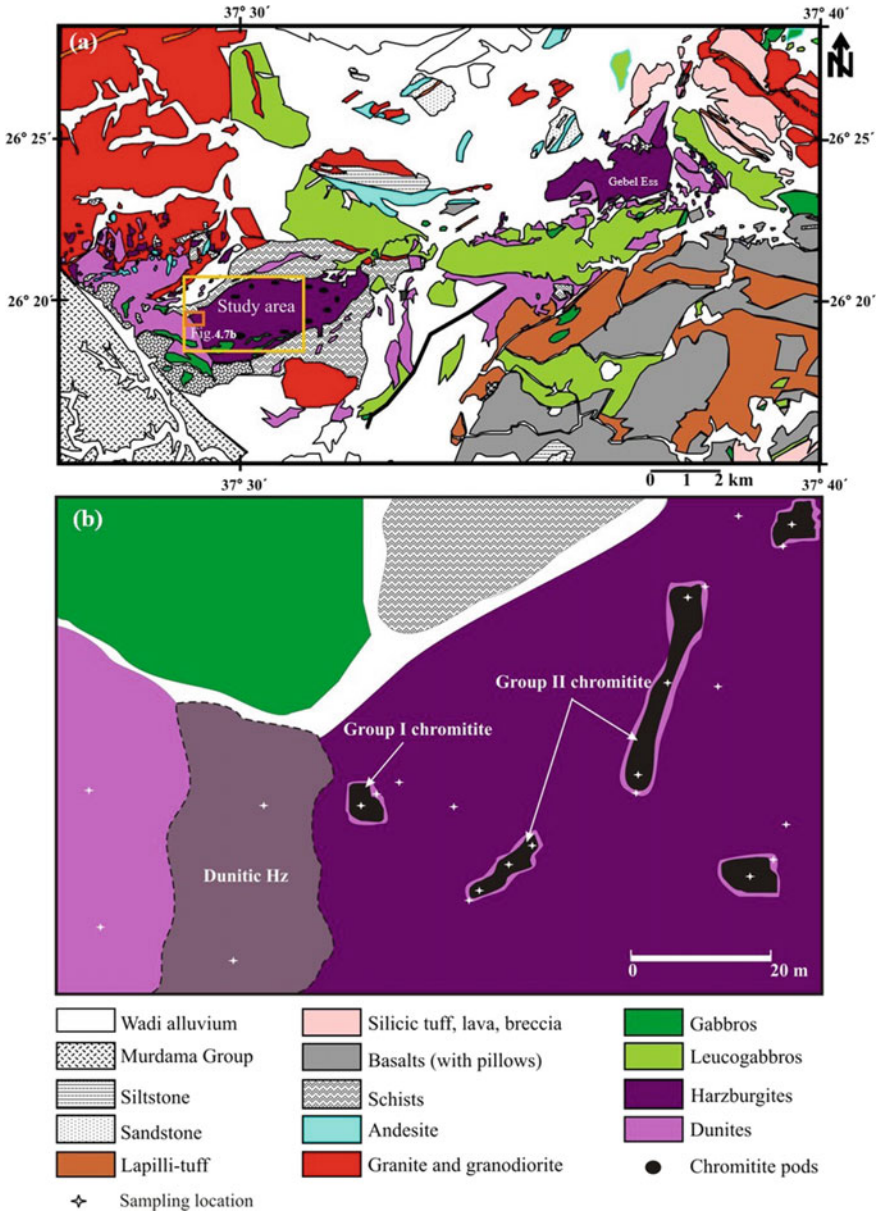

Fig. 3.7 **a** Simplified geological map of Wadi Al Hwanet and adjacent areas, and **b** geological sketch map of a part from the study area showing the relationship between dunites, chromitites and harzburgites. For details, refer to Ahmed et al. (2012)

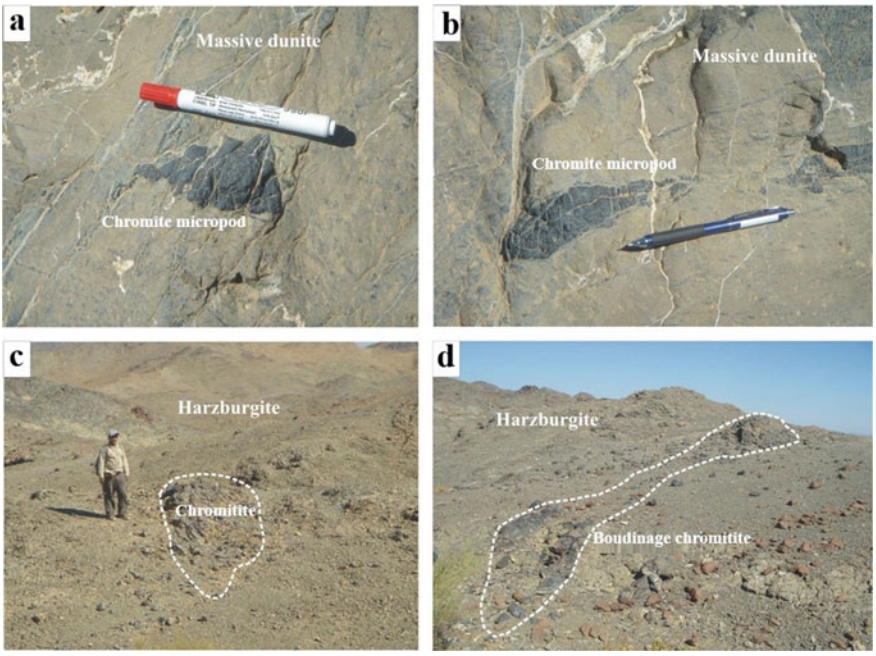

Fig. 3.8 Field photographs of the chromitite pods of Wadi Al Hwanet ophiolite (**a**, **b**) Small-scale chromitite micropods embedded within fine-grained massive dunite. **c** Small lensoidal chromitite pod within serpentinized harzburgite. **d** Boudinaged dike-like chromitite pod within serpentinized harzburgite. For details, refer to Ahmed et al. (2012)

the presence of some PGM grains as solitary inclusions within the Cr-spinel. The PGM grains show perfect polygonal crystals ranging from 10 to 30 μm in size (Fig. 3.9b). The qualitative analysis of almost PGM grains gave a composition of Ir-rich laurite ((Ru, Ir, Os)S_2). The discordant dike-like chromitite pods of Wadi Al Hwanet ophiolite occasionally contain small grains and patches of sulfide such as pyrrhotite, chalcopyrite, and pentlandite (Fig. 3.9c, d). These sulfide grains are found either as euhedral inclusions within Cr-spinel grains (Fig. 3.9c), or as irregular patches within the interstitial matrix (Fig. 3.9d). The total PGE contents in Wadi Al Hwanet chromitites vary from 200 up to 1000 ppb, depending on the chemical composition of the Cr-spinel and the sulfide contents of the ore. The sulfide-poor chromitite pods (lensoidal) are characterized by low to intermediate PGE contents with IPGE enrichment over the PPGE, and steep-negatively sloped chondrite-normalized PGE patterns, typical of ophiolitic chromitites (Fig. 3.10). The $(Pd/Ir)_N$ ratio of the sulfide-poor chromitites ranges from 0.15 to 0.28. The sulfide-rich chromitite pods (dike-like pods), on the other hand, are characterized by a general enrichment of PGE contents; being have high PPGE over the IPGE (Fig. 3.10) with remarkable positive PGE distribution patterns. The $(Pd/Ir)_N$ ratio of this chromitites ranges from 0.57 to 6.05.

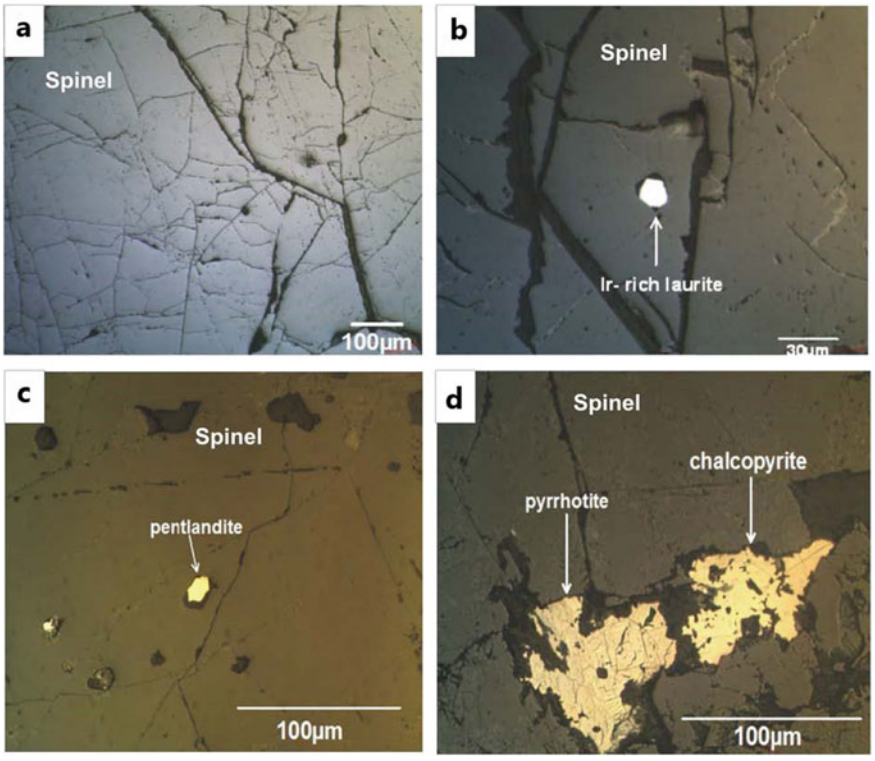

Fig. 3.9 Photomicrographs of **a** fractured Cr-spinels in massive chromitite, **b** perfect euhedral PGM grain (Ir-rich laurite) within fresh, but fractured, Cr-spinel of massive chromitite pod, **c** euhedral pentlandite grain enclosed within fresh Cr-spinel of sulfide-rich dike-like chromitite, and **d** irregular interstitial pyrrhotite and chalcopyrite grains within chromitite matrix. For detailed description, refer to Ahmed et al. (2012)

The third most important example of chromitite-bearing ophiolite in Saudi Arabia is the "*Bir Tuluhah ophiolite*"; it is located in the north central Arabian Shield along the northern margin of the Nabitah suture zone close to Hail City (Figs. 3.1 and 3.2). The Bir Tuluhah ophiolite extends about 30 km long in the NS direction and about 6 km wide (Fig. 3.11). The ultramafic rocks are strongly serpenitinized and sheared, but their harzburgite and dunite protoliths are still recognized from the bastite and mesh-textured pseudomorphs after orthopyroxene and olivine, respectively. There are about 15 chromitite bodies and occurrences at Bir Tuluhah area having different sizes and shapes, including massive pods, layers, schlieren, in situ-float boulders and mechanically-displaced float boulders (Fig. 3.12) (Al-Shanti and El-Mahdy 1988; Habtoor et al. 2017). Massive podiform chromitite lenses are mainly restricted to the northernmost part of Bir Tuluhah ophiolite, where chromitite pods are trending in the N-S directions, forming prominent outcrops in a low relief serpentinized peridotites. Chromitite pods show different shapes and sizes, ranging from elliptical to lenticular

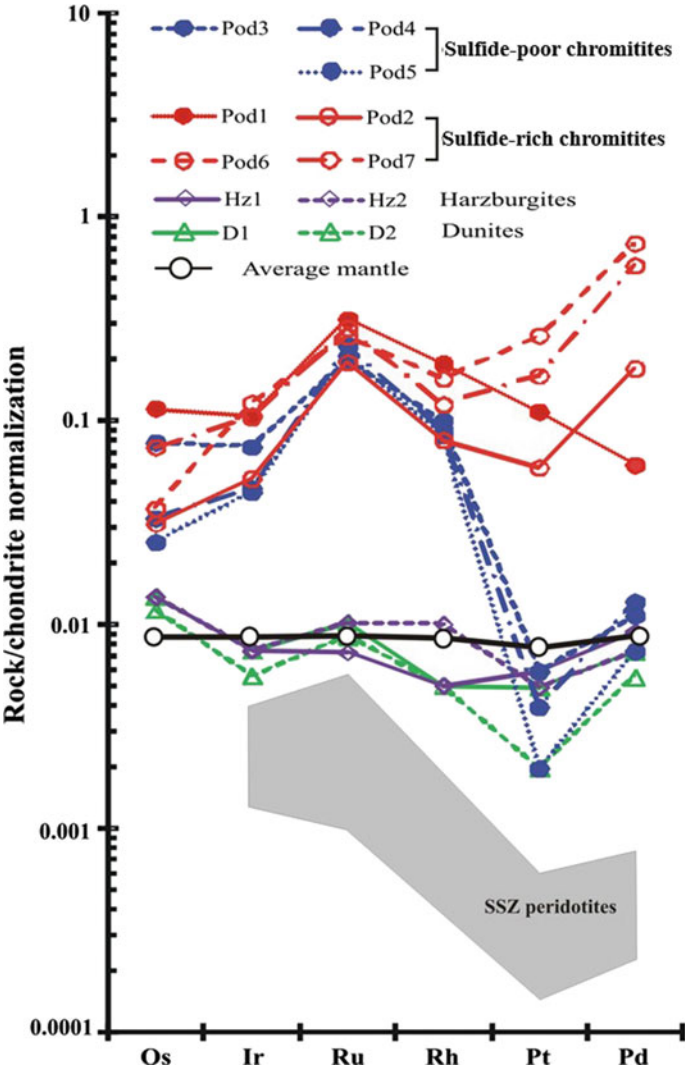

Fig. 3.10 Chondrite-normalized PGE patterns of the chromitites and associated harzburgites and dunites of Wadi Al Hwanet. For more detailed description and compositional field, refer to Ahmed et al. (2012)

individual bodies (Fig. 3.12b), but sometimes occur as elongated bodies or boudinage shape (Fig. 3.12a). The bulk composition of chromitite ores of Bir Tuluhah ophiolite gave very restricted Cr_2O_3 contents of high-Cr varieties, where the Cr_2O_3 content ranges from 52.59 to 55.86 wt% (Habtoor et al. 2017). The other major oxides in bulk chromitites composition are also vary within narrow average ranges (MgO, Al_2O_3 and Fe_2O_3 are 16.28, 10.34, and 14.9 wt%, respectively).

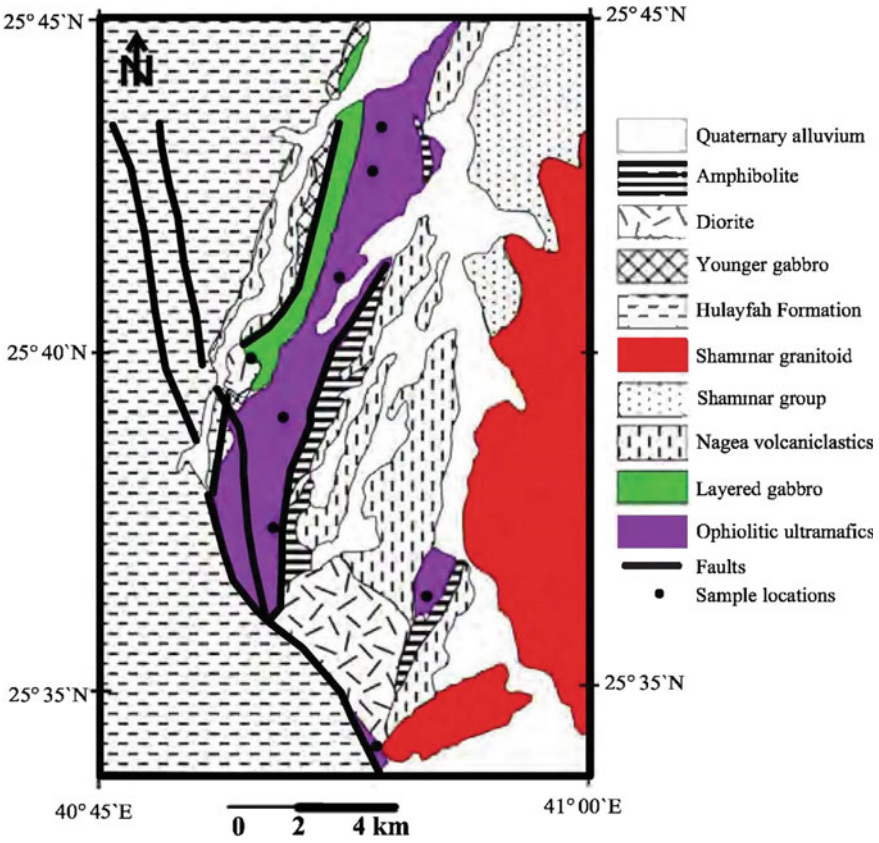

Fig. 3.11 Simplified geological map of Bir Tuluhah ophiolite showing the location of chromitite pods. For more details, refer to Habtoor et al. (2017)

The PGE contents of Bir Tuluhah chromitites are comparable with those from podiform chromitites worldwide (Fig. 3.13a). The total PGE contents of Bir Tuluhah massive chromitites vary from 142 up to 720 ppb (Habtoor et al. 2017). All the chromitite samples from the Bir Tuluhah ophiolite display a steep negative slope of PGE distribution patterns; being highly enriched in IPGE and extremely depleted in PPGE (Fig. 3.13a). The Bir Tuluhah chromitite deposits are, in terms of their PGE contents and patterns, mostly overlapped with those from the other Neoproterozoic ophiolites (e.g., Egypt, Morocco, Saudi Arabia) (Ahmed 2013; Ahmed et al. 2009, 2012; Ahmed and Habtoor 2015), and Phanerozoic ophiolite of Oman (Ahmed and Arai 2002) (Fig. 3.13a). Several PGM grains of various sizes (up to 40 μm), were identified in the Bir Tuluhah chromitite ores (Habtoor et al. 2017). Almost all PGM grains analyzed from Bir Tuluhah chromitites are Ru-rich laurite (RuS_2). Based on the PGE mineralogy and distribution patterns, the Bir Tuluhah chromitite belongs to the "unimodal" type, which is predominant by the Ru-rich laurite (Fig. 3.9b, c).

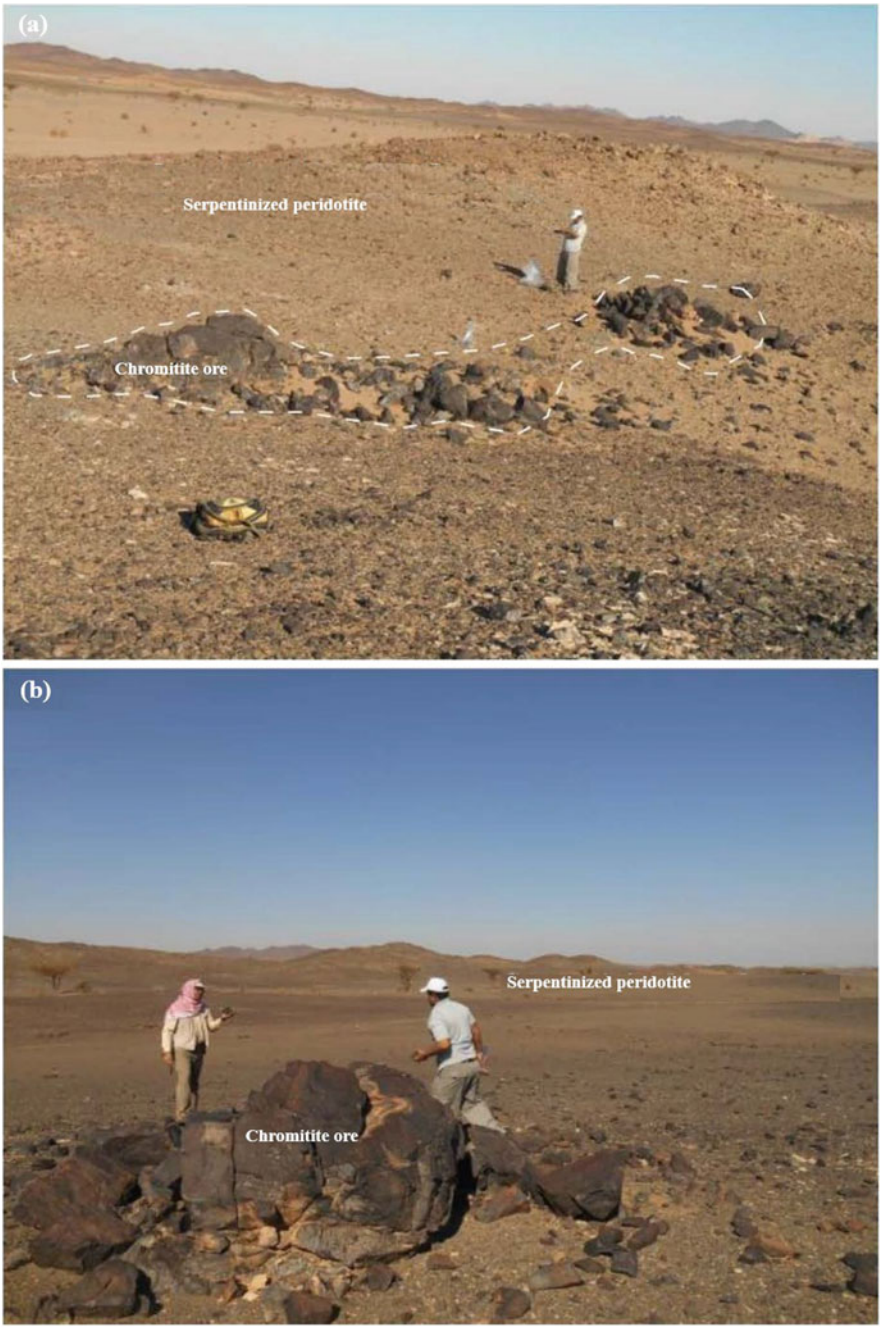

Fig. 3.12 Field photographs of **a** lensoidal fractured podiform chromitite, and **b** boudinaged structure chromitite pods, of Bir Tuluhah ophiolite. For more details, refer to Habtoor et al. (2017)

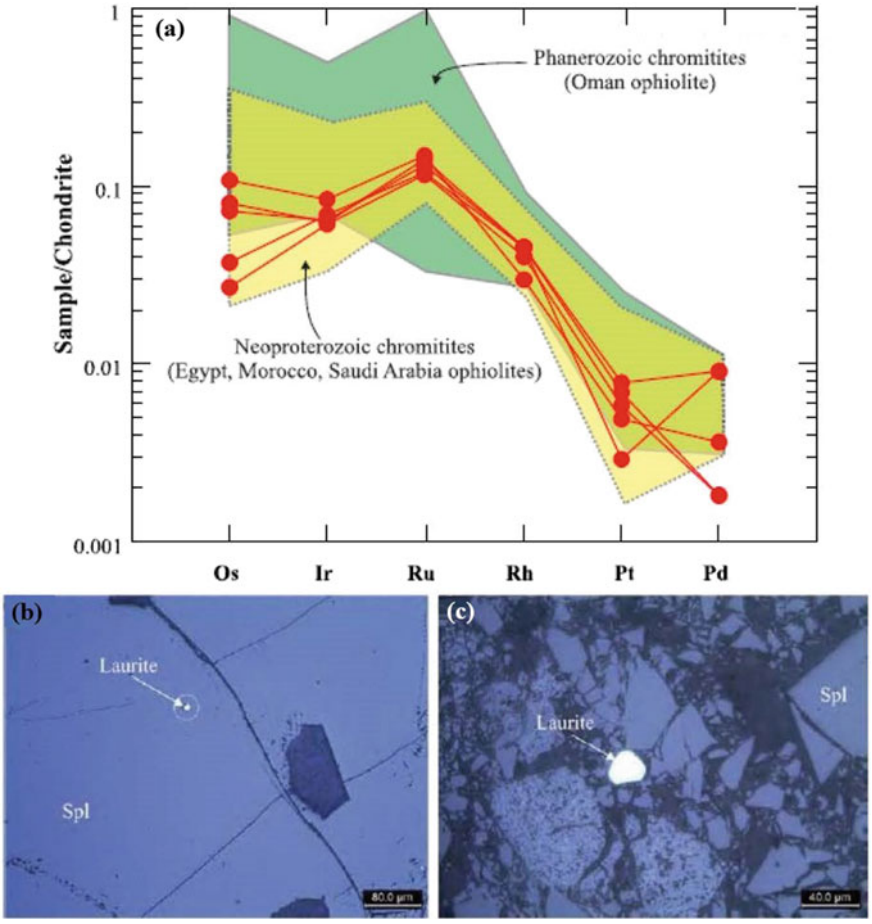

Fig. 3.13 **a** Chondrite-normalized PGE patterns of Bir Tuluhah podiform chromitites. Photomicrographs of **b** euhedral PGM grain (laurite) entirely enclosed within fresh Cr-spinel, and **c** polygonal euhedral laurite grain with interstitial matrix of brecciated massive chromitite of Bir Tuluhah ophiolite. For more detailed description, refer to Habtoor et al. (2017)

The Os and Ir average contents of laurite grains from Bir Tuluhah chromitites are relatively low (2.59, and 2.94 wt%, respectively) compared with the ordinary Os-rich laurites from other Proterozoic and Phanerozoic podiform chromitites (Ahmed and Arai 2003; Ahmed 2007; Habtoor et al. 2017).

Seeking for comparison based on the literature review, ophiolite complexes and their podiform chromitites are classified into three main formation periods in the geologic history (Arai and Ahmed 2018): (i) Archean complexes (3800–2500 Ma), (ii) Proterozoic complexes (early and late: 2500–542 Ma), and (iii) Phanerozoic complexes (<542 Ma). The Archean ophiolite complexes show narrow distribution in the Earth's geologic record compared with the other types (the late Proterozoic

and Phanerozoic ones). The size and dimensions of chromitite ores were rather small in the Archean and early Proterozoic, whereas they are much larger and abundant in the late Proterozoic and Phanerozoic. The available data on chromitites and their host peridotites of the Archean mantle (Kusky et al. 2004; Huang et al. 2004) reveal highly refractory compositions; the Cr# of Cr-spinels in chromitites is very restricted around high-Cr variety (0.7–0.9) (Fig. 3.14). The Cr# of Cr-spinel in the host peridotites is also high, ~ 0.7. The limited petrological data of chromitites and host peridotites from the early Proterozoic ophiolites (Liipo et al. 1995; Vuollo et al. 1995; Peltonen et al. 1998; Peltonen and Kontinen 2004) are rather extraordinary, where the Cr# of chromitite Cr-spinel (~0.6) is fairly lower than those of the host peridotites (0.8–0.9). Late Proterozoic ophiolites are abundant in Africa and Western Arabia; among these the ANS ophiolites in Saudi Arabia and Egypt, which are mostly containing high-Cr chromitites (Ahmed et al. 2001, 2005, 2012; Ahmed and Habtoor 2015). Although high-Al chromitite varieties were recorded in the late Proterozoic ophiolites, the high-Cr varieties with boninitic affinity represent the majority of chromitite types. During the Phanerozoic eon, ophiolite complexes are very common in the Tethyan ophiolites of the late Paleozoic to Mesozoic age (Moores 1982; Moores et al. 2000; Beccaluva et al. 2002, 2004). Podiform chromitites in the Phanerozoic ophiolites are very common and large compared with their counterpart in the Precambrian ophiolites. Their host mantle peridotites have a wide range of Cr-spinel composition;

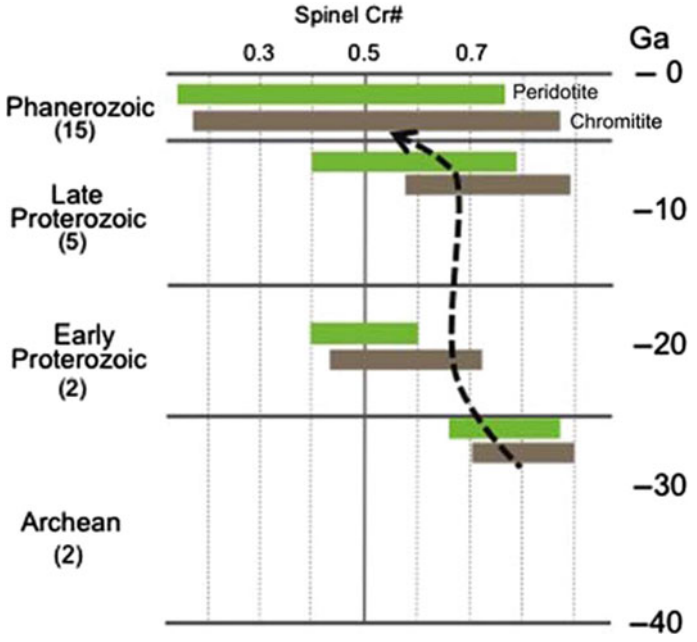

Fig. 3.14 Possible secular change of the Cr# of Cr-spinel in podiform chromitites and host peridotites. For details about description and data source, refer to Arai and Ahmed (2018)

Cr# varies from 0.2 to 0.8 (Fig. 3.14), with an intermediate average Cr# (~0.5), serving as the most common host for large chromitite ores in the Phanerozoic ophiolites (Arai 1997; Arai and Ahmed 2018). With few exceptions, all known Phanerozoic ophiolites possess less refractory peridotites and chromitites than the Precambrian ophiolites (Fig. 3.14). Diversity in Cr-spinel chemistry and PGE contents in podiform chromitites become more distinct in the Phanerozoic ophiolites compared with the older Archean and Proterozoic ones (Ahmed and Arai 2002; Arai and Ahmed 2018).

In conclusion, chromitite pods from the Precambrian ophiolites are apparently smaller than those from the Phanerozoic ones. The known Archean and early Proterozoic chromitite pods are mostly less than 20 m across (rarely up to 100 m in a longer dimension) (Li et al. 2002; Huang et al. 2004; Peltonen and Kontinen 2004). The late Proterozoic Pan-African chromitite pods (e.g., ANS ophiolites) usually show thin disc-like forms up to 30 m in length (Ahmed et al. 2012; Khedr and Arai 2013; Ahmed 2013; Ahmed and Habtoor 2015; Khedr and Arai 2016a, b Habtoor et al. 2017). In contrast, in the Phanerozoic ophiolites, large chromitite pods are rather common with diverse compositions. The largest pod that has ever been reported is the "40 Years of the KazSSR" deposit (Melcher et al. 1999; Distler et al. 2008) from the Early Paleozoic Kempirsai ophiolite, in the southern Urals, in which the chromitite dimension reached about 1.5 km × 150 m.

3.3.2 Magmatic Cu–Ni–PGE Sulfides and Fe–Ti Oxides Mineralization

Magmatic Fe–Ti oxides and Cu–Ni–PGE sulfides are both primarily formed by liquid immiscibility or by segregation of two coexisting liquid fractions from an originally homogeneous magma. The two immiscible liquids may be mineralogically similar (silicate-silicate immiscibility) or they are completely different (silicate-oxide and/or silicate-sulfide immiscibility). Liquid immiscibility is an important ore-forming process that has led to the formation of large deposits such as Kambalda magmatic Cu–Ni–PGE sulfide ores in Western Asutralia, and the Fe–Ti oxide deposits of the Bushveld Complex, South Africa. Layered mafic-ultraamafic complexes and Alaskan-type mafic–ultramafic complexes are the main host of such important magmatic Fe–Ti oxides and Cu–Ni–PGE sulfides.

In the Arabian Shield of Saudi Arabia, the available data indicate that these types of mineral deposits are present but are too low-grade or of insufficient size to be mined economically. The best examples of layered-like mafic–ultramafic complexes in Saudi Arabia that are contain low-grade Cu–Ni–PGE mineralization are the Wadi Kamal and Gebel Al Gharabah complexes, both located in the northwest of the Arabian Shield close to the Red Sea (Fig. 3.2), along the Yanbu-Al Wask suture zone. On the other hand, typical examples for the Alaskan-type concentrically zoned mafic–ultramafic complexes are those of Ha'il, Taftafan, and Lakathah are not known to have economic oxide or sulfide concentrations (Fig. 3.2).

Wadi Kamal–Wadi Murattijah mafic–ultramafic complex is the richest complex in Cu–Ni sulfides and Fe–Ti oxides occurrences in the Arabian Shield of Saudi Arabia. The Wadi Kamal complex is composed of five successive intrusive units (Fig. 3.15) (Chevremont and Johan 1982; Chevremont 1982; Harbi 2008): (1) a central dunitic unit; (2) a south mafic–ultramafic layered unit; (3) an amphibole

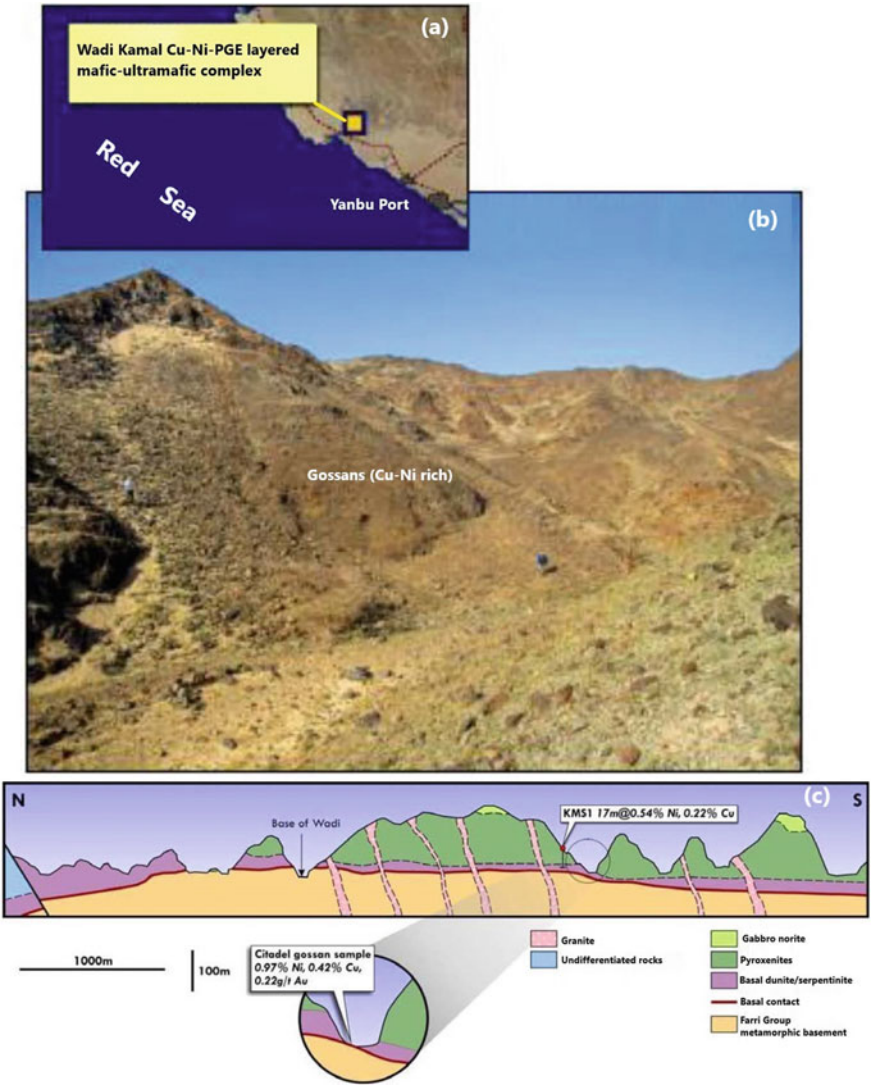

Fig. 3.15 Location of Wadi Kamal complex **a** in the Arabian Shield showing the gossans cover, **b** over the Cu–Ni–PGE sulfide occurrence. **c** Cross section through Wadi Kamal complex showing the main rock units and locations of the samples analyzed (Citadel Co. Ltd. 2010)

gabbro unit; (4) a north anorthositic-layered unit; and (5) a marginal layered gabbro unit. Wadi Kamal complex display petrologic similarities both to the Alaskan-type concentrically zoned complexes in the case of dunitic and ultramafic units (units 1 and 2), and to the upper part of the Bushveld layered complex in the case of the north mafic layered unit (unit 4). Substantial hydrothermal alteration and sulfide mineralization have been identified within each of the units 1–4. Hence, it is expected to find substantial concentrations of PGE associated with Cu–Ni sulfide mineralization in unit 4; Cu–Ni sulfide mineralization in unit 2; and sulfide + magnetite-ilmenite mineralization associated with unit 3. Disseminated Cu–Ni sulfides were reported in the gossans cover over the mafic–ultramafic layered rocks of Wadi Kamal. The analyzed gossans samples in 1974 by BRGM found to contain up to 2.3 wt% Ni and 2.5 wt% Cu. Disseminated sulfides of mainly pyrrhotite, pentlandite, chalcopyrite and pyrite, were found in many drill holes in the ultramafic units. More recent petrological and exploration studies (Harbi 2008) found that gossans and their underlying melagabbronorite samples gave low metal contents. The highest metals percentages were found in gossans, which gave 7.2 g/t Pt, 0.82 g/t Pd and 6.2 g/t Au, and the sulfide mineralization, which was intersected by drill holes, gave 0.4 g/t Pt and 0.27 g/t Pd, 0.71 wt% Ni (Collenette and Grainger 1994).

Several lenses of massive and disseminated magnetite-ilmenite-apatite (nelsonite) deposits were found in the anorthosite and gabbronorite rocks of the complex (Fig. 3.16). The nelsonite-type deposits in the central gabbroic unite display two mode of occurrences (Harbi 2008): (i) massive nelsonite bands of magnetite-ilmenite and apatite in different proportions, and (ii) massive magnetite-ilmenite ore found either as bands intercalated with nelsonite or as dike-like bodies hosted by anorthosite. The massive nelsonite (magnetite-ilmenite-apatite) mineralization is found as massive layers or bands ranging in thickness from few centimeters to several meters, and extends up to 200 m along strike. Magnetite and ilmenite with variable amounts of apatite (~25% on average) is the essential mineralogy of the massive ore. The massive ore have either sharp or gradational contacts with the disseminated mineralized gabbronorite rock (Fig. 3.16a, b). The banded massive ore is characterized by the presence of centimeters-scale ovoid xenoliths from the host gabbronorite rock, which containing fine-grained disseminated Fe-Ti oxides (Fig. 3.16c, d). The ore reserves of largest massive lens estimated to contain about 200,000–300,000 tons of ore with a general grade of 12 wt% Ti, and 51 wt% Fe (Collenette and Grainger 1994).

The Fe-Ti oxides mineralization of *Qabqab-Wadi Hayyan* area, in the most northwestern corner of Midyan terrane (Fig. 3.2), is almost similar to that at Wadi Kamal-Wadi Murattijah, which is mostly similar to the upper zone of the Bushveld complex (Chevremont and Johan 1982). The Qabqab-Wadi Hayyan mafic–ultramafic complex have several lenses of Fe–Ti oxides mineralization in a gabbro-diorite association that crops out in a ring-like complex over a total area of about 100 km^2. However, the volume of the deposit is too small to be mined, where the identified resources are about 300,000 ton with average grade of 8.5% TiO_2 and the Fe:Ti ratio is about 4.5.

Alaskan-type concentrically zoned mafic–ultramafic complexes such as: Wadi Kamal, Ha'il, Taftafan, and Lakathah complexes (Fig. 3.2) are not known to contain

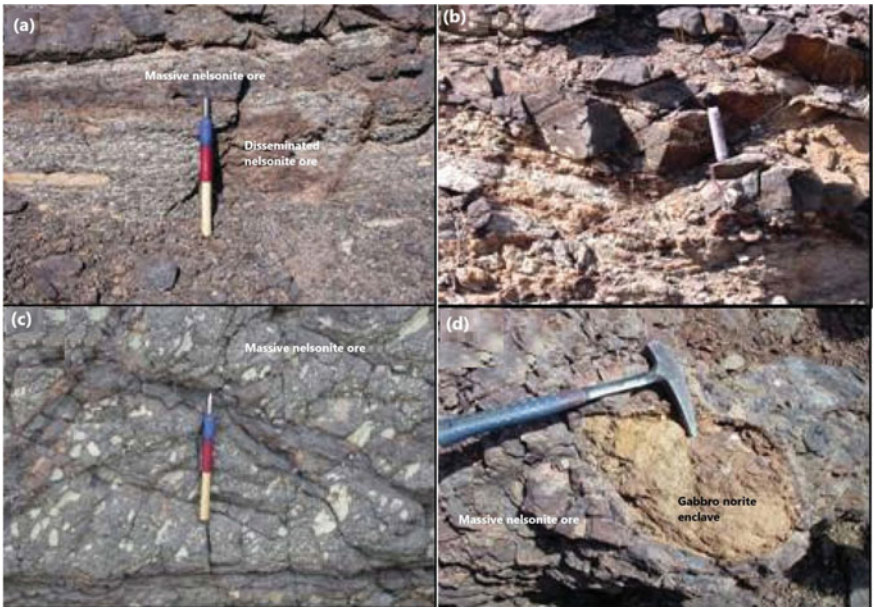

Fig. 3.16 Field photographs of Wadi Kamal layered intrusion showing **a** massive nelsonite ore intercalated with disseminated ore, **b** sharp contact between massive nelsonite ore and host gabbronorite, **c** small and **d** large enclaves of gabbronorite host within the massive nelsonite ore. For detailed description, refer to Harbi (2008)

potential ore mineralization. In Such complexes of the Alaskan-type analogues, the Cu–Ni–PGE sulfides and oxides were mainly concentrated in the high forsterite (Fo) olivine (Fo > 90) and spinel-rich ultramafic cores. The *Ha'il* mafic–ultramafic complex is composed of four petrologic units (Chevremont 1982): (i) a serpentinite unit that is locally carbonatized, amphibolitized and even tourmalinized. This srepentinite unit is sometimes containing podiform lenses of massive chromitite. (ii) Clinopyroxenite and olivine clinopyroxenite unit, which altered to hornblendite and olivine amphibolite, respectively. (iii) An amphibole gabbro unit, and (iv) an olivine gabbro unit with fresh silicate minerals compared with the ultramafic and mafic rocks of other units. The Ha'il mafic–ultramafic complex displays several similarities to the Ural Alaskan-type complex, where the serpentinized dunite core is containing high Fo olivine (Fo = 92) with chromitite lenses and concentrations.

Recent study on the petrology and geochemistry of *Gebel Taftafan* area revealed that the mafic–ultramafic complex consists of coarse-grained dunite core grading outward to hornblende- and plagioclase-bearing peridotites, troctolite, clinopyroxenite, and coarse-grained gabbroic rocks at the periphery (Habtoor et al. 2016). It forms a small oval-shaped intrusion at the upper part of the Sharqah Complex, Mekkah Quadrangle (Fig. 3.17a, b). Ore minerals in the dunite core represented mainly by disseminated Cr-spinel in the interstitial matrix and included within olivine grains, in addition to fine-grained sulfides, which are mainly chalcopyrite

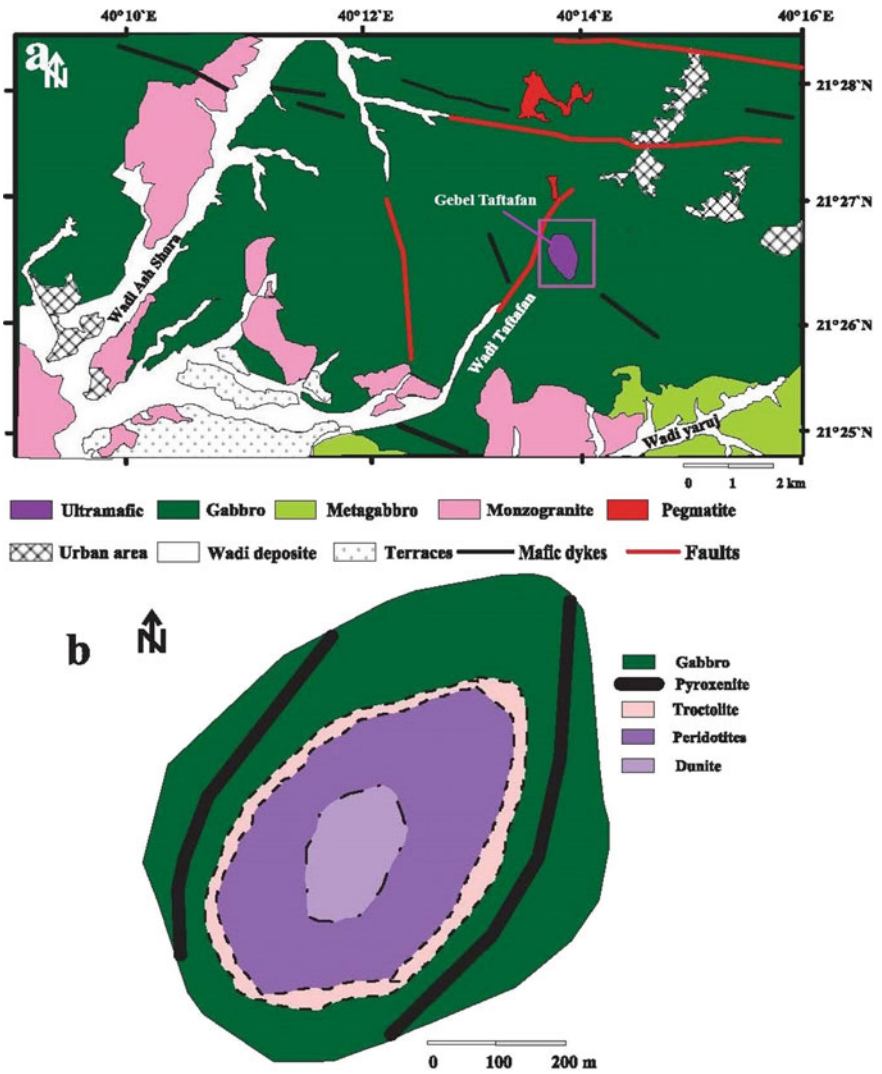

Fig. 3.17 **a** Part of the geological map of the Makkah quadrangle showing the geology of Gebel Taftafan area (Moore and Al-Rehaili 1989). **b** Lithological sketch showing the variation of rock types from ultramafic core to the marginal gabbro of Taftafan complex. For details geological description, refer to Habtoor et al. (2017)

and pyrite (Fig. 3.18a, b). The plagioclase-bearing peridotites and troctolites are characterized by spinels of anhedral to skeketal shape that separated into two parts, dark gray of Al-rich spinel, and light gray of Fe-rich spinel (Fig. 3.18c). The spinel unmixing is a characteristic feature for Alaskan-type concentrically zoned mafic–ultramafic complexes that previously described from the Nubian Shield of the Eastern

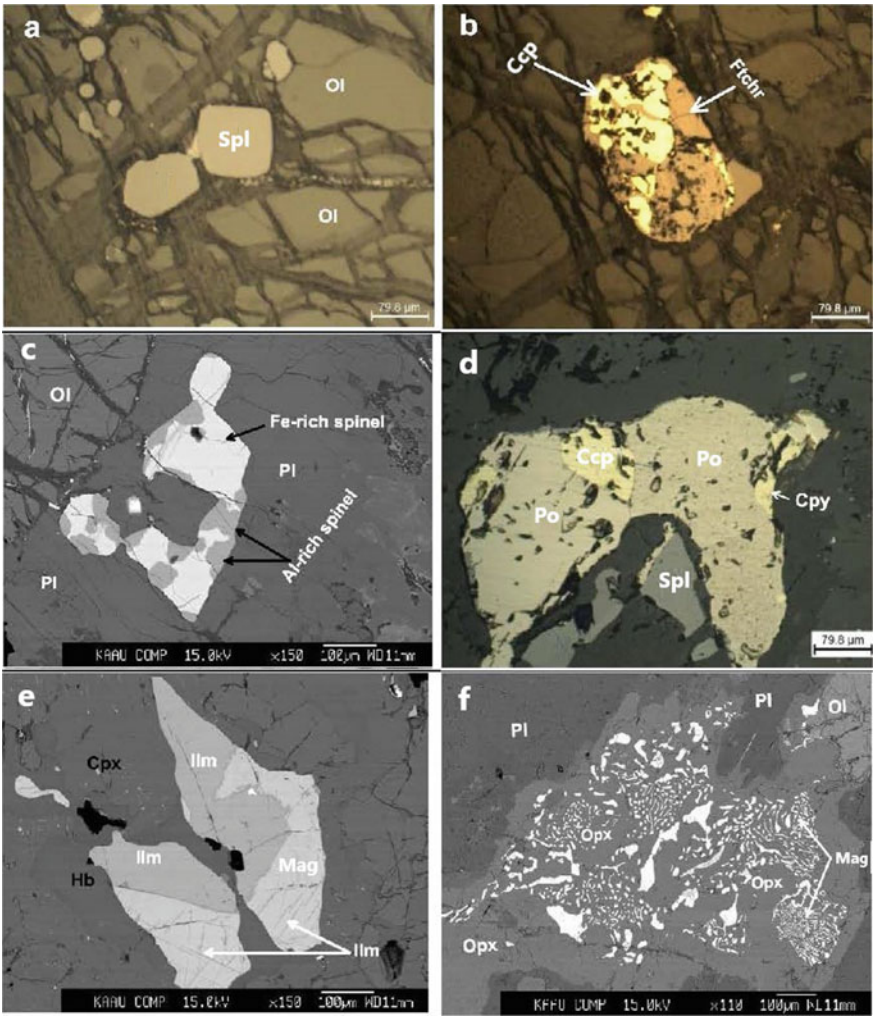

Fig. 3.18 Photomicrographs of Gebel Taftafan Alaskan-type complex showing **a** euhedral cumulus spinel grains interstitial to olivine in the dunite core, **b** composite chalcopyrite/chromite grains of peridotite, **c** anhederal to skeletal exsolved spinel types of Fe-rich and Al-rich spinels in plagioclase, troctolite rock, **d** composite chalcopyrite/pyrrhotite grains in clinopyroxenite, **e** magnetite-ilmenite grains in clinopyroxenite, and **f** symplectite texture comprising Opx and magnetite in fresh marginal gabbro. For detailed description, refer to Habtoor et al. (2017)

Desert of Egypt (Ahmed et al. 2008). Clinopyroxenite unit of the Gebel Taftafan complex contains numerous amounts of magnetite and ilmenite exsolution lamellae, as well as anhedral to subhedral composite grains of ilmenite and magnetite/hematite (Fig. 3.18e). Numerous sulfide-disseminated grains (up to 5 wt% of rock volume)

occur as net-texture of medium to coarse-grained aggregates within the coarse-grained clinopyroxenite, which are predominantly of pyrrhotite and chalcopyrite (Fig. 3.18d). Clinopyroxenite and marginal gabbro units are containing various amounts (5–8 wt% of the rock volume) of skeletal-shaped Fe-Ti oxide minerals including magnetite and ilmenite (Fig. 3.18e). In addition, tiny magnetite-ilmenite lamellae are observed, in the marginal gabbros, as exsolutions orientated along the crystallographic planes of clinopyroxene crystals (Fig. 3.18f), which known as magnetite-ilmenite symplectite. The Ni, Cu and PGE contents of the Gebel Taftafan mafic–ultramafic complex is very low (Habtoor et al. 2017); further studies are needed to locate the sulfide-rich horizons in the complex.

The *Lakathah* mafic–ultramafic complex is another well-known example of Alaskan-type mafic–ultramafic complex in the southwestern part of the Asir terrane of Saudi Arabia (Fig. 3.2), which displays a circular shape with a diameter of 10 km (Martin et al. 1979). It composed of three main units: an outer syenite ring unit, an intermediate diorite-gabbro unit, and a central pyroxenite-hornblendite core unit. The Lakathah mafic–ultramafic complex shows some characteristics that made it a good target for Cu–Ni–PGE exploration including: (1) concentric zonation from ultramafic core to mafic and altered carbonate-rich periphery; (2) small patches of massive magnetite accompanied by apatite in pyroxenite and hornblendite; and (3) the presence of sulfides (pyrrhotite and pyrite) within pyroxenite, hornblendite and carbonate rocks. Hence, the abundance of hornblendite, the presence of magnetite-ilmenite and sulfides, and the existence of dikes with carbonate alteration, all of which indicate an intense percolation of hydrothermal fluids rich in volatiles (e.g., H_2O, S, and CO_2) into the ultramafic core of the Lakathah complex. The Fe–Ti-bearing minerals at Lakathah complex found mainly in the pyroxenite-hornblendite core and associated rocks. Most of the Ti metal existed in the titaniferous magnetite, but a significant amount is also found in the kaersutite. Titaniferous magnetite ore essentially found as lenses, veins, and disseminated forms throughout the host rocks in amounts ranging from 5 to 25 wt% of the rock volume. The ore lenses are commonly ranging from 30 cm up to 3 m wide and are as much as 50 m long. The massive ore lenses are estimated to account for about 50 wt% of the rock volume. The magnetite in the Lakathah Fe–Ti mineral deposit is present as fine grains enclosed in other minerals, in cumulate interstices, and as coarsely crystalline masses.

The average TiO_2 content of the drill core samples in the Lakathah complex is about 6.2 wt%, and reached up to 10.1 wt%, and the total Fe_2O_3 content varies from 5 to 35 wt% (Martin et al. 1979). The main mineralized zone is about 500 m wide and extend for more than 1000 m long. This block contains about 175 Mt of ore for each 100 m depth; the Fe–Ti mineralized zones may extend to other parts of the central zone. The average grade of about 6.2 wt% TiO_2 of the Lakathah deposits are probably too low in grade to be worked at that time (Martin et al. 1979), but may be a future resource if there is a development in the Ti market. In addition, a large volume of the Lakathah complex has been eroded and transported to the Red Sea coast et al. Qunfudhah, about 90 km to the southwest from the complex location, and Ti–rich sands may exist on the sea margin in the form of black sands, which is very common throughout the Red Sea coast.

3.4 Magmatic Mineral Deposits in Yemen

The Precambrian rocks and tectonic belts of Yemen host significant mineral deposits. The lithology and major structures (e.g., Najd fault system and Nabitah suture zone) played an important role in the formation and remobilization of the mineralization types in Yemen (Al-Khirbash et al. 2021). The mafic–ultramafic complexes are common in the Precambrian basement of Yemen. These intrusions are metamorphosed to various extents and have suffered one or more deformational events. The Precambrian mafic–ultramafic complexes of Yemen are principally the layered/Alaskan-type intrusions. They range in size from a few square meters up to more than a hundred square kilometers. They range in composition from anorthosites through gabbros to peridotites, pyroxenites and dunites. Many of mafic–ultramafic complexes of Yemen display compositional layering and they are frequently containing massive and disseminated Cu–Ni–PGE sulfide deposits (Al-Khirbash et al. 2021). Magmatic deposits, including Ni–Cu–Co ± PGE and Fe–Ti ± V deposits, are associated with mafic/ ultramafic complexes in the Afif, Abas, and Al-Mahfid gneissic terranes. There are so few studies on the mafic–ultramafic complexes and their associated mineral deposits in Yemen; however, the available data depends mainly on some recent publications (Greenough et al. 2011; Venturi et al. 2015; Al-Khirbash et al. 2021) and on the latest reports from the Yemeni Geological Survey and Mineral Resources.

The limited studies conducted on several gossans-rich sites in the northwest, western, and southern parts of Yemen (Fig. 3.19) revealed that there are a number of Precambrian layered-like mafic–ultramafic complexes. These complexes found to contain high economic potentiality of Cu–Ni–Co–PGE and Fe–Ti–V mineralization. These areas include: Suwar-Wadi Qutabah, Byhan, Al-Qabyta, Qaifa, Wadi Mabar, Al Hamurah, and Wadi Silbah occurrences (Fig. 3.19). Following is a brief description of these mafic–ultramafic complexes and their associated mineral deposits.

3.4.1 The Suwar-Wadi Qutabah Ni–Cu–Co–PGE Occurrences

The Suwar complex is a layered mafic–ultramafic intrusion discovered by the Canadian company "Cantex Mine Development Corporation" in northwestern Yemen (Fig. 3.20a). It is located at about 80 km northwest of Sana'a, within the Precambrian basement rocks and showing a significant potential of Ni–Cu–Co-(±PGE) mineralization. Similar rock associations occur at about 30 km to the north in the Wadi Qutabah area (Fig. 3.20b); the two exposures have been considered to belong to the same intrusion (Greenough et al. 2011; Venturi et al. 2015). The U–Pb age dating of the two Suwar and Wadi Qutabah complexes gave approximately a similar age (638.46 ± 0.73 Ma and 638.58 ± 0.51 Ma, respectively), which supports being a single large intrusive complex, with a total area of about 250 km^2 (Greenough

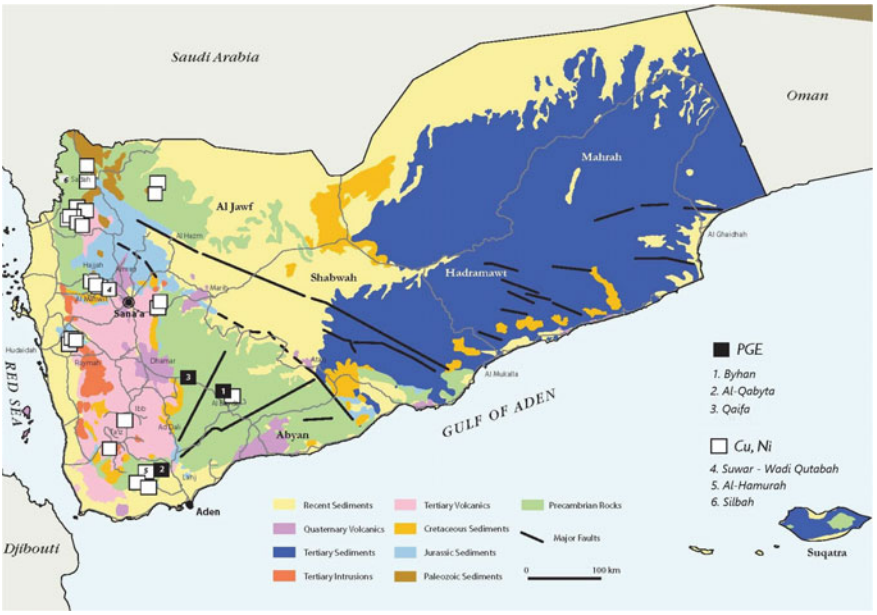

Fig. 3.19 Simplified geological map of Yemen with locations of most important mafic–ultramafic complexes and their Cu–Ni–PGE mineralization (from Mineral Resources of Yemen, 2009)

et al. 2011). The "Cantex" company estimated the total thickness of the mafic–ultramafic intrusion of Suwar-Wadi Qutabah complex by about 900 m, which is considered as one of the largest, in size and thickness, mafic–ultramafic intrusive complexes worldwide (Venturi et al. 2015). The "Cantex" company carried out exploration program involving geological, geochemical and geophysical surveys, as well as drilling of a total length of 3095 m. The Suwar-Wadi Qutabah mafic–ultramafic complex consists of three major units: gabbro, gabbronorite, and discontinuous ultramafic units. Wehrlite and troctolite layers are also recorded. Recent studies (e.g., Greenough et al. 2011; Venture et al. 2015) revealed that there are five main sulfide-rich mineralized horizons in the Suwar-Wadi Qutabah complex. These sulfide horizons are conformable with the igneous layering of the gabbroic body, which extends over an area of about 250 km^2 (Venturi et al. 2015). The size of the intrusion has not been precisely estimated as the large part of it is buried under a younger sedimentary rock cover. A minimum area extent, based on the mapping of outcrops, is about 128 km^2.

The sulfide horizons outcrop mainly as massive and disseminated gossans cover, however the fresh sulfide-rich bedrocks exposed only in steep narrow gullies where the gossans have been completely eroded. The main ore minerals described in the Suwar-Wadi Qutabah Cu–Ni–Co deposits, arranged in decreasing order of abundance, are pyrrhotite, pentlandite, chalcopyrite, and magnetite. The potential resources of the Suwar deposit were estimated by the company to be about 40 Mt

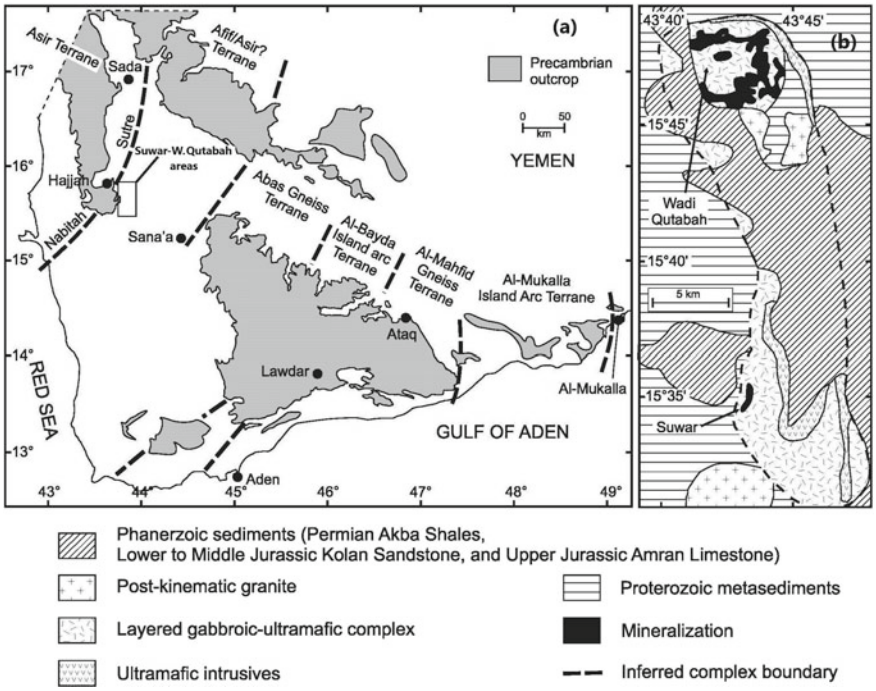

Fig. 3.20 **a** Geological map of the Pan-African terrane boundaries and Precambrian outcrops in Yemen, and **b** geological sketch map of the Suwar-Wadi Qutabah complexes (modified from Greenough et al. 2011)

with an average grade of 2% Cu, 2% Ni, and low values of Co, Pd and Pt. The mineralization essentially occurs in mafic–ultramafic rocks.

3.4.2 The Byhan Cu–Ni–PGE Occurrence

The Byhan Cu–Ni–PGE mineralization is located in the southeastern part of Yemen (Fig. 3.19), about 60 km NW of Al-Bayda city, in the Al-Bayda uplift terrane at the southeast margin of the ANS. The Cu–Ni–PGE mineralized area located in Wadi Byhan, being extends to an area of approximately 47 km in length and 43 km in width. The Byhan Cu–Ni–PGE mineralization hosted by a Neoproterozoic intrusion composed of a sequence of dunites, pyroxenites, peridotites and anorthosites. Coarse-grained pegmatitic pyroxenites are commonly observed. The Byhan mafic–ultramafic intrusive complex occurs within a northeast trending, uplifted terrane of Lower Proterozoic migmatites, biotite gneisses and marbles, bounded on both sides by two regional faults. From the structural viewpoint, the Byhan intrusion lies at the

northern slope of the Al-Bayda terrane to the north of which two well-developed deep, major faults are located. These faults cause the Al-Bayda uplifting.

Based on the available analytical data of the "Mineral Resources of Yemen, 2009", selected metallic and precious metals (Au, Pt, Pd, Cu, Ni and Co) in the Byhan mafic–ultramafic complex gave the following concentrations (Table 3.1). The mafic rock samples (gabbro and gabbronorite) have the highest Cu content. The precious metals (Pt + Pd) in the mafic lithology of Byhan intrusion varies from 10 up to 143 ppb, with an average content of 60 ppb (Table 3.1). The gossans samples over the mafic lithology of the Byhan complex show lower Cu, Ni and Co contents compared with their fresh bedrock samples (Table 3.1), however the precious metals (Pt, Pd, and Au) are much concentrated in the gossans samples. The Pt + Pd content varies, in the gossans samples, from 28 up 359 ppb, with an average of 117 ppb, while gold content varies from 7 up to 731 ppb, with an average of 88 ppm. The pyroxenite samples of the Byhan complex show the lowest metal contents compared with other rock types (Table 3.1).

Table 3.1 Chemical analysis selected metals of representative samples of the Byhan Cu–Ni–PGE layered mafic–ultramafic complex

Sample no	Rock type	Au ppb	Pt ppb	Pd ppb	Co ppm	Cu ppm	Ni ppm
RRX 174	Gossan	17	< 5	44	347	950	809
RRX 184A	Gossan	27	< 5	24	27	2230	435
RRX 184C	Gossan	28	< 5	65	11	415	161
RRX 185	Gossan	53	41	118	116	> 10,000	3880
RRX 186	Gossan	731	144	215	34	7400	1075
RRX 202	Gossan	52	< 5	106	75	484	168
RRX 208	Gossan	43	8	108	166	772	648
RRX 214	Gossan	14	7	65	253	1525	586
RRX 215	Gossan	45	20	66	106	909	206
RRX 221	Gossan	7	75	67	33	1800	473
RRX 228A	Gossan	13	18	23	43	951	198
RRX 272	Gossan	20	< 5	106	245	1285	929
RRX 184B	Mafic rocks	4	15	5	97	9050	1220
RRX 222	Mafic rocks	40	118	25	591	> 10,000	5000
RRX 228B	Gabbro	20	5	13	160	1455	879
RRX 223	Pyroxenite	15	< 5	33	284	718	2040

Source Mineral Resources of Yemen (2009)

Table 3.2 Chemical analysis of selected metals of representative samples of the Al-Qabyta layered mafic–ultramafic complex

Sample no	Rock type	Pt ppb	Pd ppb	Cu ppm	Ni ppm	Co ppm	S %
RRX 560	Ultramafic	7	18	577	34	160	2.01
RRX 590B	Gossan	22	24	572	154	65	1.08
RRX 614A	Gossan	19	6	2130	297	850	0.14
RRX 614B	Gossan	87	140	1090	210	256	0.85
RRX 641A	Gossan	15	61	589	746	13	7.37

Source Mineral Resources of Yemen (2009)

3.4.3 Al-Qabyta Occurrence

The Al-Qabyta complex is an intrusion ranging from mafic (gabbroic) to ultramafic rocks, where the ultramafic rock is frequently serpentinsed to various extents. The Al-Qabyta mafic–ultramafic intrusive complex is weakly deformed and metamorphosed under greenschist facies conditions. It intruded into a sequence of amphibolites and metasedimentary rocks; late faulting and shearing are also abundant. There is no enough information about the mineralogy and petrology about this complex, but grab samples yielded encouraging results for Ni and PGE contents. The available limited data from the Mineral Resources of Yemen (2009) shows that (Table 3.2), the gossans samples have much concentration in Cu, Ni and Co than the bedrock ultramafic samples. In the gossans samples, the highest Cu, Ni and Co contents are 2130, 746, and 850 ppm, respectively. The Pt + Pd contents in the gossans samples reached up to 227 ppb, and the sulfur content reached up to 7 wt%, which reflect the high sulfide content in the gossans samples (Table 3.2). The ultramafic bedrock shows less metal contents.

3.4.4 The Qaifa Occurrence

The Qaifa mafic–ultramafic intrusive complex comprises gabbros, norites, anorthosites, and peridotites. Some of the ultramafic rocks of this complex have been altered to serpentinites, occurring as lenses of up to 50 m wide and over than 100 m long. The Qaifa complex is intruded into a sequence of metagabbros, talc schists, metavolcanics, schistose amphibolites and quartzites. The intrusion and its wall rocks are partly covered by basalts and ignimbrites of Tertiary age.

The available limited data from the Mineral Resources of Yemen (2009) is shown in Table 3.3, where a number of fresh mafic–ultramafic bedrock samples (gabbros, metagabbros, pyroxenite) and gossans samples were analyzed for selected metals (Cu, Ni, and S), as well as precious metals (Au, Ag, Pt and Pd). Copper is the highest metal content in the bedrock samples (gabbro), which reached up to about 1 wt%, followed by Ni, which reached up to 636 ppm in the bedrock samples. The gossans

Table 3.3 Chemical analysis of selected metals of representative samples of the Qaifa layered mafic–ultramafic complex

Sample no	Rock type	Au ppb	Pt ppb	Pd ppb	Ag ppm	Cu ppm	Ni ppm	S %
RS 10 B	Metagabbro	18	7	132	< 0.2	2859	114	0.04
RSQ 48	Metagabbro	8	14	23	0.3	3455	405	0.21
RSQ 54	Gabbro	8	16	19	< 0.2	3281	636	0.06
RSQ 62	Gabbro	42	< 5	13	4	9959	208	0.05
RSQ 86	Pyroxenite	12	24	17	0.8	410	373	0.31
RSQ 15	Gossan	602	5	3	66.9	51	58	0.16
RSQ 45	Gossan	12	12	8	1.7	1373	90	1.04
RSQ 77D	Gossan	38	8	35	0.6	470	60	0.23
RSQ 78	Gossan	14	7	14	1.4	767	123	0.31
RSQ 79	Gossan	38	61	103	0.9	2272	82	0.35
RSQ 101	Gossan	8	7	12	2.4	278	97	0.78
RSQ 104	Gossan	8	27	10	1.6	790	59	0.57

Source Mineral Resources of Yemen (2009)

samples, on the other hand, show enrichment in all precious metals (Au, Ag, Pt and Pd) content compared with the bedrock samples (Table 3.3). So, as in the previous mafic–ultramafic complexes of Yemen, the sulfide-rich bedrocks of the complexes are important as a source for Cu, Ni, and to a lesser extent precious metal, whereas the leached gossans cover could be a good source for precious metals.

3.4.5 The Wadi Mabar Area

The Wadi Mabar mafic–ultramafic complex is one of the promising areas for the PGE mineralization, which was discovered by the Romanian geologists. The complex is consisting of a sequence of mafic–ultramafic rocks that mainly composed of serpentinized ultramafic rocks, talc and tremolite schist. The Pd content varies from 0.1 to 0.3 g/t. The BRGM geologists considered that PGE mineralization might occur in the Wadi Aquan layered complex, where anorthosite intrusive rocks are predominant. There is no much information about the ore resource estimation of base and precious metals in the Wadi Mabar complex.

3.4.6 The Al-Hamurah Cu–Ni Occurrence

The Al-Hamurah mineralized area is located approximately 50 km southeast of Ta'iz (Fig. 3.19); it is situated in the left slop of Wadi Al-Aghabirah Valley within the

gabbronorite that located in the middle of the biggest dioritic-lamprophyre dyke (Fig. 3.21). The lamprophyre dyke is located in the middle area between Wadi Al-Aghabirah (at the south) and Wadi Urar (at the north) (Fig. 3.21), which is a well-developed supergene alteration zone, or a large gossans surface. The Al-Hamurah area is underlain by Precambrian gneisses and amphibolites, which are

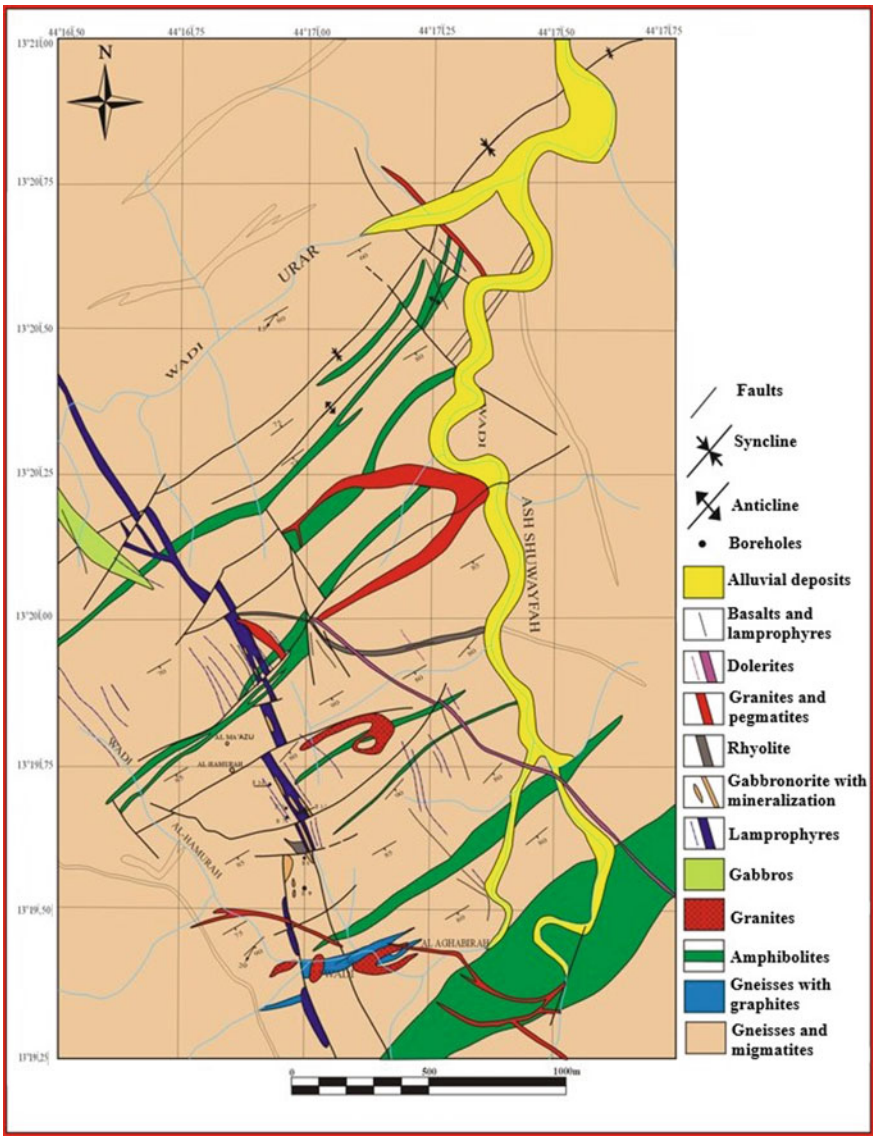

Fig. 3.21 Geological map of Al-Hamurah area, Yemen, showing the Al-Hamurah mineralization

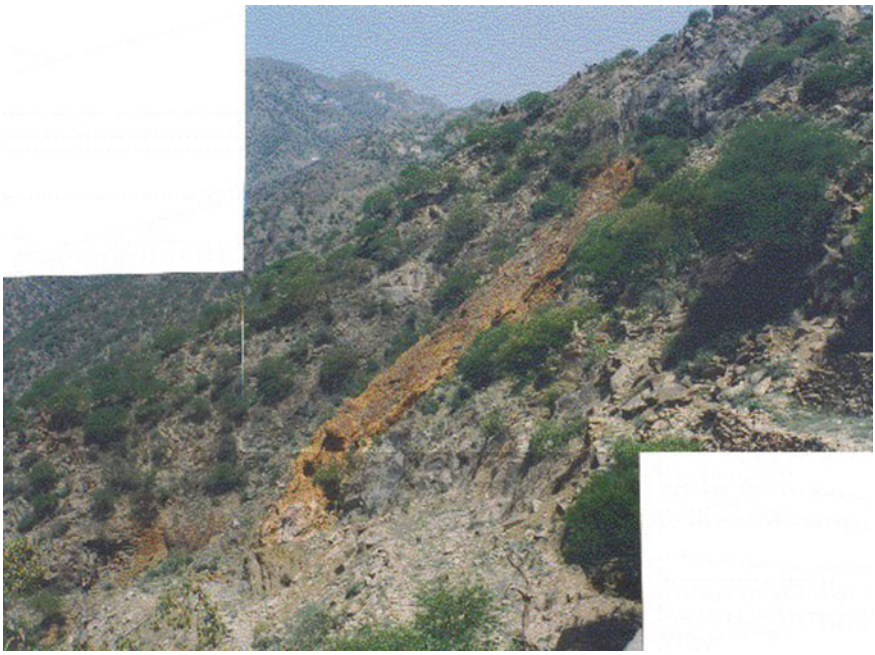

Fig. 3.22 Field photograph showing the extension of lamprophyre dyke of Al-Hamurah mafic–ultramafic complex, Yemen

cut by various fracture systems and mafic to felsic dykes (Fig. 3.21). The mineralization on the surface as well as on the underground galleries, which drilled by GEOMIN Company (1974–1984), is a sulfide-bearing gabbronorite hosted within a dioritic-lamprophyre dyke. The Cu–Ni mineralization of Al-Hamurah complex occurs in an about 7 km long NW-trending gabbroic lamprophyre dyke (Figs. 3.21, 3.22), which was emplaced during the Precambrian along a NW-striking fracture set, associated with the Al Manarah–Al-Hamurah fault. The lamprophyre dyke is up to 45 m thick, dips 60° to 80° SW, and has been investigated by drilling over more than 1000 m boreholes. The gossans cover has been examined in the Al-Hamurah area since the early 1920s by the Strojexport (a Soviet enterprise), which conducted the first detailed structural, geological and geophysical surveys and sampling the gossans area (1970). During the period from 1979 to 1983, an extensive geological, geochemical and geophysical surveys program was completed. In addition, this program is also involving 1419 m of surface drilling and 1000 m of underground drilling, as well as driving of 700 m of adit and a variety of mineralogical studies. The gabbroic lamprophyre dyke of Al-Hamurah area separated into several blocks by several transverse faults of E-W to NE-SW direction (Fig. 3.21).

The Al-Hamurah mineralization is essentially composed of sulfides and iron oxides and occurs as massive and disseminated ores or associated with quartz veins. The thickness of massive mineralization (~90% of the rock volume) is variable, which

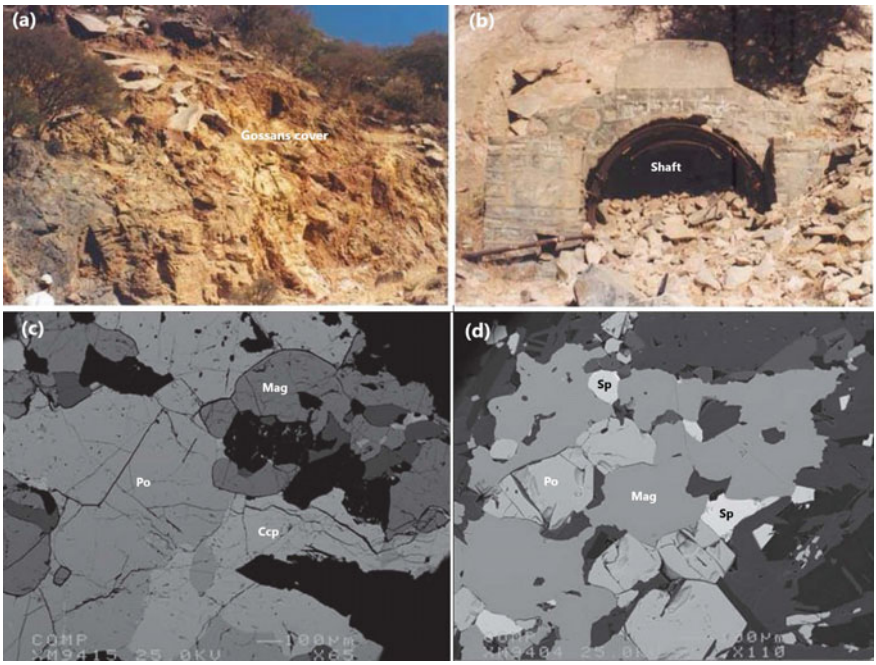

Fig. 3.23 Field photographs (**a**, **b**) showing the oxidation zone (gossans) and old shaft in the mineralized-lamprophyre dyke of Al-Hamurah area, Yemen. **c**, **d** BSE image showing the mineralogy of massive Cu–Ni sulfide deposits of Al-Hamurah mineralized lamprophyre dyke, Yemen. Abbreviation: Mag: magnetite, Po: pyrrhotite, Ccp: chalcopyrite, Sp: sphalerite

sometimes reached up to 10 m thick. The mineralization zones encountered mainly in the subsurface galleries, but on the surface, it is represented by oxidation zones "gossans" of variable dimensions (Fig. 3.23a) where several boreholes and shafts were digging (Fig. 3.23b). The depth of the oxidation zone over the Al-Hamurah layered bedrocks varies from 20 to 40 m, as has been estimated by GEOMIN Company using geophysical measurements and drilling works. Sulfide minerals in the Al-Hamura mineralization are dominated by pyrrhotite, followed by chalcopyrite and, to a lesser extent, sphalerite (Fig. 3.23c, d) as cumulus and intercumulus massive to disseminated ores. The Fe–Ti oxides (i.e. magnetite and ilmenite) are also common as cumulus and intercumulus phases in the massive and disseminated ores (Fig. 3.23c, d). The best underground drill intersection with the mineralized zone gave an average grade of 5.4 wt% Ni, and the highest Cu value was 2.2 wt%. The Felix Mining Ltd. carried out detailed work (in 1997) in the Al-Hamurah mafic–ultramafic complex investigating a number of outcropping ultramafic dykes. The gossans zones yielded the best assay results, where the highest Cu content was 9.2 wt%, up to 0.6 wt% Ni, and up to 0.1 wt% Co.

3.4.7 The Wadi Silbah Occurrence

The Wadi Silbah mafic–ultramafic complex is located to the west of Sadah (Fig. 3.19), where layered mafic to ultramafic rocks composed of gabbro, pyroxenite and peridotite with minor dunite was discovered in 1983. Small chromitite lenses and veinlets occurred in altered peridotite and sometimes in dunite. Indication of the economic potential of the Wadi Silbah mafic–ultramafic complex stems from the stream sediment samples that derived from the complex. These stream sediments contain 176–4736 ppm Cr_2O_3, 102–1778 ppm Ni, 64–151 ppm Co, and 69–214 ppm Cu. Follow-up exploration in 1992–1993 confirmed the presence of Wadi sediment anomalies and found in-situ chromite veinlets together with a boulder and floats of massive chromitite ore.

3.4.8 The Mukayras Fe–Ti–P–V Occurrence

Several localities of Fe–Ti–P–V oxide mineralization in gabbroic rocks were recorded in several localities, the Mukayras area is one of them where it is located about 20 km northwest of Al Bayda (Al-Khirbash et al. 2021). The Mukayras deposit consists of disseminated apatite-ilmenite-titanomagnetite-vanadium mineralization within the Mukayras mafic–ultramafic complex. The reporting potential mineral resource (Isakin et al. 1990) shows the presence of apatite-ilmenite-titanomagnetite-vanadium-bearing gabbroic rocks in the Mukayras magmatic complex, which estimated to be about 860 Mt of ore resource containing about 130 Mt of Fe oxide, 46 Mt of Ti oxide, 27 Mt of P oxide, and 0.15 Mt of V oxide (Al-Khirbash et al. 2021).

3.5 Magmatic Mineral Deposits in the Eastern Desert of Egypt

The Precambrian rocks in Egypt are exposed in the north, central and south of the Eastern Desert, in addition to the Sinai Peninsula. The mafic–ultramafic complexes, either ophiolitic or non-ophiolitic, are commonly distributed in the Central (CED) and Southern Eastern Desert (SED) of Egypt, along the Red Sea coast, starting from the latitude 26° N. The mafic–ultramafic complexes in the Eastern Desert of Egypt can be classified into: (1) ophiolitic complexes, and (2) non-ophiolitic complexes. The latter includes both layered mafic–ultramafic intrusions and the Alaskan-type concentrically zoned mafic–ultramafic complexes. Following is a brief description of mineral deposits found in different types of mafic–ultramafic complexes in the Eastern Desert of Egypt.

3.5.1 Chromitite–PGE Deposits in Ophiolites

Dismembered Neoproterozoic ophiolites are widely distributed mainly in the CED and SED of Egypt (Fig. 3.24), where they occur as tectonized masses and mélanges of pillowed metabasalt, metagabbro, and variably altered ultramafic bodies. Almost all of the CED ophiolites of Egypt occuras mélanges that most probably produced by tectonic disruption and deformation by the Najd fault system, rather than representing well-developed suture zones like those in the Arabian Shield of Saudi Arabia (Abdel-salam and Stern 1996; Farahat 2010; Abd El-Rahman et al. 2012). The SED ophiolites of Egypt, on the other hand, are mostly occur as well-developed elongated belts along suture zones, such as the Allaqi–Heiani-Suture (AHS) and Onib-Sol Hamed Suture (OSH) zones (Fig. 3.12). The Gabal Gerf ophiolite nappe represents the largest ophiolitic body in the Egyptian Precambrian basement, and is located midway between the AHS and OSH suture zones (Fig. 3.12). The OSH ophiolites extend in the SW trending beyond the Egyptian borders into the Sudanese territories. Nearly complete ophiolite sequences are present in some places in the Eastern Desert of Egypt such as those in the Fawakhir, Ghadir, and Gerf ophiolites (Abu El-Ela and Farahat 2010; Azer et al. 2013; Obeid et al. 2015). The nearly complete ophiolitic sequences in the Eastern Desert consist of an upper mantle unit of serpentinized peridotites (harzburgites and dunites), crustal sequence of layered and isotropic gabbros, sheeted dykes and massive or pillow lavas (e.g. Abd El-Rahman et al. 2009a, b; Abdel-Karim and Ahmed 2010; Basta et al. 2011; Abdel-Karim et al. 2016). However, the majority of the Egyptian Neoproterozoic ophiolites lack one or more of the above-mentioned lithologies (Stern et al. 2004). The Eastern Desert ophiolites span a range of estimated geologic ages from 890 to 690 Ma (e.g., Kröner et al. 1992; Stern et al. 2004; Ali et al. 2010; Bühler et al. 2014).

The main outcrops of the mafic–ultramafic complexes in the CED and SED display several forms and sizes; as huge continuous masses like those in the Gerf and Abu Dahr areas, or as lensoidal masses in many areas, as well as elongated thrust slices of many others (Fig. 3.24). In addition to the main outcrops, small tectonized mafic–ultramafic lenses and irregular bodies are present as ophiolitic mélange incorporated within the surrounding immature metasedimentary rocks. The upper mantle section of the Egyptian ophiolites consists mainly of serpentinized harzburgite, and to a lesser extent dunite and chromitite pods. Upper mantle harzburgites and dunites are, in most cases, highly altered, where almost all silicate minerals altered to secondary associations represented by serpentinites and talc-carbonate rocks. Primary igneous fresh relics of silicates (olivine and pyroxenes) and oxides (i.e., Cr-spinel) of partly serpentinized ultramafic protolith are still preserved in some localities (Azer and Stern 2007; Ahmed 2013).

Podiform chromitite deposits are widely distributed in almost all localities of the ophiolitic serpentinized ultramafic rocks in the CED and SED of Egypt (e.g., Ahmed et al. 2001; Ahmed 2013). Chromitite deposits occur mainly as small and irregular bodies of variable sizes and shapes (Fig. 3.25a, b), which in most cases are hosted by fully serpentinized peridotites, mainly harzburgite and subordinate

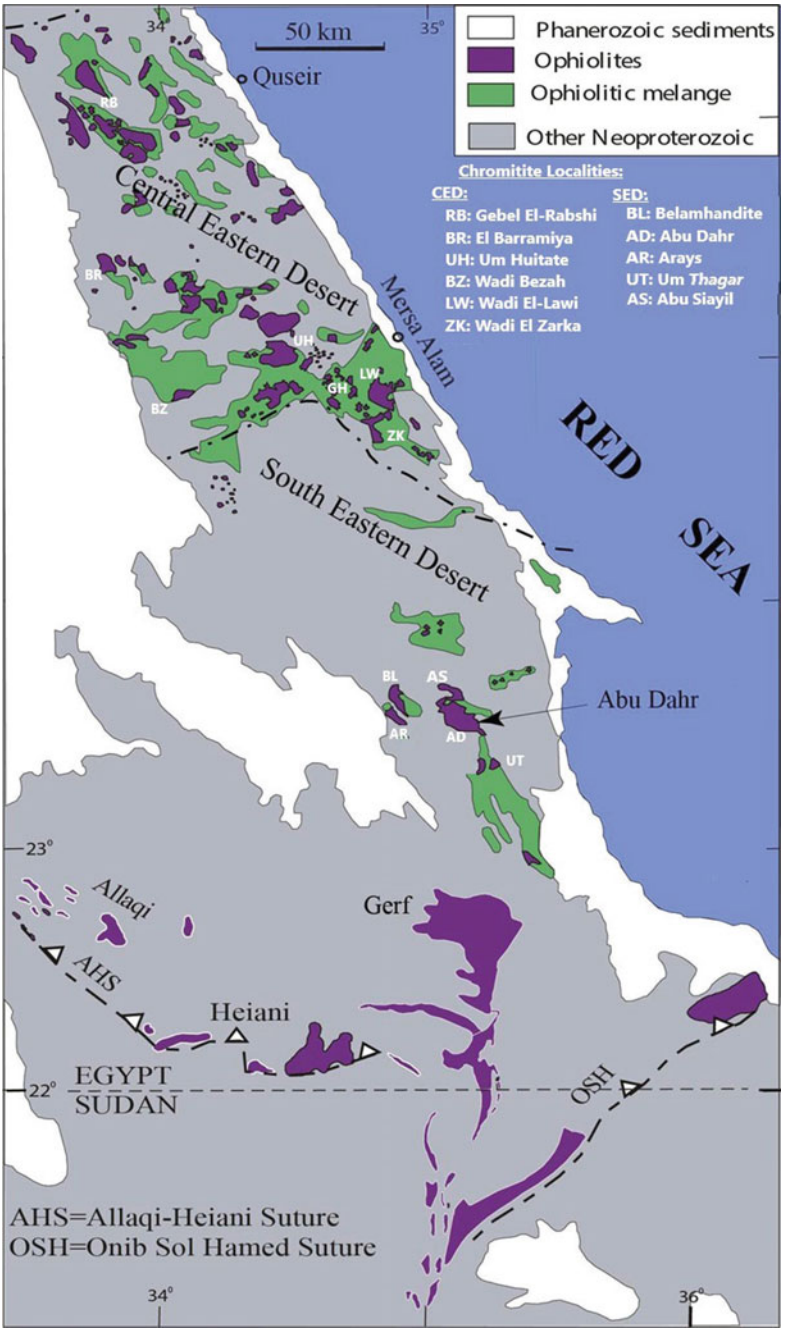

Fig. 3.24 Simplified geologic map of the Eastern Desert of Egypt showing the distribution of ophiolites and ophiolitic mélange with podiform chromitites locations in the CED and SED (modified from Azer and Stern 2007)

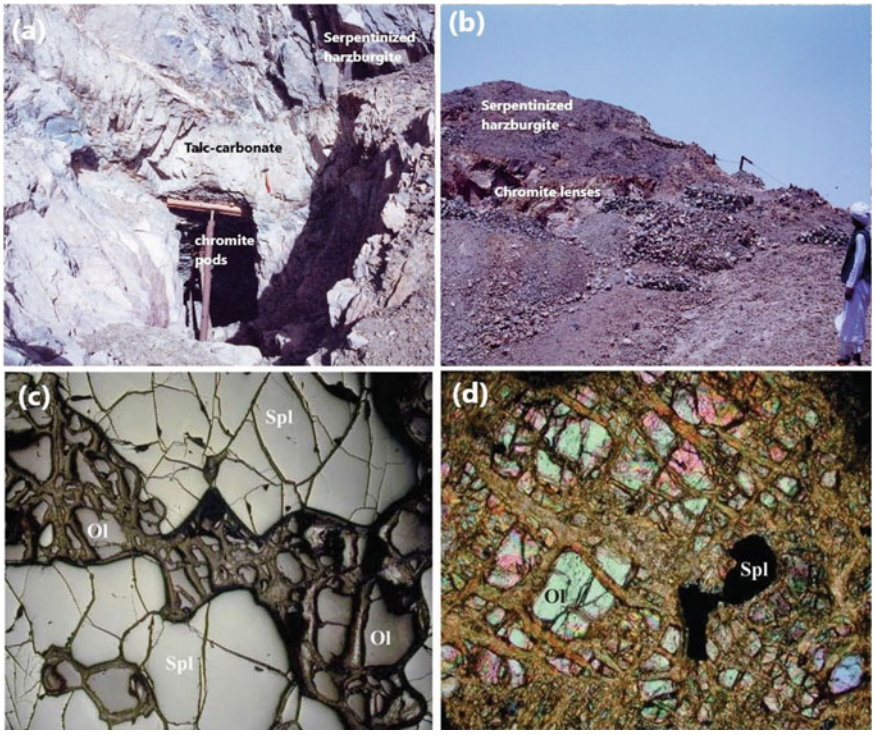

Fig. 3.25 Field photographs of mined-out chromitite pods within serpentinized/talc-carbonate rocks of belamhandite (**a**) and Um Thagar (**b**) of SED of Egypt. **c** Photomicrograph of massive chromitite with relicts of primary olivine, and **d** primary olivine and Cr-spinel in dunite envelope around chromitite pod if SED of Egypt. For more detailed description, refer to Ahmed et al. (2001) and Ahmed (2013)

dunite envelopes. The size of chromitite pods varies from few centimeters up to few tens of meters in many localions. The largest described pods are found in the Abu Dahr area, SED, which reached 50 m across; and have been mined by the Egyptian Refractory Company in the last 50 years. Continuous and discontinuous boudinaged chromitite lenses (Fig. 3.25b), up to several meters thick and few tens of meters long, are located at many places within talc-carbonate and serpentinized ultramafic rocks of the CED and SED of the Egyptian ophiolites. The SED chromitite pods, in most cases, are larger in size than the CED ones. Many of the known chromitite pods have been mined. More details about the distribution of chromitite deposits and their host ultramafic rocks can be found in the literature (e.g., Ahmed et al. 2001; Ahmed 2013; Khedr and Arai 2013, 2016a; Ahmed 2020).

Chromitite deposits of both CED and SED localities display different textures including massive, disseminated, nodular and anti-nodular textured ores. The massive chromitite contains > 90% of the rock volume Cr-spinel, the semi-massive and disseminated chromitites contain about 20–90 volume% Cr-spinel, which is more

euhedral in shape and smaller in size than in the massive ones. In the CED localities, almost all silicate minerals (olivine and/or pyroxenes) are altered to secondary minerals, whereas the SED chromitites (Abu Dahr, Abu Siayil, and Arays), the primary silicate minerals are still preserved locally (Fig. 3.25c) in the interstitial matrix (e.g., Ahmed et al. 2001; Ahmed 2013; Khedr and Arai 2013, 2016a). Dunite envelopes and harzburgite host of the chromitite lenses are, in most cases, fully serpentinized in the CED localities, whereas they are relatively fresh with remnants of primary olivine and orthopyroxene in the SED localities (Fig. 3.25d).

The bulk-rock geochemistry and Cr-spinel chemistry of chromitite deposits in the Eastern Desert of Egypt are distinguishable between the CED and SED localities. The CED chromitites have a wide compositional range from high-Al to high-Cr varieties where the Cr# of Cr-spinel (Cr# = Cr/(Cr + Al) varies between 0.5 up to 0.9 (Fig. 3.26a, b), whilst the SED chromitites are very refractory with restricted Cr_2O_3 contents around high-Cr variety, Cr# > 0.8 (Fig. 3.26a, b). Almost all the chromitite pods from the CED and SED localities are closely located to the Cr–Al join of the Cr–Al–Fe ternary diagram; being display a wide range of Al–Cr contents in the CED case, but high-Cr variety in the SED case, and both of them show low Fe^{3+} contents (Fig. 3.26a). They are all entirely plotted within the ophiolitic chromitites (Fig. 3.26a). The TiO_2 content is very low in all chromitites deposits of all localities in the Eastern Desert of Egypt, which is a common feature of ophiolitic chromitites. The Cr-spinels composition in dunite envelopes of the CED and SED localities usually have comparable Cr_2O_3 contents to those from the associated chromitites, while those in harzburgites are compositionally distinct, being have intermediate Cr# (~ 0.5) in the CED and relatively higher Cr# ($\geq$ 0.7) in the SED ones.

In general, the PGE (platinum-group elements) contents of chromitite deposits are distinctly higher than the associated dunites and harzburgites in all of the Eastern Desert localities. Consistent with Cr-spinel chemistry, the SED chromitites show uniform chondrite-normalized PGE distribution patterns with general negative slope from Ru to Pt, which is a common feature of all ophiolitic chromitites (Fig. 3.27) (Ahmed 2007, 2013). The total PGE contents of the SED chromitites vary from 140 to 320 ppb, where all chromitite pods show strong negative Pt anomalies (Fig. 3.27). The $(Ru/Pt)_N$ value is very high ranging from 11 up to 61, which indicating to a strong decoupling of the IPGE (Os, Ir and Ru) and PPGE (Rh, Pt and Pd). The $(Pd/Ir)_N$ value is very low in chromitites of all SED chromitites; it ranges from 0.04 up to 0.19. The dunites and harzburgites host of the SED chromitites have low PGE, mostly < 50 ppb; being display relatively unfractionated chondrite-normalized PGE patterns. On the other hand, the CED chromitites show variable PGE contents and distribution patterns from locality to locality. Some chromitite deposits in the CED show unusually high PGE contents reached up to 3200 ppb and their dunite envelopes have unexpectedly high PGE content up to 2300 ppb (Ahmed 2007, 2013). The PGE-rich chromitites of the CED commonly exhibit gentle negative slopes of PGE distribution patterns (Fig. 3.27); being enriched in both IPGE and PPGE, whereas the associated dunites exhibit U-shaped patterns due to enrichment in Os, Pt and Pd (Ahmed 2007). The PGE-poor chromitites from other CED localities show low to intermediate PGE contents ranging from 58 to 365 ppb displaying negative slopes

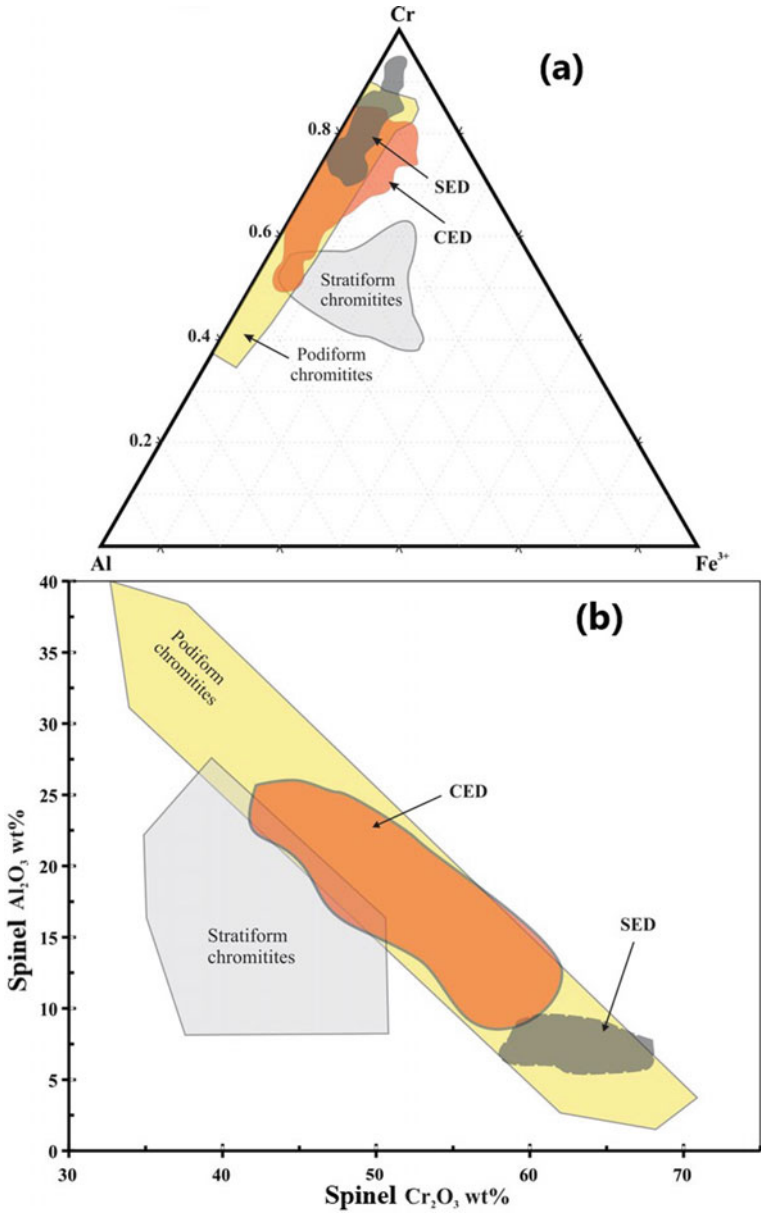

Fig. 3.26 **a** Triangular variation diagram of Cr–Al–Fe^{3+} (atomic ratios), and **b** Cr_2O_3 versus Al_2O_3 wt% variation diagram of Cr-spinels in the chromitite deposits of CED and SED of Egypt. For details, refer to Ahmed (2020)

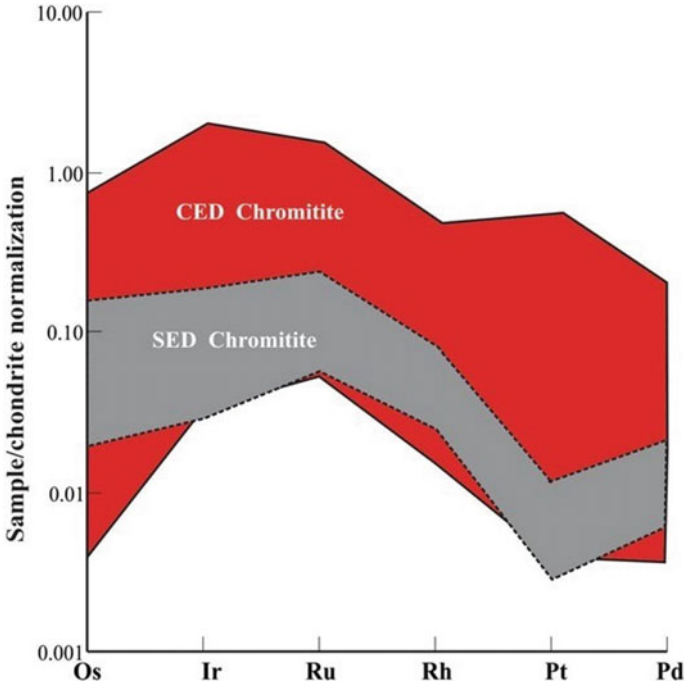

Fig. 3.27 Chondrite-normalized PGE distribution patterns of CED and SED chromitites of Egypt

as in almost all ophiolitic chromitites. Harzburgite hosts in all of the CED and SED localities show approximately flat unfractionated PGE patterns; exhibiting restricted PGE contents (up to 89 ppb) (Ahmed 2007, 2013).

Platinum-group minerals (PGM), especially those of Os, Ir and Ru, are commonly associated with Cr-spinel of chromitite ores. Very few studies were carried out for PGE mineralogy in podiform chromitites (El Haddad 1996; Styles et al. 1996). However, PGE mineralogy and in situ Os isotope geochemistry of the Egyptian chromitites have been thoroughly investigated recently by Ahmed et al. (2006) and Ahmed (2007). These studies found that almost all the chromitite deposits in the CED and SED of Egypt contain various PGM. In general, there are three mineralogical groups of PGM in podiform chromitites of the Eastern Desert of Egypt, arranged in decreasing order of abundance as: (i) sulfides, (ii) alloys, and (iii) arsenides-sulfarsenides. The Wadi El-Lawi PGE-rich chromitite of the CED is the most enriched locality in PGE and PGM among the other studied localities (Ahmed 2007). Consistent with the differences in Cr-spinel chemistry between CED and SED chromitites, there is also a PGM diversity between the two-chromitite domains. The CED chromitites characterized by the predominance of Os-rich laurite as the most popular PGM species, while the Os–Ir alloys are the dominant PGM in the SED chromitites (Fig. 3.28). Os-rich laurite (RuS_2) counts about 54% of the total encountered PGM grains in all the CED studied areas, whereas the least abundant PGM

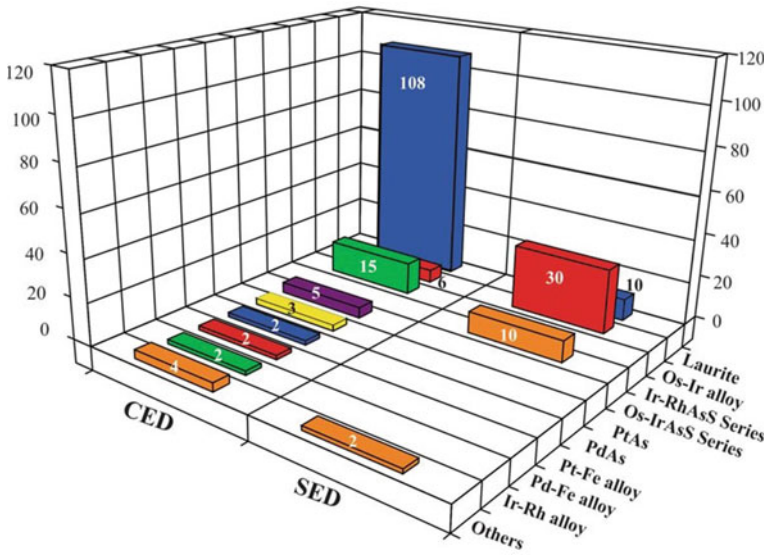

Fig. 3.28 Frequency distribution histograms of PGM in the CED and SED chromitites of Egypt. For detailed description, refer to Ahmed (2007, 2020)

phase is (Pt–Pd)–Fe alloys (Fig. 3.28). In most cases, the PGM grains are predominantly monophase and subordinately show polyphase PGM associations. The most common PGM associations are laurite + osarsite and Os–Ir alloy + laurite. PGE-sulfides (mainly laurite and erlishmanite) form the main PGM grains in the CED chromitites, comprising about 77% (Figs. 3.28 and 3.29) of the total PGM found in the CED chromitites. The grain size of PGE sulfides reached up to 40 μm across, which found exclusively as solitary euhedral crystals embedded within chemically fresh Cr-spinel (Fig. 3.30a). Upon weathering, Os-rich laurite has been altered to porous and ragged Os-poor laurite or to heterogeneous composite grains of Os-rich and Os-poor laurites surrounded by osarsite (OsAsS) (Fig. 3.30b). The Pt–Fe, Pd–Fe alloys and native Pd are the main Pt and Pd phases found as small aggregates, of composite grains in the altered Cr-spinels of the CED chromitites (Fig. 3.30c). Irarsite (IrAsS) and hollingworthite (RhAsS), with wide range of solid solution between them, are the main PGE sulfarsenides in the CED chromitites of Egypt. On the other hand, the PGE mineralogy in the SED chromitites is much simpler than those of the CED examples, comprising mainly of Os–Ir alloys (Fig. 3.30d), few small grains of Os-poor, Os-free, and Os-rich laurites (Fig. 3.30e), and osarsite–irarsite sulfarsenides (Fig. 3.30f). Os–Ir alloys are accounting for 75% of the total PGM grains found in the SED chromitites (Figs. 3.28 and 3.29). For more details about PGM distribution and mineralogy in the Egyptian chromitites, it is recommended to refer to Ahmed (2007).

In-situ Os isotope systematics, in combination with other geochemical characteristics, can provide unique information about the geological settings at which this

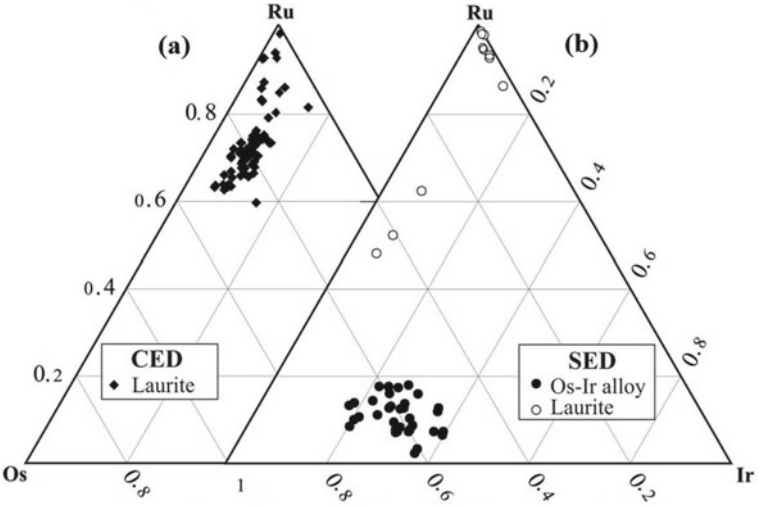

Fig. 3.29 Compositional variation diagram of laurite and Os–Ir alloys in terms of Ru–Os–Ir composition in the CED and SED of the Egyptian chromitites. For detailed description, refer to Ahmed (2007, 2020)

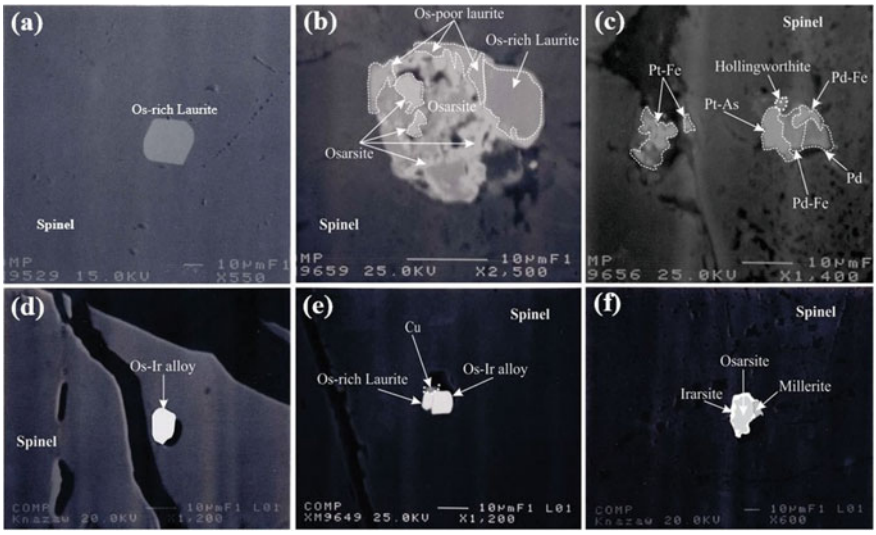

Fig. 3.30 BSE images of PGM grains included within Cr-spinel of the Egyptian CED chromitites (**a**–**c**), and SED chromitites (**d**–**f**). For detailed description, refer to Ahmed (2007, 2020)

PGE mineralization has been formed, as well as about the crustal recycling process in subduction zones. The Os-rich PGM grains encapsulated within fresh Cr-spinel are likely the best materials to constrain the initial $^{187}Os/^{188}Os$ isotope values. Based on the in-situ analysis of Os-rich PGM in both CED and SED chromitites (Ahmed et al. 2006), there is a clear difference in Os isotope ratios between the two chromitite domains. The Os-rich PGM grains from the CED chromitites have a sub-chondritic average $^{187}Os/^{188}Os$ of 0.12261, while those from the SED chromitites have a supra-chondritic $^{187}Os/^{188}Os$ of 0.12928. The isotopic heterogeneity of mantle rocks was attributed to at least two factors: (1) addition or subtraction of Re, and (2) addition of Os with different isotope ratios to the depleted mantle source (Walker et al. 1996; Ahmed et al. 2006). The least radiogenic values are most probably characteristic of the primary magmatic mantle system, whereas the more radiogenic ones are attributed to the crustal assimilation materials (Walker et al. 1996). Therefore, it can be concluded that, if the CED chromitites with primary Os-rich laurite and sub-chondritic Os-isotope ratios represent the primary composition of the mantle in the late Proterozoic ophiolite of Egypt, the chromitites in the SED with the primary Os–Ir alloys and supra-chondritic Os-isotope ratios may represent a modification by subduction components along the subduction zone setting. Therefore, the Egyptian chromitites of Neoproterozoic ophiolite have the following characteristics: (1) diversity of PGM inclusions in Cr-spinel from the CED to the SED chromitites, (2) sub-chondritic and supra-chondritic Os-isotope ratios of Os-rich PGM in the CED and SED chromitites, respectively, and (3) identical petrological characteristics (wide range of Cr-spinel chemistry from high-Al to high-Cr varieties). All of these features are indicating that the mantle rocks of the late Proterozoic ophiolite of Egypt are equivalent to the depleted mantle lithosphere initially formed in mid-ocean ridge setting and then extensively modified in a supra-subduction zone setting (Ahmed et al. 2001, 2006; Ahmed 2007, 2013).

3.5.2 Non-ophiolitic Cu–Ni–PGE Sulfide Occurrences

There are several non-ophiolitic mafic–ultramafic complexes in the central part of the SED of Egypt, which are aligned approximately E-W around 22–24°N (Fig. 3.31). Some of these mafic–ultramafic complexes have the petrological characteristics of Alaska-type concentrically zoned rock associations, whereas others show generally attributable to layered mafic intrusions (Helmy and El Mahallawi 2003; Ahmed et al. 2008; Helmy et al. 2014; Khedr and Arai 2016b; Azer et al. 2017). Examples of these mafic–ultramafic complexes are: Gabbro Akarem, Abu Hamamid, Genina Gharbia, Dahanib, Abu Swayel, El Motaghairat, and Zabargad island in the Red Sea (Fig. 3.31). In most cases, these mafic–ultramafic intrusions have more or less similar lithological characteristics, including a dunite core, then fractionated outward to hornblende peridotite, hornblende gabbro, and then marginal gabbro/gabbronorite. Most of these mafic–ultramafic complexes in the SED have potentially economic to sub-economic Cu–Ni–PGE deposits, such as those in the Gabbro Akarem and

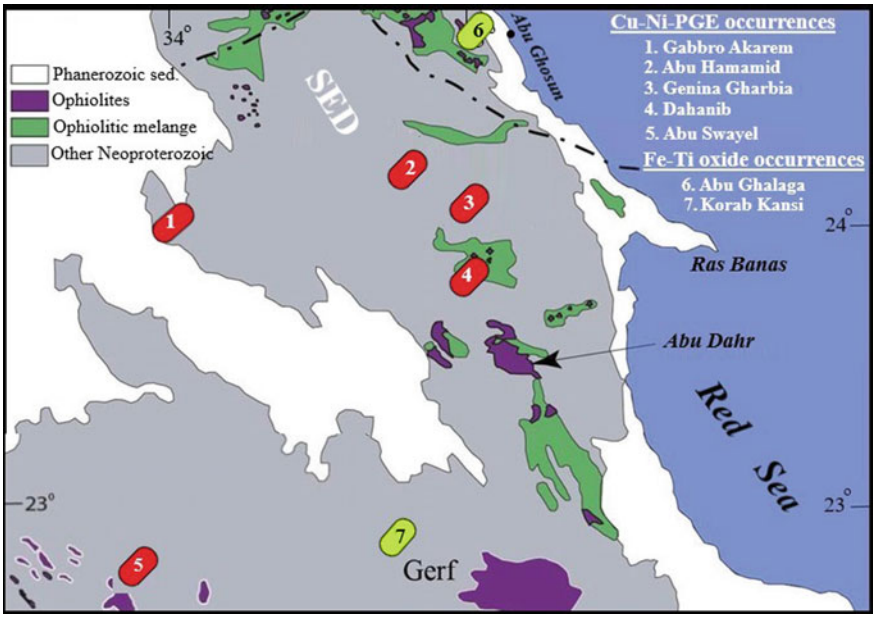

Fig. 3.31 Part of geological map of the Eastern Desert of Egypt showing the distribution of non-ophiolitic (layered/Alaskan-type) mafic–ultramafic complexes, where the Cu–Ni–PGE sulfides and Fe–Ti oxides deposits are located

Genina Gharbia complexes. The Cu–Ni–PGE sulfide mineralization occurs as small massive pockets and disseminations in the ultramafic portions of these complexes (e.g., Abu Swayel, Gabbro Akarem and Genina Gharbia). Other Alaskan/layered-type mafic–ultramafic intrusions of Abu Hamamid, Dahanid and Zabargad Iisland are are sulfide-poor but oxide-rich (Cr-spinel, magnetite and ilmenite). The following is a brief description of the Cu–Ni–PGE mineralization in sulfide-rich mafic–ultramafic occurrences that represented by Abu Swayel, Gabbro Akarem and Genina Gharbia complexes.

The *Abu Swayel* Cu–Ni–PGE sulfide mineralization is one of the famous occurrences for economic to sub-economic mineral deposits in the SED of Egypt. It is located about 185 km southeast of Aswan (Fig. 3.31). The Abu Swayel area covered mainly by metasedimentary rocks and metamorphosed mafic–ultramafic rocks. Non-metamorphosed granitoid intrusions are also common. Hornblende and biotite schists, gneisses and marble are representing the metasedimentary rocks in the Abu Swayel area. The mafic–ultramafic rocks form large bodies, about 500 m long and up to 30 m thick, which conformably interlayered with the metasedimentary rocks (Helmy 2005). All rock units in the Abu Swayel area suffered amphibolite facies metamorphism (4–5 kbars and 650 °C), at about 636 ± 10 Ma ago (Helmy et al. 1995; Finger and Helmy 1998). The sulfide mineralization of Abu Swayel

occurrence occurs mainly as small massive lenses, micro-veinlets, and disseminations in the metamorphosed ultramafic rocks. The massive sulfides fill the interstices between the large plagioclase and garnet porphyroblasts, along the syn-metamorphic shear zone (Helmy 2005). Sulfides also found as veinlets that fill the cracks in the deformed silicate crystals. The main sulfide minerals in the Abu Swayel Cu–Ni–PGE occurrence represented by chalcopyrite, pyrrhotite, pentlandite, pyrite, cubanite ($CuFe_2S_3$) and violarite ($FeNi_2S_4$), whereas sphalerite, mackinawite (FeNiS) and valleriite ($Cu_2Fe_4S_7$) are accessory minerals (Helmy 2005). No primary magmatic textures of sulfide minerals were preserved. However, most of the sulfide minerals were considered as hypogene minerals that exsolved subsequently from a metamorphic monosulfide solid solution during the metamorphic cooling event. Platinum-group minerals (PGM) were observed as micron-size inclusions within chalcopyrite, and they comprise michenerite (PdBiTe), froodite ($PbBi_2$), merenskyite ($PdTe_2$), palladian bismuthian melonite $(PdNi)(TeBi)_2$, sudburyite (PdSb) and geversite (PtSb) (Helmy 2005). The PGM grains occasionally associated with hessite (Ag_2Te), Te-rich electrum (AuAg) and altaite (PbTe). Massive sulfide samples from the Abu Swayel mineralization gave high concentrations of Pd and Pt (13 and 2 ppm, respectively) (Helmy 1996). The Abu Swayel Cu-Ni–PGE mineralization is assumed to be magmatic in origin, which was subsequently remobilized and recrystallized during the amphibolite facies metamorphism. The regional geologic setting of the Abu Swayel area and the mode of occurrence of the mineralized ultramafic bodies suggests that other hidden mineralized ultramafic bodies could be present in the area (Helmy 2020).

The *Gabbro Akarem* mafic–ultramafic intrusion is a typical Precambrian analogue of Alaskan-type complexes; it is concentrically zoned with dunite core enveloped by pyroxenites and marginal gabbros (Helmy and El Mahallawi 2003). It is located in the center of SED of Egypt, about 130 km east of Aswan (Fig. 3.32). The Gabbro Akarem mafic–ultramafic complex consists of eastern and western bodies, about 1.5 km apart. The eastern body is about 7 × 2 km, and the western body of the complex is about 3 × 0.5 km, both of which composed of, in decreasing order of abundance, plagioclase-hornblendite, olivine-plagioclase hornblendite and peridotite (Fig. 3.32). Plagioclase hornblendite is the major rock type; being forms the outer margins of the intrusion in contact with the metasedimentary host rocks. The ultramafic rock units form the inner part of the intrusion as elongated bodies oriented in a NE–SW direction, parallel to the regional trend of the intrusion (Fig. 3.32). The peridotite cores of the eastern body are highly mineralized (about 30% of the rock volume is sulfides), but the margins of the intrusion are less mineralized (<10% sulfides by volume) (Helmy and El Mahallawi 2003). The Gabbro Akarem intrusion was dissected, brecciated, and displaced by a large number of normal faults; one of them has displaced the intrusion into two parts. The available estimation of ore reserves, based on surface showings and drill cores (total 1888 m), was about 700,000 tons of ore, with average grade of 0.95% (Cu + Ni), and less than 1.0 ppm (Pt + Pd) (Helmy and Mogessie 2001). The sulfide mineralization is closely associated with

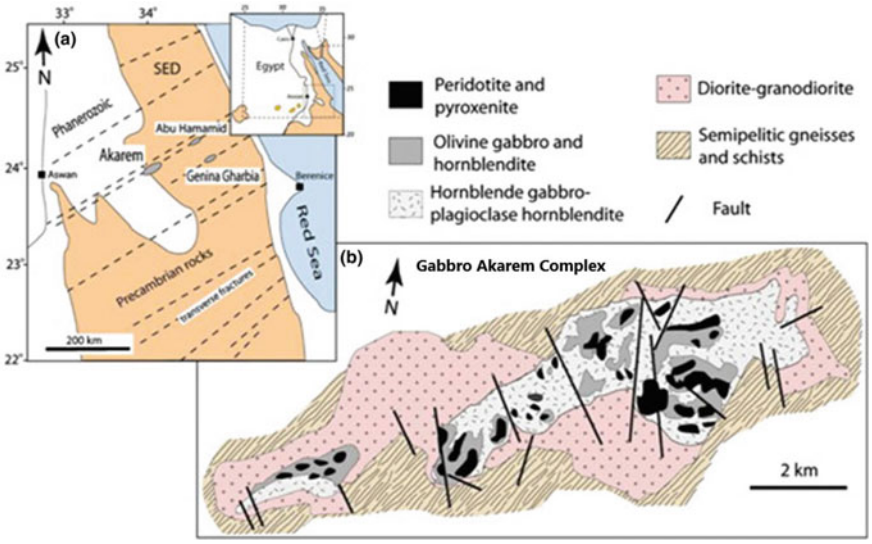

Fig. 3.32 **a** Location map of the Alaskan-type mafic–ultramafic complexes in the Eastern Desert of Egypt, and **b** a geologic map of Gabbro Akarem intrusion (from Helmy 2020)

the inner olivine-rich cores (dunite-dominated pipes), where the massive and disseminated sulfide minerals found as net-textured ore. Sulfides are occasionally associated with Al-Mg-rich spinel and Cr-rich magnetite. The sulfide mineralogy is mainly pyrrhotite, pentlandite, chalcopyrite and minor cubanite, which show typical primary magmatic textures. Meresnkyite [$(Pd,Pt,Ni)(Te,Bi)_2$], michenerite [(Pd,Pt)BiTe], and Pd-bearing bismuthian melonite [$(NiPd)(TeBi)_2$] are commonly form as micron-size inclusions in pyrrhotite and along cracks of other sulfides. The magmatic textures are overprinted partly by post-intrusion shearing, which resulted in minor redistribution of sulfides by post-magmatic fluids (Helmy and Mogessie 2001).

The *Genina Gharbia* mafic–ultramafic complex, which located at about 40 km east of Gabbro Akarem (Figs. 3.31 and 3.32), is also a concentrically zoned intrusion that covering a total area of about 9 × 3.5 km. The complex comprises mainly of hornblende harzburgite, hornblende-bearing peridotite, hornblende pyroxenite, and marginal gabbros, which intruded into Precambrian metasedimentary and metavolcanic rocks (Helmy 2005; Helmy et al. 2014). The Genina Gharbia intrusion is essentially unmetamorphosed, but it is strongly faulted and sheared where most of the original igneous contacts have been obliterated. The common abundance of hornblende, biotite, and apatite in various rock units of the intrusion is a characteristic feature of a hydrous parent magma (Helmy 2004). The sulfide ore was traced on surface and by four exploratory drill cores with a total of 621 m. Ore reserves were estimated based on drill cores at about 270,000 tons of ore, with an average grade of 1.5 wt% (Cu + Ni) and Cu/Ni ratio less than unity (Helmy 2004). To our knowledge so far, no mining activities have been carried out in the Genina Gharbia area. The

Cu–Ni–PGE mineralization of the Genina Gharbia complex found either as massive batches in hornblende gabbro or as disseminated ore in hornblende harzburgite. The sulfides mineralogy consists of pyrrhotite, pentlandite, chalcopyrite, pyrite, violarite, cubanite, and to a lesser extent, cobaltite-gersdorffite, nickeline, sphalerite, molybdenite and valleriite (Helmy 2005). The wide compositional range of Pd melonite and the common presence of native Te led to the suggestion that the Genina Gharbia Cu–Ni–PGE mineralization most probably formed in the late magmatic stage of the mafic magma crystallization (Helmy 2004, 2005).

3.5.3 Non-ophiolitic Fe–Ti Oxide Occurrences

Several non-ophiolitic (layered/Alaskan-type) mafic–ultramafic occurrences are present in the CED and SED of Egypt; some of them are hosting economic to sub-economic Fe–Ti oxide deposits. The host rocks of these magmatic Fe–Ti oxides mineralization are mostly fresh gabbroic rocks, including olivine gabbros, melanorite, and anorthosite. The best examples of these Fe–Ti oxides-bearing complexes are (Fig. 3.31) Abu Ghalaga, Umm Effein, Umm Ginud, Korab Kansi, Wadi Rahaba, Abu Dahr, Hamra Dome and Wadi El-Miyah (Amin 1954; Basta and Takla 1968; Khedr et al. 2020a, b). Except of Abu Ghalaga area, all other occurrences have too small tonnage and low-grade ores to be mined economically. Following is a brief description of the famous Fe–Ti oxide mafic–ultramafic occurrences in the Eastern Desert of Egypt.

The ***Abu Ghalaga*** Fe–Ti oxides mineralization (also called in the literature as Abu Ghalaga ilmenite) is the most promising economic magmatic Fe–Ti oxide occurrence in Egypt. It is located at about 20 km to the west from the Abu Ghosun port on the Red Sea coast (Fig. 3.31). The Abu Ghalaga Fe–Ti oxide deposits occur either as massive lenses and layers, or as disseminated ores throughout the host gabbros and anorthosite. The mineralized zone may attain layer thicknesses of up to 150 m, which trend NW-SE and dips 30°–45° with an extension up to 350 m (Amin 1954; Basta and Takla 1968). The ore-rich zone in the Abu Ghalaga area exists as surface oxidized massive ore rich in hematite (~80% of the rock volume) with up to 71% ilmenite, and as disseminated ore (~55% of the rock volume) with up to 62% ilmenite (Basta and Takla 1968). The Abu Ghalaga massive ore is dominated by ilmenite (about 67% on average), in addition to subordinate amount of titano-magnetite (4–17%), hematite (13–18%) and up to 2% sulfides (Khalil 2001). Hematite-ilmenite or hemo-ilmenite intergrowths are the most common ore textures of the Abu Ghalaga Fe–Ti oxide mineralization. The Abu Ghalaga Fe–Ti oxide occurrence underwent several evaluation programs to estimate the ore reserves and extension by the Geological Survey of Egypt and other authorities, where more than 30 diamond-drill boreholes of about 3000 m length were investigated. The available data of Abu Ghalaga ore reserves revealan indicated resourceof about 40 Mt, with an average grade of about 35% TiO_2 (Hussein 1990).

The *Korab Kansi* mafic–ultramafic intrusion is another important Fe–Ti oxide occurrence in the SED of Egypt, which is located to the west of Gebel El Gerf (Figs. 3.31 and 3.33) and covers an area of about 100 km^2, where a considerable ore reserve was estimated (Nasr et al. 2000; Makhlouf et al. 2008; Khedr et al. 2020b). The Korab Kansi area lies along the E-W Allaqi-Heiani suture zone, and cut by the N-S Hamisana shear zone (HSZ) (Stern et al. 1989). The HSZ separats the Korab Kansi intrusion from the ophiolitic mafic–ultramafic bodies to the east, which includes El-Gerf and Abu Hudeid ophiolitic massifs. The area consists of a Neoproterozoic (741–720 Ma, Kröner et al. 1992; Zimmer et al. 1995) mafic–ultramafic intrusion

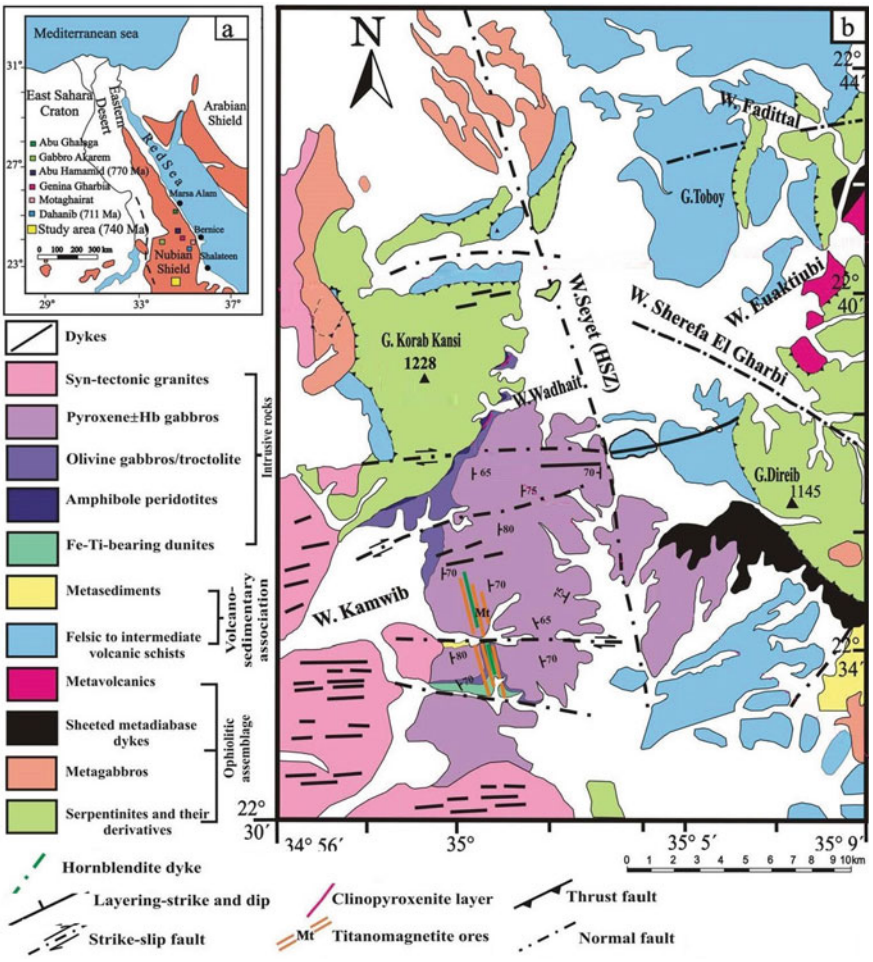

Fig. 3.33 **a** Location map of the layered/Alaskan-type mafic–ultramafic complexes in the Eastern Desert of Egypt, and **b** a geologic map of Korab kansi intrusion in the SED (modified from Khedr et al. 2020b)

in the southern part, and ophiolitic mélange represented by serpentinites and talc carbonates in the northern part (Khedr et al. 2020b). The Korab Kansi mafic–ultramafic body cuts the ophiolitic mélange rocks along their southern to southeastern margin (Fig. 3.33). The lithology of the Korab Kansi intrusion is composed mainly of dunite layers, pyroxene gabbro, pyroxene-hornblende gabbro, with subordinate olivine gabbro, troctolite, and gabbronorite. The Fe–Ti oxides are either found as massive concordant layers parallel to the igneous layering of the complex, or as disseminated ore throughout the dunite and gabbroic layers. The Fe–Ti oxides mineralization occurs as multiple discontinuous parallel lenses, as well as irregular bodies and layers (Fig. 3.34a, b) in the form of dyke-like bodies within the gabbroic rocks. The Fe–Ti oxides are present within troctolite rock. The igneous layering of the Korab Kansi intrusion strikes mostly N-S and steeply dipping toward east except in the eastern side where the layering steeply dipping toward west. The Fe-Ti oxide layers vary in width from 1.5 to 5 m and can be traced NNW-SSE for about 600 m, but sometimes can be extended up to 2.5 km along strike (Makhlouf et al. 2008). The dunite bodies are coarse-grained adcumulate rocks composed mainly of various proportions of olivine, titano-magnetite, ilmenite and accessory sulfides. The mineralogy of Fe–Ti oxides is represented by titano-magnetite, magnetite and ilmenite, which found as intercumulus oxide phases between cumulus olivine (Fig. 3.34d). Primary magmatic textures are well-preserved in the Fe–Ti oxide minerals and their

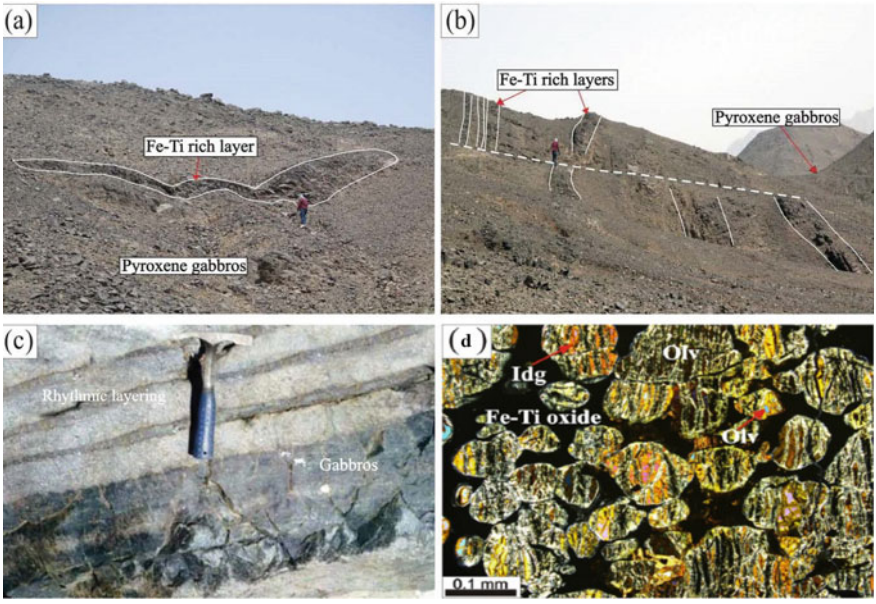

Fig. 3.34 Field photographs **a**–**c** of the Fe–Ti rich layers (**a**, **b**), and rhythmic layering (**c**), and photomicrograph (**d**) of the Fe–Ti oxides mineralization of the Korab Kansi mafic–ultramafic intrusion, SED of Egypt (quote from Khedr et al. 2020b). For detailed description, refer to Khedr et al. (2020b)

host rocks, with small-scale rhythmic layering of massive oxides intercalated and/or associated with hornblendite bands (Fig. 3.34c) (Makhlouf et al. 2008; Khedr et al. 2020b).

At the *Abu Dahr* occurrence, the mineralization zone is striking NE-SW as discordant dyke-like body in metagabbros. The Abu Dahr ore consists of considerable amount of apatite, which can be considered as a nelsonite ore (apatite-Fe–Ti oxide ore) hosted by anorthosite. This nelsonite-like deposit at Abu Dahr occurrence is mostly similar to those in the Wadi Kamal occurrence in Saudi Arabia (Arabian Shield) that described by Harbi (2008). The Fe–Ti oxide deposits in the Eastern Desert of Egypt are similar to those distributed worldwide, which are most probably formed by in situ fractional crystallization of Fe–Ti-P from a volatiles-rich gabbroic magma followed by injection into the anorthositic/gabbroic lithology at high fO_2. An alternative mechanism is also suggested for the formation of Fe–Ti oxide deposits in mafic–ultramafic complexes by a liquid immiscibility model between silicate-rich melt and oxide-rich melt (Duchesne and Liégeois 2015).

3.6 Magmatic Mineral Deposits in Sudan

In general, mineral occurrences in Sudan are concentrated mainly in some belts of the country including (Fig. 3.35): (1) the Red Sea Hills area of NE Sudan, (2) Bayuda Desert (North Central Sudan), (3) the Gebel Abyed and Gebel Rahib areas (NW Sudan), (4) the Ingessana Complex (Eastern Sudan), (5) Gebel Marra area (Western Sudan), and (6) the Nuba Mountains (South Central Sudan). The mafic–ultramafic complexes in Sudan have ophiolitic upper mantle-lower crust associations, whereas layered/Alaskan-type complexes are rare or absent (Ministry of Minerals, Geological Research Authority of Sudan-GRAS). Podiform chromitite deposits and Ni–sulfide (and Ni-laterite) ores are the most important orthomagmatic mineral deposits associated with mafic–ultramafic rocks in Sudan. Anomalous Ni values have been found in some lateritic profiles associated with ophiolite mafic–ultramafic rocks at Ingessana Hills, Gebel Rahib, and Nuba Mountains (Fig. 3.36). Chromitite ore deposits in Sudan occur mainly in the Ingessana Hills in the Blue Nile region, as well as in some other occurrences such as Hammissana, Sol Hamid in the Northern Red Sea Hills, the Nuba Mountains in Southern Kordofan, Gebel Rahib Northwest Sudan, and Gebel El-Tawil in Central Butana in Southern Sudan (Fig. 3.36). The chemistry of chromitite ore shows different grades from high-Al to high-Cr varieties (Table 3.4). Podiform chromitite occurrences in Sudan were first reported at early of the 1930s, and have been processed as small-scale minessince the 1950s. Detailed geological studies have shown the existence of many localities of Neoproterozoic Alpine-type ultramafic massifs, as parts of dismembered ophiolites along highly strained suture zones of the Pan-African ANS.

The ultramafic mantle sequence of these dismembered ophiolites contains numerous pods of chromitite ore, where at some localities considered as economic

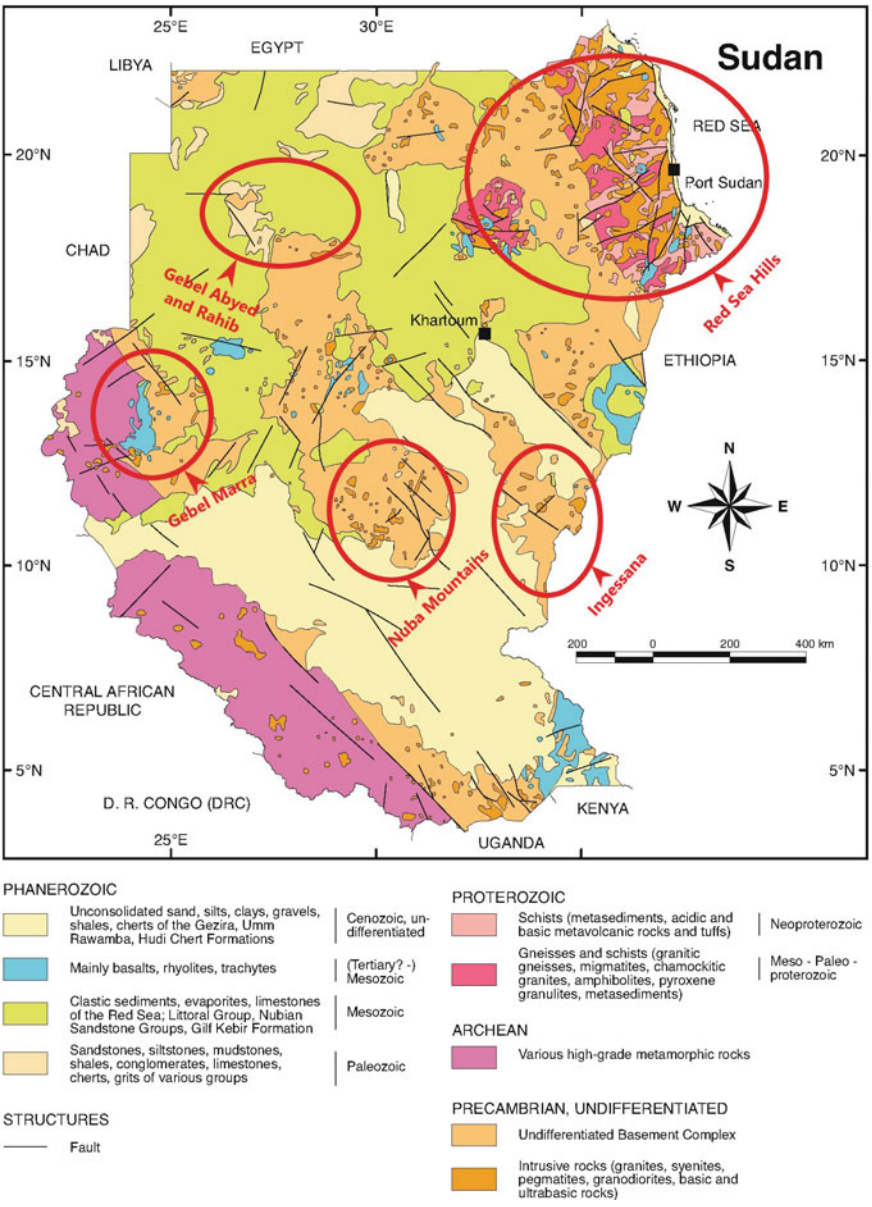

Fig. 3.35 Simplified geological map showing the main mineralized sectors of the Sudan

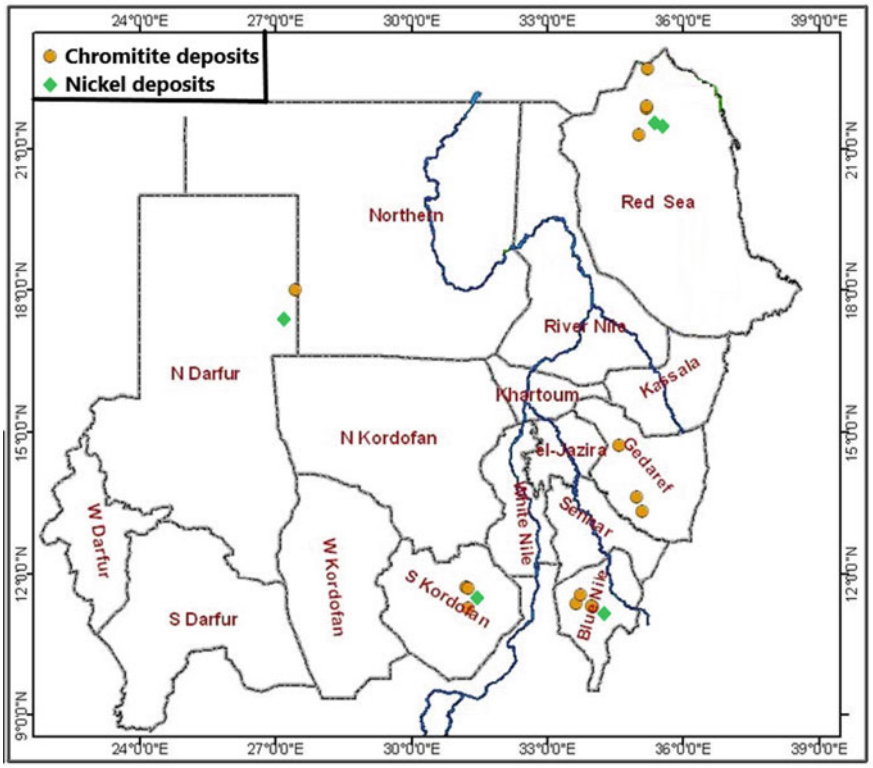

Fig. 3.36 Location distribution map of Chromite-Ni deposits in the mafic–ultramafic complexes of Sudan

Table 3.4 Average geochemical analyses of podiform chromitite deposits from different localities of Sudan (Ministry of Minerals, Geological Research Authority of Sudan-GRAS)

Locality	Cr_2O_3	Fe_2O_3	Al_2O_3	SiO_2
Ingessana	58.57	3.04	11.42	0.22
Qala En Nahak	25–37.8	16.00	01.87	10.56
G. Rahib	57.00	2.28	14.23	0.032
Oshib	55.52	2.44	1.85	0.17
Hamissana	28.0	3.21	17.19	0.28
Nuba Mt	30.00	22.00	12.00	12.00

deposits. Following is a summary of the some of these economically important areas, based on their potentialities and available information.

3.6.1 Ingessana Hills Area

The Ingessana Hills area is located in the southern Blue Nile of Sudan, about 80 km from the Ed Damazine city, the capital of Blue Nile Governorate (Fig. 3.37). This area is famous for gold, chromite, and Ni-laterite occurrences, and is promising for further mineral exploration. The basement rock assemblages of the Ingessana area comprises various types of granitoids, schist, marble and ophiolitic mafic–ultramafic rocks that are variably altered to serpentinite, and to talc-carbonate mineral assemblages (Fig. 3.37). The Ingessana complex is a large Neoproterozoic mafic–ultramafic massif representing the main and central parts of the Ingessana-Kurmuk Ophiolite Belt, which extends from the Nile to the northwest of the Red Sea Hills as major thrust slices (Fig. 3.37). The protolith of mafic–ultramafic units of the complex is extensively serpentinized and silicified dunite and harzburgite at the contact with the granite intrusions. The lower, highly serpentinized ultramafic rocks are overlain by less serpentinized peridotite, minor pyroxenite, layered gabbro and dolerite. The chromitite mineralization zones are associated with NE-SW trending shear zones. In addition to the podiform chromitites, mineralization in the Ingessana Hills that associated with ophiolitic belts includes asbestos, talc, and base metal (Cu, Ni, Co) mineralization. The Ingessana chromitite ore is considered as one of the largest chromite ore deposits in Sudan. There are more than a hundred chromitite

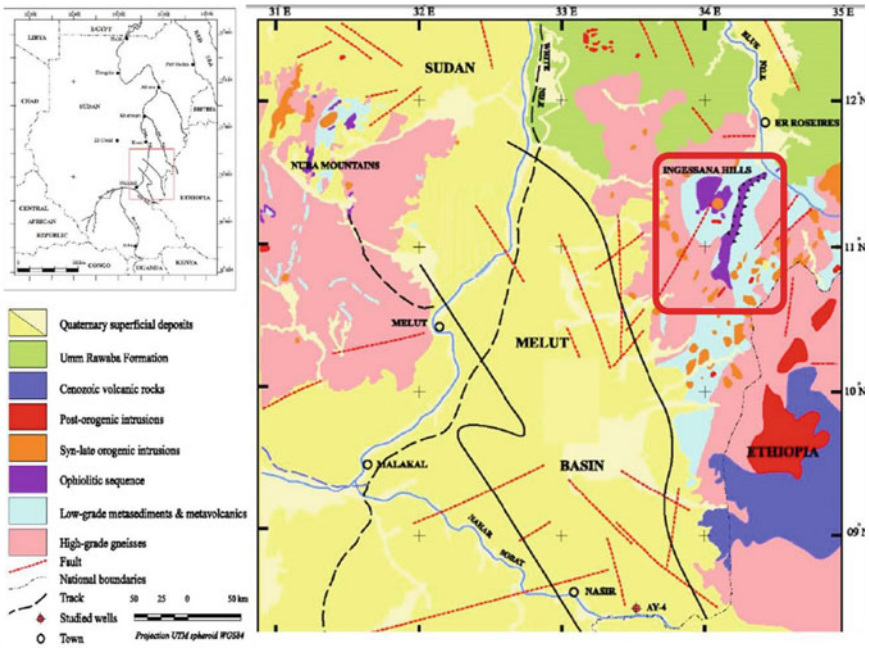

Fig. 3.37 Simplified geological map of the Ingessana Hill and surrounding areas, showing the extension of the ophiolitic mafic–ultramafic rocks

occurrences in the Ingessana massif hosted by the lower part of serpentinized dunite-harzburgite and associated talc carbonates. Chromitite pods are mainly lenticular in shape and range in size from 10 to 50 m long, 1 to 3 m thick, and extend from 30 to l00 m down-dip. The chromitite ore is mainly massive, compact, often sheared, and consists of coarse-grained brecciated Cr-spinel. The ore is chemically classified as a metallurgical grade, with a high Cr/Fe ratio. The ore reserves have been estimated at about 2 Mt with an average grade of 58.57 wt% Cr_2O_3, 3.04 wt% Fe_2O_3, 11.42 wt% Al_2O_3, and 0.22 wt% SiO_2 (Table 4.4) (Habashi and Bassyouni 1982; Ahmed 1998; Ministry of Minerals, Geological Research Authority of Sudan-GRAS). Systematic underground chromite mining started in 1963 by a state-owned company with an annual capacity of about 11,020 tons. The largest reserve in the Ingessana Hills is located in the Gam Mining area, which is leased to the national "Advanced Mining Works Company". With progress of the mining operations, it is anticipatedthat a much resource will be developed.

In addition to the high-grade massive ores, disseminated low-grade banded chromitite ores are common in the Ingessana Hills area, with up to 25 wt% Cr_2O_3. Furthermore, low-grade ore reserves in the dumps of the old mines were calculated totaling of about 120,000 tonnes with average grade of 22.6 wt% Cr_2O_3. New discoveries of chromitite ores of variable grades were reported everywhere in the Ingessana area. In addition, the oxidized capping of ultramafic rocks is strongly serpentinized forming a lateritic discontinuous zone with anomalous Ni concentration of an average grade up to 2.8 wt% Ni over an extensive length of about 200 km aligned to the NE–SW of the Ingessana Hills. The weathered lateritic profiles of Ingessana Hills are significant potential targets for Ni-laterite deposits in the region.

3.6.2 Qala En Nahal—Umm Saqata Areas

The Qala En Nahal—Umm Saqata area is located in the southwestern part of El-Gadarif State, Eastern Sudan, close to the Sudanese-Ethiopian border (Fig. 3.38). The area is located to the northeast of the Blue Nile–Dinder–Rahad Rivers. The Qala En Nahal—Umm Saqata area is a transition area between the northern and southern terrains of the Neoproterozoic Pan-African ANS. The main rock units in the Qala En Nahal—Umm Saqata areas include: (1) mafic–ultramafic massifs known as Qala En Nahal–Umm Saqata ophiolitic complex, which structurally overlying a layered sequence of low-grade volcano-sedimentary units, and (2) syn- to late- and post-orogenic granitoid complexes intruded the previous sequences. The dismembered ophiolite complex represents the oldest rock units in the area, and has been thrust over a low-grade metavolcano-sedimentary sequence. The mafic–ultramafic complex consists of, from the bottom upward, chromite-rich highly serpentinized peridotites, overlain by mafic–ultramafic cumulates comprising peridotite and pyroxenite, and grading upward into layered gabbro. Chromitite deposits at Qala En Nahal and Umm Saqata areas found as small pods, lenses of massive ore hosted in serpentinized dunite–harzhurgite association. Chromitite pods vary in length between 3 and 6 m,

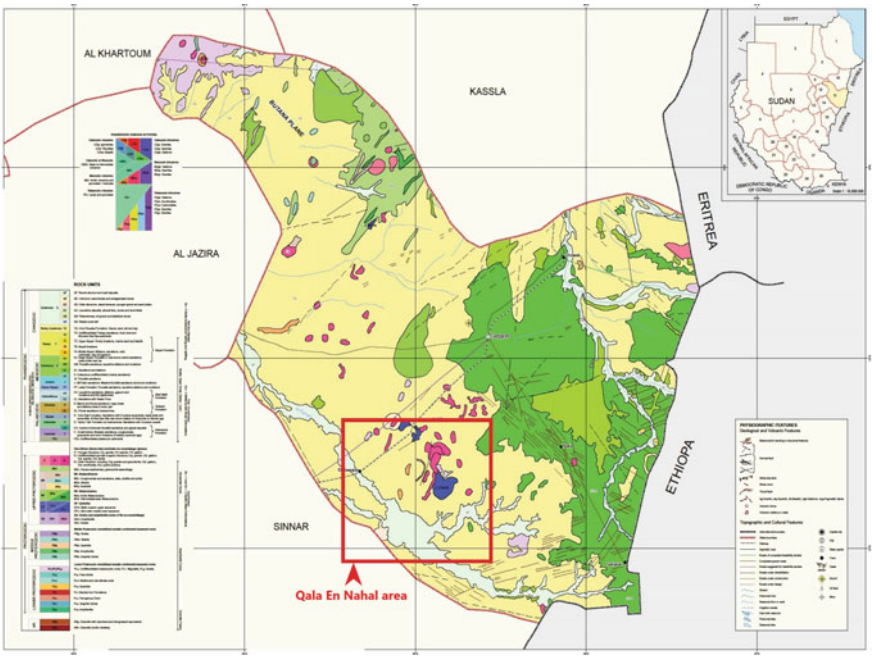

Fig. 3.38 Simplified geological Map of Qala En Nahal–Umm Saqata areas showing the distribution of mafic–ultramafic complexes and their mineralization

thickness between 1.5 and 2 m, and ore grade ranging between 25 and 38 wt% Cr_2O_3 (Table 3.4). The ore reserve estimation of Qala En Nahal—Umm Saqata areas exceeds 600,000 tons, but some occurrence in the area are not estimated (Suleiman 1994; Ahmed 1998; Al-Tigani et al. 2019). Recent mineral resource estimates by wet chemical analysis (Al-Tigani et al. 2019) revealed that the ore grade of Qala En Nahal—Umm Saqata areas is relatively low, containing 24.9 wt% Cr_2O_3; 8.6 wt% Fe_2O_3; 24.2 SiO_2%; 13.1% MgO; 0.02% CaO; and low average Cr/Fe ratio of about 2.9. This obtained result from this study explained that the mineralization style is a disseminated type and the main gangue materials are silicates (e.g., serpentine) with low Cr/Fe ratio (Al-Tigani et al. 2019).

3.6.3 The Nuba Mountains

The eastern and western margins of the Nuba Mountains, in the central Sudan (Fig. 3.35) is predominantly covered by low-grade metamorphosed volcano-sedimentary sequence with dismembered ophiolitic rocks. The lower part of the ophiolite sequence comprises serpentinized dunite-hatzburgite rocks that contain podiform chromitite lenses. More than 26 chromite occurrences have been recorded in

the mafic–ultramafic rocks of the Nuba Mountains area (German-Sudanese Technical Corporation Project Reports 1971–1984). The assay analyses indicated an average grade containing about 30 wt% Cr_2O_3; 12 wt% Al_2O_3; 22 wt% Fe_2O_3 and 12 wt% SiO_2 (Table 3.4). The ore is mainly composed of Cr-spinel grains intimately associated with interstitial silicates. An anomalous Cu–Zn–Ni metals concentration has been reported from discontinuous gossans outcrops in the Nuba Mountains area. The average Ni content in the different gossans cover ranges between 112 g/t in the Biteria area and 5744 g/t in the Gebel Tumluk area, which show the highest Ni value of about 1.00 wt.%.

3.6.4 The Red Sea Hills Region

The Red Sea Hills region (also named central-eastern Bayuda Terrane) of Eastern Sudan is an integral part of the Neoproterozoic Pan-African ANS. It comprises distinct terranes of volcano-sedimentary arc sequences, and plutonic equivalents, in which all are separated by ophiolite-decorated suture zones (Fig. 3.39). The mafic–ultramafic rocks of the Red Sea Hills consist mainly of olivine-gabbronorite, olivine-websterite to lherzolite and serpentinite at a locality just adjacent to central Dam El Tor FTB (Barth and Meinhold 1979). Pyroxenites, metagabro, and metachert have been also reported at Wadi Kurmut and Abu Harik (Essamaldeen 2005), and in the east of the Nile (Lissan 2003; Evuk 2007; Lissan and Bakheit 2011). In addition, small outcrops of serpentinized ultramafic rocks and suspected pillow basalt were found west and in the central part of Dam El Tor FTB (Figs. 3.39) (Evuk et al. 2014). Pyroxenites were also encountered at Azuma, El Shereikh and Absol area. These rocks are interpreted in NE Sudan as dismembered Neoproterozoic ophiolites (Abdel-Rahman 1993, Abdelsalam et al. 1998) that are representing suture zones. In the Red Sea Hills, there are three major suture zones. From the north to the south, they are (Figs. 3.39): (1) Onib-Sol Hamid, (2) Nakaseib, and (3) Barka sutures. Chromitite deposits have been reported from the basal units of these ophiolitic ultramafic rocks within the three suture zones. However, only the Onib ophiolite occurrences are considered as the economic interest. The Onib ophiolite has a number of chromitite pods as small lenses and schilieren in Wadi Sudi area. The most important occurrence is found in Wadi Hamissana area where massive and sub-massive podiform chromitite lenses are scattering within the basal serpentinite units. The largest chromitite body reached up to about 250 m long, 5 m average thickness, and extends about 100 m down-dip. The geochemical assay gave an average grade of 28 wt% Cr_2O_3, with 2.5 Cr/Fe ratio. In addition, small pockets of massive chromitite have been reported from highly serpentinized ultramafic rocks of the Oshib ophiolite in the Nakaseib suture (Fig. 3.39). The geochemical analysis of the Oshib chromitite ore shows metallurgical grade with high average Cr_2O_3 contents (Table 3.4).

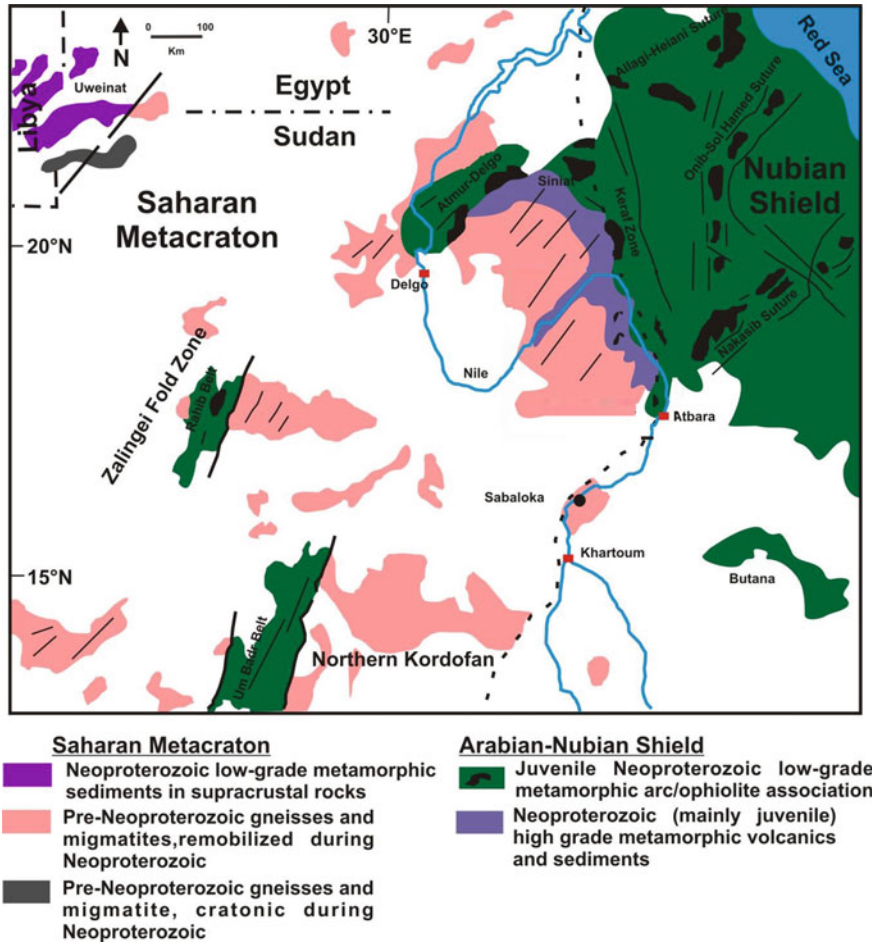

Fig. 3.39 Simplified geologic map of the Neoproterozoic rocks in the northeastern Sudan (Red Sea Hills) and their extension into the Saharan Metacraton, showing the main suture zones and ophiolitic complexes (after Küster et al. 2008)

3.6.5 The Gebel Rahib Occurrences

The Gebel Rahib area is located in the northern Darfur State (Figs. 3.35 and 3.39). The lithology of Gebel Rahib area is dominated by a low-grade metamorphosed sequence of rift-type sedimentary rocks with complete, but dismembered, Neoproterozoic ophiolite complexes. The mafic–ultramafic rocks were recorded in the western and eastern parts of Gebel Rahib area, associated with folded metasedimentary rocks (Abdel Rahman et al. 1990). The contact between the mafic–ultramafic rocks and the associated folded metasedimentary rocks is obviously a tectonic contact, where there is no evidence for contact metamorphism. The chromitite-bearing ultramafic

rocks are generally highly serpentinized and being occur in the topographically higher levels of the ridges. These chromitite-bearing ultramafic ridges apparently overlain by peridotitic, gabbroic and hornblende-pyroxenite cumulates, which commonly show discontinuous layering. Three zones of chromite mineralization were identified in the eastern and western parts of Gebel Rahib ultramafic rocks, the major of which extends for more than one km and is about 200 m wide in a NNE-SSW direction. The zone contains several pods of chromitite ore some of which may attain 50 m in length and about 2–3 m in thickness that hosted by highly serpentinized dunite-harzburgite lithology. The ore is coarse-grained, very compact, massive and sometimes disseminated. The mineralization is promising, with metallurgical grade variety of an average grade of 57 wt% Cr_2O_3, 2.28 wt% Fe_2O_3, 14.23 wt% Al_2O_3, and 0.03 wt% SiO_2 (Table 3.4). The high bulk-rock Cr_2O_3 content of the chromitite pods along with high Cr# of Cr-spinel in chromitites and ultramafic host rocks of Gebel Rahib occurrences suggested that the ophiolite complex of Gebel Rahib was originated in a supra-subduction zone environment (Abdel Rahman et al. 1990). The oxidized cap of Gebel Rahib mafic–ultramafic rocks forms a laterite profile with a thickness of about 25 m cover an area of about 1000 km^2, being contains a high Ni concentration that encourages exploration for lateritic Ni deposits.

3.6.6 The Southern Sudan Occurrences

Chromitite deposits have been reported in the Southern Sudan from two different areas; the Juba and Kapoeta-Nagishot areas. In the River Kit area, to the southeast of Juba town, a chromitite ore occurrence was discovered on the footpath between River Kit and River Afoyi to the east. The chromitite mineralization of this area is as small lenses (2–3 m long) associated with talc schist, in a banded biotite gneiss succession. The chromitite pods composed of a massive and brecciated Cr-spinel grains. The chemical analyses of chromitite ore in this area gave an average grade of about 37 wt% Cr_2O_3, low Cr/Fe ratio of 2, and relatively low Fe_2O_3 content of approximately 13 wt%. Although the chromitite deposits in Southern Sudan are small and of relatively low grade, this occurrence could be a significant source of chromitite deposits in case of the possibility of discovering more extensive source in the area. On the other hand, the mafic–ultramafic rocks in Kapoeta-Nagishot area crop out as dyke-like bodies in the south and southwest of the Southern Sudan. The reported chromitite deposits hosted in serpentinized ultramafic rocks and talc schist are of metallurgical grade variety (48–50 wt% Cr_2O_3). The chromitite pods found as lens-shaped veins of 0.5–l0 m widths, and extend on surface along strike to several tens of meters lengths.

3.6.7 The Northern Sudan Occurrences

The Atmur-Delgo dismembered ophiolite in the central north Sudan extends from the Nile to the NE of the Red Sea Hills, where the mafic-ultrarnafic massifs have been found with the major thrust slices (Fig. 3.39). Chromitite pods of different sizes and shapes are often associated with highly serpentinized dunite-harzburgite rocks in the western parts of the massifs. Chromitite pods vary from centimeter scale schilieren to lenses of more than one meter in length and up to a half meter in thickness. The chromitite ore is generally massive, with local high strain zones that have lenses that exhibit boudinage structure. The chromitite ore in the Northern Sudan is located between the River Nile and Wadi Halfa-Atbara railway line and is mainly of refractory type where the Cr_2O_3 content of Wadi Akasha area reached up to 31 wt%.

3.7 Magmatic Mineral Deposits in Eritrea

Magmatic mineral deposits associated with mafic–ultramafic rocks in Eritrea are negligible in terms of their spatial distribution and economic importance. There are two main types of Precambrian mineralization in Eritrea: (1) polymetallic sulfide deposits, and (2) gold-bearing quartz veins hosted in shear zones (orogenic gold deposits). These deposits are broadly grouped into those of the Asmara, Augaro and Bisha mineral districts, which will be discussed in detail in the next chapters. The approximately absence of mafic–ultramafic mineralization type is mostly due to the nature of the Precambrian basement complex of Eritrea, which essentially composed of metamorphic, volcanosedimentary and metasedimentary rock associations.

As mentioned in Chap. 2 of this book, the basement rocks in Eritrea can be subdivided into four tectonic segments, separated by tectonic boundaries. Three of these segments, the western (Barka terrane), central (Hagar Terrane), and eastern (Nakfa Terrane) segments, are covering the northern and central Eritrea, whilst the fourth (Danakil Terrane) segment, entirely occurs in the southeastern part of the country. The Barka Terrane is separated from the Haya Terrane, of the southern Red Sea Hills in Sudan by what so called “Barka lineaments”, which is characterized by the presence of highly serpentinized mafic–ultramafic rocks. This contains non-economic occurrences of chrysotile asbestos, garnerite (Ni-Mg hydrosilicates), magnesite, and very few chromitite pods. The Barka Terrane made up of amphibolite, amphibolite-facies metamorphic pelitic schists containing kyanite and staurolite, quartzites and marble. The Hagar Terrane, in the central north Eritrea, extends from the Barka River up to the Adobha Abi valley in the east, and dominantly composed of oceanic and accretionary wedge materials. The Hagar Terrane comprises mainly of layered sequences of chloritic schists interlayered with epidotic and chloritic metabasalts, thin and discontinuous marbles, and manganiferous and ferruginous cherts. Although there is no documented occurrence of chromitite and associated

mineralization, the Hagar Terrane is known to be prospective for chromitite and Ni–Cu–Au–PGE mineralization.

The Nakfa Terrane is exceptionally dominated by gabbroic complex (the Bisha complex), about 275 km^2, which is a mafic layered intrusion forming elevated hills in the southern and central parts of the Terrane. The complex extends in a NNE-SSW direction for 35 km and has a maximum E-W width of about 12 km (Barrie et al. 2007). The Bisha layered gabbroic complex comprises medium-to coarse-grained cumulate gabbroic rocks, with lesser gabbronorite, pyroxenite, and ferroan gabbro containing up to 8% of rock volume Fe–Ti oxides. The Nakfa Terrane is bounded by the Adobha Abi valley in the west and by the Red Sea escarpment to the east. It is essentially consisting of calc-alkaline volcanic and volcanoclastic rocks conformably overlain by a metasedimentary sequence of chlorite schists, grits and polymictic conglomerates with occasional pelitic sericite schists and carbonates. The Nakfa Terrane is considered to represent a relict island arc assemblage, where several volcanogenic massive sulfide (VMS) base metal occurrences and gold showings are associated with this tectonic unit.

3.8 Magmatic Mineral Deposits in Ethiopia

In general, the Precambrian basement rocks underlie a large area in the northern (Northern Greenstone Belt) and western Ethiopia (Western Greenstone Blet), and smaller areas in the south and east (Southern Greenstone Belt) of the country (Fig. 3.40). As previously mentioned, the general tectono-stratigraphic classification of Precambrian rocks in Ethiopia can be subdivided into three major complexes: (1) Lower Archean complex, (2) Middle Paleo- to Mesoproterozoic complex, and (3) Upper Neoproterozoic complex. The majority of the Precambrian rocks (granite-gneiss, volcano-sedimentary and ophiolitic suites) of Ethiopia have apparently been belonging to the Pan-African orogeny of a Neoproterozoic age (Ayalew et al. 1990; Gichile 1992; Teklay et al. 1998; Gerra 2000). Most of the Precambrian metallic mineral deposits in Ethiopia is concentrated in the low-grade metamorphic rocks that belong to the ANS, which can be classified into three main domains (Tadesse et al. 2003): the northern greenstone belt, the western greenstone belt, and the southern greenstone belt (Fig. 3.40). Each of these three domains characterized by specific types of mineral deposits that will be discussed in details in the coming chapters. The mafic–ultramafic rocks are exclusively belonging to the ophiolitic type, which are entirely existence in the above-mentioned greenstone belts. Following is a brief description of the magmatic mineral deposits associated with mafic–ultramafic rocks of Ethiopia.

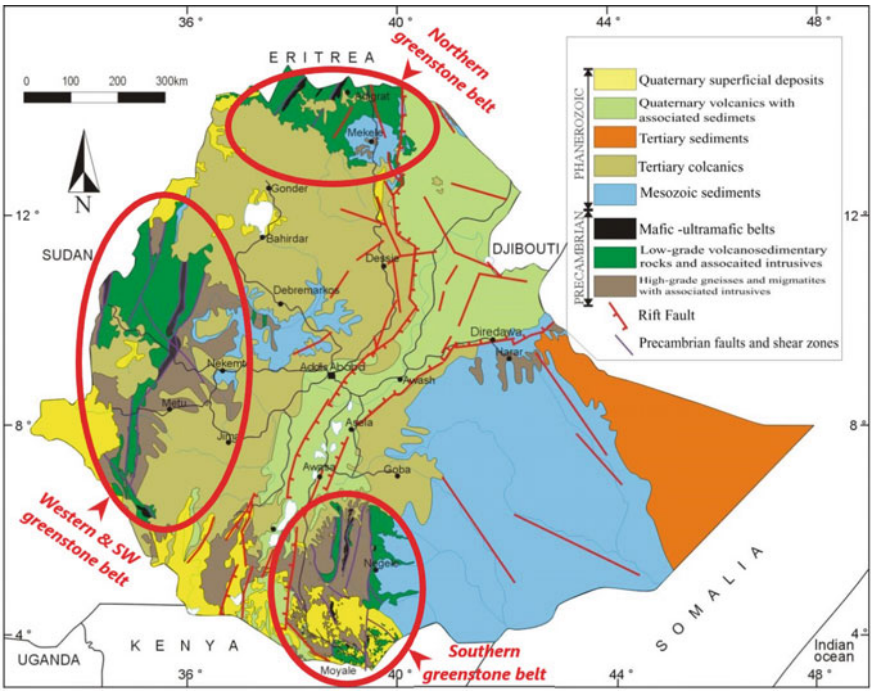

Fig. 3.40 Simplified geological map of Ethiopia showing the main mineralization greenstone belts domains (modified from Tefera et al. 1996)

3.8.1 PGE Mineralization in Western Ethiopia

The Precambrian of Western Ethiopia (western greenstone belt) is the largest Precambrian block in the country, which extends northwards for about 650 km in length and varies in width from about 200–250 km in the north, and to about 20–50 km in the south (Fig. 3.41). The western Ethiopian mafic–ultramafic assemblage found as linear, but discontinuous, masses that exposed in several places, particularly, from south to north, at Akobo, Yubdo, Daletti, Tulu Dimtu, Meti, Sire Banti and Baruda (Fig. 3.41). None of these massifs was mined on a commercial scale but Pt-Fe alloys are known in some of these bodies and their surrounding placers. The mafic–ultramafic rocks of these bodies are covered by a thick laterite profile, which is frequently exceeds 15 m thick. These mafic–ultramafic bodies were interpreted as a dismembered ophiolite sequence (Kazmin 1978; de Wit and Chewaka 1981; Alemu and Abebe 2000; Tadesse and Allen 2005). They separated the lithotectonic domains in what so-called "Sekerr-Yubdo-Tulu Dimtu-Barka" suture zone (Berhe 1990) or "Barka-Tulu Dimtu" suture zone (Abdelsalam and Stern 1996). However, some workers argued against the ophiolitic origin of these mafic–ultramafic bodies in western Ethiopian domain (e.g., Braathen et al. 2001), and they interpreted them as Alaskan-type concentrically zoned intrusions in volcano-sedimentary rocks.

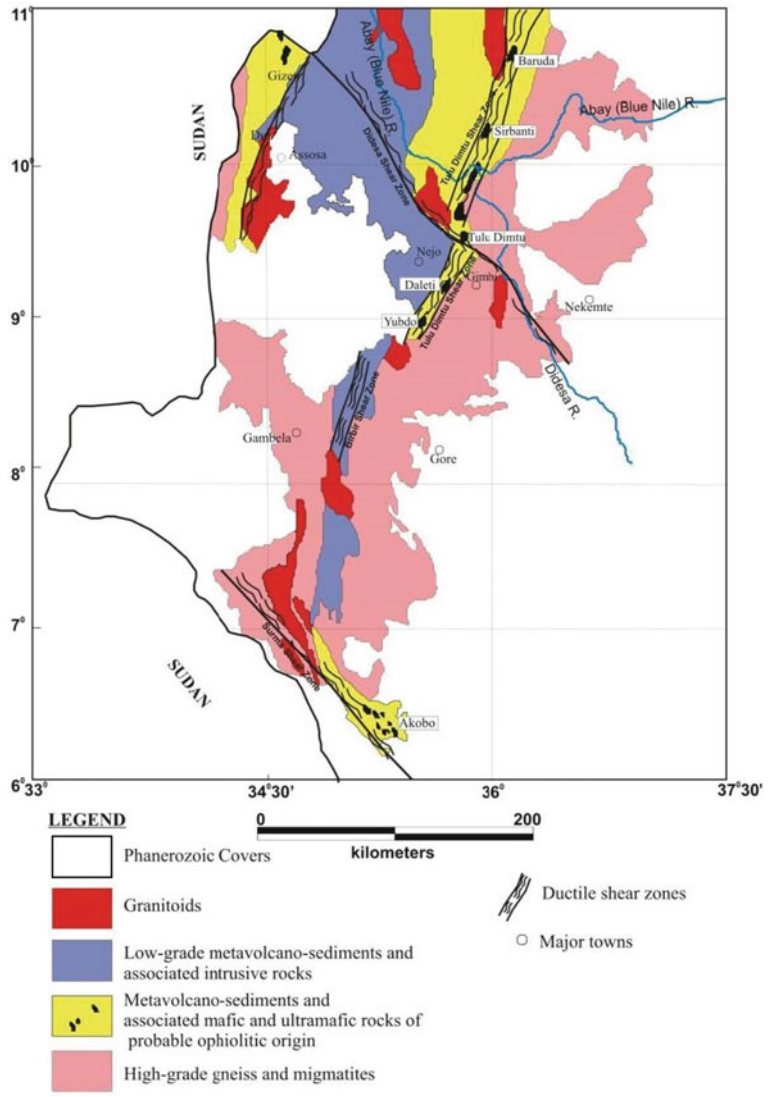

Fig. 3.41 Simplified geological map of the Precambrian rocks of Western Ethiopia showing the distribution of mafic–ultramafic belts and their mineralization localities (after Alemu and Abebe 2000)

Recently, one of the mafic–ultramafic bodies in the western Ethiopia (Tulu Dimtu Complex) has been petrologically examined (Sofiya et al. 2017). Based on the petrological characteristics of primary olivine and Cr-spinel relicts, it was concluded that the Tulu Dimtu complex is a part of dismembered ophiolite sequence similar to that of the ANS ophiolites (e.g., Stern et al. 2004). The Cr# value of Cr-spinel of the Tulu

Dimtu mafic–ultramafic complex overlaps with the variations of most ANS ophiolite bodies, such as those in Southern Ethiopia, Kenya, Sudan, and Egypt (Sofiya et al. 2017). In general, the mafic–ultramafic rocks of Western Ethiopia are dominantly represented by massive serpentinized dunite, with minor intercalations of talc schist, talc-carbonate schist and amphibolite. The serpentinized dunite occasionally contains disseminated chromitite pods and magnetite.

One of the famous mafic–ultramafic complexes in Western Ethiopia is the Yubdo massif, the southernmost mafic–ultramafic body, which consists of serpentinized dunite core, clinopyroxenite, peridotite, serpentine schist, and listwaenite/birbirite (silica-rich cap) units (Fig. 3.42). The Yubdo mafic–ultramafic complex is located about 520 km to the west from Addis Ababa; it is a well-known complex for Pt deposits and alteration zones for the last many years. The Yubdo mafic–ultramafic body is found along the Barka-Tulu-Dimtu shear zone; it is interpreted as an Alaskan-type concentrically zoned intrusion with both surface and bedrock PGE mineralization along sub-vertical alteration zones. The Yubdo mafic–ultramafic complex is essentially zoned; being have dunite at the core, with peridotite then pyroxenite at the margins. In some places, especially in the eastern and southern parts of the intrusion, peridotites intercalated with dunite (Mogessie et al. 1999). Several drill cores were carried out in the Yubdo mafic–ultramafic complex, almost all of them were sunk into the dunite zone and they only intersected dunite and peridotite layers. Some of the drill cores intersected thin magnetite veinlets, which extend along fault zones and talc-chlorite dykes.

The Minerva Resources Company of Ethiopia evaluated the platinum potential of the Yubdo mafic–ultramafic complex in 2006. The examined locality is to the southwest of the small-scale mining operation southeast of Yubdo village. A total thirty pits were completed on a 60 m × 60 m square grid, which covering an area of 420 m × 240 m, and a pit depth of about 10 m. Channel sampling at one meter intervals down the side of the pits gave an average grade reached up to 1.8 g/t Pt. Based on the results of the drilling program of the whole area, a total resource was estimated to be about 23,760 oz (793 kg) of Pt within 1.5 Mt ore of laterite materials with an average grade of 0.54 g/t Pt. It is noteworthy that, the average grade of the laterite below 1.5 m barren surfaces of soil layer was 0.82 g/t Pt. The geological mapping of the area (Fig. 3.42) shows that the potentially mineralized laterite profile extends for several kilometres along strike in the Yubdo mafic–ultramafic intrusion. In addition, the mapping of exposed bedrock in the pits and in outcrop shows fractures system containing quartz-carbonate veins, veinlets, and planar fracture fillings with boxworks-like pyrite occurring in zones trending NE with general steep westward dips, cutting the serpentinised dunites and pyroxenites of the Yubdo mafic–ultramafic complex.

Several grains and nuggets of PGM have been found in both the bedrocks and placer deposits around Yubdo mafic–ultramafic complex. Sperrylite ($PtAs_2$) and Pt-Fe alloys are the dominant primary PGM systematically found in chromite, dunite and pyroxenite of the Yubdo mafic–ultramafic complex (United Nations 1971; Belete et al. 2000). In addition, sperrylite was also discovered in birbirite (silica-rich capping) samples from the Yubdo complex. All nuggets reported from Yubdo

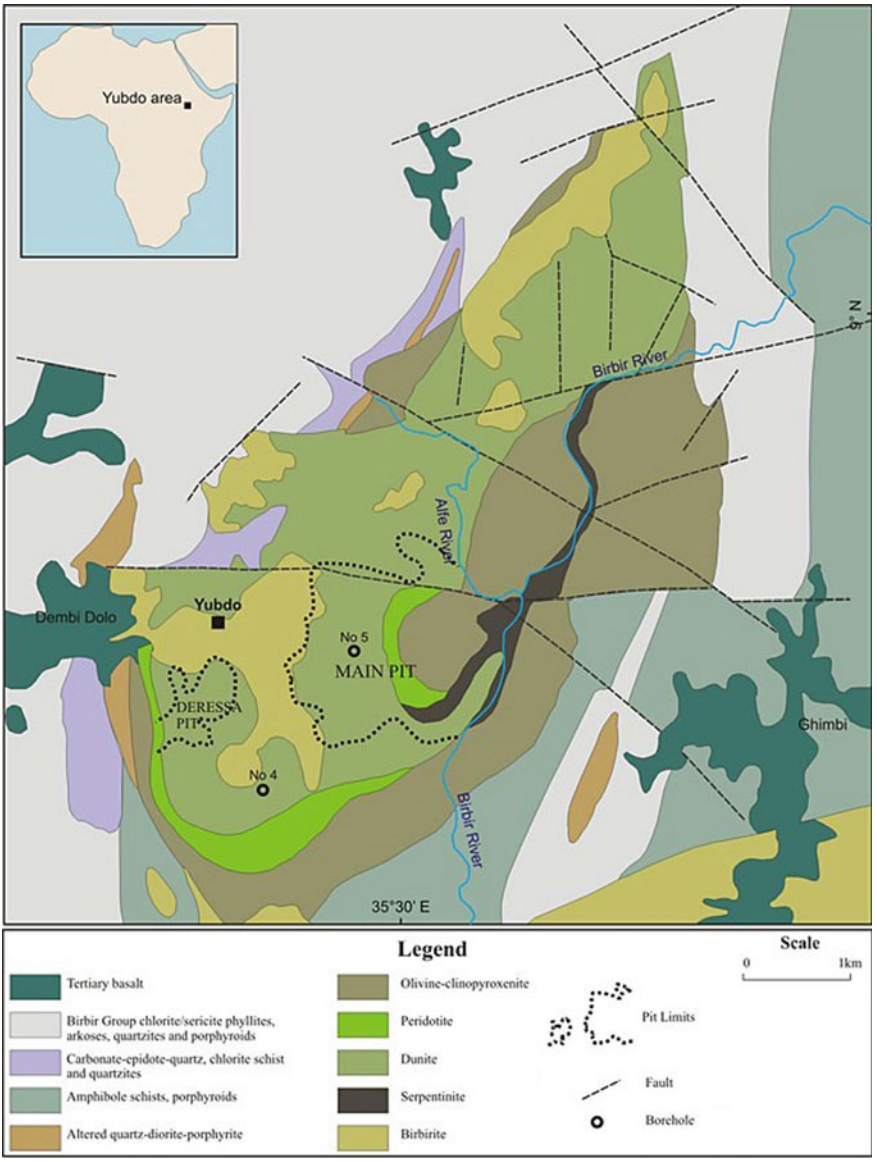

Fig. 3.42 Simplified geological map of the Yubdo mafic–ultramafic complex and the mineralization localities (modified from Alemu and Abebe 2000)

complex are Pt-Fe in composition; however, wide varieties of PGM inclusions were found within these nuggets (Belete et al. 2000). The most abundant PGM inclusions found were hollingworthite (RhAsS), genkinite ($(Pt,Pd)_4Pb_3$), irarsite (IrAsS), platarsite (PtAsS) and native Os. The average composition of the Pt-Fe nuggets from the Yubdo mafic–ultramafic complex is 79.48 wt% Pt, 0.49 wt% Pd, 0.75 wt% Rh, 0.8 wt% Ir, 1.41 wt% Os-Ir, and 0.49 wt% Au. Iron forms the remaining percentage. Other metallic minerals in association include tulameenite, osmiridium, electrum, pentlandite and chalcocite in trace amounts (Belete et al. 2000; Selassie and Reimold 2000; Tadesse et al. 2003).

The other four mafic–ultramafic bodies along the Barka-Tulu-Dimtu shear zone (Tulu-Dimtu, Kingy, Daleti and Ankori) are less well-studied than the Yubdo complex. All the five bodies are highly altered and the degree of serpentinization is greater than 50% (Mogessie et al. 1999; Tadesse and Allen 2005). Other PGE occurrences have also been reported together with gold from several occurrences in Western Ethiopia (Wollega) (e.g., Tulu Dimtu, residual and Soddu, placer). The sources of Pt-Fe nuggets that have been found in the rivers in western Ethiopia are likely from the mafic–ultramafic complexes.

3.8.2 Southern Ethiopian Ni–Co–Cu Mineralization

The Precambrian basement of southern Ethiopia consists of high-grade ortho- and para-gneisses and migmatites, as well as low-grade ophiolitic belts and granitoids. It occupies an important position between the Pan-African Mozambique Belt, to the south, and the ANS to the northeast, which, together, form the East African Orogen (Stern 1994). The mafic–ultramafic complexes in Southern Ethiopia (Southern Greenstone Belt) composed from three parallel zones: the Adola belt, the kenticha blet, and the Negelle area of Southern Ethiopia (Fig. 3.43). These three parallel mafic–ultramafic belts referred in the literature in a broad sense as the "Adola-Moyale Belt". All the three mafic–ultramafic zones are entirely fault bounded. The Adola-Moyale Belt extends approximately in a N–S direction for about 350 km. The Moyale mafic–ultramafic rocks occur south of the well-documented Adola mafic–ultramafic complex of southern Ethiopia.

More than 20 occurrences of Ni-rich mafic–ultramafic rocks have been found in association with serpentinite bodies belong to the Adola and Kenticha belts. Estimation of ore resources in these occurrences gave about 17 Mt of ore with an average grade of 1.3 wt% Ni. The main deposits are those located at Ula Ulo, which gave about 4 Mt ore with an average grade of 1.33 wt% Ni and 0.01 wt% Co, and Tulla, which gave about 6.6 Mt ore with an average grade of 1.12 wt% Ni. There are some other similar Ni-rich occurrences reported in Sidamo district such as those in Kilta, Big Dubicha, Small Dubicha, Fulanto, Monissa, Burjiji and Lolotu, in which for example at Kilta area gave about 2 Mt ore with an average grade of 1.5 wt% Ni (Tadesse et al. 2003). All of the above-mentioned occurrences are hosted in serpentinized ultramafic rocks. The Ni-rich mineralization is essentially hosted in oxidized

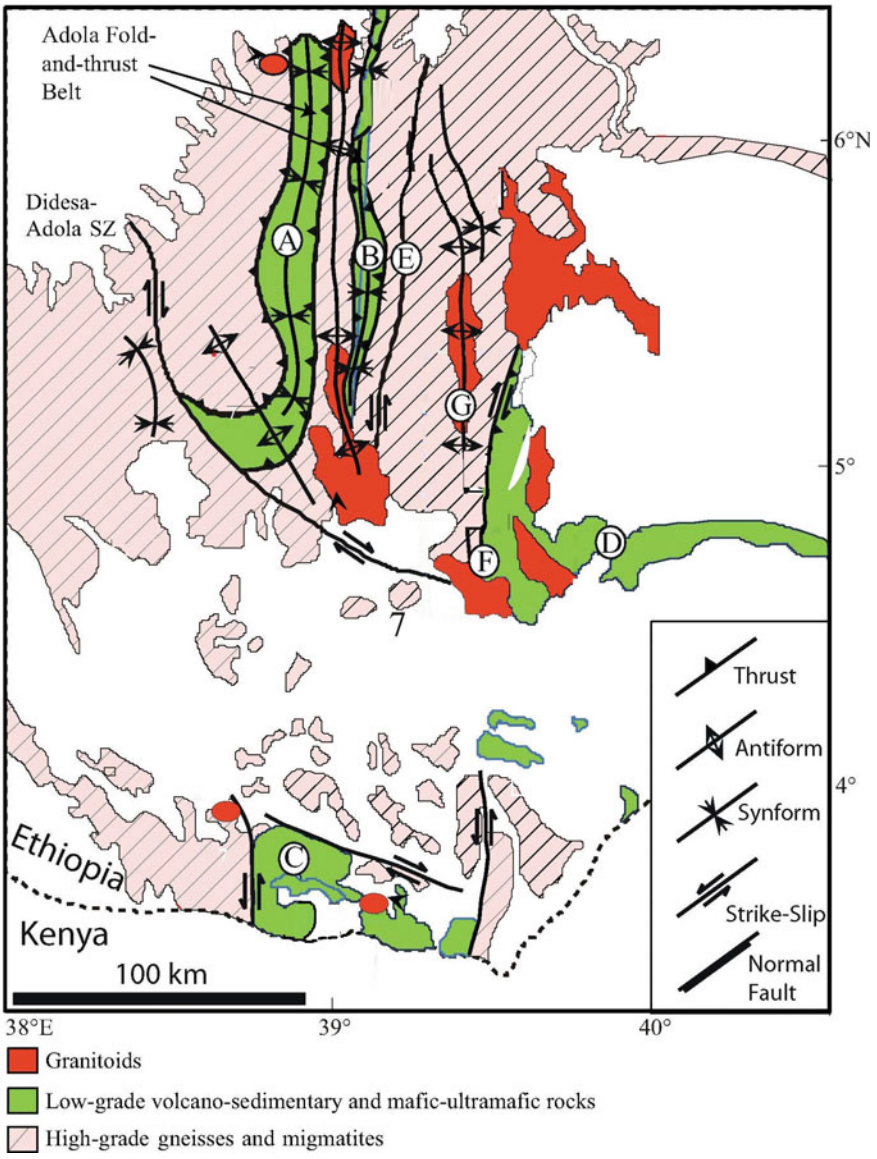

Fig. 3.43 Simplified geological map of the Southern Ethiopia showing the distribution of mafic–ultramafic belts and their mineralization localities (modified from Stern et al. 2012). A: Megado belt; B: Kenticha belt; C: Moyale belt; D: Bulbul belt; E: Wadera shear zone; F: Bulbul shear zone; and G: Alghe Terrane/Melka Guba Domain

capping of laterite zones over serpentinized ultramafic bodies, which are consisting of serpentine minerals, talc and bands of talc schists, tremolite, chlorite schists and actinolite schists. The mafic–ultramafic bedrocks have low metals content with an average of 0.1–0.3 wt.% Ni, 0.02 wt% Co, and about 1 wt% Cu.

3.8.3 Chromitite-Fe–Ti Mineralization in Western and Southern Ethiopia

There are some occurrences of high-grade chromitite deposits in southern Ethiopia (e.g., Kenticha Hill, Sidamo, Metti-Gola, Dubicha-Gudda, Dermidama, Molicha) and in Western Ethiopia (Wolega area, especially in the Yubdo-Dalleti-Tulu Dimto Belt). The ore reserves of these occurrences have not estimated. Chromitite deposits of these areas are essentially associated with the Pt mineralization in the mafic–ultramafic complexes. The most famous studied chromitite deposits in Ethiopia is the Kenticha Hill chromitites in Southern Ethiopia (Bonavia et al. 1993). The Kenticha Hill mafic–ultramafic complexes found as sheared and tectonized bodies that separated by mylonites. Both chromitite pods and their host peridotites display boudinaged structures that preserved from intense tectonic events and surrounded by mylonites. Several small-scale massive chromitite pods of maximum a half meter across are found within serpentinized peridotites of Kenticha Hill, Southern Ethiopia. The chemistry of Cr-spinel in chromitite pods of the Kenticha Hill is mainly high-Cr variety (Cr# ~ 0.9), but the petrological characteristics of the host peridotites was not determined due to the intense shearing and metamorphism (Bonavia et al. 1993). Due to the intense deformation, it was difficult to recognize the igneous textures of host peridotite and whether they are ophiolitic or Alaskan-type concentrically zoned mafic–ultramafic remnants.

Several occurrences of iron deposits are also found in many areas in Ethiopia such as those in Tigray (Adua, Entichio) and Wollega, Western Ethiopia (Koree, Gordoma, Chago or Mai Gudo). The Fe deposits in Ethiopia belong to three main types: (i) Precambrian mafic intrusion-hosted Fe–Ti deposits (Bikilal, Melka Arba), (ii) banded iron formation (BIF) deposits associated with Precambrian ferruginous quartzites (Koree, Gordoma, Chago), and (iii) secondary laterite and/or gossans-related deposits (e.g. Melka Sedi). The earlier type (Fe–Ti oxide deposits associated with mafic–ultramafic intrusions) is the main Fe deposits in Ethiopia, which is discovered at Western Ethiopia at Bikilal in Wollega district. These Fe–Ti–P deposits formed by magmatic segregation processes from mafic magma, where the Fe–Ti ore bodies are confined to the mafic–ultramafic zone, which consists of ore-bearing actinolite rich rocks, olivine pyroxenite, meta-hornblendite, apatite bearing meta-hornblendite and meta-gabbro (Tadesse et al. 2003). The dimension of the mafic–ultramafic zone is about 1 km wide and 12 km long, while the size of the ore-bearing zone is about 200–1400 m in length, 2–6 m in width and 200–300 m in depth. The dominant ore minerals in the Bikilal Fe-Ti deposits are magnetite (~40 wt%) and ilmenite

(~29 wt%) that mixed with interstitial silicate minerals (~30 wt%). Sulfide minerals such as pyrrhotite-pyrite (2–2.5 wt%), chalcopyrite-pentlandite (<1%), as well as apatite (0.6 wt%), are the most common accessory minerals in the Fe-Ti deposits. The gangue minerals represented mainly by amphiboles, chlorite, olivine, pyroxene and plagioclase. The Fe-Ti deposits of Western Ethiopia are chiefly found as massive to disseminated ores. The estimated ore reserves of Bikilal Fe–Ti deposit is about 58 Mt with an average grade of 41 wt% total Fe. The ore reserves of P-rich zones (apatite-rich ore) are estimated to be about 127 Mt of apatite ore with an average grade of 21.8% total Fe.

References

Abd El-Rahman Y, Polat A, Dilek Y, Fryer B, El-Sharkawy M, Sakran S (2009) Geochemistry and tectonic evolution of the Neoproterozoic Wadi Ghadir ophiolite, Eastern Desert. Egypt Lithos 113:158–178

Abd El-Rahman Y, Polat A, Dilek Y, Fryer BJ, El-Sharkawy M, Sakran S (2009) Geochemistry and tectonic evolution of the neoproterozoic incipient arc–forearc crust in the Fawakhir area, central Eastern Desert of Egypt. Precambr Res 175:116–134

Abd El-Rahman Y, Polat A, Dilek Y, Kusky TM, El-Sharkawy M, Said A (2012) Cryogenian ophiolite tectonics and metallogeny of the central Eastern Desert of Egypt. Int Geol Rev 54:1870–1884

Abdel Rahman EM (1993) Geochemical and geotectonic controls of the metallogenic evolution of selected ophiolite complexes from the Sudan. Berliner Geowissenschaftliche Abhandlungen/A 145:175

Abdel Rahman EM, Harms U, Schandelmeier H, Franz G, Darbyshire DPF, Horn P, Muller-Sohnius D (1990) A new ophiolite occurrence in NW Sudan: constraints on Late Proterozoic tectonism. Terra Nova 2:363–376

Abdel-Karim AAM, Ali S, Helmy HA, El-Shafei SA (2016) A fore-arc setting of the Gerf ophiolite, Eastern Desert, Egypt: evidence from mineral chemistry and geochemistry of ultramafites. Lithos 263:52–65

Abdel-Karim AM, Ahmed Z (2010) Possible origin of the ophiolites of Eastern Desert, Egypt, from geochemical perspectives. Arab J Sci Eng 35:115–143

Abdelsalam MG, Stern RJ (1996) Sutures and shear zones in the Arabian–Nubian Shield. J Afr Earth Sc 23:289–310

Abdelsalam MG, Stern RJ, Copeland P, Elfaki E, Elhur B, Ibrahim FM (1998) The Neoproterozoic Keraf suture in NE Sudan: sinistral transpression along the eastern margin of west Gondwana. J Geol 106:133–148

Abu El Ela FF, Farahat ES (2010) Neoproterozoic podiform chromitites in serpentinites of Abu Meriewa-Hagar Dungash district. Eastern Desert, Egypt: Geotectonic Implications Metamorphism: Island Arc 19:151–164

Ahmed AAM (1998) Sudan industrial mineral & rocks. Center for Strategic Studied, Khartuom, Sudan, pp 76–106

Ahmed AH (2007) Diversity of platinum-group minerals in podiform chromitites of the late Proterozoic ophiolite, Eastern Desert, Egypt: genetic implications. Ore Geol Rev 32:1–19

Ahmed AH (2013) Highly depleted harzburgite-dunite-chromitite complexes from the Neoproterozoic ophiolite, south Eastern Desert, Egypt: a possible recycled upper mantle lithosphere. Precambr Res 233:173–192

Ahmed AH (2020) Mineral resources in Egypt (I): Metallic Ores—chromite deposits in Egypt. In: Hamimi et al (eds) The geology of Egypt, regional geology reviews. Springer Nature Switzerland, pp 565–564. https://doi.org/10.1007/978-3-030-15265-9-14

Ahmed AH, Arai S (2002) Unexpectedly high-PGE chromitite from the deeper mantle section of the northern Oman ophiolite and its tectonic implications. Contrib Miner Petrol 143:263–278

Ahmed AH, Arai S (2003) Platinum-group minerals in podiform chromitites of the Oman ophiolite. Can Mineral 41:597–616

Ahmed Z, Harriri MM (2008) Neoproterozoic ophiolites as developed in Saudi Arabia and their oceanic and pericontinental domains. Arab J Sci Eng 33:17–54

Ahmed AH, Habtoor A (2015) Heterogeneously depleted Precambrian lithosphere deduced from mantle peridotites and associated chromitite deposits of Al'Ays ophiolite, Northwestern Arabian Shield, Saudi Arabia. Ore Geol Rev 67:279–296

Ahmed AH, Arai S, Attia AK (2001) Petrological characteristics of the Pan African podiform chromitites and associated peridotites of the Proterozoic ophiolite complexes. Egypt. Mineralium Deposita 36:72–84

Ahmed AH, Arai S, Yaser MA, Ikenne M, Rahimi A (2009) Platinum-group elements distribution and spinel composition in podiform chromitites and associated rocks from the upper mantle section of the Neoproterozoic Bou Azzer ophiolite, Anti-Atlas, Morocco. J Afr Earth Sc 55:92–104

Ahmed AH, Arai S, Yaser MA, Rahimi A (2005) Spinel composition as a petrogenetic indicator of the mantle section in the Neoproterozoic Bou Azzer ophiolite, Anti-Atlas, Morocco. Precambr Res 138:225–234

Ahmed AH, Hanghøj K, Kelemen PB, Hart SR, Arai S (2006) Osmium isotope systematics of the Proterozoic and Phanerozoic ophiolitic chromitites: in-situ ion probe analysis of primary Os-rich PGM. Earth Planet Sci Lett 245:777–791

Ahmed AH, Harbi HM, Habtoor AM (2012) Compositional variations and tectonic settings of podiform chromitites and associated ultramafic rocks of the Neoproterozoic ophiolite at Wadi Al Hwanet, northwestern Saudi Arabia. J Asian Earth Sci 56:118–134

Ahmed AH, Helmy HM, Arai S, Yoshikawa M (2008) Magmatic unmixing in spinel from late Precambrian concentrically-zoned mafic-ultramafic intrusions, Eastern Desert. Egypt Lithos 104:85–98

Alemu T, Abebe T (2000) Geology of the Gimbi area: geological survey of Ethiopia, Memoir 15, Addis Ababa, Ethiopia, Geological Survey of Ethiopia, 158 p

Ali KA, Azer MK, Gahlan HA, Wilde SA, Samuel MD, Stern RJ (2010) Age of formation and emplacement of neoproterozoic ophiolites and related rocks along the Allaqi Suture, south Eastern Desert, Egypt. Gondwana Res 18:583–595

Al-Khirbash S, Heikal MTS, Whitehouse MJ, Windley BF, Al Selwi K (2021) Evolution and mineralization of the Precambrian basement of Yemen. In: Hamimi Z et al (eds) The geology of the Arabian–Nubian shield, regional geology reviews, pp 633–657. https://doi.org/10.1007/978-3-030-72995-0_24

Al-Shanti AM, El-Mahdy OR (l988) Geological studies and assessment of chromite occurrences in Saudi Arabia: KACST Project No. AT-6-094

Al-Tigani MMH, Mohamed AA, Seifelnasr AA (2019) Mineralogical and chemical characterization of disseminated low-grade sudanese chromite ore in gedarif state at Umm Saqta-Qala Elnahal. J Environtal Anal Chem 6:261

Amin MS (1954) The ilmenite deposit of Abu Ghalqa, Egypt. Econ Geol Bull Soc Econ Geol 49:77–87

Arai S (1997) Control of wall-rock composition on the formation of podiform chromitites as a result of magma/peridotite interaction. Resour Geol 47:177–187

Arai S, Ahmed AH (2018) Secular change of chromite concentration processes from the Archean to the Phanerozoic. In: Mondal SK, Griffin WL (eds), Processes and ore deposits of Ultramafic-Mafic Magmas through space and time, pp 139–157. https://doi.org/10.1016/B978-0-12-811159-8.00006-8

Ayalew T, Bell K, Moore JM, Parish RR (1990) U-Pb and Rb–Sr geochemistry of the western Ethiopian Shield. Geol Soc Am Bull 102:1309–1316
Azer MK, Stern RJ (2007) Neoproterozoic serpentinites in the Eastern Desert, Egypt: fragments of fore-arc mantle. J Geol 115:457–472
Azer MK, Gahlan HA, Asimow P, Al-Kahtany KM (2017) The late Neoproterozoic Dahanib mafic-ultramafic intrusion, South eastern Desert, Egypt: is it an Alaskan-type or a layered intrusion? Am J Sci 317:901–940
Azer MK, Samuel MD, Ali KA, Gahlan HA, Stern RJ, Ren M, Moussa HE (2013) Neoproterozoic ophiolitic peridotites along the Allaqi-Heiani Suture, South Eastern Desert, Egypt. Mineral Petrol 107:829–848
Barrie CT, Nielsen FW, Aussant CH (2007) The Bisha volcanic-associated massive sulphide deposit, Western Nakfa Terrane, Eritrea. Econ Geol 102:717–738
Barth H, Meinhold KD (1979) Mineral prospecting in the Bayuda Desert. Part I. Sudanese German Exploration Project, Technical Report, BGR, Hannover, 336 p
Basta EZ, Takla MA (1968) Mineralogy and origin of Abu Ghalaga ilmenite occurrence, Eastern Desert, Egypt. J Geol 12:87–124
Basta FF, Maurice AE, Bakhit BR, Ali KA, Manton WI (2011) Neoproterozoic contaminated MORB of Wadi Ghadir ophiolite, NE Africa: geochemical and Nd and Sr isotopic constraints. J Afr Earth Sci 59:227–242
Beccaluva L, Coltorti M, Di Girolamo P, Melluso L, Milani L, Morra V, Siena F (2002) Petrogenesis and evolution of Mt. Vulture alkaline volcanism (Southern Italy). Mineral Petrol 74:277–297
Beccaluva L, Coltorti M, Giunta G, Siena F (2004) Tethyan vs. Cordilleran ophiolites: a reappraisal of distinctive tectono-magmatic features of supra subduction complexes in relation to the subduction mode. Tectonophysics 393:163–174
Belete KH, Mogessie A, Hoinkes K (2000) Platinum and gold deposit of Yubdo mafic-ultramafics, western Ethiopia: a late stage hydrothermal mineralization. In: Symposium 200: Geology and Ore Deposits 2000, the great basin and beyond. A Geological Society of Nevada Symposium, Reno, pp 583–589
Berhe SM (1990) Ophiolites in northeast and east Africa: implication for Proterozoic crustal growth. J Geol Soc Lond 147:41–57
Bonavia FF, Diella V, Ferrario A (1993) Precambrian podiform chromitites from Kenticha Hill. Southern Ethiopia: Econ Geol 88:198–202
Braathen A, Grenne T, Selassie MG, Worku T (2001) Juxtaposition of Neoproterozoic units along the Baruda-Tulu Dimtu shear belt in the East African Orogen of western Ethiopia. Precambr Res 107:215–234
Bühler B, Breitkreuz C, Pfänder JA, Hofmann M, Becker S, Linnemann U, Eliwa HA (2014) New insights into the accretion of the Arabian–Nubian Shield: depositional setting, composition and geochronology of a mid-Cryogenian arc succession (North Eastern Desert, Egypt). Precambr Res 243:149–167
Chevremont P (1982) Core drilling in the Wadi Kamal area, Saudi Arabian Deputy Ministry for Mineral Resources Open-File Report, KSA, BRGM-03-7, 66 pp
Chevremont P, Johan Z (1982) Wadi al Hwanet-Jabal Iss Ophiolite Complex. BRGM-OF-02-14. Saudi Arabia Deputy Ministry for Mineral Resources
Collenette P, Grainger DJ (1994) Mineral resources of Saudi Arabia. Not including oil, natural gas and sulfur, DGMR Special Publication SP-2, pp 55–68
De Wit MJ, Chewaka S (1981) Plate tectonic evolution of Ethiopia and mineral deposits: an overview. In: Chewaka S, De Wit MJ (eds) Plate tectonics and metallogenesis, some guidelines to Ethiopian mineral deposits: Ethiopian Institute of Geological Surveys Bulletin, vol 2, pp 115–119
Distler VV, Kryachko VV, Yudovskaya MA (2008) Ore petrology of chromite-PGE mineralization in the Kempirsai ophiolite complex. Mineral Petrol 92:31–58
Duchesne JC, Liégeois JP (2015) The origin of nelsonite and high-Zr ferrodiorite associated with Proterozoic anorthosite. Ore Geol Rev 71:40–56

El Haddad MA (1996) The first occurrence of platinum group minerals (PGM) in a chromitite deposit in the Eastern Desert, Egypt. Miner Deposita 31:439–445
Essamaldeen A (2005) Geology and structural evolution of Abidiya area, Sudan: remote sensing, structural and geochemical approaches. M.Sc. thesis, Al Neelain University, Khartoum, Sudan, 170 pp
Evuk DO (2007) Structural geology and tectonic setting of Umtrambish shear zone, Berber Province, River Nile State, Sudan. M.Sc. thesis, Juba University, Sudan, 143 pp
Evuk DO, Franza G, Frei D, Lucassen F (2014) The Neoproterozoic evolution of the central-eastern Bayuda Desert (Sudan). Precambr Res 240:108–125
Farahat ES (2010) Neoproterozoic arc–back-arc system in the Central Eastern Desert of Egypt: evidence from supra-subduction zone ophiolites. Lithos 120:293–308
Finger F, Helmy HM (1998) Composition and total-Pb model ages of monazite from high-grade paragneisses in the Abu Swayel area, southern eastern desert, Egypt. Mineral Petrol 62:269–289
Gerra S (2000) A short introduction to the geology of Ethiopia. Chronique De La Recherche Minière 540:3–10
Gichile S (1992) Granulites in the Precambrian basement of southern Ethiopia: geochemistry, P-T conditions of metamorphism and tectonic setting. J Afr Earth Sci 15:251–263
Greenough JD, Kamo SL, Theny L, Crowe SA, Fipke C (2011) High-precision U-Pb age and geochemistry of the mineralized (Ni–Cu–Co) Suwar intrusion, Yemen. Can J Earth Sci 48:495–514
Habashi F, Bassyouni FA (1982) Mineral resources of the Arab Countries, 2nd edn, Quebec, Canada, p 46
Habtoor A, Ahmed AH, Harbi HM (2016) Petrogenesis of the Alaskan-type mafic–ultramafic complex in the Makkah quadrangle, western Arabian Shield, Saudi Arabia. Lithos 263:33–51
Habtoor AM, Ahmed AH, Akizawa N, Harbi H, Arai S (2017) Chemical homogeneity of high-Cr chromitites as indicator for widespread invasion of boninitic melt in mantle peridotite of Bir Tuluha ophiolite, Northern Arabian Shield, Saudi Arabia. Ore Geol Rev 90:243–259
Harbi HM (2008) Geology and lihostratigraphy of ultramafic–mafic rocks and associated mineralization Wadi Khamal area, Western Saudi Arabia. King Abdulaziz Univ J Earth Sci 19:119–157
Helmy HM (1996) Precious metal and base metal sulphide mineralization at Abu Swayel and Um Samiuki, Eastern Desert, Egypt. PhD Thesis, Minia University, Egypt
Helmy HM (2004) Cu-Ni-PGE mineralization in the Genina Gharbia mafic-ultramafic intrusion, Eastern Desert, Egypt. Can Mineral 42:351–370
Helmy HM (2005) Melonite group minerals and other tellurides from three Cu–Ni–PGE prospects, Eastern Desert, Egypt. Ore Geol Rev 26:305–324
Helmy HM (2020) Mineral resources in Egypt (I): metallic ores—sulfides and precious metal in Egypt. In: Hamimi et al (eds) The geology of Egypt, regional geology reviews. Springer Nature, Switzerland, pp 543–549. https://doi.org/10.1007/978-3-030-15265-9-14
Helmy HM, Mogessie A (2001) Gabbro Akarem, Eastern Desert Egypt: Cu–Ni–PGE mineralization in a concentrically zoned mafic-ultramafic complex. Miner Deposita 36:58–71
Helmy HM, El Mahallawi MM (2003) Gabbro Akarem mafic-ultramafic complex, Eastern Desert, Egypt: a late Precambrian analogues of Alaskan-type complexes. Mineral Petrol 77:85–108
Helmy HM, Abd El-Rahman YM, Yoshikawa M, Shibata T, Arai S, Tamura A, Kagami H (2014) Petrology and Sm-Nd dating of the Genina Gharbia Alaskan-type complex (Egypt): insights into deep levels of Neoproterozoic island arcs. Lithos 198–199:263–280
Helmy HM, Stumpfl EF, Kamel OA (1995) Platinum group minerals from the metamorphosed Abu Swayel Cu-Ni-PGE mineralization, South Eastern Desert, Egypt. Econ Geol 90:23–50
Huang X, Li J, Kusky TM, Chen Z (2004) Microstructures of the Zunhua 2.50 Ga podiform chromite, North China Craton and implications for the deformation and rheology of the Archean oceanic lithospheric mantle. In: Kusky TM (ed) Precambrian ophiolites and related rocks, developments in precambrian geology vol 13, pp 321–337
Hussein AA (1990) Mineral deposits. In: Said R (ed) The geology of Egypt. Balkema, Rotterdam, pp 511–566

Isakin MM, Lobunets SS, Yegorov IV (1990) Explanatory note to the map of mineral distribution of the PDRY, scale: 1:200,000. Ministry of Energy and Minerals, Department of Geology and Mineral Exploration, Aden, 34 pp

Kazmin V, Shiferaw A, Balcha T (1978) The Ethiopian basement: stratigraphy and possible manner of evolution. Geol Rundsch 67:531–546

Kerr A, Leitch AM (2005) Self destructive sulfide segregation systems and the formation of high-grade magmatic ore deposits. Econ Geol 100:311–332

Khalil KI (2001) Mineralogical and mineralogcal studies on the origin of the Abu Ghalaga ilmenite ore, southeastern Desert, Egypt. MERC Ain Shams Univ 15:94–118

Khedr MZ, Arai S (2013) Origin of Neoproterozoic ophiolitic peridotites in south Eastern Desert, Egypt, constrained from primary mantle mineral chemistry. Mineral Petrol 107:807–828

Khedr MZ, Arai S (2016a) Chemical variations of mineral inclusions in Neoproterozoic high-Cr chromitites from Egypt: evidence of fluids during chromitite genesis. Lithos 240–243:309–326

Khedr MZ, Arai S (2016b) Petrology of a Neoproterozoic Alaskan-type complex from the Eastern Desert of Egypt: implications for mantle heterogeneity. Lithos 263:15–32

Khedr MZ, Arai S, Morishita T (2020a) Formation of banded chromitites and associated sulphides in the Neoproterozoic subarc deep-crustal magma inferred from the Alaskan-type complex, Egypt. Ore Geol Rev 120:103410

Khedr MZ, El-Awady A, Arai S, Hauzenberger C, Tamura A, Stern RJ, Morishita T (2020b) Petrogenesis of the ~740 Korab Kansi mafic-ultramafic intrusion, South Eastern Desert of Egypt: evidence of Ti-rich ferropicritic magmatism. Gondwana Res 82:48–72

Kröner A, Todt W, Hussein IM, Mansour IM, Mansour M, Rashwan AA (1992) Dating of late Proterozoic ophiolites in Egypt and the Sudan using the single grain zircon evaporation technique. Precambr Res 59:15–32

Kusky TM, Li J, Glass A, Huang X (2004) Origin and emplacement of Archean ophiolites of the Central Orogenic belt, North China craton. In: Kusky TM (ed) Precambrian ophiolites and related rocks, developments in precambrian geology vol 13, pp 223–274

Kuster D, Liegeois J-P, Matukov D, Sergeev S, Lucassen F (2008) Zircon geochronology and Sr, Nd, Pb isotopes geochemistry of granitoids from Bayuda Desert and Sbaloka (Sudan): evidence for a Bayudian event (920–900 Ma) preceding the Pan-African orogenic cycle (860–590 Ma) at the eastern boundary of the Saharan Metacraton. Precambr Res 164:16–39

Li J, Kusky TM, Huang X (2002) Archean podiform chromitites and mantle tectonites in ophiolitic mélange, North China Craton: a record of early oceanic mantle processes. GSA Today 4–11

Liipo J, Vuollo J, Nykänen V, Pirainen T, Pekkarinen T, Tuokko I (1995) Chromites from the early Proterozoic Outokumpu-Jormua Ophiolitic Belt: a comparison with chromitites from Mesozoic ophiolites. Lithos 36:15–27

Lissan NH (2003) Geology, lithochemistry, geotectonic setting and gold mineralization in the area east of Artoli Village, Berber Province, River Nile State, Sudan. M.Sc. thesis, University of Juba, Sudan, 144 pp

Lissan NH, Bakheit AK (2011) Geochemistry and geotectonic setting of Neoproterozoic granitoids from Artoli Area, Berber Province, Northern Sudan. J Appl Sci 11:752–767

Makhlouf A, Beniamin NY, Mansour MM, Mansour SA, El-Shrbeni H (2008) Mafic-ultramafic intrusion of South Korab Kansi area with emphasis on titanomagnetite ores, south Eastern Desert, Egypt. Ann Geol Surv Egypt V(XXX):1–20

Martin C, Roberts RJ, Stoeser DB (1979) Titaniferous magnetite in the layered intrusive complex at Lakathah. Kingdom of Saudi Arabia: USGS Saudi Project Report 238: 36 p

Melcher F, Grum W, Thalhammer TV, Thalhammer OAR (1999) The giant chromite deposits at Kempirsai, Urals: constrains from trace element (PGE, REE) and isotope data. Mineral Petrol 34:250–272

Mogessie A, Belete K, Hoinkes G, Ettinger K (1999) Platinum mineralization in the Yubdo ultramafic rocks, western Ethiopia. In: Stanley et al (eds) Proceeding of the 5th Biennial SGA meeting and the 10th quadrennial IAGOD symposium. Mineral deposits: process to processing, London, vol 1, pp 751–754

Moores EM (1982) Origin and emplacement of ophiolites. Rev Geophys Space Phys 20:735–760
Moore TA, Al-Rehaili MH (1989) Geological map of the Makkah quadrangle, Sheet 21D. In: Saudi Arabian Directorate General of Mineral Resources Geoscience Map GM 107, Kingdom of Saudi Arabia, 62 p, scale 1:250,000
Moores EM, Kellogg LH, Dilek Y (2000) Tethyan ophiolites, mantle convection, and tectonic 'historical contingency'; a resolution of the 'ophiolite conundrum'. In: Dilek Y, Moores E, Elthon D, Nicolas A (eds) Ophiolites and Oceanic Crust: New Insights from Field Studies and the Ocean Drilling Program: Special Paper. Geological Society of America, vol 349, pp 3–12
Nasr BB, Sadek MF, Masoud MS (2000) Some new occurrences of layered titanomagnetite, Egypt. Annal Geol Surv Egypt V(XXXIII):679–690
Nehlig P, Genna A, Asfirane F (2002) Review of the Pan-African evolution of the Arabian Shield. GeoArabia 7:103–124
Obeid MA, Khalil AES, Azer MK (2015) Mineralogy, geochemistry and geotectonic significance of the Neoproterozoic ophiolite of Wadi Arais area, south Eastern Desert, Egypt. Int Geol Rev 58:687–702
Peltonen P, Kontinen A, Huhma H (1998) Petrogenesis of the mantle sequence of the Jormua Ophiolite (Finland): melt migration in the upper mantle during Palaeoproterozoic continental break-up. J Petrol 39:297–329
Peltonen P, Kontinen A (2004) The Jormua ophiolite: a mafic-ultramafic complex from an ancient ocean-continent transition zone. In: Kusky TM (ed) Precambrian ophiolites and related rocks, Developments in precambrian geology, vol 13, pp 35–71
Prichard HM, Fisher PC, Nearly CR, Ohara MJ (2008) PGE-rich podiform chromitites in the Al'Ays ophiolite complex, Saudi Arabia: an example of critical mantle melting to extract and concentrate PGE. Econ Geol 103:1507–1529
Selassie MG, Reimold WU (2000) A review of the metallic mineral resource potential of Ethiopia. Chronicle Miner Res Explor 540:11–32
Shackleton RM (1994) Review of the Late Proterozoic sutures, ophiolitic melanges and tectonics of Eastern Egypt and Northern Sudan. Geol Rundsch 83:537–546
Sofiya A, Ishiwatari A, Hirano N, Tsujimori T (2017) Relict chromian spinels in Tulu Dimtu serpentinites and listvenite, Western Ethiopia: implications for the timing of listvenite formation. Int Geol Rev 59:1621–1631
Stern RJ (1994) Arc assembly and continental collisions in the Neoproterozoic East African Orogen: implication for the consideration of Gondwanaland. Annu Rev Earth Planet Sci 23:319–351
Stern RJ, Johnson PJ, Kröner A, Yibas B (2004) Neoproterozoic ophiolites of the Arabian–Nubian Shield. In: Kusky T (ed) Precambrian ophiolites and related rocks. Elsevier, Amsterdam, pp 95–128
Stern RJ, Kroner A, Manton WI, Reischmann T, Mansour M, Hussein IM (1989) Geochronology of the late Precambrian Hamisana shear zone, Red Sea Hills. Sudan and Egypt. J Geol Soc Lond 146:1017–1030
Stern RJ, Ali KA, Abdelsalam MG, Wilde SA, Zhou Q (2012) U-Pb zircon geochronology of the eastern part of the Southern Ethiopian Shield. Precambr Res 206–207:159–167
Stowe CW (1994) Compositions and tectonic settings of chromite deposits through time. Econ Geol 89:528–546
Styles MT, Nasr BB, Connor EAO (1996) Several occurrences of platinum group minerals in the Nubian Shield of Eastern Egypt. Internal Report, Geological Survey of Egypt, pp 793–808
Suleiman Y (1994) Economic potenialty of mineral and rocks in Gala Enhal & Umm Saqata. M.Sc. Thesis, Khartoum University, Sudan
Tadesse G, Allen A (2005) Geology and geochemistry of the Neoproterozoic Tuludimtu Ophiolite suite, western Ethiopia. J Afr Earth Sci 41:192–211
Tadesse S, Milesi J-P, Deschamps Y (2003) Geology and mineral potential of Ethiopia: a note on geology and mineral map of Ethiopia. J Afr Earth Sc 36:273–313
Tefera M, Cherenet T, Haro W (1996) Geological map of Gore area (1:2000, 000): Ethiopian Institute of Geological Surveys

Teklay M, Kröner A, Metzger K, Oberhänsli R (1998) Geochemistry Pb–Pb single zircon ages and Nd–Sr isotope composition of Precambrian rocks from southern and eastern Ethiopia: implications for crustal evolution in East Africa. J Afr Earth Sci 26:207–227

Venturi CM, Greenough JD, Ulansky C, Fipke C (2015) Stratigraphy, thickness, tectonic environment, and economic implications of the giant Suwar—Wadi Qutabah layered mafic complex in northwestern Yemen. Can J Earth Sci 52:134–146

Vuollo J, Liipo J, Nykänen V, Pirainen T, Oekkarinen L, Tuokko I, Ekdahl E (1995) An early proterozoic podiform chromitite in the Outokump Ophiolite, Finland. Econ Geol 90:445–452

Walker RJ, Hanski E, Vuollo J, Liipo J (1996) The Os isotopic composition of Proterozoic upper mantle: evidence for chondritic upper mantle from the Outokumpu ophiolite, Finland. Earth Planet Sci Lett 141:161–173

Zhou MF, Robinson PT, Malpas J, Li Z (1996) Podiform chromitites in the Luobusa ophiolite (southern Tibet): implications for melt-rock interaction and chromite segregation in the upper mantle. J Petrol 37:3–21

Zimmer M, Kröner A, Jochum KP, Reischmann T, Todt W (1995) The Gabal Gerf complex: a Precambrian N-MORB ophiolite in the Nubian Shield, NE Africa. Chem Geol 123:29–51

Chapter 4
Magmatic—Hydrothermal Deposits (Intrusion-Related Deposits)

Contents

4.1 Introduction . . . 168
4.2 Magmatic-Hydrothermal Deposits in Saudi Arabia . . . 169
4.2.1 Porphyry Cu–Mo–Au Mineralization . . . 169
4.2.2 Epithermal Au–Ag Vein-Type Mineralization . . . 172
4.2.3 Greisen-Related Mineralization . . . 178
4.2.4 Granite-Related Mineralization . . . 184
4.3 Magmatic-Hydrothermal Deposits in Yemen . . . 186
4.3.1 Skarn-Related Sn–W Mineralization . . . 187
4.3.2 Granite-Related Radioactive and REE Mineralization . . . 188
4.4 Magmatic-Hydrothermal Deposits in Eastern Desert of Egypt . . . 189
4.4.1 Porphyry Cu–Au Mineralization . . . 190
4.4.2 Skarn-Related Mineralization . . . 199
4.4.3 Epithermal Vein-Type Mineralization . . . 203
4.4.4 Granite- and Pegmatite-Related Mineralization . . . 204
4.5 Magmatic-Hydrothermal Deposits in Sudan . . . 222
4.5.1 Porphyry Cu–Au Deposits . . . 223
4.5.2 Granite-Related Mineralization . . . 226
4.6 Magmatic-Hydrothermal Deposits in Eritrea . . . 228
4.7 Magmatic-Hydrothermal Deposits in Ethiopia . . . 228
4.7.1 Rare-Metals Granitic Pegmatites . . . 229
4.7.2 Beryllium (Emerald) Mineralization . . . 233
References . . . 237

A. Hassan Ahmed, *Mineral Deposits and Occurrences in the Arabian–Nubian Shield*,
Earth and Environmental Sciences Library,
https://doi.org/10.1007/978-3-030-96443-6_4

4.1 Introduction

Magmatic-Hydrothermal Deposits (Intrusion-Related Deposits)

Concentration of metals during magma formation and subsequent cooling and crystallization

(a) Porphyry (Cu–Mo–Au–W) deposits
(b) Epithermal-vien (Au–Ag) deposits
(c) Skarn polymetallic deposits
(d) Greisen deposits
(e) deposits associated with felsic intrusions

- Mineral deposits in granites
- REE-bearing pegmatites

In Chap. 3, several mineral deposits have been described in the ANS, which have segregated within the magma chamber. Those mineral deposits are collectively called "magmatic mineral deposits", which are directly formed from magmatic activity and are mostly associated with mafic–ultramafic intrusions. In this chapter, other economically important mineral deposits will be described, which are not directly segregated from a crystallizing magma but are formed by hydrothermal activity associated with felsic to intermediate intrusions. This group of mineral deposits is termed as "magmatic-hydrothermal deposits", or as "intrusion-related deposits". Intrusion-related ore systems are formed when a magma intrudes into a shallow level of the Earth's crust. Such intrusions essentially cool slowly in the crustal magma chamber resulting in the formation of coarse-grained rocks such as granite. Some of these rocks may contain larger crystals and a relatively smaller counterparts (bimodal) set in a finer-grained or glassy groundmass, forming a characteristic texture called 'porphyritic' texture. As a result of complete crystallization and solidification of these felsic to intermediate porphyritic rocks, a large volume of hot brine (salt-rich) fluids are produced that can potentially carry significant amounts of base metals such as Cu, Mo, Au, W, Sn and other metals.

Several economically important mineral deposits are related to the felsic to intermediate porphyritic igneous rocks (magmatic-hydrothermal deposits), including: (1) porphyry copper deposits, (2) polymetallic skarn deposits, (3) epithermal Au–Ag vein deposits, (4) greisen-related deposits, and (5) granite-pegmatite related deposits (see Table 2.1). Polymetallic epithermal Au–Ag veins and skarn deposits, greisen-related and granite/pegmatite-related deposits are the most common deposit types in the ANS. These mineral deposits are typically associated with, and occur within, the same geological environments as for porphyry copper deposits, which is therefore can be considered as a direct evidence for the presence of porphyry copper deposits in the ANS countries. Most of these deposits/prospects are associated with Neoproterozic (mostly Ediacaran) granitic intrusions within volcanic to volcano-sedimentary rocks. Many of these occurrences and prospects are located in the

Arabian Shield of Saudi Arabia and Nubian Shield in the Eastern Desert of Egypt, Red Sea Hills of northeastern Sudan, as well as in the greenstone belts of Western and Southern Ethiopia.

Following are detailed descriptions of the most common magmatic-hydrothermal deposit types (intrusion-related ore deposits) in the ANS. It is notable that this group of mineral deposits has been carefully and extensively studied in both the Arabian Shield of the Kingdom of Saudi Arabia and the Nubian Shield in the Eastern Desert of Egypt, where these deposits are abundant. At present, this group of deposits is under-represented in the rest of the Nubian Shield in Sudan, Eritrea and Ethiopia, likely due to lack of exploration. Therefore, the focus of this chapter will be on the mineral deposits present in the Kingdom of Saudi Arabia and the Eastern Desert of Egypt.

4.2 Magmatic-Hydrothermal Deposits in Saudi Arabia

The complex geologic history and the diversity of rock types of the Arabian Shield in Saudi Arabia is favorable for the formation of various types of metallic mineral deposits in the shield rocks. The evolution of the Arabian Shield has gone through various geologic stages (which resulted in the formation of such diversity of metallic mineral deposits), including: (1) island arcs accretion at convergent plate margins, (2) subduction of juvenile oceanic crust, (3) divergent movements involving the formation of early to middle Neoproterozoic intra-oceanic and continental margin volcanic-magmatic arcs, (4) the deposition of middle to late Neoproterozoic sedimentary and volcano-sedimentary successions, and (5) the emplacement of an enormous amount of late- to post-tectonic granitic and lesser mafic intrusions. The Arabian Shield therefore hosts various types of metallic mineral deposits such as Au, Cu, Zn, Pb, Fe, REE, and other metallic mineral deposits related to the active convergent/divergent plate tectonics and associated orogenic systems.

In this chapter, intrusion-related mineral deposits including porphyry Cu–Mo–Au deposits, epithermal vein-type Au–Ag deposits, greisen-related deposits, and granite/pegmatite-related deposits in the Arabian Shield of Saudi Arabia are discussed. Although garnetiferrous and calcic skarns were described in the SW of the Arabian Shield (Ahmed and Harriri 2006; Surour and Moufti 2009), the metallic skarn deposits are not reported until now in Saudi Arabia.

4.2.1 Porphyry Cu–Mo–Au Mineralization

Porphyry deposits are considered considered to be one of major sources of copper (Cu), molybdenum (Mo), and gold (Au) (Sillitoe 1997, 2010; Hedenquist et al. 1998; Ulrich et al. 1999; Halter et al. 2002; Heinrich et al. 2004; Cooke et al. 2005). Porphyry deposits are characterized by very large volume of mineral resources but low- to medium-grade of Cu–Mo–Au concentrations, which occur as disseminated

vein-, stockwork-, and breccia-hosted mineralization associated with porphyritic acidic intrusions (Singer 1995; Rowins 2000; Seedorff et al. 2005; Cooke et al. 2005; Berger et al. 2008). Porphyry deposits are typically formed from aqueous solutions at temperatures lower than 500 °C in island and continental arc environments in a close association with subduction-related, calc-alkaline silicic magmas (Richards 2003; Seedorff et al. 2005; Sillitoe 2010; Siddiqui et al. 2015). Generally, there are several characteristic features of porphyry system, which can distinguish them from other base-metal deposits such as the volcanogenic-massive sulfide (VMS) deposits. These features include: (1) close relation to porphyritic stocks, dikes, and sills with a composition ranging from granodioritic to quartz monzonitic, (2) have a simple ore mineralogy, comprising chalcopyrite, pyrite, and molybdenite, (3) show characteristic types and distribution pattern of alteration zones, and (4) common abundance of hydrothermal breccias and quartz-vein sets overlain the porphyritic intrusions.

Porphyry-type mineralization with one or more of the above features has been recently recognized in the Arabian Shield of Saudi Arabia (Nehlig et al. 2002; Johnson and Kattan 2012). In general, there is a common geochemical zonation associated with the K-rich intrusive rocks, characterized by Cu–Mo anomalies in the core, Sn–W anomalies near the margin/contact, and Pb–Zn–Ag–Au quartz veins farther out in the country rocks. They are mainly found in an inter-arc crustal setting, or in younger sedimentary basins such as the Murdama and Jibalah groups. Most of the global porphyry/epithermal deposits are characterized by "adakitic" signature, which is also identified in the Arabian Shield. Examples of these porphyry systems in the Arabian Shield are documented in the Al Amar and Samran belts, and at Gebel Ghadarah-Bir Tawilah (Fig. 4.1). The known porphyry-type occurrences in the Arabian Shield at present are clustered in eight major districts (Nehlig et al. 1999). These occurrences include the Fawarah Murdama basin, the Baid ad Jimalah—Umm Hadid belt, the Ar Ruwaydah belt (west of Al Amar), the Wadi Salamah—Al Khushaymaiyah Murdama basin, the South Afif terrane, the Ghurayrah block north of Khamis Mushayt, the Musayna'ah district (Cu–Au) west of Nuqrah, and the Al Ula—Khaybar district.

Some occurrences and prospects of Cu–Au mineralization are reported along the northwest margin of the Ar Rayn terrane, in the *Ad Dawadimi* province (Fig. 4.1), such as Al Eitaby and Umm ash Shash, and are interpreted as possible surface expressions of potential porphyry Cu system at depth (Doebrich et al. 2007). These occurrences contain Cu-bearing vein and stockwork zones associated with porphyritic granitic intrusions and alteration zones typical for porphyry-type mineralization. The ore minerals in these areas include chalcopyrite, malachite, magnetite, and hematite. Recently, Saudi Geological Survey (SGS) (according to the State-Owned News Agency) has discovered large quantities of porphyry Cu–Mo deposits in the area of Ad Dawadmi province, which extends to the north of Al-Quway'iyah. Based on the kingdom's mining regulations, the ministry of petroleum and mineral resources will seize the area, which will be considered as a potential Cu mining reserve.

In addition to the Ad Dawadmi Cu prospects, there are several occurrences of porphyry Cu–Mo–Au mineralization throughout the Arabian Shield. One of the largest well-known Cu-bearing areas in Saudi Arabia is the *Musayna'ah* prospect in the As Safra-Musayna'ah district (Fig. 4.1), ~6 km long, Cu–Au mineralization of

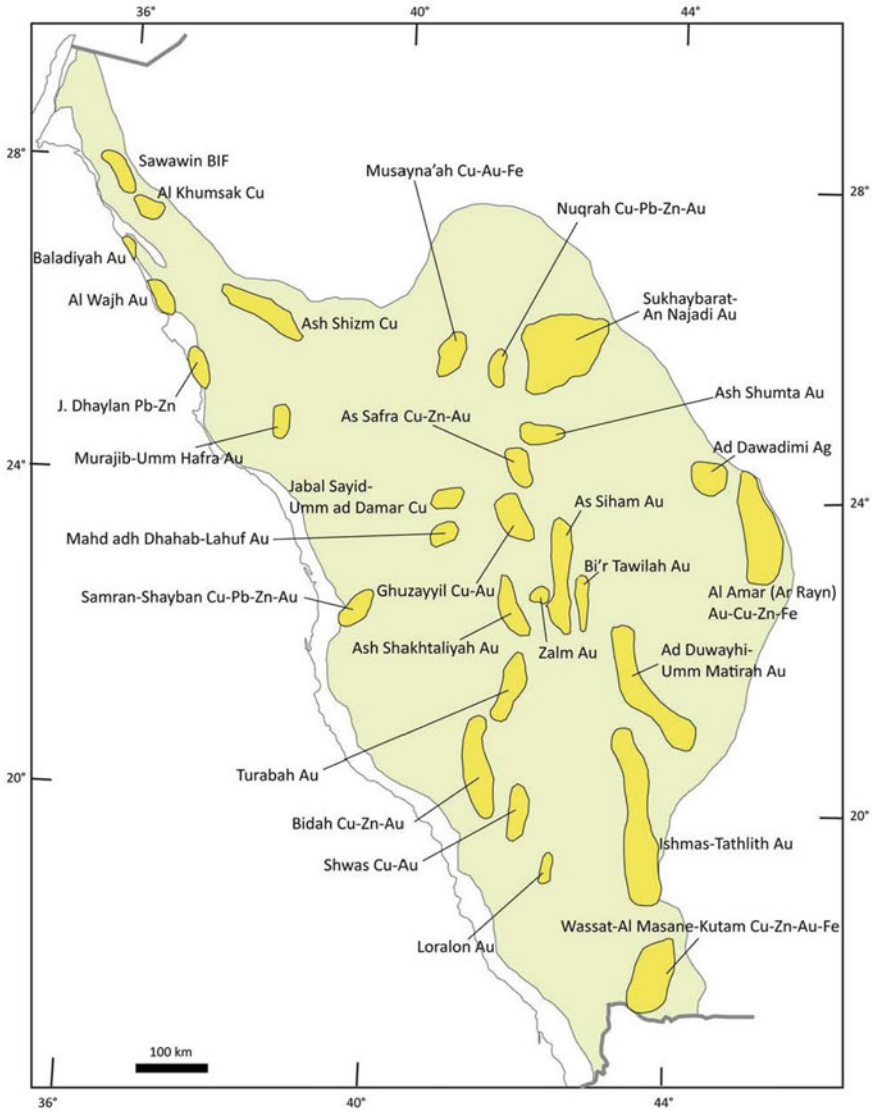

Fig. 4.1 Mineral districts and metallic mineral grouping in the Arabian Shield of Saudi Arabia (taken from Johnson and Kattan 2012)

various forms, including: (1) disseminated Cu sulfides (i.e., chalcopyrite) in andesitic breccia, with minor Au–Cu in veinlets and stockworks cutting andesite and rhyolite dikes. The Cu mineralization (mainly cuprite and tenorite) is mostly associated with the potassic alteration zone (K-feldspar, biotite, magnetite, and hematite). Propylitic alteration zone is also developed laterally with chalcedony, chlorite, carbonate, and

auriferous pyrite, all suggestingthe presence of a large porphyry system related to the syntectonic granodioritic intrusion. (2) Vein-rich and disseminated Cu–Au (up to 14 g/t Au in gossans cover) in breccias displaying cockade texture/structure; and (3)) Cu occurrences associated with Fe oxides in south of the Hamra intrusion and skarn-type associations are also known farther north (Nehlig et al. 1999).

Some other Cu–Mo–Au occurrences are also documented in the *Sukhaybarat-Silsilah* district (Fig. 4.1), where several Cu–Mo–Au–Ag occurrences, around and within granitic intrusions, were described as porphyry-type mineralizations (Nehlig et al. 1999). Among these occurrences (1) *Al Habla* occurrence, east of Sukhaybarat, has a wide area of old workings extending over 3.7 km with an average dumps grade of around 7.8 g/t Au. (2) The *Mibari* Cu–Mo–Au occurrence, where shallow drilling delineated a very wide area of propylitic alteration zone, characteristic of porphyry system, giving very large tonnage (~80 Mt) but low-grade ore (0.18 g/t Au, 0.12% Cu). Although this low-grade/high tonnage occurrence is not attractive for the traditional ancient time miners, it might be a potential for the new Cu–Mo–Au target if further detailed exploration conducted. (3) The *Hibshi* prospect, located near a major shear fault, is known to contain a Cu–Mo, and to a lesser extent Au, mineralization.

In the *Baid Ad Jimalah-Ad Dawadimi* district (Fig. 4.1), there are several small-scale Cu–Mo–Ag occurrences related to sub-volcanic or young peralkaline intrusions, which are considered as potential sources of the porphyry-style mineralization such as those in the Ar Ruwaydah complex. Furthermore, a Sn–Mo–Cu–Ag anomalies were interpreted (by induced polarization method) in a breccia zone in the northeast of the prospect intersecting a quartz porphyry intrusion. At *Wadi Garrah*, of *Al Amar* district (Fig. 4.1), porphyry-type mineralization occurrs in the form of a circular peralkaline granite cupola of about 100 m diameter within gneissic tonalite rocks, where diffused quartz stockworks and a flat-lying quartz veins in a ring system are common. Analysis of oriented rock-samples yielded significant average grades of Mo (up to 0.6%), Au (up to 0.8 g/t) and Cu (up to 0.6%).

4.2.2 Epithermal Au–Ag Vein-Type Mineralization

Epithermal vein-type deposits are commonly hosted in volcanic rocks forming the upper part of sub-volcanic K-rich intrusions, and most frequently overlying the porphyry systems in a subduction-related arc setting. In the Arabian Shield of Saudi Arabia, there are two major epithermal Au–Ag telluride vein-type deposits: Mahd Adh Dhahab and Al Amar deposits (Fig. 4.2). The *Umm Hadid* Ag occurrence and some other occurrences of Mn–Ba–Ag mineralization may also belong to the same group of epithermal vein-type mineralization.

Several gold deposits and occurrences are intensively explored and developed in the Arabian Shield of Saudi Arabia (Fig. 4.2). Some of these deposits are currently being mined (e.g., Mahd Adh Dhahab, Al Amar, and Al Sukhaybarat), but some others are already mined out. The *Mahd Adh Dhahab* “Cradle of Gold” gold mine is

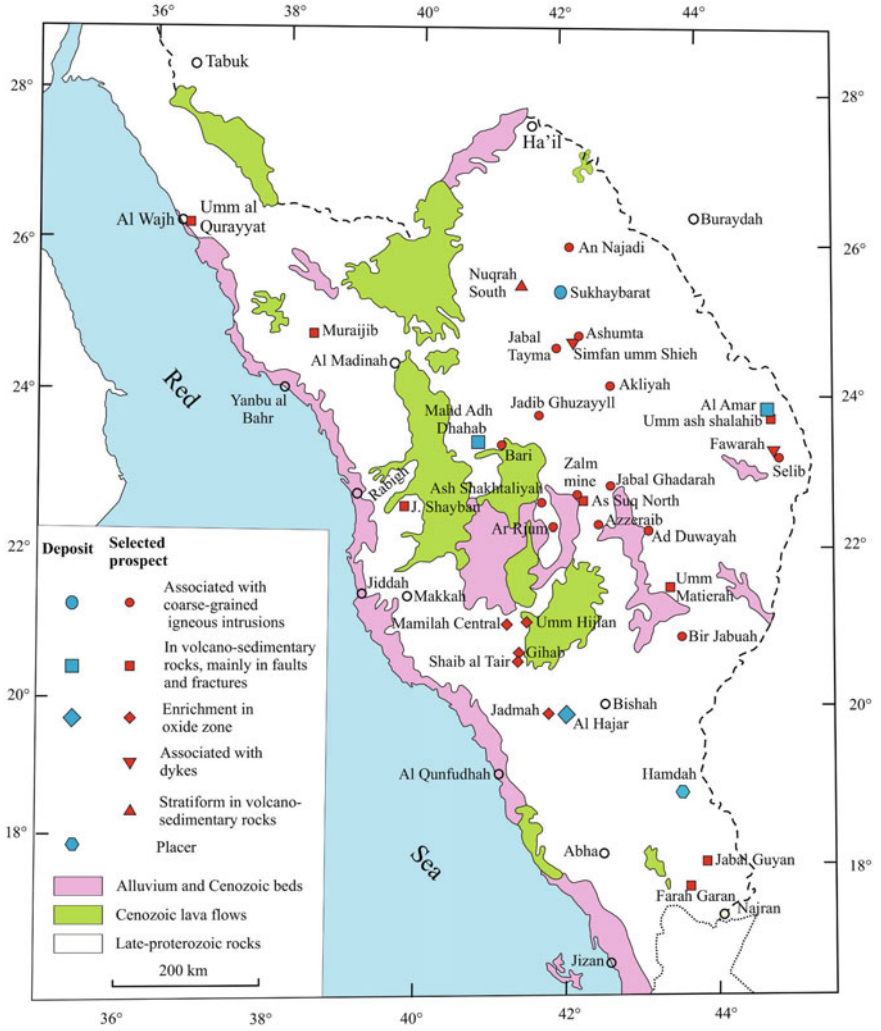

Fig. 4.2 Distribution of gold deposits and occurrences in the Arabian Shield of Saudi Arabia, showing the location of Mahd Adh Dhahab and Al Amar epithermal gold vein deposits (modified from Collenette and Grainger 1994)

one of the largest polymetallic Au–Ag telluride vein-type epithermal deposits in the Arabian Shield. The age of the Mahd Adh Dhahab mineralization was constrained at 649 Ma (Afifi 1990). The Mahd Adh Dhahab area is located 380 km northeast of Jeddah (Fig. 4.2) in the west-central part of the Arabian Shield. The mineralized area is hosted by the Mahd group rocks (Clavez and Kemp 1982), which are unconformably underlain by the metamorphosed calc-alkaline granitoid basement rocks of Dhukhur batholith (Kemp et al. 1982; Afifi 1990). The Mahd group rocks

in the mine area were intruded by granitic and gabbroic intrusions and subsequently covered by conglomerates, epiclastic sandstones and dacitic lavas of the Ghamr group rocks (Fig. 4.3). From the oldest to the youngest, the stratigraphic succession of the Mahd area, consists of andesite, lower agglomerate, lower tuff, upper agglomerate and upper tuff (Luce et al. 1976; Doebrich and LeAnderson 1984). The layered sequence of the Mahd area was lately intruded by rhyolite porphyry, which host the most extensive ancient workings along fault-related quartz veins (Fig. 4.4a). Rhyolite porphyry commonly contains fine-grained disseminated base-metal sulfides. The latter is oxidized and is now a reddish color secondary surficial material at surface exposures (Fig. 4.4b).

The gold mine of Mahd Adh Dhahab is located along the eastern edge of the Mahd Mountain in a wide zone of quartz veins, alteration, and fault systems. The mineralized structure or/and area of Mahd Adh Dhahab is located at a few kilometers from the southwestern edge of the Najd fault system, which contains the ancient and current mining activities. The mineralized quartz veins in the Mahd Adh Dhahab area are mostly fault-related fracture fillings, trending north/northeast, and to a lesser extent, northwest/west directions. The mineralized quartz veins are mostly banded (Fig. 4.4c) and brecciated (i.e., stockworks), which indicate multi-phase injections

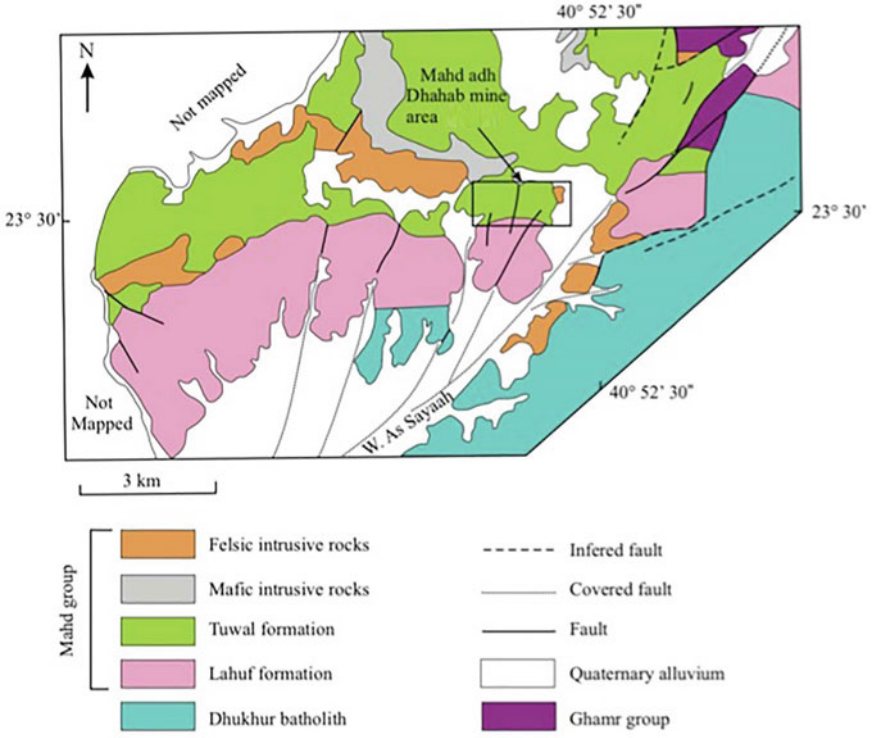

Fig. 4.3 Geologic map showing the general geology of Mahd Adh Dhahab district (modified from Afifi 1990)

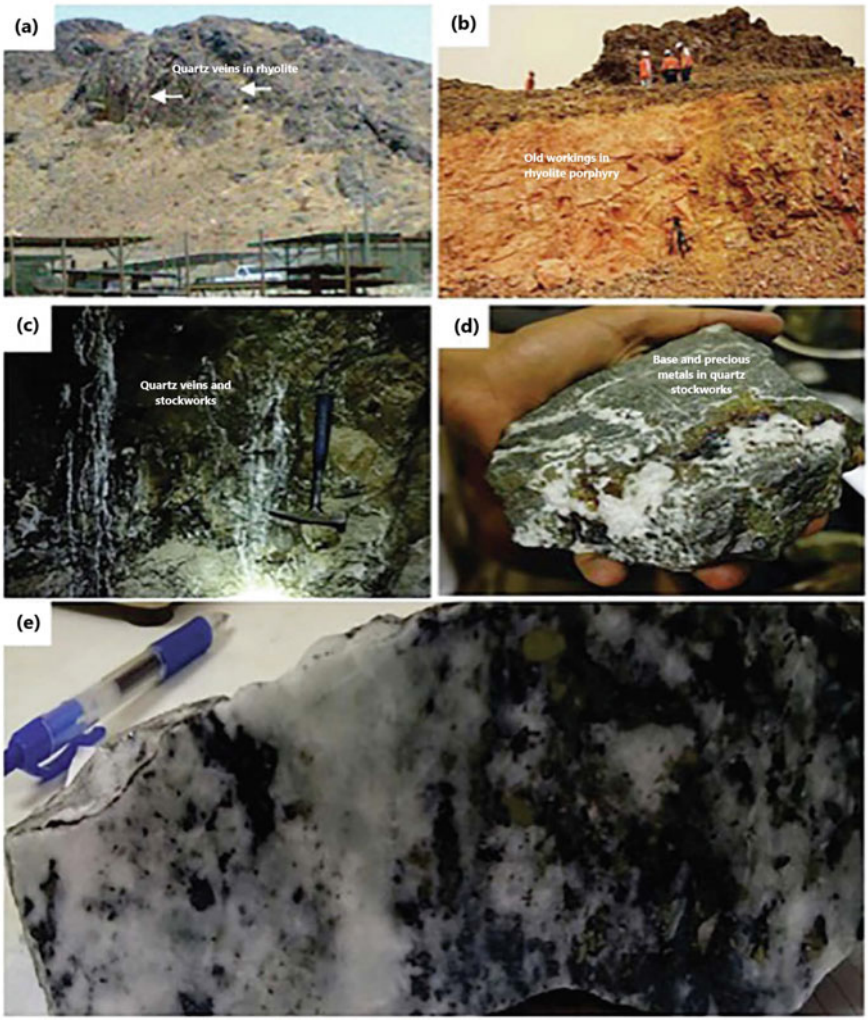

Fig. 4.4 Field photographs (**a**–**c**) and hand specimens (**d**, **e**) of Mahd Adh Dhahab gold mine. **a** Part of the Mahd Adh Dhahab mountain with sets of parallel quartz veins, **b** excavated rhyolite porphyry intrusion within the upper agglomerate unit of the Mahd Group, **c** multiphase quartz veins and veinlets sets (white) cross-cutting the rhyolite porphyry, underground mine, **d** hand specimen showing stockwork-bearing sulfides in quartz veins, underground mine, and **e** polished rock slab showing quartz-chlorite breccias with minor sulfides, underground mine of Mahd Adh Dhahab area (taken from El-Shafei et al. 2020)

(El-Shafei et al. 2020). In the eastern side of the southern mining area, the quartz veins are mainly occurred as massive stockworks (Fig. 4.4d) up to 30 m wide dipping to the west by 10–60°. The multi-stage veining in the Mahd Adh Dhahab area is manifested by variably mineralized veinlets intersecting each other, where different generations of milky and smoky quartz veins are recognized. The milky quartz veins represent the earlier generations and comprise both massive and banded types. The massive milky quartz veins contain traces of pyrite (Fig. 4.4e) whereas banded quartz veins are composed of crustified quartz, chlorite, sulfides (sphalerite and chalcopyrite) and Au–Ag tellurides. The smoky quartz veins constitute the later generations and include two subsequent stages; the first stage consists of comb-structure quartz, chalcopyrite and sphalerite with minor carbonate. The second stage of smoky quartz veining is commonly calcareous where carbonate exceeds quartz and contains only sparse sulfides, mostly pyrite and minor chalcopyrite. The primary base-metal sulfide minerals include, in a decreasing order of abundance, sphalerite, chalcopyrite, galena, and pyrite, however in places, sulfides are predominant as pyrite-sphalerite veins (Sangster and Abdulhay 2005).

Precious metals (Au and Ag) are present as Au–Ag tellurides, mainly represented by hessite (Ag_2Te), petzite (Ag_3AuTe_2), and sylvanite ($(Au, Ag)_2Te_4$), while gold occurs in native form as inclusions in sphalerite, along grain boundaries, and as small grains in quartz (El-Shafei et al. 2020). The distribution of Au and Ag is erratic and their grades in the mine are highly variable. In addition, Bi tellurides are also present as tetradymite and tellurobismuthite, while altaite is the only described Pb-telluride. It is noteworthy that, Au, Ag and Bi tellurides are commomly related to chalcopyrite, whereas sphalerite is almost devoid of any tellurides (El-Shafei et al. 2020). It is also noted that propylitic alteration and silicification are widespread in and around the mine area. The potassic alteration is abundant at the Mine Hill and close to mineralization, and disseminated pyrite is common in vein of the wall rocks. The depth of oxidation penetrates as much as 50–100 m below the surface, and supergene enrichment is unevenly distributed between depths of 20 and 50 m as a zone of few meters thick. The Mahd Adh Dhahab gold mine is a world-class Au–Zn–Cu–Ag mine, with estimated average ore grades of 24 g/t Au, 92 g/t Ag, 0.65% Cu and 3.11% Zn, with a total historic production of more than 180 ton of Au, 4.5 ton Ag, 249 ton Zn, and 425 ton Cu. The Mahd Adh Dhahab mine is currently producing more than 3 ton of Au per annum.

The Au–Ag telluride mineralization, at Mahd Adh Dhahab is interpreted to be formed from varying proportions of mixed magmatic and meteoric fluids (El-Shafei et al. 2020). The ascending magmatic fluids originated from the alkaline magma were originally rich in Te. Several lines of evidence indicate that the Au mineralization was formed through a multi-stage process, including: (1) alternating bands of smoky and milky quartz, (2) alternating sphalerite-rich and chalcopyrite-rich bands, (3) various types of compositionally and texturally different chlorites, and (4) the close association of Au- and Ag-tellurides with certain types of chlorite and sulfide phases. The Au, Ag and Te contents of the fluid pulses were likely variable to produce the observed mineralogical differences (El-Shafei et al. 2020).

Furthermore, epithermal vein-type mineralization has also been explored in the region nearby the Mahd Adh Dhahab mine, in Mahd group rocks at the *Lahuf* area,

about 12 *km* along strike west of Mahd Adh Dhahab mine. Quartz-veins and stockworks, up to several meters wide are present at the *Gebel Ram Ram* volcanic caldera, ~25 km west of Mahd Adh Dhahab. *Bari* area, located at ~30 km southeast of Mahd Adh Dhahab mine is characterized by Au–Ag–Zn–Cu-quartz veins in tonalite and quartz diorite.

The *Al Amar* Au–Ag deposit is the second largest polymetallic epithermal deposit, similar to the Mahd Adh Dhahab counterpart, in the eastern margin of the Arabian Shield (Fig. 4.2). The Al Amar deposit is currently in production by the Ma'aden Company. It is located in the Al Amar arc, which is part of the Ar Rayn terrane. The latter is one of the richest provinces in metallic mineral deposits in the Arabian Shield (Fig. 4.1). The Al Amar arc is a late Cryogenian-Ediacaran (>689–615 Ma) continental-margin volcanic-arc assemblage, exposed along strike of ~200 km at the extreme eastern edge of the Arabian Shield. It further continues for at least 300 km to the north beneath the Phanerozoic sedimentary cover (Johnson and Stewart 1995). Mineralization in the Ar Rayn terrane are concentrated in the Al Amar group rocks, in the western part of the terrane, at the contact with the Ad Dawadimi terrane. The rock types of Al Amar group are mostly low-grade tholeiitic to calc-alkaline basaltic to rhyolitic volcanic and volcaniclastic rocks with subordinate tuffaceous sedimentary rocks and carbonates (Doebrich et al. 2007). The Al Amar epithermal Au–Ag deposits are hosted in volcanic-arc assemblage comprising mafic to intermediate pyroclastic rocks and subordinate andesite flows, felsic volcaniclastic rocks and lava, and felsic to intermediate tuffs and pyroclastics (Fig. 4.5).

The Al Amar ore deposits mainly occur in two subvertical northwest-trending veins (Fig. 4.5), the north- and south-vein zones, which are composed of polymetallic sulfides (pyrite, sphalerite, chalcopyrite, and galena), and Au-bearing veins associated with beds and lenses of talc, barite, and Ca–Fe–Mn carbonates (Lofts et al. 1986). In addition to the existence of free Au and electrum, Au–Ag tellurides are also common in the sulfide minerals. Similar geologic setting and ore mineral assemblages of the Al Amar and Mahd Ad Dhahab deposits suggest, the similarity in their genesis. However, the formation of native Au and electrum in the Al Amar deposits indicates lower Te activity, which could be due to low Te concentrations in the source (El-Shafei et al. 2020). The estimated ore reserves of Al Amar deposit are 1.55 Mt as measured and indicated reserves, with an average grade of 12.31 g/t Au, 21.07 g/t Ag, 6.16 wt% Zn, and 0.92 wt% Cu, in addition to 3.0 Mt inferred reserve with an average of 5.1 g/t Au.

There are several other occurrences and prospects in the Arabian Shield that are considered as an epithermal vein-type deposits but needs further investigations. Examples of such occurrences include the epithermal veins associated with carbonates at *As Safra* area and those veins associated with younger volcanic rocks at *Asfar al Hadawi* area in As Safra-Musayna'a district (Fig. 4.1). In the As Safra prospect, there are extensive old workings in a shear-zone developed in rhyolitic tuff associated with carbonates and intruded by subvertical rhyolitic dikes (Nehlig et al. 1999). In the Asfar al Hadawi occurrence, northwest of Hulayfah, the mineralization consists of fractures filled with barite, and Ag- and U-bearing minerals, which could represent an Au-depleted high-sulfidation epithermal mineralization. In Al Amar district,

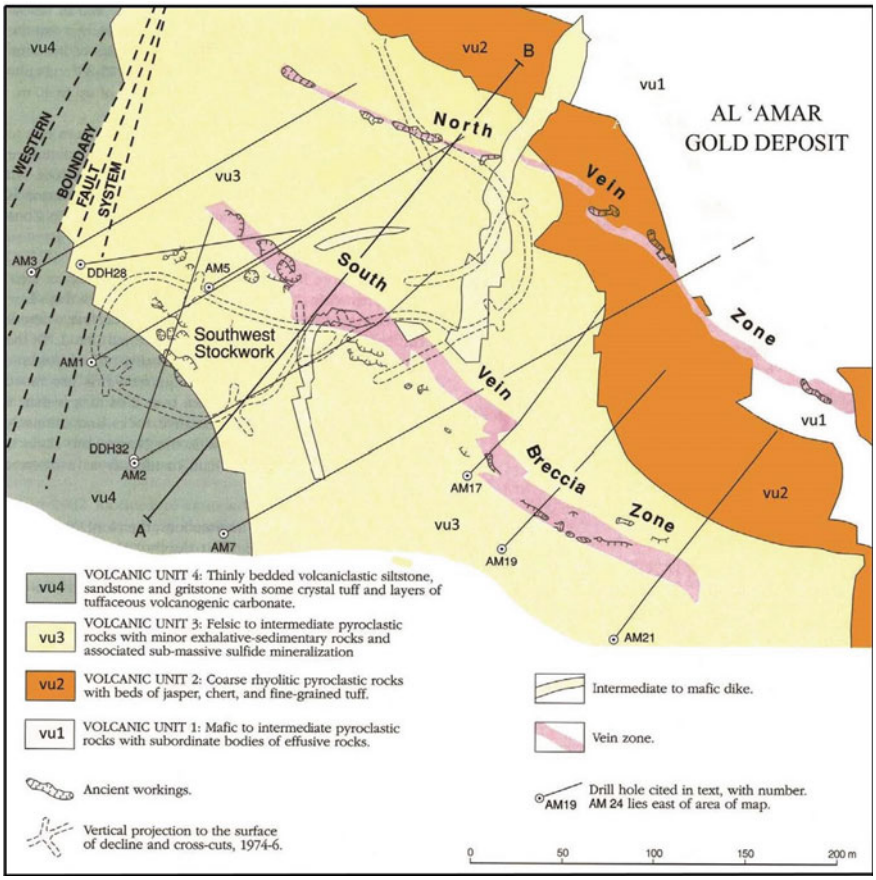

Fig. 4.5 Geologic map of Al Amar gold deposits, eastern Arabian Shield of Saudi Arabia (taken from (Collenette and Grainger 1994)

several occurrences of the same epithermal mineralization, but with few old workings and much abundant hydrothermal alteration, such as those in *At Taybi* (south of Al Amar) where Zn–Cu–Ag sulfides were intersected, *Umm Ad Dabah*, *Umm ash Shalahib* Cu–Zn–Au, and *Marjan* Au–Ag–Cu–Zn prospects.

4.2.3 Greisen-Related Mineralization

Greisenization is a granite-related post-magmatic (i.e., metasomatic) process, in which the micas (biotite and/or muscovite) and feldspars become unstable and replaced by complex smaller aggregates of micas (mainly muscovite), quartz, topaz, fluorite and tourmaline. In many cases, economic to sub-economic metallic deposits

of tin (Sn), tungsten (W), molybdenum (Mo) and beryllium (Be) are associated with greisenization. The distribution and occurrences of greisen are limited to the high-SiO_2 metalliferous granitic plutons (especially in their apical parts or cupola) (Stemprok 1987).

In the Arabian Shield of Saudi Arabia, most Sn and W mineralizations are related to highly differentiated "silica-rich" granites enriched in volatiles (F, P, Li). Few examples of greisen-related mineralizations were found in the Shield, these are: the *Bir Tawilah W–Sb–Bi–Mo* mineralization occurring as veins around granite cupolas, the *Silsilah Sn–W* mineralization related to greisen alteration within a peraluminous granite intruding the Murdama metasedimentary rocks, and fluorite deposits associated with greisen alteration of *Gebel Ablah*. These greisen-related occurrences represent small-stocks that are not economic at present, but their potential, especially those at Gebel Ablah and Gebel Silsilah need further assessments.

The *Gebel Silsilah* granitic complex forms a huge ring structure (Fig. 4.6) of ~12 km in diameter, and is dated at 587 Ma (du Bray 1985, 1986). The core of

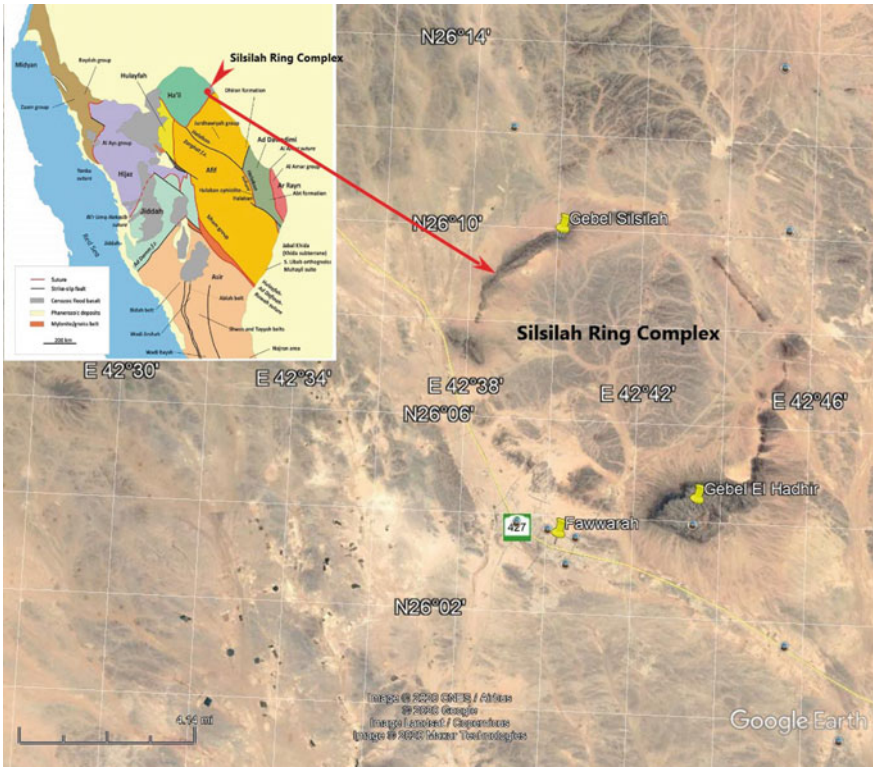

Fig. 4.6 Google Image Landsat showing the Silsilah granitic ring complex of Saudi Arabia. Inset map shows the location of Silsilah ring complex in the Arabian Shield

the Silsilah complex is composed of alkali granite, with a rim of aplite and peralkaline commendites. The Silsilah ring complex consists of three principal intrusive rock-types (Fig. 4.6); the northwestern and southeastern parts are composed of Silsilah alkali granites, and the southwestern part is represented by Fawwarah alkali-feldspar granite. The El Hadhir aplite in the southeastern part of the complex forms a sill-like body capping the alkali-feldspar granite. The alkali granite of the complex is intensively affected by a greisen-type alteration with muscovite and topaz containing disseminated cassiterite mineralization. Simple pegmatite, with quartz and K-feldspar, forms a sheet-like body in the area between the Fawwarah alkali-feldspar granite and El Hadhir aplite, as well as a plug of ~1 km long inside the southwestern margin of the ring complex. Two strongly mineralized greisenized pods occur near this plug. Weakly mineralized pods of greisen also crop out at several localities in the SW part of the complex and within the Fawwarah alkali-feldspar granite. All the above plutonic units are cut by numerous quartz veins.

The mineralized greisen underlies El Hadhir aplite and pegmatitic rocks at its base in the southwestern part of the Silsilah complex. Other sheet- or cupola-like bodies may also present beneath thin outcrops of aplite and/or Maraghan lithic greywacke (du Bray 1986). Degree of greisenization decreases downwards and the greisen grades into incompletely greisenized alkali-feldspar granite within a few meters below the surface. The greisen is entirely covering two small hills less than 1 km long inside the outer rim of the southwestern part of the ring complex, with an irregular outcrop pattern (Fig. 4.6). The metallic mineralization occurs as disseminated cassiterite grains that constitute up to 10% of the quartz-topaz rich rock with traces of opaque oxide and white mica. In some places of the complex, small elliptical pods ranging in size from 0.05 to 5 m in diameter contain about 50–90 volume % cassiterite. The less greisenized granite at the periphery of greisen, comprises various proportions of quartz, white mica, topaz and trace amounts of albite and cassiterite. They occur as isolated pods within the Fawwarah alkali-feldspar granite, particularly in the south of the complex, near the two small masses of alkali-feldspar granite cropping out inside the ring structure. These pods are approximately ellipsoidal in shape and range in size from 10 to 200 m across. Although Sn and W are the only metals of economic interest, some other elements such as Ag, B, Bi, Mo, Nb, Pb, Zn, As, and F, are also present in anomalous concentrations in these rocks compared with values in the host low-Ca granite (du Bray 1985, 1986). The estimated resources of the Silsilah occurrence were about 1.5 Mt with an average grade of 0.19% Sn. The complete economic potential of the complex needs further assessment.

The *Gebel Ablah* greisenized alkali granite/pegmatite is one of the famous locality for fluorite deposits in the Kingdom of Saudi Arabia. The Ablah area is known for ancient mining activities that are commonly small, but with unusual mineral occurrences for fluorite as well as Ag, Cu, Au, and Mo, in greisenized alkali feldspar granite and pegmatite body (Collenette and Grainger 1994). The Gebel Ablah mine site is a prominent white cone-shaped hill near the northern margin of the composite Shuwas pluton of the Asir terrane (Fig. 4.7). The Ablah prospect is located ~75 km west/northwest of Bishah, where a pegmatite forms a small hill of ~150 m height. This pegmatite plug intruded diorite/tonalite pluton, which lies on the northern edge of a syenite ring structure. The fluorite mineralized body forms a sub-circular pipe

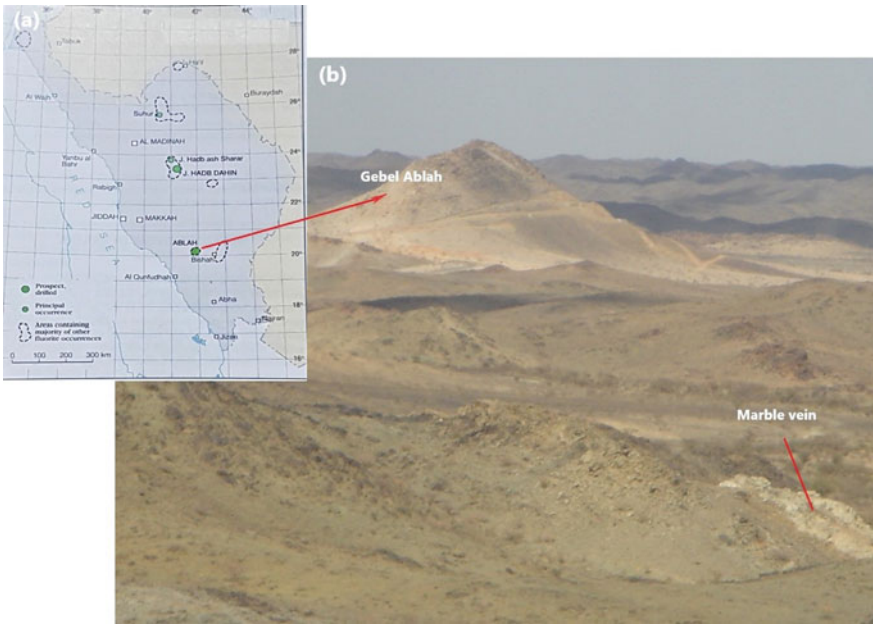

Fig. 4.7 **a** Location map of fluorite deposits in Saudi Arabia, and **b** field photograph showing Gebel Ablah and its pegmatite and fluorite deposit

of about 20 m in diameter, cropping out in a brecciated pegmatite near the top of the hill (Fig. 4.8). The fluorite pipe is composed of colorless to pale yellow-green massive fluorite ore with ~80–90 volume percentage of fluorite mineral (Fig. 4.9a). On the periphery of the pipe, the ore deposit is altered with clear enrichment in limonite, quartz, and muscovite that bear traces of malachite and iron carbonates. The alteration zone was mined (~2 m wide) to a depth of ~50 m in ancient times, probably for Au and Cu. The main body of Gebel Ablah white cone is composed essentially of pegmatite breccia (hydrothermal breccia) that consists of variable sizes of randomly oriented K-feldspar and quartz blocks (Fig. 4.9b). The brecciated pegmatite body is intensively greisenized, where the K-feldspar and quartz blocks are cemented by fine-grained muscovite and quartz (Fig. 4.9c). In addition to various blocks, quartz is also found as veins and veinlets cross cutting the brecciated pegmatite. Quartz veins and blocks occasionally contain exotic minerals such as tourmaline crystals and ore mineral aggregates (galena and cassiterite). Greisenized brecciated pegmatite is also sometimes stained with green and brown colored malachite and iron oxide minerals.

The western side of the lower part of Gebel Ablah is characterized by fresh pegmatite body displaying a simple mineral zonation such that large (meter sized) quartz crystals are surrounded by fresh K-feldspar. Furthermore, several quartz crystal cores are randomly distributed in the lower part of the white cone. The area around Gebel Ablah has been extensively explored where several base metal anomalies were detected. Grab samples from a nearby fluorite mineralization, displayed Au value of over 6 g/t (Collenette and Grainger 1994). In addition, Au values ranging

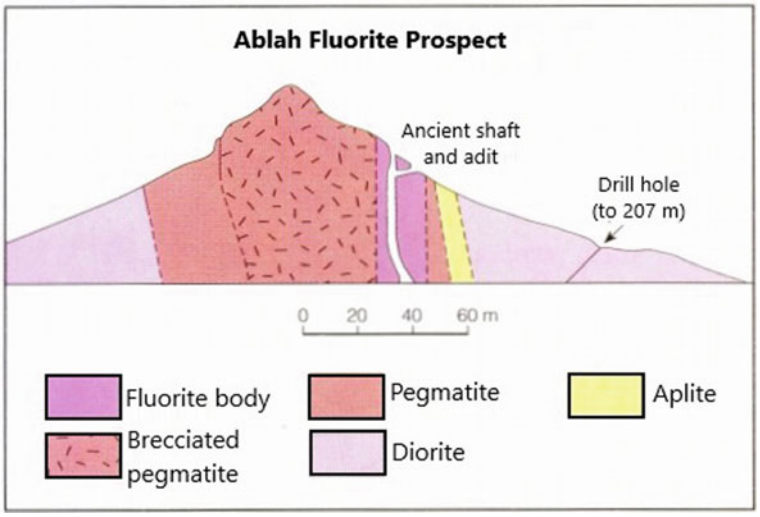

Fig. 4.8 Geologic cross-section of Gebel Ablah pegmatite and fluorite deposit (taken from Collenette and Grainger 1994)

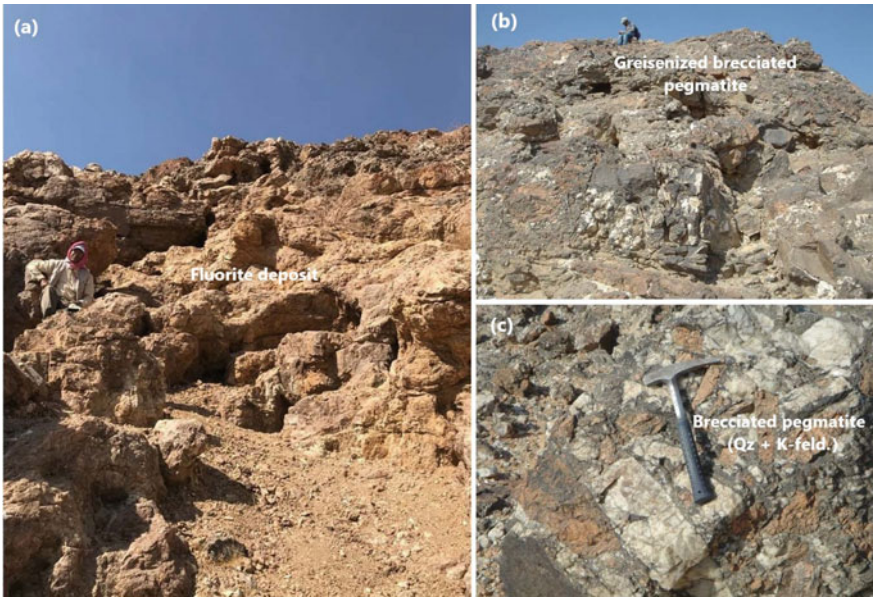

Fig. 4.9 Field photographs showing **a** fluorite deposit, **b** greisenized brecciated pegmatite, and **c** brecciated pegmatite of Gebel Ablah

from 0.5 to 8 g/t were recorded in surface samples collected from the vicinity of the fluorite mineralization during an exploration program for gold in 1989. The estimated fluorite reserves were ~20,000 metric tons of acid-grade fluorite, which was previously used as flux materials in the Cu–Au production, where large amounts of slag materials are discarded in the area.

Although production of metallic deposits are not recently commenced in the Gebel Ablah area, detectable amounts of some metals such as Cu, Pd, Zn, Au, Bi and W, were recoded as disseminated metallic minerals associated with fluorite deposits and greisenized pegmatite. These metallic minerals commonlyoccur as fissure-filling materials, where Cu-carbonate staining (i.e. malachite) is widespread in the area filling the cracks between fluorite grains, and usually associated with galena and Zn-bearing minerals (Fig. 4.10). Galena is very common in the greisenized pegmatite of Gebel Ablah, especially within fluorite deposits, which is present either as crack-filling between the K-feldspar and fluorite grains, or as small aggregates within fluorite grains (Fig. 4.10). Galena is commonly altered to cerussite (Pb carbonates). Bismuth mineral (Bi_2O_3) is also common in the greisenized pegmatite of Gebel Ablah, especially with fluorite mineralization, which is found as filament-like vermicular aggregates within quartz crystals intergrown with fluorite (Fig. 4.11). Where present, Bi mineral is commonly associated with galena and malachite within fluorite and

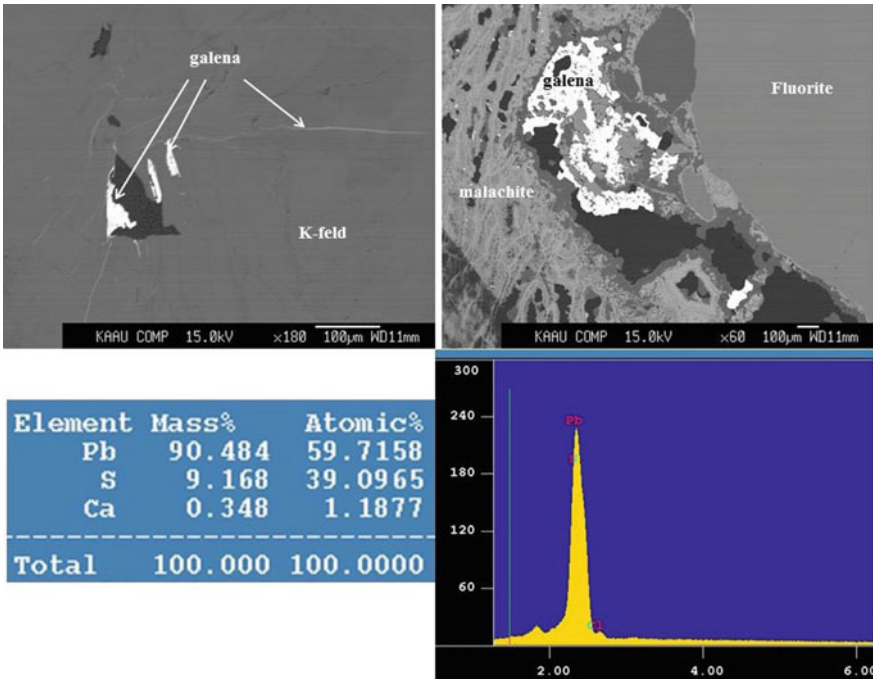

Fig. 4.10 Back-scattered electron (BSE) images and semi-quantitative analyses/chart of Gebel Ablah fluorite deposit, showing galena and malachite minerals associated with fluorite

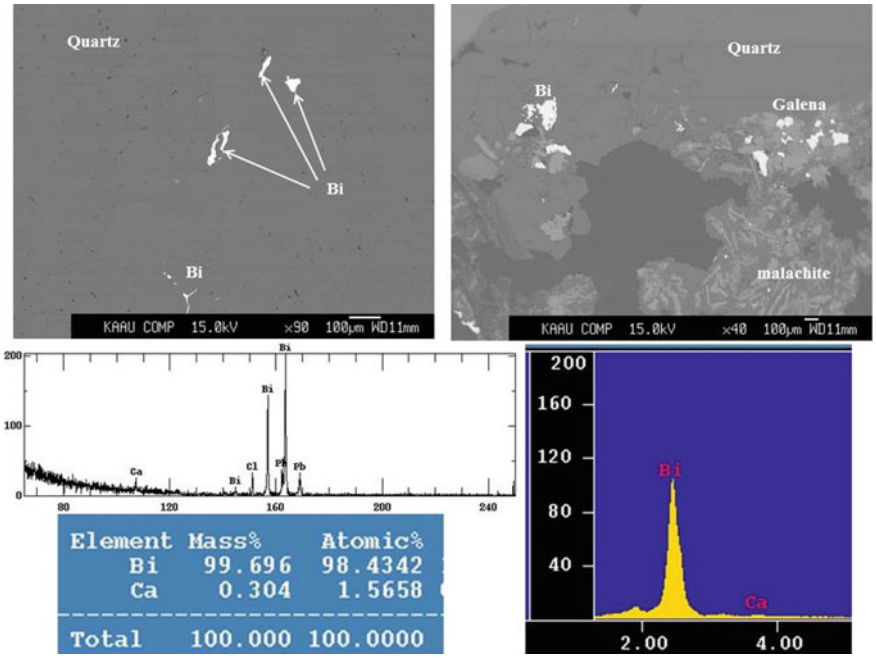

Fig. 4.11 BSE images and semi-quantitative analyses/chart of Gebel Ablah fluorite deposit, showing bismuth, galena and malachite minerals associated with fluorite

quartz grains. Although the greisen system is very famous for Sn–W deposits elsewhere in the world, the Gebel Ablah greisenized pegmatite contains few amounts of W minerals but devoid of Sn mineralization. Tungston-bearing mineral (e.g., wolframite_Fe, Mn) WO_4) of Gebel Ablah commonly associated with fluorite either as an euhedral small-sized crystals entirely included within fluorite or as an anhedral aggregates within cavities of fluorite (Fig. 4.12). Wolframite is commonly associated with other accessory minerals such as rutile, galena and malachite. The high Ca content in the semi-quantitative analyses of wolframite is due to the contamination from the surrounding fluorite (Fig. 4.12).

4.2.4 Granite-Related Mineralization

Granitoid rocks of late- to post-tectonic settings are widespread in the Arabian Shield of Saudi Arabia, and they are important sources of Au, Sn–W, and Nb–Y–REE mineralizations. Mesothermal quartz veins, within and at the contact zones of granitoid rocks of dioritic-tonalitic-granodioritic composition are suitable for gold mineralization. The veins may be controlled by faults or thrusts in the country rocks and granitic intrusions themselves. Small Sn and W occurrences are mostly associated with syenogranite and alkali-feldspar granite, for example at *Silsilah* and *Ba'id al Jimalah* areas. The mineralization is concentrated in the apical parts of small plutons

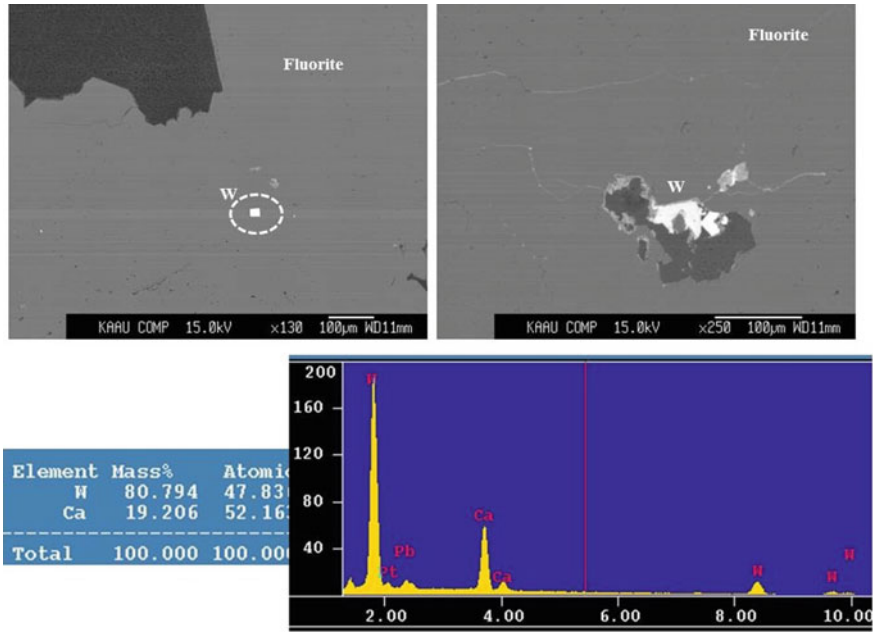

Fig. 4.12 BSE images and semi-quantitative analyses/chart of Gebel Ablah fluorite deposit, showing wolframite and veinlets of galena associated with fluorite

and stocks, although there is an unusual occurrence of W mineralization in gabbro at *Gebel Marya* in the southern part of the Arabian Shield. Other small intrusions and stocks of alkali-feldspar granite are enriched in Nb, Y, REE, and U. These intrusions were previously investigated for U but are now important as potential sources of transition metals and REE. A comprehensive review of metallic-mineral occurrences associated with felsic-plutonic rocks in the Arabian Shield is given by Jackson (1986), and descriptions of individual occurrences are provided in the DMMR Bulletin 29: Felsic plutonic rocks and associated mineralization of the Kingdom of Saudi Arabia (Drysdall et al. 1984).

Granitoid rocks hosting such mineralization can be divided into five types (Jackson 1986):

(1) Alkali granite associated with Nb, Zr, Y, REE, Sn, Ta, U, Th, and F.
(2) Low-Ca Muscovite-bearing granite associated with Sn, W, Ta, Pb, Zn, Bi, Ag, Mo, Be, and F.
(3) High-Ca Biotite-bearing granite and granodiorite associated with Mo, W, Sn, Bi, Cu, Pb, Zn, Ag, and As.
(4) Diorite, tonalite and granodiorite associated with Au, Ag, Cu, Pb and Zn.
(5) Low-Ca syenite associated with Nb, Zr, REE and F.

The alkali-granite intrusions are the most important hosts for Nb, U, Th, and REE in Saudi Arabia. *Ghurayyah* prospect, in the northwestern part of the Midyan terrane

is hosted by a circular stock of porphyritic albite-microcline alkali microgranite, and it contains potentially very large amounts of Ta, Nb, REE, Zr, and Y. Mineralization consists of uniformly disseminated columbite-tantalite, zircon, and thorite, which are the principal sources of the elements Nb, Ta, U, tin, and some Y. Other alkali granites in the Arabian Shield contain promising concentrations of these elements on the apical parts of small stocks and on their hydrothermal derivatives (pegmatites, aplites, and silexites). Occurrences include *Gebel Tawlah, Umm al Birak, and Gebel Sayid*.

The low-Ca granitoid intrusions are the main host of most Sn and W resources in the Kingdom of Saudi Arabia. Examples for such mineralizations include the *Gebel Silsilah*, which comprises low hills of greisenized granite in the apical part and cupolas of an alkali-feldspar granite stocks (pegmatites), surrounded by a large ring of alkali and alkali-feldspar granite ~6 km in diameter. The mineralization consists of hydrothermally altered alkali-feldspar granite with pods and disseminations of cassiterite in topaz-quartz and topaz-muscovite-quartz greisen. Another locality is the *Ba'id al Jimalah* prospect, which is located at a small intrusion of greisenized and quartz-veined porphyritic microgranite emplaced in sedimentary rocks of the Murdama group. The mineralization is possibly occurs at the apex of an intrusion composed of interconnected and merging sills and dikes that connect with a larger sill ~100 m below the surface. Mineralization, comprising wolframite, cassiterite, scheelite, and sulfides, is associated with quartz veins and phyllic-altered microgranite, locally replaced by coarse-grained quartz-muscovite greisen. Furthermore, well-known examples of mineralization associated with biotite-bearing, high-Ca granite and granodiorite are the *Khushaymiyah* (Mo–W–Bi), *Bi'r Tawilah* (W–Mo–Sn), and the *Ad Dawadimi* Ag district (Pb–Zn–Ag).

Characteristic types of syenite granites named alkali-feldspar syenite, quartz alkali-felspar syenite and quartz syenite, particularly their fine-grained apical varities, are associated with mineralized breccia pipes, REE-bearing pegmatites and silexites, and contact Fe-replacement mineralization (skarn). Such rock types are not common in the Arabian Shield. *Ablah* fluorite pipe and *Gebel Hamra* are the largest known fluorite-bearing Y and highest-grade REE occurrences, respectivel. The Ablah mineralization (described above) occurs in a breccia pipe is emplaced in a pegmatite-aplite breccia of 300 m long and 150 m wide, which in turn is emplaced in a diorite host. *Gebel Hamra* is a lenticular vertical body of fine-grained silexite, an igneous rock composed essentially of primary quartz (60–100%), intruded into a quartz-alkali-feldspar syenite. The pipe, approximately 300 m by 100 m, carries disseminated Nb-, Ta-, Sn-, REE-, Y-, Th-, U-, and Zr-bearing minerals. The host syenite contains pegmatite with Nb, Zr, Y, and REE minerals.

4.3 Magmatic-Hydrothermal Deposits in Yemen

The mineralization potential of the ANS in Yemen is generally poorly understood. Therefore, there is an urgent need for a comprehensive mineral exploration in order to assess its potential metal endowments. A notable reconnaissance study by the

Yemeni Geological Survey and Mineral Resources Board (YGSMRB), documented a descriptive overview of mineral resources of Yemen, entitled "The Geology and Mineral Resources of Yemen" and published in 1994. This publication was subsequently, reprinted in 2001 and 2009. Recently, Al-Khirbash et al. (2021) compiled the most important mineral deposits and occurrences in the Precambrian rocks of the Arabian Shield of Yemen. Neither porphyry Cu nor epithermal vein-type deposits were reported from the shield rocks of Yemen. Base metal sulfides and precious metal (Au and Ag) deposits were largely associated with auriferous shear zones and Au-bearing quartz veins, mainly in greenstone belts of hydrothermally altered metavolcanic and meta-diorite rocks. These types of mineralization are classified as "mesothermal" or "orogenic deposits", which will be discussed in detailed in the next chapter of this book. The only intrusion-related (magmatic-hydrothermal) deposits found in the Precambrian basement rocks of Yemen are the Sn–W skarn deposits and granite-related radioactive and REE deposits.

4.3.1 Skarn-Related Sn–W Mineralization

Tin-tungsten mineral deposits and occurrences are present in several geological environments in Yemen; most of these mineralization are associated with post-orogenic granites in northwestern part of the country. There are three types of W-bearing occurrences in southern Yemen (Table 4.1) (Shallan and Heikal 1989; Isakin et al. 1990): (1) skarn scheelite-molybdenite at the contact between granitoids and carbonate rocks such as those in the *Sarban* occurrence, (2) hydrothermal vein scheelite in volcanogenic sedimentary rocks such as those in the *Al Jafiyah* occurrence, and (3) metamorphic scheelite-skarnoid in volcanogenic-sedimentary and amphibolite rocks (e.g., the *Majab* and *Sabahan* occurrences). In addition, a low-grade Sn–W mineralization occurs in skarns in the southwestern part of *Gebel as Sa'adi* granite in the Jabali area, near Sana'a. Furthermore, a well known Sn-bearing granite occurs in *Gebel Gahlalah*, which is located about 3 km southeast of Sadah. The granite pluton measures ~3 km by 5 km and is exposed over an area of ~12 km^2. It consists of a slightly alkaline biotite-bearing metaluminous granite cut by numerous aplite and pegmatite dykes. Cassiterite mineralization is present in the narrow (~0.5 m thick) east-trending quartz-feldspar pegmatites. The Gebel Gahlalah granite contains 400–1035 ppm W, which indicates the presence of minor amounts of scheelite.

In the *Majab* W occurrence, southwest of Ataq, the mineralization is confined to amphibolite and skarnitized amphibolite, which forms lenticular bodies within the north-trending Wasr Formation. The size of these mineralized zones ranges from 0.4 × 10 to 0.7 × 15 m. The analyzed samples from this occurrence contain from 0.1 to 0.82 wt% W, with high concentrations of Cu, Mo, Au, Sn and Zn. In addition, four molybdenite mineralized occurrences were recorded in granitic pegmatite in the *Hayfan* area (GEOMIN 1980). Table 4.1 summarizes the significant Sn and W deposits/occurrences in Yemen.

Table 4.1 Important Sn and W deposits/occurrences in Yemen (Frick and Al-Jawadi 2009)

Deposit/Occurrence name	Metallogenic setting	Status	Metallogenic province
Skarn deposits that host Sn, W, and Mo			
Occurrences: Al Jafiyah Sabahan	Metamorphic scheelite-bearing skarn occurrences associated with volcanogenic-sedimentary rocks	Occurrences	Southern Yemen
Sarban occurrence	*Carbonate-hosted skarn with scheelite and molybdenite*	*Occurrence*	*Southern Yemen*
Gebel as Sa'adi granite	Magnetite-bearing skarn with Sn and W	Occurrence	Jabali Area
Majab W occurrence	*Skarn deposits in amphibolite*	*Occurrence*	*Wasr Formation*
Granite hosted magmatic and pegmatitic occurrences			
Occurrences: Gebel Gahlalah Hayfan area Wadi Wassat Wadi al Qaradah Wadi Haniyah	*Mo, Sn, and W anomalies associated with Tertiary and Precambrian granites*	*Occurrences and anomalies*	*Different areas in Yemen*

4.3.2 Granite-Related Radioactive and REE Mineralization

The Precambrian terranes in western Yemen are characterized by granitic intrusions of different ages, some of which are known to host variable amounts of various lithophile elements, especially Nb, Ta, Sn, Ce, Be, Th, and U. In addition, some pegmatite bodies that are associated with the granite intrusions are also known from the western and northwestern Yemen, and also contain the same assemblages of lithophile elements. These deposits and occurrences are summarized in Table 4.2 (Frick and Al-Jawadi 2009).

Furthermore, the roll-front type U mineralization has been found in the Cretaceous Wajid ferruginous sandstones and conglomerates in southwestern Yemen, which is unrelated to the Precambrian Shield rocks (Table 4.2).

The REE mineralization occurs in southeast of Lawder, in three continuous, linear and vein-like carbonatite bodies with an average thickness of 3 m, 50 to 60 m long, and crop out over a total area of ~2 km^2 (Frick and Al-Jawadi 2009). The carbonatite bodies are confined to a northeasterly trending fault zone, which contains lenses and disseminated monazite as well as pyrocholre $(Na, Ca)_2Nb_2O_6(OH, F)$, hatchettolite $(U, Ca, Ce)_2$ $(Nb, Ta)_2O_6(OH, F)$, and fergusonite (Y, REE) NbO_4. The estimated ore resources to a depth of 100 m are ~5.1 Mt with an average grade of 4% monazite. Presence of U, Nb, REE mineralization is also reported in various localities in southern Yemen including *Manif*, the *Shasir* granite, the *Al-Masharij*

Table 4.2 Radioactive and REE deposits and occurrences in Yemen (Frick and Al-Jawadi 2009)

Deposit/Occurrence name	Metallogenic setting	Status	Metallogenic province
Ahwar occurrence	*Roll-front U occurrence in lenses in a ferruginized sandstone*	*Occurrence*	*Roll-front deposit*
Other occurrences in ferruginized conglomerates Wadi Marwan, Wadi Nshur, Wadi Aquam, Wadi Abdi	Uranium anomalies in a ferruginized conglomerate at the base of the Wajid sandstones	Anomalies	Stratigraphically confined to the Wajid Sandstones
Near Lawder	*Lenses of monazite, pyrochlore, and fergusonite in carbonatites veins and lenses*	*Occurrence*	*Carbonatite-bearing mineralization*

granite, the *Harat* granite, the *Jarar* granite and in the *Gebel Al-In* area. Another Nb-REE occurrence was also reported in the *Umm Shat* area in Wadi Mahgaga acid volcanic rocks. Nb–Zr–REE occurrence was also reported in felsic intrusive rocks of *Gebel Kharaz* (Frick and Al-Jawadi 2009).

The layered sequence of Precambrian Shield rocks of Yemen is intruded by numerous post-tectonic granite plutons, some of which are extensively evolved to be peraluminous in composition. Some of these peraluminous granites are reported to contain disseminated coarse-grained corundum crystals, which could be a source for REE deposits. In addition, coarse-grained granitic pegmatite rocks containing high concentrations of rare metals such as Be, Sn, Nb, Ta, Ce, and Rb, as well as some rare earth minerals such as euxenite and xenotime have been reported in some areas of the northern shield terranes of Yemen, (Frick and Al-Jawadi 2009).

4.4 Magmatic-Hydrothermal Deposits in Eastern Desert of Egypt

Almost all types of the magmatic-hydrothermal deposits are well documented in the Precambrian Nubian Shield rocks of the Eastern Desert of Egypt, including porphyry Cu–Au deposits, skarn deposits, epithermal vein-type Au–Ag deposits, and granite/pegmatite-related deposits. The following is brief descriptions of these mineral deposit types.

4.4.1 Porphyry Cu–Au Mineralization

Several studies were attempted to describe the Cu mineralization in the Precambrian basement rocks in the Eastern Desert and Sinai of Egypt (e.g., Ivanov 1972; Hilmy and Osman 1989; Hussein 1990; Botros and Wetait 1997; Botros 1999; Helmy and Kaindl 1999; Salem et al. 2013; Mamedov et al. 2014). Some of these studies were based mainly on the presence of alteration zones and no other evidence for porphyry mineralization were recognized. No Cu minerals but pyrite, were identified either on the surface exposure or in drill holes at some of these sites (Ivanov 1972; Hussein 1990). Few studies have documented the presence of porphyry mineralizations in Wadi Ranga and Hamash areas in the Southern Eastern Desert (SED) of Egypt (Helmy and Kaindl 1999; Ahmed and Gharib 2016). Field relationships, petrographic observations, ore mineralogy, and fluid inclusion data were used to characterize the mineralizing fluids of Au–Cu bearing quartz veins, which are spatially associated with a granite-porphyry. Some geological features such as association of the deposits with island-arc granite porphyry and volcanics, extensive deformation, systematic alteration zones and frequent abundance of gossans cover and copper staining along fault planes and joints were used to confirm the presence of porphyry Cu mineralization in the Eastern Desert of Egypt (e.g., Helmy and Kaindl 1999; Ahmed and Gharib 2016). Previous studies (e.g., Ivanov 1972; Hussein 1990) suggested that two main porphyry Cu mineralizations are present in the SED: Hamash and Um Garayat occurrences. Recently Ahmed and Gharib (2016) identified Ranga area near Hamata district, as a potential candidate for the occurrence of porphyry Cu mineralization. Following is a brief description of these possible porphyry Cu occurrences.

In the *Wadi Ranga* area of SED, typical features of porphyry Cu mineralization were recently reported, which are virtually similar to those of the worldwide examples (Ahmed and Gharib 2016). The Wadi Ranga area is bounded by Gebel Sarubi metavolcanic rocks to the north, by metagabbro–diorite complex to the northeast, and by quartz-diorite–granodiorite older granitoids to the west (Fig. 4.13b). The detailed study of the Ranga volcanic rocks revealed that the area consists mainly of two volcanic sequences: the older mafic sequence, composed essentially of pyroclastics and the associated lava flows, and the younger sequence cutting the older counterparts, is represented by pitchstone porphyry intrusion (e.g., Gharib and Ahmed 2012; Maurice et al. 2012). Compositionally, the Wadi Ranga mafic volcanic rocks are not comparable with the Dokhan volcanics or any Neoproterozoic volcanicity in the North Eastern Desert (NED) and Sinai (Gharib and Ahmed 2012). The older mafic volcanic rock sequence is crosscut by small porphyritic granitic plugs (Fig. 4.14a). In some places, the contact between granite porphyry and mafic volcanic rocks is well exposed on the surface, and the red gossans cover can easily be used to identify the mineralized rocks. The Wadi Ranga volcanic rocks commonly crosscut by numerous hydrothermal breccia pipes and quartz-vein sets (Fig. 4.14b, c), which are common features of porphyry systems worldwide (Hattori and Keith 2001; Sillitoe 2010). The vertical extension of hydrothermal breccia pipes reached up to several meters with widths of few tens of centimeters (Fig. 4.14b), which are sometimes

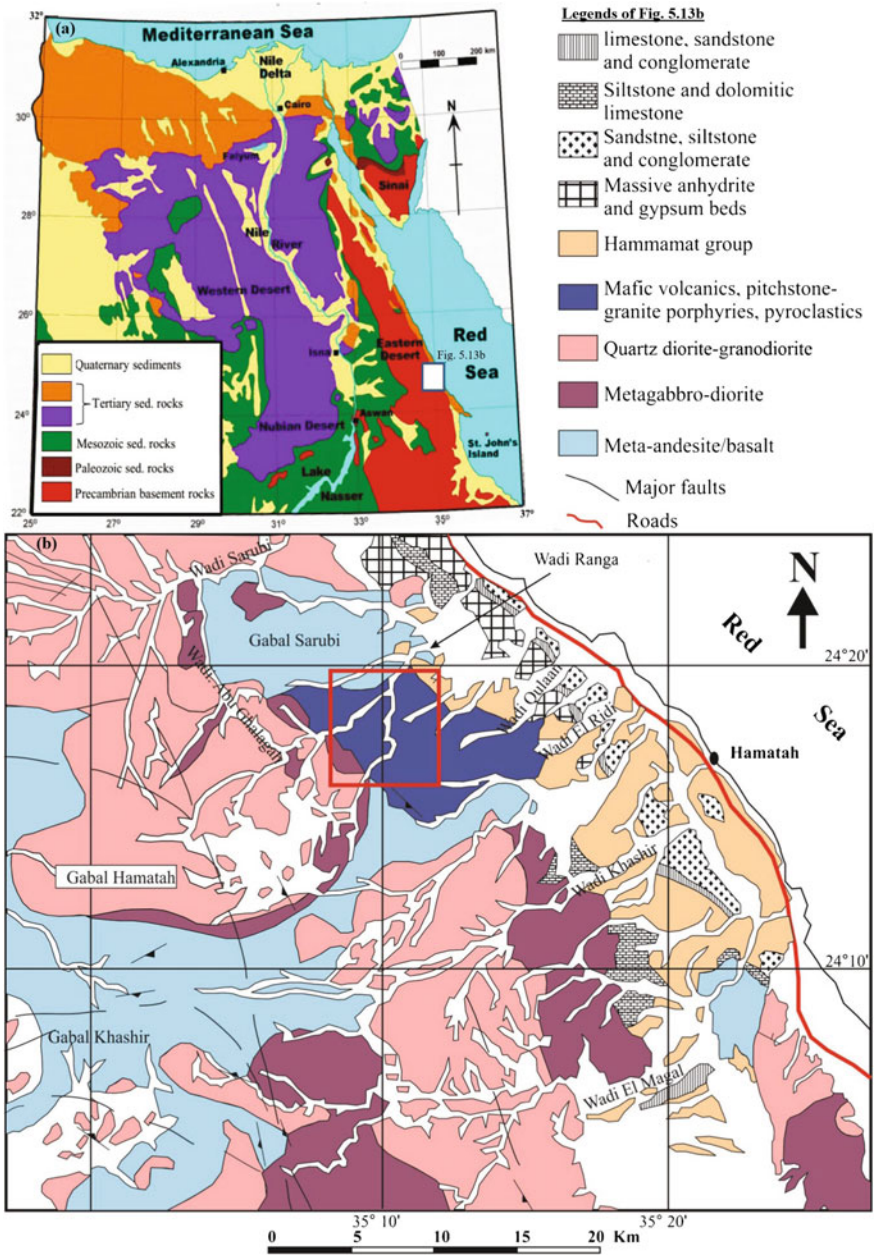

Fig. 4.13 **a** Outline geologic map of Egypt showing the location of the possible porphyry Cu mineralization in Wadi Ranga area. **b** Simplified geologic map of Hamata area where the porphyry mineralization occurred (taken from Ahmed and Gharib 2016)

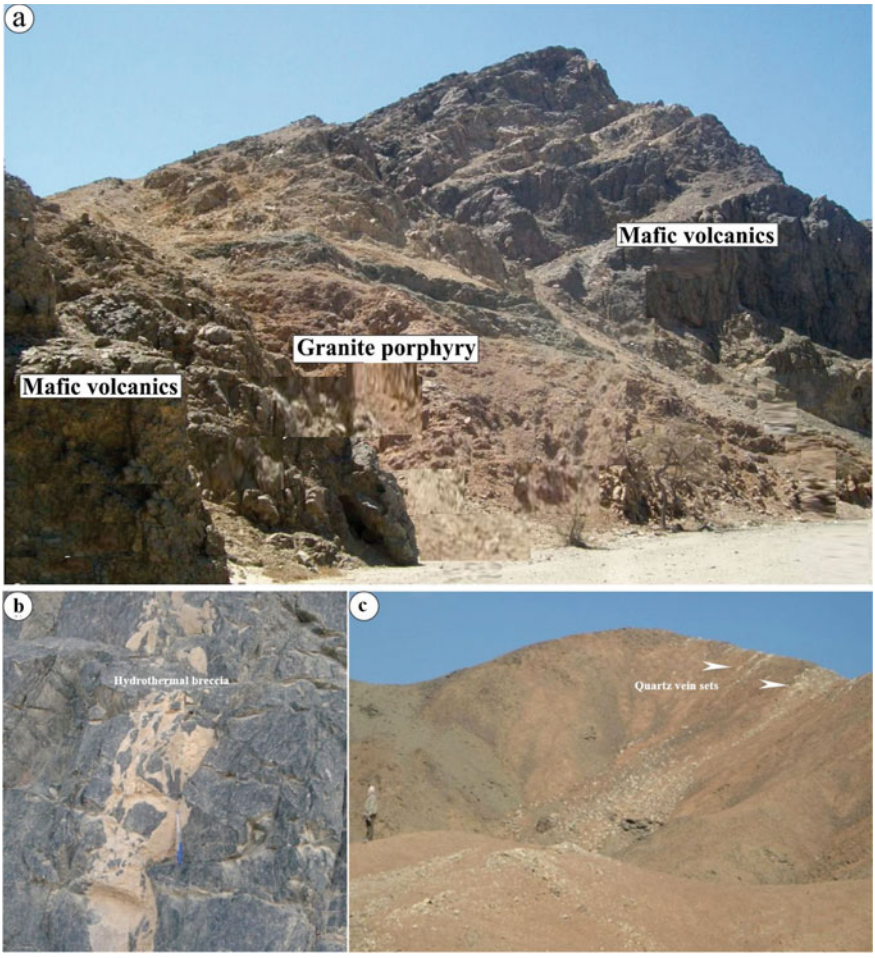

Fig. 4.14 Field photographs showing features of porphyry Cu mineralization in Wadi Ranga area, SED of Egypt. **a** Granite porphyry intrusion in the root zone of mafic volcanic rocks, **b** hydrothermal breccia pipe cross cut the overlying volcanic rocks showing the braided or stockwork pattern, and **e** quartz-vein sets cross cutting the volcanic rocks overlying the porphyritic intrusion (modified from Ahmed and Gharib 2016)

locally mineralized with disseminated sulfide aggregates. The volcanic rocks above the porphyry intrusion are also crosscut by quartz-vein sets trending eastwest to southeast/northwest directions (Fig. 4.14c). The quartz veins range in thickness from few centimeters to few meters with several hundred meters lateral extension (Fig. 4.14c). The presence of quartz veins above porphyry intrusions is akin to the epithermal veins commonly associated with porphyry systems (Chang et al., 2011).

Wide area of surface exposures of mineralization in the Wadi Ranga is marked by dark-brown, deeply weathered, strongly oxidized and leached surface (Fig. 4.15a).

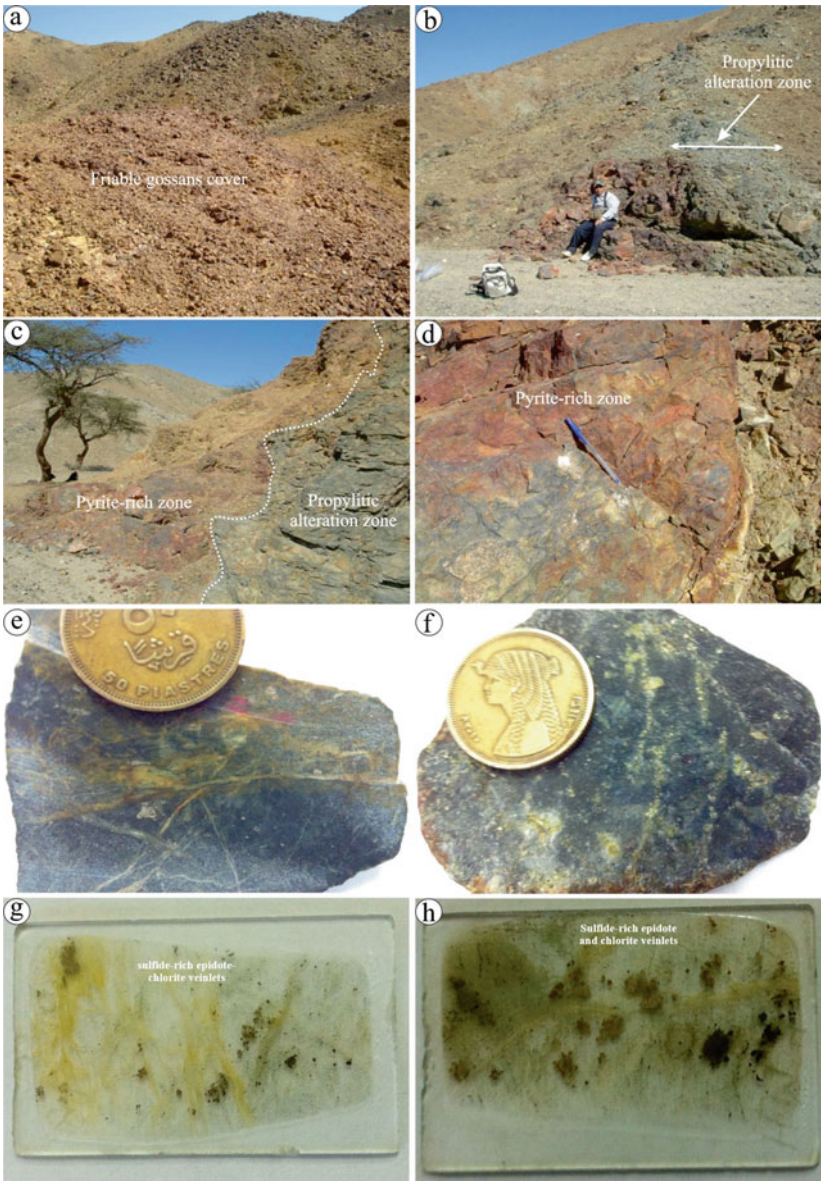

Fig. 4.15 Field photographs (**a**–**d**) of the pyrite-rich zone, hand specimens (**e**, **f**), and polished thin sections (**g**, **h**) of pyrite-rich rocks. **a** Highly weathered thick goethite-hematite gossans cover in a host mafic volcanics, **b** pyrite-rich lens with thin goethite crust in highly weathered volcanic rocks, **c** sharp irregular contact between pyrite-rich lens and highly weathered country rocks, **d** close up of (**c**), **e** hand specimen showing chlorite and epidote veinlets of the propylitic alteration zone, **f** chlorite-epidote veinlets and stockworks in the pyrite-rich mafic volcanic rocks, and **g**, **h** polished thin sections showing sulfide patches along chlorite-epidote veinlets of the pyrite-rich volcanic rocks (taken from Ahmed and Gharib 2016)

Pyrite-rich zone and Cu disseminations as several lenses of various sizes are commonly distributed in the area (Fig. 4.15b, c). Epidote- and chlorite-rich zone (propylitic alteration zone), and to a lesser extent argillic alteration zone, are very common in the contact zone with the pyrite-rich lenses (Fig. 4.15b). The contact between pyrite-rich lenses and surrounding altered mafic volcanic rocks is quite sharp and irregular (Fig. 4.15c). The pyrite-rich lenses are a few tens of meters wide and several tens of meters long showing a reddish-brown Fe staining cover (Fig. 4.15d). Quartz, epidote, and chlorite veins and veinlets are very common and rich in sulfides in the altered volcanic rocks (Fig. 4.15e, f). Sulfide mineralization occurs as aggregates and disseminations throughout the chlorite, epidote, and silica-rich veins and veinlets (Fig. 4.15g, h). In addition to the mineralized mafic volcanic rocks, the porphyritic intrusion itself is partially mineralized, and hydrothermal alteration of volcanic rocks is extensive and typically zoned close to the porphyry intrusion. Chemical analysis of the porphyry intrusion in the Ranga area shows low Cu contents, ranging from 4 to 10 ppm, while the pyrite-rich mafic volcanic rocks show anomalous Cu contents ranging from 86 to 321 ppm (Ahmed and Gharib 2016). Gold and silver contents are very low in the Ranga volcanic rocks, except in the mineralized pyrite-rich bodies, which have relatively higher values of Au up to 8 ppb.

The mineralogy of sulfides in the mineralized rocks is simple containing, in decreasing order of abundance: pyrite, chalcopyrite, pyrrhotite, covellite, and sphalerite, all of which are hypogene minerals, except covellite, which is a supergene after chalcopyrite. Pyrite and chalcopyrite are the most abundant hypogene minerals in the exposed mineralization and occur primarily as disseminations, fractures filling, and in quartz-epidote veins. Pyrite occurs as disseminated crystals and seems to be fracture controlled. Pyrite content ranges from 10 up to 20% of the rock volume in the pyrite-rich bodies, while chalcopyrite ranges between 1 and 3 vol% of the rock. The pyrite/chalcopyrite ratio of the mineralized outcrops commonly exceeds 10. Chalcopyrite occurs as irregular aggregates interstitial to pyrite (Fig. 4.16a, b). Numerous small chalcopyrite grains are also found as inclusions of rounded to anhedral grains scattering throughout and totally enclosed within pyrite crystals (Fig. 4.16c, d and f). Pyrrhotite and sphalerite are associated with pyrite and chalcopyrite as accessory hypogene minerals in the pyrite-rich bodies. Where present pyrrhotite essentially occurs as interstitial crystals to, and as small solitary inclusions within, pyrite and chalcopyrite (Fig. 4.16e, f). Pyrrhotite is less common in most porphyry Cu systems worldwide, although there are some deposits that have been found to contain pyrrhotite, indicating their formation under relatively reducing conditions (e.g., Rowins et al. 1997; Rowins 2000; Ahmed and Gharib 2016). The high pyrite/chalcopyrite ratio ($\geq$10) in conjunction with field and petrographical evidence, strongly suggest that the mineral assemblages of surface exposures of Wadi Ranga area are typically consistent with the pyrite shell or pyrite mineralization zone of the porphyry Cu system. The common presence of hydrothermal breccia pipes and quartz vein sets in the area are further evidence for the linkage with the porphyry Cu mineralization. All of the above field, petrological and mineralogical evidences suggests that the area is potential for a porphyry copper mineralization

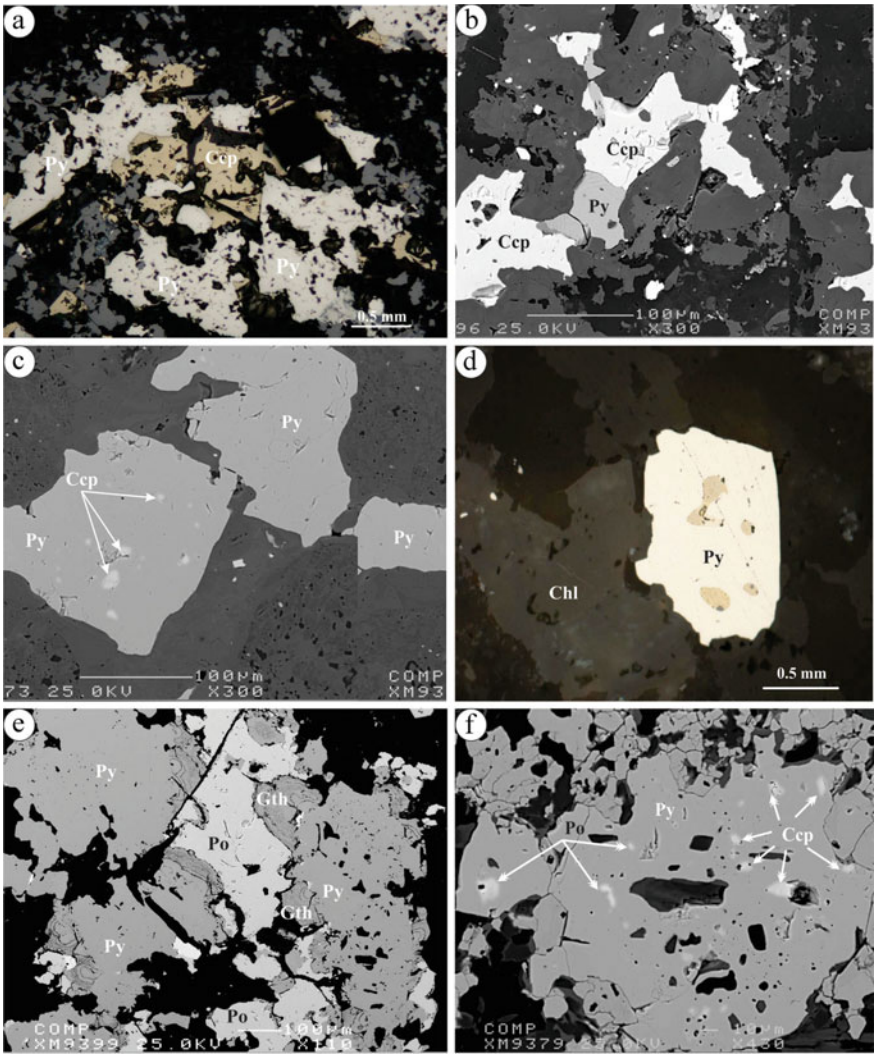

Fig. 4.16 Photomicrographs (**a**, **d**) and BSE images (**b**, **c**, **e**, and **f**) of sulfide mineralization in the pyrite-rich mafic volcanic rocks of Wadi Ranga area, SED, Egypt. **a** Irregular aggregates of pyrite (Py) and chalcopyrite (Ccp) association, **b** BSE image of irregular Py/Ccp intergrowths surrounded by epidote and chlorite patches in phyllic-argillic alteration zone, **c** BSE image of euhedral to subhedral Py crystals consisting fine-grained blebs of Ccp, **d** subhedral py crystal contains numerous Ccp grains of different sizes, **e** BSE image of large Py aggregates partly altered to goethite (Gth) intergrown with intercumulus pyrrhotite (Po) aggregates, and (f) BSE image of large Py crystal containing numerous fine-grained Ccp and Po crystals (taken from Ahmed and Gharib 2016)

and therefore, recommended for detailed exploration and further petrologic studies (see also Ahmed and Gharib 2016).

The *Harmash* area is another promising locality for the occurrence of porphyry Cu mineralization; it is historically known for its gold mineralization. In addition, it is also noted that several localities in the area have intensive hydrothermal alterations and show malachite staining along joints and fractures. Among these localities are the *Um Hagalig*, *Ara East*, *Ara West*, *Harnash North* and *Um Tundub* (lvanov 1972). The Hamash area is composed essentially of volcanic rocks of wide range of composition, intruded by sub-volcanic granodiorite porphyry intrusions. The granodiorite porphyry intrusion records intensive alteration zones at the Um Hagalig locality including propylitization, sericitization, kaolinization and silicification. It is crosscut by several quartz veins with malachite staining exposed due to previous excavation. Anomalous values of Cu (up to 0.5 wt%) were found close to the quartz veins, but did not extend into the granodiorite porphyry, and Mo values reached up to 50 ppm in some scattered samples. Characteristic quartz-sericite-pyrite alteration zones were noted in the Ara East and Ara West localities. Anomalous Cu (up to 200 ppm) and Mo (80 ppm) concentrations were determined in these localities, where the drill holes penetrated vertically (to a depth of 200 m) through rocks intersected with a zone of up to 30 vol% pyrite, but with no other sulfide minerals (Bugrov 1972). The locality of Harnash North is geologically much more interesting, where quartz veins are abundant with pyrite-chalcopyrite mineralization, as well as the presence of gossans cover and hydrothermal alteration zones up to 500 m long and 100 m wide, within the andesite-granodiorite porphyry. The analysis of alteration zones yielded anomalous Cu concentrations (from 200 to 5000 ppm) and Mo (from 10 to 50 ppm) (Bugrov 1972).

The *Um Tundub* locality was considered as the most promising locality at the Hamash area. Two vertical drill holes (250 m each), were intersected a zone of intensive alteration and development of pyrite. Pyrite is disseminated and fills the cracks and fractures through out the whole length of the core. The pyrite-rich zone is estimated to contain about 500 Mt of pyrite but no other sulfide minerals were identified. It is well-documented that in the porphyry-systems, Cu is always located towards the inner margins of the pyrite zone. Helmy and Kaindl (1999) reported four generations of genetically related quartz veins in the Hamash Au mine area. Two types of alteration zones are developed close to the quartz veins; sericite-quartz-pyrite and chlorite-epidote-pyrite-sericite alterations. The main sulfide minerals in decreasing order of abundance are pyrite, chalcopyrite, bornite, chalcocite and covellite. Gold essentially occurs as inclusions in and/or interstitial to pyrite grains and as free-Au grains in quartz veins (Fig. 4.17a–d) (Helmy 2020). The geological, mineralogical and fluid inclusion evidences suggest that the Hamash Cu–Au mineralization records characteristic features/signatures of both porphyry- and epithermal-type deposits (Helmy and Kaindl 1999).

Therefore, it can be concluded that there are high chances of the presence of porphyry Cu deposits at Hamash area (Hussein 1990; Helmy and Kaindl 1999). The apparent absence of porphyry Cu mineralization at Hamash area does not necessarily mean that no economic porphyry Cu deposit was developed in the area. Perhaps

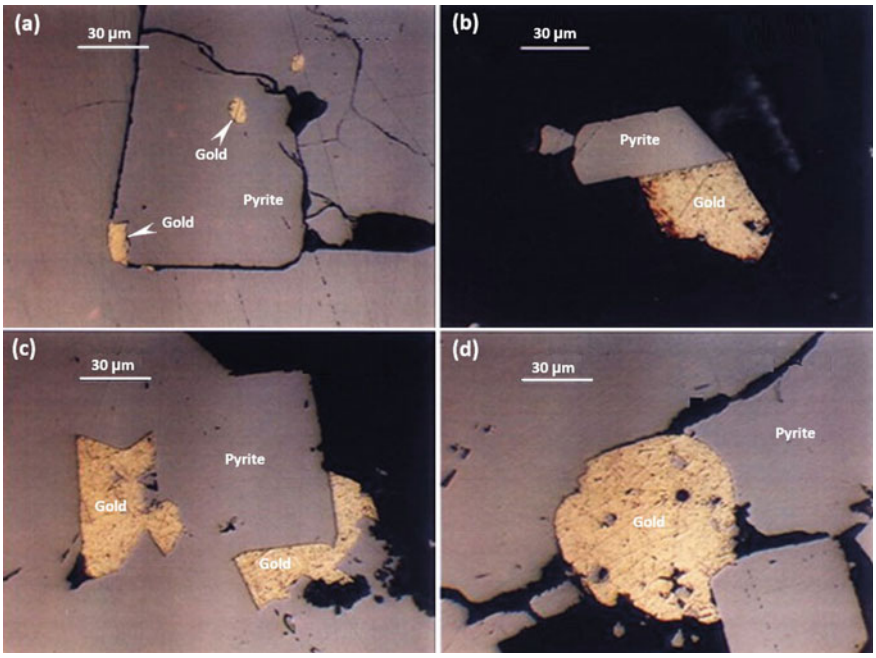

Fig. 4.17 Gold inclusions within large pyrite crystals of Hamash porphyry Cu–Au mineralization (modified from Helmy 2020)

apparent absence of the deposit is attributed to: (1) mineralization fluids were poor in Cu (2) the present level of erosion is above the zone of Cu ore shell, implying that mineralization could be present at depth but the drill holes locations and drilling orientation (direction) may have been incorrect.; (3) the porphyry intrusion and its associated mineralization, of Proterozoic age, has been intensively eroded well below the level of mineralization. The available data (unpublished data of the author), support the second possibility for the apparent lack of Cu at exposure hence discovery of such deposits.

The *Um Garayat* area is part of the 50-km-wide zone of deformation of the Allaqi-Heiani belt in the Neoproterozoic Nubian Shield of the SED (Fig. 4.18) (Abdelsalam et al. 2003; Zoheir and Klemm 2007; Zoheir et al. 2018). In addition to the widely known historical Au localities of Um Garayat and Haimur Au deposits, the Wadi Allaqi district contains numerous occurrences of Au mineralization such as those in the Um Ashira, Hariari, Naguib, Nile Valley Block, Marahiq, Atshani, Feilat, and Wadi Murra occurrences (Fig. 4.18). The rocks of Um Garayat area consists of different assemblages of granodiorite and quartz-andesite porphyries. The granodiorite porphyry intrusion shows complete concentric hydrothermal alteration zones with prominent intensive oxidation gossans cover. The central granodiorite core of quartz porphyry suffered intensive silicification and sericitization, and development of minor hydrobiotite and pyrophyllite (Hussein 1990). These alteration zones grade

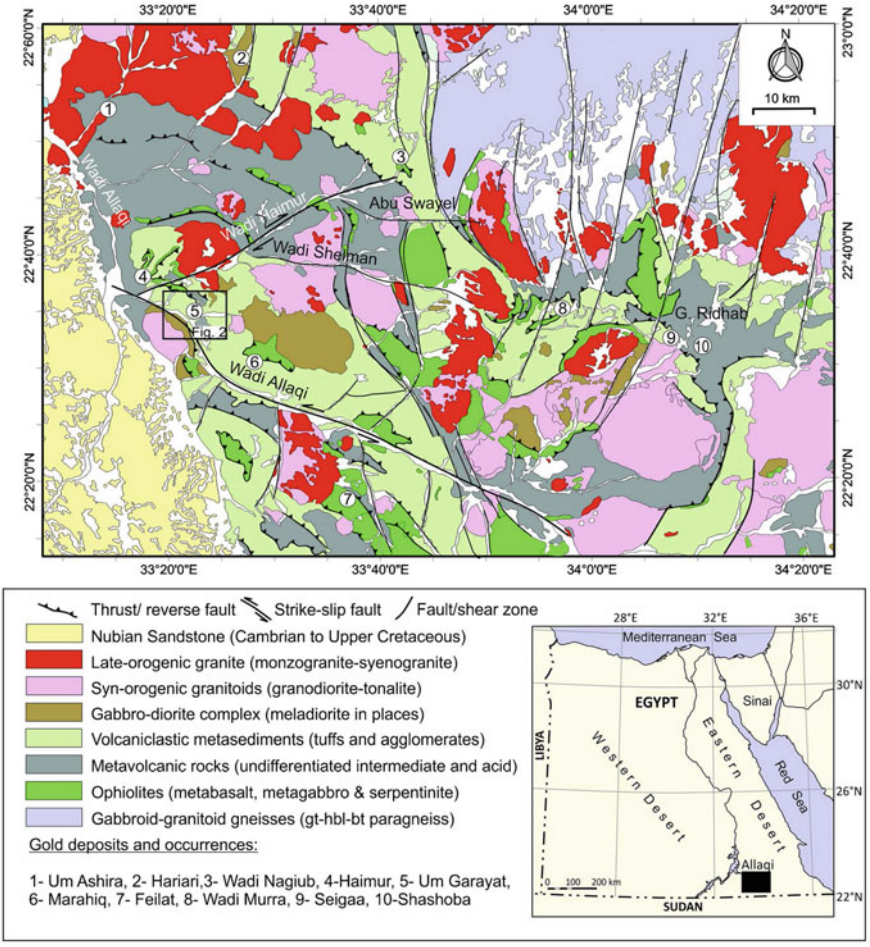

Fig. 4.18 Simplified geological map of the western Allaqi district, where the location of gold occurrences is given in numbers and names in the legend. The Um Garayat area is also shown on the map (from Zoheir et al. 2018)

outwards into kaolinization and propylitization, where pyrite mineralization is superimposed on these alteration zones, gradually pass into less altered rocks, then fresh rocks. Minor quartz veins and lenses with apatite, tourmaline and occasional specks of native Au are encountered in the silicified core of the granodiorite intrusion.

The Um Garayat gold mine area is underlain by metavolcanic and metasedimentary rocks, which are strongly foliated in places and cut by metagabbro-diorite and granodiorite-tonalite intrusions. The metavolcanic rocks comprise meta-andesite, meta-andesitic tuffs, metadacite, and metarhyolitic tuffs. The host metavolcanic and metasedimentary rocks crosscut by numerous dykes of andesite, diorite, and trachyte, as well as quartz veins and veinlets in several directions (Zoheir et al. 2018). The

Au-bearing quartz veins are hosted by sheared silty and graphite-bearing metasedimentary and tuffaceous rocks. Some of the mineralized veins extend for more than 1 km and have a width of up to 1.8 m in the swelling zones (e.g., El-Makky 2000; Zoheir et al. 2018). In the previous studies, no sulfide minerals, except pyrite, were reported in the Um Garayat area. However, a pervasive sulfidation process adjacent to the Au-bearing quartz veins was reported in the area represented by the common presence of chalcopyrite, covellite, chalcocite, and pyrite in the altered wall rocks (e.g., Oweiss and Khalid 1991; Zoheir et al. 2018). Magnetic anomalies on the alteration zone of metavolcanic rocks east of the Um Garayat mine led Hussein (1990) to propose the presence of a buried ore body. Core samples down to 212 m-deep showed the presence of a thick body of massive sulfides beneath ~70-m-thick layer of altered metavolcanic rocks (Hussein 1990). Like the case of Hamash occurrence, the absence of Cu in surface exposures of the Um Garayat area is attributed to two possibilities: (1) Cu mineralization was not developed due to the Cu-poor mineralizing fluids, or (2) it was formed but subsequently completely leached out from the oxidation zone but could be occurred deeper in the supergene enrichment zone.

4.4.2 Skarn-Related Mineralization

In general, skarn deposits represent a very diverse class of polymetallic mineralization in terms of their geologic setting and ore metals. Skarn deposits constitute the main sources of W in the world (>70% of the world's W production); major sources of Cu; important sources of Fe, Mo, and Zn; as well as minor sources of Co, Au, Ag, Pb, Bi, Sn, Be, REE, F, and B (Einaudi et al. 1981; Misra 2000; Meinert et al. 2005). Skarn deposits occur in a broad spectrum of geologic environments and range from Precambrian to late Tertiary in age, however most economic skarn deposits are relatively young, and related to magmatic-hydrothermal activities associated with dioritic to granitic plutonism in orogenic belts. The modem usage of the term "skarn" refers to a wide variety of generally coarse-grained calc-silicate rocks (garnet + pyroxene + epidote) that are rich in Ca, Fe, Mg, Al, and Mn, regardless of their metallic mineral associations. Skarn deposits are essentially formed by replacement of originally carbonate-rich rocks by metasomatic processes (Einaudi et al. 1981). Carbonate-rich rocks (limestones and dolostones) are the most common protoliths of skarns, although shales, quartzites (Atkinson and Einaudi 1978), and igneous rocks (Einaudi et al. 1981; Harris and Einaudi 1982; Vidal et al. 1990) have also been reported to host skarn deposits. Skarns and skarn deposits are formed by either contact or regional metasomatic processes.

Skarns and skarn deposits are not so common in the Precambrian basements of the Eastern Desert of Egypt; only two main occurrences of skarn mineralization were reported including: (1) Pan-African skarn occurrence associated with banded iron formation (BIF) at Um Nar area, CED (El Habaak 2004), and (2) Neoproterozoic skarn-type Zn–Pb–Ag mineralization at Wadi Kid area, SE Sinai (Helmy et al. 2014a).

Following is a brief description of these skarn occurrences in the Eastern Desert of Egypt.

The *Um Nar* area is a part of the basement complex of Egypt that exposed in the CED (~40 km north of the southern limit of the CED) (Fig. 4.19). It is one of thirteen localities of banded iron formation (BIF) occur in an area extending over 30,000

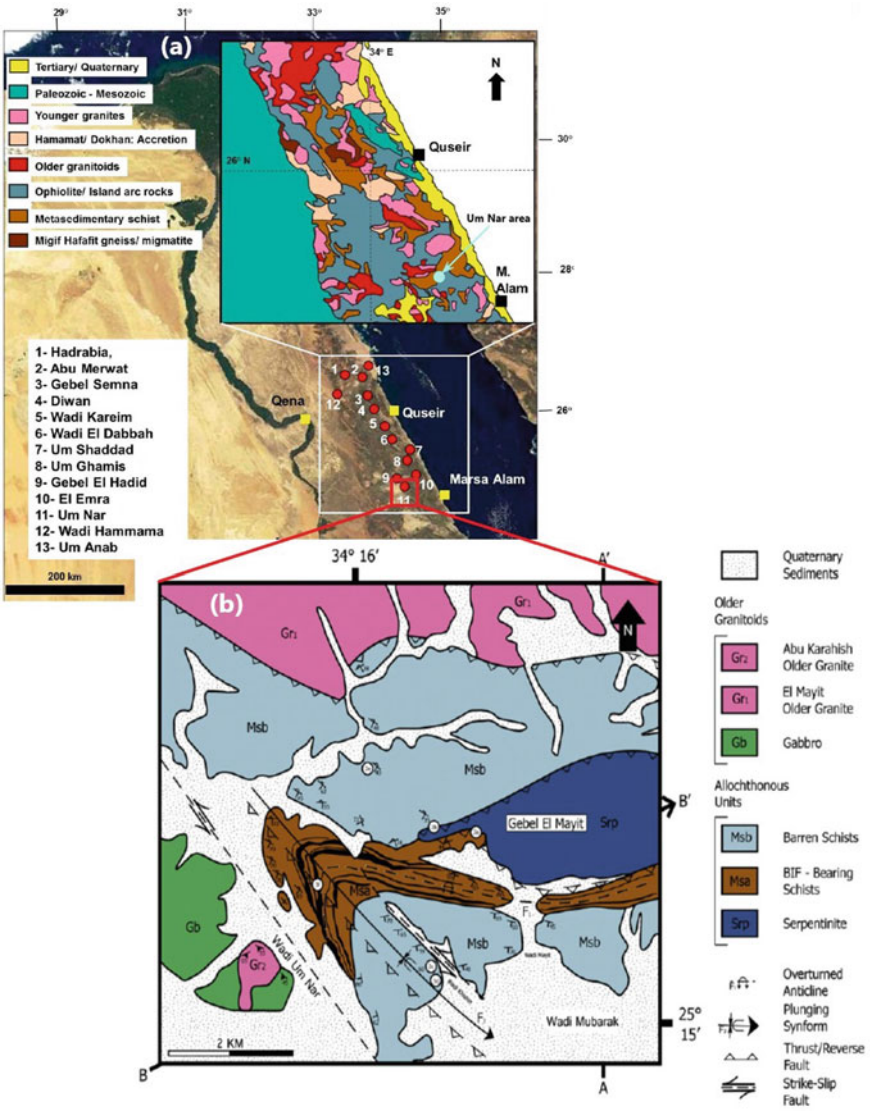

Fig. 4.19 **a** Landsat image of Egypt showing the location of banded iron formations (BIF). Inset is a simplified geological map of the area outlined in the box. **b** Simplified geological map of the Um Nar area (from El-Shazly and Khalil 2014)

km^2 in the CED; it is located in the southernmost exposure of the BIF in the Eastern Desert (Fig. 4.19a). Two distinct types of iron ore are found in the Um Nar area in the same succession (El Habaak 2004): the first type is quite similar to the normal Pan-African BIF described from different localities in the Eastern Desert (Fig. 4.19a), which are associated with island arc assemblages such as those in Wadi Kareim and El Dabbah BIF. The second type is rich in coarse-grained calc-silicate minerals such as andradite, diopside, epidote and amphiboles, which is in many aspects similar to skarn deposits from elsewhere in the world (Einaudi et al. 1981). Type 2 skarn is the subject of this section, while type 1 (normal Pan-African BIF) will be described in detail in the subsequent chapters of this book.

The geology of Um Nar area consists of different rock units that can be arranged from older to younger as (e.g., El-Shazly and Khalil 2014) (Fig. 4.19b): (1) ophiolitic serpentinite masses with small disrupted bodies of amygdaloidal basalts and locally rodingitized gabbros partially rimmed by blackwalls (ophiolitic mélange), (2) two types of schists intercalated with meta-dacites/meta-rhyolites that thrusted on top of the ophiolitic mélange, (3) a gabbroic intrusion, and (4) two granitic intrusions (Al-Mayit cataclastic mylonitic granite and Abu Karahish older granite; Fig. 4.19b). The Um Nar skarn mineralization are hosted in a metamorphosed clastic and calcareous sedimentary succession, which represents the topmost part of the ophiolitic mélange. The metamorphosed sedimentary rocks were intruded by granodiorite, post-tectonic granite and olivine gabbro, and felsite (aplite) dykes. In the Um Nar area, numerous BIF bands are mainly confined to the biotite schist, where the BIF is composed of alternating iron-rich and chert bands. The protolith of Um Nar BIF composed of calcareous (carbonate-rich) BIF and oxide-rich BIF interbedded with chert bands. The carbonate-rich BIF bands are susceptible for chemical changes by metasomatic fluids and mostly transformed into skarn deposits, whereas the oxide bands are more resistant to metasomatizm. The mineralogy of BIF protolith is simple, comprising fine-grained magnetite, hematite, calcite (±siderite), and quartz. The skarn-rich zone shows a gradational contact with the surrounding biotite schist, and shows a rhythmic alternation of dark magnetite-rich and pale calc-silicates laminae, which are essentially medium- to coarse-grained. The formation of BIF-related skarn in the Um Nar area began with the recrystallization of the BIF-forming minerals accompanied by increasing in the grain sizes and gradual metasomatic replacement by calc-silicate and sulfide minerals. The majority of the original carbonate minerals were consumed in the formation of calc-silicates, although remnants of calcite and siderite are partially preserved.

The *Wadi Kid* area, southeastern Sinai, is another important locality where a polymetallic Precambrian skarn-type mineralization was discovered (Helmy et al. 2014a). The Wadi Kid area is located to the west of Gulf of Aqaba in southeastern Sinai; it comprises continental margin volcano-sedimentary succession, which was deformed and intruded by syn-tectonic granite–diorite complexes (e.g., Moghazi et al. 1998; Fowler et al. 2010). The Wadi Kid area is characterized by many occurrences of sulfide-rich ores such as those in the Um Zeriq I, II, and II, Samra occurrences and Shalal (Fig. 4.20). Sulfides occur as either disseminations or massive lenses and veinlets in various types of host rocks. Drilling by the Geological Survey of Egypt in Um

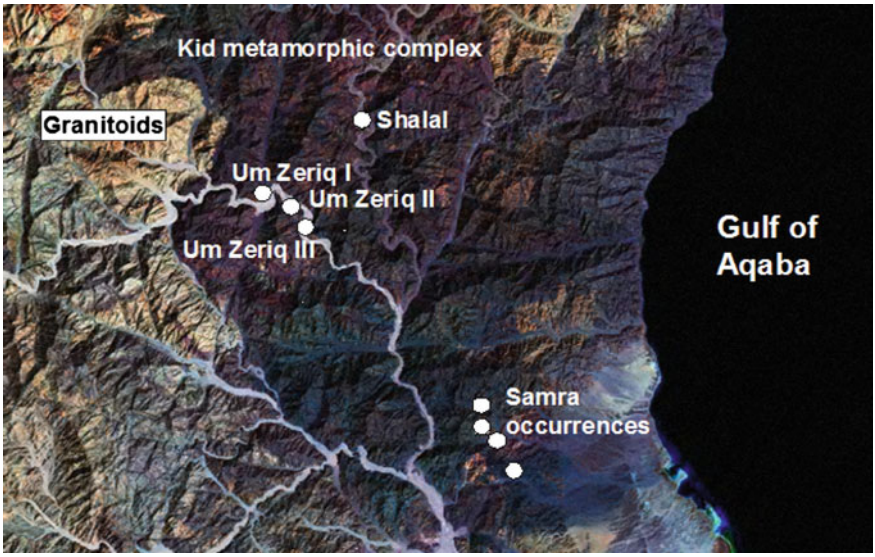

Fig. 4.20 Location map of sulfide mineralizations in Southeast Sinai, Egypt (from Helmy et al. 2014a)

Zeriq II led to the discovery of massive sulfide zones hosted in metapelites (Helmy et al. 2014a). Generally, the Wadi Kid metamorphic complex forms a thick (~4.5 km) sequence of volcano-sedimentary rocks, deposited in active continental margin of back-arc, remnant arc, and intra-arc environments (Fowler et al. 2010). The Kid metamorphic complex contains four volcano-sedimentary rock formations; from bottom to top these are Um Zeriq, Malhaq, Tarr and Heib Formations. The polymetallic skarn-type mineralization occurs in the Um Zeriq area, which forms the lower stratigraphic unit of the Kid complex (Helmy et al. 2014a). The Um Zeriq Formation (>1500 m thick) consists of schists and phyllites, derived from pelites, psammites, and feldspathic lithic greywackes. Calcareous rocks of impure dolomites form minor components of the pelitic rocks at the lower stratigraphic level. The metapelites of Um Zeriq Formation was dated at 660±25 Ma using Th–Pb isochrone age for the metamorphic monazite (Helmy et al. 2014a).

Sulfide mineralization at Um Zeriq II and III is located along the fault zone forming the Wadi Kid, where the sulfide ores can be identified on the surface by the presence of gossans cover of few meters long in highly sheared rocks (up to 20 m wide and 500 m long). Some pockets and lenses of massive sulfides, which are mainly made of galena, are preserved in the gossans cover. The mineralized zones were identified in the drill hole of Um Zeriq II (Helmy et al. 2014a) are: (1) the surface oxidized gossans cover (1–2 m thick) with massive galena, hematite and goethite. (2) Disseminated-ore zone extending from a depth of 27 to 37 m, in which sulfide minerals constitute about 8 modal % of the core. (3) Disseminated to massive ore zone extending between 78 and 82 m depth along shear zone. Massive sulfide

lenses and veinlets are found when approaching the shear plane. The gangue silicate mineral assemblage is dominated by garnet–biotite–andalusite and quartz.

Based on the host rock and metal contents, two types of large-scale metal zoning mineralization were identified in the Wadi Kid area; Cu–Zn–Co hosted in calc-silicate rocks, and Zn–Pb–As–Ag in metapelites (Helmy et al. 2014a). Primary magmatic textures of sulfide mineralization and host rocks are largely obliterated by the intense amphibolite facies metamorphism. Ore minerals in disseminated and massive sulfide occurrences consist of variable amounts of sphalerite, arsenopyrite, pyrite, löllingite, galena, and pyrrhotite, as well as some Ag minerals and sulfosalts. The P–T conditions, based on the sphalerite geobarometry and arsenopyrite geothermometry, estimated a peak metamorphic pressure of ~3–3.6 kbar and temperatures of ~540±40 °C. The role of metasomatic fluids in the formation of these polymetallic skarn deposits can be inferred from the extensive transformation of primary silicate mineral assemblage into chlorite and by the enrichment of the original disseminated to massive sulfide bodies. The presence of Ag minerals suggests the formation of Wadi Kid skarn deposits at low temperatures during retrograde metamorphism (i.e., cooling) of sulfide ore. Polymetallic variation and mineralogical zoning of the Wadi Kid mineralization are characteristic features of skarn deposits, which commonly show large-scale metal zonation as a result of different distances from the granitic intrusion. The Wadi Kid area is highly promising for Cu, Zn, Pb and Ag mineralization hence a candidate for future exploration. Much attention should be focused on the highly sheared areas and into the depth where the source of heat and metals (i.e., granitic intrusion) is probably located (Helmy 2020).

4.4.3 Epithermal Vein-Type Mineralization

Vein-type deposits in the ANS, in general, and in Egypt in particular, found to host the most important precious and base metal deposits. More than a hundred Au occurrences are known in the Eastern Desert of Egypt; most of them were exploited by traditional exploration and mining activities of ancient Egyptians. In most cases, Au occurrences are restricted to quartz veins, occupying the pre-existing fractures, which are essentially, comprised massive quartz with disseminated Au and base metal sulfide minerals. In addition, there are some occurrences where the Au ore is either associated with felsic dikes, as stockworks of minor quartz veinlets, or contained in disseminated pyrite grains throughout the whole mass of the dike. The host rocks of the mineralized veins are quite varied including serpentinized ultramafic rocks, metamorphosed volcanic and sedimentary rocks, intrusive gabbros and different granitoid rocks. The mineralized veins are structurally controlled; being fissure fillings, confined to fault planes, or zones of intensive fracturing.

The sulfide mineralogy of most Au-bearing vein deposits in the Eastern Desert of Egypt is dominated by pyrite, arsenopyrite, and pyrrhotite, with subordinate chalcopyrite, sphalerite, galena and tetrahedrite. The gangue minerals associated with these vein-type Au deposits are mainly white mica, chlorite, and carbonate, typical

of orogenic gold deposits (Zoheir et al. 2019). The orogenic Au deposits are widely recognized in both Phanerozoic mobile belts and older cratonic blocks. This class of Au deposit is characteristically associated with deformed and metamorphosed mid-crustal rocks in close spatial association with major crustal structures (Goldfarb et al. 2001, 2005). In contrast, the intrusion-related epithermal vein-type Au deposits typically occur in metaluminous sub-alkalic plutonic bodies of felsic to intermediate composition, mainly in convergent plate boundaries (Lang and Baker 2001). In the Eastern Desert of Egypt, many Au occurrences are located along sheared margins to granitic intrusions or along contacts between different lithologies, where sheared silica- and carbonate-altered ultramafic rocks along many fault zones (Zoheir et al. 2019). The genesis of most vein-type precious and base metal deposits are still debated, such that whether they related to epithermal or mesothermal (orogenic) deposits. Based on the most recent study (Bouabdellah and Slack 2016; Zoheir et al. 2019), orogenic model is preferred for most of vein-type deposits in the Eastern Desert. Orogenic deposits are discussed in the next chapter (i.e., Chap. 5) of this book.

4.4.4 Granite- and Pegmatite-Related Mineralization

Granite intrusions and related pegmatite-hosted trace elements (Ta–Nb–Sn–W–F) and REE mineralization are widely distributed in the Proterozoic terranes of the ANS. These granitic intrusions are mostly pre-, syn-, and post-tectonic plutons of Late Proterozoic (Tonian to Ediacaran) age. Based on the age, felsic granitic rocks in the ANS are generally classified into two main groups: Tonian-Cryogenian and Cryogenian–Ediacaran felsic intrusions, where each category has its own mineralization type. The Tonian-Cryogenian granitic plutons mainly hosts Au deposits, whereas the Cryogenian–Ediacaran granitic intrusions mainly hosts rare-element deposits such as Ta–Nb–Sn–W–Mo–F–Be–Y and REE. These rare-metals deposits are commonly associated with rare-metal granites and granitic pegmatites in the ANS. The rare-elements mineralization essentially occurs in peraluminous rare-metal granites and pegmatites in the ANS (e.g., Kenticha, Ethiopia; Abu Dabbab and Nuweibi, Egypt; Umm Al Suquian, Saudi Arabia), and in peralkaline rare-metal granites (e.g., Ghurayyah, Saudi Arabia) (Fig. 4.21). These granite-related mineralizations are associated with a post-tectonic magmatic phase ranging in age from 610 Ma in the north to 530 Ma in the south of the ANS (Küster 2009). Granites, in general, are broadly classified into "magnetite series" and "ilmenite series" granites; the former is usually associated with sulfide mineralization whereas lithophile elements such as Mo, Sn and W are related to the latter granites. In Egypt, the magnetite series granites are represented by "G1" granites (described below), which is known to be generally barren or associated with minor Cu, Zn osr Pb sulfides. The "G3", and to lesser extent "G2" granites, are ilmente series granites, and they are likely associated with Sn–W mineralizations (Hussein et al. 1982). A similar study was also carried out in Saudi Arabia (Jackson et al. 1983) and concluded that most of the central Higaz

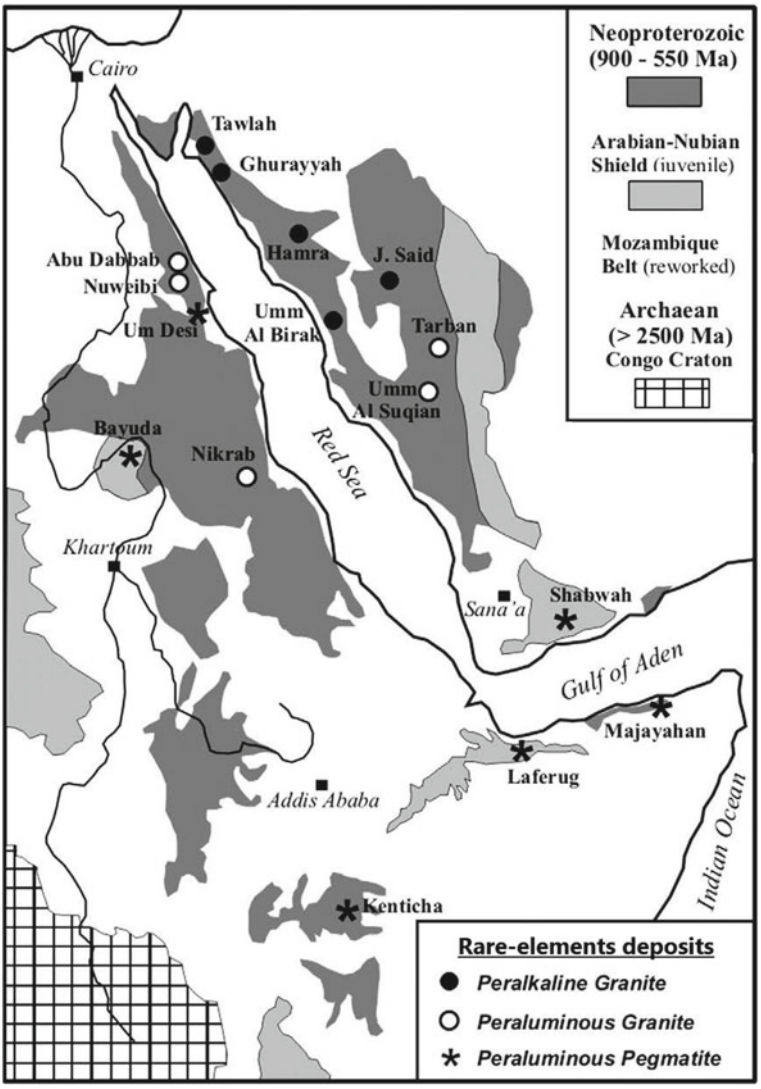

Fig. 4.21 Geological sketch map of northeastern Africa and Arabia showing major crustal segments and the locations of tantalum deposits and mineralization (from Küster 2009)

granites belong to the magnetite series granites and are likely to host Cu–Mo sulfide mineralization.

In Egypt, granitoid rocks constitute about 40% of the Proterozoic shield rocks, cropped out mainly in the southern Sinai, Eastern Desert, and the southernmost part of the Western Desert. Proterozoic granitic rocks of Egypt are generally classified into three groups (Hussein et al. 1982): Gl, G2 and G3 categories. The G1 granites

are a subduction related, and are characterized by: (1) calc-alkaline in composition, (2) closely associated with island arc volcanics, (3) formed under compressional environments, and (4) are related to I-type granites. The G1 granites usually form large plutons that include rocks ranging in composition from diorites to granites, with SiO_2 contents not exceeding 65% (Hussein 1990). The G1 granites are previously referred in the literature to as "Old", "Shaitian", "Grey", "Syn-orogenic" or "Aswan" granites, which are very poor in the Nb, REE, and radioactive elements contents. The G2 granites, on the other hand, were formed due to suturing and are related to S-type, ilmenite series, and calc-alkaline granites, which formed in compressional environments. They tend to form relatively small plutons with a narrow range of composition, always granitic, with SiO_2 contents higher than 65 wt%. The G2 granites are previously referred in the literature to as "Younger", "Gattarian", "Pink", "Red" or "Post-orogenic" granites. Although G2 granites have low contents of Nb, REE and radioactive elements, they may contain accessory monazite, zircon and cassiterite. The G3 granites include small and simple intrusions of alkali to peralkaline intraplate anorogenic granites. They are related to the S-type, ilmenite series granites that formed under extensional environments. In addition they have a very limited range of composition, with SiO_2 contents ranging between 70 and 75 wt%. This type of granite is rich in Nb, REE and radioactive elements, and the accessory minerals may be monazite, zircon and cassiterite. The G3 granites are frequently partly greisenized and/or albitized (Hussein 1990).

Several occurrences of granite-related mineral deposits in Egypt are associated with these granitic rocks that covering wide varieties of mineralization and spread over the NED and CED parts of Egypt, where these granitic rocks are predominate. Most of the Sn, W, Mo, Nb–Ta, REE, Be, and F deposits are associated mainly with the G3 granites, although some of them may also be associated with G2 granite plutons. The G1 granites type, on the other hand, do not have appreciable amounts of mineralization, being only show some scattered minor base metal bearing quartz veins. Three main classes of granite/pegmatite-related mineral deposits are discussed in this part, including: (1) Molybdenum (Mo) mineralization, (2) tin (Sn)-tungsten (W) mineralization, and (3) niobium (Nb)-tantalum (Ta) mineralization. Some other mineralizations related to granites are also, briefly discussed, including, uranium, fluorite and beryl.

(A) ***Molybdenum vein-type mineralization***

The Mo-bearing quartz veins in the Eastern Desert of Egypt are essentially found cutting across the G2 or Pink granites. They are distributed in six occurrences in the NED (Fig. 4.22); *Gebel Gattar*, *Abu Harba*, *Wadi Dib*, *Abu Marwa*, *Um Disi*, and *Homret Akarem* (Hussein 1990; Salem et al. 2020).

The *Gebel Gattar* granitic batholith is exposed over an area of ~450 km^2 in the NED (Fig. 4.22). It is located ~70 km southwest of Hurghada, Red Sea coast. The Gattar granite intruded into metavolcanic rocks, which is found as roof-pendant over the granitic batholith. The country rocks in the area also include arc granitoids and Hammamat sedimentary rocks (molasse-type sediments) with low topographic elevations (Fig. 4.23). The Gattar granitic batholith is divided into two parts by the

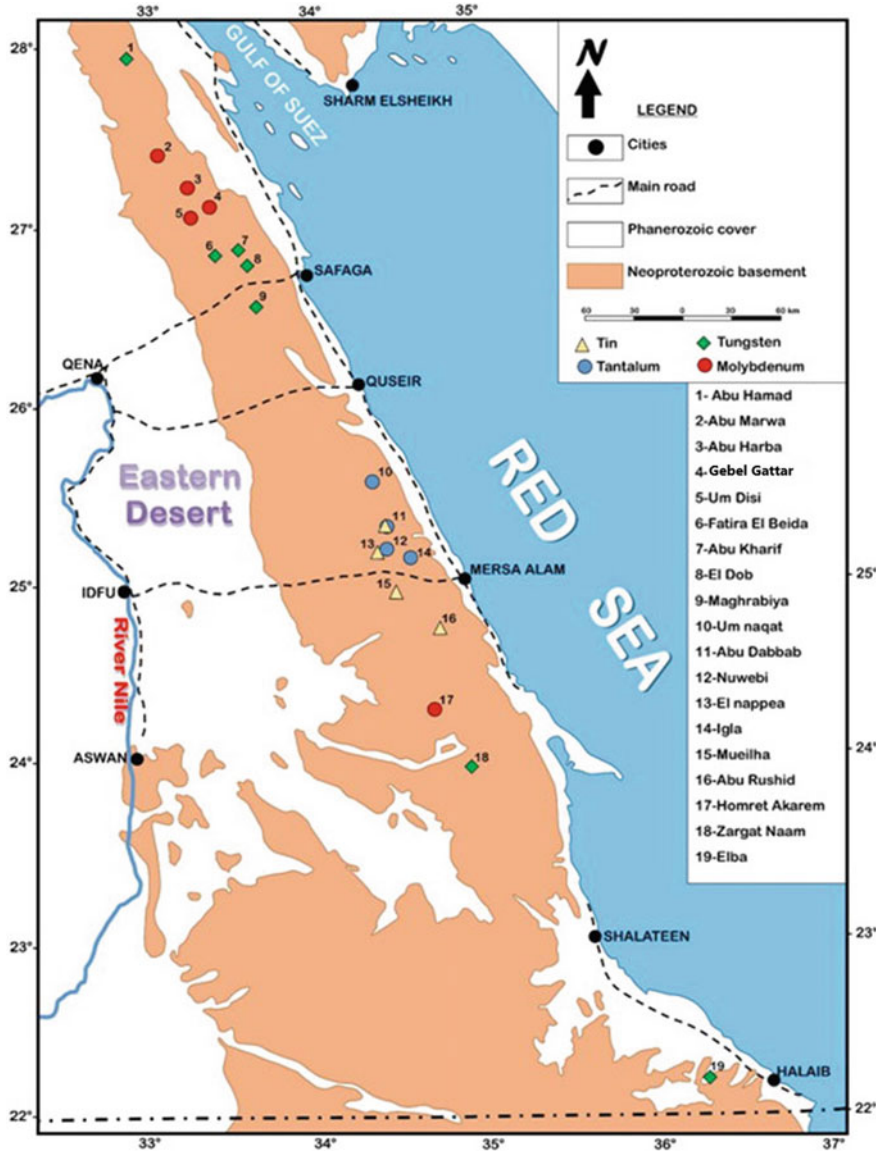

Fig. 4.22 Sketch map of Egypt showing the mineral deposits and occurrences of Sn, W, Ta, and Mo deposits in the Eastern Desert of Egypt (from EGSMA 1998; Abdelnasser 2020)

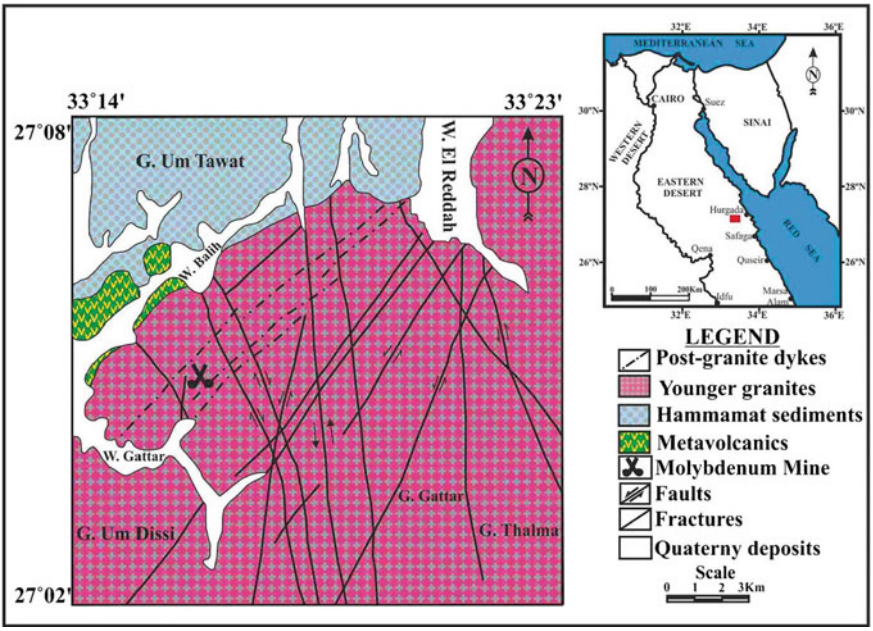

Fig. 4.23 Simplified geological map showing the location of Gebel Gattar granitic pluton (after Salem et al. 2020)

Wadi Al Ghoza; the southern part is composed of pink granite, and the northern part is composed of red granite (Figs. 4.23). The contact between the Gattar red granite and the Hammamat sedimentary rocks is remarkably sharp. Red granite offshoots are obviously penetrating into, and fills the fractures, of the Hammamat sedimentary rocks (Helmy et al. 2014b). In addition, xenoliths from the Hammamat sedimentary rocks are sometimes encountered within the red granite. The Gattar red granite is highly deformed and affected by NNE–SSW sinistral and NW–SE dextral fault systems in its northern margin near the Hammamat sedimentary rocks. The Mo and Bi–Ag–U–F mineralization (Helmy et al. 2014b; Mahdy et al. 2015; Salem et al. 2020) is mainly restricted to the NNE faulting with a sinistral displacement that represents the latest phase of deformation. The Mo-bearing quartz veins are commonly follow this trend especially at the conjugated fault system (Mahdy et al. 2015), which is represented by magmatic-hydrothermal alteration of the host rocks. Where intersected with structural elements (faults and/or shear zones), the red granite is highly brecciated and fractured with the development of coarse-grained (up to 0.5 cm) euhedral fluorite crystals. In the highly deformed rugged granite, the U-F mineralization is concentrated, where the color of the red granite changes into dark-red violet in the mineralized zones due to hematitization and development of coarse-grained violet fluorite (Helmy et al. 2014b).

The mineralization forms a zone of veins of ~25 m wide and 500 m long, cutting across the pink granites of Gebel Gattar, where the individual veins vary from 1 mm

up to 10 cm. The mineralized zone extends from the surface to underground with the same attitude and thickness down to depths of 46 to 136 m below the surface. Molybdenite occurs as massive patches in quartz veins and as disseminations within the host granite forming coarse crystals (1 to 3 cm across), concentrated within the veins and/or along their contacts with the country rocks (Hussein 1990). Molybdenite is the principal ore mineral in the studied quartz veins although commonly associated with chalcopyrite, sphalerite, pyrite, galena, gold, bismuth and silver. The estimated ore reserve of the Mo-bearing zone at Gebel Gattar is ~4500 t Mo, with an average grade ranging from 0.27 to 2.25 wt% Mo. Molybdenum mineralization is also observed in small occurrences in nearby Gebel Gattar area of the NED, named *Abu Marwa*, *Abu Harba* and *Um Disi* (Fig. 4.22, occurrences# 2, 3 and 5). 1n these small occurrences, the ore occurs in quartz veins cutting across red granite, and the veins are always bordered by narrow (5 to 10 cm) zones of greisenized granite. Based on the estimated reserves and grades of the ore in these occurrences, Dardir and Gad Allah (1969) and Hussein (1990) concluded that any of these occurrences are economically significant.

Homret Akarem area is one of the famous occurrences for Mo mineralization in the southernmost part of the CED (Fig. 4.22, occurrence# 17). In this area, polymetallic mineralization including Be, Sn, Mo, Bi, W, and Cu anomalies were reported, and therefore Searle (1974) studied this deposit in detail. The Homret Akarem area was found to contain a zone of quartz veining, covering an area of ~1100 m by 875 m, but a narrow zone of this area (~240 m^2) is considered to be of economic interest, where the mineralized vein intensity reached up to 30 vol% of the vein outcrop. The Mo mineralization occurs in zones, such that the central zone represents the intense quartz veining with molybdenite, which is followed outwards by a narrow zone of cassiterite enrichment in a greisenized granite. The outer zone of the mineralized area contains Cu sulfides of mainly chalcopyrite and chalcocite. Fluorite is commonly found within the Sn-bearing zone, and a geochemical anomaly of Be is present in all of the mineralized zones. Five drill-holes were carried out in the area and drilled a total of 1375 m. Four of them were inclined and one was vertical. The estimated ore reserves from the drill holes gave ~8.3 Mt of ore, with an average grade of 0.03 wt% Mo (Searle 1974; Hussein 1990).

(B) ***Tin-Tungsten (Sn–W) vein-type mineralization***

Tin (Sn) and tungsten (W) in the Eastern Desert of Egypt display two modes of occurrence, vein-type and disseminated-type of mineralization (Hussein 1990). Tin essentially occurs as cassiterite, and W occurs as wolframite. Cassiterite and wolframite are commonly associated with quartz veins, which are mainly found at the NED and, to a lesser extent, in the CED and SED (Fig. 4.22). The main occurrences of Sn mineralization are at *Igla*, *Nuweibi*, *Abu Dabbab* and *Mueilha*, while the main occurrences of W mineralization are at *Abu Hamad*, *Fatira El Beida*, *Abu Kharif*, *El Dob*, *Magharabiya*, *Um Bisilla*, *Zargat Naam* and *Qash Amir* (See numbers in Fig. 4.22 for locality names). Most of Sn–W-bearing quartz veins from the CED and SED of Egypt were intersected the Precambrian metasedimentary and metavolcanic rocks, and they are always associated with albite granite.

The *Mueilha* Sn mine area is located ~3 km northwest of Gebel El Mueilha granite mass and covers an area up to 500 m^2. The area consists essentially of Precambrian metsediments, metavolcanics, diorite, serpentinites, and greizenized albite granite (Mohamed 2013), which are all (except serpentinites) cut by mafic and felsic dykes, as well as mineralized quartz veins (Fig. 4.24a). The host rocks of the mineralized veins in Mueilha Sn–W occurrence are represented mainly by intensively greisenized and albitized granites. More than seventy quartz veins were mapped in the mine area, and many of them are carrying cassiterite and wolframite, others are carrying only cassiterite, and some of them are barren. The Sn–W quartz veins range in width from few cm up to 1 m, and length from 50 to 500 m. Greisenization zone of up to 2 cm is well developed at the contact between quartz veins and country rocks, which is composed of mica and cassiterite intergrowths (Mohamed 2013). Two modes of occurrence of Sn–W mineralization are known in the Mueilha mine area as fissure filling quartz veins and greisen zones. The mineralized quartz veins are composed mainly of massive milky quartz with a contact zone rich in mica, beryl, topaz, cassiterite and wolframite. The inner part of quartz veins contain vugs and cavities up to 10 cm across, which are usually filled by elongated quartz grains and sometimes associated with chalcopyrite, fluorite, and calcite. In addition, disseminated Sn–W mineralization was also discovered during the verification of an airborne radiometric anomaly at Gebel Mueilha area, ~3 km to the southeast of the old mine site. This was followed by the discovery of similar Sn–W deposit at Igla, Abu Dabbab, Nuweibi and many other occurrences. The greisenized and albitized zones of Mueilha granite are also associated with anomalous concentrations of Sn (500–1000 ppm), Nb (500–800 ppm), Bi (up to 300 ppm) and Be, where the estimated average grade of Sn ranges from 0.1 to 0.3 wt% (Hussein 1990).

The *Igla* mine was previously known for the production of Sn, where the ruins of the Sn smelter is still there. The host rocks in the Igla mine area are acidic to intermediate volcanic rocks and tuffs intruded by a small mass of apogranite (a lithium albite granite) with disseminated cassiterite and wolframite. However, in some occurrences (e.g., Abu Hamad, Fatira El Beida, Abu Kharif, El Dob, Magharabiya, Um Bisilla, Zargat Naam and Qash Amir, see Fig. 4.22), wolframite is the principal mineral over cassiterite. Wolframite-bearing quartz veins are of limited length and thickness, where they are cross cutting the younger pink granites. The mineralized quartz veins occur at the contact between apogranite masses and the country rocks, where they are carrying cassiterite, wolframite and beryl. The estimated proven ore reserves are ~1700 t of ore containing about 7 t of Sn, while the estimated probable reserves may contain more than 60 t of Sn (Hussein 1990).

In the *Abu Dabbab* area, which is located at ~30 km north Marsa Alam in the CED (Fig. 4.22), there are some 58 cassiterite-bearing quartz veins cutting the post-orogenic granitoid stocks, known as the "apogranite" in the literature. The apogranite of Abu Dabbab area contains essentially Ta–Nb mineralization (see section C below). In the *Abu Dabbab* area, a small apogranite stock intruded into metasedimentary country rocks. The cassiteritebearing quartz veins and veinlets range from 50 to 600 m in length and from 10 to 50 cm in thickness. The veins consist essentially of massive quartz with cassiterite, some wolframite, zinnwaldite, fluorite and topaz.

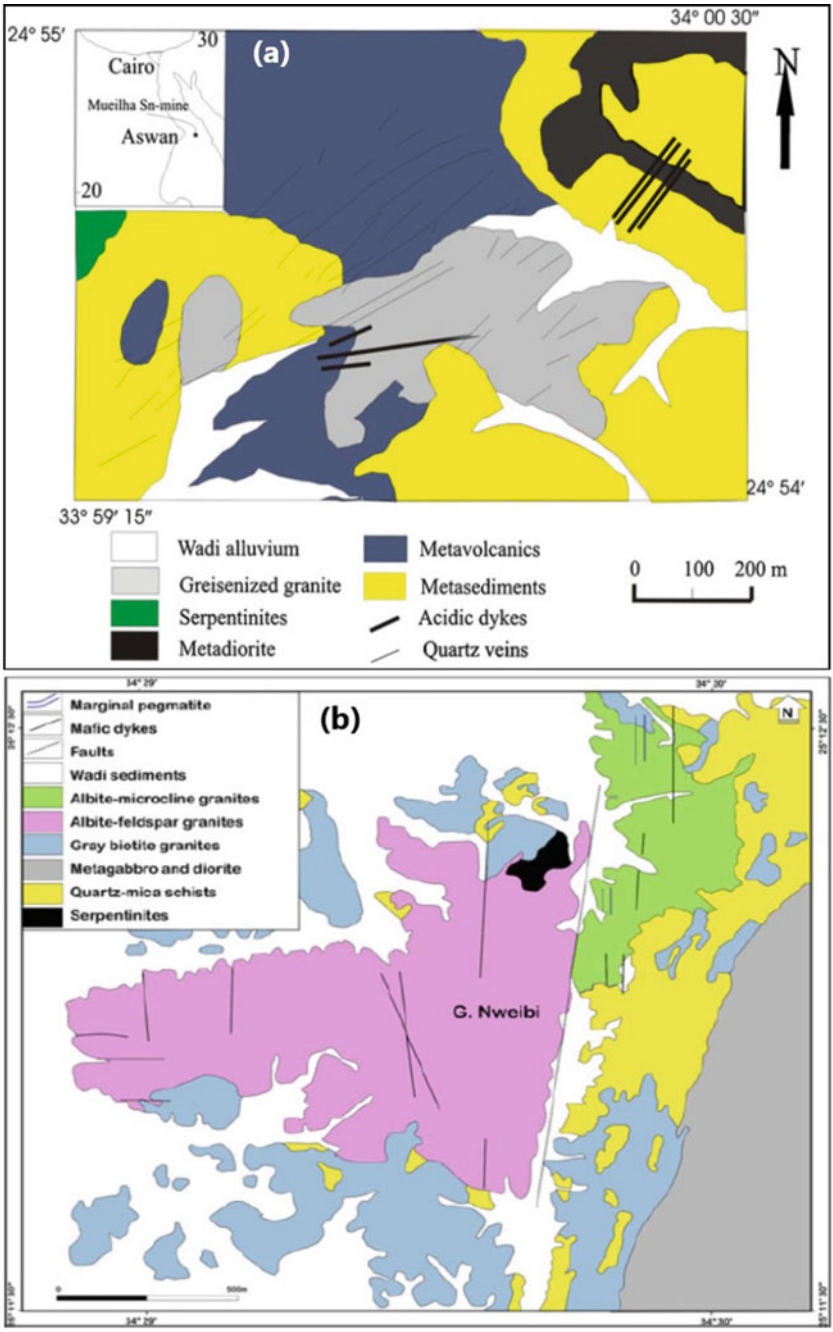

Fig. 4.24 Simplified geological map of **a** Mueilha Sn mine area (from Mohamed 2013), and **b** Nuweibi area (after Gaafar 2014)

The estimated ore reserves in the mineralized veins of Abu Dabbab area are very limited, about 16,000 t of ore, in addition to ~500,000 t of alluvium ore with an average grade of 0.1 wt% Sn (Hussein 1990).

The *Nuweibi* area is located in the CED, ~30 km north of Marsa Alam and ~33 km west of the Red Sea coast (Fig. 4.22). It is covering an area of ~135 km^2, mainly consisting of metasedimentary rocks, serpentinites, metagabbros, grey granites, albite granites, post and pre-albite granite dykes (Fig. 4.24b). The Nuweibi area is also well-known for Nb–Ta mineralization, and the mineralization is present as impregnation zones within the Nuweibi apogranite mass, whereas the Sn mineralization is present in quartz cassiterite veins. The cassiterite-bearing veins occurs as zones east of the apogranite mass, including more than seventy quartz veins ranging in length from 100 to 800 m and in thickness from 25 to 30 cm. The mineralized quartz veins contain thick mica selvages and are made up of massive milky quartz with cassiterite, wolframite, some molybdenite, tantalite, beryl, malachite, azurite, and limonite. The estimated ore reserves in the veins and alluvial sediments are ~94,000 t of ore with an average grade varying from 0.003 to 0.3 wt% Sn (Kochin and Bassiuni 1968; Hussein 1990).

There are several occurrences of W mineralization, concentrated mainly in the NED, and to a lesser extent, in the CED, some of which are represented by Abu Hamad, Fatira El Beida, Abu Kharif, El Dob, Maghrabiya, Um Bisilla, Zargat Naam, Gash Amer, and Gebel Atud (Fig. 4.22, see numbers for locality names). Tungsten mineralization in these occurrences mostly present as vein-type mineralization. The quartz veins in the *Abu Hamad* area are mostly associated with red granite, which in turn, cut by dolerite dikes. The mineralized quartz veins are approximately vertical, 2–30 *cm* thickness and consist mainly of quartz, feldspar and mica, as well as tungstate minerals of wolframite and scheelite. No reserve estimation data are available for the W mineralization in the Abu Hamad area. In the *Fatira El Beida* area (Fig. 4.22), the mineralized quartz veins are characterized by a thickness of 10–30 cm and up to 500 m long, trending northeast/southwest direction and dipping 30° toward northwest. These veins are always associated with granite and contain less amount of wolframite.

The *Abu Kharif* area (Fig. 4.22) contains two sets of wolframite-bearing quartz veins: the older set trends east/west and dips 30° toward north. It ranges in thickness from 20 to 150 cm and up to 150 m long. These quartz veins consist of irregularly distributed wolframite pockets. The younger quartz-vein set is oriented in northeast/southwest direction, approximately vertical and consists of quartz, orthoclase, fluorite, mica, and less amount of wolframite. In the *El Dob* area (Fig. 4.22), the wolframite-bearing quartz veins are locally associated with the greisenized granite. Walframite-bearing quartz veins are trending northeast/southwest direction, dipping toward the southeast, ranging in thickness from 20 to 45 cm, and extending up to 1 km along strike. These veins are essentially composed of milky quartz, orthoclase, mica, and irregularly distributed pockets of wolframite. The *Maghrabiya* area (Fig. 4.22) contains three wolframite-bearing quartz veins cross cutting locally greisenized and kaolinized granite. The wolframite-bearing quartz veins are trending north/south and/or northeast/southwest direction, approximately vertical, and up to 150 m long

and 30 cm thick. Wolframite is the only ore mineral that irregularly distributed in quartz veins.

The *Um Bisilla* area (Fig. 4.22) contains small-mineralized quartz veins cutting through muscovite-albite apogranite, which intruded the Hammamat sedimentary and volcanic rocks. These quartz veins are trending northwest/southeast direction, dipping toward northeast, and composed essentially of quartz, subordinate calcite, chlorite, muscovite, and barite. Wolframite is the main W minerals associated with subordinate magnetite, pyrite, chalcopyrite, and malachite. The ore reserves of the Um Bisilla area are limited with an average grade ranging from 0.006 to 0.01 wt% W (El-Ramly et al. 1970). The *Zargat Naam* and *Gash Amer* areas (Fig. 4.22) have low amounts of W mineralization in which small wolframite-bearing veins and veinlets are found either in the marginal contact of the granitic masses, in the Zargat Naam area, or along the fractures in younger granite, in the Gash Amer area (Hussein 1990). Wolframite mineralization in the *Atud* area (Fig. 4.22) is associated with auriferous quartz veins, at the base of the Gebel Atud. These veins have a thickness of ~30 cm and extending for 20 m in the northwest/southeast direction within the altered gabbro-diorite mass.

(C) ***Niobium-Tantalum (Nb–Ta) mineralization***

The primary igneous niobium (Nb) and tantalum (Ta) mineralization occasionally commonly associated with other rare metals such as Li, Cs, Rb, Be, Sn, W, U, Zr, REE, which is hosted by geochemically and mineralogically unique rare-metal granitoid rocks. Based on the geological and geochemical composition of the host granitic rocks, the Nb–Ta mineral deposits are generally classified into four different types (e.g., Černý 1989; Pollard 1989; Fetherston 2004; Kuster 2009) including: (1) peraluminous rare-element granitic pegmatites characterized by Nb, Ta, Li, Cs, Be, Sn; (2) peraluminous rare-metal granites, also known as Li-mica albite granites, Li–F granites or "apogranites" characterized by Ta, Sn, Be, Li, Nb; (3) peralkaline granites and quartz syenites characterized by Zr, REE, Nb, Ta, Sn, U, Th; and (4) carbonatites and nepheline syenites characterized by Nb, REE, P, Zr, Ta. The first two types of granites (peraluminous granites and pegmatites) are the main hosts of the Nb–Ta deposits, whereas the other two types (peralkaline granites and carbonatites) contain less amounts of Nb–Ta as accessory metals.

The Nb–Ta mineralization, along with other rare-metals, are concentrated mainly in the CED of Egypt (Fig. 4.22). The Nb–Ta mineralization is commonly associated with Li-mica albite granite "apogranite", which are found at some occurrences in the CED including *Igla*, *Nuweibi*, *Abu Dabbab* and *Humr Waggat*. The Nuweibi and Abu Dabbab are the most thoroughly studied and hence well known occurrences (Fig. 4.22). As in the most Precambrian outcrops of the CED, the *Nuweibi* and *Abu Dabbab* areas are made up of gneisses, migmatites, ophiolite and ophiolitic mélange, syn-orogenic metagabbro–diorite complexes, late to post-orogenic granitoid intrusions, as well as post-accretionary volcanics and molasses-type sedimentary rocks (e.g., Helba et al. 1997).

The apogranite of *Nuweibi* area is divided into eastern and western parts by strike–slip fault along Wadi Nuweibi (Fig. 4.24b). Granite in the eastern part has intruded the

metasediments, metavolcanics, and serpentinite rocks, whereas the western part is mostly grey granites. The Nuweibi Nb–Ta mineralization is found mainly as disseminations through the apogranite and within quartz-cassiterite veins, as well as in the greisenized zones (Abouzeid and Khaled 2011). The ore mineralogy of Nb–Ta bearing apogranites in Nuweibi area revealed the presence of columbite [(Fe, Mn) Nb_2O_6], cassiterite, magnetite, ilmenite, zircon, topaz, barite, and trace amounts of apatite, rutile and monazite (Hussein 1990). Mineralized zone at Nuweibi area records that the Ta_2O_5 and Nb_2O_5 contents vary from 0.018 to 0.024 wt%, and from 0.005 to 0.009 wt%, respectively. The Ta_2O_5: Nb_2O_5 ratio ranges from 2: 1 to 5: 1. It is also noted that the eastern part of the apogranite mass is potentially more important for mineralization, although Ta and Nb contents are substantial lower (0.004% Ta_2O_5 and 0.002% Nb_2O_5) (Sabet et al. 1973). There is a potential zone of ~1000 m long and 450 m wide with a continuous mineralization down to 50 m depth. The average concentrations Ta_2O_5 and Nb_2O_5 inthis zone gare 0.018 and 0.009 wt%, respectively, and the Ta_2O_5: Nb_2O_5 ratio is 2: 1. The estimated proven ore reserve is ~20 Mt of ore containing about 3600 t Ta_2O_5 and 1800 t Nb_2O_5. More recently, ore reserve was also estimated in Nuweibi area to be ~114.7 Mt of ore with average grades of 0.022 wt% Ta_2O_5 and 0.2 wt% Nb_2O_5 (Naim et al. 1996; Abouzeid and Khaled 2011).

The *Abu Dabbab* Nb–Ta mineralization is primarily a Ta deposit, which occurs in a sheet to stock-like apogranite intrusions. The latter forms strongly altered alkali-feldspar granite of peraluminous geochemical characteristics/features. Abu Dabbab granitic mass intruded within early to middle Cryogenian ophiolitic mélange of metasedimentary, metavolcanic and talc carbonate rocks (Kuster 2009). The mineralized stock has an ellipsoidal shape trending in an east/west direction, and covering an area of ~3.2 km^2, which is made up of quartzalbite or quartz-albite-amazonite lithionite. Mineralization is most intensive in the northeastern side to be ~30 m wide contact zone of the mass. The estimated proven ore reserves of Abu Dabbab Nb–Ta mineralization are ~10 Mt ore, containing 2800 t Ta_2O_5, and 800 t Nb_2O_5 (Sabet 1976). The Ta_2O_5 content ranges from 0.0095 to 0.075 wt%, with an average of 0.028 wt%, and the Nb_2O_5 values varied from 0.002 to 0.029 wt%, with an average of 0.008 wt%, and average Ta_2O_5: Nb_2O_5 ratio of 3: 1.

(D) ***Beryllium (emerald-beryl) mineralization***

In addition to the above mentioned granite-related mineralization (Mo, Sn–W and Nb–Ta), there are anomalous mineralization of beryl/emerald, fluorite and uranium, also related to granite. sEmerald is a dark-green chromium (Cr)-vanadium (V)-rich variety of beryl ($Be_3Al_2Si_6O_{18}$). It is the third most valuable gemstone (after diamond and ruby). Beryl is also economically important as a major source of the metal beryllium (Be), which is important in the nuclear industry. The Egyptian emerald/beryl mines are mainly located in the SED (Upper Egypt) ~40–60 km south of Marsa Alam city (Fig. 4.25). These occurrences have an immense historical value, where emerald was well known and mined for the first time in the Graeco-Roman period between 30 BC and 312 AD. The famous "*Cleopatra Mine*" of Ancient Egypt, located at Wadi Sikait of Marsa Alam area, is the oldest known source of emeralds, where mining is

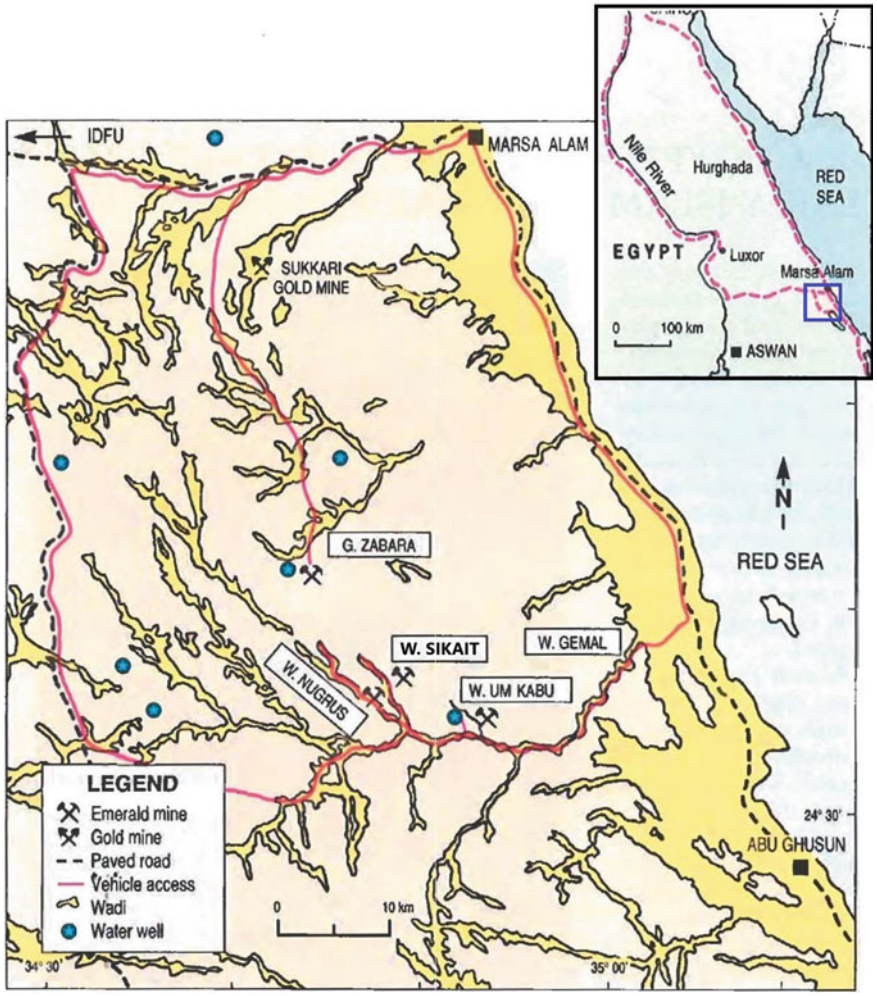

Fig. 4.25 Simplified geographic map showing the emerald-bearing province of upper Egypt, which lies in the hills inland from the coast of the Red Sea, west of Marsa Alam (from Jennings et al. 1993)

thought to have been carried out 4000 years before present. Egypt is believed to be the only source of emerald and other beryl minerals for the ancient civilizations of Europe and the Mediterranean region. The Egyptian emerald/beryl was mined from several localities in the SED, all of them are situated within 15 km from *Wadi Sikait*, including *Gebel Zabara* to the northwest, *Wadi Nugrus* and *Wadi Abu Rusheid* to the west, *Wadi Um Kabu* and *Wadi Um Debaa* to the southeast, and *Wadi El Gemal* to the southwest (Fig. 4.25). A summary of key geologic features of emerald deposits at the above localities is given below.

The geology of emerald-bearing localities displays a wide variety of igneous and metamorphic rock types of basement complex (Fig. 4.26), including metasedimentary and metavolcanic rocks, intruded by granites (Hassan and El-Shatoury 1976; Jennings et al. 1993). The emerald deposits of Upper Egypt occur within a northwest-southeast trending belt of emerald-bearing schistose rocks that extends for ~45 km from Gebel Zabara in the northwest to Wadi Um Kabu in the southeast (Fig. 4.26). The beryl/emerald mineralization is commonly linked to the intrusive contact between a gneissic biotite granite and the overlying mica schists (Soliman 1986). The emeralds and other beryl minerals occur as isolated crystals within biotite schists, biotite-actinolite schists, and biotite-tourmaline schists along this contact, as well as in quartz veins and pegmatite dikes that commonly crosscut the emerald-bearing zones in these mica schists (Jennings et al. 1993). The ancient emerald mines in the SED were located along stream valleys where erosion exposed the

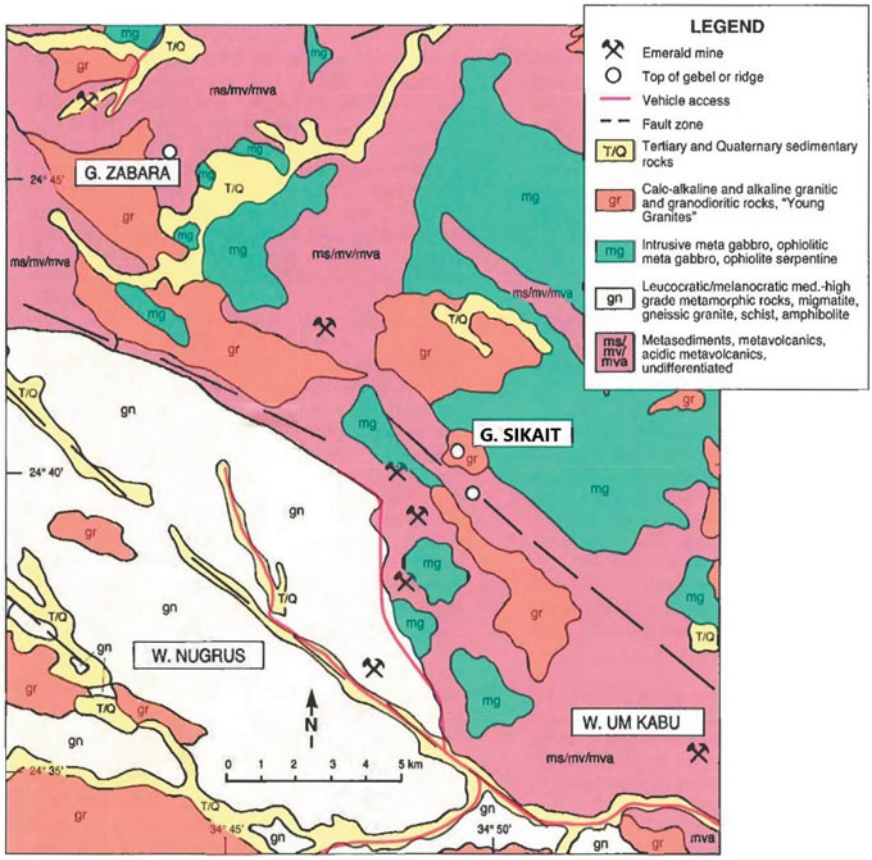

Fig. 4.26 Simplified geologic map of the emerald localities in the SED of Egypt shows the general NW–SE trend of the mines (after Geologic Map of Egypt, Gebel Hamata Sheet 1987; Jennings et al. 1993)

mineralization along the contact zone. Emerald fragments were also abundant in the alluvial deposits of these streams. It appears that most of these emerald concentrations in the region were mined out a long time ago, with a limited/little chances of finding emerald fragments by today's explorers. The northwest-southeast linear distribution of beryl mineralization and emerald mines in the region suggest that the presence of a northwest-southeast trending deep-seated tectonic zone/structure in the Precambrian. The beryl mineralization is believed to be formed along this northwest-southeast trending zone due to magmatic-hydrothermal processes associated with the episodic emplacement of younger granites during the Precambrian (Soliman 1986; Hussein 1990; Jennings et al. 1993).

The *Zabara* area has the most famous beryl (emerald) deposits among the other emerald mineralizations in the SED. Basta and Zaki (1961) and Hassan and El-Shatoury (1976) discussed the geology of beryl occurrences in the Zabara area. Emerald and green beryl were mined from the schistose rocks at their contact with the underlying gneissic granite intrusion, where the contact between them is commonly covered by talus from the steep canyon walls. In some cases, however, the contact is well exposed on both sides of the narrow wadi, and there are numerous shafts along its entire length. There are numerous quartz veins and fractures cutting across the schists and underlying gneissic granites. The beryl mineralization occurs in limited and discontinuous zones along the contact, with mica schists. The gem quality of beryl tends to occur more frequently in the mica schist than in the quartz veins and veinlets. Greisenized and albitized parts of the gneissic granite of the Zabara area gave ~80 ppm Be. Molybdenum, Sn, and W have been identified in quartz veinlets in the area. Fragments of emerald and green beryl were also recovered from the tailings associated with the mines and from alluvial gravels in the floor of the narrow valley (Wadi).

Sikait-Nugrus area was extensively mined in the ancient times. At *Sikait-Nugrus area* beryl mineralization is restricted to the contact zone of mica schists with the quartzo-feldspathic gneissic granite of Wadi Abu Rushaid and Wadi Nugrus. The geology of the beryl occurrences in the Sikait/Nugrus localities has been described in detail by Hume (1934), Basta and Zaki (1961), and Hassan and El-Shatoury (1976). Grubessi et al. (1990) documented geology of this area, a reason behind which the present excursion was initiated to this locality and hence many fine ancient ruins (dwellings and temple) were seen (Fig. 4.26a). The main temple at Wadi Sikait, carved into the canyon walls, has been served as a landmark for many travelers to the area (Fig. 4.27b). The most extensive workings for emerald at this locality is present on the southwest slopes of Gebel Sikait, midway along Wadi Sikait near the temple, and on the northeast side of Wadi Nugrus, near the ruined dwellings (Fig. 4.27a). Similarly, the best occurrence of beryl in these Wadis is restricted to the mica schist-gneissic granite contact zone (Fig. 4.27c). Beryl is concentrated in discontinuous zones of schistose rocks along this contact, and in quartz veins cutting the schists and underlying gneissic granites. This contact is often covered by alluvium or by tailings from the numerous mines, where in most places, the contact between the beryl-bearing schistose rocks and the underlying gneissic granite is unclear but inferred. The beryl-bearing schists are exposed on the slopes of Gebel Sikait, and

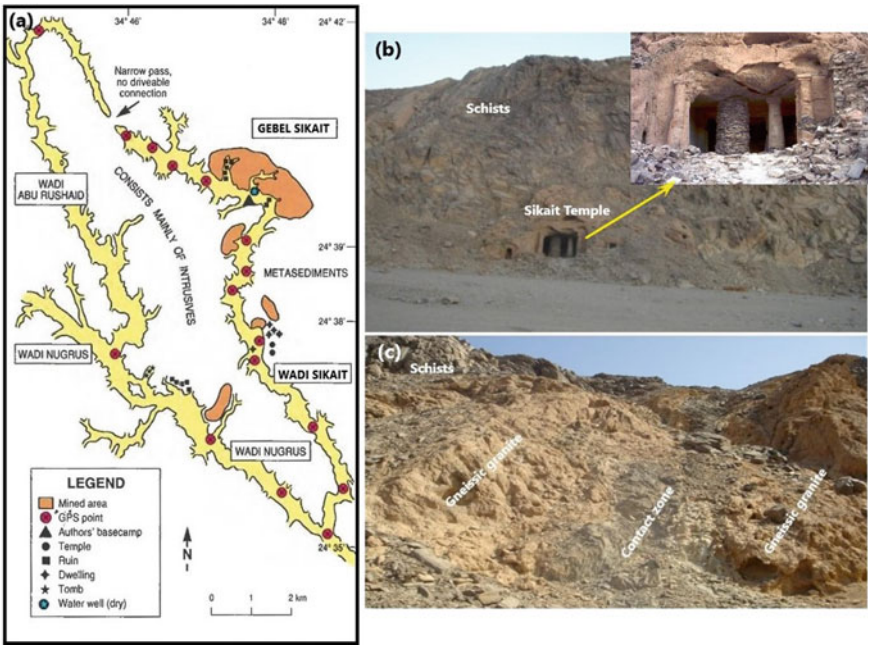

Fig. 4.27 **a** Sketch map of the emerald mines of Wadi Sikait and Wadi Nugrus (from Jennings et al. 1993). **b** Temple of Wadi Sikait, and **c** field photo shows the occurrence of beryl in Wadi Sikait, which is restricted to the mica schist-gneissic granite contact zone

to the southeast along Wadi Sikait, toward the ruins. The deposits on the slopes of Gebel Sikait occur in four bands of mica schist and talc schist, which have fault contact with the gneissic granite.

The *Um Kabu* beryl occurrence is shown in Figs. 4.25 and 4.26, where the emerald mines and workings are accessed from two Wadis that branch north/northeast from Wadi El Gemal (Fig. 4.25). Despite extensive mining activities at *Um Kabu* area, very little information has been published on Um Kabu beryl mineralization. such an extensive ancient mining suggests that the Um Kabu beryl mineralization was once a major source of emerald (Jennings et al. 1993). The beryl occurrence at Um Kabu, as at the other localities, is believed to be formed due to the emplacement of granites into mica schists (Hassan and El-Shatoury 1976; Soliman 1986). Small exposures of gneissic granite and white granite were observed in the lower reaches of Wadi Um Kabu, and where the occurrences of beryl are indicative of the presence of granitic intrusion very close to the surface. Abundant fragments of green beryl and emerald were found along the narrow Wadis that lead to the emerald workings of Um Kabu. Emerald in this locality occurs as small (few millimeters across), loose, hexagonal prisms, as single crystals and occasional as clusters embedded in quartz and biotite schist. Fragments of green beryl and emerald were also found in the tailing piles.

The *Homret Akarem* and *Homret Mikpid* beryl occurrences lie on an east/west trend ~20 km apart, southwest of Marsa Alam in the SED (Fig. 4.28a). Beryl mineralization in both occurrences is linked to stock-like bodies of alkali feldspar granites. Beryl mineralization typically occurs as beryl veinlets and disseminations in massive pegmatoidal lenses and pegmatite veins intruding the alkali granite, as well as in quartz veins at the contact between the alkali granite and the country rocks. The Homret Akarem is located at Wadi Khashab, ~20 km west of the conspicuous landmark of Gebel Homret Mikpid; it is built up of pelitic metasedimentary rocks, grey gneissose granite, pink alkali granite forming Gebel Homret Akarem, and a

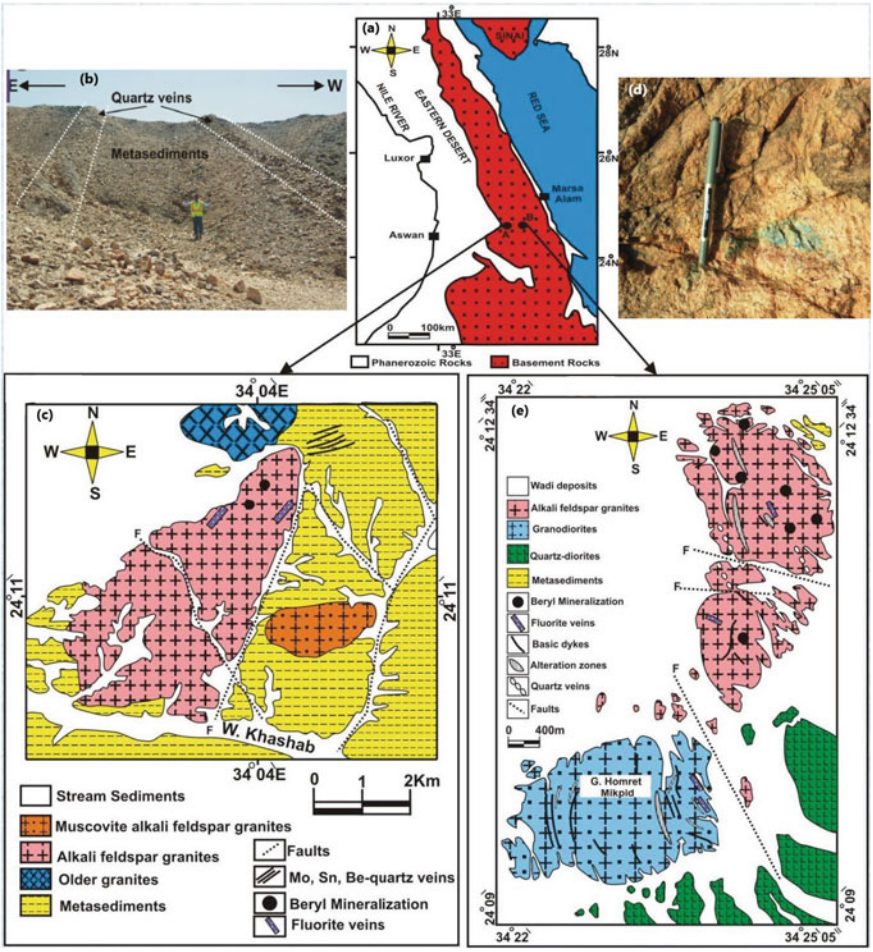

Fig. 4.28 **a** Location map of the Homret Mikpid and Homret Akarem beryl occurrences, SED of Egypt. **b** Cassiterite/molybdenite-bearing quartz veins cross cutting the metasedimentary rocks of Homret Akarem beryl occurrence. **c** Geologic map of Homret Akarem area. **d** Pale green beryl crystal within peralkaline granite of Homret Mikpid area. **e** Geologic map of Homret Mikpid area

smaller body of muscovite granite (Fig. 4.28c). Beryl mineralization at Homret Akarem occurs in different modes (Hassan and El-Shatoury 1976) including: (1) small pegmatoidal lenses (20 × 80 cm) of massive beryl within alkali feldspar granite, (2) in the selvage zone between the cassiterite-molybdenite-bearing quartz veins and the metasedimentary rocks (Fig. 4.28b), and (3) in pegmatite dikes cutting across the alkali feldspar granite. On the other hand, the Homret Mikpid area is located between Wadi Abu Natash (a tributary of Wadi Khashab) and Wadi El Kharit in the SED (Fig. 4.28e). The Gebel Homret Mikpid, which is a conspicuous landmark in the area, consists of alkali feldspar granite intruding metavolcanic rocks, diorite and granodiorite (grey granite) (Fig. 4.28e). As for Homret Akarem, Beryl mineralization at Homret Mikpid also occurs in different modes including: (1) disseminated in alkali feldspar granite (Fig. 4.28d), (2) in pegmatites, and (3) in quartz veins and veinlets cutting the alkali feldspar granite and surrounding metavolcanic rocks.

(E) ***Uranium (U) mineralization***

In addition to the U-bearing granites, U mineralization in Egypt is known in various environments, including Carboniferous and Cretaceous black shales, in phosphorite deposits, and Oligocene sandstones and associated rocks at Gebel Qatrani, where U content reached up to 0.3 wt% U_3O_8. In this section, the U mineralization related to Proterozoic granite rocks will be discussed, where it occurs either as disseminations in the metasomatically altered granites (greisens and albitites), or where it forms veinlets and stringers across granite masses (Hussein et al. 1982). The more important U occurrences (e.g., El Missikat, El Erediya, El Atshan, Um Doweila) are highlighted below (Fig. 4.29).

The *El Missikat* area is one of the most important U occurrences in the Eastern Desert. It is located in the CED between latitude 26° 23´ and 26° 33´N and longitudes 33°15´ and 33° 30´ E, to the south of Safaga-Qena road (Fig. 4.29). It covers an area of ~350 km^2, which is composed essentially of basement rocks of Precambrian and the Phanerozoic Nubian Sandstone. The El Missikat younger granite plutons host a significant U mineralization (Abu Dief 1992; Abu Dief and El-Tahir 2008). The radioactivity of El Missikat area is related to U mineralization associated with highly brecciated black and jasperoid silica veinlets, confined to minor faults and fractures striking east/northeast direction. Uranium mineralization is represented on the surface by uraophane and soddyite minerals, which were observed visually as thin films or aggregates of acicular crystals or as a paint on fractures and cavities. It is always associated with sulfide minerals such as pyrite, chalcopyrite, galena, sphalerite and molybdenite, and the gangue minerals are mainly fluorite and Fe–Mn oxides (Attawiya 1983; Hussein 1990). The U mineralization in El Missikat area is associated with silicification, sericitization and kaolinization of granite. It is lithologically and structurally controlled, connected to black and jasperoid siliceous materials representing two younger generations of silica filling the fracture shear zones. The mineralized shear zones are intensively oxidized at the surface as a result of oxidation and leaching.

The *EI Erediya* area is characterized by U mineralization. It is part of the CED, ~50 km away from El Missikat area (Fig. 4.29). and it covers ~25 km^2. The El

Fig. 4.29 Google satellite map showing the most important U occurrences in the NED and CED of Egypt

Erediya mineralization forms the southwestern portion of Gebel El Erediya granitic mass along Wadi El Erediya, ~30 km south of Qena-Safaga road. Gebel El Erediya is an oval-shaped pink granite striking northwest/southeast direction with a length of ~ 6.5 km and width of 2.5 km. It is cut by aplites, pegmatite and jasper dikes and veins and a few basaltic dikes. Radioactive anomalies and U mineralization have been discovered by airborne radiometric survey and ground survey (Ammar 1973). These studies revealed that the radioactive anomalies in the area are attributed to the secondary U mineralization associated with jasperoid veins. Other significant radioactive showings are associated with a set of northeast/southwest trending parallel fractures cutting the southwestern part of the granitic mass. High radioactivity was also recorded in the extreme southern part of the mineralized shear zone, where disseminated pitchblende and secondary U minerals (uranophane with subordinate soddyite and renardite) are present.

Some minor but important U deposits were also recorded in El Atshan, Um Doweila, Abu Zawal and Um Shilman areas. The *El Atshan* is one of the earliest U deposits discovered in the Quseir area (Fig. 4.29), where pitchblende and atshanite

occur as fracture filling in the contact zone between a microgranite dikes and country rocks of slates and low-grade schists. It is believed that the U-bearing hydrothermal solutions represent the late stage of magmatic differentiation. Like the El Atshan area, the *Um Doweila* occurrence is part of the SED and is the longest U-bearing microgranite dikes (bostonite). It extends in a northeast direction for ~11 km and ranges in thickness from 2 to 20 m. The northern barren and non-altered part are composed essentially of grey alkaline microgranite with aegirine, riebeckite and arfvedsonite minerals (Hussein, 1990). The alkaline microgranite cuts across the non-metamorphosed country volcanic and pyroclastic rocks. Mineralization was discovered by a very pronounced airborne radiometric signature, followed by ground scintillometric and Radon emanometric surveys, which record strong radioactivity and highest U contents localized in two separate segments totaling about 3 km in length. These two segments are intensively sheared, brecciated, ferruginated, and the sodic amphiboles and pyroxenes are completely replaced by hematite and goethite, with extensive silicification of the matrix. At the *Abu Zawal* area, the southernmost part of the NED (Fig. 4.29), radioactivity is associated with pegmatite veins in altered pink alkali granites indicating the presence of allanite in these veins. Similarly, in the wider area of Wadi El Gemal, several radioactive anomalies are also related to the concentrations of allanite in granite pegmatites associated with white granites. At the *Um Shilman* occurrence, in the SED, the radioactive apogranite zone occurs at the margin of the Um Shilman granitic pluton. It contains disseminated secondary U minerals and anomalous concentrations of trace metals such as Pb, Zr, Y, Nb and Ta. The metasomatically altered apogranites are always intensively silicified, albitized and greisenized, and are carrying accessory thorite, uranothorite, zircon and kasolite, together with their abnormal concentrations of r trace metals such as Sn, Be, Ta, Zr, Li and REE.

4.5 Magmatic-Hydrothermal Deposits in Sudan

The magmatic-hydrothermal mineral deposits in Sudan are represented by the recently discovered porphyry Cu–Au deposits in the Gebel Ohier (Bierlein et al. 2016, 2020) and the Cu–Au porphyry deposits in the Atbara area (Sasmaz 2020) of the Red Sea Hills of northeastern Sudan. Granite-related Sn–W, fluorite, and rare metal deposits are also found in the Red Sea Hills and Nuba Mountains. To the author's knowledge, the epithermal vein-type and skarn deposits are not reported from Sudan. The following sections present a brief description of these magmatic-hydrothermal deposits in Sudan.

4.5.1 Porphyry Cu–Au Deposits

The mineral resources of Sudan have not been fully explored. although there are some important new discoveries recently. Examples include the porphyry Cu–Au deposits in the *Gebel Ohier* (Bierlein et al. 2016, 2020) and the porphyry Au–Cu deposits in the *Atbara* region (Sasmaz 2020) of the Red Sea Hill of northeastern Sudan. Gebel Ohier deposit is a Cu–Au rich stockwork mineralization, where intensive alteration zones (potassic, advanced argillic and propylitic) are well developed around the mineralized systems (Bierlein et al. 2016). The wide mineralization area, the stockwork mineralization style, the distinctive well-developed alteration zones, and the close association of the mineralization with acidic porphyry intrusions, suggest that the Gebel Ohier deposit is typical of porphyry Cu–Au mineralization. It is quite distinctive from the previously recognized orogenic gold style mineralization in the Red Sea Hills (Klemm et al. 2001) and from those of the well-documented Cu–Zn–Au volcanogenic massive sulfide (VMS) mineralization in the Ariab district.

The *Gebel Ohier* is located in a remote area of Sudan, ~300 km to the west/northwest of Port Sudan (Fig. 4.30). Historically, exploration at Gebel Ohier was commenced in the early 1980s, during a reconnaissance fieldwork carried out by the "Bureau de Recherches Géologiques et Minières" (BRGM), as a part of the

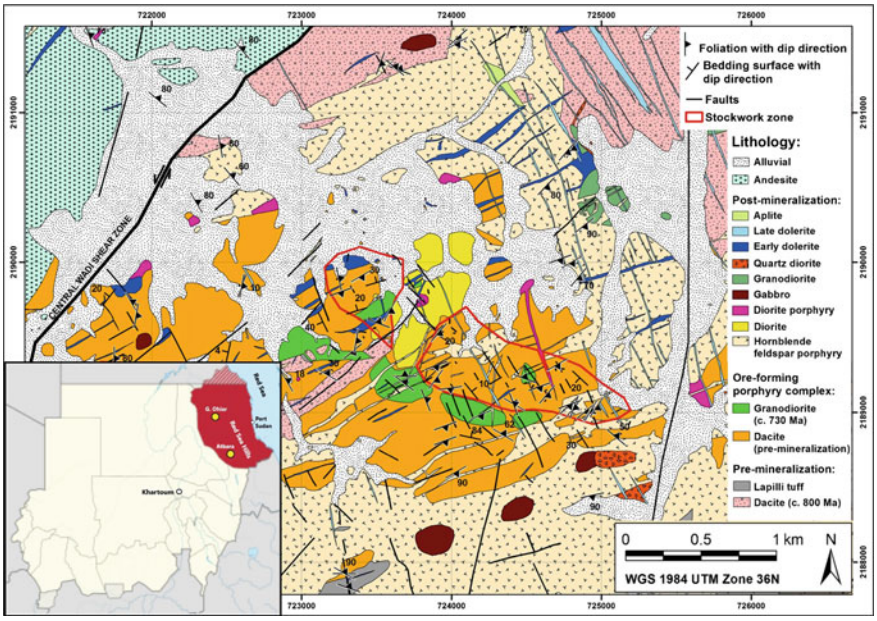

Fig. 4.30 Simplified geological map of the Gebel Ohier and Atbara areas showing major rock units, structural trends, and extent of the stockwork zone (from Bierlein et al. 2016). Inset is a sketch map of Sudan showing the, ocation of the Red Sea Hills and Geber Ohier area

regional exploration program for metal deposits. Following this early reconnaissance study, the Anglo-American Corporation geologists were revisited the Gebel Ohier area in 1995, for further prospectivity assessment (unpublished report for Qatar Mining Sudan Co Ltd "QMSD"). A regional geochemical sampling program, grid soil and rock-chips sampling at the Gebel Ohier prospect was, conducted by the "Geological Research Authority of Sudan" (GRAS) in 2004 and 2005 (Adde 2004, 2005). Recently, the "QMSD" has conducted a detailed geochemical sampling and geological mapping, followed by a preliminary exploratory drilling of ~ 5600 m during the period of September 2014 to February 2015 (Bierlein et al. 2016). The results of exploratory drilling program gave an average grade of between 0.2 and 1.5 wt% Cu and depth of 35 to 75 m. Anomalous concentration of Cu (>0.5 wt%) and Au (up to 0.45 g/t) have been intercepted at multipile depths of drill cores below the base of the oxide zone to about 200 m depth. The lateral and vertical extensions of the mineralized zone areunconstrained, and the resource estimation has not been carried out yet.

The Gebel Ohier area is characterized by intrusive and extrusive rocks ranging in composition from gabbroic to granodioritic-dacitic. Porphyry intrusion was emplaced into an older andesitic to dacitic, and in places tuffaceous volcanic sequence. The mineralization and associated alteration zones occur in a thick massive to laminated dacitic rocks (Fig. 4.30). The granodiorite and dacite rocks were intruded by a distinct post-mineralization porphyritic intrusive suite, termed as "hornblende-feldspar porphyry", as well as a series of post-mineralization intermediate to mafic intrusive plugs, stocks and dykes (Bierlein et al. 2016). The alteration zones are well developed around the mineralization, covering an area of ~4 × 1.5 km, and represented mainly by pervasively quartz-sericite-chlorite alteration, and in places, strongly silicified and pyritized dacite and granodiorite. A phyllic sericite ± pyrite-dominated zone, advanced argillic and argillic alteration zones, and a peripheral zone of weakly developed propylitic epidote-carbonate-chlorite alteration zone are all well developed around the hydrothermal stockwork mineralization system (Bierlein et al. 2016).

The mineralized stockwork zone in the Gebel Ohier prospect comprises veins of variable thicknesses and extensions that range from thin veinlets (1–25 mm across) to thicker massive veins (20–100 mm across), and sometimes laterally continuous, laminated to massive, asymmetric, and irregular-shaped veins. The veinlets are typically discontinuous and erratically orientated containing rare disseminated sulfides. The hypogene zone is typically containing characteristic sulfide-Fe-oxide-carbonate central domains and narrow sericitic selvages (Bierlein et al. 2016). A variably thick layer of chrysocolla with minor malachite commonly coats the oxidized outcrop. The veining patterns and distinctive development of stockwork sequence at Gebel Ohier closely resemble those widely described from many porphyry Cu–Au deposits worldwide, such as those at El Salvador, Ok Tedi and Grasberg (e.g., Gustafson and Hunt 1975; Sillitoe 2010). All features recognized at the Gebel Ohier porphyry mineralization are mostly similar to those reported from Wadi Ranga and Hamash porphyry mineralization of the SED of Egypt (Ahmed and Gharib 2016; Helmy and Kaindl 1999). As in many porphyry systems from elsewhere, the mineralogy of Gebel Ohier

porphyry mineralization is very simple, where the main sulfide phases are pyrite and chalcopyrite, which occur as disseminated phases. Chalcopyrite typically fringes and penetrates pyrite grains along fractures. Low-Fe sphalerite (1.5–6 wt% Fe), galena, bornite, and rare pyrrhotite inclusions in pyrite occur as subordinate phases in stockwork veins, and rarely as disseminated grains in the silicified dacite (Bierlein et al. 2016). Disseminated magnetite represents an early hydrothermal phase in the more mafic-intermediate host rocks, as well as associated with pyrite and chalcopyrite in stockwork veins. When present, bornite is replaced by covellite and/or chalcocite. Very few Au grains have been observed as tiny visible grains in quartz and feldspar veins, and within cracks of the main sulfide minerals.

The ore minerals assemblage and the low-Fe content of sphalerite can be used to estimate the formation temperature of spahlerite at ~400 to 450 °C at Gebel Ohier (Scott 1983; Bierlein et al. 2016). Furthermore, the presence of few molybdenite grains within large pyrire aggregates, and the presence of accessory phases, such as empressite-hessite, sylvanite, altaite, and enargite, associated with the main sulfides in stockworks, suggest that their precipitation occurred under progressively lower hydrothermal temperature conditions from a moderately to hyper-saline fluids (e.g., Bodnar 1995; Sun et al. 2013).

Another recent discovery of porphyry Au–Cu mineralization in the Red Sea Hills of northeastern Sudan is the *Atbara* deposit (Sasmaz 2020), which is located close to the boundary between Gebeit and Haya terranes, at ~300 km northeast of Khartoum (inset of Fig. 4.30). The Haya terrane, hosting Atbara Au–Cu mineralization is characterized by the granodioritic-gabbroic intrusive rocks and associated volcano-sedimentary rocks (Reischmann and Kröner 1994). Late-orogenic granites occupy large low topographic areas in the northern and northeastern part of Atbara area, whereas several post-collisional alkaline syenite intrusions form elevated hills.. The thickness of mineralized zones ranges between 0.10 and 3.0 m and the length between 100 and 300 m. Three types of mineralization were identified in the Atbara area, including Au-bearing quartz veins of different colors (brown and white/grey), and low-grade Au mineralization associated with Cu-rich zones (Sasmaz 2020). The Au concentrations in quartz veins and wall rocks show significant variations, which are mainly controlled by the extension and deformation occurred in the alteration zones (kaolenization, sericitization, and silicification) in granitic and dioritic rocks. The common ore minerals in the Atbara Au–Cu mineralization are represented mainly by native Au, chalcopyrite, pyrite, galena, pyrrhotite, tetrahedrite, covellite-chalcocite, goethite, psilomelane and hematite (Sasmaz 2020). The gangue minerals are dominated by brown and white/grey quartz, calcite, chlorite, epidote and feldspar. Native Au is mainly hosted in brown and white/grey quartz veins, and as disseminated or veinlets in quartz, but not associated with chalcopyrite. Despite detailed field, mineralogical and geochemical studies of the Atbara Au–Cu porphyry deposits (Sasmaz 2020), there is no resource/reserve estimation for the mineralized area.

4.5.2 Granite-Related Mineralization

The granite-related mineralization is represented mainly by Sn–W and fluorite occurrences in some localities in the central part of Sudan. A Sn–W-bearing stockwork has been described from the *Sabaloka* igneous complex of Neoproterozoic-Cambrian granites, ~90 km north of Khartoum. The mineralized stockwork is recognized within a small 300 m long lens-shaped mass of greisen, on the contact of a porphyritic microgranite ring dyke with the host gneissic rocks. Individual quartz veins within the stockwork are commonly less than 5 cm wide, and they are rich in cassiterite, wolframite, goethite, limonite, jarosite, powellite, galena, fluorite, molybdenite, scheelite, calcite and malachite, in approximate order of abundance. The greisen lens contains numerous miarolitic cavities lined with quartz and/or cassiterite. The source of greisen and mineralizing fluids may have been from the nearby mass of biotite-muscovite granite.

The Nuba Mountains ofCentral Sudan, represent a major geological feature hosting several mineral deposits within the Precambrian basement rocks, including fluorite, Au, Cu, Fe, talc, Zn, graphite, Mn, U, and chromite (e.g., Shaddad et al. 1979; Khalil 1980; Abdel Galil 2008). The Nuba Mountains occupying an area of ~140,000 km^2; it is situated ~550 km southwest of Khartoum (Fig. 4.31) in the South Kordofan State. The basement complex of the Nuba Mountains comprises two lithological units (Abdelsalam and Dawoud 1991): (1) older high-grade gneisses in the west, and (2) younger low-grade volcano-sedimentary sequence to the east (Fig. 4.31). Both the older and younger unites are cross cutting by post-tectonic intrusive bodies of various compositions, ranging from gabbroic to granitoid rocks. The intrusive rocks, together with associated extrusive equivalents are concentrated

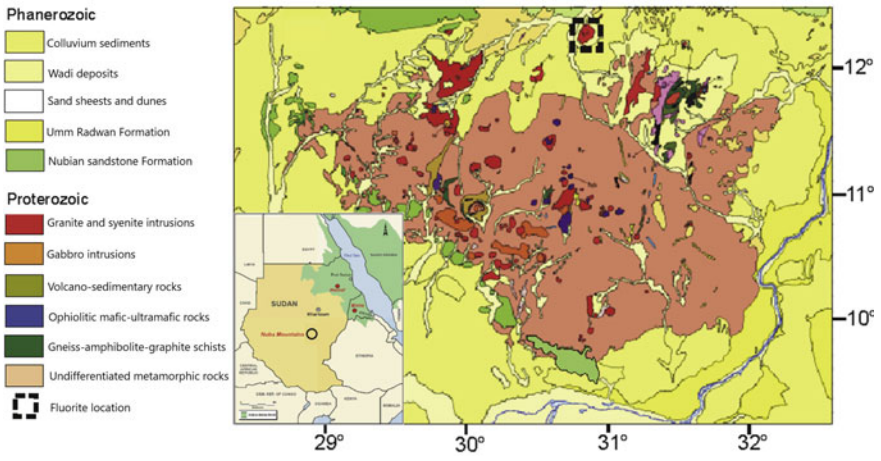

Fig. 4.31 Geological map of the Nuba Mountains, central Sudan showing the location and geological units of the fluorite deposits (from Ismail et al. 2015). Inset is the location map of Nuba Mountain in the central Sudan

mainly along three belts: southwestern, central and northeastern belts. In the third belt, scattered syenitic and granitic intrusions (Gebel Ed Dair, Kadero, Dumbier, El Semieh, and Tibna) are common, and in some places (i.e., Dumbier) carbonatite has been reported (e.g., Ismail et al. 2015 and references therein).

Fluorite occurrences in the Nuba Mountains are concentrated mainly in the northern part of the area, where they occur as lenses and veins in several localities. The thickness of fluorite veins ranges from a few centimeters to 1 m (Fig. 4.32) with sharp contact with the country rocks. The host rocks are mainly orthoclase-rich pink granite and pegmatite rocks. The color of the fluorite varies from purple, pink to pinkish white, and yellowish white to white (Fig. 4.32). Fluorite is generally massive in the core of the veins, but when exposed to the surface they become soft due to weathering. The fluorite veins are, in most cases, associated with milky white to yellowish white quartz veins of approximately 20–30 cm in thickness, as well as colorless to grayish white carbonatite veins and lenses up to 50 cm in thickness (Ismail et al. 2015).The gangue minerals associated with fluorite include quartz, calcite, orthoclase, and muscovite.

The fluorite deposits of Nuba Mountains is characterized by high concentrations of REEwith the total REE ranging from 541 to 10,430 ppm (average of 3234 ppm) (Ismail et al. 2015). The chondrite-normalized REE patterns of different types of fluorite show similar general trend, being highly enriched in light rare earth elements

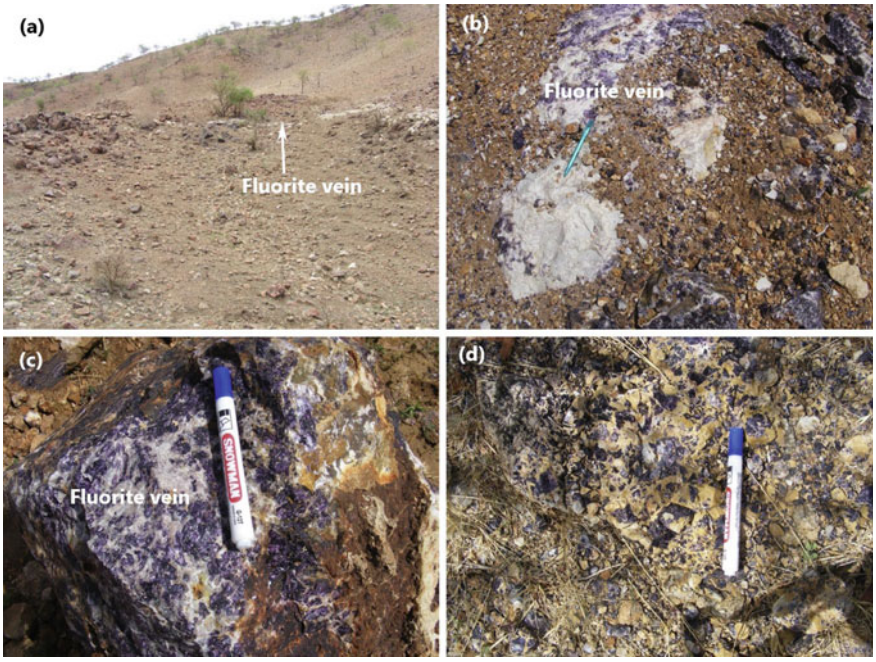

Fig. 4.32 **a** and **b** Field photographs showing the occurrence of fluorite-bearing veins in the country rocks, and **c** and **d** is a close up of the pinkish fluorite vein (taken from Ismail et al. 2015)

(LREE) and strongly depleted in heavy rare earth elements (HREE). Fluorite has three possible genetic models for its formation, including: (1) high-temperature pegmatite, (2) medium-temperature hydrothermal, and (3) low-temperature sedimentary settings (e.g., Möller et al. 1976). These models hence fluorite types can be distinguished based on petrographical, fluid inclusions and geochemical ground. (Dolnicek and Slobodnik 2001; Ackerman 2005; Sasmaz and Yavuz 2007). For example, fluorites from the Nuba Mountains are plotted in the high-temperature pegmatite field in the Tb/Ca versus Tb/La variation diagram, consistent with the late crystallization environment of the host granitic magma. The late magmatic-hydrothermal origin of fluorites from the Nuba Mountains is supported by their compositional heterogeneity, abundant of growth zoning, irregular shape of fluorite grains, and the presence of fluorite as inclusions in other magmatic minerals. The hydrothermal fluorite, on the other hand, is characterized by homogeneous composition, appearance, and the absence of growth zones (Dolnicek and Slobodnik 2001; Ismail et al. 2015).

4.6 Magmatic-Hydrothermal Deposits in Eritrea

Magmatic-hydrothermal mineralization in Eritrea is poorly understood. In other words, this style of mineralization in most part of Eritrea is not well studied. Locally, for example near the border with Ethiopia, there are some copper mineralization associated with the porphyry granite intrusion of the Firfira Complex in Tsehafi Emba. In this area mineralization is present in the form of veinlets and disseminated minerals of chalcopyrite and pyrite hosted in metamorphic gabbroic rocks, syenites, fine-grained mafic volcanic rocks and granite. Aplites and simple pegmatite veins associated with swarms of quartz veinlets in greisenized granite including calcite, muscovite, tourmaline, pyrite, and locally beryl (Binda et al. 1993) are common in the areas surrounding the Firfira Complex. No further information are available regarding magmatic-hydrothermal style of mineralization in Eritrea.

Poly-metallic volcanogenic massive sulfide (VMS) deposits (e.g., Debarwa, Adi Nefas North, Amba Derho, and Bisha), and gold-bearing quartz veins (orogenic gold) hosted in shear zones (e.g., Augaro, Medrizien, and Adi Shimaglle), will be discussed in subsequent chapters.

4.7 Magmatic-Hydrothermal Deposits in Ethiopia

The magmatic-hydrothermal mineralization in Ethiopia is represented mainly by granite- and granitic-pegmatite-related mineral deposits, in the Southern Ethiopian Greenstone Belt, and in the Wollega and Kenticha areas of the Adola belt (Fig. 4.33). These rare metal granitic pegmatites contain high concentrations of trace and REE including Ta, Nb, Mo, Sn, W, Be, Li, U, Th, etc. Information about porphyry, skarn

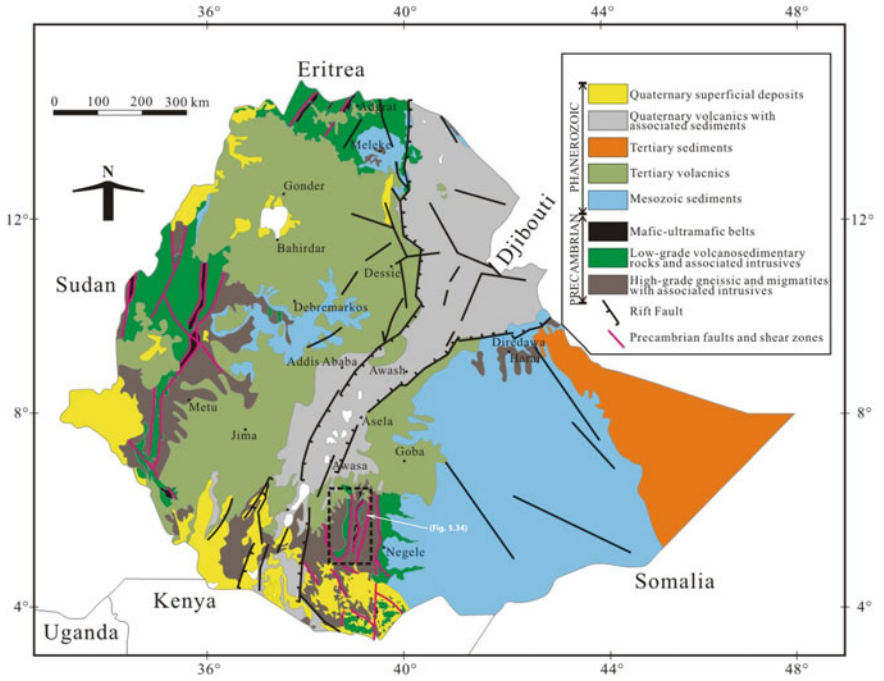

Fig. 4.33 General geological map and location of the rare-metals pegmatite area of Ethiopia (after Kazmin 1971)

and epithermal mineral deposits in Ethiopia is very scarce andtherefore, in this we focus on the granitic pegmatite-related deposits, the only subject discussed here, which include the rare-metals pegmatite and emerald-bearing rocks near the contact zone between the mica schist and silica-rich fluids from granitic batholiths and pegmatite veins.

4.7.1 Rare-Metals Granitic Pegmatites

In general, and as described in Chap. 2, the Neoproterozoic basement rocks of southern Ethiopia are classified into two principal lithotectonic units (Küster 2009): (1) granite-gneiss complexes (GGC) consisting of high-grade para- and orthogneisses, i.e., deformed and metamorphosed granitoids, biotite-hornblende gneiss and amphibolite, and (2) ophiolitic fold and thrust belts (OFTB), consisting of low-grade, mafic–ultramafic rocks and sedimentary rock assemblages. These different rock units are juxtaposed in many places along thrust and shear zones (Fig. 4.34). The orthogneisses and deformed dioritic to granitic batholiths are common and locally represent the dominant rock type. Four lithological granite–gneiss complexes GGC

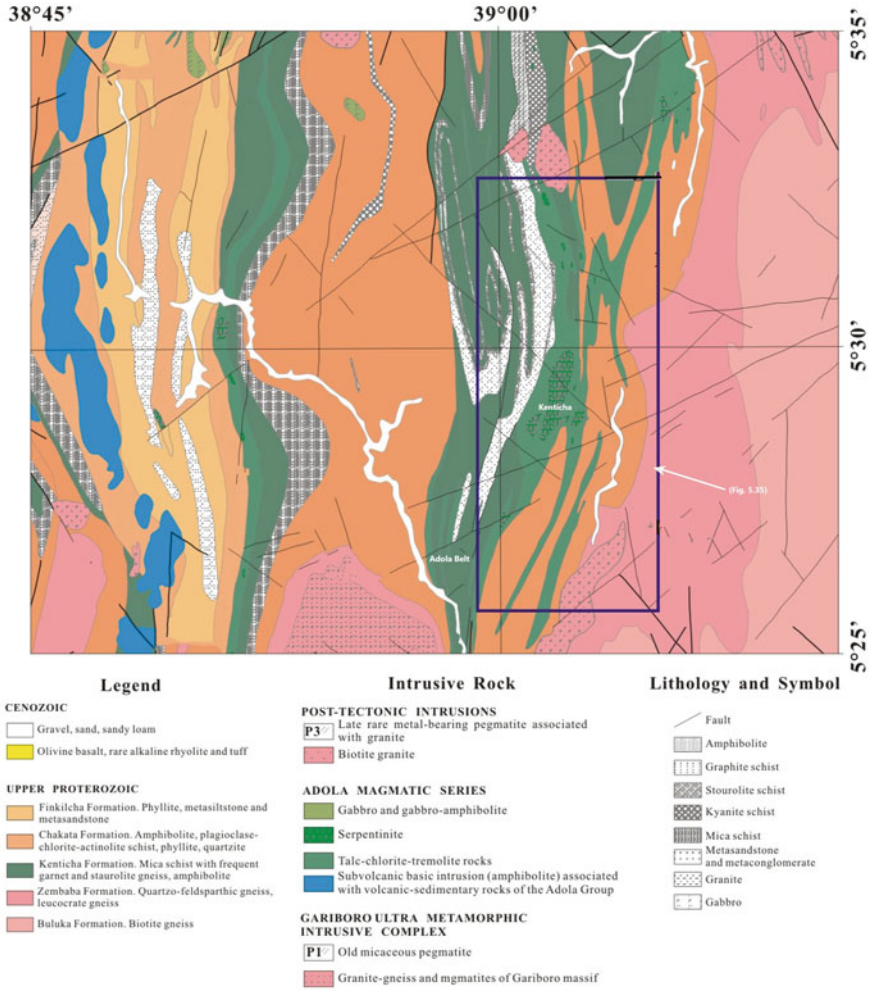

Fig. 4.34 Regional geological map of the Adola Belt showing the locations of the rare-metal pegmatite (taken from Kim et al. 2013, after Ethiopian Mapping Agency 1988)

(*Adola, Genale*, *Burji-Finchaa* and *Moyale-Sololo*), separated by major regional shear zones, are distinguished (Yibas et al. 2002). Ophiolitic fold and thrust belts (OFTB) are essentially composed of mafic and ultramafic metavolcanic and metasedimentary rocks (Yibas et al. 2002; Küster 2009). Four lithological OFTBs (*Megado*, *Kenticha*, *Bulbul*, and *Moyale-El Kur*) are also distinguished based on chemical composition of their metabasalts, the presence of boninitic rocks and contrasting proportions of ultramafic and metasedimentary rocks. The contact between the OFTBs and the adjacent GGCs is marked by zones of multiple deformation, indicating thrusting and strike-slip shear faulting. The Adola Belt includes, from older

to younger, the Aflata and Kenticha Formations, Adola metamorphic rock series and early Paleozoic post-orogenic granites and pegmatites (Fig. 4.34). The Kenticha Formation along a narrow synclinal structure, comprises, from older to younger, biotite-, muscovite-, garnet amphibolite- and quartz-feldspatic-gneisses, fine grained amphibolite-, staurolite-garnet-biotite-, garnet-staurolite-mica-schists, and marble (Yibas et al. 2002; Küster 2009; Mohammedyasin 2017).

Granitic pegmatites of southern Ethiopia are found in all lithotectonic units of the Adola Belt (Poletayev et al. 1991), particularly in the Kenticha Hill, west of Chuni Hill, where distinct clusters of pegmatites are present (Fig. 4.35). These pegmatite clusters are referred, in the literature, to as the "Kenticha pegmatite field", which is distributed in an area of ~2500 km^2 (Yibas et al. 2002; Küster 2009; Mohammedyasin 2017). The rare-metals pegmatites of Kenticha Hill were emplaced close to, but mainly west of, the NNE–SSW striking Kenticha thrust shear zone (Fig. 4.35). The mineralized pegmatities intruded the greenschist to lower amphibolite facies talc–tremolite schists, chromite-bearing serpentinites, and pelitic to graphitic mica schists. Most of the rare-metals pegmatites of the Kenticha field strike N–S to NNE–SSW (Figs. 4.35 and 4.36); and are characterized by considerable differences in size (from a few tens of meters to more than 1 km in length), shape (steeply dipping dykes to almost flat lying sheets), internal zoning, mineralogy, and geochemistry (Poletayev et al. 1991; Kim et al. 2013; Mohammedyasin 2017). Pegmatite is found as stratified bodies; with obscured lower contact, but the upper contact with serpentinite is clear and sharp (Fig. 4.36a and b).

The boundary between pegmatites and host granite is clear in the outcrop and in mineralogy. The muscovite and two-feldspar granite in the lower zone grades upward into albite, muscovite-, quartz-microcline and muscovite-quartz-albite-microcline pegmatite zones (Fig. 4.36c) (Küster 2009; Mohammedyasin 2017). The middle zone is dominated by muscovite-spodumene-microcline-albite pegmatite superimposed by albitized and greisenized units. The upper zone of pegmatite is the most differentiated zone, containig spodumene, large quartz cores (Fig. 4.36d), microcline and ambigonite montebrasite blocks, and spodumene-quartz zones (Kim et al., 2013). Elongated spodumene veins and veinlets commonly associated with blocky quartz, are ubiquitous in the upper pegmatite zone (Fig. 4.37a, b). Tantalite is easily observed with the naked eye in the surface outcrops, where it reaches to centimeters size, commonly associated with coarse-grained quartz and albite (Fig. 4.37c, d). In the upper part of pegmatite, fine-grained unoriented tantalite grains are also associated with chlorite (Fig. 4.37e), and elongated grains of lepodolite (centimeters size) are also common (Fig. 4.37f). The Ta content increases upward, where it is occasionally associated with the columbite-tantalite group minerals forming flattened and short prismatic small grains of ~5–7 cm length (Kim et al. 2013; Mohammedyasin 2017). Based on mineral paragenesis and trace element systematics, the Kenticha pegmatite is classified into rare-metals pegmatites and barren pegmatites (Zerihun 1991; Zerihun et al. 1995). There are several types of rare-metals pegmatites in Kenticha Hill area including, (1) Ta-poor pegmatites (Kilkele and Bupo), (2) Ta-rich beryl-columbite subtype (Kilkele and Dermidama), (3) complex spodumene type,

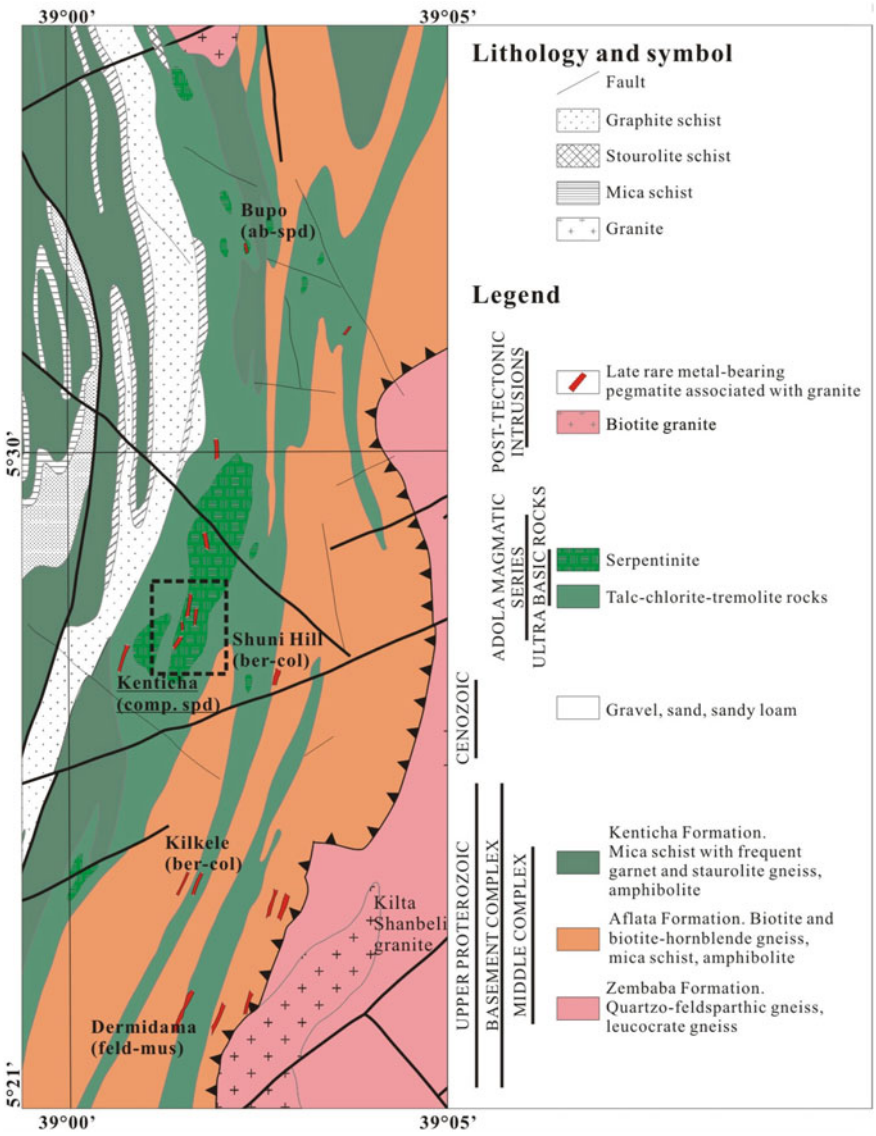

Fig. 4.35 Local geological map of the Kenticha area showing the distribution of the rare-metals pegmatite (taken from Kim et al. 2013, after Ethiopian Mapping Agency 1988)

and (4) albite spodumene type (Bupo) (Fig. 4.35). Similarly, there are regional mineralogical zoning in Kenticha pegmatite field including Li-silicates accommodated in lepidolite, spodumene, holmquistite, albite and swinfordite, and Li-phosphates in the form of amblygonite and lithiophyllite (Dill 2015). Many pegmatite veins and

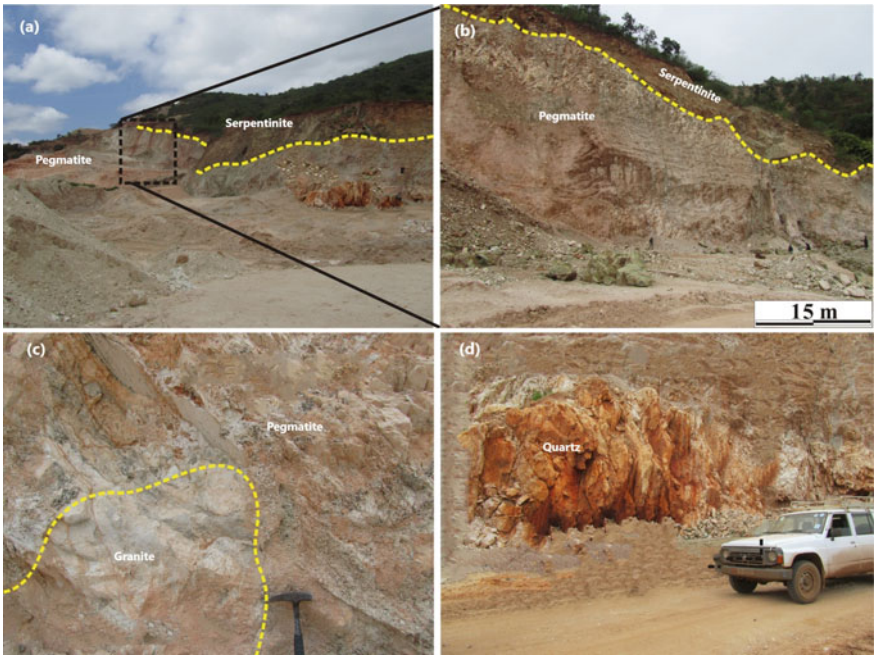

Fig. 4.36 Field photographs of the Kenticha rare-metals pegmatite. **a** and **b** Upper pegmatite showing the sharp contact with serpentinite, **c** gradual contact zone between lower leucocratic granite and intermediate quartz-albite-muscovite-microcline pegmatite, and **d** massive quartz unit (taken from Kim et al. 2013)

dikes in Kenticha area show inward mineralogical and textural changes parallel to the degree of pegmatite fractionation (Tadesse 2001).

4.7.2 Beryllium (Emerald) Mineralization

As for the beryllium-bearing minerals (beryl/emerald) in the Eastern Desert of Egypt, emeralds (the gem form of beryl) in Ethiopia also found close to the contact zone between the mica schist and granitic batholiths and pegmatite veins. Like many other industrial minerals including quartz, feldspar, opal, garnet, peridot and sapphire, Ethiopia is now mining and trading emeralds, which creates new jobs for thousands of Ethiopians. The emerald mineralization was recently discovered in Ethiopia in 2016, which is located in the south-central part of the country, ~20 km south of Shakiso town (Fig. 4.38). This area hosts various mineral deposits, including Au, tantalum, quartz and feldspar, which are commonly associated with the rare-metals granitic pegmatites in Kenticha Hill. As described above, this whole region is situated within the northern portion of an orogenic belt known as the "Mozambique metamorphic

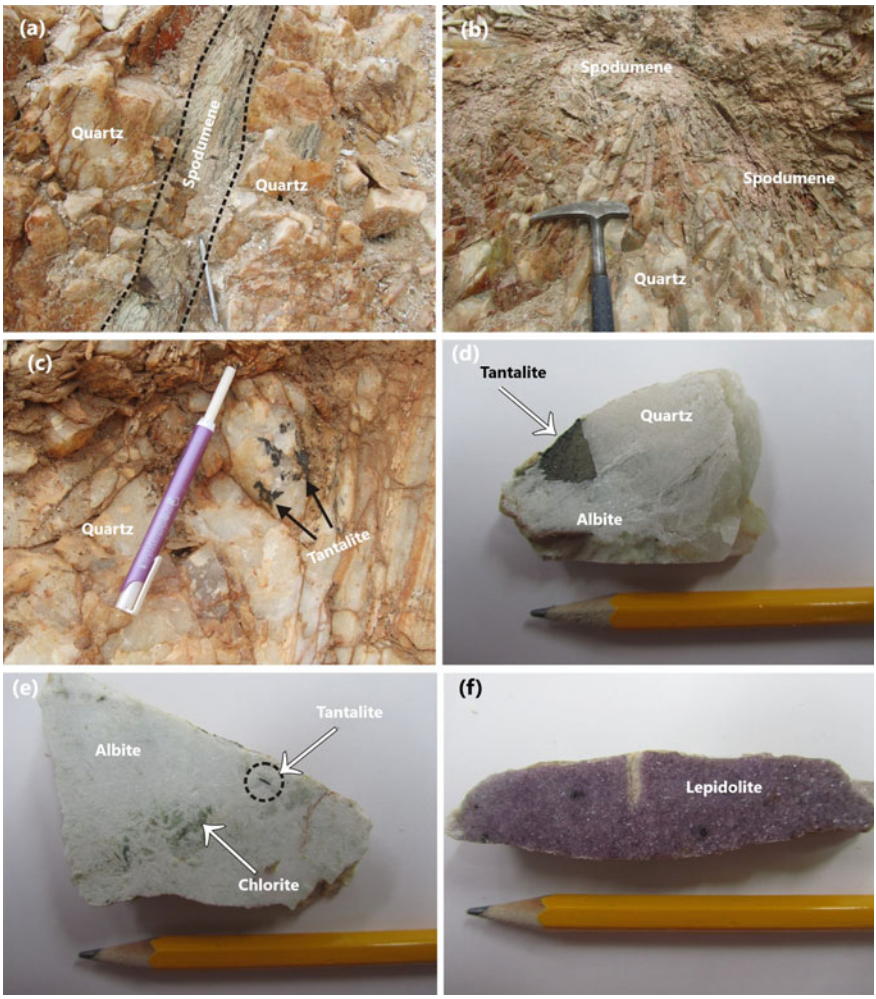

Fig. 4.37 Mode of occurrences of rare-metal minerals in Kenticha pegamtite. **a** and **b** wedge and radial shape spodumene associated with quartz, **c**–**e** Mn-tantalite in massive quartz-spodumene and sacchroidal albite, and **f** lepidolite with albite (taken from Kim et al. 2013)

belt" extending from the Red Sea all the way to Mozambique and as far as eastern and southern Madagascar. The belt is a major suture that formed during the late Neoproterozoic, with main metamorphic events occurring between 500 and 650 Ma ago, where the mafic and ultramafic rocks were compressed and uplifted as a result of the extensive Pan-African geologic event. Relatively high P–T conditions in the uplift areas resulted in substantial changes in the composition and texture of pre-existing rocks, transformed them into metamorphic rocks (schists and amphibolites) during cooling (Schluessel and Schuessel 2018). The emerald mineralization in Ethiopia is relatively small-scale mining (Fig. 4.38a) but yields gem- to semi-gem quality

Fig. 4.38 Sketch map of Ethiopia showing the location of the new emerald deposit, which is located near the town of Shakiso

crystal materials (Fig. 4.38b). It can be faceted into exquisitely fine, clean, and unique emeralds that are comparable to those mined from the world class varieties such as those in Chivor, Colombia. The emerald mineralization was thought to be formed through metasomatic process in and near the contact zone between the mica schist and silica-rich fluids generated from granitic batholiths and pegmatite veins.

The emeralds are mined in and near Kenticha area (Seba Boru district), to be subsequently brought to Shakiso where gemstone dealers from Addis Ababa buy the rough materials. The emerald at Kenticha Hill is neither the first nor the only occurrence in Ethiopia, but it is the most promising site both in terms of quality and quantity. From the mine, the emeralds are transported by car on to Shakiso; despite the presence of a small airport, most emerald dealers prefer to drive 10 h to the capital city (Schluessel and Schuessel 2018). Access to the mining area has been barred to anyone without a permit from the Ethiopian Ministry of Mines. Optical and physical properties of the Ethiopian emeralds are similar to the other schist-hosted emeralds from elsewhere, particularly those from Minas Gerais in Brazil and Zambia. The emerald crystals weight reached up to 10 ct when faceted, but stones over 20 ct and even exceeding 30 ct have been recorded. The color ranges from very pale green to very intense green (Fig. 4.39a, b), more saturated emeralds commonly exhibit a slight bluish secondary color (Schluessel and Schuessel 2018) (Fig. 4.39a, b).

Fig. 4.39 **a** The Haloo mine, one of the several emerald mines that are worked in a traditional way using hand tools, **b** mixed-grade rough Ethiopian emeralds

References

Abdel Galil MY (2008) Geology and mineralization related to anorogenic igneous complexes of Northern Nuba Mountains and Northern Kordofan-Sudan (Ph.D. thesis). Al Neelain University, Sudan, p 213

Abdelnasser A (2020) Mineral resources in egypt (I): metallic ores—Industrial metal oxides (Sn, W, Ta, Nb, and Mo). In: Hamimi et al. (eds) The geology of egypt, regional geology reviews. Springer Nature Switzerland, pp 550–556, https://doi.org/10.1007/978-3-030-15265-9-14

Abdelsalam M, Dawoud AS (1991) The Kabus ophiolitic melange, Sudan, and its bearing on the western boundary of the Nubian shield. J Geol Soc London 148:83–92

Abdelsalam MG, Abdeen MM, Dowaidar HM, Stern RJ, Abdelghaffar AA (2003) Structural evolution of the Neoproterozoic Western Allaqi-Heiani suture, southeastern Egypt. Precambr Res 124:87–104

Abouzeid AM, Khaled AM (2011) Mineral industry in Egypt—Part I: metallic mineral commodities. Nat Resour 2:35–53

Abu Dief A, El-Tahi M (2008) A new uranium occurrence, gabal el-missikat prospect, central eastern desert, egypt. J King Abdilaziz Univ (Earth Sci Sect), Jeddah, KSA 19:85–97

Abu Dief A (1992) The relation between the uranium mineralization and tectonics in some Pan-African granite, West Safaga, Eastern Desert, Egypt. Ph.D. thesis, Faculty of Science, Assiut University, Egypt, p 218

Ackerman L (2005) Magmatic vs. hydrothermal origin of fluorites from Vlastejovice Bohemian massif. J Czech Geol Soc 50:35–41

Adde AE (2004) Preliminary geochemical gold exploration at Jebel Oheir Area. Geological Research Authority of Sudan (GRAS), Sudan (unpublished), NE Sudan

Adde AE (2005) Phase 2 geochemical gold exploration at Jebel Oheir Area. Geological Research Authority of Sudan (GRAS), Sudan (unpublished), NE Sudan

Afifi AA (1990) Environments of gold telluride mineralization in the Mahd adh Dhahab district, Arabian shield: Ann Arbor, University of Michigan, Ph.D. dissertation, p 285

Ahmed AH, Gharib ME (2016) Porphyry Cu mineralization in the eastern desert of Egypt: inference fromgeochemistry, alteration zones, and ore mineralogy. Arab J Geosci 9:179. https://doi.org/10.1007/s12517-015-2107-x

Ahmed Z, Hariri MM (2006) Formation and mineral chemistry of a calcite skarn from Al-Madhiq, SW Saudi Arabia. Chem Erde 66:187–201

Al-Khirbash S, Heikal MTS, Whitehouse MJ, Windley BF, Al Selw K (2021) Evolution and mineralization of the Precambrian basement of Yemen. In: Hamimi Z et al (eds) The geology of the Arabian–Nubian shield, regional geology reviews, pp 633–657. https://doi.org/10.1007/978-3-030-72995-0_24

Ammar AA (1973) Application of aerial radiometry of the geology of Wadi El Gdami area, Eastern Desert; Ph.D. Thesis, Faculty of Science, Cairo University, p 424

Atkinson Jr WW, Einaudi MT (1978) Skarn formation and mineralization in the contact aureole at Carr Fork, Bingham, Utah. Econ Geol 73:1326–1365

Attawiya M (1983) Mineralogical study of El Erediya-I Uranium occurrence. Eastern Desert, Egypt: Arab J Nucl Sci Technol 16:221–236

Basta EZ, Zaki M (1961) Geology and mineralization of Wadi Sikheit area, South-Eastern Desert. J Geol U.A.R., 5(1):148

Berger BR, Ayuso RA, Wynn JC, Seal RR (2008) Preliminary model of porphyry copper deposits, U.S. Geological Survey Open-File Report 2008, 1321, 55

Bierlein FP, McKeag S, Reynolds N, Bargmann CJ, Bullen W, Murphy FC, Al-Athbah H, Brauhart C, Potma W, Meffre S, McKnight S (2016) The Jebel Ohier deposit—a newly discovered porphyry copper–gold system in the Neoproterozoic Arabian–Nubian Shield, Red Sea Hills, NE Sudan. Miner Deposita 51:713–724

Bierlein FP, Potma W, Cernuschi F, Brauhart C, Robinson J, Bargmann CJ, Bullen W, Henriquez JF, Davies I, Kennedy A (2020) New insights into the evolution and age of the neoproterozoic jebel ohier porphyry copper deposit, red sea hills, Northeastern Sudan. Econ Geol 115:1–31

Binda PL, Omenetto P, Warden (1993) Mineral deposits and occurrences in the Precambrian of northeast Africa and Arabia: A Review. From Geology and Mineral Resources of Somalia and Surrounding Regions, 1st Agron. Oltremare, Firenze, Relaz. e Monogr. 113:429–516

Bodnar RJ (1995) Fluid-inclusion evidence for a magmatic source for metals in porphyry copper deposits. In: Thompson JFH (ed) Magmas, fluids, and ore deposits. Mineralogical Association of Canada short course series 23, p 139–152

Botros NS (1999) Acid sulphate alteration type at south Um Monqul, North Eastern Desert, Egypt. Arab Gulf J Sci 17:15–34

Botros NS, Wetait MA (1997) Possible porphyry copper mineralization in South Um Monqul, Eastern Desert, Egypt. Egypt J Geol 41:175–196

Bouabdellah M, Slack JF (2016) Geologic and metallogenic framework of North Africa. In: Bouabdellah M, Slack JF (eds) Mineral deposits of North Africa, mineral resource reviews. Springer International Publishing Switzerland, https://doi.org/10.1007/978-3-319-31733-5_1

Bugrov V(1972) Mineral potential of Aswan region. Geochemical operations July 1968–June 1972 UNDP Technical Report 3 New York, pp 31–33, 63

Calvez JY, Kemp J (1982) Geochronological investigations in the Mahd adh Dhahab quadrangle, central Arabian Shield: Saudi Arabian Deputy Ministry for Mineral Resources Technical Record BRGM-TR-02-5, p 41

Černý P (1989) Characteristics of pegmatite deposits of tantalum. In: Möller P, Černý P, Saupé F (eds) Lanthanides, tantalum and niobium. Springer, Berlin, pp 195–239

Chang Z, Hedenquist JW, White NC, Cooke DR, Roach M, Deyell CL, Garcia JJr, Gemmell JB, McKnight S, Cuison AL (2011) Exploration tools for linked porphyry and epithermal deposits: example from the Mankayan intrusion-centered Cu–Au district, Luzon, Philippines. Econ Geol 106:1365–1398

Collenette P, Grainger D (1994) Mineral resources of Saudi Arabia. DGMR special publication, Ministry of Petroleum and Mineral Resources, Jeddah, KSA

Cooke DR, Hollings P, Walsh JL (2005) Giant porphyry deposits: characteristics, distribution, and tectonic controls. Econ Geol 100:801–818

Dardir AA, Gad Allah A (1969) Report on expedition 7168, Eastern desert. Internal report, Geological Survey Egypt. Davidson, GE 1986

Dill H (2015) Pegmatites and aplites: Their genetic and applied ore geology. Ore Geol Rev 69:417–561

Doebrich JL, Al-Jehani AM, Siddiqui AA, Hayes TS, Wooden JL, Johnson PR (2007) Geology and metallogeny of the Ar Rayn terrane, eastern Arabian shield: evolution of a Neoproterozoic continental-margin arc during assembly of Gondwana within the East African Orogen. Precambr Res 158:17–50

Doebrich JL, LeAnderson PJ (1984) Geology and hydrothermal alteration of the Mahd adh Dhahab epithermal precious-metal deposit, Kingdom of Saudi Arabia: Saudi Arabian Deputy Ministry for Mineral Resources Open-File Report USGS-OF-04-32, p 33, scale 1:2,000 (U.S. geological Survey Open-File Report 84–640)

Dolnicek Z, Slobodnik M (2001) The neoidic fluorite mineralization in the Brno Massif: interaction between fluid and rock. Geolines 13:51–52

Drysdall AR, Jackson NJ, Ramsay CR, Douch CJ, Hackett D (1984) Rare element mineralization related to Precambrian alkali granites in the Arabian shield. Econ Geol 79:1366–1377

du Bray EA (1985) Jabal as Silsilah tin prospect. In: Drysdall AR, Ramsay CR, Stoeser DB (eds) Felsic plutonic rocks and associated mineralization in the Kingdom of Saudi Arabia: Saudi Arabian Deputy Ministry for Mineral Resources Bulletin, vol 29, pp 237–247

du Bray EA (1986) Specialized granitoids in the southeastern Arabian shield–case history of a regional assessment. J Afr Earth Sc 4:169–176

EGSMA (1998) Metallogenic map—Arab Republic of Egypt, Meatllic ores and non-metallic deposits, Scale 1:1,000,000. Egyptian geological survey and mining authority, pp Exploration Sheet

Einaudi MT, Meinert LD, Newberry RJ (1981) Skarn deposits. Econ Geol 75:317–391

El Habaak GH (2004) Pan-African skarn deposits related to banded iron formation, Um Nar area, central Eastern Desert, Egypt. J Afr Earth Sci 38:199–221

El-Makky AM (2000) Applications of geostatistical methods and zonality of primary haloes in geochemical prospecting at the Um Garayat gold mine area, south Eastern Desert, Egypt. Delta J Sci 24:159–192

El-Ramly M, Budanov VI, Hussein AA, Dereniuk NE (1970) Ring complexes in the South–Eastern Desert of Egypt. Studies on some mineral deposits of Egypt. The Egyptian Geological Survey, Cairo, pp 181–194

El-shafei SA, Abdel-Maksoud KM, Helmy HM, Ahmed AH (2020) J Asian Earth Sci 201:104510

El-Shazly AK, Khalil KI (2014) Banded iron formations of Um Nar, Eastern Desert of Egypt: P-T–X conditions of metamorphism and tectonic implications. Lithos 196–197:356–375

Fetherston JM (2004) Tantalum in Western Australia. Mineral Resources. Bulletin 22. Geol Surv West Aust (153 S.)

Fowler A, Hassen IS, Osman AF (2010) Neoproterozoic structural evolution of SE Sinai, Egypt: II. Convergent tectonic history of the continental arc Kid Group. J Afr Earth Sc 58:526–546

Frick CN, Al-Jawadi ZY (2009) Mining strategy for republic of Yemen. United Nations Economic and Social Commission for Western Asia (UNESCWA), in cooperation with Yemen Geological Survey and Mineral Resources Board (YGSMRB), p 114

Gaafar I (2014) Geophysical mapping, geochemical evidence and mineralogy for Nuweibi rare metal albite granite, Eastern Desert, Egypt. Open J Geol 4:108–136

GEOMIN (1980) Report on geological, geophysical and geochemical investigations carried out in the Precambrian formations south-east of Taiz. Yemen Arab Republic, Geomin-Yominco, Bucharest, p 252

Gharib ME, Ahmed AH (2012) Late Neoproterozoic volcanics and associated granitoids at Wadi Ranga, south Eastern Desert, Egypt: a transition from subduction related to intra-arc magmatism. Lithos 155:236–255

Gmbessi O, Aurisicchio C, Castighoni A (1990) The Pharoahs' forgotten emerald mines. J Gemmol 22:164–177

Goldfarb RJ, Baker T, Dube B, Groves DI, Hart CJR, Gosselin P (2005) Distribution, character, and genesis of gold deposits in metamorphic terranes. Econ Geol 100th Anniversary 407–450

Gustafson LB, Hunt JP (1975) The porphyry copper deposit at El Salvador, Chile. Econ Geol 70:857–912

Halter WE, Pettke T, Heinrich CA (2002) The origin of Cu/Au ratios in porphyry type ore deposits. Science 296:1844–1846

Harris NB, Einaudi MT (1982) Skarn deposits in Yerington district, Nevada: metasomatic skarn evolution near Ludwig. Econ Geol 77:877–898

Hassan MA, El-Shatoury HM (1976) Beryl occurrences in Egypt. Mining Geol 26:253–262

Hattori KH, Keith JD (2001) Contribution of mafic melt to porphyry copper mineralization: evidence from Mount Pinatubo, Philippines, and Bingham Canyon, Utah, USA. Miner Deposita 36:799–806

Hedenquist JW, Arribas AJr, Reynolds,TJ (1998) Evolution of an intrusion-centered hydrothermal system: far Southeast-Lepanto porphyry and epithermal Cu-Au deposits, Philippines. Econ Geol 93:373–404

Heinrich CA, Driesner T, Stefánsson A, Seward TM (2004) Magmatic vapor contraction and the transport of gold from the porphyry environment to epithermal ore deposits. Geology 32:761–764

Helba H, Trumbull R, Morteani G, Khalil S, Arslan A (1997) Geochemical and petrographic studies of Ta mineralization in the Nuweibi albite granite complex, Eastern Desert, Egypt. Miner Deposita 32:164–179

Helmy HM, Kaindl R (1999) Mineralogy and fluid inclusion studies of the Au-Cu quartz veins in the Hamash area, South-Eastern Desert, Egypt. Mineral Petrol 65:69–86
Helmy HM, Kaindl R, Shibata T (2014a) Genetically related Mo-Bi-Ag and U-F mineralization in A-type granite, Gabal Gattar, Eastern Desert, Egypt. Ore Geol Rev 62:181–190
Helmy HM, Shalaby IM, Abdel Rahman HB (2014b) Large-scale metal zoning in a late-Precambrian skarn-type mineralization, Wadi Kid, SE Sinai, Egypt. J Afr Earth Sci 90:77–86
Helmy HM (2020) Mineral resources in egypt (I): metallic ores—Sulfides and precious metal in Egypt. In: Hamimi et al. (eds) The geology of egypt, regional geology reviews. Springer Nature Switzerland, pp 543–549, https://doi.org/10.1007/978-3-030-15265-9-14
Hilmy ME, Osman A (1989) Remobilisation of gold from a chalcopyrite–pyrite mineralisation Hamash gold mine, Southeastern Desert, Egypt. Miner Deposita 24:244–249
Hume WF (1934) Geology of egypt, vol 2. Part 1: The metamorphic rocks. Government Press, Cairo, pp 105–125
Hussein AA, Ali MM, El Ramly MF (1982) A proposed new classification of the granites of Egypt. J Volcanol Geoth Res 14:187–198
Hussein AA (1990) Mineral deposits. In: Said R (ed) Geology of Egypt, Ch. 26, Balkema, Rotterdam, pp 511–566
Isakin MM, Lobunets SS, Yegorov IV (1990) Explanatory note to the map of mineral distribution of the PDRY, scale: 1:200,000. Ministry of Energy and Minerals, Department of Geology and Mineral Exploration, Aden, 34 pp
Ismail I, Baioumy HM, Ouyang H, Mossa H, Aly HF (2015) Origin of fluorite mineralizations in the Nuba Mountains, Sudan and their rare earth element geochemistry. J Afr Earth Sc 112:276–286
Ivanov HAA (1972) Report on geological operations in the assessment of the mineral potential of the Aswan region. Internal report, Aswan Mineral Survey Project, Geological Survey of Egypt
Jackson NJ (1986) Mineralization associated with felsic plutonic rocks in the Arabian Shield. J Afr Earth Sc 4:213–227
Jackson NJ, Basahel AN, Cooray PG, Darbyshire DPF (1983) Late Precambrian (Sequence A) rocks of the east central shield of Saudi Arabia: Jeddah. King Abdulaziz Univ Fac Earth Sci Bull 5:119–134
Jennings RH, Karnmerling RC, Kovaltchouk A, Calderon GR, El Baz MK, Koivula JI (1993) Emeralds and green beryls of Upper Egypt. Gems Gemol 29:100–115
Johnson PR, Kattan FH (2012) The Geology of the Arabian Shield. Saudi Geological Survey, p 466
Johnson PR, Stewart ICF (1995) Magnetically inferred basement structure in central Saudi Arabia. Tectonophysics 245:37–52
Kazmin V (1971) Precambrian of Ethiopia. Nature 230:176–177
Kemp J, Gros Y, Prian J-P (1982) Geologic map of the Mahd adh Dhahab quadrangle, Sheet 23E, Kingdom of Saudi Arabia: Saudi Arabian Deputy Ministry for Mineral Resources Geologic Map GM-64, P 39, scale 1:250,000
Khalil B (1980) Geology and prospecting for mineral deposits in the precambrian basement complex of the Nuba Mountains. In: Sudan 6th conference of the geological society of Africa, Nairobi, p 23
Kim E-J, Kim S-Y, Moon D-H, Koh S-M (2013) Fractionation and rare-element mineralization of Kenticha Pegmatite, Southern Ethiopia. Econ Environ Geol 46:375–390. https://doi.org/10.9719/EEG.2013.46.5.375
Klemm D, Klemm R, Murr A (2001) Gold of the pharaohs—6000 years of gold mining in Egypt and Nubia. J Afr Earth Sc 33:643–659
Kochin GG, Bassyuni FA (1968) The mineral resources of the U.A.R. Report on generalization of geological data on mineral resources of the UAR carried out under Contract 1247 (1966–1968), part I: metallic minerals. Geol Surv Egypt
Küster D (2009) Granitoid-hosted Ta mineralization in the Arabian–Nubian Shield: ore deposit types, tectono-metallogenetic setting and petrogenetic framework. Ore Geol Rev 35:68–86
Lang JR, Baker T (2001) Intrusion-related gold systems: the present level of understanding. Miner Deposita 36:477–489

Lofts PG, Bognar B, Howes DR, McHugh JJ, Saleh YT (1986) Exploration of the al amar prospect: Saudi Arabian Deputy Ministry of Mineral Resources Open-File Report RF-OF-06–1, p 54
Luce RW, Bagdady A, Roberts RJ (1976) Geology and ore deposits of the Mahd Adh Dhahab mine, Kingdom of Saudi Arabia: U.S. Geological Survey open-file report (IR) SA-195
Mahdy NM, Kalioubi BA, Wohlgemuth-Ueberwasser CC, Shalaby MH, El-Afandy AH (2015) Petrogenesis of U- and Mo-bearing A2-type granite of the Gattar batholith in the Arabian Nubian Shield, Northeastern Desert, Egypt: evidence for the favorability of host rocks for the origin of associated ore deposits. Ore Geol Rev 71:57–81
Mamedov EA, Ahmed ES, Chiragov MI (2014) Copper–gold–sulphide mineralization associated with late Precambrian volcanic ring structures, southern Sinai, Egypt. Arab J Sci Eng 39:273–286
Maurice A, Fawzy B, Ali K (2012) Neoproterozoic nascent island arc volcanism from the Nubian Shield of Egypt: magma genesis and generation of continental crust in intra-oceanic arcs. Lithos 132–133:1–20
Meinert LD, Dipple GM, Nicolescu S (2005) World skarn deposits. Econ Geol 100th Anniversary 299–336
Misra KC (2000) Skarn deposits. In: Understanding mineral deposits. Springer, Dordrecht. https://doi.org/10.1007/978-94-011-3925-0_9
Moghazi AM, Andersen T, Oweiss GA, El Bouseily AM (1998) Geochemical and Sr–Nd–Pb isotopic data bearing on the origin of Pan-African granitoids in the Kid area, southeast Sinai, Egypt. J Geol Soc 155:697–710
Mohamed MA-M (2013) Evolution of mineralizing fluids of cassiterite–wolframite and fluorite deposits from Mueilha tin mine area, Eastern Desert of Egypt, evidence from fluid inclusion. Arab J Geosci 6:775–782
Mohammedyasin MS (2017) Geology, geochemistry and geochronology of the Kenticha rare metal granite pegmatite, Adola Belt, Southern Ethiopia: A review. Int J Geosci 8:46–64
Möller P, Parekh PP, Schneider HJ (1976) The application of Tb/Ca-Tb/La abundance ratios to problems of flourspar genesis. Minr Deposita 11:111–116
Naim G, El-Melegy A, Soliman K (1996) Tantalum-Niobium-Tin mineralization in Central Eastern Desert, Egypt, a Review. In: Proceedings of geological survey, pp 599–622
Nehlig P, Genna A, Asfirane F (2002) Review of the Pan-African evolution of the Arabian Shield. GeoArabia 7:103–124
Nehlig P, Salpeteur I, Asfirane F, Bouchot V, Eberle JM, Genna A, Kluyver HM, Lasserre JL, Nicol N, Recoche G, Shanti M, Thieblemont D, Tournleier B (1999) The Arabian Shield Project Participants. Miner Potential Arab Shield Reassessment, p 19, in www.gisarabia.brgm.fr
Oweiss KA, Khalid AM (1991) Geochemical prospecting at Um Qareiyat gold deposits, South Eastern Desert, Egypy. Ann Geol Surv Egypt 17:145–151
Poletayev J, Verbvsky O, Teweldemedhin T, Musa E, Alemayehu B, Manaye Y (1991) The geology and rare metal potential of the Kenticha pegmatite deposit. Internal Report (unpublished), Ethiopian Mineral Resource Development Corporation, Ministry of Mines and Energy, Addis Ababa
Pollard P (1989) Geologic characteristics and genetic problems associated with the development of granite-hosted deposits of tantalum and niobium, Lanthanides, Tantalum and Niobium. Springer, Berlin, pp 240–256
Reischmann T, Kroner A (1994) Late Proterozoic island arc volcanics from Gebeit, Red Sea hills, north-east Sudan. Geol Rundsch 83:547–562
Richards JP (2003) Tectono-magmatic precursors for porphyry Cu-(Mo–Au) deposit formation. Econ Geol 98:1515–1533
Rowins SM (2000) Reduced porphyry copper-gold deposits: a new variation on an old theme. Geology 28:491–494
Rowins SM, Groves DI, McNaughton NJ, Palmer MR, Eldridge CS (1997) A reinterpretation of the role of granitoids in the genesis of Neoproterozoic gold mineralization in the Telfer dome, Western Australia. Econ Geol 92:133–160
Sabet A (1976) Tin-tantalum deposit of Abu Dabbab. Ann Geol Surv Egypt 6:180–190

Sabet A, Chabanenco V, Tsogev V (1973) Tin-tungsten and rare metal mineralization in the Central Eastern Desert of Egypt. Ann Geol Surv Egypt 3:75–86
Salem SM, Arafa SA, Ramadan TM, El Gammal EA (2013) Exploration of copper deposits in Wadi El Regeita area, Southern Sinai, Egypt, with contribution of remote sensing and geophysical data. Arab J Geosci 6:321–335
Salem IAN, El Dosuky BT, El Bahariya GA, Refaey EF (2020) Mineralogy and fluid inclusions evidence for the genesis of molybdenite mineralization at Gabal Gattar, North Eastern Desert, Egypt. Arab J Geosci 13:369. https://doi.org/10.1007/s12517-020-05322-w
Sangster DF, Abdulhay GJS (2005) Base metal (Cu-Pb-Zn) mineralization in the Kingdom of Saudi Arabia: Jeddah. Saudi Geol Surv, p 128
Sasmaz A, Yavuz F (2007) REE geochemistry and fluid-inclusion studies of fluorite deposits from the Yaylagözü area in Central Turkey. Neues Jahrb Für Mineral Abh 183:215–226
Sasmaz A (2020) The Atbara porphyry gold–copper systems in the Red Sea Hills, Neoproterozoic Arabian–Nubian Shield, NE Sudan. J Geochem Explor 214:106539
Schluessel R, Schuessel NH (2018) Emeralds from Ethiopia. Gemworld International, Gemguide, 1–5
Scott SD (1983) Chemical behavior of sphalerite and arsenopyrite in hydrothermal and metamorphic environments. Mineral Mag 47:427–435
Searle DI (1974) Assessment of the mineral potential of Aswan Region, Arab Republic of Egypt. The geology and mineralization of the Homr Akarem area. Egyptian Geological Survey, Internal Report
Seedorff E, Dilles JH, Proffett JM, Einaudi MT, Zurcher L, Stavast WJA, Johnson DA, Barton MD (2005) Porphyry deposits: characteristics and origin of hypogene features. Econ Geol 100th Anniv 251–298
Shaddad MS, Kropachev SM, Khalil B (1979) Regional geological setting of the Nuba Mountains in Sudan. Ann Geol Surv Egypt IX:446–454
Shallan MB, Heikal MTS (1989) Distribution of opaque minerals in the Precambrian rocks at Hajjah district, Yemen Arab republic. Ann Geol Surv Egypt 16:189–196
Siddiqui RH, Khan MA, Jan MQ, Kakar MI, Kerr AC (2015) Geochemistry and petrogenesis of Oligocene volcaniclastic rocks from the Chagai arc: implications for the emplacement of porphyry copper deposits. Arab J Geosci. https://doi.org/10.1007/s12517-015-1815-6
Sillitoe RH (1997) Characteristics and controls of the largest porphyry copper-gold and epithermal gold deposits in the circum-Pacific region. Aust J Earth Sci 44:373–388
Sillitoe RH (2010) Porphyry copper systems. Econ Geol 105:3–41
Singer DA (1995) World class base and precious metal deposits—a quantitative analysis. Econ Geol 90:88–104
Soliman MM (1986) Ancient emerald mines and beryllium mineralization associated with Precambrian stanniferous granites in the Nugrus-Zabara Area, Southeastern Desert, Egypt. Arab Gulf J Sci Res 4:529–548
Stemprok M (1987) Greisenization (a review). Geol Rundsch 76:169–175
Sun WD, Liang HY, Ling MX, Zhan MZ, Ding X, Zhang H, Yang XY, Li YL, Ireland TR, Wei QR, Fan WM (2013) The link between reduced porphyry copper deposits and oxidized magmas. Geochim Cosmochim Acta 103:263–275
Surour AA, Moufti AMB (2009) A new occurrence of garnetiferous skarn rocks in Saudi Arabia: a case study from Bahrah area, Jeddah-Makkah Al Mukaramah highway. Arab J Geosci 4:879–897
Tadesse S (2001) Geochemistry of the pegmatitic rocks and minerals in the Kenticha Belt, Southern Ethiopia: Implication to geological setting. Gondwana Res 4:97–104
Ulrich T, Gunther D, Heinrich CA (1999) Gold concentrations of magmatic brines and the metal budget of porphyry copper deposits. Nature 399:676–679
Vidal CE, Injoque-Espinoza J, Sidder GB, Mukasa SB (1990) Amphibolitic Cu-Fe skarn deposits in the central coast of Peru. Econ Geol 85:1447–1461

Yibas B, Reimold WU, Armstrong R, Koeberl C, Anhaeusser CR, Phillips D (2002) The tectonostratigraphy, granitoid geochronology and geological evolution of the Precambrian of southern Ethiopia. J Afr Earth Sc 34:57–84

Zerihun D, Garbarino C, Valera R (1995) Granite pegmatite system in Kenticha (Adola, Sidamo, Ethiopia) rare metal pegmatite belt: petrochemistry, regional pegmatite zoning and classification. SINET 18:119–148

Zerihun D (1991) Le mineralizzazioni a Ta-Nb: classificazione, prospezione, valutazione. Il caso di Kenticha (area di Adola, Sidamo—Ethiopia). unpublished Ph.D. thesis, Univ of Milan, p 365

Zoheir BA, Klemm DD (2007) The tectono-metamorphic evolution of the central part of the Neoproterozoic Allaqi-Heiani suture, south Eastern Desert of Egypt. Gondwana Res 12:289–304

Zoheir BA, Emam A, Pitcairn IK, Boskabadi A, Lehaye A, Cooper MJ (2018) Trace elements and isotope data of the Um Garayat gold deposit, Wadi Allaqi district, Egypt. Miner Deposita 54:101–116

Zoheir BA, Johnson PR, Goldfarb RJ, Klemm DD (2019) Orogenic gold in the Egyptian Eastern Desert: Widespread gold mineralization in the late stages of Neoproterozoic orogeny. Gondwana Res 75:184–217

Chapter 5
Hydrothermal Mineral Deposits in Orogenic Environments

Contents

5.1 Introduction . . . 245
5.2 Orogenic Mineral Deposits in Saudi Arabia . . . 247
5.2.1 Orogenic Au Deposits . . . 247
5.2.2 Iron Oxide–Copper–Gold Deposits . . . 263
5.3 Orogenic Gold Deposits in Yemen . . . 264
5.4 Orogenic Mineral Deposits in the Eastern Desert of Egypt . . . 268
5.4.1 Allaqi–Sol Hamed Block . . . 269
5.4.2 Um Samiuki–Abu Dahr Block . . . 275
5.4.3 East Nugrus Block . . . 276
5.4.4 Mubarak–Hamash Block . . . 277
5.4.5 Meatiq–Sibai Block . . . 283
5.5 Orogenic Deposits in Sudan . . . 293
5.6 Orogenic Deposits in Eritrea . . . 304
5.7 Orogenic Deposits in Ethiopia . . . 307
References . . . 316

5.1 Introduction

Hydrothermal deposits: ore minerals precipitated from high-temperature aqueous fluids of different origins.

(a) *Deposits in orogenic environments*

- Orogenic Au deposits
- Carlin-type Au deposits
- Iron oxide–copper–gold (IOCG) deposits

A. Hassan Ahmed, *Mineral Deposits and Occurrences in the Arabian–Nubian Shield*,
Earth and Environmental Sciences Library,
https://doi.org/10.1007/978-3-030-96443-6_5

(b) *Deposits in volcano–sedimentary environments*

- Volcanogenic massive sulfide (VMS) deposits
- Mississippi Valley–type (MVT) deposits
- Sedimentary exhalative (SEDEX) deposits
- Red-bed copper deposits
- Uranium deposits.

The mineralizing fluids of hydrothermal deposits derived from sources other than magmatic solutions include those formed from metamorphic dehydration reactions (orogenic environments), from the expulsion of pore fluids during compaction of sediment (connate water), from meteoric waters, and from seawater. These hydrothermal deposits can be subdivided into two main parts:

(1) *Hydrothermal deposits of orogenic environments* (metamorphic hydrothermal fluids), which are represented by Table 2.1:

(i) orogenic Au deposits,
(ii) Carlin-type Au deposits, and
(iii) iron oxide–copper–gold (IOCG) deposits.

This part will be discussed in the present chapter.

(2) *Hydrothermal deposits of volcano–sedimentary environments*, which are represented by various deposit types including (Table 2.1):

(i) volcanogenic massive sulfide (VMS) deposits,
(ii) Mississippi Valley–type (MVT) deposits,
(iii) sedimentary exhalative (SEDEX) deposits,
(iv) red-bed copper deposits, and
(v) uranium deposits.

This part of hydrothermal deposits will be discussed in Chap. 6.

For hydrothermal deposits of orogenic environments, there are three important types of hydrothermal Au and Au-Cu deposits, which form during the regional metamorphism in the host geological terranes:

Orogenic Au deposits: also known as *lode*, *quartz-vein*, *Au-only*, or *mesothermal* Au deposits. These deposits exist as vein and replacement Au deposits in metamorphic and intrusive igneous rocks; they are mostly formed during periods of regional metamorphism.

Carlin-type Au deposits: also known as *sediment-hosted* or *disseminated* Au deposits, based on the host rocks and the nature of the ore. They are found as replacement ore bodies in metasomatically altered impure carbonate and calcareous siliciclastic sedimentary rocks.

IOCG deposits: the major Fe-bearing minerals in this type of ores are iron oxides (magnetite and/or hematite) rather than iron sulfides. This deposit type is an important

source for Cu and Au, but also many of them are producing other metals (U, Ag, light rare-earth elements (LREEs)) as by- and coproducts.

Although the role of magmatic fluids of these mineral deposit types is not completely ruled out, none of these types has a direct relationship to magmatic activities. Instead, metamorphic fluids and deeply convecting meteoric fluids are the main fluid sources responsible for the formation of these deposit types. The metamorphic fluids are those derived from the dehydration/devolatilization of mineral reactions that resulted in release of the volatile components such as H_2O, CO_2, or H_2S during the prograde regional or contact metamorphism in the crust and/or in the mantle. After the metamorphic dehydration reactions, the expelled fluids will circulate through the rock, escape upward through the crust, and dissolve minerals along their pathways. The channelways of fluid escape are marked by the generation of many quartz carbonate veins that are a common component of metamorphic terranes. On the other hand, the deep circulation of surface-derived water sources (e.g., meteoric and seawater) in the tectonically and magmatically active terranes will also act as an important agent for ore formation. The temperature of these surface-derived fluids can reached up to 300–350 °C in such deep levels within the crust.

Following are detailed descriptions of these orogenic mineral deposit types in the Arabian–Nubian Shield (ANS) countries.

5.2 Orogenic Mineral Deposits in Saudi Arabia

5.2.1 Orogenic Au Deposits

Although many orogenic Au deposits are individually mined at a small scale, it is the source for ~one-third of the worldwide Au production; they are essentially mined only for Au, and very rarely for producing As and Sb as co-products or byproducts. One of the characteristic features of this type of deposit is the Ag-poor character, where the Ag:Au ratio is much lower than either the average crustal abundances or the ratio in other hydrothermal ore deposit types (e.g., VMS and epithermal deposits). The orogenic Au deposits are mostly formed in active metamorphic belts and are mainly hosted by regionally metamorphosed igneous rocks. They are mostly form at relatively high-pressure conditions, between ~1.5 and 5 kbar (at depths of ~4–15 km), and a temperature formation lower than any magmatic hydrothermal deposits, 300–450 °C. The Au-bearing fluids of this deposit type typically have a common composition of low salinity and high CO_2 contents. The common host rocks of orogenic Au deposits are mainly metamorphosed to the greenschist facies.

In the Arabian Shield of Saudi Arabia, the orogenic Au deposits/occurrences consist of simple-to-complex quartz carbonate vein systems that are variably associated with brittle–ductile shear zones, volcano–sedimentary rocks, and mafic-to-intermediate intrusive rocks (Robert 1996; Johnson and Kattan 2012). Gold in this

deposit type occurs mainly disseminated in the quartz carbonate veins or in the adjacent country rocks. The Au-bearing veins typically occur in low- to medium-grade metamorphic belts of brittle–ductile deformation, most probably under compressive conditions at intermediate depths within the crust. Except for the epithermal gold-vein deposits (e.g., Mahd adh Dhahab and El Amar) that are described in Chap. 4, and those of VMS-bearing Au deposits, which will be discussed in Chap. 6 of this book, the Au-bearing quartz carbonate veins of the orogenic type constitute the most widespread Au mineralization in the Arabian Shield of Saudi Arabia (Fig. 5.1). The orogenic quartz carbonate Au-bearing veins are widespread in all geologic terranes; they are widely distributed from the Hijaz terrane to the strongly sheared rocks along the Nabitah fault zone. They are located in a variety of structural settings ranging from little- or moderately deformed sedimentary and plutonic rocks as in the Sukhaybarat–An Najadi gold district, to such thrust systems as those in the Al Wajh district (Johnson and Kattan 2012) (Fig. 5.1). These types of mineral deposits/occurrences are also called *mesothermal quartz veins* or *shear-zone related mineralization*, since they mostly have a common mode of occurrence and general characteristics.

The *Sukhaybarat–An Najadi* area is one of the most important Au-bearing districts (Fig. 5.2) in the Kingdom of Saudi Arabia because it contains the historical Sukhaybarat gold mine (~1000–3000 years old); the first orogenic Au deposit that developed in modern times in the Arabian Shield. The Sukhaybarat–An Najadi district consists of Late Cryogenian sedimentary rocks of the Murdama group and plutonic rocks of the Idah suite in the northern part of the Afif terrane (Fig. 5.3). It is bounded on the north by faults along the Hibshi formation, on the south by part of the Halaban-Zarghat fault zone, and from the east by contacts with the Suwaj sub-terrane and Kishaybi suite of granitoids (Johnson and Kattan 2012). The Sukhaybarat gold mine is located at the southern end of the district, ~550 km northwest of Riyadh and 250 km northwest of Mahd Adh Dhahab in the Nuqrah–As Safra area. This area is the center of historical Au and Cu workings that were discovered in the 1930s. The Sukhaybarat is one of a large number of ~40 Au occurrences in the Sukhaybarat–Silsilah district; include An Najadi, Wadi Shabah, Meshaheed, and other occurrences close to the Riah thrust zone (Fig. 5.3). Au mineralization is essentially found at shear zones and hosted either in Murdama volcano–sedimentary or post-amalgamation Murdama group rocks, and in small diorite, quartz diorite, and tonalite intrusions belonging to the Idah suite. Modern development of the deposit began in 1986 with a feasibility study investigated by the Saudi Company for Precious Metals (SCPM), a joint venture between Petromin and Boliden (a Swedish mining company). In 1991, this partnership began open-pit mining of the Sukhaybarat reserves. The estimated total mineable ore reserve in 1991 was 17.6 t, with an average cut-off grade of 1.1 g/t Au (Al-Dabbagh and Dowd 1996).

Geologically, the mineralization at Sukhaybarat mine is located close to the contact between the Murdama group and Idah suite intrusions. The ore is located in two connected systems of shallow dipping quartz veins and veinlets of the Nabitah fault system and hosted in altered stockwork zones of granodiorite/tonalite intrusion and adjacent layered volcanic rocks. The ore zone consists of clusters of Au-bearing quartz veins ranging in thickness from a few centimeters to ~1 m, flanked

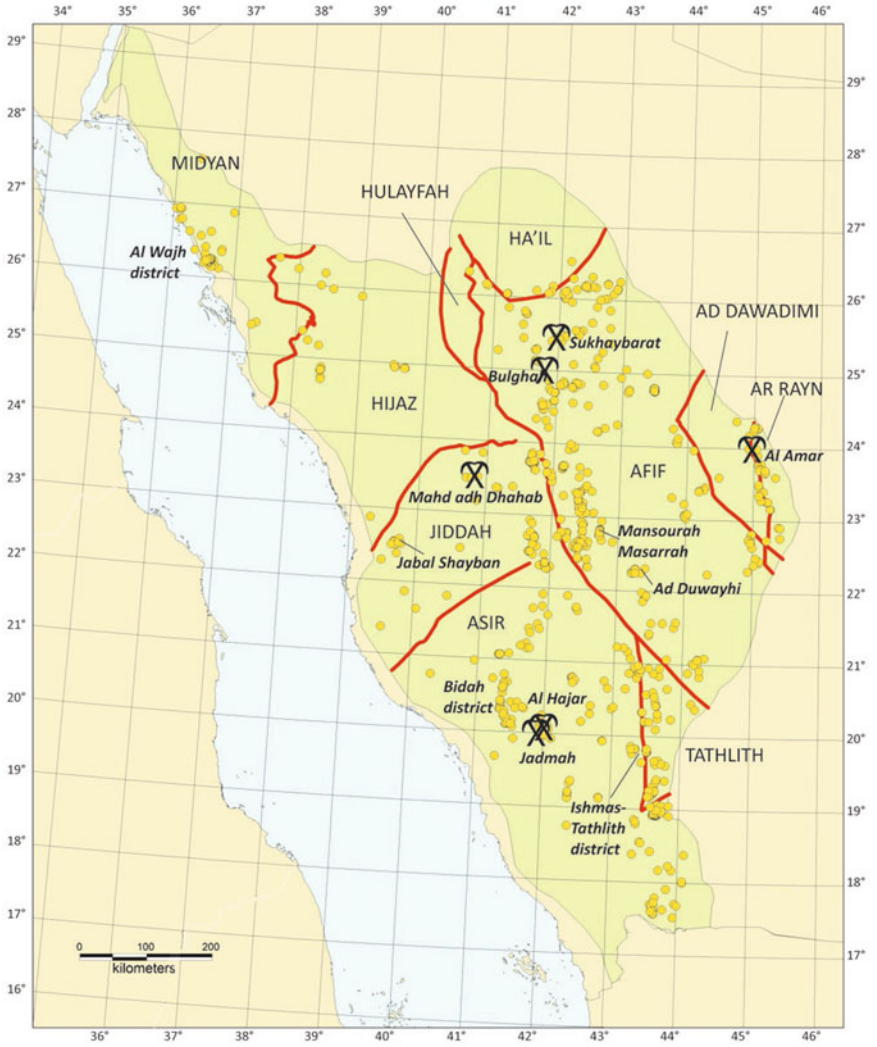

Fig. 5.1 Locations of Au occurrences and mines in the Arabian Shield of Saudi Arabia (compiled by Johnson and Kattan 2012). The terrane boundaries are also shown

by envelopes of arsenopyrite-rich, Au-bearing altered diorite/tonalite or metamorphosed Murdama group siltstone. The individual vein might carry up to 30 g/t Au, and sometimes as much as 60–200 g/t Au (Albino et al.1995). The Au-bearing quartz veins concentrate in two-ore zones, the principal zone being an east/west-trending system of conjugate veins developed along an north/northeast-directed thrust (Malmgren and Anderson 1994), or zone of shortening. At the An Najadi occurrence, the mineralization consists of Au-bearing quartz and quartz carbonate veins, mostly

0.5–5 cm in thickness but sometimes ranging up to 1 m, flanked by thin, sulfide-bearing alteration selvages. In addition, the Au-bearing veins at all occurrences in the Sukhaybarat–An Najadi district contain varying amounts of sulfide minerals such as arsenopyrite, pyrite, sphalerite, galena, chalcopyrite, and stibnite, in the range of <1 to 5 vol.% (Lewis and Schull 1994; Albino et al.1995).

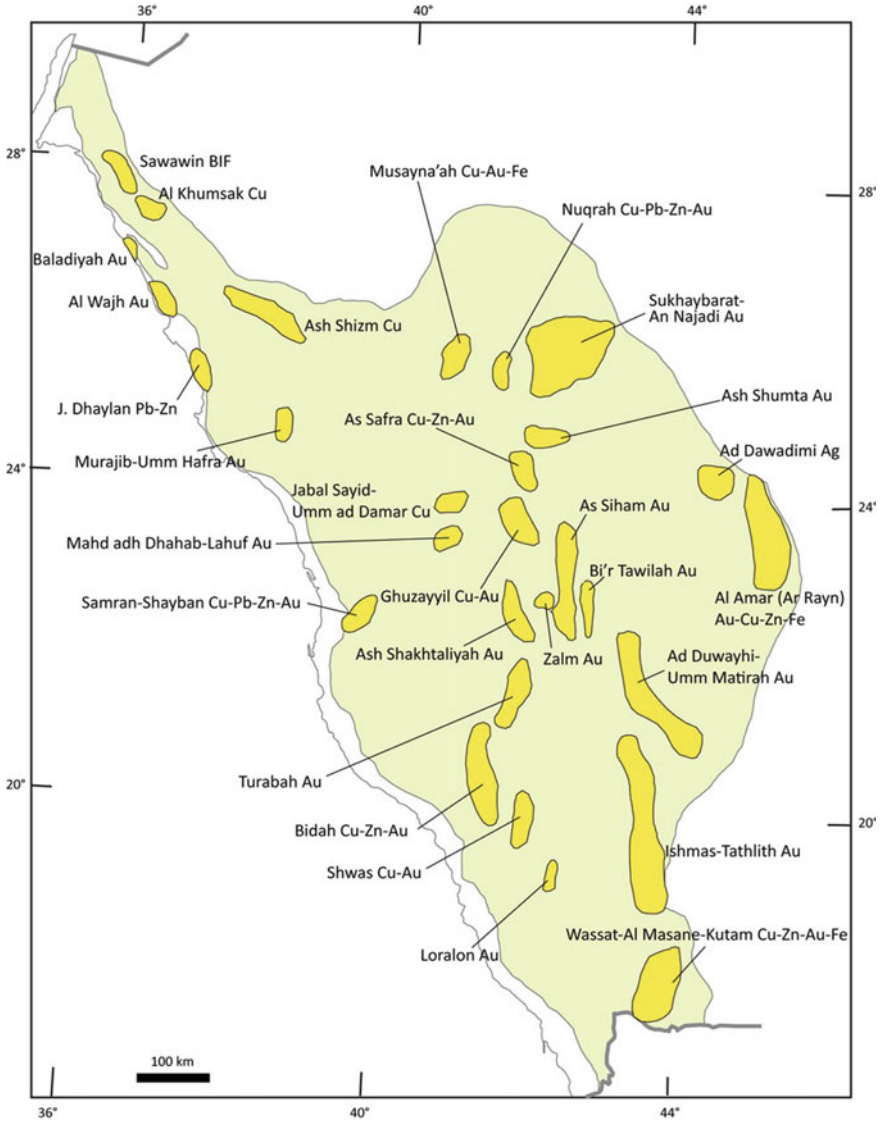

Fig. 5.2 Mineral districts and metallic mineral grouping in the Arabian Shield of Saudi Arabia (taken from Johnson and Kattan 2012)

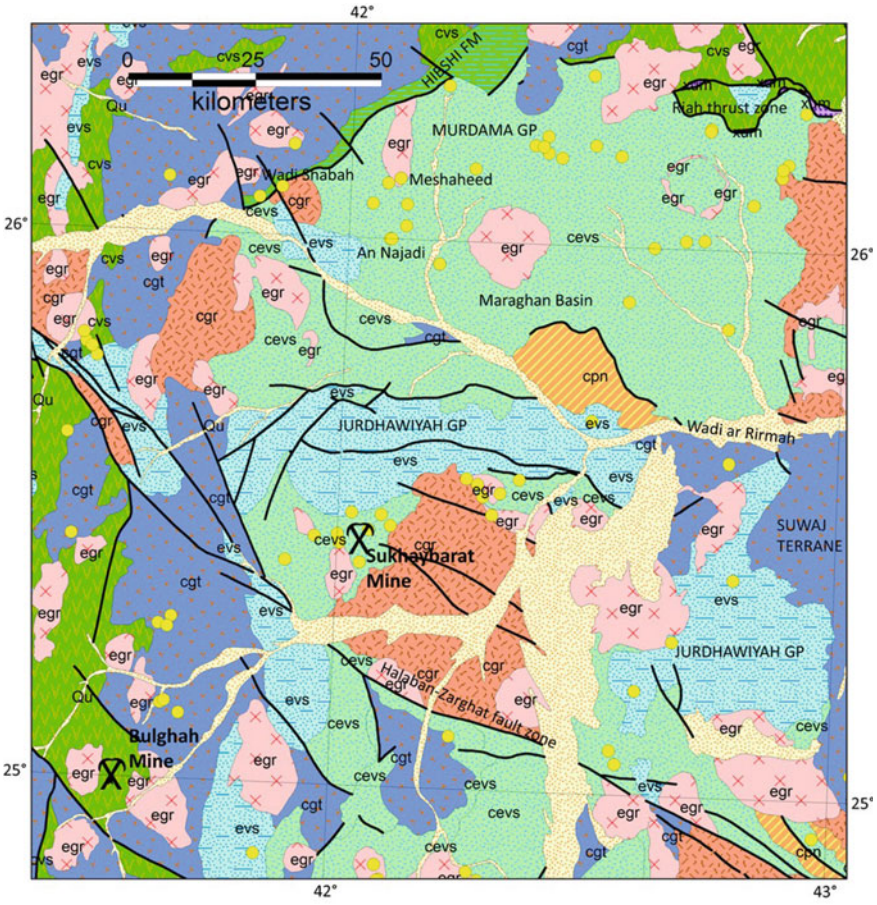

Fig. 5.3 Geologic map of the Sukhaybarat–an Najadi Au district. Yellow dots are the main Au occurrences

A significant large group of orogenic Au deposits/occurrences is also present in the *Zalm*, *As Siham*, *Bi'r Tawilah*, and *Ad Duwayhi-Umm Matirah* districts in the central Arabian Shield (Fig. 5.2), along the western and southern margins of the Afif terrane (Fig. 5.4). These occurrences are mostly formed along fractures or shear zones, or in the country rock of the shear zones, which represent examples of structurally controlled mesothermal veins. Some occurrences are located at the contacts between granitic intrusions and country rock and may be classified as intrusion-related deposits.

The *Zalm* Au occurrence is located in an area of ancient workings scattered over ~5 × 2 km, where the main host rock is granite to gabbro of the Humaymah suite (630–560 Ma), and small metamorphosed volcano–sedimentary rocks of the Siham group.

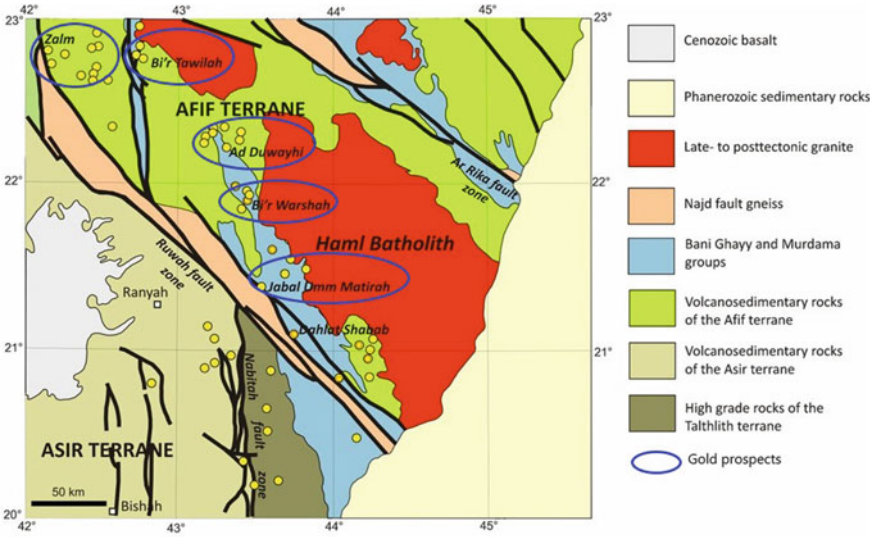

Fig. 5.4 Simplified geologic map of the region between Zalm and the eastern margin of the shield, showing the main gold occurrences (yellow dots) (modified from Johnson and Kattan 2012)

The western part of the prospect area (Fig. 5.4) intruded by a gabbroic to granitic-layered complex (647 ± 6 Ma) (Leistel and Eberlé 1999). The quartz veins in the Zalm prospect are controlled by an anastomosing system of normal faults, trending mainly N55 °E with a dip of 35° to the southeast. The veins and their alteration halos form gently dipping lens-shaped orebodies parallel to the fault system. Individual veins are as much as 20-cm thick, with strike and down-dip extents of a few hundred meters. They consist of quartz, carbonate, and small amounts of sulfides such as pyrite, arsenopyrite, ±galena, ±sphalerite, ±chalcopyrite, with a common visible native Au. Gold is commonly present in the quartz carbonate veins, but also alteration halos contain low- to medium-grade ore. Alteration zones around the mineralized veins are characterized by the presence of sericite, carbonate, local epidote, rutile, and disseminated sulfides.

In the *As Siham* Au district, the Au-bearing quartz carbonate veins are hosted by weakly metamorphosed sedimentary and volcanic rocks of the Siham group, and by a variety of mafic to intermediate rocks, pre- to posttectonic tonalite–trondhjemite–granodiorite (TTG) rocks, and granite (Fig. 5.5). Overall, the district trends north, parallel to the ultramafic-decorated Lamisah thrust, which extends along the axis of the Siham group (Figs. 5.2 and 5.5). In places, the Lamisah thrust is marked by a series of lenses of listwaenite (carbonatized ultramafic rocks) with gold–pyrite–quartz veinlets concentrated at the contacts between listwaenite and Siham-group black shale and andesite (Johnson and Kattan 2012). The estimated ore grades are in the range of <1 g/t to >7 g/t Au for veins, and 0.1–3.0 g/t Au for the country rock (Gaukroger and Morfett 1982). The wall-rock alteration typically includes silicification, carbonatization, as well as sulfide and oxide ferruginization (pyrite and hematite). The specific

structural control on the veins is not certain; however, a late-stage fracturing associated with sinistral strike–slip faulting on the Najd faults is suggested to cut the region. The spatial relationship with the Lamisah thrust suggests there may be other controls of the type found at Au-bearing ultramafic-decorated shear zones.

Along the southern extension of the As Siham Au district, the *As Suq* open-pit mine is located within the western section of the Afif terrane, within the eastern Nabitah "mobile belt." It is located in Makkah Al Mukarramah Province of Saudi Arabia, ~25 km southeast of Zalm (Fig. 5.5), and ~90 km northwest to west-northwest of the Ad Duwayhi gold mine. The deposit lies within a site of ancient Au workings, where the Au mineralization is localized in narrow, shallow dipping quartz veins associated with a north/south trending zone of flat-dipping quartz veins and associated stringer zones within altered sedimentary and volcanic rocks of the Al Siham formation. This formation, on a district scale, is composed of steeply dipping, 750–685 Ma metavolcanic and subsidiary metasedimentary rocks. The metavolcanic rocks include intermediate to mafic lava and pyroclastic rocks with subordinate silicic volcanic rocks. The pyroclastic rocks are laminated, fine-grained basaltic to andesitic lithologies and agglomerates. The sedimentary rocks within this sequence comprise claystones and sandstones. The mineralized quartz vein system extends over a horizontal length of ~1.2 km and persist to a vertical depth of at least 120 m. The feasibility study on the As Suq occurrence was completed in 2010 and construction commenced, to be completed in January 2014, with the first commercial production in March of that same year. The estimated total pre-mining ore resources up to December 2012 were ~8.6 Mt, with an average grade of 1.78 g/t Au (15.3 t of Au; Ma'aden Annual Report 2012). The estimated ore reserve on December 2018 was ~5.7 Mt, with an average grade of 1.59 g/t Au for 9 t of Au (cut-off grade variable from 0.33 to 0.42 g/t Au).

The *Ad Duwayhi* Au deposit is located in the east central part of the Arabian Shield (Figs. 5.2 and 5.4); it is one of the newest Au discoveries in Saudi Arabia. Exploration to date has identified a resource of greater than 1.82 million ounces (Moz) of Au with significant potential for expansion. The mineralization of this district is affected by various tectonic events that resulting in the formation of more than 45 occurrences in one of the biggest mineralized belts in the Arabian Shield (Fig. 5.4). They created the pathways for mineralized fluid circulation and for the emplacement of intrusions that further activated such fluid circulation and allowed the early magmatic–hydrothermal mineralization of Ag-Sn-W-Mo-Bi deposits. The Au mineralization at Ad Duwayhi occurs in quartz veins filled the fractures in mafic to felsic intrusive or volcano–sedimentary rocks (Doebrich et al.2004). The estimated ore resource by drilling up to 2004 is ~31 Mt of ore (1 Moz Au); the current resource available is unknown. The Ad Duwayhi Au mineralization consists of Au-bearing quartz veins and breccia in and along the margins of the granite stock and Au-bearing stockwork, quartz veins, and massive to banded quartz-rich tabular veins spatially associated with quartz porphyry. The early quartz–molybdenite veining phase appears to be poor in Au mineralization, the mineralized zones are poor in sulfides and base-metal contents, and the Au:Ag ratio is ~6:1. Re-Os dating at Ad Duwayhi of molybdenite from a quartz–molybdenite vein and a tabular quartz vein with cogenetic Au yields robust ages of 655.6 ± 2.7 and 649 ± 2.3 Ma, respectively (Doebrich et al.2004). The result implies that

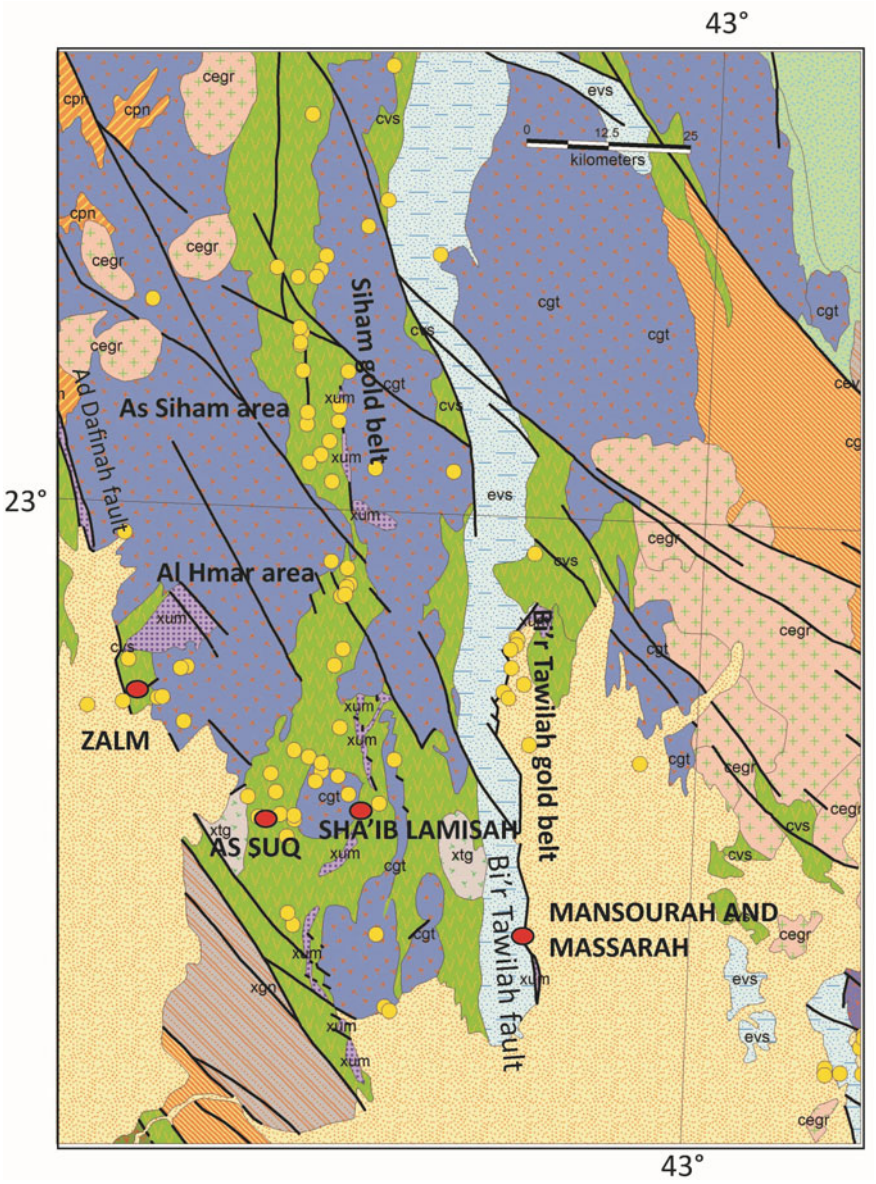

Fig. 5.5 Detailed geologic map of the Bi'r Tawilah and southern part of the Siham Au district, Au prospects shown as yellow dots, and red dots indicate significant prospects (Johnson and Kattan 2012)

mineralization was contemporary with emplacement of the quartz porphyry and, more distantly, with the early phase of emplacement of the Haml batholith. The occurrence is thus an example of intrusive-related mesothermal gold veins. This mineralization appears to be slightly older than that at Zalm and at least 30 Ma older than mineralization found at Sukhaybarat. The main mineralized thrust zone is typically 2–10 m in thickness, containing heavily deformed cataclastic rocks that host well-developed mineralized quartz veins. Thin, high-grade Au-bearing veins are also found outside the main mineralized vein system. The mineralized area characterized by hydrothermal alteration comprising silicification, quartz–sericite–pyrite (phyllic), potassic and propylitic alteration assemblages. The Au mineralization is most closely associated with the phyllic alteration zone. Gold is principally associated with pyrite and tetrahedrite, which occupy ~3–5 vol.% of the ore zone and occur as fine-grained (>5 μm) free gold grains that is not locked within other sulfides, although some is found as Au–Ag tellurides. Gold is also present as placer accumulations nearby the deposit, and within the colluvial materials. The estimated total pre-mining ore resource up to July 2007 is ~17.1 Mt, with an average grade of 3.9 g/t Au for 66.65 t of total Au content. The estimated remaining ore reserves up to the end of December 2018 are ~19.18 Mt, with an average grade of 2.38 g/t Au for 45.5 t of total Au.

The *Murayjib–Umm Hafra* gold district is located in the Midyan terrane, in the northwestern Arabian Shield (Figs. 5.2 and 5.6), in which the orogenic Au-bearing veins existed in a different geologic setting (Al-Otaibi et al.1995; Lewis et al.1997). This Au-bearing district comprises four ancient gold mines (Fig. 5.6) and placer workings, named *Murayjib, Bil'iwy, Hashayim, and Umm Hafra* (Fig. 5.6), in a general north/south alignment along a subsidiary anticline in the western part of the synclinorium. Gold mineralization consists of low sulfide (<5% vol.%) quartz and quartz–albite–carbonate veins. The veins have low to very low base-metal contents (<30 ppm Pb, <30 ppm Cu, <160 ppm Zn, <10 ppm Sb, <1000 ppm As). They are in steeply dipping, east/west-striking joints that developed perpendicularly to the main fold trends as a result of extension along the axis of the synclinorium. In the *Murayjib* and *Bil'iwy*, fractures are developed preferentially in pebbly wacke and massive mafic volcanic rocks, at the Umm Hafra in diorite, basaltic andesite, and sedimentary rocks. The timing of gold mineralization is not certain. However, structural evidence that the extensional joints were contemporary with folding, and that both the Hadiyah and underlying Al Ays groups were folded together and intruded by Jar-Salajah tonalite (~745–695 Ma), is permissive of the Au being emplaced prior to 695 Ma. This suggests that Au mineralization in this part of the shield occurred significantly earlier than the mesothermal gold mineralization present, for example, in the Sukhaybarat–An Najadi and Zalm–Ad Duwayhi areas (Johnson and Kattan 2012). The estimated grades in the veins from Murayjib contain up to 2.36 g/t Au, but most samples of veins and drill core contain < 1.5 g/t (Lewis et al.1997). The Au-bearing veins from Bil'iwy yield 0.5–1.1 g/t Au, with an average of 0.65 g/t Au (Al-Otaibi et al.1995). The quartz veins and stockworks at the Umm Hafra occurrence contain values of <0.35 g/t Au.

The *Al Wajh* Au district, northwest of the Yanbu suture, consists of Au-bearing low-sulfide quartz carbonate veins in a stack of thrusts superimposed by sinistral

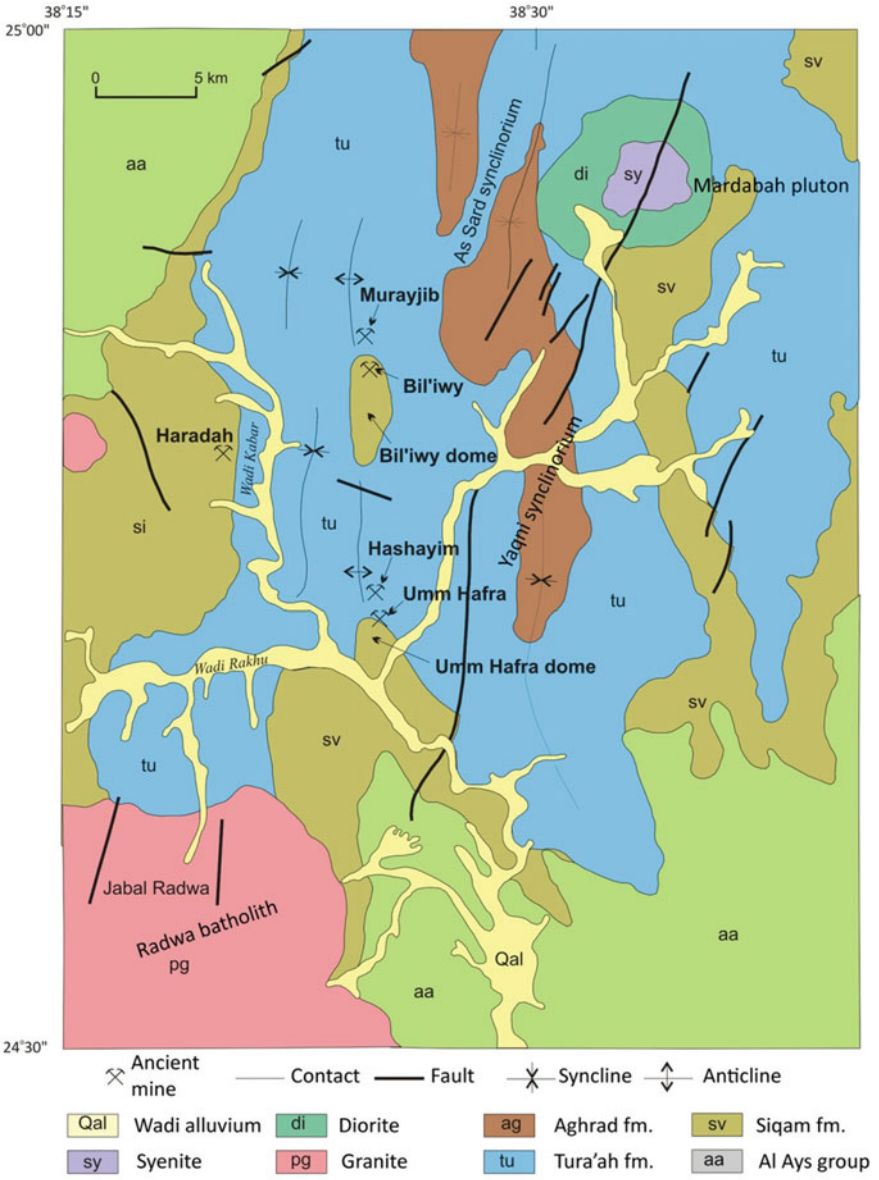

Fig. 5.6 Geologic map of ancient Au mines in the Murayjib–Umm Hafra Au district (after Al Otaibi et al. 1995)

strike–slip shears (Johnson and Offield 1994; LeAnderson et al.1995). The Au-bearing quartz carbonate veins are chiefly hosted by low-grade mafic to felsic tuffs, basalt, andesite, and volcaniclastic wacke belonging to an early Cryogenian immature volcanic arc assemblage of the Zaam group (760–710 Ma) (Fig. 5.7). Some quartz carbonate veins, such as those at *An Nahdayn*, *Ash Shuwaytah South #1*, and *Ash Shuwaytah South #2*, are located at S-bends in subvertical sinistral shear zones. The largest ancient working in the district, at Umm al Qurayyat (LeAnderson and Yoldash 1990), is in a stack of thick quartz sheets that are interpreted as being emplaced in the hanging wall of a regional thrust in massive metabasalt (Fig. 5.7). The estimated ore resources for in situ quartz and dump material at Umm al Qurayyat range variously from 80,200 t, with an average grade of 3.57 g/t Au, to 155,634 t, with an average grade of 3.8 g/t Au (Johnson and Offield 1994). The average grade of 13 quartz vein samples at Umm al Qurayyat gave ~3.12 g/t Au (range, 0.4–20.5 g/t) and 16 samples of sericite–pyrite-altered rocks gave an average of 3.91 g/t Au (range, 0.3–7.4 g/t). Overall, Au grades in quartz samples in the district range from <0.2 to 7.0 g/t, with exceptional values of 20 g/t Au. The sheared and altered wallrocks contain mostly low values (<1 g/t Au), but exceptionally sometimes contain 10 g/t Au or more. The timing of sinistral shearing and, therefore, possible mineralization, is unknown, but if structurally related to the Ajjaj shear zone, may be some time between 630 and 560 Ma (Johnson and Kattan 2012).

Other Au- and sulfide-bearing occurrences belong to the shear-zone environment, which is mostly similar in mode of occurrence and characteristics to the orogenic environment. These are represented by Au mineralization at the *Al Mansourah*, *Masarrah*, and *Bi'r Tawilah* occurrences, or as Cu and Zn occurrences such as those at *Kutam* and *Khnaiguiyah.* In the last few years, the Saudi Ma'aden Mining Company carried out an exploration program for Au and associated noble metals in the area to the south of Bi'r Tawilah. The exploration program concentrated at two occurrences: Al Mansourah and Masarrah. The main aim of the extensive diamond drilling was Au mineralization in carbonatized ultramafic rocks (i.e., listwaenite), where the assay results gave pronounced Au anomalies in the listwaenite rocks. The Al Mansourah and Masarrah occurrences are associated with sheared and carbonatized ultramafic rocks along the Bi'r Tawilah thrust, whereas the exact origins of Kutam and Khnaiguiyah are uncertain, which may be sheared, remobilized VMS deposits (Johnson and Kattan 2012). The Bi'r Tawilah, Masarrah, and Al Mansourah open-pit resources are members of an ~50-km-long (Fig. 5.5), north/south-oriented string of Au deposits and occurrences distributed along the major regional Ad Dafinah thrust fault zone. Bi'r Tawilah, which is ~50 km east of Zalm, is ~5 km north of Masarrah, which is, in turn, ~ 8 km north of Al Mansourah (Fig. 5.5). They are located at ~460 km northeast of Jeddah and 460 km west/southwest to southwest of Riyadh in Saudi Arabia. The Bi'r Tawilah area contains ancient Au and W mine workings.

In the *Al Mansourah* occurrence, the thrust contact between the Siham group schists and younger, less deformed, Bani Ghayy group is marked by a variably altered serpentinized ultramafic unit and diorite and quartz–feldspar porphyry intrusions. The thrust zone is repeatedly offset by sinistral strike–slip faults of the Najd fault

system, which also offset mineralization and the youngest intrusions. The serpentinized ultramafic rocks are commonly altered to listwaenite to an assemblage of quartz–carbonate–fuchsite. Remnants of the serpentinite occur along the margins of the listwaenite, particularly along the footwall side. Gold mineralization is closely associated with quartz veins and breccia zones that are preferentially developed within listwaenite. Mineralization is developed over thicknesses ranging from a few meters up to 60 m, both within quartz veins and listwaenite wall rock, with good continuity over a strike length of ~1 km. Quartz veins and mineralization are developed to a lesser extent within the diorite and porphyry intrusions, which have been deformed and are sub-parallel to the regional structure. Gold mineralization has also been intersected within footwall greywackes and shales of the Bani Ghayy group, but forms narrower and less continuous zones compared to that in the listwaenite. High-grade mineralized zones are associated with an assemblage of chlorite–graphite–pyrite–arsenopyrite in fractures or in brecciated quartz veins, as disseminated and as semi-massive pyrite–arsenopyrite veinlets in sheared diorite. Low-grade zones are associated with networks of centimeter-scale quartz stockworks in listwaenite–breccia zones and with disseminated pyrite–arsenopyrite in almost all fractured rocks including the younger footwall sediment and quartz–feldspar porphyry dykes. The deposit is thought to represent intrusive related orogenic vein and disseminated type Au mineralization (SRK Consulting 2007).

The *Masarrah* prospect has the same geological and structural setting as described above for the Al Mansourah prospect, where the Au mineralization has been traced over a strike length of 3 km. The Au mineralization is hosted mainly by carbonatized ultramafic rocks (listwaenite) and is closely associated with sulfide-bearing quartz veins. The Al Mansourah and Masarrah occurrences have been suggested to represent a single deposit displaced by 6.5 km across the Najd fault system structures. Mineralization has developed over the entire widths within quartz veins and breccia zones that preferentially developed within listwaenite (SRK Consulting 2007). In the *Bi'r Tawilah* gold deposit, both hypogene and supergene ores are well represented, where the hypogene Au mineralization is hosted by intermediate to felsic intrusions that occur along the north/south structural belt, as described above. The four lithological rock units recognized in the mineralized belt of Bi'r Tawilah, from oldest to youngest, are serpentinites and related listwaenites, diorites, granitic rocks, and porphyritic acidic rocks. All rock types of this zone are affected by hydrothermal alteration, which are represented by chlorite, sericite, carbonates, and silica. Sulfide mineralization is mostly associated with carbonate alteration, while chloritization of biotite leads to the formation of abundant rutile. The Bi'r Tawilah mineralization is confined to northwest-trending shears related to north/south slip of the pre-existing thrust interpreted to have been due to activation within the Najd fault system. Sulfides and Au mineralization occur in most rock types, with a sulfide assemblage represented by pyrite and relatively lesser amounts of arsenopyrite, as well as minor chalcopyrite, sphalerite, and galena, where the abundance of arsenopyrite increases with depth. The highest Au grade reached up to 5.4 g/t Au, which is mostly attributed to the supergene alteration that took place during weathering above the water table at a depth of ~20–25 m (Surour et al.2014).

The estimated ore resources, reserves, and grades of the Al Mansourah, Masarrah, and Bi'r Tawilah deposits/prospects are reported here (Ma'aden Annual Report 2018). At the Al Mansourah prospect, the total (measured + indicated + inferred) resources are 46.80 Mt ore, with an average grade of 2.14 g/t Au. The total (proved + probable) reserves are 27.70 Mt ore, with average grades of 2.53 g/t Au. At the Masarrah prospect, the total (measured + indicated + inferred) resources are 43.70 Mt ore, with average grades of 1.59 g/t Au. The total (proved + probable) reserves are 17.30 Mt or, with an average grade of 1.99 g/t Au. At the Bi'r Tawilah deposit, the total (indicated + inferred) resources are 41.00 Mt ore, with average grades of 0.87 g/t Au. The Au contents of the estimated resources are 100 t in the Al Mansourah, 69.5 t at Masarrah, and 35.5 t Au at Bi'r Tawilah.

A large number of shear zone-related Au-bearing quartz veins are also found in the *Ishmas–Tathlith* gold district along the Nabitah fault zone in the southern part of the Arabian Shield (Worl 1980) (Fig. 5.2). The Ishmas–Tathlith gold district consists of quartz carbonate veins hosted by strongly deformed rocks along the Nabitah fault zone, as well as occurrences to the east that are hosted by the high-grade metamorphic rocks of the Tathlith terrane or are associated with a serpentinite thrust sheet intruded by aplite at *Hamdah*. More than 30 gold occurrences are known in this district, ranging in size from small ancient workings on isolated outcropping quartz veins, to large clusters of workings on quartz vein systems, as well as placer workings in alluvium deposits. The suture between the Tathlith and Asir terranes represents the northern part of the Nabitah fault zone, which consists of serpentinite-decorated subvertical brittle–ductile to brittle shears, individually as much as 0.5 km across, in a zone as much as 5 km wide. Quartz veins and quartz-rich breccias in zones as much as 1 m wide and 50 m long occur along or close to this northern part of the Nabitah fault zone. In addition, other occurrences spread over areas up to 80 m wide and 600 m long, consisting of quartz veins, pods, breccias, and stringer zones in sheared and altered rocks. Gold occurs as small flakes in quartz and in vugs, along fractures in quartz, and as specks adjacent to or within chlorite, pyrite, and chalcopyrite.

The *Ishmas* area is located at the northern end of the Nabitah fault zone, where there is a series of quartz veins trending along a northwest fault zone west of the main Nabitah fault. Quartz veins are mainly hosted by gabbro, chlorite schist, carbonatized gabbro, and carbonatized schist rocks (White and Doebrich 1988). Many Au-bearing occurrences and old workings occur along the main Nabitah fault zone east of Ishmas and aligned along north/northwest- or northeast-trending faults in dacite, quartz dacite, and monzodiorite, such as those et al. Suwaydah and Nabitah, Umm Shat Gharb, and Umm Shat Sharq. The *Al Lugatah*, also referred in the literature as *Lakathah*, in the southern part of the Nabitah fault zone, comprises quartz veins and bodies of altered and veined quartz porphyry in a lens of relatively unsheared rock bounded by zones of more strongly sheared rocks along the axis of the Nabitah fault zone.

The *Hamdah* gold mineralization is located within the southern section of the Nabitah mobile belt where it defines the boundary between the Asir and Tathlith terranes. There are a large group of ancient Au workings in the southern half of the Arabian Shield within Asir Province, ~150 km northeast of the provincial

capital Abha and ~700 km southwest of Riyadh. Ancient lode and placer workings and archaeological remnants of mining camps suggest mining has been undertaken during early Islamic times, ~1000 ya. The country rocks of the Au-bearing veins are layered metamorphic units, composed of quartz–biotite, hornblende, carbonaceous, and chlorite–epidote schists of metavolcanic and metasedimentary origin, and belong to the Malahah subgroup of the Halaban greenstone belt. Deformed serpentinite sheet overlies the hornblende, quartz–biotite, and carbonaceous schists, but underlies the chlorite–epidote schists. All of these rock units have intruded by diorite to granite intrusions, and by mafic to felsic dykes and sills (Hariri and Makkawi 2004). Gold mineralizations are essentially hosted by altered phyllonite, but mostly occur in listwaenite above the felsic sills, and within the sills themselves. Gold here is mainly associated with magnetite, pyrrhotite, pyrite, minor arsenopyrite, and loellingite, with traces of electrum, chalcopyrite, sphalerite, and galena. Gold with sulfide mineralization is found hosted within quartz carbonate veinlets, as well as being sparsely disseminated mainly in hydrothermally altered and thrust zones within the host rocks (Bookstrom et al.1994). Two main mineralized zones have been outlined in the district; the first is to the northeast of the district, up to 21 m below the surface, ranging from 0.5 to 14 m in thickness, with Au grades ranging from 0.1 to 3.13 g/t Au. The second zone is larger than the first one and located to the southwest of the district; both of the two zones have largely been exhausted by the ancient workings. The estimated ancient working's production totals ~ 0.2 Mt ore, with an average grade of 3.8 g/t Au for 0.76 t of Au content. The estimated measured reserve in placers and ancient dumps is ~0.911 Mt ore, with an average grade of 2.89 g/t Au for 2.6 t of Au content. The estimated indicated resource in bedrock is ~0.059 Mt ore, with an average grade of 18.8 g/t Au for 1.1 t of Au content.

The *Khnaiguiyah* occurrence is a sulfide-rich mineralization, of uncertain origin, in strongly sheared rocks in the northern part of the Ar Rayn terrane. It consists of four stratiform ore bodies, called Zone1, Zone2, Zone3, and Zone4, comprising sulfide–oxide mineral assemblages of magnetite; hematite; pyrite; sphalerite; chalcopyrite; rhodochrosite; rhodonite; Ag, Pb, and Bi tellurides; and barite in carbonate-altered shear zones. The ore bodies are hosted by discontinuous bands of carbonatized rocks in a sequence of rhyolitic tuff, lahars and pyroclastic flows, ignimbrite, and subordinate andesitic tuff assigned to the Shalahib formation of the Al Amar group. The rock associations are pervasively affected by greenschist-facies metamorphism and locally develop skarn-type mineral assemblages at the contacts with the granodiorite intrusion. Several hypotheses were suggested for the ore genesis, one of them is that the carbonates and their oxide–sulfide contents are the products of hydrothermal exhalation contemporary with the enclosing volcanic rocks (Testard 1983; Pouit and Bournat 1982). An alternative interpretation is that the carbonates and mineralization are the result of hydrothermal alteration along post-metamorphic, post-tectonic shear zones (BRGM Geoscientists 1993). An epigenetic origin by replacement of carbonates and volcaniclastic rocks controlled by post-metamorphic, post-folding shear zones was also suggested (Sangster and Abdulhay 2005). The mineralization bodies are submassive to disseminated and commonly have a pseudo-stratiform appearance. Previous drilling of >45,000 m in ~345 RC and diamond drill holes at Khnaiguiyah

by BRGM and Ma'aden (Saudi Arabian Mining Company) had outlined substantial Zn-Cu mineralization in two zones—Zone2 and Zone3, as well as significant additional mineralization in Zone1 and Zone4 (ASX report dated at 22 December 2015). The Zn grades range between 10 and 33 wt% and Cu up to 1.5 wt% in the massive mineralization (referred to as "chlorite facies"). Disseminated ore (referred to as "mottled facies") contains <5 wt% Zn and less Cu content. The estimated resource published by BRGM Geoscientists (1993) indicate a "drill-measured total resource" of 24.81 Mt ore, with an average grade of 4.11 wt% Zn and 0.56 wt% Cu. The Zone3, the largest mineralized body at Khnaiguiyah, contains ~65% of the total Zn resource.

The *Kutam* occurrence is located in the southern Saudi Arabia, ~80 km SSW of Al Masane, ~690 km southeast of Jeddah, and is within 10 km north of the Yemen border; it is in the far southwest of the Wassat-Al Masane-Kutam mineral district (Fig. 5.2). The Kutam occurrence is another example of a polymetallic sulfide deposit of uncertain origin that is structurally controlled by shearing. Kutam is a disseminated and stringer sulfide mineralization, hosted by the ~750–730 Ma Malahah volcanic succession. Similarly, it looks like the Al Masane deposit; it falls within the Khadra structural belt of the Asir composite terrane and is within the Nabitah mobile belt. It consists of locally discordant but generally stratiform and stratabound bodies of disseminated and stringer chalcopyrite, sphalerite, and sparse pyrite, tetrahedrite, and galena. The Kutam occurrence is surrounded by extensive ancient workings and piles of smelter slags. The occurrence was rediscovered by geologists of the US Geological Survey (USGS) in 1974 and drilled by the USGS and Noranda in 1976–1977, defining a steeply dipping zone of disseminated and stringer-style Cu–Zn mineralization. The regional stratigraphy in the district comprises three major assemblages. Lowest is a sequence of felsic metavolcanic rocks with minor interbedded sedimentary rocks, hosting the Kutam mineralization, and overlain by mafic volcanic rocks. At middle depths is a more complex sequence composed of grey phyllites overlain by a series of intercalations between felsic and mafic volcanic rocks, chloritic phyllite, sericitic phyllite, and siliceous chemical sedimentary rocks. At the uppermost level is a succession of mafic volcanic rocks grading to the south into greywacke and other sedimentary rocks, all capped by a grey phyllite after carbonaceous mudstone (Independent Technical Report, Coffey Mining Pty Ltd 2012). The geology of the Kutam mineralized area is dominated by sheared mafic-to-intermediate volcanic rocks (Fig. 5.8), chiefly metabasalt to meta-andesite. These volcanic rocks intercalated with quartz porphyry of porphyritic metadacite to metarhyolite in composition. The youngest rocks are north/south-trending mafic dykes that cut the foliation in the volcanic rocks, all of which have been metamorphosed to amphibolite facies. The mineralized bodies are overall concordant but locally discordant; show zones of disseminated and stringer sulfides occurring as thin, conformable sheet-like bodies; and lack any development of massive sulfides. Mineralization on the footwall (northeast) side of the prospect has high Cu/Zn ratios, whereas on the hanging-wall side the reverse is evident with high Zn/Cu ratios (Legg 1983). The Kutam mineralization has been variably interpreted as an epigenetic sulfide replacement of sheared rocks (Smith et al.1977), or as a sheared Cu–Zn-rich VMS deposit (Legg 1983). Sangster and Abdulhay (2005) also suggested a VMS origin for the Kutam prospect. The

estimated (indicated + inferred) ore resources by MineMap Consulting Pty Ltd for Petrohunt Middle East Limited (2010) are 16.43 Mt ore, with an average grade of 1.03 wt% Cu, 0.51 wt% Zn, and 0.1 g/t Au.

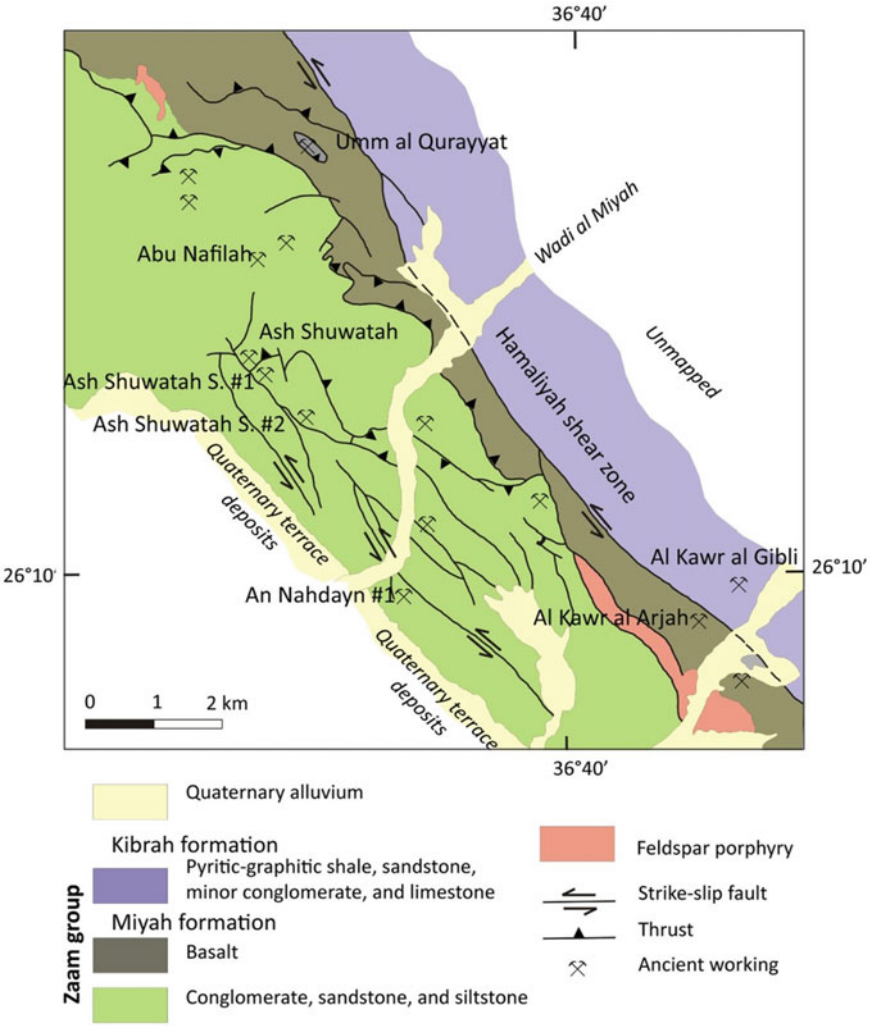

Fig. 5.7 Geologic map of the southern part of the Al Wajh Au district, northwestern Arabian shield (after Johnson and Kattan 2012)

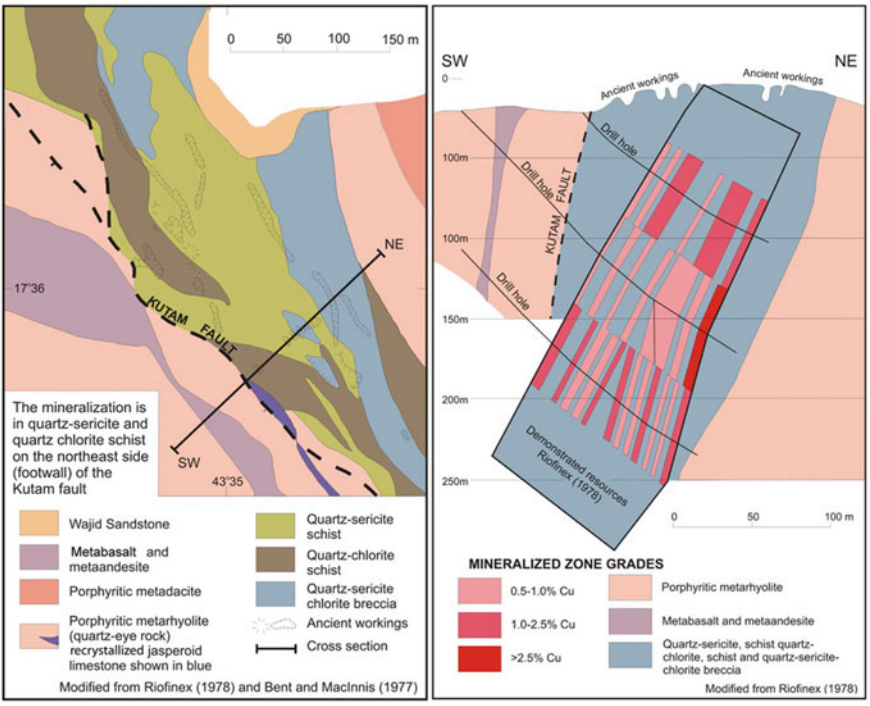

Fig. 5.8 Geologic map (left) and cross-section (right) of the Kutam deposit, Asir terrane (after Johnson and Kattan 2012)

5.2.2 Iron Oxide–Copper–Gold Deposits

The mineral deposits of this type are generally characterized by the levels of iron oxides, such as magnetite and/or hematite in tabular bodies, breccia fillings, veins, disseminations, and replacements in dominantly felsic volcano-plutonic settings (Gandhi and Bell 1996). The deposits range from essentially monomineralic (Fe) to polymetallic (Fe + Cu ± U ± Au + Ag + rare-earth elements (REEs)). These deposits range in size from small (<10 Mt) to very large (100–500 Mt) to extremely large (>2000 Mt). They typically occur in late tectonic or anorogenic continental environments, but occurrences that may belong to this type have been identified over the past ten years in the Arabian Shield in convergent-margin settings in the Ar Rayn terrane and possibly the Hulayfah and Asir terranes (Johnson and Kattan 2012).

In the Ar Rayn terrane, the IOCG occurrences are essentially represented by *Gebel Idsas*, but others are known along the western margin of the terrane; they are either magnetite- or hematite-rich. The mineralized occurrences of these deposit types are hosted by Al Amar group volcanic and volcaniclastic rocks and formed as metasomatic replacement bodies of disseminated magnetite and smaller fault-controlled bodies of massive magnetite (Doebrich et al. 2007). Gebel Idsas was previously

explored over several years as an iron-ore resource, but sampling by Doebrich et al. (2007) has suggested an IOCG mineralization. The Gebel Idsas deposit consists of magnetite, apatite, hematite (martite), actinolite, chalcopyrite, chalcocite, and covellite associated with amphibole (actinolite), tourmaline, epidote, and sericite. The magnetite-rich deposits are enriched in LREE, whereas hematite-rich deposits are more enriched in Cu and Au. The estimated ore resources of the fault-controlled massive lenses at Gebel Idsas are ~1.3–6.7 Mt ore, with ore grades at 64–65 wt% Fe, whereas ore resources in disseminated magnetite deposit gave ~300 Mt ore, with ore grades at 18–20 wt% Fe (Ashworth and Abdulaziz 1978).

Possible IOCG occurrences in the Hulayfah terrane are in the *Musayna'ah* mineral district (Fig. 5.2), west of the Bi'r Tuluhah ophiolite and the Hulayfah fault zone in the most northern Arabian Shield. The country rocks consist of low-grade basalt and andesite, basaltic breccia, andesitic tuff, sandstone, conglomerate, and marble of the Hulayfah group (>720 Ma), with diorite, gabbro, and granodiorite intrusions. The mineralization comprises as many as eight small occurrences of Cu and Cu-Au-Fe (magnetite or hematite) in volcano–sedimentary rocks close to contacts with granite and diorite intrusions. The mineralized occurrences were initially explored as sources of iron, but further exploration indicated that the magnetite contains as much as 2.5 g/t Au. The prospects were trenched and drilled in the 1970s, included in a review of geology and mineral resources of the wider Bi'r Tuluhah area in the 1980s (Johnson et al.1989), and mapped and resampled in the early 2000s by Saudi Geological Survey (SGS) (Jannadi et al.2005).

In the Asir terrane, the possible IOCG occurrences are found in the *Bidah* mineral district along the main Bidah shear zone (Fig. 5.2). The mineral occurrences were the sites of ancient Au mining developed on quartz stringers and stockworks within lenses of ferruginous chert or diorite and granodiorite intrusions (Worl and Smith 1982) at *Bani Sar*, *Umm ar Raha*, and *Shib an Nahl*. The ferruginous chert lenses appear to be in the same lithostratigraphic unit that hosts the Rabathan Cu–Zn occurrence. Samples of quartz veins have Au contents from as low as 0.1 to as high as 53.5 g/t Au, but mostly 1.0–1.5 g/t Au. Silver content is low, mostly 0.9–1.6 g/t Ag. The *Mamilah*, *Mamilah North*, and *Mamilah South* ancient Au mines at the north end of the mineral belt are associated with Fe-rich rocks ranging from massive jasperitic chert to friable ironstone. Gold grades reported by Bureau de Recherches Géologiques et Minières (BRGM) in the Mamilah area are erratic, the highest value being present in pyritic carbonate–altered schist in the footwall of one of the veins. One trench averaged 19.2 g/t Au over 8 m, but drill intersections were in the range of 9.2 g/t Au over 1.35 m to 0.7 g/t Au over 0.25 m. The estimated measured resource by BRGM in the area gave ~ 0.237 Mt ore at 4.11 g/t Au to a depth of 50 m.

5.3 Orogenic Gold Deposits in Yemen

Historically, Yemen was the seat of the Sabayans (known as the Queen of Sheba), a nation that was well known for its wealth in Au. Although there appears to be

evidence that the west of Yemen was the source of much of this Au, it is surprising that in modern times there are very few records of Au mining in Yemen in general. The Sabayans were famous for Au mining, and it was said that they were one of the richest peoples in the region because of the large number of Au mines in their land. The doors, ceilings, and walls of their palaces and temples were decorated with Au, Ag, and gemstones. The limited modern exploration coverage in terms of reconnaissance geochemical and geological surveys has located many Au occurrences in Yemen. The Geological Survey and Mineral Resources Board (GSMRB) publication "Mineral Resources in Yemen 2009" stated that there are over 40 known Au and/or Ag occurrences, among of which ~12 sites are the subject of exploration by international companies.

In general, Au occurs in three different geological settings: auriferous shear zones and Au-bearing quartz veins (orogenic Au) in Precambrian basement, mainly in greenstone belts; Tertiary volcanic-hosted Au; and sediment-hosted, disseminated Au associated with rifting in Cretaceous rocks. Here the discussion will focus only on the first category, the auriferous shear zones and Au-bearing quartz veins in the Precambrian basement rocks. Almost all of these Au-bearing occurrences are related to the orogenic Au deposits (Al-Shameery and Sun 2011), which will be discussed below. The most promising Au occurrences of the auriferous shear zones and Au-bearing quartz veins in the Precambrian basement of Yemen are those at *Wadi Madan, Hiru, Musayani, Al-Hariqah, and Wadi Sharis* Au occurrences (Fig. 5.9).

The *Wadi Madan* Au occurrence, Hadramout, is located in the eastern part of Yemen, ~70 km northwest of the port city of Al Mukalla from the Arabian Sea (Fig. 5.9). It is the largest Au mineralization in Yemen. The host rocks represent a window of Precambrian greenstones consisting of a succession of mafic metavolcanic and metasedimentary rocks with intercalated felsic metavolcanic rocks. The Wadi Madan Au occurrence consists of at least 12 parallel north/south-trending shear zones varying in width from 1 to 5 m and dipping to the east at high angles (Frick and Al-Jawadi 2009). The Au-mineralization zone has been traced in the field over a distance of ~2.5 km. Several research and exploration groups have investigated the Wadi Madan Au occurrence including the "Soviet Geological Mission" carrying out trenching and diamond drilling. The estimated ore reserves that were carried out in 1992 are shown in Table 5.1. A new drilling program was carried out in 2008 with new resource estimates, but it is not available to be cited here. The available resource estimate, which was completed in 2006, yielded an indicated Au resource of ~1 million oz at an average grade of 6.99 g/t Au. There are several other occurrences nearby the Wadi Madan occurrence, but they have been not properly explored as have those of the *Nagab* occurrence of Au and Cu mineralization, which occurs in oxidized quartz veins 0.25–0.4 m wide and 100 m long. The average assay of grab samples from the quartz veins shows values up to 41 g/t Au.

The *Hiru* occurrence is located very close to the Wadi Madan occurrence (Fig. 5.9). It comprises a zone of altered quartz veins of 8–10 cm thickness and 200 m length, and is localized at the contact of a granodiorite dyke. The assay of four grab samples from the veins contained 50–110 g/t Au (Frick and Al-Jawadi 2009). At the *Mohamadiyin* occurrence, the Au mineralization is associated with pyrite, quartz, and carbonate in

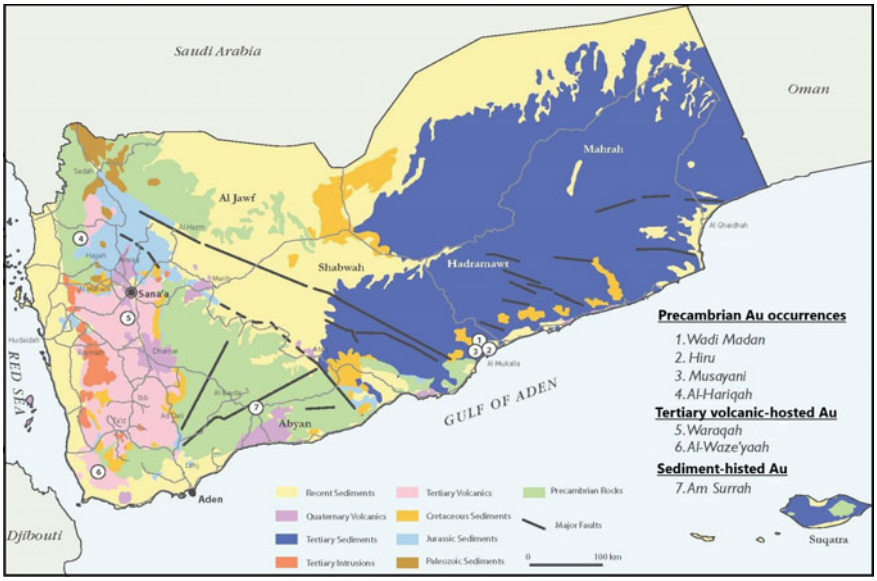

Fig. 5.9 Simplified geological map of Yemen showing the most promising Au occurrences of different mineralization types

Table 5.1 Tonnage and Au contents in different blocks of Wadi Madan occurrences (Mineral Resources in Yemen 2009)

Zone	Blocks	Mass (t)	Au (ppm)	Ag (ppm)
A1	12	13,616	12.66	nd
A2	40	34,224	15.2	8.99
A3	1	9178	8.04	nd
A4	3	13,797	23.2	4.96
B1	31	28,894	14.96	18.96
C1	3	948	21.86	nd
D1	1	2,831	16.80	nd
H1	7	9097	17.25	nd
K1	14	16,521	11.22	11.59
L1	5	2041	18.39	nd
M1	4	2036	9.45	nd
M2	4	2385	10.5	nd
S1	3	1069	45.05	nd
	128	136,187	15.07	11.94

a gently dipping altered shear zone cutting Precambrian meta-andesite. The quartz carbonate veins are up to several meters thick and containing 2–20 g/t Au within the shear with a strike length of 600 m. The *Musayni* occurrence (Fig. 5.9) comprises moderately dipping quartz veins of ~10–15 cm in thickness, where Au is associated with cerussite ($PbCO_3$) and minor galena. The *Ntaisha* area comprises five occurrences located ~5 km southeast of the Wadi Madan area, where 19 mineralized and altered quartz carbonate veins have been identified in metavolcanic rocks intruded by numerous syenitic to dioritic dykes (Frick and Al-Jawadi 2009). Gold values of up to 55.5 g/t were found in a zone up to 900 m in length and ranging 0.12–0.8 m in width.

The *Al-Hariqah* Au occurrence is situated in the Aflah Asham district of northwest Yemen (Fig. 5.9), ~110 km northwest of Sana'a. The Al-Hariqah Au occurrence occurs in two parallel zones oriented in north/northwest directions. The occurrence is more than 4 km long, and hosted in a sequence of foliated, variably metamorphosed Proterozoic–Archean volcaniclastic–sedimentary and metadiorite intrusive rocks (Cantex 2000). The two zones are 50 m in width or more in the northern part of the occurrence but progressively narrow to ~30 m in width in the southern part of the occurrence. The mineralized zones are hydrothermally altered and which mostly consist of quartz, sericite, arsenopyrite, and pyrite (Cantex 2000). The Au mineralization is characterized by high-grade pods that are contained within a low-grade country rock. Gold is predominantly associated with arsenopyrite, pyrite, and rare galena with other secondary minerals. In the oxidation zone, which comprises the top 30 m of the occurrence, Au-bearing quartz veins and stockworks with free Au grains are locally common (Cantex 2000). The estimated ore resources carried out for the drill holes by Cantex in 2005–2006, where the Al-Hariqah occurrence is estimated to contain more than 40 Mt of ore, with an average grade of 1.5 g/t Au or greater (Cantex 2000).

The *Wadi Sharis* Au occurrence is located ~10 km to the east of Hajjah Province, ~260 km to the west of Sana'a; it was discovered in 1996 by the Canadian Mountain Company during a detailed prospecting and exploration campaign. The Au mineralization of this occurrence is considered to be an orogenic-vein-type Au deposit, which occurs in quartz veins hosted in Neoproterozoic metavolcanic and metavolcano–sedimentary rocks (Al-Shameery and Sun 2011). The orebody is extended from Wadi Sharis in the south to Wadi Alharirah in the north over a distance of ~30 km. The Wadi Sharis orogenic Au is basically hosted by a variety of rock types including Neoproterozoic low-grade metasedimentary and volcano–sedimentary rocks, which consist of amphibolite, carbonaceous quartz–biotite–schist, chlorite–actinolite schist, quartz–amphibolite–biotite schist, serpentinite and graphitic quartzite and ophiolitic mafic to ultramafic bodies. The greenschist- and amphibolite-facies metamorphic rocks are intruded by calc-alkalic and alkalic granites of Pan-African age (600 Ma) consisting of granite, aplite, and pegmatite bodies. Both the metamorphic and intrusive granitic rocks are highly sheared, especially close to the fault contacts between the two rock units. The ore zone is intersected by diamond drilling at a depth of ~150 m. Gold mineralization is mainly associated with intense silicification, sericitization, carbonatization, and sulfide-rich alteration zones. Gold

deposit occurs along metamorphic brittle–ductile shear zones, where the arsenopyrite is the dominant mineral hosted by quartz veins. Mineralization in the Wadi Sharis occurrence comprises Au- and sulfide-bearing quartz veins and veinlets. The Au is commonly associated with arsenopyrite, pyhrrotite, and pyrite, which are confined in a variety of sulfide-rich quartz carbonate veins. The veins situated along north/south-trending structures, and the mineralized zones are mainly parallel to the schistosity (foliation) of the metamorphic units. The veins vary in size from a few centimeters to as much as 50 cm in width and a few tens of centimeters to 35 m in length (Al-Shameery and Sun 2011). The estimated inferred ore reserves contain ~4,100 oz of Au, with an average grade of 1.5 g/t Au, whereas the possible ore reserve is ~40,000 oz of Au, with an average grade of 1.2 g/t Au. The *Sa'dah/Al-Jawf* district has many ancient gold mines in the Al-Lawdh/Al-Marazig area, which is located northeast of Sa'dah and close to Al-Jawf, within the At Talh composite terrane, and close to the Silbah suture on the eastern edge of the Amlah terrane (Al-Khirbash et al.2021). The Sa'adah/Al-Jawf mineralization district contains the most significant Au-bearing quartz veins that were mined by the ancient Yemenis. The Au mineralization in this area is associated with northeast- and northwest-oriented veins that dip steeply to the west and undergo multi-phases deformation of folding, faulting, and shearing in mafic metavolcanic rocks and in late alkaline granite intrusions (Al-Khirbash et al. 2021). In addition, several (Au–Ag–Cu)-bearing occurrences were reported by Petromine Company during its exploration programme during 2012–2014 in southeast Taiz and northwest Lahj, to the south/southwest of Sana'a (i.e., Haifan–Al Qabaitah complex). These occurrences are associated with quartz veins and pegmatitic granites, such as at Gebel Dhmran, Hasn-Al Hitary, Al Rojimah, Al Zabirah, and Hamedk (Al-Khirbash et al. 2021).

5.4 Orogenic Mineral Deposits in the Eastern Desert of Egypt

In the Eastern Desert of Egypt, orogenic mineralization environments are represented only by orogenic-Au deposits, there is no strong evidence to support the presence of IOCG and Carlin-type Au deposits. Lately, the term *orogenic-Au deposits* is being expanded to include the majority of Au mineralization in the Eastern Desert of Egypt (Zoheir 2008; Johnson et al. 2017; Abdel Monsef et al. 2018; Zoheir et al. 2019a). Numerous Au deposits/occurrences are widely distributed throughout the ANS (Fig. 5.10) in general and in particular in the Eastern Desert of Egypt, where hundreds of Au-bearing sites are identified by trenches, adits, and dumps (Fig. 5.11), as well as by placer Au workings in alluvium sediments (Klemm et al. 2001; Zoheir et al. 2019a). The majority of these ancient workings were directed to the Au-bearing quartz carbonate veins in metamorphic terranes, which typically are classified as orogenic-Au deposits. One of the best examples that are currently active in Au production is the Sukari gold mine in the Central Eastern Desert (CED) of Egypt, which

is presently operated as a large-scale open-pit and high-grade underground mining site. Other possible types of Au mineralization, including the intrusion-related or porphyry-Au deposits (such as those at Hamash, Wadi Dara, and Um Mongul), have already been discussed in Chap. 4 of this book (Helmy and Kaindl 1999; Ahmed and Gharib 2016; Abd El-Rahman et al. 2018). Another category of Au-bearing deposits in the Eastern Desert of Egypt and some other places in the ANS is the VMS deposits, which will be discussed in Chap. 6 of this book.

As mentioned before in Chap. 2 of this book, the Eastern Desert of Egypt, which forms the northwestern flank of the ANS, can be lithologically and structurally subdivided into three main subdivisions: (1) the North Eastern Desert (NED), composed of Ediacaran (635–541 Ma) granite, with scattered outcrops of Ediacaran volcanic and sedimentary rocks, and minor exposures of arc volcanic rocks; a situation similarly found in Sinai (Stern and Hedge 1985); (2) CED characterized by ensimatic (oceanic) arc rocks and high-grade schist and gneiss; and (3) South Eastern Desert (SED) dominated by ophiolitic, metavolcanic, and metasedimentary rocks. However, smaller subdivisions of these three lithological parts of the Eastern Desert were made based on differences in structural trends; where nine structural blocks (Fig. 5.12) were recognized (Zoheir et al. 2019a). These structural blocks are the Allaqi–Sol Hamed, Abu Swayel, Um Samiuki-Abu Dahr, Hafafit-Natash, East Nugrus, Mubarak-Hamash, Meatiq–Sibai, Fatira-Um Anab, and Wadi Dara-Um Monqul blocks. The contacts between these structural blocks are mostly major faults and shear zones, in some cases are well-established or inferred suture zones, and, in a single case, the margin is coincident with an apparent change in crustal thickness. Detailed lithological and structural descriptions of these blocks can be found in Zoheir et al. (2019a), which are used here as the basis for a useful framework to describe the distribution of orogenic-Au occurrences/deposits in the Eastern Desert. In general, the distribution of Au occurrences in the Eastern Desert is heterogeneous (Fig. 5.11); however, they are mainly concentrated in five structural blocks (Fig. 5.12). Following are brief descriptions of the main orogenic-Au occurrences in the Eastern Desert blocks, which are based mainly, but with some extra details, on the study by Zoheir et al. (2019a).

5.4.1 Allaqi–Sol Hamed Block

The *Allaqi–Sol Hamed block* is located in the southernmost part of the SED, where there are more than 20 orogenic-Au occurrences, most of which are controlled by extensional structures in response to the Hamisana shear zone. The most studied and promising orogenic-Au occurrences in the Allaqi–Sol Hamed block include the *Haimur deposit* and *Um Garayat deposit* and the *Seiga*, *Shashoba*, *Um El-Tuyor*, *Betan*, and *Romite occurrences* (Figs. 5.11, 5.12). The *Haimur Au deposit* is located at the western end of the Allaqi–Sol Hamed suture zone (Fig. 5.11), and hosted by silica- and carbonate-rich altered serpentinite rocks (listwaenite), metagabbro, and metabasalt (El-Shimi 1996; Klemm et al.2001; Kusky and Ramadan 2002; Emam and

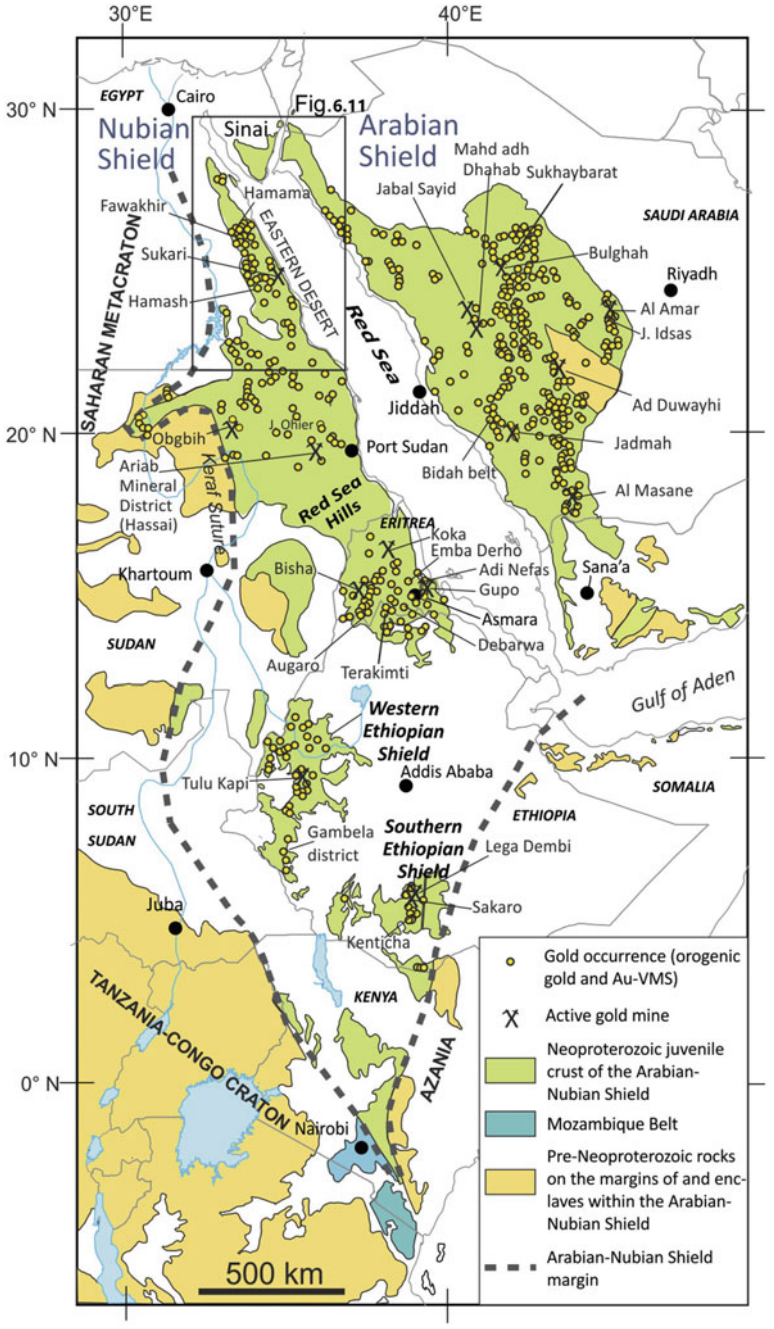

Fig. 5.10 Distribution of Au occurrences and active Au mines in the Arabian–Nubian Shield (after Johnson et al. 2017a, b)

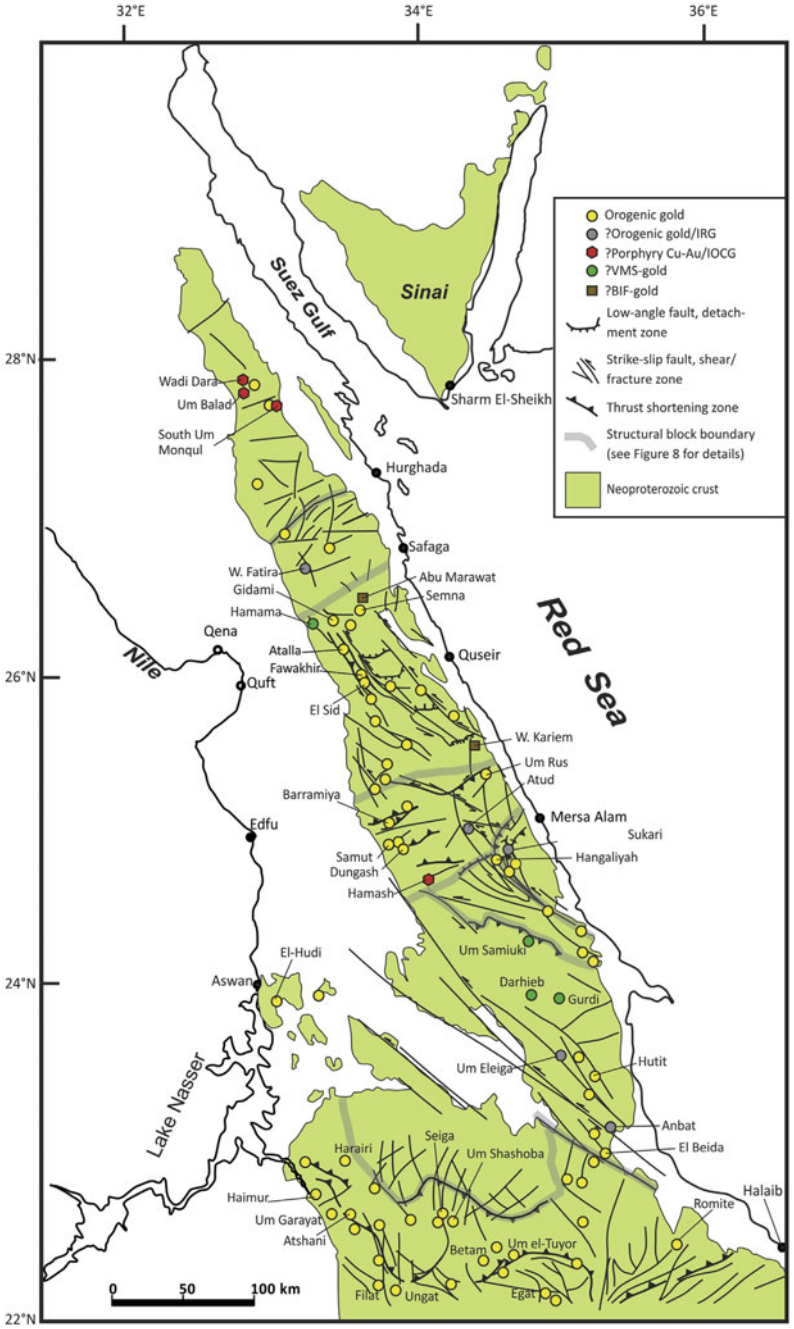

Fig. 5.11 Distribution of Au occurrences, of different mineralization types, in the Eastern Desert of Egypt (after Johnson et al. 2017a, b)

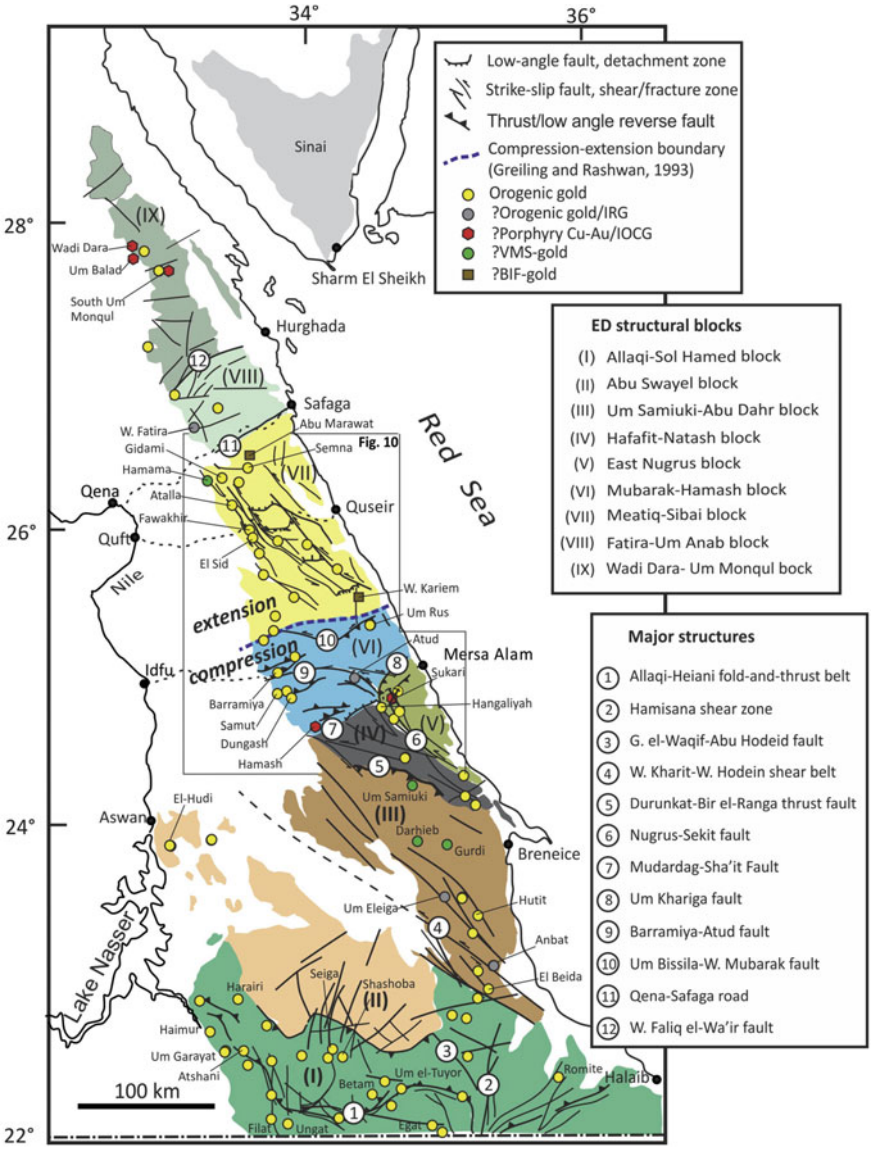

Fig. 5.12 Distribution of Au occurrences in structural blocks in the Eastern Desert of Egypt (Zoheir et al. 2019a)

Zoheir 2013; Zoheir and Emam 2014). The Au mineralization is mainly concentrated in carbonate- and sulfide-bearing milky and grey quartz veins in highly tectonized listwaenite. The veins are narrow in width (2–100 cm) but as long as 25 m along strike. The Au assay of the Haimur deposit reached up to 35 g/t Au (Ramadan 1997; Ramadan et al. 1999), which mainly occurs as fine disseminated grains associated with sericite, chlorite, and carbonates. Early sulfide mineral assemblages are represented by chalcopyrite, gersdorffite, arsenopyrite, pentlandite, and pyrrhotite, while pyrite and free Au grains represent later hydrothermal phases (Zoheir et al. 2019a).

The *Um Garayat* Au deposit is a part from the 50-km-wide zone of deformation of the Allaqi–Heiani belt in the Neoproterozoic Nubian Shield of the SED (Fig. 5.12). The origin of the Um Garayat deposit is uncertain, sometimes considered to be orogenic-Au deposit (Zoheir et al. 2019a), but sometimes considered to be intrusion-related porphyry Cu-Au deposit (Hussein 1990; Zoheir et al. 2008). The Um Garayat deposit is a historical Au occurrence in the Wadi Allaqi district; it is present as north/northwest-trending sulfide-rich quartz and quartz carbonate veins cutting through variably deformed island arc metavolcanic and metavolcaniclastic rocks. The quartz carbonate veins and altered wallrocks (metavolcaniclastic/metasedimentary rocks) are characterized by disseminated hydrothermal pyrite. Anomalous Au concentrations, locally up to 17 g/t, are only reported in arsenopyrite-rich parts of the quartz veins. Ore mineralogy in the Um Garayat deposit includes pyrrhotite, pyrite, chalcopyrite, sphalerite, arsenopyrite, and galena, where the Au mainly presents as refractory Au in pyrite and arsenopyrite, but sometimes also occurs as free-milling Au inclusions in sulfides and quartz veins (Zoheir et al. 2008).

The *Seiga* Au occurrence is located in the northern part of the Allaqi–Sol Hamed block (Fig. 5.12), and comprises quartz veins in the north/northwest-trending, steeply northeast dipping fractures, and hosted by strongly foliated meta-andesites and slates. The shear fabrics at the Seiga occurrence suggests that the quartz veins were formed concurrently with the deformation of the host rocks. The mineralized zone extends for ~800 m, and the discontinuous zones of mineralized veins extend over 1.2 km along strike. The estimated inferred ore resource is ~1.1 Mt of ore, with an average grade of 2.3 g/t Au, over a horizontal length of ~525 m along strike and to a maximum depth of 150 m. The *Shashoba* Au occurrence is located ~6.5 km southeast of the Seiga occurrence (Fig. 5.12), at the foot of Shashoba Mountain. The occurrence comprises north- and north/northwest-trending Au-bearing quartz veins that cut across altered carbonate–metagreywacke and metaconglomerate of undifferentiated metasedimentary or metavolcanic origin. Silicification and carbonatization are widespread in the ancient working mined area, where the networks of quartz veinlets were selectively mined out. The estimated mineralized materials from the old mining activities have ~1300 t of tailings and 4311 t of dump rocks. An anomalous Au-bearing zone was identified based on the assay results of channel samples, consistent with an north-trending shear zone close to the ancient workings. The assay results of quartz veins gave Au content up to 4 g/t, with an average of 2.2 g/t (Klemm and Klemm 2013).

The *Um El Tuyor* Au occurrence is located in the extreme south of the Eastern Desert of Egypt, between latitudes 22° 05′ N and 22° 25′ N and longitudes 34° 27′ E

and 34° 50′ E, near the border with Sudan (Fig. 5.12). The area extends for more than ~1000 km^2, in the eastern part of the Wadi Allaqi region. The area consists of massive and laminated quartz and quartz carbonate veins that formed along brittle–ductile dextral shear zones parallel to the Hamisana shear zone, extending and trending to the north/northwest to northwest. The shear zones cut pelitic metasedimentary rocks comprising garnet–biotite schist intercalated with metamorphosed mudstone and greywacke. The mineralized area is intensely sheared, consistent with the characteristic features of the central part of the Allaqi–Sol Hamed block. Hydrothermal alteration of sericite–carbonate–chlorite assemblage overprints the metamorphic assemblages in the wallrocks, which indicate the Au mineralization postdated peak metamorphism. The Au mode of occurrence is essentially as microscopic blebs within arsenopyrite and pyrite, along fractures and grain boundaries in quartz, and as fine disseminations in chlorite ± sericite—and carbonate-altered wallrock (Zoheir et al. 2019a).

The *Betam* occurrence is one of several Au occurrences at the extreme part of SED of Egypt, in the Wadi Allaqi district (Fig. 5.12). It comprises Au-bearing milky and grey quartz veins in conjugate northwest- and northeast-trending brittle–ductile shear zones in tectonized metagabbro and metasedimentary rocks in the vicinity of small granite intrusions (Zoheir 2008; Zoheir and Qaoud 2008; Zoheir et al. 2013). The abundant stone huts, millstones, dumps and tailings observed in the mine area indicate significant mining activities in the past. The Au-bearing quartz veins were mined on surface through several trenches and in the underground through shafts and adits. Gold mineralization zone represented mainly by auriferous quartz veins and veinlets along a brittle–ductile shear zone cutting through schistose pelitic metasedimentary rocks. The average grade assay of ore dump at the mine area is ~6 g/t Au (Zoheir and Qaoud 2008). Elongated surface alteration zone trending northwest/southeast associated with central sheared auriferous quartz veins, where the hydrothermal alteration includes pervasive silicification, sericitization, chloritization and albitization. The intensity of alteration correlates positively with the thickness of the silicification zone and quartz veins. Alteration includes a proximal quartz–pyrite–sericite ± albite assemblage adjacent to the veins, an intermediate zone of sericite–chlorite–pyrite ± biotite, and a distal zone of chlorite + calcite + biotite + pyrite ± epidote. Most free-milling Au is associated with a paragenetically late galena–tetrahedrite–chalcopyrite sulfide assemblage. However, an early Fe–As sulfide assemblage shows minor invisible (refractory) Au. Geochemical data define widespread dispersion of Au, Ag, Sb, Cu, and Pb near intersecting shear zones and in altered wallrocks (Zoheir et al. 2013).

The *Romite* Au occurrence is located in the extreme southern part of the Eastern Desert (Fig. 5.12), ~90 km south of the coastal village of Shalateen. It is a part of the major curvilinear Allaqi–Heiani–Onib–Sol Hamed suture, which is commonly marked by ophiolite mafic and ultramafic rocks. The entire area was later deformed by the north-trending Hamisana shear zone, which is a complex belt of deformation characterized by east/west crustal shortening fabrics, steep folds, and thrust faults. The Romite occurrence comprises Au-bearing quartz and quartz carbonate veins and disseminated Au in Fe-stained, carbonate-altered, and silicified quartz diorite.

Gold mineralization is mostly associated with sulfide minerals, including pyrite, arsenopyrite, and lesser chalcopyrite and pyrrhotite. The mineralized veins trend north-northeast along the shear zone and dip steeply to the northwest. Based on the morphology, the asymmetrical pinch-and-swell structures, and quartz textures, it was suggested that Au-bearing veins were formed synkinematically with movement on the north-northeast-trending shear (Zoheir 2012). The veins reached up to 300 m long and 5–150 cm wide. The estimated Au assay of grab samples of quartz vein contain up to 7 g/t Au, while the altered wallrock samples mostly contain <1 g/t Au.

5.4.2 Um Samiuki–Abu Dahr Block

The number of orogenic-Au occurrences in the Um Samiuki–Abu Dahr block is relatively very few compared with those in the Allaqi–Sol Hamed block, they are mostly in the southern part of the block, close to and along the northwest-trending shears of the Wadi Kharit–Wadi Hodein shear belt (Fig. 5.12). The *El-Beida* and *Anbat* Au-bearing occurrences are the most famous and studied in this structural block. The *El-Beida* Au occurrence is located at the southern margin of the block, and hosted by polydeformed ophiolitic, island-arc volcanic and plutonic rocks along and subparallel to the northwest-trending shear zone (Zoheir et al. 2019a). The Au-bearing quartz veins occur in secondary shear zones, which are considered to be a southernmost part of the Najd fault system that controls most of the Au mineralization in the Eastern Desert (Obeid et al. 2001; Zoheir et al. 2019a). The ore mineralogy in quartz veins contains pyrite, chalcopyrite, chalcocite, covellite, marcasite, and subordinate pyrrhotite and sphalerite, which have average assay grades of 2–6 g/t Au. The wallrock surrounding the quartz veins is strongly hydrothermally altered, including an inner zone of quartz–sericite–pyrite assemblage and an outer zone of quartz–chlorite–calcite assemblage.

The *Anbat* Au mining area is located a few kilometers north of El-Beida (Fig. 5.12). It comprises Au-bearing quartz ± carbonate veins in pervasively silicified, highly sheared ophiolitic, metavolcanic rocks, as well as in porphyritic granite along a kilometer-scale wide shear zone that is part of the Wadi Kharit–Wadi Hodein shear belt (Zoheir 2011). The kinematic indicators in the Anbat area suggest transpressional deformation along the shear zones, where the area was affected by west-southwest/east-northeast compression, west-southwest–verging thrusting, and development of conjugate sinistral northwest-striking and dextral northeast-trending strike–slip faults (Zoheir et al. 2019a). The Au mineralization occurs as quartz veins, sulfide-rich granitic rocks, and pervasively silicified, sulfidized metavolcaniclastic rocks and listwaenite along shear zones. Gold generally occurred as free grains in quartz veins, and in silicified host rocks associated with pyrite, arsenopyrite, and gersdorffite. Because some Au-bearing veins are hosted by quartz–feldspar porphyry and granodiorite, the Anbat occurrence has been referred to as an intrusion-related Au system. The estimated Au resource is ~17 t Au, with an average grade at 58 m depth

of 2.09 g/t Au and at 24 m of ~4.38 g/t Au (Thani Stratex Resources Limited website, downloaded June 2018).

5.4.3 East Nugrus Block

The East Nugrus block is located to the northeast of the Hafafit–Natsh block (Fig. 5.12), and separated from it by the Nugrus–Sekit fault. The entire block is an allochthon, comprising a stack of northwest-verging thrusts that curve to the northeast from the north-northwest–trending Nugrus–Sekit fault (Makroum 2017; Abd El-Wahed et al.2016). The East Nugrus block contains few Au localities; among the most important and famous Au occurrences include the *Sukari* and *Hangaliya* deposits (Fig. 5.12).

The *Sukari* gold mine in the CED is the largest in the ANS and the first modern mining operation in Egypt; it is located ~20 km to the southwest of Marsa Alam, between the Red Sea coast and the Hafafit gneiss dome (Figs. 5.12 and 5.13). The Sukari area has a long history of mining activities, from the predynastic era (~3200 BC), through the Ptolemaic, Roman, and Arab eras, through the British Colonial period, to the present day. The ancient Sukari Au mining activities were mainly confined to the Au-bearing quartz veins without any attention to the associated alteration zones. The Sukari gold mine is currently operated as a joint venture between Centamin plc and the Egyptian government. The mine is situated within Late Neoproterozoic granitoids that intruded into older volcano–sedimentary successions and an ophiolitic assemblage (Fig. 5.13a) that is known as Wadi Ghadir mélange. The volcano–sedimentary succession is composed of andesites, dacites, rhyodacites, tuffs, and pyroclastics. Magmatic rocks are of calc-alkaline affinity and were formed in an island-arc setting (El Gaby et al.1990; Akaad et al. 1996). The dismembered ophiolitic succession is represented by a serpentinite at the base that locally altered to listwaenite (Helmy et al.2004), followed upwards by a metagabbro–diorite complex and sheeted dykes. Metagabbro–diorite rocks and serpentinites form lenticular bodies (1–3 km^2) as well as small bodies occurring conformably scattered in the volcano–sedimentary arc assemblage (Harraz 1991) (Fig. 5.13a). All rocks are weakly metamorphosed (lower greenschist metamorphic facies), intensely sheared, and transformed into various schists along shear zones. Mineralized quartz veins and talc carbonate veinlets are common.

The Sukari gold mine is mined as a large-scale open-pit (Fig. 5.14) and a high-grade underground mine. The mineralization comprises Au-bearing quartz stockworks and sheeted veins in brittle–ductile shears (Fig. 5.13a, b) within the 689 ± 3 Ma Sukari intrusion (Abd El-Wahed et al.2016). The host intrusion is variably identified as an I-type, magnetite-bearing granodiorite to monzogranite (Helmy et al.2004) or monzogranite, syenogranite, and alkali–feldspar granite (Mohamed et al.2018). The mineralized zone trends north-northeast/south-southwest for ~2.3 km and is 100–600 m wide; it extends in a down dip as much as 1200 m below the surface. Ore mineralogy in the quartz veins, stockworks, and alteration zones are represented by

pyrite and arsenopyrite, and, less commonly, sphalerite, chalcopyrite, galena, and gold. The higher Au inclusions are mainly found to be associated with arsenopyrite. The mineralized quartz veins are essentially controlled by shears, which have been inferred to be part of the late Cryogenian–early Ediacaran regional-scale system of north/northwest- and northeast-trending conjugate zones of transpression and thrusting that characterizes the East Nugrus block (Abd El-Wahed et al.2016). The Sukari gold mine includes an open-pit mine, underground mine, ore-processing plant, and Au-extraction room (Rabeiy et al.2017; Abdelaal et al.2021). The open-pit operations in the mine began in 2010 and underground operations started in 2011. The Sukari Gold Mine Co. mined and processed ~6.4 Mt and ~4.5 Mt ore, respectively, in 2012, producing ~8.175 tons Au (Taib 2015). The most recent estimated total open-pit mineral resources were ~386 Mt ore, with an average grade of 1.03 g/t Au (~366 t/12.9 Moz) Au; the estimated underground resources were ~ 4.67 Mt ore, with an average grade of 6.8 g/t Au (~29 t/1.02 Moz) Au (Franzmann et al.2015). In March 2018, the total Au reserves were reported at 227 t and the total ore resources at ~344 Mt, with a predicted lifetime of 15 years (Centamin 2018).

The *Hangaliya* gold occurrence is located ~25 km southwest of the Sukari gold mine (Fig. 5.12), which comprises milky quartz veins along the northwest-trending line of the Nugrus shear zone, where it intersects the Gebel Nugrus monzogranite pluton. Gold-bearing quartz veins form boudinages along the shear zone and are enclosed by a wallrock alteration assemblage that includes sericite, fluorite, and sulfides. Gold is associated with pyrite and chalcopyrite in quartz veins and adjacent wallrocks (Raslan and Ali 2010). It occurs as both free-milling Au grains and as refractory Au in chalcopyrite.

5.4.4 Mubarak–Hamash Block

The Mubarak–Hamash block is located in the middle of the CED (Fig. 5.12) and contains a number of very-famous ancient large gold mines, including *Um Rus*, *Atud*, *Barramiya*, *Dungash*, *Samut*, and *Hamash* deposits/occurrences. The *Um Rus* gold deposit is located ~55 km northwest of Mersa Alam on the Red Sea (Fig. 5.12), which is a well-known occurrence of Au-bearing quartz veins associated with a late- or postorogenic I-type tonalite–granodiorite intrusion. The Um Rus intrusion (Fig. 5.15) exhibits a simple zoning pattern with a granodiorite core that grades outwards to a tonalitic margin. The meladiorite zone, ~200 m wide, is characterized by abundant mafic xenoliths, surrounds the Um Rus intrusion, and separates it from the country gabbroic rocks (Klemm and Klemm 2013; Zoheir et al. 2020). The crystallization age of the Um Rus intrusion was determined by in situ sensitive high-resolution ion microprobe (SHRIMP) $^{206}Pb/^{238}U$ and $^{207}Pb/^{235}U$ measurements on accessory monazite grains. The resultant monazite U–Pb mean age (643 ± 9 Ma) roughly overlaps the existing geochronological data for similar granitic intrusions that are confined to major shear systems and are locally associated with Au mineralization in the CED (e.g., Fawakhir and Hangaliya). Gold mineralization is essentially hosted

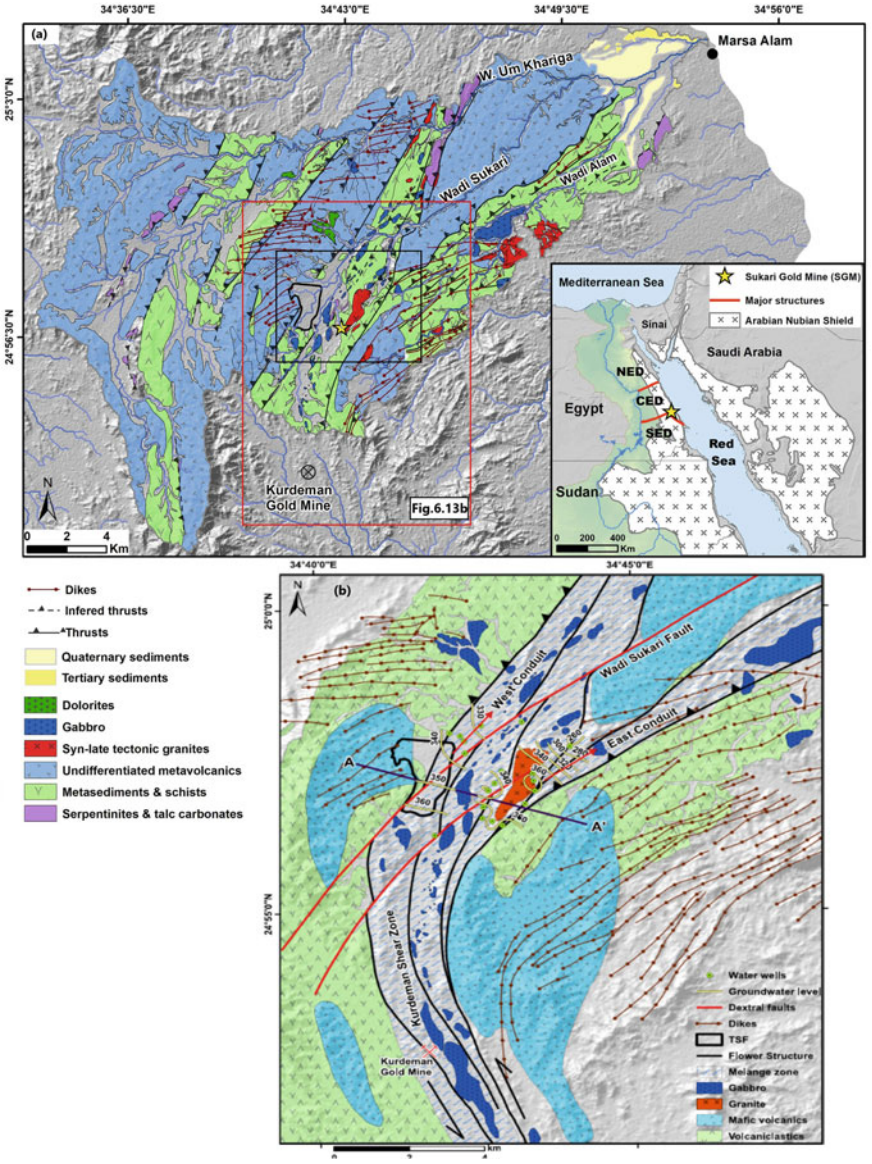

Fig. 5.13 **a** Simplified geological map for the Sukari Au mine and surroundings draped over a digital elevation model (after Abdelaal et al.2021). Inset shows the distribution of the ANS outcrops, the subdivisions of the Eastern Desert (NED, CED, and SED), and the location (asterisk) of the Sukari Au mine. **b** Enlargement of the map area outlined by the red box in Fig. 5.13a showing the major rock units and structural trends (after Abdelaal et al.2021)

Fig. 5.14 General overview of the large-scale open-pit Sukari Au mine of the Eastern Desert of Egypt

in north-northwest–, north- and north-northeast–trending milky and smoky quartz veins, with variable abundances of carbonate and Fe-Cu–Zn–Pb sulfides (Harraz and El-Dahhar 1993; Klemm and Klemm 2013). The geometry and structural styles (i.e., pinch-and-swell, bifurcation, brecciation) of the auriferous quartz veins indicate that hydrothermal fluids migrated along synthetic and antithetic shears of the Wadi Mubarak system, and deposited Au in D3 structures (Zoheir et al. 2020).

Modern exploitation of the Um Rus gold mine was commenced between 1900 and 1907 when 19,000 t of ore were excavated, containing 3055 oz of Au and 11.9 oz of Ag (Harraz and El-Dahhar 1993). First estimation of ore reserves in the mine was carried out in 1937–1938 by the Um Rus expedition of the "The Central Administration of Mines and Quarries", providing 10,352 t of ore containing 3985 oz of Au. This was performed through drilling down some 500 feet and sampling of the old workings in the upper three main lodes at 6 ft intervals. In 1940, further development of the mine was carried out, proving an additional 5800 t of ore with an average grade of 10.85 g/t Au. During the period of 1943–1946, some 9370 t of the ore were mined, leaving ~6782 t in situ. The Um Rus gold deposit is promising in terms of its commercial

concentration of Au and regularity in downward increase of Au content in the quartz veins. The total assured reserves are 16,000 t, with an average grade of 11 g/t Au (Hussein 1990).

The *Atud* gold occurrence is located in the CED, ~60 km west of Marsa Alam and ~5 km south of the Idfu–Marsa Alam asphaltic road; it is mostly located in the central part of the Mubarak–Hamash block (Figs. 5.12 and 5.16a). The Atud gold mine was excavated, for the first time since Pharaonic times, between 1952 and 1969; it has not produced ore since then. During this latter period, three expeditions have been carried out by the Geological Survey of Egypt, performing surface and underground prospecting work in the main Atud area. During these expeditions, the first, second, and third levels were excavated; drifting was done on the three levels along strike of the main lode (north-northwest to south-southeast directions) for more than 200 m for each level. The width of each level is ~2 m and the vertical distance between levels is ~22 m. Three inclined shafts, known as the north shaft, intermediate shaft, and main shaft, were dug into the mine down the dip of the lode at variable distances; depths for these shafts range from <20 m to 50 m.

The Atud gold deposit is considered to be an orogenic-Au deposit, where it occurs in quartz veins mainly hosted in Neoproterozoic dioritic rocks of Gebel Atud (Harraz 2002). However, Abdelnasser and Kumral (2017) suggested that the Atud gold occurrence is an intrusion-related deposit, due to its relationship to the diorite intrusion. The Atud gold deposit is spatially and genetically associated with a metagabbro–diorite complex called "the Atud gabbro–diorite intrusion" that is emplaced at shallow levels within serpentinite, metavolcanic, and metasedimentary rocks (Fig. 5.16b) (Harraz 2002; Stern et al., 2020). The Atud gabbro–diorite intrusion is a small Neoproterozoic plutonic body (3 × 3 km) in the Eastern Desert of Egypt that intruded into metasedimentary and ophiolitic rocks (Fig. 5.16b). The eastern half of the intrusion is dioritic and the western half is gabbroic in composition (Fig. 5.16b). The hornblende diorite is comparatively highly altered and is generally thought to be significantly older than the gabbro; it is the main host of the Au mineralization in the Atud area (Stern et al. 2020). The Au mineralization of the Atud occurrence comprises north-northwest-dipping Au- and sulfide-bearing quartz and quartz carbonate veins in a southwest-verging thrust in dioritic wallrocks. Early Au-poor, pyrrhotite–arsenopyrite–pyrite–bearing quartz veins were paragenetically followed by the formation of Au-rich, sphalerite–arsenopyrite–pyrite–galena–chalcopyrite–bearing quartz veins, and then later by pyrite–galena–bearing quartz carbonate veins. Gold occurs as free Au inclusions (ranging in size from 5 to 20 μm in diameter) in quartz and as smaller inclusions (<5 μm in diameter) in arsenopyrite and pyrite (Abdelnasser and Kumral 2017). Gold is also present in fractures and at grain boundaries of pyrite, arsenopyrite, and base metal sulfides.

The *Barramiya* gold occurrence is one of the most-studied gold deposits in Egypt overall, in the Mubarak–Hamash block in particular. The Barramiya gold mine lies in the southwest of Barramiya district, which in turn is located in the western flank of the basement rocks of the CED (Figs. 5.12 and 5.17). The Barramiya district is dominated by ophiolitic rocks, ophiolitic mélange, and syntectonic granitoids (Figs. 5.17 and

5.18a). The ophiolitic rocks are represented mainly by serpentinites and their derivatives (talc carbonates, graphite schists, and listwaenites). The ophiolitic mélange is dominated by repeated slices of highly sheared serpentinites and metavolcanic and metasedimentary rocks formed by frequent thrusting (Zoheir and Lehmann 2011). The Barramiya gold occurrence (main lode) is hosted in one of these thrust slices with sepentinites and their sheared derivatives on the hanging-wall and metavolcanic and metasedimentary rocks on the footwall (Fig. 5.19). The main Au-bearing quartz vein (main lode) extends within the sheared rocks of the hanging-wall along the strike (east/west direction) for >1 km (Fig. 5.19). The mineralized zone consists of quartz and quartz carbonate veins, which are 10 cm–1 m wide and extending as much as 1 km along strike and 400 m down dip.

The Au-bearing quartz veins of the Barramiya Au occurrence as a whole are hosted in the graphite schist and are known (by local mining workers) as the main lode, Taylor's reef, Caunter lode, and New Caunter lode. The main lode extends for ~1 km in an east/west direction, dipping steeply (80°) northwards, shows several pinches and swells with an average thickness of ~1 m, and splits into and is accompanied by smaller parallel veinlets and stringers. It represents the main Au-bearing quartz vein, which is commonly grey-to-bluish-grey in color, variably fractured and brecciated, and occasionally cut by younger carbonate veins. Taylor's reef is only found underground, without surface outcrops, to the north of the main lode. It is almost vertical and extends for ~75 m along the strike in the east/west direction (almost parallel to the main lode), with an average thickness of 0.6 m. The Caunter and New Caunter lodes are two auriferous quartz veins extending in the northeast/southwest direction, dipping steeply to the southeast. They are considered to be the two main underground branches of the main lode that are mostly without surface outcrops. The Caunter lode is built up of a group of auriferous quartz veinlets with small slivers of mineralized graphite schist in between, forming the lode zone, with an average thickness of 60 cm. It was mined for 130 m along strike and 75 m down dip. New Caunter lode is similar in nature to Caunter lode, but with a greater average thickness of ~1 m. It was mined for 90 m along strike and ~115 m down dip. The underground workings in the Barramiya gold mine showed that most of the Au lodes are ended out and lost at a depth of ~150 m.

Sulfide minerals in the quartz carbonate veins and adjacent wallrocks are essentially represented by arsenopyrite and lesser pyrite, with trace amounts of chalcopyrite, sphalerite, tetrahedrite, pyrrhotite, galena, gersdorffite, and Au also present. Gold occurs as free grains and as grains of Au–Ag alloy along microfractures in quartz but mostly as auriferous arsenopyrite. Individual grains of arsenopyrite contain as much as 2200 ppm Au, altered wallrock samples contain as much as 1.37 ppm Au, and quartz veins average 1.59 ppm Au (Botros 2004; Zoheir and Lehmann 2011). The veins are mainly contained in dextral shears, typically in the center of the shear zones, although some veins are in Riedel fractures oblique to the shear zones (Fig. 5.18a, b) (Zoheir et al. 2019a). The estimated ore reserves of different quartz lodes in the Barramiya Au-mineralized area were summarized by Hussien (1990), and are given here, as follows: In the main lode, the still-present ore was estimated to be ~20,000–27,000 t, with Au content of 2.2–15.5 g/t. The ore reserves of Taylor's reef are

estimated to be ~13,800 t, with an average grade of 16.5 g/t Au. The richest bonanza has been recorded in Taylor's reef, which was estimated to contain up to 105 kg/t. The ore reserves of Caunter lode are estimated to be ~2740 t, with Au content ranging 18.69–43.09 g/t, and for New Caunter lode, the average Au content is estimated to be ~8.4 g/t, decreasing with depth. Last, based on trench sampling along the main lode, ACA Howe International Ltd reported an Au content of up to 14.13 g/t (Annual report of Centamin Egypt 2004).

The *Dungash* area is part of the Meulha–Dungash district (Figs. 5.12, 5.17 and 5.18), which belongs to the Pan-African (550–650 Ma) ophiolite zone in the CED; it is located ~20 km south of the Barramiya (Fig. 5.18a, c). The district is mainly covered by metasedimentary and metavolcanic rocks, as well as serpentinites and metagabbro–diorite rocks. The entire rock sequence is interpreted to be a remnant of obducted oceanic crust that has recently been intruded by calc-alkaline (older) and subalkaline to alkaline (younger) granitoid rocks (El-Gaby et al.1990; Khalil et al.2003). The rocks of the Meulha–Dungash district are strongly folded along northwest/southeast- and northeast/southwest-trending axes and are cut by several faults trending in northeast/southwest and northwest/southeast directions. Gold mineralization occurs in an east/west-trending quartz carbonate vein system of ~1.5 km length and ~1–4 m width. The Au-bearing veins contain pyrite, arsenopyrite, chalcopyrite, and galena and are surrounded by alteration zones that pass from proximal quartz–sericite, to sericite, carbonate–sericite, and distal chlorite–sericite alteration (Zoheir et al. 2019a). Mineralogical and textural relationships indicate an early assemblage of arsenopyrite–pyrite–gersdorffite ± pyrrhotite, a transitional pyrite–arsenopyrite ± gersdorffite assemblage, and a late assemblage of tetrahedrite–chalcopyrite–sphalerite–galena–Au. Gold is also present as inclusions in arsenopyrite in the carbonate–sericite alteration zone, along microfractures in pyrite, and along grain boundaries of quartz (Khalil et al. 2003). There is no available ore reserve estimation of for the Dungash Au mine; however, Au concentrations in rock chips and grab samples vary between 1 and 21 ppm (Internal report of the Egyptian Mineral Resources Authority 2006).

The *Samut* gold occurrence is a part from the Muilhah–Dungash district, which is located at the central part of the Mubarak–Hamash block in the CED, ~15 km south of the Barramiya gold mine and very close to the Dungash gold prospect (Figs. 5.12 and 5.20). The Samut Au occurrence is one of the historical small-scale Au mines in the Eastern Desert where abundant ruins of Ptolemaic buildings are widespread at the mine area. It is a proper orogenic-Au type deposit where it is hosted in north- to north/northeast-trending sheared and brecciated quartz veins with abundant clay alteration of gabbro–diorite and quartz–diorite host rocks. The mineralized veins show intense brecciation and comb quartz textures, suggesting repeated episodes of fragmentation (Zoheir et al. 2019b). Gold mineralization was found as free-milling Au grains, which is common in association with deformed pyrite crystals and in recrystallized quartz veins. Fluid inclusion data revealed a minimum vein formation temperature of ~300 °C for the early hydrothermal event. The wide range of pressure estimates for ore-related aqueous carbonic inclusions (~1–3 kbar) suggest the late Au and sulfide deposition was syn-brittle hydrofracturing and vein growth. Pyrite in the

mineralized veins evolved from As-poor to As-rich varieties over the paragenesis. A transitional variety of pyrite, characterized by abundant inclusions of chalcopyrite, galena, and sphalerite, is enriched in As and Au (Zoheir et al. 2019b).

The *Hamash* gold deposit has been discussed in Chap. 4 of this book, where it was considered to be a magmatic–hydrothermal or intrusion-related deposit; however, it is sometimes considered to be of IOCG type. The Hamash mineralization is located at the most southern part of the Mubarak–Hamash block (Fig. 5.12), and consists of north/northwest-trending Au- and sulfide-bearing quartz veins, within a dipping 30–60° west shear zone at the contact between the Hamash granite and meta-andesitic rocks. The Hamash granite is a porphyritic I-type trondhjemite that intrudes island-arc metavolcanic rocks and ophiolitic metagabbro and serpentinite. The mineralized zone extends over a distance of >350 m. Ore mineralogy includes pyrite, chalcopyrite, bornite, chalcocite, arsenopyrite, tetrahedrite, and free Au grains (Hilmy and Osman 1989).

5.4.5 Meatiq–Sibai Block

The Meatiq–Sibai block is one of the most famous regions for historical Au mining in Egypt; it includes the well-known *Fawakhir*, *El Sid*, and *Atalla* gold occurrences. The northern part of the Meatiq–Sibai block is currently the focus of extensive Au exploration by private companies, including Aton Resources Inc. (formerly Alexander Nubia International Inc.), in a concession area extending from the Abu Marawat to the Hamama occurrences. There are numerous Au occurrences and deposits in this district, including *El Sid, Fawakhir, Atalla, Gidami, Abu Marawat, Semna*, and many other occurrences (Fig. 5.12). The El Sid, Fawakhir, and Atalla gold deposits are the famous ones, which are located along the north/northwest-trending Atalla shear zone, part of the Najd fault corridor of the CED (Fig. 5.21). The Atalla shear zone contains the Fawakhir pluton that hosts the auriferous quartz veins at Fawakhir and El Sid, and the Atalla pluton that hosts the Atalla occurrence (Fig. 5.21). Other lithologies along and west of the shear zone include ophiolitic serpentinites, metagabbros, metabasalt, meta-andesite, and metasedimentary rocks of the Abu Ziran group that are presumably correlative with the 760–735 Ma island arc assemblage more widely developed in the Wadi Kareim–Wadi El Dabbah area (Zoheir et al. 2015), as well as the Dokhan volcanics and Hammamat group of molasses sediments (Fig. 5.22).

The *Fawakhir–El Sid* mining district is one of the most important Au-producing districts in ancient Egypt. It is located midway between the Nile River and the Red Sea, along the Quseir-to-Quft asphaltic road in the CED (Fig. 5.12). Ancient Au mining in the area is documented since the Old Kingdom (~2700 BC), with peaks in Au production during the New Kingdom (~1500 BC), the Ptolemaic period (~200 BC), and the Arab period (~1200 AD) (Klemm and Klemm 2013; Zoheir et al. 2015). Ruins of an ancient mining settlement, including numerous stone huts, ceramics, and different types of millstones, are dispersed close to an old freshwater well (Bir Um Fawakhir) (Fig. 5.22). There is evidence for Pharaonic up to Coptic/Byzantine mining

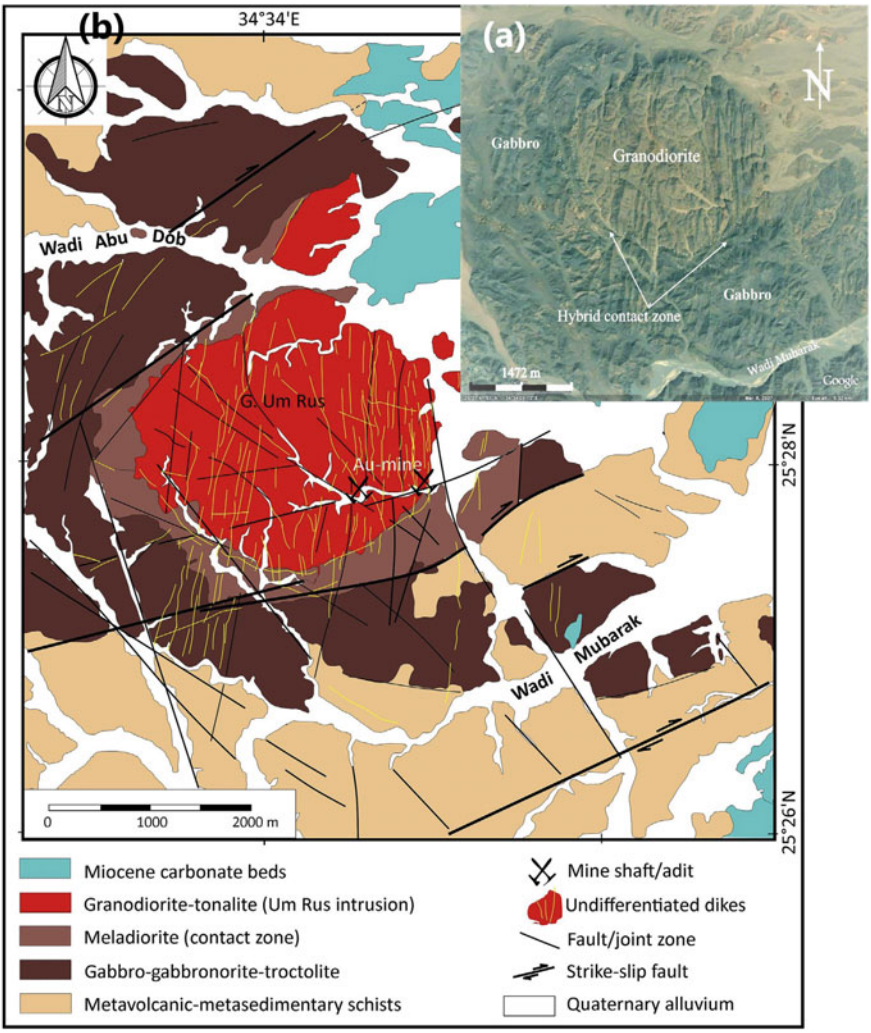

Fig. 5.15 **a** Satellite image showing the Um Rus granodiorite intrusion and surrounding hybrid contact zone with gabbro. **b** Geological map of the Um Rus tonalite–granodiorite intrusion and Au mine area (after Zoheir et al.2020)

activity in the area; the extensive heliographic inscriptions on rock surfaces along the Wadi Hammamat attest to mining for Au and ornamental stones since the New Kingdom's Nineteenth Dynasty (Harrell and Brown 1992; Klemm and Klemm 2013). At the Fawakhir area, the Au-bearing lodes extend east/northeast at a sharp angle in the main direction of the shear zone, and dip toward the south in a ~40-m-wide zone of shearing and hydrothermal alteration. Individual veins extend for several hundred meters along strike and vary in width from a few centimeters to greater than one

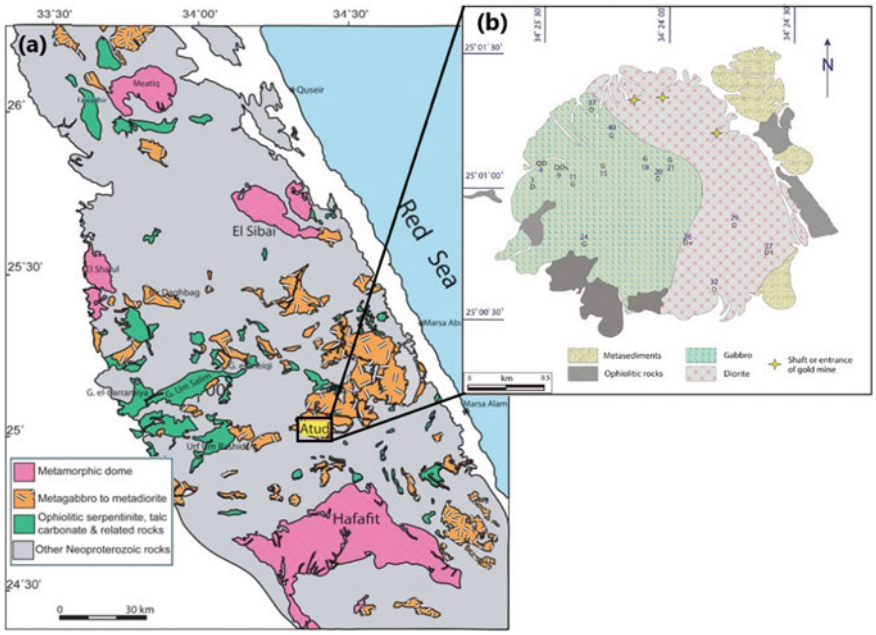

Fig. 5.16 **a** Simplified geological map of the CED of Egypt showing the distribution of Neoproterozoic basement rocks and the location of Atud Au mine area. **b** Simplified geological map of the Atud intrusion showing the Au mine area, letters refer to the lithology and numbers are sample numbers from Stern et al. (2020)

meter (Zoheir et al. 2015). At the El Sid area, the veins form a stockwork that is ~100 m across. The Fawakhir ores are composed of massive and laminated quartz with subordinate calcite and sericite. Ore mineralogy at both Fawakhir and El Sid includes early Fe-As ± Cu-sulfides replaced, in part, by Zn-Pb-Sb sulfides, Au, and Bi-tellurides (Harraz 2000; Zoheir and Moritz 2014). The mineralized quartz veins were mined through a number of pits, trenches, adits, and vertical shafts. The El Sid Mining Company produced ~5 t Au from quartz veins, with an average grade of ~30 g/t, from the underground mining until 1958. Although there is no recent ore resources/reserves estimation, the mineralized veins at both the Fawakhir and El Sid occurrences gave average grades from 1.5 to 22.6 g/t Au, and locally as much as 30 g/t Au (Hussein 1990; Harraz 2000).

The *Atalla* Au occurrence is located ~20 km north of the Fawakhir occurrence (Figs. 5.12 and 5.21) in the CED. It is hosted by the Atalla monzogranite intrusion along north/northwest-trending major sinistral shear zone, namely the Atalla shear zone. The Atalla gold occurrence has a long history of mining and exploration since Pharaonic times until the early twentieth century. Most ruins of old mining in the area belong to the Early Arab Period (Klemm and Klemm 2013); however, significant tailings and workings are related to mining activities during British colonization in the early twentieth century. Gold-bearing quartz veins in the Atalla area are confined

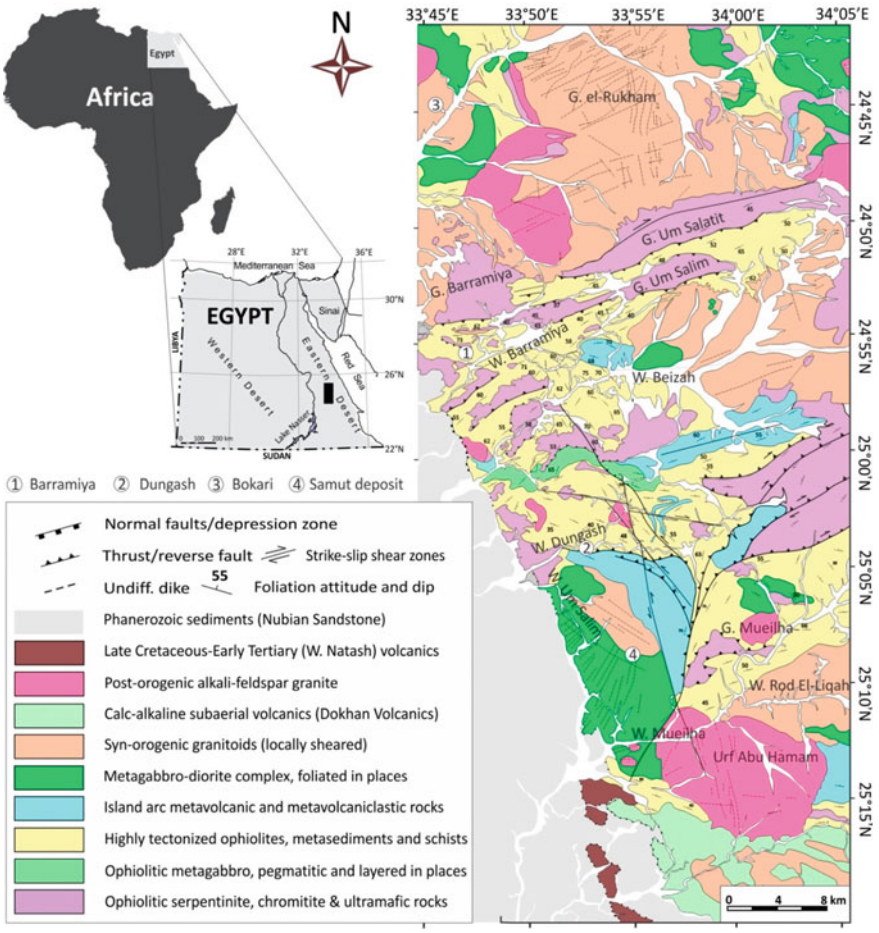

Fig. 5.17 Simplified geological map of the Barramiya–Mueilha sector in the western part of the CED of Egypt (after Zoheir et al. 2019b)

to fault/shear zones that cut mainly the Atalla granitic intrusion. The association with late tectonic granitoid intrusions along the same controlling shear zone assumes that the Atalla and El Sid Au mineralization have identical genetic models related to the same tectonic and/or magmatic activities in the period of ~600 Ma (Zoheir and Moritz 2014; Zoheir et al. 2015). The auriferous veins consist of milky, greyish-white, and smoky fragmented quartz along brittle–ductile northeast- and east/northeast-trending shear zones in the monzogranite, perpendicular to the Atalla shear zone. The main Au-bearing quartz vein extends for ~274 m in a northeast direction and was worked to a depth of >100 m. The age of mineralization was deduced using $^{40}Ar/^{39}Ar$ dating and gave a plateau age of 601 ± 5.5 Ma, which is very close to the age of the Fawakhir Au-forming event at 601 ± 17 Ma (Zoheir et al. 2015).

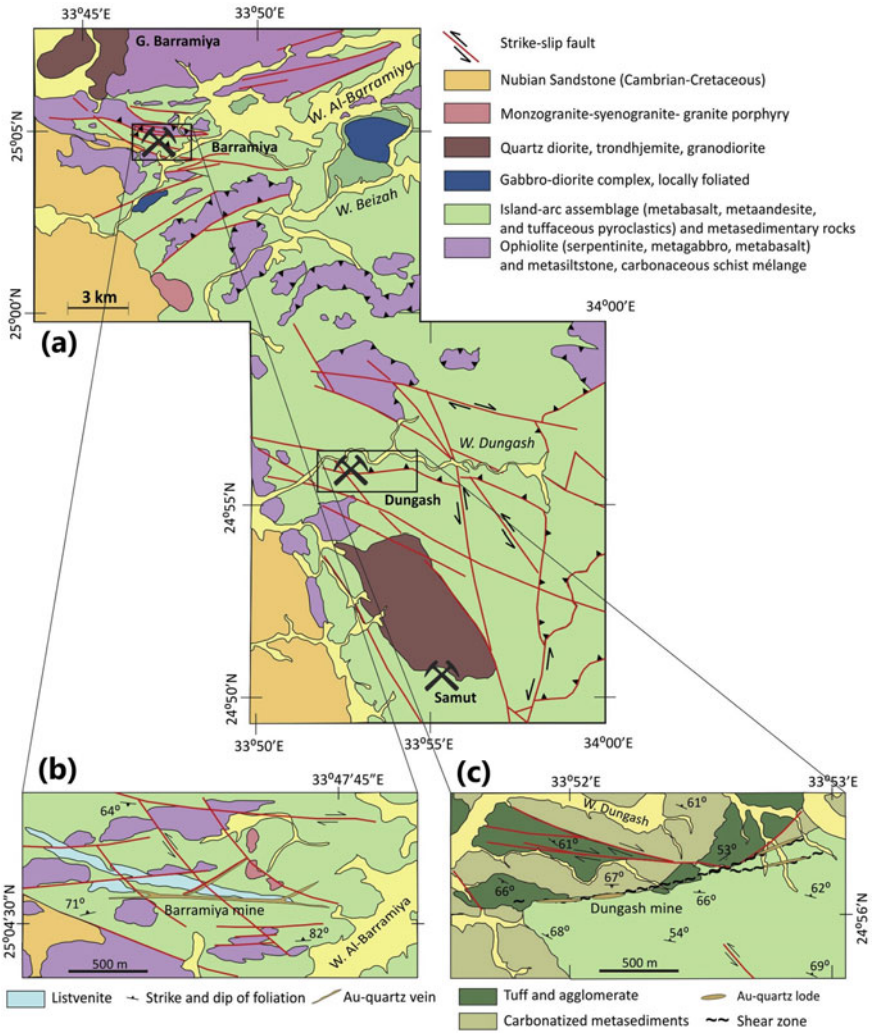

Fig. 5.18 **a** Simplified geological map of the Barramiya–Dungash area of the Mubarak–Hamash block, **b** deposit scale geology of Barramiya Au mine, and **c** deposit scale geology of Dungash Au deposit (after Zoheir et al. 2019a)

The *Abu Marawat* concession (owned by Aton Resources) is located in the CED, ~200 km north of Centamin's Sukari Au mine. It contains more than eighteen Au prospects of various deposit types including: polymetallic epithermal VMS occurrences as those in Hamama and Rodruin that containing Au–Ag mineralization in an iron oxide cap developed above a primary sulfide zone (Bampton 2017; Ordūna 2018), Au-Cu mineralization in quartz veins, anomalous Au mineralization in banded iron formation (Botros 2004), and many of them classified as orogenic-Au deposits.

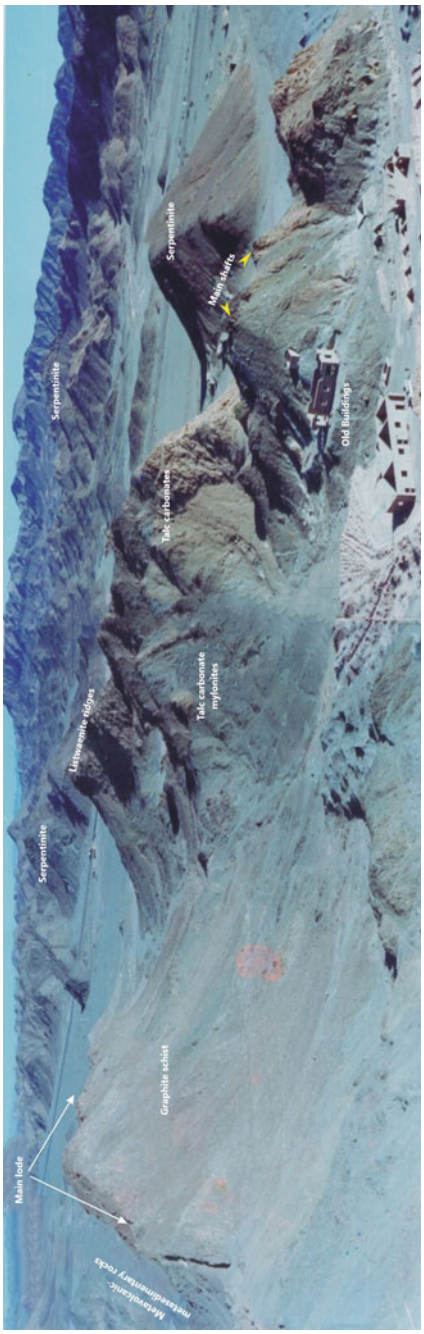

Fig. 5.19 Panoramic field view of the Barramiya Au mine and surrounding lithology showing the old buildings and different rock types in the Barramiya area

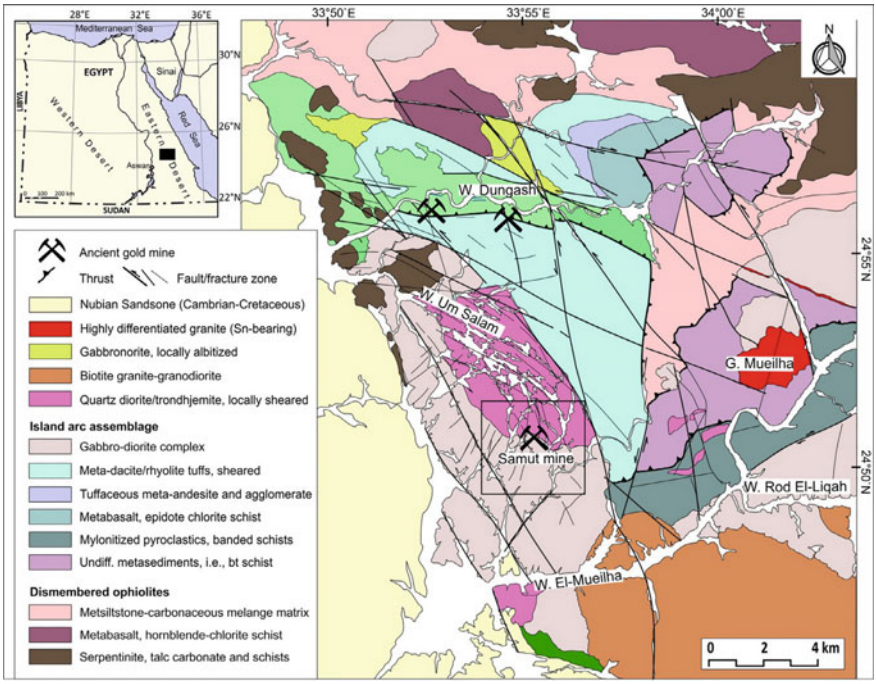

Fig. 5.20 Geological map of the Mueilha–Dungash terrane in the CED of Egypt (after Zoheir et al. 2019b)

Aton has identified numerous Au occurrences throughout the entirety of the concession area, including the Hamama deposit in the west and the Abu Marawat polymetallic deposit in the northeast (Fig. 5.23). The genesis of Au-bearing quartz veins in the Abu Marawat area is controversial; they have been interpreted as a reef- or breccia-vein type, or as a sheared VMS deposit (Valliant and Salmon 2012), as well as they have also some characteristic features of orogenic Au deposit (Zoheir and Akawy 2010). The Abu Marawat Au mineralization comprises a system of north-trending massive and sheared, milky quartz-sulfide veins hosted by an intensely altered sequence of island-arc metavolcanic and metavolcaniclastic rocks and banded iron formation, very close to a north-trending Najd fault containing sheared serpentinite (Zoheir and Akawy 2010). The Au-bearing quartz veins have a complex history including shearing textures, repeated filling and deposition, microbrecciation, and crack-seal quartz precipitation. Sulfide minerals essentially include pyrite and lesser amounts of chalcopyrite, pyrrhotite, sphalerite, and galena. Gold presents as refractory in pyrite and chalcopyrite, and is locally present as visible native Au, electrum, and Au-tellurides. The vein system comprises two main quartz veins and subparallel less-mineralized quartz veins extending over ~800 m along strike and 20–250 m depth. Quartz-rich gossans are the main surface expression of the Au-bearing quartz

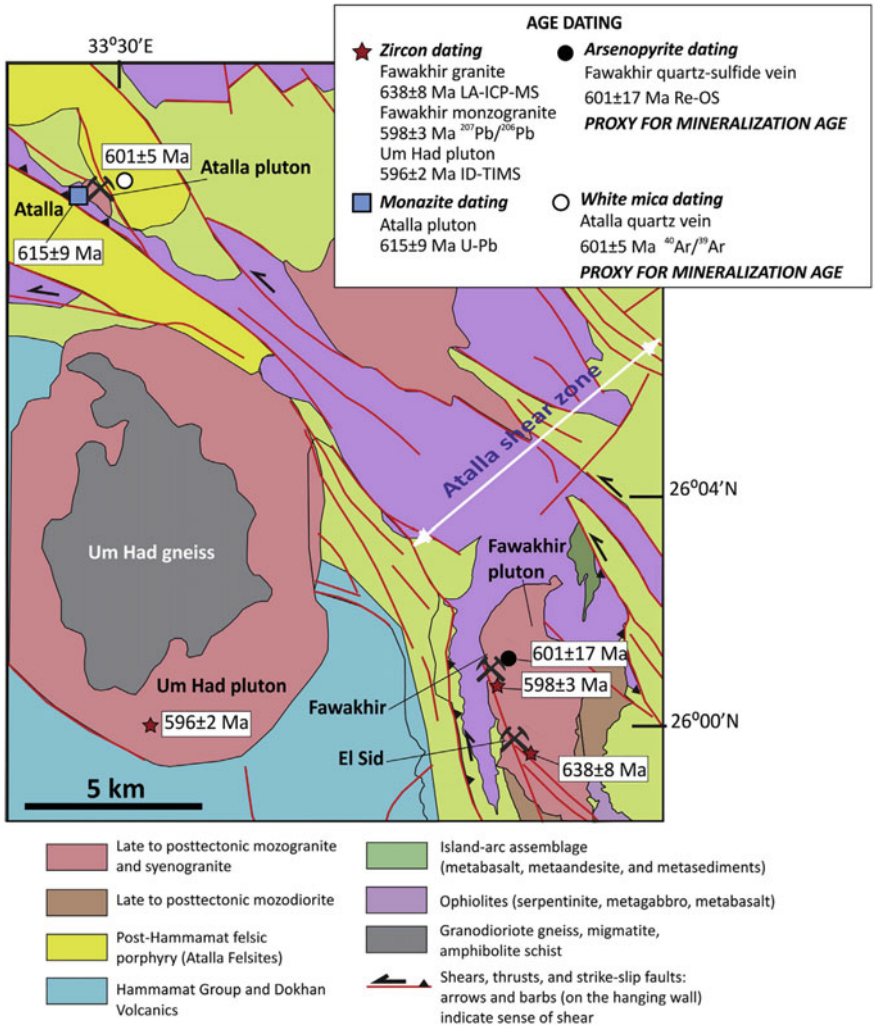

Fig. 5.21 Simplified geological map of the Fawakhir–Atalla area of the Meatiq–Sibai block showing the locations of Au occurrences in relation to the Najd faults and adjacent plutons, and available geochronologic information (after Zoheir et al. 2019a)

veins. Hydrothermal alteration includes pervasive silicification, pyritization, sericitization, and carbonatization. The estimated inferred ore resources of the deposit based on 98 diamond drill holes of a total 19,573 m is 2.9 Mt ore, with average grades of 1.75 g/t Au, 29.3 g/t Ag, 0.77% Cu, and 1.15% Zn (Bampton 2017).

The *Semna* Au occurrence is located ~10 km southwest of the Abu Marawat deposit (Figs. 5.12 and 5.23). The Semna area has a long history of Au mining, during both ancient and modern times; it contains archaeological evidence suggesting that

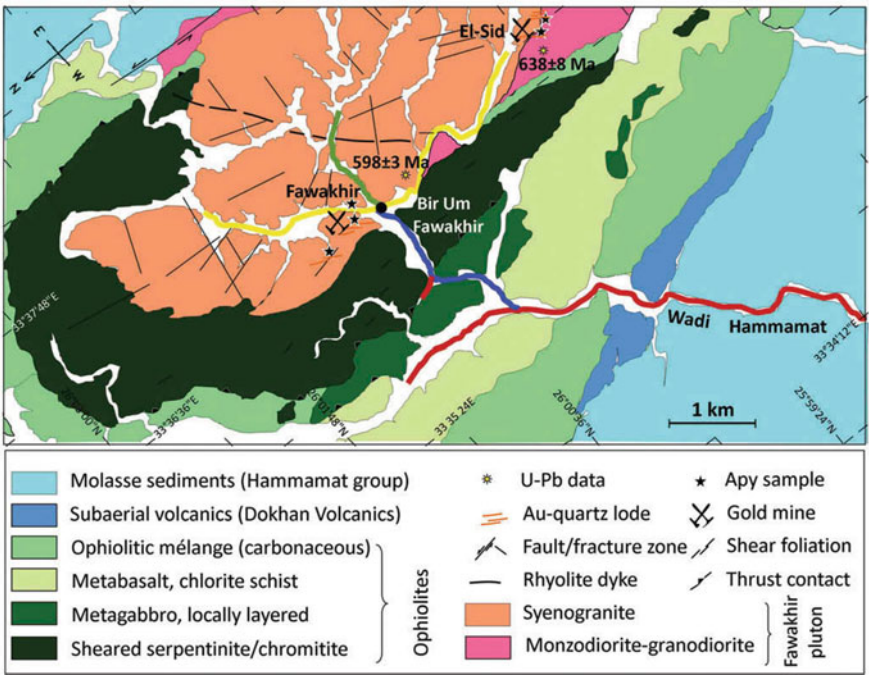

Fig. 5.22 Geological map of the Fawakhir–El Sid Au district (Zoheir et al.2015). The arsenopyrite sampling locations and the locations of two rock samples dated by U–Pb geochronology on zircon are also given

Semna was first mined during the Old Kingdom period, > 4500 years ago. In modern times, Semna was exploited by the British during the early twentieth century. The exploited Au-bearing quartz vein at Semna is the widest vein mined by the British in Egypt, reaching up to 6 m in width in places, with mining grades > 2 oz/t being reported. The ore pillars found within ancient stopes assayed up to 5.5 oz/t. The Au mineralization at Semna is essentially hosted in a quartz diorite body that has intruded into a package of metasedimentary rocks with banded iron formation horizons. The mineralization zone is strongly structurally controlled and is hosted in a series of steeply dipping shear zones that contain at least four zones of Au-bearing quartz veins that noticeably pinch and swell. The orebodies exhibit a complex structure of massive and brecciated quartz, where the textural, structural, and mineralogical evidence suggest vein formation during active faulting. The ore mineral assemblage includes pyrite, chalcopyrite, and subordinate arsenopyrite, galena, sphalerite, and gold. The exact deposit type of Semna, whether it is an orogenic Au type or epithermal-vein type, is uncertain, because the mineralogy of the occurrence is strongly suggestive of high-sulfidation epithermal mineralization (Zoheir et al. 2019a). Channel sampling at the surface (Aton Resources Inc., November 2020) returned mineralized intervals

including 9.7 m with an average grade of 5.17 g/t Au, 6.9 m with grade 4.24 g/t Au, and 10.8 m with average grade of 2.43 g/t Au.

The *Sir Bakis* (*Gidami*) Au mine is located ~10 km northwest of the Rodruin, ~12 km northeast of the Hamama, and ~24 km southwest of the Abu Marawat occurrences (Figs. 5.12 and 5.23). It was operated by the British from 1904 to 1906 and exploited a 1.5-m-wide quartz vein underground, which can be traced for ~1.5 km at the surface. There are also very extensive remains of ancient mine workings and settlements in the general Sir Bakis area, dating back to the New Kingdom and Ptolemaic periods. In addition to the extensive individual high-grade auriferous quartz veins at Sir Bakis, there is also evidence for potential intrusion-related Au mineralization in a sheeted vein swarm, associated with the intrusion of late post-orogenic pink alkali granites into older grey granites. To the northwest of the main auriferous vein, swarms of smaller north/northwest- or north-trending veins were extensively mined out during the ancient times. Most of the mineralized quartz veins

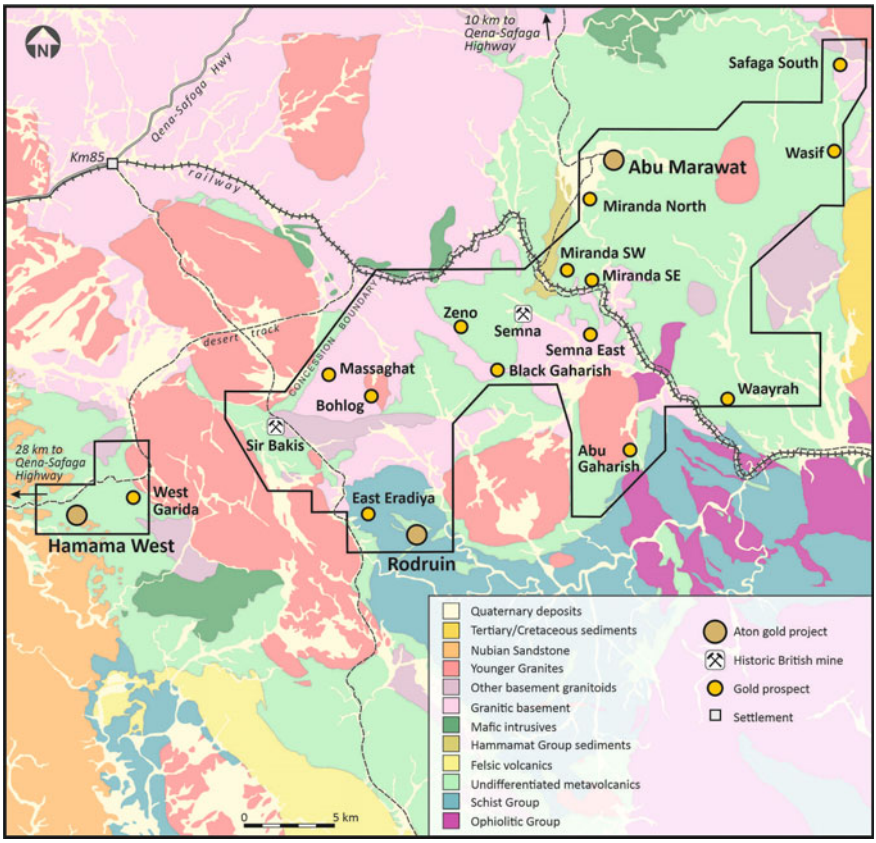

Fig. 5.23 Simplified geological map of the Abu Marawat concession of NED of Egypt showing the locations of numerous Au prospects of different mineralization styles (Aton Resources Inc 2020)

cut a granite and diorite intrusive complex, and less commonly extend beyond the boundary between the intrusion and siltstone conglomerate of the Hammamat group molasses sediments. The mineral assemblage includes Au, pyrite, sphalerite, chalcopyrite, and galena. The presence of disseminated calaverite and hessite in the mineralized quartz veins suggested Au deposition from aqueous carbonic fluids at ~250 °C (Klemm et al.2001). Aton Resources carried out surface sampling in 2017 at Sir Bakis, returning assays of high-grade ore that demonstrated 150, 32.9, and 29.5 g/t Au from individual samples. In addition, excavator-dug trenches over the sheeted vein system returned mineralized intervals of 109.1 m with an average grade of 0.21 g/t Au, and at 45.85 m gave average grades of 0.36 g/t Au, suggesting a potential for the development of a low-grade ore body of intrusion-related style of mineralization at Sir Bakis.

The *Abu Gaharish* occurrence is located at ~ 16 km south of the Abu Marawat mine (Fig. 5.23). It is a Sukari-style structurally controlled potential intrusion-related Au mineralization covering an area more than 5 km along strike of the the eastern margin of the Gaharish granite. The Au-bearing quartz veins are confined to the eastern boundary of an oval (north/south) granitic intrusion (Gebel Abu Gaharish) emplaced within siltstone and conglomerate (Hammamat group), with a well-developed hornfels zone (Klemm and Klemm 2013). The occurrence is considered to be a reduced intrusion-related Au deposit (Ordūna 2018); however, more information is needed to accurately classify this occurrence. Auriferous quartz veins occur in two main zones (Abu Gaharish, both north and south). Assaying of more than 100 grab and channel samples (https://www.atonresources.com/) returned significant Au concentrations of up to 27 g/t. Surface channel sampling results included 31.2 m with an average grade of 1.04 g/t Au, and at 3.6 m with an average grade of 11.05 g/t Au.

5.5 Orogenic Deposits in Sudan

As summarized in Chap. 2 of this book, the ANS in Sudan is composed of three main juvenile Neoproterozoic volcanic terranes that formed in an island arc/back-arc basin setting and were subsequently metamorphosed to greenschist facies during accretion/East African Orogeny (Fig. 5.24). These Neoproterozoic terranes are referred to as the Barka–Nafka (870–840 Ma), Haya (870–790 Ma), and Gebeit/Gabgaba (830–720 Ma) terranes (Fig. 5.24). The earliest major tectonic features of the ANS in Sudan are the arc–arc accretionary sutures that formed during the collision and accretion of these terranes and now form the boundaries between them. There are four main suture zones separated by these tectonic terranes: the Nakasib, Onib–Sol Hamed, Barka, and Atmur Delgo suture zones (Fig. 5.24). The Atmur Delgo suture zone is a greenschist facies Neoproterozic oceanic/island arc formed during the collision of the Palaeoproterozoic Bayuda and Halfa terranes during the accretion of the ANS to the Sahara/Nile craton. During the East African Orogeny (~650–600 Ma), the largely formed ANS collided with the Sahara/Nile craton along a north/south-trending suture zone, extending from southern Kenya to southern Egypt (Burke and

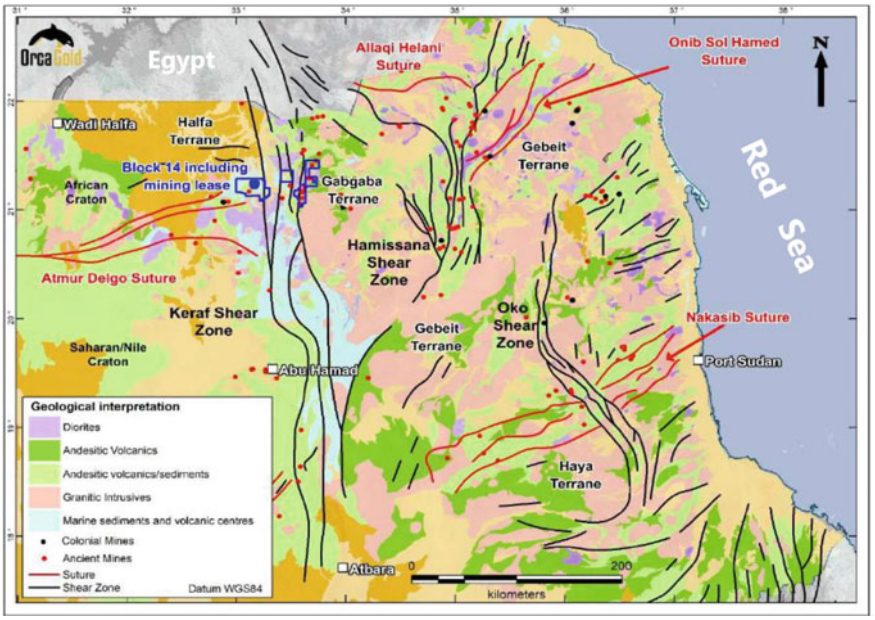

Fig. 5.24 Regional schematic geologic map of northeastern Sudan showing the assemblage of arc-accretionary belts of the Neoproterozoic age accreted to the African craton to the west. Points indicate the locations of ancient and colonial mining activities (after Abanyin et al. 2015)

Sengor 1986; Johnson et al.2013). In Sudan, the exposure of this suture zone is known as the *Keraf suture zone*; it is an arc-continental suture with a complex, polyphase deformation history extending for ~500 km long, trending in the north/south direction (Fig. 5.24). It is a fault-bound wedge of metamorphosed marine sediments varying in width from 30 km in the south to 80 km in the north. The Keraf suture zone is a complex belt that varies from north to south in terms of lithology, deformation, metamorphic history, and intrusive events (Gaboury et al.2020). Lithologies in the Keraf suture zone comprise siliciclastic and carbonate-rich metasediments, which intercalate with sills of metabasalt and microdiorite and post-tectonic granitoids and diorites.

In the Nubian Shield of Sudan, the orogenic mineral deposits are essentially represented by orogenic Au deposits, which are widespread in northern and eastern Sudan in the Red Sea Hills area, as well as in the Nubian Desert of north central Sudan (Fig. 5.25). In general, Au in the northern part of Sudan has been mined since the Pharaonic period, ~6000 years ago (Klemm et al.2001; Klemm and Klemm 2013). Sudan ranked as the third-leading producer for Au in Africa, after South Africa and Ghana. Although Sudan has a substantial Au endowment and long history of Au production, there are so few recent scientific studies of Au deposits (e.g., Almond et al. 1984; Cheng et al. 2017; Adam et al. 2020; Perret et al. 2020; Gaboury et al. 2020), mostly due to the political instability, sanctions, and embargos that have

restricted physical access in recent decades. The intensive prospecting and exploration work carried out by the Geological Research Authority of the Sudan (GRAS), through its joint ventures, have permitted assessment of the precious metal potential in Sudan in general and the Red Sea Hills region in particular. New mineralization styles have been discovered and additional information is being gained regarding Au mineralization in conjunction with the Pan-African tectonic evolution of the region (Elsamani et al. 2001). It is noteworthy that the majority of ancient Au mines and prospects in Sudan are located in the central and northern parts of the Red Sea Hills (Fig. 5.25). Geographically, Au-bearing deposits in Sudan are distributed along three tectoni belts (Elsamani et al. 2001): Ariab–Arbaat, Sinkat–Serakoit, and Abirkateb–Hamisana, which correspond to three suture zones separating three domains: Gebeit-Sasa, Gabgaba, and the southern Red Sea Hills (Fig. 5.25). Other Au prospects and ancient mines lie along the Nile in the Northern Province.

Genetically, Au mineralization occurred in different forms corresponding to at least the three following geological environments: volcanogenic-associated massive sulfides (Au-bearing VMS), associated with silica and massive lenticular barite bodies, and orogenic Au in quartz veins along shear zones. The majority of Au-bearing occurrences, of different styles, in Sudan have been, and are to this day, mined through small-scale artisanal Au mining activities (Fig. 5.26), which contribute ~85% of the national Au production of the country; detailed information is not available ~many of these occurrences. The Hamisana shear zone overprinted and displaced the Allaqi–Heiani–Onib–Sol Hamed suture zone at the southern end of the Eastern Desert terrane (Fig. 5.25) by as much as 50 km (Stern et al. 1990). The Oko shear zone overprinted and sinistrally offset the Nakasib suture by as much as 10 km. The main controls on Au mineralization in this part of the Nubian Shield are the Hamisana and Oko shear zones, the Keraf suture zone, and volcanic assemblages along the Nakasib, Allaqi–Heiani–Onib–Sol Hamed, and Keraf sutures (Johnson et al. 2017a, b).

Orogenic Au mineralization in the Sudanese Nubian Shield rocks is essentially concentrated along the Hamisana shear zone, as well as along the Keraf, Allaqi–Heiani–Onib–Sol Hamed, and Nakasib sutures (Fig. 5.25). This type of Au mineralization is the most abundant throughout the region; it occurs exclusively in the form of auriferous quartz veins from which considerable amounts of Au have been extracted. The quartz veins are confined to either first- or second-order shear zones. The *Gabgaba* (also called Qbgbih) deposit is the oldest occurrence at which mining activates were started in the area along the Keraf suture zone, along which more than 20 Au-bearing sites are located. Exploration is underway elsewhere along the Keraf suture at the *Gabgaba*, *Galat Sufa South*, *Negeim*, *Kimaweit*, *Artoli*, and *Umtrambiesh* prospects, and along the Nakasib suture at *Kamoeb* (Fig. 5.27). All of these Au mineralization sites are hosted by quartz veins and veinlets with very low sulfide contents (<1%) and traces of muscovite, sericite, biotite, chlorite, and carbonate minerals. The north central Sudan Au occurrences are considered to be an orogenic-Au type because they share the same characteristics, in terms of structural settings, styles, and hydrothermal alterations, as classic orogenic-Au deposits (Gaboury et al. 2020).

In some cases, Au is associated with the disseminated sulfide minerals in the wall rocks. Commercial Au mining in Sudan is presently restricted to the Gabgaba area operated by Manum, a subsidiary of the Moroccan mining group Managem. The *Hassai* Au mine, the first commercial Au mine in Sudan, which produced Au from oxidized massive sulfide lenses (Barrie et al. 2016), closed in 2014 after 21 years of production. Other significant Au deposits, such as the Galat Sufar South and nearby Wadi Doum deposits (Orca Gold Ltd.), are at the development stage. In addition, another major obstacle is the lack of reliable modern tectonostratigraphic geological maps, although the rocks are generally well-exposed. Following is a summary of the available information ~of the orogenic-Au deposits/occurrences in north central Sudan.

The *Wadi Gabgaba* region is famous for Au mineralization since ancient times; it was mined by the Nubians, the ancient Egyptians, the Ottomans, and the British. The Gabgaba occurrence, along with many other Au-bearing deposits in the region, is located within the broad Keraf suture zone (Fig. 5.27). The Wadi Gabgaba and nearby Au-bearing deposits in the region are hosted by rocks dominated by greenschist to amphibolite siliciclastic and carbonate-rich metasedimentary rocks (turbidites) intercalated with sills of metabasalt and microdiorite and some pillow basaltic lavas, with lesser amount of high- to intermediate-grade gneisses, ophiolitic nappes and molasses-type sedimentary rocks cut by various types of syn- to post-tectonic granitic intrusions (Fig. 5.27) (Bailo et al. 2003). More than 20 Au-bearing sites and deposits are distributed in an area of 250 km (northwest-to-southeast) × 100 km (southwest-to-northeast) in northern Sudan (Fig. 5.28). Gold mineralization zones have been systematically exposed by artisanal mining or by commercial operation. Based on the interpreted structural elements in the area (Gaboury et al. 2020), there are two main Au-bearing structural north/south-trending corridors, the East Corridor and the West Corridor, in addition to numerous intrusive bodies, which are mostly subcircular, and ranging in size from 2 to 25 km (Fig. 5.28). The West Corridor extends for more than 250 km and hosts numerous Au-bearing deposits/occurrences including, from north to south: West Gabgaba (WG-03), Central (C02-C04), UTM, WG-14, Toubi, Anas, northwest, and Shereik occurrences (Fig. 5.28). The East Corridor, on the other hand, extends for ~300 km and hosts some Au-bearing sites, including the Negeim, southwest, and Yasmine mineralized occurrences (Fig. 5.28) (Gaboury et al.2020).

Recent studies (Gaboury 2015; Gaboury et al. 2020) identified and characterized three main Au deposits in the Gabgaba area: *WG-03*, *UTM*, and *Central* (Fig. 5.28). The WG-03 deposit is a complicated structurally controlled (orogenic) Au deposit hosted in a metamorphosed gabbroic complex (Gaboury 2015). Gold occurs in three different modes: early east/west-trending shallow north-dipping S1 shear zones manifested by amphibole foliation, north/south-trending subvertical S2 shear zones manifested by biotite schistosity, and late extensional centimeter-size quartz veins oriented east/west and dipping moderately north. These later veins also occur in S1 and S2 shear zones. The WG-03 deposit is hosted close to the east-trending Atmur–Delgo suture, ~30 km from the north-trending Keraf shear zone (Figs. 5.27 and 5.28). The Central deposit includes two zones, CO_2 and CO_4, in which the Au-bearing quartz

veins are hosting by felsic dykes (up to 15 m in thickness), which are oriented approximately north/south with a steep dip to the east. These felsic dykes cut across vertical sedimentary sequences of greywacke and shales. Felsic dykes and their host rocks display very strong iron carbonate hydrothermal alteration. The UTM deposit is the only commercial production site, corresponding to a north/south-trending shallow east-dipping quartz vein system hosted in a S2 shear zone, as indicated by C-S fabrics and down-dip stretching lineations. The Au mineralization zone in the UTM site occurs as fault-filled quartz veins of meters-size thickness; it is traced for kilometers and is developed at the contact between a large dioritic intrusion and metavolcanic rocks (Gaboury et al. 2020).

Based on fluid inclusions study (Gaboury et al. 2020), six types of hydrothermal fluids have been distinguished, most of them can be related to fluid evolution by hydrothermal reactions and/or phase separations from a primitive fluid of metamorphic origin. The common presence of ethane as a main component in the fluid inclusions is a good indication that fluids were generated by the metamorphism of carbonaceous pyritic sedimentary rocks (Gaboury 2013). These organic compound–rich sedimentary rocks are considered to be one of the best sources for providing ligands and Au for the formation of orogenic-Au deposits (Gaboury 2019). The Keraf shear zone in north central Sudan, which is composed mainly of turbidites, provided

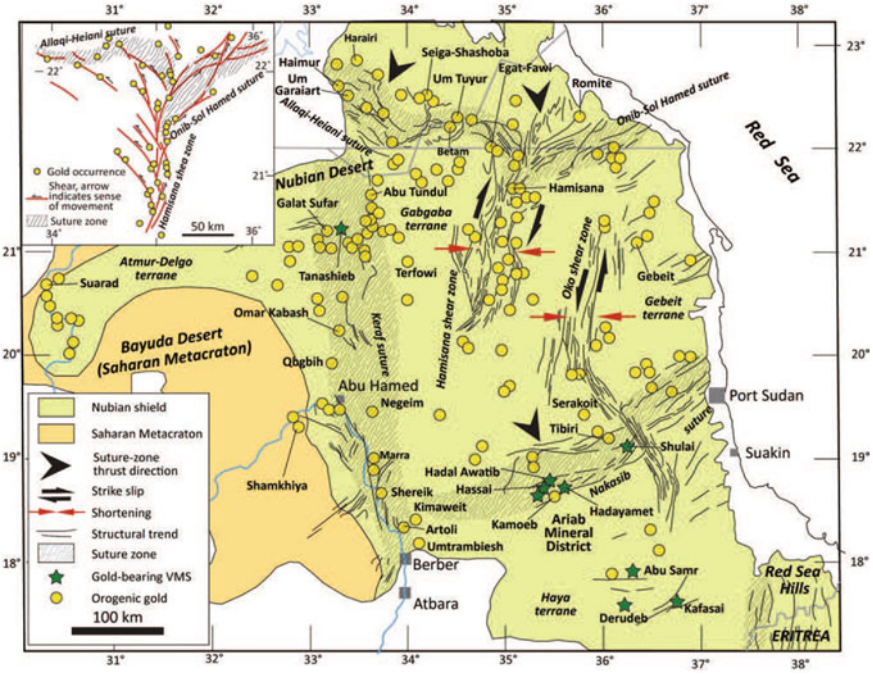

Fig. 5.25 Locations of Au occurrences in the Nubian Shield in Sudan and part of southern Egypt (after Klemm et al. 2001; Johnson et al. 2017a, b)

Fig. 5.26 Small-scale traditional artisanal Au mining activities in Sudan by which the majority of Au production (~85%) are carried out in Sudan

such source rocks deeper in the suture zone and below the adjacent cratons during the collision. The orogenic-Au sites and deposits in north central Sudan in various structural contexts and metamorphic facies are thus attributed to the deeper metamorphism of these specific rock types, where Au extraction by metamorphism of primary pyrite in organic-rich sediments were favorable for Au enrichment (Gaboury et al. 2020).

The *Galat Sufar South* (*GSS*) Au deposit is another famous example for a typical orogenic-Au deposit. It is located in the western part of the Block 14 area, close to the eastern margin of the Halfa terrane, at the junction between the north/south Keraf suture zone and the east/west Atmur–Delgo structure (Fig. 5.24). The Block 14 area is dominated by two distinct geological domains: the andesite-dominated Gabgaba terrane of the ANS rocks to the east and the marine sediments of the Keraf suture in Western Gabgaba; the two domains are separated by the Eastern Gabgaba fault system. The GSS area is located at the central portion of the Western Gabgaba anticlinorium on the southern flanks of a fold interference culmination called the Galat Sufar andesite domain with an axial surface trace trending east/northeast. This structure comprises peripheral mafic volcanic rocks surrounding a package of intermediate-subalkalic volcanic and calcareous metasedimentary rocks that host the Au deposit on the southern flanks of the structure. The GSS Au deposit is situated just south of the contact between marine sediments to the north, marked by the silicified dolomite

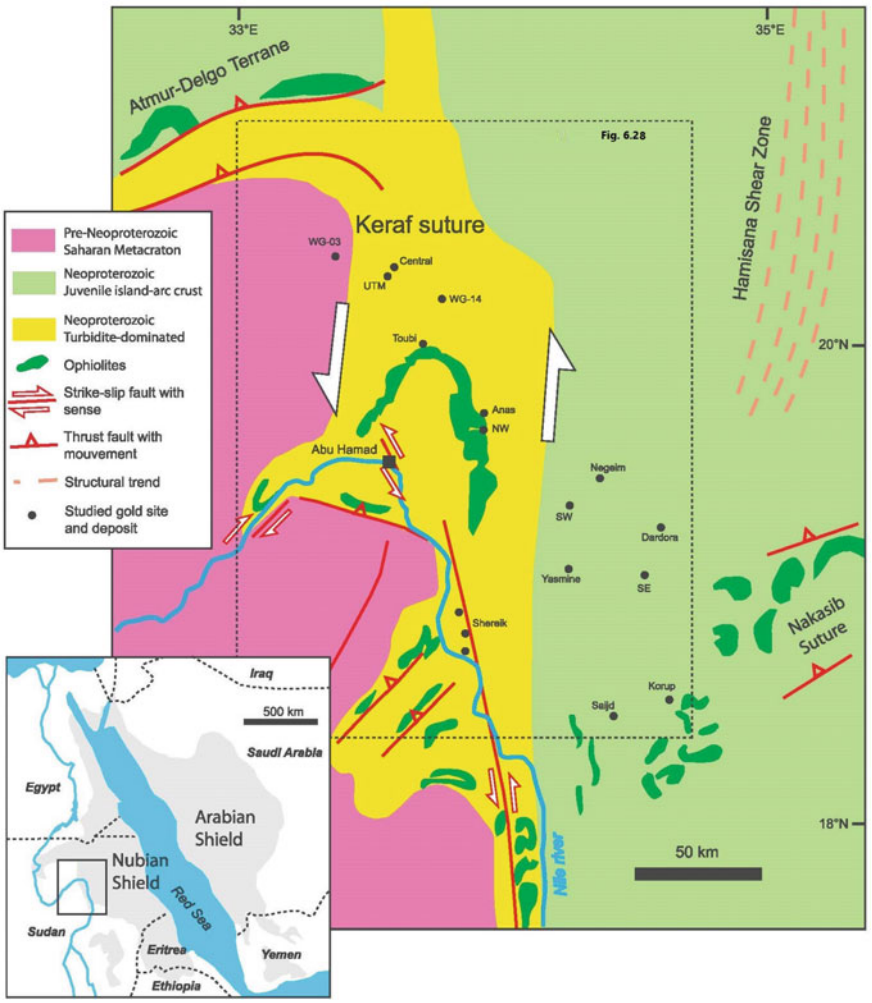

Fig. 5.27 Simplified geological map showing the boundaries of Keraf suture zone with the most known Au sites and occurrences (after Gaboury et al.2020). The Hamisana shear zone location is from Stern et al. The inset map shows the regional distribution of the ANS

marker unit that dominates a ridgeline, and an andesitic volcanic sequence to the south (Fig. 5.29). The andesitic sequence is compositionally heterogeneous comprising lava flows, pyroclastic deposits and volcanic breccia (Duckworth 2020). Within the andesitic dome (Fig. 5.29) is a core of marine sedimentary rocks (limestones, marls, and pelites), which are thought to be a remnant of the Keraf sediments that have been structurally interleaved and folded with the andesites. The northeastern apices of this doubly plunging antiform hosts the Galat Sufar north prospect, whilst other prospects are located on its northern flanks.

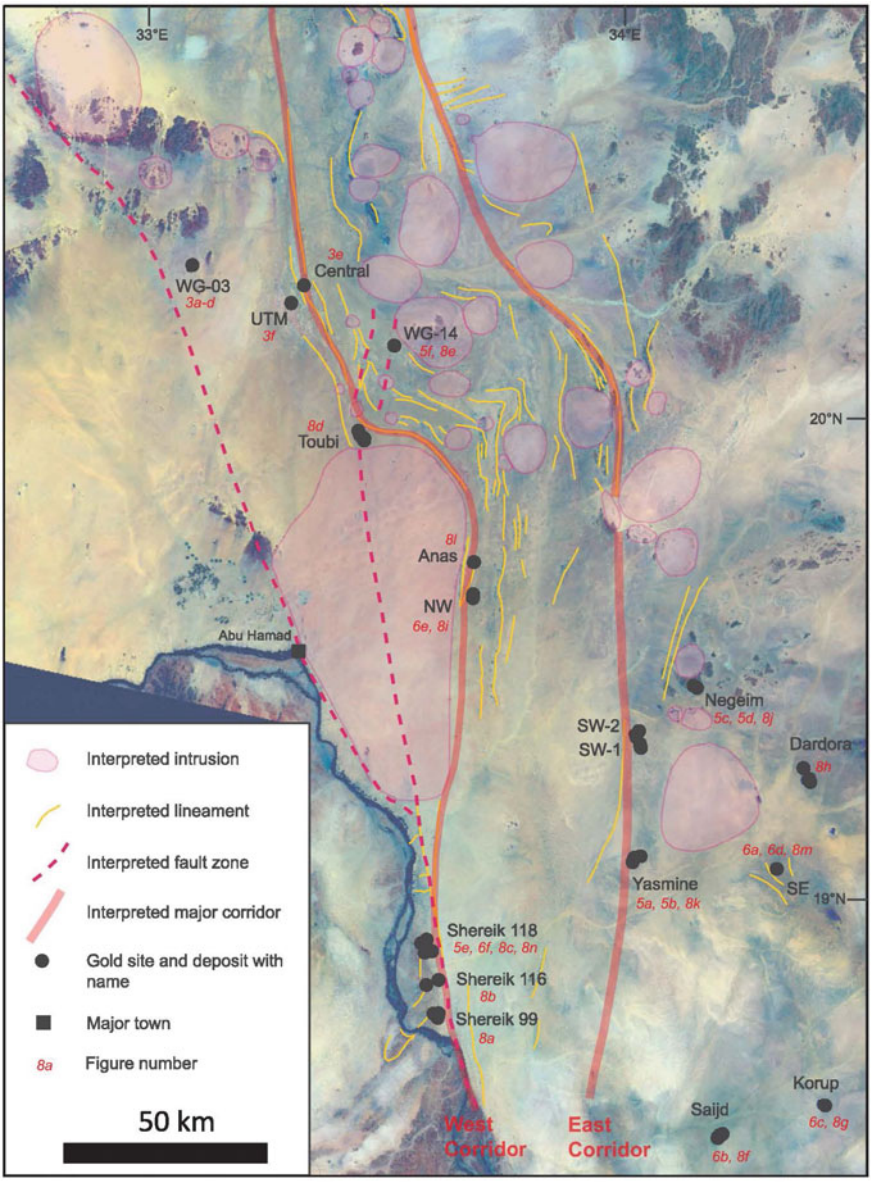

Fig. 5.28 Landsat 8 satellite image with the interpreted lineaments and intrusive bodies and the locations of some Au-bearing sites and deposits (after Gaboury et al. 2020)

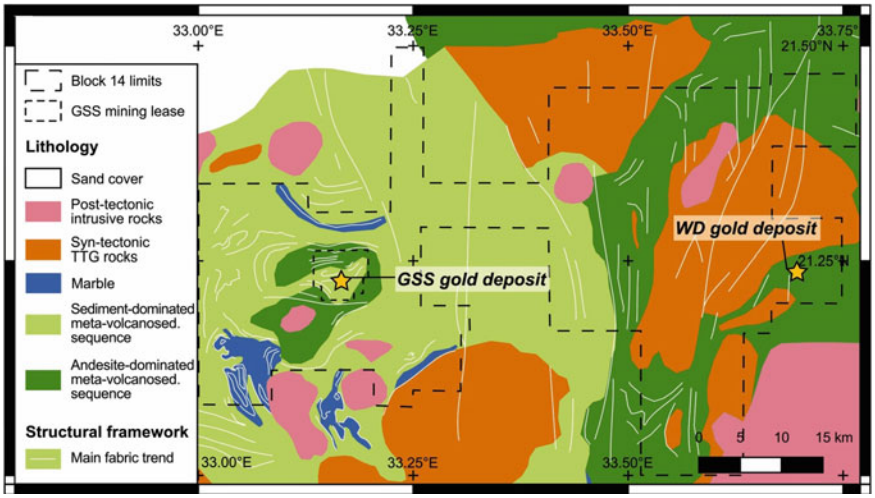

Fig. 5.29 Lithostructural framework of the Block 14 area (northeast Sudan) showing the Block 14 limits and the location of Galat Sufar South (GSS) and Wadi Doum (WD) Au deposits (after Perret et al. 2020)

The mineralization zones in the GSS is essentially associated with an intensely altered and silicified core. The deposit-scale units are pervasively altered and defined by their alteration assemblages, which are variably zoned outward from the Au mineralization. Quartz veins are present within all of the mineralized intersections but are rarely observed at the surface due to strong exploitation by artisanal workings. The quartz veins show multiple generations of development, are themselves mylonitized, and brecciated in the mineralized Main Zone. Quartz blow is present throughout the region and outside of the GSS site carries no Au mineralization. At the GSS site, however, quartz veins are brecciated (Fig. 5.30), have sheared contacts and contain significant Au enrichment. Gold mineralization is primarily associated with intense sericite–carbonate alteration, the presence of pyrite, zones of moderate silicification, and quartz veining ranging in size from the millimeter scale to a maximum of 1.5 m. The best mineralization zones occur in areas of strong deformation, with the widest and best-developed shear zones containing the largest Au resources. The Au mineralization zones are predominantly restricted to foliated quartz–sericite–pyrite schist or to silicified host rock. Significant mineralization was intersected over broad intervals of widths of approximately 15 to >80 m, with average grades of 1.25 to 5 g/t Au and 0.5 to 6 g/t Ag (Abanyin et al.2015). Gold occurs either as free-milling Au grains disseminated within the host rock or in association with pyrite and within Ag-Au tellurides (e.g., petzite, Ag_3AuTe_3). Free Au grains are rarely visible, mostly occurring as very fine (1–10 μm) grains, which contain up to 20% Ag (in the form of electrum). In addition, minor amounts of Au also occurs in quartz carbonate veins. Some refractory Au content (~16–18%) is locked in sulfides and/or disseminated (~2–4%) in the host rocks. The sulfide content in mineralized zones rarely exceeds

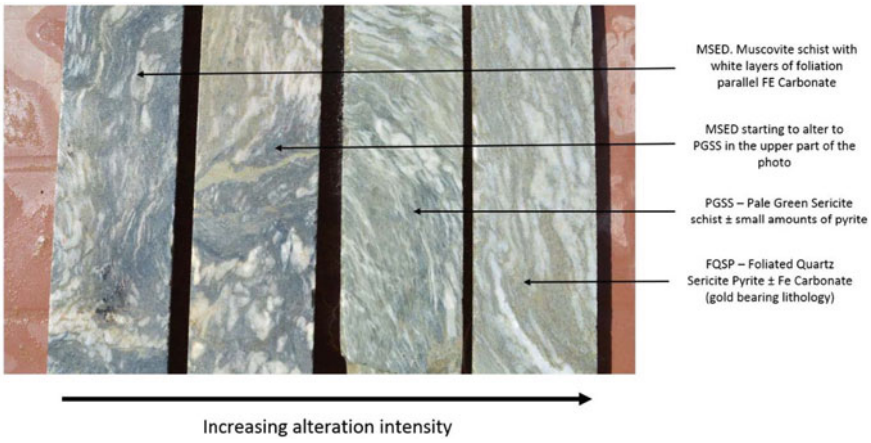

Fig. 5.30 Bisected core samples of the GSS Au-bearing quartz veins showing the alteration and brecciation of quartz veins (Orca Gold Inc. Report3209-43-101-14-Sep-20.pdf)

5%, in which pyrite is the dominant sulfide minerals with subordinate amount of chalcopyrite, sphalerite, galena and tennantite/tetrahedrite.

In the mineralized area of GSS, there are multiple generations of quartz veining, which have subsequently been mylonitized and brecciated in the main ore zones (Fig. 5.30). The first phase of quartz veining occurred as milky-white, fused quartz blows that are randomly oriented, crosscut by shear zones, and associated with subsequent veining. In the GSS area, there are six fault-separated mineralized domains (Abanyin et al.2015), defining as east/northeast trending zones ~1500 m in length. These are, from west to east (Fig. 5.31): (1) The 320 Zone, which occurs as discontinuous ribbons and plunging shoots within a 140°-oriented shear zone that is parallel with the local schistosity. This zone contains high-grade ore (>10 g/t Au). (2) The Main Zone (up to 90 m wide, laminar), a 150-m strike-length zone that represents a set of 10°-trending shears crossing a rigid body of syenite/K-feldspar–altered diorite in the footwall. It is a high-grade mineralized zone that juxtaposed with the 320 Zone. (3) The 050 Zone, a narrow domain linking the East Zone (to the east) and a north/south-trending set of mineralized quartz veins in an area known as *The Gap* (in the west). (4) East Zone, which is hosted by an ~100°-oriented corridor, which contains several small, often brecciated and dismembered intrusive stocks. Shear fabrics wrap around the intrusive bodies. The approximate width of this zone is ~90 m in its central sections, while it is much smaller mineralized structures in its north and south parts. A barren plug of alteration zone occurs adjacent to high-grade tectonic breccias and may be associated with quartz blows observed at the surface. (5) Far East Zone has a similar trend to the East Zone, having discontinuous mineralization hosted by a sheared sericitized microdiorite, within steep-to-vertical mineralized trends. (6) Shareg Zone, a steep, north/south-striking trend, hosted by a sericite/carbonate–altered diorite to microdiorite. It separates the Far East Zone of

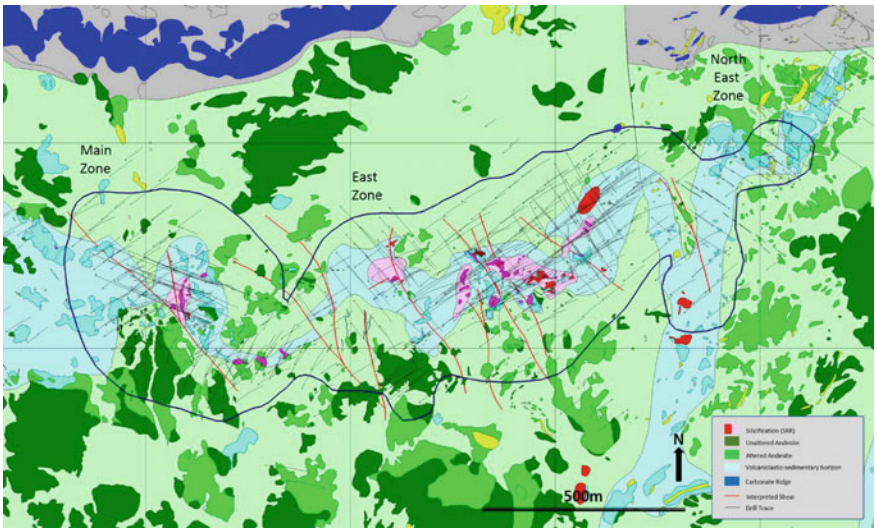

Fig. 5.31 Geology, mineralization, and drill sites of the GSS Au deposit of the NE Sudan showing the different mineralization zones and veining types (Orca Gold Inc. Report3209-43-101-14-Sep-20.pdf)

the GSS deposit from the Northeast Zone, which is a braided, >1-km-long shear and containing components of the main shear trends.

The estimated ore resources/reserves of the GSS deposit, as of 14 September 2020 (Orca Gold Inc., Report3209-43-101-14-Sep-20.pdf), are based on 2-m down-hole composited Au grades from RC and diamond drilling. The resource dataset comprises 49,069 composites with Au grades ranging from 0.002 to 126 g/t, with an average of 0.55 g/t Au, and silver grades ranging from 0.005 to 294 g/t, with an average of 0.92 g/t. The dataset is dominated by composites from RC holes, which represent 74% of the mineralized domain composites. The total ore resources are ~92.5 Mt, with an average assay of 1.26 g/t Au and 1.47 g/t Ag, for 116 t of contained Au. These mineral resources include a total ore reserve of ~77.4 Mt, with an average grade of 1.07 g/t Au.

The *Wadi Doum* Au deposit is located ~50 km east of GSS in the Block 14 region (Fig. 5.29). It is much smaller in size but of higher-grade Au mineralization than the GSS site (~3×) that is outcropping at the base of the hill and is hosted by a strongly sulfidic volcaniclastic unit in contact with a distinct rhyolite unit to the immediate east. The volcanoclastic unit dips at an angle of 20° to the southwest, and the rhyolite is bounded to the east by a dacitic unit intruded by syn-tectonic altered syenite/diorite body that forms the summit of the main Wadi Doum hill. The Au mineralization on the hill is associated with stringer zones within the altered syenite/diorite body and in places within smaller shears. The mineralization at the Wadi Doum area is divided into a western volcaniclastic unit containing some of the best intercepts and characterized by a dark-colored, fine-grained sulfide-rich zone (>10–15%), and a central

unit of pale, sulfide-rich felsic volcaniclastic rocks containing deformed sulfide veinlets and a lower-grade footwall unit of largely undeformed felsic volcaniclastic rocks. The dominant sulfide mineral is pyrite with subordinate amount of sphalerite, galena, chalcopyrite, and freibergite.

The main alteration types are represented by sericitization within the felsic volcanic rocks and a wider halo of carbonate alteration. Silicification is noticeably absent or weak within the high-grade part of the ore deposit. The area is dominated by a strong and pervasive, north/south-trending schistosity, which is largely followed by the late dykes. The high-grade mineralization often appears unaffected by structure whereas the mineralization hosted by the syenite/diorite on and around the summit of the hill does appear structurally controlled. The estimated ore resource dataset (Orca Gold Inc., Report3209-43-101-14-Sep-20.pdf) comprises ~6,465 composites with Au grades ranging from 0.005 to 388.6 g/t, with an average of 0.90 g/t, and Ag grades ranging from 0.00 to 122.6 g/t and averaging 3.37 g/t. The dataset is dominated by composites from RC holes, which represent 94% of the mineralized domain composites. The total estimated ore resources (indicated and inferred) are ~5.9 Mt ore, with an average grade of 1.71 g/t Au and 4.95 g/t Ag, for 10 t of contained Au. These mineral resources include a total ore reserve of ~2.588 Mt ore, with an average grade of 2.36 g/t Au.

5.6 Orogenic Deposits in Eritrea

As was previously mentioned early in Chap. 2 of this book, more than 60% of Eritrean territory is part of the southern Nubian Shield. The geology of Eritrea is essentially made up of three major stratigraphic successions: The basement rocks constituting the Precambrian greenstone volcano–sedimentary assemblages, Paleozoic and Mesozoic sedimentary and volcanic rocks unconformably overlying the Precambrian rocks, and sedimentary and volcanic rocks of the Paleogene to Quaternary ages. Based on lithological and structural characteristics, the Eritrean Neoproterozoic basement rocks have been divided into five tectonostratigraphic terranes (Drury and Berhe 1993; Teklay et al.2001; Drury and Filho 1998): (1) Barka terrane in the west is mainly composed of upper amphibolite to granulite metasedimentary and mafic gneiss complexes. (2) Hagar terrane in the north is dominated by oceanic affinity of suprasubduction mafic and felsic volcanic rocks. (3) Adobha Abiy terrane in the central and western parts is mainly composed of highly deformed ophiolites and post-accretionary basinal sediments. (4) Nakfa terrane occupying more than half of the basement complex in Eritrea contains greenschist facies volcano–sedimentary and syn- to post-collision granitoid rocks. (5) The easternmost Arig terrane is a narrow belt of high-grade gneiss and syn- to late-tectonic granitoid rocks along the Red Sea lowlands.

Orogenic mineral deposits in Eritrea are essentially represented by orogenic-Au deposits, which are concentrated in belts of transpressional deformation; the same

belts that contain VMS deposits (Fig. 5.32). Most of the VMS type and quartz vein–hosted Au ± sulfide (lode Au) deposits and occurrences in Eritrea are concentrated along NNW- and NNE-trending narrow zones in the southern Nubian Shield (Johnson et al. 2017a, b). These mineralization zones are the Augaro–Adobha belt (AAB) and the Asmara–Nakfa belt (ANB) (Ghebreab et al. 2009). Both the world-class Bisha VMS and Koka orogenic-Au deposits are located along the AAB Cu and Au metallogenic belt (Fig. 5.32) (Barrie et al. 2007; Zhao et al. 2019). The VMS deposits in the ANS will be discussed in detail in Chap. 6 of this book. Following, however, is a brief description of the Koka orogenic-Au deposit, the only known lode Au deposit, in the northwest of Eritrea.

The *Koka* Au deposit is located in northwestern Eritrea, which has a long mining history extending back to the Egyptian Pharaohs. However, modern mining at the Koka area began in the early twentieth century, starting during the Italian colonization, until it was terminated due to the war for independence. Since independence in 1991, several foreign mining companies from China, South Africa, India, Japan, the United Kingdom, Australia, and Canada have been involved in exploring the mineral potential of Eritrea. Despite several years of exploration and exploitation, the Koka Au deposit still has promising prospects. The origin and style of mineralization of the Koka Au deposit is debatable. However, recent studies have suggested, based on field observations and fluid inclusion chemistry, that the Koka deposit is a vein-type Au deposit, which is controlled by shear zones and Koka granite, and is thus considered to be an orogenic-like Au deposit (Zhao et al. 2019).

The Koka Au mine is located in the Elababu shear zone (ESZ) that separates the Nakfa terrane in the east from the Adobha Abiy terrane in the west. The ESZ is the dominant ore- and granite-controlling structure in the area, where the ore bodies are strictly distributed in the north/south-striking ESZ. The ESZ is characterized by the occurrence of thrust nappe faults (strike to ~10°–20°, tending to the southwest) and low-grade metamorphic volcano–sedimentary rocks upright folds (the dip angle of limbs is 75°–90°) along the different lithologic interfaces (Zhao et al. 2019). The formation of the ESZ is related to the north/south-striking extrusion caused by the collision of the Neoproterozoic Gondwana continent. Granite occurring along the ESZ is characterized by strong mylonitization, where the preferred orientation of sericite defined the main foliation anastomosing around rotated K-feldspar porphyroclasts. The mineralization commonly occurs as reticular veins, with branching and converging features, and has locally expanded to form lens-shaped bodies. Ore-bearing quartz veins are essentially hosted by a relatively fine- to medium-grained grey-colored granitic body (Fig. 5.33b), which is bounded by greenschist facies metamorphic rocks. In the eastern part of the Nakfa terrane, the host rock consists of intermediate-to-felsic volcanic and pyroclastic units and post-tectonic granitoids. In the western part of the Adobha Abiy terrane, the host rock consists of sequence of siliciclastic metasedimentary and metavolcanic rocks, including tuffaceous greywacke, sandy mudstone, shales and mafic metabasaltic flows, and associated syn-tectonic granitoid rocks (Fig. 5.33b).

The Koka Au mineralization developed within a relatively elongated NNE-trending microganitic body dated back to 851.2 ± 1.9 Ma (Dean et al. 2010) that was

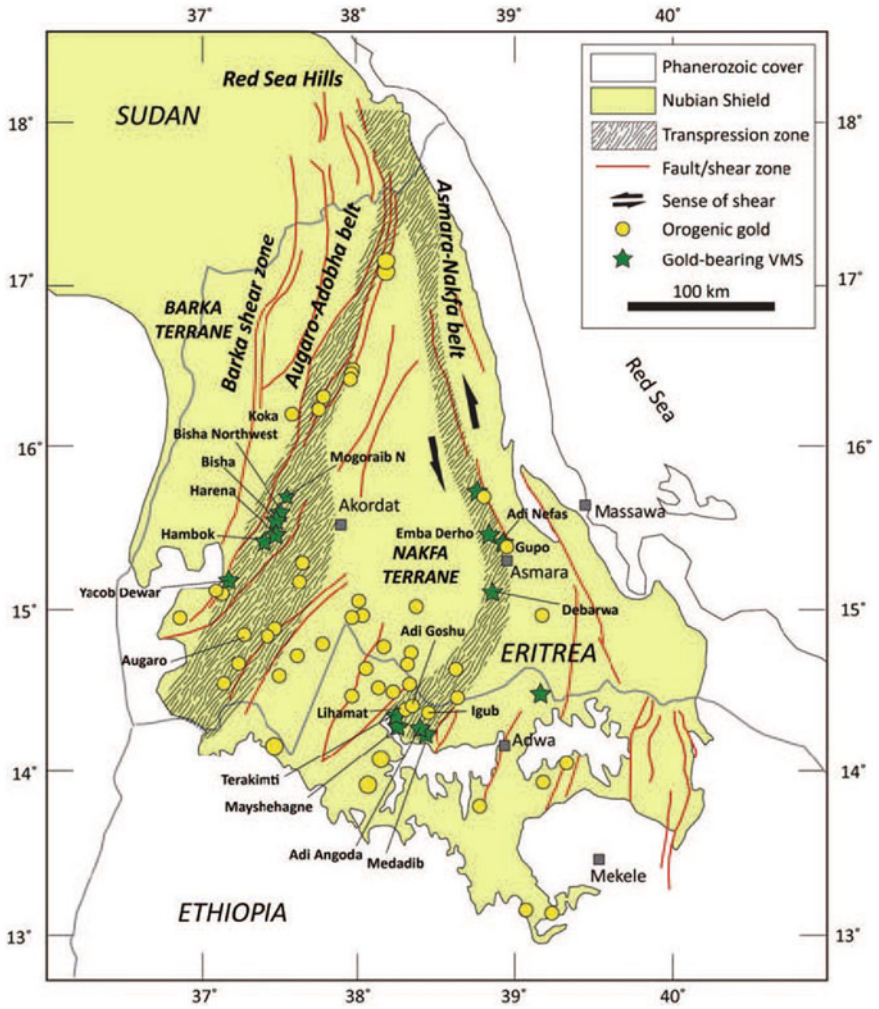

Fig. 5.32 Selected Au occurrences in the Nubian Shield of Eritrea and northern Ethiopia, showing the prevalence of north to NNE structural trends (after Johnson et al. 2017a, b)

highly fractured during the post-magmatic deformation events. The main Au mineralization zones can be classified into two categories: quartz-vein type and wall-rock alteration type (Zhao et al. 2019). The former is characterized by intense alteration, where the main mineralization zone localized in a 10-m-wide stockworks of quartz veins and veinlets of ~50–80 m from the contact of the footwall within the microgranite body. The second mineralization type, the wall-rock alteration, mainly developed in the contact zone between the Koka microgranite and footwall metavolcano–sedimentary rocks. The diamond-drilling program (Dean et al. 2010) had constrained that the Koka Au orebody was traced over a strike length of ~650 m, with an average

depth of >165 m below the surface. The average Au grade is ~5–6 g/t, with proven Au reserves of ~26.13 t. Gold is essentially found in quartz veins in the form of native Au, associated mainly with pyrite, chalcopyrite, galena, and sphalerite. The gangue minerals are mainly represented by quartz, calcite, and sericite. The types of alterations closely related to Au mineralization are silicification, sericitization, pyritization, and carbonation, which are superimposed on each other in zonation patterns in the mining area. Silicification is particularly consistent with the main mineralization, whereas the sericitization and pyritization, as a sericite + pyrite altered halo, are beyond the distribution of the mineralization zone. The carbonation alteration zone often occurred in the surrounding rocks mainly as carbonated veins, accompanied with other alterations or found separately. Two main stages of Au mineralization are recognized in the Koka Au deposit (Zhao et al. 2019): stage I is characterized by the development of quartz–sulfide–Au veins, in which Au occurs as xenomorphic grains distributed between pyrite and quartz, and stage II is characterized by the development of milky-white quartz veins poor in sulfide minerals. In the latter stage, the mineral assemblage is relatively simple, where only a small amount of chalcopyrite and fine-grained pyrite can be observed.

Based on the fluid inclusions and stable isotopic (C–H–O–S) compositions, combined with geological features and ore-forming fluid characteristics, the Koka Au deposit is mostly similar to those of orogenic Au deposits (Zhao et al. 2019). Hence, the Koka deposit might be an orogenic Au deposit related to granite, where the ore-forming fluids could have originated from metamorphic strata with a considerable magmatic contribution, and the metals were most probably derived from magma. Along the same mineralization as the AAB, the *Konate* prospect, ~6 km south of and virtually along strike from Koka (Fig. 5.33) is an area of artisanal workings on quartz stockwork in silica–sericite altered microgranite. The mineralization and alteration characteristics of the Konate prospect are mostly similar to that in the Koka mining site, which support a similar mineralization type (orogenic Au deposit). In addition, there are several Au prospects along a shear zone in the ANB, including those at the *Gupo* deposit (Fig. 5.32), which comprises Au and sulfides in stockworks and quartz veins (Ross and Martin 2012). *Adi Goshu* and *Lihamat* (Fig. 5.32), along the same belt in northern Ethiopia, also contain Au mineralization close to the contact between a northeast-trending elongate body of quartz–feldspar porphyry and sericite-altered mafic and felsic volcanic and volcaniclastic rocks (Archibald et al. 2014; Johnson et al. 2017a, b).

5.7 Orogenic Deposits in Ethiopia

In general, Precambrian basement rocks (~23%), Paleozoic and Mesozoic sediments (~25%), Tertiary volcanic rocks (~34%), and Quaternary sediments and younger volcanic rocks (~18%) constitute the essential geology of Ethiopia. The Precambrian basement rocks are well-exposed in the northern, southern, eastern, western, and southwestern parts of the country and host most of the known metallic and

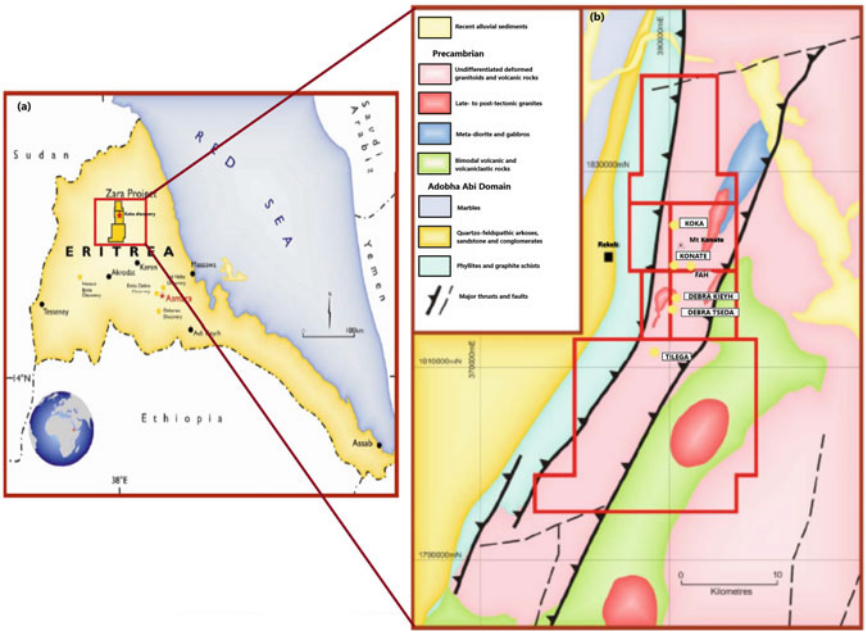

Fig. 5.33 **a** Location map of Eritrea showing the Zara project where the Koka Au deposit is located. **b** Simplified geologic map of the Zara project area showing the location of Koka and nearby Au deposits and prospects in central Eritrea (after Chalice Gold Mines Limited as of 24 November 2009)

nonmetallic mineral deposits. The Adola Gold Exploration Project (AGEP), an Ethiopian–Soviet joint team, investigated the region after 1978 for metallic and nonmetallic mineral deposits. As a result, the Lega Dembi Au mine and the Kenticha and Buanbuawuha pilot plants were established for the mining of Au, tantalum, and kaolin, respectively. Since then, different mining companies have carried out exploration for various minerals such as Au, base metals, and industrial minerals. The Au mineralization in the Ethiopian Precambrian basement occurs essentially in intensely sheared, hydrothermally altered greenschist facies volcano–sedimentary rocks of Megado and Kenticha belts in the southern part (Fig. 5.34) (Deksisa and Koerbel 2004); Meli, Weri, and Werkamba area in the northern part (Abraham et al. 2015); and in granitoid rocks of the Western Ethiopian Shield (Fig. 5.32). Orogenic Au deposits in Ethiopia are mainly concentrated in the Western and Southern Ethiopian shields, of which the *Tulu Kapi*, *Lega Dembi*, and *Okote* Au deposits/prospects (Fig. 5.34) are the most famous localities.

The *Tulu Kapi* Au deposit is located in western Ethiopia, ~350 km due west from the capital of Addis Ababa. Tulu Kapi is found in the Western Ethiopian Shield (WES), also called the Western Greenstone Belt, which is one of the western-most exposures of the Neoproterozoic ANS (Fig. 5.35a). Unlike the Southern Ethiopian

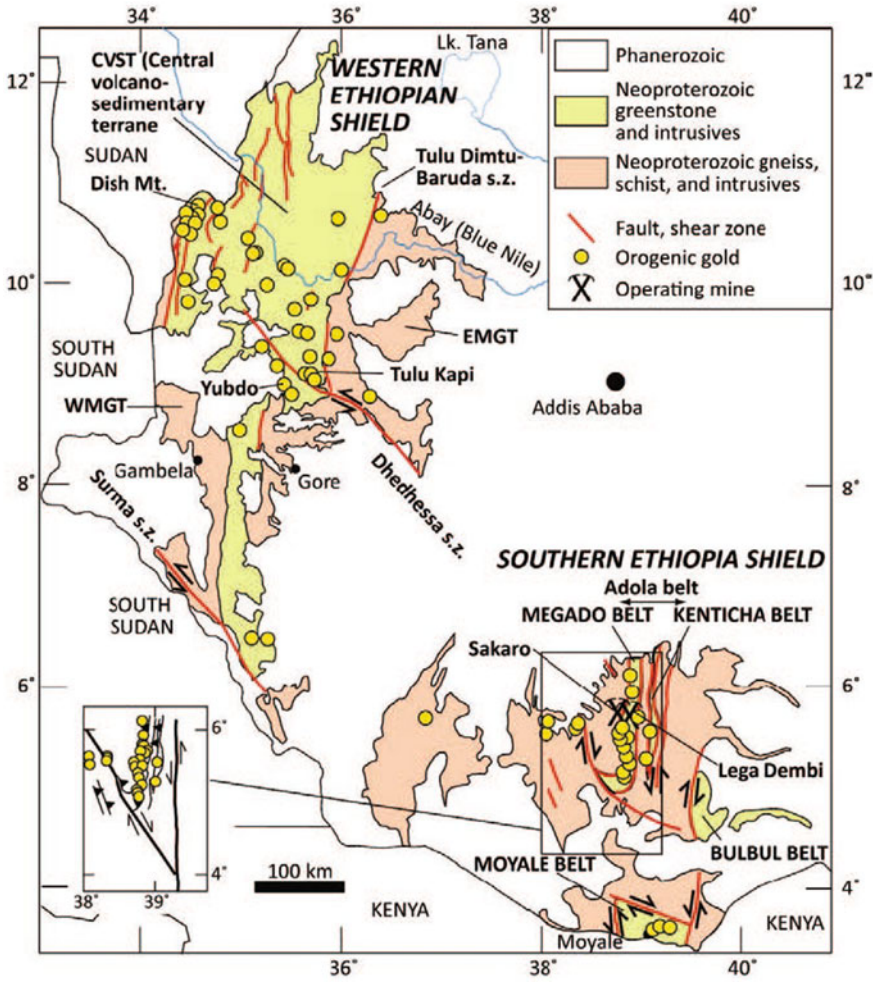

Fig. 5.34 A simplified map showing the Au occurrences and producing mines of Precambrian geology in western and southern Ethiopia (after Johnson et al. 2017a, b)

Shield (SES), the WES has no record of primary Au mining, but only alluvial workings, which is most probably due to the difficulty of access as well as extensive development of regolith cover that complicates the Au exploration. One of the few documented Au deposits in the WES is Tulu Kapi. The WES stretches more than 600 km from Akobo–SW Ethiopia, and its average width varies from 50 to 200 km. Geologically, this belt comprises chlorite, sericite, and graphitic schists, phyllites, quartzites, and andesitic to rhyolitic volcanic rocks, hosting auriferous veins and alteration zones. The WES is divided into five lithotectonic domains (Allen and Tadesse 2003); from east to west are (Fig. 5.35b) Didesa, Kemashi, Dengi, Sirkole, and Daka. The Tulu Kapi deposit is hosted in the Kemashi domain, which consists

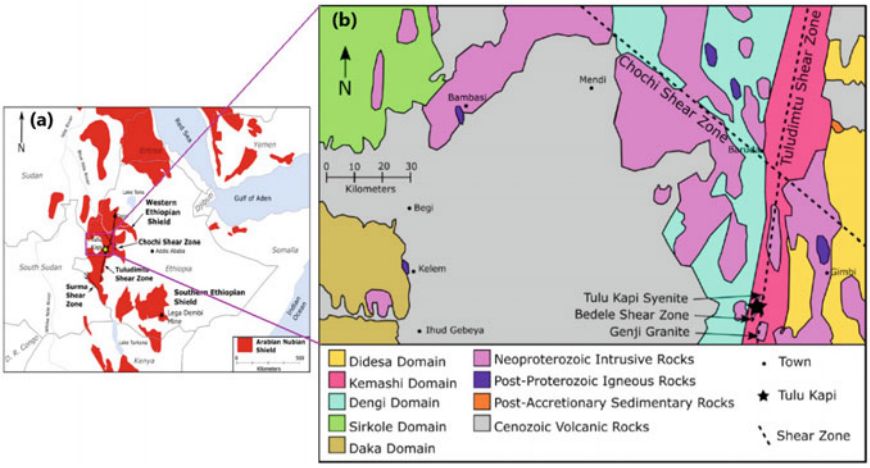

Fig. 5.35 **a** The distribution of ANS rocks showing the Tulu Dimtu shear zone and the location of Tulu Kapi Au deposit in the Western Ethiopian Shield. **b** Domain map of the Western Ethiopian Shield showing the location of the Tulu Kapi Au deposit (after Molnar 2019)

of low-grade metasedimentary and ultramafic–mafic metavolcanic rocks intruded by ultramafic-to-intermediate plutons (Allen and Tadesse 2003; Alemu and Abebe 2007). The intruding plutons include the deformed Tulu Kapi syenite and the undeformed Genji granite (Fig. 5.35b), which date back to 584 ± 10 Ma (Blades et al. 2015). The Tulu Kapi syenite is located along the Tulu Dimtu shear zone, which represents the central feature of the WES (Fig. 5.35b).

The Tulu Kapi Au deposit is hosted by the Tulu Kapi syenite pluton with minor Au mineralization hosted in the eastern part of the Kapi gabbro (Molnar 2019; Oljira and Warkisa 2020). The syenite and gabbroic plutons bordered by the Bedele shear zone to the southeast and the Guji shear zone to the west (Fig. 5.36). The Bedele shear zone, found on the southeast of the deposit, join the Tulu Dimtu shear zone a few kilometres to the north of Tulu Kapi (Figs. 5.35 and 5.36). The Tulu Kapi syenite pluton lies on the western side of the Tulu Dimtu shear zone and in the hanging wall of its splay fault, the Bedele shear zone (Fig. 5.36). Quartz veins are widely distributed throughout the syenite pluton and are mostly consistent with the brittle behavior during deformation. The margin of the syenite pluton is intensely sheared at the contact with the Bedele shear zone (Molnar 2019; Oljira and Warkisa 2020). The Kapi gabbro occurs mostly to the east of the Tulu Kapi syenite (Fig. 5.36), and the contact between gabbro and syenite appears to be intrusive contact, but with some shearing or detachment with proximity to the Bedele shear zone (Fig. 5.36).

The Au mineralization and its associated alterations of Tulu Kapi deposit are found in rocks containing quartz + sulfide ± carbonate veins, where the veining is mainly found in the eastern side of the elongated syenite pluton in the contact with the Bedele shear zone. There are four different vein types at the Tulu Kapi area, three of them are found in the alteration zones associated with Au mineralization,

and the fourth one along a lithotectonic contact between the Tulu Kapi syenite and Bedele shear zone (Molnar 2019; Oljira and Warkisa 2020). All of these quartz veins within syenite pluton and that at the contact with the shear zone are found to host Au mineralization. The Kapi gabbro, on the other hand, hosts Au-mineralized quartz lone veins but not in en échelon arrays. In addition to Au mineralization, sulfide minerals are also found in the syenite, dykes, gabbro, the trachyte, and the Bedele shear zone. The most common sulfides are pyrite, pyrrhotite, and lesser amount of galena, sphalerite and chalcopyrite, which are mostly restricted to the syenite, gabbro, and syenite dykes. In quartz veins, Au is found along grain boundaries of pyrite or pyrrhotite, enclosed within quartz, filling fractures in pyrite, or as inclusions in pyrite. Visible Au grains are found in breccia veins and fractures near the footwall of the syenite, mostly at depths ~300 m below the surface in the deposit, in an area referred to as the *deep shoot*. Gold concentration in the deep shoot is more than twice that of shallower levels (Granitzio et al. 2015). The shoot features superimposed vein sets and dense fracture networks resulting in a quartz vein stockwork. Throughout the deposit, Au lodes contain compositionally heterogeneous veins called *polyphase veins*, comprising zoned quartz, carbonate, and sulfide minerals that reflect multiple accommodated fluid phases (Molnar 2019). These veins exhibit zoning of early and late hydrothermal quartz, multiple sulfides phases and carbonates.

Thus, the main mineralization stage at Tulu Kapi is composed of an assemblage of hydrothermal minerals, including quartz, albite, carbonate, biotite, muscovite, epidote, sulfides, and Au (Molnar 2019; Oljira and Warkisa 2020). The Au mineralization commonly occurs in veins, crackle zones, and minor breccia zones, where the albitized syenite is one of the main hostings for the Au mineralization. It has been widely overprinted by a multistage hydrothermal system that is essentially controlled by fractures and minor breccia zones (Pollard 2008). The Tulu Kapi Au mineralization is mostly associated with sulfide-bearing albite alteration quartz veins and structurally controlled following the fracture fillings and orientation of the foliations (Pollard 2008; Molnar 2019). The estimated total ore resources (indicated + inferred) as of April 2015 (KEFI Minerals website, viewed November 2020) is ~20.2 Mt ore, with an average grade of 2.65 g/t Au, for ~53.5 t of Au. The estimated total probable ore reserves are ~15.4 Mt of ore, with an average grade of 2.12 g/t Au, for a total of 32.65 t Au.

In the SES, the orogenic-Au occurrences are mainly hosted in greenstone belts and sheared gneiss and schist in a structural scissor between north- and northwest-trending shear zones (Fig. 5.34). Famous localities of orogenic-Au deposits in southern Ethiopia include *Lega Dembi*, a surface and underground mine, and *Sakaro*, an underground mine, and *Okote* prospect at the southern part of the Adola Au field (Fig. 5.34).

The *Lega Dembi* and *Sakaro* Au deposits are located ~365 km south of Addis Ababa in southern Ethiopia. Lega Dembi is ~6 km south/southwest of the town of Shakisso (Fig. 5.37), and Sakaro is a further 4 km to the southwest. They are situated within the SES, in the southwestern section of the ANS, specifically within the Adola granite–greenstone belt that covers an area of ~5000 km^2. Historically, numerous primary and placer Au deposits have been known from various regions in

Ethiopia in general, and in the Adola belt in particular. The primary Lega Dembi and Sakaro Au deposits were first discovered in 1975 by artisanal miners, and subsequently by the intensive and detailed exploration program carried out by the Ethiopian Mineral Resources Development Corporation (EMRDC) in 1979. Initially, the EMRDC mined the Lega Dembi deposit as an open pit before it was sold to the Saudi-backed MIDROC Gold Mine plc in 1997, and then MIDROC continued mining by open pit before going underground. Gold reserves at Lega Dembi were exhausted in 2018 and the mine was closed. EMRDC had mined alluvial and eluvial Au from the Sakaro deposit from 1986, with ~896 kg being recorded by 1991 (Billay et al.1997). The MIDROC Gold then commenced mining at Sakara as an underground operation in 2009. Geologically, the Adola greenstone belt comprises two linear, north/south trending blocks of metamorphosed supracrustal rock; each is ~5–15 km wide and are ~10 km distant from each other (Fig. 5.37). The Megado volcano–sedimentary belt is in the west, composed of ultramafic and tholeiitic mafic volcanic rocks and intrusives that are intercalated with predominantly arkose, feldspathic quartzite, quartzite and pelite, together with subordinate polymictic conglomerate and greywacke. Small pod- or lens-like, mainly tonalitic bodies intrude into the mafic rocks. The eastern margin of this belt is tectonic, regionally known as the Lega Dembi–Aflata shear zone (Worku and Yifa 1989; Worku and Schandelmeier 1996). The western margin is marked by the development of gneissose tonalite, which has primary intrusive contacts with the supracrustal assemblages. The Kenticha ultramafic belt is in the east and is dominated by ultramafic rocks, with subordinate amphibolites and sedimentary rocks, occurring as biotite schists and minor graphitic schists and marbles.

The *Lega Dembi* Au deposit, considered to be the largest Au producer in Ethiopia, situated in late-Precambrian metamorphosed sediments of the north/south-trending, volcano–sedimentary Megado Belt, forms part of the late-Proterozoic Adola granite–greenstone terrane in southern Ethiopia. The lode-Au mineralization at Lega Dembi occurs in a north/south-trending, steep westerly-dipping quartz vein system that follows the structural contact between feldspathic gneisses and the volcano–sedimentary sequence of the Megado belt (Billay et al. 1997). This contact also marks the northernmost extension of the regional-scale, sinistral strike–slip Lega Dembi–Aflata shear zone. Gold mineralization and intense quartz veining is best developed in graphite-rich metasedimentary rocks within an area less than 80 m away from this tectonic contact. The main mineralized area is characterized by three main composite quartz vein systems that are each up to 10 m thick: the Eastern, Central and Western veins, although thin foliation-parallel quartz veinlets also occur throughout the metasedimentary succession. The principal vein system in the Northern pit has a strike extent of ~250 m and semi-continuously persists down-dip for >350 m (Billay et al. 1997). The Eastern vein is hosted by muscovite–quartz–plagioclase schist, whereas the Central and the Western veins are within laminated, graphite-bearing arkose and quartz wacke hosts. Sulfide minerals essentially occur as fine disseminations in quartz veins and in wall rocks. Sulfides in the quartz veins comprise, in decreasing order of abundance, chalcopyrite, galena, pyrrhotite, and pyrite, with minor to rare sphalerite, gersdorfite, arsenopyrite, molybdenite, tellurides, Ag-rich tetrahedrite, and Au. Microscopic Au grains occur along sericite alteration within

quartz veins. Gold is typically spatially associated and intergrown with galena, and is commonly associated with chalcopyrite, pyrrhotite, and tellurides (hessite and stuetzite). Inclusions of Au in pyrrhotite, galena, tellurides, and chalcopyrite are rare.

Hydrothermal wall-rock alteration is broadly zoned on a deposit scale, although the pattern is confused by the intense and multiple quartz veining and associated alteration overprint, as well as variations in host rock lithologies. The broad zonation include (Billay et al. 1997): (1) Chlorite–carbonate–epidote, which occurs between the Western and the Central veins, and is distal to the vein system in wall rocks, giving the rocks a distinct greenish coloration. It may also occur as foliation-parallel anastomosing bands. Minor chlorite is also developed after muscovite within the quartz veins. (2) Actinolite/tremolite–biotite–calcite, which is pervasive and the most characteristic alteration at Lega Dembi. It developed within 15–20 m of the main quartz veining. Gold mineralization occurs preferentially in the sericite alteration zone, where it is closely associated and intergrown with galena.

The *Sakaro* Au deposit is located ~4 km SW of Lega Dembi. Gold mineralization is hosted in an en échelon quartz vein system developed in graphitic metapelites parallel to the contact between massive amphibolites and metasedimentary rocks, the latter being correlated stratigraphically with the metasediments of the Lega Dembi area. The ore is hosted by Au-rich and sulfide-poor quartz veins that are 1–9.3 m thick and occupy fault planes and follow foliation and rock contacts in the Neoproterozoic low-grade metamorphic host rocks. The veins, which strike northeast and dip at 45° to 80° northwest, form a mineralized zone that is ~760 m in strike length and up to at least 150 m in vertical extent. The veins are mainly composed of quartz, containing partings, streaks, and fragments of the altered wall rocks, particularly graphite. Within each quartz vein, three distinct hypogene mineralized zones have been recognized, from vein margin to center, involving marcasite–chalcopyrite in the peripheries, to galena–chalcopyrite–marcasite, to sphalerite–high galena-chalcopyrite in the center. Gold is present in all the three zones, although it is strongly enriched in the latter one, the sphalerite–high galena–chalcopyrite, in the vein cores, followed by the hanging wall marcasite–chalcopyrite zone, and least in footwall zone of the same sulfide assemblage (MIDROC Gold website, viewed 2020).

There is an outward metal zonation in the Sakaro deposit from Au–Ag-Pb within the vein core to Ag-Pb-Cu on the vein margins and proximal wall rock to as much as 3 m from the vein. This passes into a halo in the wall rocks enclosing the veins comprising an inner wolframite–scheelite–Fe sulfides (W–As–Cu) zone and an outer marcasite–pyrrhotite-chalcopyrite (Fe–Co–Ni–Mo–Cu) periphery extending to as much as 20 m from the vein. This halo is gradually diminished downward. The mineralogy of the veins suggests their development was via multiple episodes of vein opening and filling characterized by wolframite–scheelite–quartz, sulfide–Au–quartz and disulfide–carbonate stages. The generalized paragenetic sequence is an early wolframite + scheelite stage, followed by an early sulfide event involving arsenopyrite + pyrrhotite + Au, then a late sulfide stage with chalcopyrite + sphalerite + galena + Au, and a disulfide–carbonate stage of marcasite + melnicovite–pyrite + siderite. The estimated total endowment at Lega Dembi in the open pit is

~66 t of Au, with an average grade of 3.7 g/t Au, which equates to a total reserve of ~17.8 Mt of ore. The underground total endowment is ~11 t of Au, with an average grade of 3.6 g/t Au, which equates to a total reserve of ~3 Mt of ore (MIDROC Gold website, viewed 2020). The estimated underground ore resource at Sakaro deposit is ~20 t of Au (MIDROC Newsletter June 2014); where the inferred resource at East Sakaro is ~2 Mt of ore, with an average grade of 9.8 g/t Au, for ~19.6 t of Au.

The *Okote* Au prospect is situated in the most southern part of the Adola Au field in the southern Precambrian basement rocks of Ethiopia; it is located ~610 km south of Addis Ababa (~100 km south of the Lega Dembi Au mine) (Fig. 5.37). The Adola Au belt is the place where the high-grade Mozambique belt intercalated with the low-grade ANS rocks (Fig. 5.37, inset map), in which the best mineralization types were formed in Ethiopia including Au, REEs, and gemstone-like beryl and corundum. Geologically, the Okote prospect is part of the southern extension of the metavolcano–sedimentary rocks of the Adola belt, where the high elevation Burjiji–Gariboro gneiss (Ranu granitic gneiss) can be observed ~2 km east of the prospect area. The western side of the prospect is lower in elevation than the eastern side and characterized by intercalation of metagranodiorite and amphibolite and mostly covered with thick younger quartz vein, which can be grouped in the last phase of deformation (Abu Wube 2005). The Okote prospect area is mostly covered by felsic and mafic metavolcanic rocks that are often mylonitized at their contacts. The felsic rocks are represented by metagranodiorite and aplitic dykes and the intermediate-mafic/ultramafic sequences are represented by metagabbro, amphibolite, metadiorite, chlorite–amphibole schist, chlorite schist, and talc schist (Geda 2019). The felsic rocks can be observed crosscutting and intruding the mafic rocks, where mafic xenoliths hosted by granodiorite are common features of the contact area.

Gold mineralization in the Okote prospect is essentially localized to quartz veins, veinlets as well as the wall-rock alteration. The primary Au mineralization of Okote prospect is confined to subparallel shear zones trending at ~northeast within the metagabbro and epidote quartz chlorite schist, of ~3 to 10 m wide and ~3 km strike length in northeast trend. Minor intercalations of talc and talc–tremolite–actinolite and metagranodiorite are also found. Gold occurs as native Au inclusions in chalcopyrite, pyrite, calcite (both in veins and wall rock) and as free Au in the quartz matrix. High Au values were detected in trenches, miner excavations, and drill holes, where the ore zone has been interpreted to lie flat or plunge at a high angle in a northeast-southwest direction with discrete zones of intense deformation resulting in pinch and swell structures (Abu Wube 2005). Gold mineralization occurs in all units and is dominantly associated with quartz veining, alteration zones, and pyrite. Okote valley bisects the area into northern and southern sections and it is rich in alluvial Au placers. Gold is also present in the young tributary valleys and streams of Okote. The greatest Au concentrations are found around the primary quartz veins and alteration zones, which show pinch and swell within the metamorphosed mafic host rocks. Gold mineralization of the Okote prospect is mostly associated with base metal mineralization; whenever anomalous concentrations of base metals exist, it should be inferred that anomalous Au concentrations are likely to existed (Abu Wube 2005).

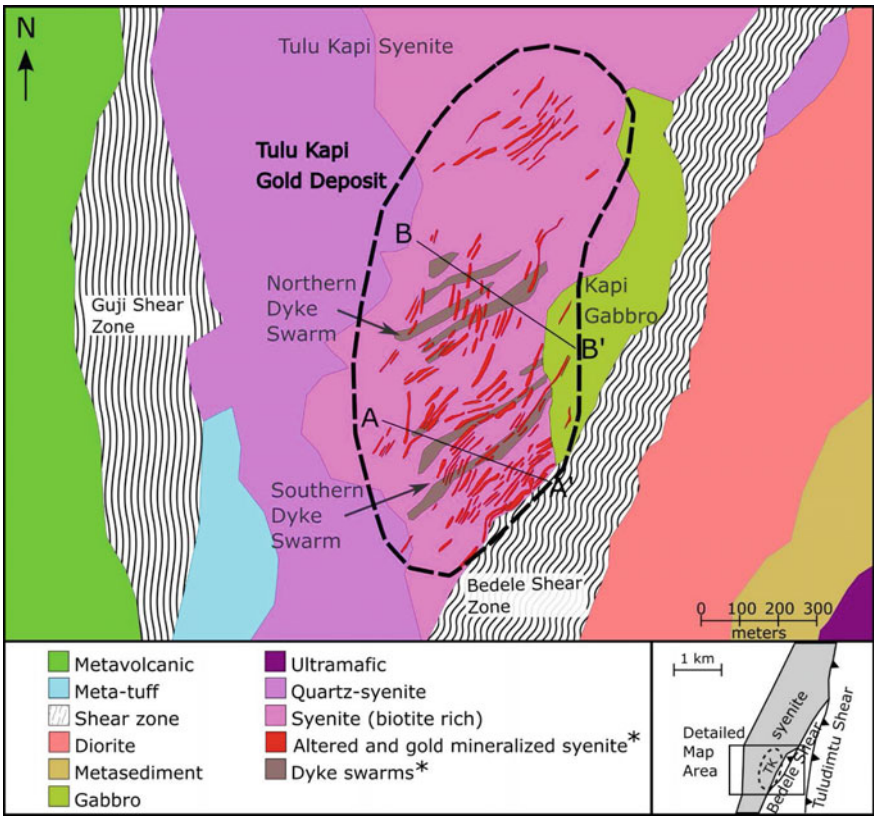

Fig. 5.36 Geological location map of Tulu Kapi Au deposit area (after Molnar 2019, modified)

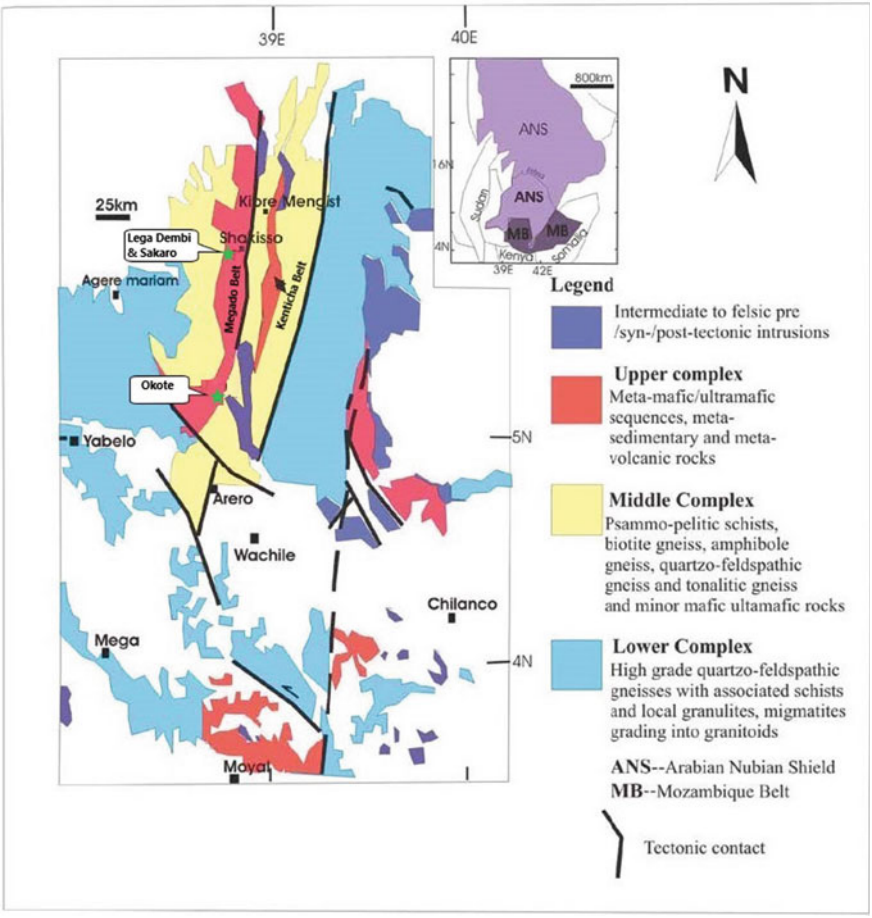

Fig. 5.37 Geological map of the Precambrian rocks of southern Ethiopia with interfingering relationship of the ANS and the Mozambique Belt (MB) showing the location of Lega Dembi, Sakaro and Okote Au deposits (after Abu Wube 2005)

References

Abanyin E, Abdel Salam B, Ackah E, Appiah M, Mohamedy M, Mills S, Stuart H (2015) The discovery and geology of the Galat Sufar south deposit, Republic of the Sudan. In: New GenGold 2017, Conference, Case Histories of Discovery, Perth Western Australia, Paydirt Media, Perth, Conference Proceedings, pp 115–130

Abd El-Monsef M, Slaem I, Slobodnik M, Ragab A (2018) Fluid evolution of Au-Cu zones in Um Balad area, North Eastern Desert of Egypt: implications from mineral chemistry and fluid inclusions. J Afr Earth Sci 143:321–338

Abd El-Rahman Y, Seifert T, Said A (2018) The South Um Mongul Cu-Mo-Au prospect in the northern Eastern Desert of Egypt: Tonian porphyry-style mineralization with an Ediacaran hydrothermal iron-oxide overprint. Ore Geol Rev 99:217–234

Abd El-Wahed MA, Harraz HZ, El-Behairy MH (2016) Transpressional imbricate thrust zones controlling gold mineralization in the Central Eastern Desert of Egypt. Ore Geol Rev 78:424–446

Abdelaal A, Sultan M, Elhebiry, M, Krishnamurthy RV, Sturchio N (2021) Integrated studies to identify site-specific parameters for environmentally benign mining operations: a case study from the Sukari Gold Mine, Egypt. Sci Total Environ 750:141654

Abdelnasser A, Kumral M (2017) The nature of gold-bearing fluids in Atud gold deposit, Central Eastern Desert, Egypt. International Geology Reviews 59:1845–1860

Abraham S, Bheemalingeswara KV, Gebreselassie S (2015). Geology of volcanogenic massive sulfide deposit near Meli, northwestern Tigray, northern Ethiopia. Momona Ethiopian J Sci (MEJS) V7(1):85–104

Adam MMA, Lv X, Rahman AAA, Stern RJ, Abdalrhman AAA, Ullah Z (2020) In-situ sulfur isotope and trace element compositions of pyrite from the Neoproterozoic Haweit gold deposit, NE Sudan: Implications for the origin and source of the sulfur: Ore Geol Rev 120:103405

Ahmed AH, Gharib ME (2016) Porphyry Cu mineralization in the eastern desert of Egypt: inference fromgeochemistry, alteration zones, and ore mineralogy. Arab J Geosci 9:179. https://doi.org/10.1007/s12517-015-2107-x

Akaad MK, Noweir AM, Abu El Ela AM (1996) Geology of the Pan-African basement rocks of the Jabal al Hadid, Wadi Mubarak District, Eastern Desert, Egypt (covering parts of sheet NG 36 G 3, 6 and NG 36 H 1, 4). Rep Geol Surv Egypt 73

Albino GV, Jalal S, Christensen K (1995) Neoproterozoic mesothermal gold mineralization at Sukhaybarat East mine. Trans Inst Mining Metallur (Sect B: Appl Earth Sci) 104:B157–B170

Al-Dabbagh MH, Dowd PA (1996) Sukhaybarat Gold Mine, Saudi Arabia. Mineral Industry International, July 16–21

Al-Khirbash S, Heikal MTS, Whitehouse MJ, Windley BF,Al Selwi K (2021) Evolution and mineralization of the Precambrian basement of Yemen. In: Hamimi Z et al.(eds) The geology of the Arabian-Nubian Shield, Regional Geology Reviews:633–657. https://doi.org/10.1007/978-3-030-72995-0_24

Alemu T, Abebe T (2007) Geology and tectonic evolution of the Pan-African Tulu Dimtu Belt, Western Ethiopia. Online J Earth Sci 1:24–42

Allen A, Tadesse G (2003) Geological setting and tectonic subdivision of the Neoproterozoic orogenic belt of Tuludimtu, western Ethiopia. J Afr Earth Sci 36:329–343

Almond DC, Ahmed F, Shaddad MZ (1984) Setting of gold mineralization in the Northern Red Sea Hills of Sudan. Econ Geol 79:389–392

Al-Otaibi RH, Lewis RS, Ben Talib M, Christian RP (1995) Geology and gold mineralization of the Bil'iwy prospect, Murayjib-Umm Hafra region, Kingdom of Saudi Arabia. Saudi Arabian Deputy Ministry for Mineral Resources Technical Report USGS-TR-95-2

Al-Shameery MA, Sun FY (2011) Geology and fluid inclusion of Wadi Sharis Neoproterozoic orogenic gold deposits in northwestern Yemen. Global Geol 14:21–28. https://doi.org/10.3969/j.issn.1673-9736.2011.01.04

Archibald SM, Martin C, Thomas DG (2014) NI 43-101 Technical report on a mineral resource estimate at the Terakimti Prospect, Harvest Property (centered at 38° 21′ E, 14° 19′ N), Tigray National Region, Ethiopia. Prepared for Tigray Resources Inc

Ashworth KL, Abdulaziz MI (1978) Economic geology and evaluation of the Jabal Idsas magnetite deposits: Saudi Arabian Directorate General of Mineral Resources Open-File Report DGMR-664

Bailo T, Schandelmeier H, Franz G, Sun CH, Stern RJ (2003) Plutonic and metamorphic rocks from the Keraf suture (NE Sudan): a glimpse of Neoproterozoic tectonic evolution on the NE margin of W. Gondwana. Precambr Res 123:67–80

Bampton M (2017) Hamama West Deposit, Abu Marawat concession, Arab Republic of Egypt. NI 43-101 Independent Technical Report prepared for Aton Resources Ltd

Barrie CT, Abdalla MAF, Hamer D (2016) Volcanogenic massive sulphide-oxide gold deposits of the Nubian Shield in Northeast Africa. In: Bouabdellah M, Slack JF (eds) Mineral deposits of North Africa. Mineral resource reviews. Springer, Berlin, pp 417–435. https://doi.org/10.1007/978-3-319-31733-5_17

Barrie CT, Nielsen FW, Aussant CH (2007) The Bisha volcanic-associated massive sulfide deposit, western Nakfa terrane, Eritrea. Econ Geol 102:717–738
Billay AY, Kisters AFM, Meyer FM, Schneider J (1997) The geology of the Lega Dembi gold deposit, southern Ethiopia: implications for Pan-African gold exploration. Miner Deposita 32:491–504
Blades ML, Collins AS, Foden J, Payne JL, Xu X, Alemu T, Woldetinsae G, Clark C, Taylor RJM (2015) Age and hafnium isotopic evolution of the Didesa and Kemashi Domains, western Ethiopia. Precambr Res 270:267–284
Bookstrom AA, Bosch PS, Jannadi EH, Komi MB (1994) Hamdah gold deposit. In: Collenette P, Granger DJ (eds) Mineral resources of Saudi Arabia, not including oil, natural gas, and sulfur. DGMR Special Publication Sp-2
Botros NS (2004) A new classification of the gold deposits of Egypt. Ore Geol Rev 25:1–37
BRGM Geoscientists (1993) Khnaiguiyah zinc-copper deposit prefeasibility study; synopsis of geology and mineralization: Saudi Arabian Directorate General of Mineral Resources Technical Report BRGM-TR-13-4
Burke K, Sengör C (1986) Tectonic escape in the evolution of the continental crust. In: Barazangi M, Brown L (eds) Geodynamics Series. American Geophysical Union, Washington, DC, pp 41–53
Cantex (2000) Intern Geological Report on the Suwar Ni-Cu Prospect, Northwest Region, Republic of Yemen, vol 1. Report No 00821 Prepared for Canadian Mountain Minerals, Yemen Ltd by Vince Roberts and Associates Pty Ltd, Perth, Western Australia
Cheng XH, Xu JH, Wang JX, Xue QP, Zhang H (2017) Carbonic fluids in the Hamadi gold deposit, Sudan: Origin and contribution to gold mineralization: Can J Earth Sci 54:494–511
Dean C, David L, David G (2010) Technical report on the Koka Gold Deposit, Eritea; Chalice Gold Mine Ltd, Asmara, Eritrea
Deksissa DJ, Koeberl C (2004) Geochemistry, alteration, and genesis of gold mineralization in the Okote area, southern Ethiopia. Geochem J 38:307–331
Doebrich JL, Al-Jehani AM, Siddiqui AA, Hayes TS, Wooden JL, Johnson PR (2007) Geology and metallogeny of the Ar Rayn terrane, eastern Arabian shield: evolution of a Neoproterozoic continental-margin arc during assembly of Gondwana within the East African Orogen. Precambr Res 158:17–50
Doebrich JL, Zahony SG, Leavitt JD, Portacio JS Jr, Siddiqui AA, Wooden JL, Fleck RJ, Stein HJ (2004) Ad Duwayhi, Saudi Arabia: geology and geochronology of a Neoproterozoic intrusion-related gold system in the Arabian shield. Econ Geol 99:713–741
Drury SA, Berhe SM (1993) Accretion tectonics in northern Eritrea revealed by remotely sensed imagery. Geol Mag 130:177–190
Drury SA, De Souza Filho CR (1998) Neoproterozoic terrane assemblages in Eritrea: review and prospects. J Afr Earth Sc 27:331–348
Duckworth G (2020) Feasibility study Ni 43-101 Technical Report Block 14 Gold Project, Republic of the Sudan, Report Date: 14 September 2020. Orca Gold Inc, Report 3209-43-101-14-Sep-2020
El Gaby S, List FK, Tehrani R (1990) The basement complex of the Eastern Desert and Sinai. In: Rushdi S (ed) The geology of Egypt. Balkema, Rotterdam, pp 175–184
Elsamani Y, Almuslem AA, El Tokhi M (2001) Geology and geotectonic classification of Pan-African gold mineralizations in the Red Sea Hills, Sudan. Int Geol Rev 43:1117–1128
El-Shimi KA (1996) Geology, structure and exploration of gold mineralization in Wadi Allaqi area (SW, Eastern Desert, Egypt). Dissertation, Ain Shams University, Egypt
Emam A, Zoheir B (2013) Au and Cr mobilization through metasomatism: microchemical evidence from ore-bearing listvenite, South Eastern Desert of Egypt. J Geochem Explor 125:34–45
Franzmann D, Smith P, Johnson N, Zammit M (2015) Mineral resources and mineral reserve estimate for the Sukari Gold Project, Egypt. $2-101F1 report prepared for Centamin plc
Frick CN, Al-Jawadi ZY (2009) Mining strategy for Republic of Yemen. Geol Surv Mineral Resour Board Internal Report
Gaboury D (2013) Does gold in orogenic deposits come from pyrite in deeply buried carbon-rich sediments? Insight from volatiles in fluid inclusions. Geology 41:1207–1210

Gaboury D (2015) Geometrical characteristics and origin of the gold mineralisation at the WG-03 deposit, Gabgaba project, Sudan. Unpublished report to Manum, 14 June
Gaboury D (2019) Parameters for the formation of orogenic gold deposits. Appl Earth Sci 128:124–133
Gaboury D, Nabil H, Ennaciri A, Maacha L (2020) Structural setting and fluid composition of gold mineralization along the central segment of the Keraf suture, Neoproterozoic Nubian Shield, Sudan: implications for the source of gold. Int Geol Rev. https://doi.org/10.1080/00206814.2020.1838336
Gandhi SS, Bell RT (1996) Kiruna/Olympic Dam-type iron, copper, uranium, gold, silver. In: Eckstrand OR, Sinclair WD, Thorpe RI (eds) Geology of Canadian mineral deposit types. Geology of Canada, vol 8. Geological Survey of Canada, Ottawa, Canada, pp 513–522
Gaukroger KF, Morfett EM (1982) Exploration for gold in the Zalm-As Siham area, southeast Najd. Saudi Arabian Directorate General for Mineral Resources Open-File Report RF-OF-02-30
Geda S (2019) The role of intrusion in orogenic poly phase gold mineralization, Okote area (Southern Ethiopia). Dissertation, Addis Ababa Science and Technology University, Addis Ababa, Ethiopia
Ghebreab W, Greiling RO, Solomon S (2009) Structural setting of Neoproterozoic mineralization, Asmara district, Eritrea. J Afr Earth Sc 55:219–235
Granitzio F, Rayner J, Aregay T (2015) Tulu Kapi Gold Project: a history of repeated discoveries in Western Ethiopia. https://www.kefi-minerals.com/files/files/KEFI-NewGenGold-Paper-TuluKapi-web.pdf
Hariri MM, Makkawi MH (2004) Gold mineralization distributions within rock units at the Hajr gold mine, southwest Saudi Arabia. Arab J Sci Eng 29(2A):111–121
Harraz HZ (1991) Lithochemical prospecting and genesis of gold deposits in El Sukari gold mine, Eastern Desert, Egypt. Dissertation, Tanta University
Harraz HZ (2000) A genetic model for a mesothermal Au deposit: evidence from fluid inclusions and stable isotopic studies at El-Sid Gold Mine, Eastern Desert. J Afr Earth Sci 30:267–282
Harraz HZ (2002) Fluid inclusions in the mesozonal gold deposit at Atud mine, Eastern Desert, Egypt. J Afr Earth Sci 35:347–363
Harraz HZ, El-Dahhar MA (1993) Nature and composition of gold forming fluids at Um Rus area, Eastern Desert, Egypt: evidence from fluid inclusions. J Afr Earth Sci 16:341–353
Harrell JA, Brown VM (1992) The world's oldest surviving geologic map: the 1150 B.C. Turin Papyrus from Egypt. J Geol 100:3–18
Helmy HM, Kaindl R (1999) Mineralogy and fluid inclusion studies of the Au-Cu quartz veins in the Hamash area, South-Eastern Desert, Egypt. Mineral Petrol 65:69–86
Helmy M, Reinhard K, Fritz H, Loizenbauer J (2004) The Sukari Gold Mine, Eastern Desert-Egypt: structural setting, mineralogy and fluid inclusion study. Miner Deposita 39:495–511
Hilmy ME, Osman A (1989) Remobilization of gold from a chalcopyrite-pyrite mineralization Hamash gold mine, Southeastern Desert, Egypt. Mineral Deposita 24:244–249
Hussein AA (1990) Mineral deposits. In: Said R (ed) The geology of Egypt. Balkema, Rotterdam, pp 511–566
Jannadi EH, Khalil I, Al Harbi ZM, Siddiqui AA (2005) Assessment and regional exploration of the Musayna'ah district. Saudi Geological Survey Open-file Report SGS-OF-2005-9
Johnson PR, Halverson GP, Kusky TM, Stern RJ, Pease V (2013) Volcanosedimentary basins in the Arabian-Nubian Shield: markers of repeated exhumation and denudation in a Neoproterozoic accretionary orogen. Geosciences 3:389–445
Johnson PR, Kattan FH (2012) The geology of the Arabian Shield. Saudi Geological Survey, p 466
Johnson PR, Offield TW (1994) Structural setting of mineralization in the Al Wajh gold district. Saudi Arabian Deputy Ministry for Mineral Resources Technical Report USGS-TR-94-2, Kingdom of Saudi Arabia
Johnson PR, Quick JE, Kamilli RJ (1989) Geology and mineral resources of the Bi'r Tuluhah quadrangle, Kingdom of Saudi Arabia. Saudi Arabian Directorate General of Mineral Resources Technical Record USGS-TR-09-1

Johnson PR, Zoheir BA, Ghebreab W, Stern RJ, Barrie CT, Hamer RD (2017) Gold-bearing volcanogenic massive sulfides and orogenic-gold deposits in the Nubian Shield. S Afr J Geol 120:63–76

Johnson PR, Zoheir BA, Ghebreab W, Stern RJ, Barrie CT, Hamer RD (2017) Gold-bearing volcanogenic massive sulfides and orogenic-gold deposits in the Nubian Shield. South African. J Geol 120:63–76

Khalil KI, Helba HA, Mücke A (2003) Genesis of the gold mineralization at the Dungash gold mine area. Eastern Desert, Egypt: A mineralogical-microchemical study. J Afr Earth Sci 37:111–122

Klemm D, Klemm R, Murr A (2001) Gold of the Pharaohs: 6000 years of gold mining in Egypt and Nubia. J Afr Earth Sci 33:643–659

Klemm R, Klemm D (2013) Gold and gold mining in ancient Egypt and Nubia. In: Natural science in archaeology. Springer, Berlin, p 341

Kusky TM, Ramadan T (2002) Structural controls on Neoproterozoic mineralization in the SE Desert, Egypt. An integrated field, Landsat TM, and SIR C/X approach. J Afr Earth Sci 35:107–121

LeAnderson J, Yoldash M (1990) An evaluation of the Umm al Qurayyat gold deposit, Al Wajh district, Sheet 26D. Saudi Arabian Directorate General of Mineral Resources Open-File Report DGMR-OF-09-19

LeAnderson PJ, Yoldash M, Johnson PR, Offield TW (1995) Structure, vein paragenesis, and alteration in the Al Wajh gold district, Saudi Arabia. Econ Geol 90:2262–2273

Legg CA (1983) Metal zoning in the Kutam copper-zinc deposit (17/43): Saudi Arabian Deputy Ministry for Mineral Resources Open-File Report DGMR-OF-04-15

Leistel JM, Eberle JM (1999) The Zalm gold deposit, in IUGS/UNESCO, Base- and precious-metal deposits in the Arabian shield: Deposit-modeling workshop, November 12–19, 1999. Saudi Arabian Deputy Ministry for Mineral Resources, Jiddah, Saudi Arabia

Lewis RS, Albino GV, Johnson PR (1997) Geology and gold mineralization of the Murayjib-Umm Hafra mineral belt, Kingdom of Saudi Arabia. Saudi Arabian Deputy Ministry for Mineral Resources Technical Report USGS-TR-97-2

Lewis RS, Schull HW (1994) Geology and gold mineralization of the An Najadi mineral belt and comparison to the Sukhaybarat gold mine. Saudi Arabian Deputy Ministry for Mineral Resources Technical Report USGS-TR-94-6, Kingdom of Saudi Arabia

Makroum F (2017) Structural interpretation of the Wadi Hafafit culmination: a Pan-African gneissic dome in the central Eastern Desert, Egypt. Lithosphere 9:759–773

Malmgren K, Andersson W (1994) Sukhaybarat gold mine. In: Collenette P, Grainger DJ (compilers) Mineral Resources of Saudi Arabia: Saudi Arabian Directorate General of Mineral Resources Special Publication DGMR-SP-2, pp 111–115

Mohamed HA, Ali S, Sedki T, Abdel Khalik I (2018) The Sukari Neoproterozoic granitoids, Eastern Desert, Egypt: petrological and structural implications. J Afr Earth Sci 149:426–440

Molnar ZBK (2019) The Tulu Kapi gold deposit of the Western Ethiopian Shield: structural framework, U-Pb zircon geochronology and paragenesis. M.Sc. thesis, Waterloo, Ontario, Canada

Obeid MA, Hussein AM, Abdallah MA (2001) Shear zone-hosted gold mineralization in the Late Proterozoic rocks of El Beida area, south Eastern Desert, Egypt. Trans Inst Mining Metallur (Sect B: Appl Earth Sci) 110:192–204

Oljira T, Warkisa G (2020) Geology, geochemistry and geochronology of the gold mineralization hosting Syenite, Tulu Kapi, Western Ethiopia: a review. Preprints 2020, 2020090598. https://doi.org/10.20944/preprints202009.0598.v1

Ordūna J (2018) Gold and base metal deposits of the Abu Marawat concession, Egypt. Presentation for Aton Resources Inc, downloaded 10 January 2019. Aton resources gold and base metal deposits of the Abu Marawat Concession

Perret J, Eglinger A, André-Mayer A-S, Aillères L, Feneyrol J, Hartshorne C, Abanyin E, Bosc R (2020) Subvertical, linear and progressive deformation related to gold mineralization at the Galat Sufar South deposit, Nubian Shield, NE Sudan. J Struct Geol 135:104032

Pollard PJ (2008) Gold mineralisation and associated alteration at the Tulu Kapi prospect, Ethiopia. Recommendations for future work. Private report, Minerva Resources Pty Ltd

Pouit G, Bournat G (1982) Volcanosedimentary Cu-Pb-Zn(-Ag) sulfide mineralization in Saudi Arabia; review of geologic and gitologic context and its application to mineral exploration. Saudi Arabian Deputy Ministry for Mineral Resources Open-File Report BRGM-OF-02-4

Rabeiy RES, El Tahlawi MR, Boghdady GY (2017) Occupational health hazards in the Sukari Gold Mine, Egypt. J Afr Earth Sci 146:209–216

Ramadan TM (1997) Shear zone gold mineralization at Marsa Sha'b area, South Eastern Desert, Egypt. In: Fourth Biennial SGA Meeting, Turku, Finland, pp 293–296

Ramadan TM, Abdelsalam MJ, Stern RJ (1999) Mineral exploration with Landsat TM and SIR-C/X SAR images: Wadi Allaqi suture, South Eastern Desert, Egypt. In: South-Central Geol Society of America Meeting, 1, Lubbock, Texas, p A33

Raslan MF, Ali MA (2010) Mineral chemistry of polymetallic mineralization associated with altered granite, Hangaliya area, South Eastern Desert, Egypt. Geologija 53:129–138

Robert F (1996) Quartz-carbonate vein gold. In: Eckstrand OR, Sinclair WD, Thorpe RI (eds) Geology of Canadian mineral deposit types. Geology of Canada, vol 8. Geological Survey of Canada, Ottawa, pp 350–366

Ross AF, Martin CJ (2012) Sunridge gold corp: mineral resource estimate update, Emba Derho Deposit, Adi Nefas Property, Eritrea. NI 43-101 Technical report prepared by Snowden Mining Industry Consultants Inc for Sunridge Gold Inc with contributions by Blue Coast Metallurgy Ltd

Sangster DF, Abdulhay GJS (2005) Base metal (Cu-Pb-Zn) mineralization in the Kingdom of Saudi Arabia. Saudi Geological Survey, Jeddah

Smith CW, Anderson RE, Dehlavi MR (1977) Geology and ore deposits of the Kutam mine, Kingdom of Saudi Arabia. U.S. Geological Survey Saudi Arabian Project Report 211, 51 p

Stern RJ, Ali KA, Asimow PD, Azer MK, Leybourne MI, Mubarak HS, Ren M, Romer RL, Whitehouse MJ (2020) The Atud gabbro–diorite complex: glimpse of the Cryogenian mixing, assimilation, storage and homogenization zone beneath the Eastern Desert of Egypt. J Geol Soc 177:965–980

Stern RJ, Hedge CE (1985) Geochronologic constraints on late Precambrian crustal evolution in the Eastern Desert of Egypt. Am J Sci 285:97–127

Stern RJ, Nielsen KC, Best E, Sultan M, Arvidson RE, Kroner A (1990) Orientation of late Precambrian sutures in the Arabian Nubian shield. Geology 18:1103–1106

Surour AA, Harbi HM, Ahmed AH (2014) The Bi'r Tawilah deposit, central western Saudi Arabia: Supergene enrichment of a Pan-African epithermal gold mineralization. J Afr Earth Sc 89:149–163

Taib M (2015) The mineral industry of Egypt. In: U.S. Geological survey mineral yearbook

Teklay M, Kröner A, Mezger K (2001) Geochemistry, geochronology and isotope geology of Nakfa intrusive rocks, northern Eritrea: products of a tectonically thickened Neoproterozoic arc crust. J Afr Earth Sc 33:283–301

Testard J (1983) Khnaiguiyah, a synsedimentary hydrothermal deposit comprising Cu-Zn-Fe sulfides and Fe oxides in an ignimbritic setting. Saudi Arabian Deputy Ministry for Mineral Resources Open-File Report BRGM-OF-03-9

Valliant WW, Salmon B (2012) Technical report on the Abu Marawat Concession, Egypt. NI 43-101 Indpendednt technical report prepared for Alexander Nubia International Inc

White WH, Doebrich JL (1988) Gold deposits of the Ishmas district, Kingdom of Saudi Arabia: Saudi Arabian Directorate General of Mineral Resources Technical Record USGS-TR-07-5

Worku H, Schandelmeier H (1996) Tectonic evolution of the Neoproterozoic Adola Belt of southern Ethiopia: evidence for a Wilson Cycle process and implications for oblique plate collision. Precambr Res 77:179–210

Worku H, Yifa K (1989) The tectonic evolution of the Precambrian metamorphic rocks of the Adola belt (Southern Ethiopia) and its implication on gold mineralization. Report, EIGS, Addis Ababa

Worl RG (1980) Gold deposits associated with the Jabal Ishmas-Wadi Tathlith fault zone. In: Cooray PG, Tahoun SA (eds) Evolution and mineralization of the Arabian–Nubian shield. King Abdulaziz University Faculty of Earth Sciences, Jeddah. IAG Bull 3(4):61–69

Worl RG, Smith CW (1982) Reconnaissance investigations of ancient gold mines in the southern part of the Wadi Bidah district, Jabal Ibrahim and Al'Aqiq quadrangles. Saudi Arabian Deputy Ministry for Mineral Resources Open-File Report USGS-OF-02-43

Wube A (2005) Mineralization and associated structures of Okote prospect, Southern Ethiopia. M.Sc. thesis, Addis Ababa University, Addis Ababa, Ethiopia

Zhao K, Yao H, Wang J, Ghebretnsae GF, Xiang W, Xiong Y-Q (2019) Genesis of the Koka gold deposit in Northwest Eritrea, NE Africa: constraints from fluid inclusions and C-H–O–S isotopes. Minerals 9:201. https://doi.org/10.3390/min9040201

Zoheir B, Abdel-Fattah MG, El-Alfy SM (2013) Geochemistry and mineral chemistry of lode gold mineralisation, SE Egypt: implications for ore genesis and exploration. Arab J Geosci 6:4635–4646

Zoheir BA (2008) Characteristics and genesis of shear zone-related gold mineralization in Egypt: a case study from the Um El Tuyor mine, south Eastern Desert. Ore Geol Rev 34:445–470

Zoheir BA (2011) Transpressional zones in ophiolitic mélange terranes: potential exploration targets for gold in the South Eastern Desert, Egypt. J Geochem Explor 111:23–38

Zoheir BA (2012) Controls on lode gold mineralization, Romite deposit, South Eastern Desert, Egypt. Geosci Front 3:571–585

Zoheir B, Akawy A (2010) Genesis of the Abu Marawat gold deposit, central Eastern Desert of Egypt. J Afr Earth Sci 57(4):306–320

Zoheir BA, Akawy A, Hassan I (2008) Role of fluid mixing and wallrock sulfidation in gold mineralization at the Semna mine area, central Eastern Desert of Egypt: evidence from hydrothermal alteration, fluid inclusions and stable isotope data. Ore Geol Rev 34:580–596

Zoheir BA, Creaser RA, Lehmann B (2015) Re-Os geochronology of gold mineralization in the Fawakhir area, Eastern Desert, Egypt. Int Geol Rev 57:1418–1432

Zoheir BA, Emam A (2014) Field and Aster imagery data for the setting of gold mineralization in western Allaqi-Heiani belt, Egypt; a case study from the Haimur deposit. J Afr Earth Sc 99:150–164

Zoheir BA, Goldfarb R, Holzheid A, Helmy HM, El Sheikh A (2020) Geochemical and geochronological characteristics of the Um Rus granite intrusion and associated gold deposit, Eastern Desert, Egypt. Geosci Front 11:325–345

Zoheir BA, Johnson PR, Goldfarb RJ, Klemm DD (2019) Orogenic gold in the Egyptian Eastern Desert: Widespread gold mineralization in the late stages of Neoproterozoic orogeny. Gondwana Res 75:184–217

Zoheir BA, Lehmann B (2011) Listvenite-lode association at the Barramiya gold mine, Eastern Desert, Egypt. Ore Geol Rev 39:101–115

Zoheir BA, Moritz R (2014) Fluid evolution in the El Sid gold deposit, Eastern Desert, Egypt. In: Garofalo PS, Ridley JR (eds) Gold-transporting hydrothermal fluids in the Earth's crust. Geological Society, London, Special Publications, p 402. https://doi.org/10.1144/SP402.3

Zoheir BA, Qaoud NN (2008) Hydrothermal alteration and geochemistry of the Betam gold deposit, south Eastern Desert, Egypt: mass-volume-mineralogical changes and stable isotope systematics. Appl Earth Sci (trans Inst Mining Metallur B) 117:55–76

Zoheir BA, Steele-MacInnis M, Garbe-Schönberg D (2019) Orogenic gold formation in an evolving, decompressing hydrothermal system: genesis of the Samut gold deposit, Eastern Desert, Egypt. Ore Geology Rev 105:236–257

Chapter 6
Hydrothermal Mineral Deposits in Volcano–Sedimentary Environments

Contents

6.1 Introduction . . . 323
6.2 Volcano–Sedimentary Mineral Deposits in Saudi Arabia . . . 327
6.2.1 Volcanogenic–Massive Sulfide Deposits . . . 327
6.3 Volcano–Sedimentary Mineral Deposits in Yemen . . . 340
6.3.1 Jabali Mississippi Valley–Type Zn–Pb–Ag Deposit . . . 348
6.4 Volcano–Sedimentary Mineral Deposits in the Eastern Desert of Egypt . . . 352
6.4.1 Introduction . . . 352
6.4.2 The Hamama West Prospect (Abu Marawat Mineral District) . . . 354
6.4.3 The Um Samiuki Mineral District . . . 359
6.4.4 The Derhib–Abu Gurdi Mineral District . . . 362
6.5 Volcano–Sedimentary Mineral Deposits in Sudan . . . 367
6.5.1 Oxidized Surface Zones (Gossans) . . . 371
6.5.2 Hypogene Cu–Zn–Au–Ag Volcanogenic Massive Sulfide Deposits . . . 371
6.6 Volcano–Sedimentary Mineral Deposits in Eritrea . . . 378
6.6.1 Bisha Volcanogenic Massive Sulfide District . . . 379
6.6.2 Asmara Volcanogenic Massive Sulfide District . . . 390
6.7 Volcano–Sedimentary Mineral Deposits in Ethiopia . . . 397
References . . . 406

6.1 Introduction

Hydrothermal deposits: ore minerals precipitated from high-temperature aqueous fluids of different origins.

(a) *Deposits in orogenic environments*

- Orogenic gold deposits

A. Hassan Ahmed, *Mineral Deposits and Occurrences in the Arabian–Nubian Shield*,
Earth and Environmental Sciences Library,
https://doi.org/10.1007/978-3-030-96443-6_6

- Carlin-type gold deposits
- Ironoxide–copper–gold (IOCG) deposits.

(b) *Deposits in volcano–sedimentary environments*

- Volcanogenic massive sulfide (VMS/VHMS) deposits
- Sedimentary exhalative (SEDEX) deposits
- Mississippi-Valley Type (MVT) deposits
- Red-bed copper deposits

Mineral deposits of volcano–sedimentary environments, island arcs, and mid-ocean ridges are of great economic importance in extracting many metallic elements, such as Cu, Zn, Pb, Au, Ag, and other economically important metals. The components of these volcano–sedimentary associations are derived mainly from submarine volcanic sources called *volcanic exhalations*, which are precipitated in volcano–sedimentary or sedimentary basins, and are therefore referred to as *double-origin deposits*. This group of mineral deposits includes a number of ores, including *volcanogenic massive sulfide* (VMS) *deposits* (or *volcanic-hosted massive sulfide* (VHMS) *deposits*), *sedimentary exhalative* (SEDEX) *deposits*, *Mississippi Valley–type* (MVT) *deposits*, and *red-bed deposits*, which are all major sources of base-metal sulfides.

Hydrothermal mineral deposits in volcano–sedimentary environments represent the dominant source worldwide of Pb, Zn, Cu, Co, and U and are significant sources of Ag and, to a lesser extent, Au. The major types of ore deposits are those of base-metal sulfide deposits. Mineral deposits in volcano–sedimentary basins are either syngenetic, which are formed at the same time of sedimentation of the host rocks, or epigenetic, which are formed after sedimentation of the host rocks. Most host basins were not sites of magmatic activity during mineralization. Neither magmatic hydrothermal fluids nor magmatic heat-driving fluid flow are thus considered to be factors in the formation of these mineral deposits in sedimentary basins. Instead, metal-carrying solutions migrate long distances through the sedimentary rocks of the basin and in some cases also through underlying basement (Ridley 2013). The hydrothermal fluids in volcano–sedimentary basins are at relatively low temperatures, ranging ~00–150 °C, but sometimes reaching up to ~250 °C. Efficient transport and precipitation of ore minerals from migrating low-temperature fluids are required for specific geochemical environments.

Hydrothermal fluids of non-magmatic origin in the volcano–sedimentary basins are called *basinal fluids* and include seawater and meteoric water origin that have infiltrated from above into the basin, as well as the connate and diagenetic waters that are derived from within the basin itself. The metal contents of seawater and meteoric waters are low; however, their metals are most probably have been dissolved into the basinal hydrothermal fluids either during fluid circulation or via diagenetic reactions. In either case, these fluids are derived by leaching of the sedimentary rocks in the basin or from underlying basement rocks. There are empirical relationships between the

type of hydrothermal mineral deposits in the volcano–sedimentary basins and the type of sedimentary rocks that form the major aquifers in the sedimentary basins (Fig. 6.1). The Zn-rich deposits occur in carbonate-dominated sequences, while the Pb-rich deposits are found in close association with sandstones, and the Cu-rich deposits commonly associated with sequences of either continental red-bed sandstones or oceanic basaltic lavas, or both (Fig. 6.1; Ridley 2013). These relationships suggest that the metal content of the fluid is mainly controlled by metal availability in specific rocks of the volcano–sedimentary basin. For example, in Zn-rich deposits, Zn would be potentially released from limestone via replacement of calcite by dolomite. In the case of Pb-rich deposits, Pb can be in relatively high concentrations in feldspars of clastic sediments, and these are replaced in many basins by clay minerals during diagenesis, potentially releasing Pb. On the other hand, in Cu-rich deposits, Cu can be concentrated via adsorption onto hematite or iron hydroxide coating of quartz grains in red-bed sandstones and these coatings may be dissolved during syndiagenetic fluid flow. Copper can be also sourced from ocean-floor basalts to form VHMS (VMS) deposits, and may thus also be sourced from mafic rocks interbedded with sedimentary rocks in the volcano–sedimentary basin, most likely when primary mafic silicate minerals are replaced by lower-temperature hydrous minerals such as chlorite and epidote (Ridley 2013).

The base-metal sulfide mineral deposits in volcano–sedimentary basins may be syngenetic, syndiagenetic, or epigenetic, where the ores have the following common characteristics (Ridley 2013): (1) Hosted in sedimentary and/or volcano–sedimentary basins. (2) "Syngenetic ores are generally stratiform and stratabound. Syn-diagenetic and epigenetic ores are generally stratabound." (3) Mineral deposits of these types are formed at relatively low temperatures between approximately 60 and 250 °C. (4) In many cases, the ore fluids have salinity higher than seawater. (5) Many ores have an intimate relationship with either abundant sedimentary organic matter or with migrated hydrocarbons (oil or gas). The classification of these volcano–sedimentary base-metal deposits are based mainly on the metal content, host-rock type, and the timing of mineralization relative to sedimentation. The main classes of volcano–sedimentary mineral deposits can be categorized under the following types:

(i) ***Volcanogenic massive sulfide (VMS) deposits*** (or *volcanic-hosted massive sulfide* (VHMS) *deposits*): These are mainly found as stratabound and sometimes-stratiform bodies of hydrothermal massive sulfide ores. The VMS deposits occur in a variety of tectonic settings but are typically related to precipitation of metals from hydrothermal solutions circulating in volcanically active submarine environments. They are polymetallic deposits, containing variable metal sulfides such as Cu, Zn, and Pb, in addition to Au and Ag; where the host rocks are submarine volcanic rocks and/or deep-sea sedimentary rocks intercalated with volcanic rocks. There are some geological and geochemical criteria for targeting VMS mineralization (Gibson et al. 2007), which can be summarized as follows: (1) VMS deposits commonly occur in clusters that define the VMS districts. VMS districts occur within large volcanic edifices, calderas, and crustal structures. (2) Some of the largest

deposits (>50 Mt ore) may be associated with a major long-lived crustal structure, or with thick successions of volcaniclastic rocks, or occur in more-stable rifted continental margin settings. The large deposits tend to be associated with widespread, low-temperature alteration systems, felsic volcaniclastics and thin, but laterally extensive Fe and Fe–Mn formations. (3) Deposits associated with mafic-dominated terranes tend to be Cu- and Cu–Zn-endowed. Continental margin or successor rifted arc-hosted deposits with felsic volcaniclastic–sedimentary host rocks have a higher Pb–Zn endowment. (4) Strongly metamorphosed deposits commonly found in Archean or Proterozoic terranes tend to have coarser-grained sulfides and consequently metal recovery is commonly better than for the finely crystalline sulfides in some less metamorphosed districts. Recrystallization can also mechanically purify deposits of metals such as Hg, As, and Sb.

(ii) ***Sedimentary exhalative (SEDEX) deposits***: In contrast to the VMS deposits, SEDEX deposits are dominated by Zn–Pb (with lesser Cu, but commonly Ba- and Ag-rich) hosted in sedimentary rocks of early Proterozoic to Mesozoic age. Barite can also be accumulated near SEDEX deposits. SEDEX deposits are also related to hydrothermal fluids venting onto the sea floor, but without an obvious or direct link to volcanism.

(iii) ***Mississippi Valley–Type (MVT) deposits***: These occur as epigenetic Pb–Zn sulfide deposits in solidified carbonate rocks, at up to ~10 wt%, with equal grades of Pb and Zn metals. MVT deposits can contain other metals as byproducts, including one or more of Ag, Ge, Cd, Cu, barite, or fluorite.

(iv) ***Red-bed copper deposits***: These occur as large, laterally extensive, stratabound Cu deposits, with Co and minor amounts of Ni, Ag, Zn, Pb, and U as important byproducts. This deposit type provides ~30 wt% of the world's Cu supply. The host rock of this deposit type is largely red-bed sandstones overlying black shales of shallow marine or lacustrine origin. It is thus distinct from those of MVT and SEDEX deposits.

In the Arabian–Nubian Shield (ANS), the mineral deposits of volcano–sedimentary environments are essentially found in many places of various tectonic settings including volcano–sedimentary associations, island arcs, and mid-ocean ridges. Most of these mineral deposit types are represented by VMS deposits, and to a lesser extent, sometimes by MVT deposits and stratabound/stratiform red-bed base-metal hosting deposits. Following is a detailed description of most famous localities of these types of mineral deposits and/or occurrences in the ANS, with the same approach used in the previous chapters starting with the Arabian Shield (Saudi Arabia and Yemen) and then the Nubian Shield (Egypt, Sudan, Eritrea, and Ethiopia).

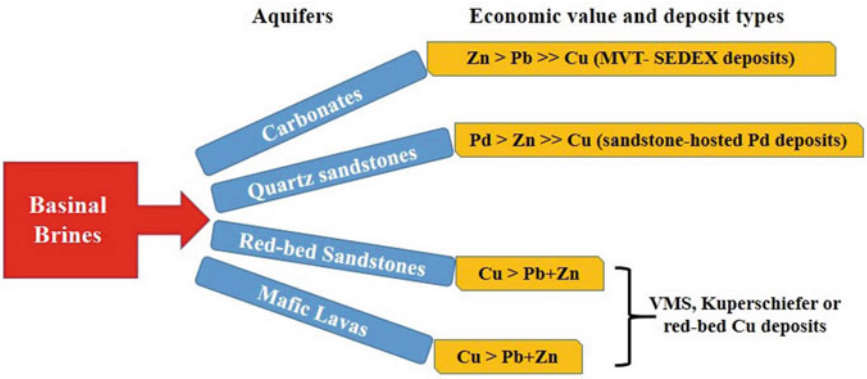

Fig. 6.1 Empirical relations between aquifer rock type and metal content of sediment-hosted hydrothermal ore deposits and examples of each deposit type (modified from Ridley 2013). The ore composition indicates the relative economic value of the metals rather than the concentrations

6.2 Volcano–Sedimentary Mineral Deposits in Saudi Arabia

There are numerous mineral deposits related to the volcano–sedimentary environments in the ANS, in general, and in the Arabian Shield of Saudi Arabia, in particular (Fig. 6.2), including those of island arc and the mid-ocean ridge associations. These mineralizations are mainly represented by VMS and SEDEX mineral deposits/occurrences, which are found in several tectonic terranes of the Arabian Shield including: (1) the Midyan terrane in the northwest, (2) Jiddah terrane in the central-western shield, (3) the Asir terrane in the southwest, (4) the Afif–Ar Rayn terranes in the northeastern Arabian Shield, and (5) the Al Amar terrane in the eastern Arabian Shield (Fig. 6.2). Following are detailed descriptions of the well-known deposits and/or occurrences of these deposit types.

6.2.1 Volcanogenic–Massive Sulfide Deposits

Globally, VMS deposits are major sources of Cu, Zn, Pb, and Ag (± Au); they formed throughout the Earth's history (see, e.g., Lydon 1988, 2007; Hannington et al. 2011). The VMS deposits form in a variety of tectonic settings, including back-arc, intra-arc basins, and mid-ocean ridges (Tornos et al. 2015). The volcanic-arc assemblages of the Arabian Shield are highly favorable for polymetallic VMS deposits, which are concentrated mainly in the western juvenile arc-terranes in the shield that originated at convergent margins in intra-oceanic settings. The host rocks of these VMS deposits are mostly Cryogenian, ranging from ~850 Ma in the Bidah and Shwas districts to ~700 Ma in the Al Amar district (Johnson and Kattan 2012).

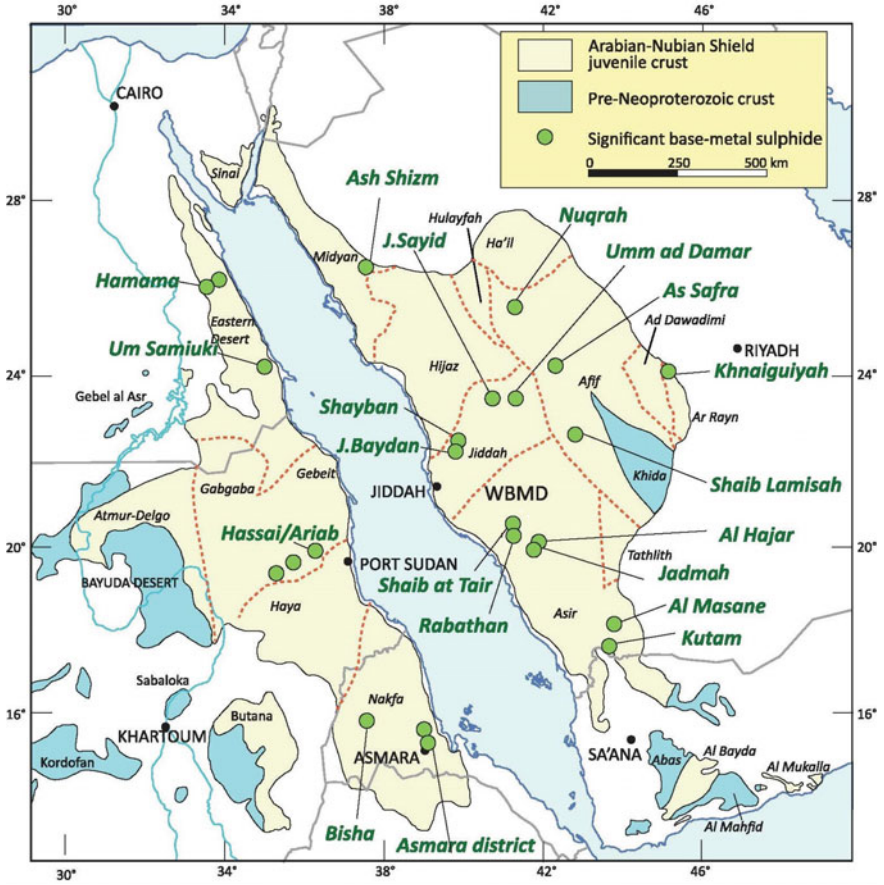

Fig. 6.2 Distribution of major significant base-metal sulfide occurrences in the Arabian–Nubian shield, including the typical VMS as well as Cu–Zn sulfide occurrences of uncertain deposit type (after Volesky et al. 2017)

Many of these mineral deposits are classic examples of VMS mineralization but some others are highly sheared and are of unknown or uncertain deposit type. The VMS deposits are hosted by bimodal mafic-to-felsic volcanic rocks, particularly where the volcanic sequences contain packages of exhalative carbonates and chert, and range in size from small-sized deposits (a few million tons) to large-sized deposits (>150 million tons) of mineralized rock. The most famous occurrences of classic large-sized VMS deposits include *Al Masane* and *Gebel Sayid*. Examples of smaller, but underexplored, VMS deposits are at *Umm ad Damar*, *Ash Shizm*, *Farah Garan*, and *Gebel Baydan*. Weathering zones of some VMS deposits, enriched in supergene gold, have been worked at Al Hajar and are being worked at Jadmah.

Volcanogenic massive sulfide deposits in the Midyan terrane: Cu–Zn mineralization is found in the *Ash Shizm* district, which is located to the northwest of the

city of Al-Ula (Fig. 6.2). The site is located within a volcanic assemblage, including diabase and metabasalt dykes, surrounded on three sides by a plutonic complex of gabbro, diorite, trondhjemite, and granite cut by porphyritic rhyolite dykes. The volcanic assemblage comprises four lithostratigraphic units (Sangster and Abdulhay 2005); the first three volcanic units are interpreted to be members of the Farri group, where a major unconformity separates these rocks from the uppermost unit, which is correlated with the dominantly sedimentary Al'Ays group. The main sulfide deposits and associated alterations consist of a funnel-shaped discordant chloritic alteration aureole extending upward from within Unit I to the top of Unit II. The aureole is ~150 m in width and ~300 m in height and terminates with a red jasper layer at the top of Unit II. A wide mineralization zone (~300 m) of disseminated pyrite surrounds the chloritic aureole at the lower rhyolitic lava facies of Unit II. The host rocks are completely transformed by intense alteration to massive chloritite containing veinlets, amygdules, and irregular spots of silica, epidote, and calcite. The red jasper layer forms a cap to the chloritic funnel-shaped alteration, and irregular patches of sericite occur within and toward the top of the chlorite zone. Sulfide mineralization occurs within the chloritite aureole as a stockwork that begins deep in Unit I as chlorite–sulfide veins. In Unit II, the stockwork increases in breadth to ~100 m and consists of sulfide-bearing veinlets accompanied by chlorite and epidote. The top of the stockwork penetrates a silicified and chloritized breccia containing disseminated sulfides. This is then capped by a band of magnetite-bearing red jasper up to 5 m thick, and at its base, the jasper is brecciated and cemented with pyrite, chalcopyrite, and galena. The entire mineralized complex strikes north/northeast parallel to a bounding fault on the west. The core and base of the stockwork contain mainly chalcopyrite grading upward and outward to increasing amounts of sphalerite, pyrite, and galena. A small body consisting of blocks and fragments of massive sulfide occurs on the footwall of the jasper layer. A second zone of alteration ~200 × 100 m in width is elongated in a north/south direction and located ~1.8 km NE of the main mineralization zone; it lies within the hornfels zone of a nearby granite body. Drill holes into this alteration zone yielded values up to 0.2 wt% Cu and 0.6 wt% Zn (Sangster and Abdulhay 2005).

The principal ore minerals in Gebel Ash Shizm deposit comprise, in decreasing order of weight percent, chalcopyrite, sphalerite, magnetite, bornite, and minor/trace amounts of cobaltite, various tellurides and selenides, titanium-bearing minerals, enargite, and argentite. Supergene weathering mineral products such as malachite, native silver, and greenockite are also present. Gangue minerals are represented mainly by chlorite, epidote, quartz, calcite, muscovite, and sericite. The common presence of ancient workings, in addition to the piles of waste and slag in the area, indicate that this site was previously exploited. Studies confirmed that the exploitation process took place during the Abbasid state. The mineralization of Gebel Ash Shizm appears to possess many of the characteristics of a stringer zone or vent complex of the VMS deposit. The position of the deposit at the transition from a mafic to a felsic volcanic sequence and the association with synvolcanic faulting permit consideration of Gebel Ash Shizm as a VMS deposit (Sangster and Abdulhay 2005). Furthermore, the intense chloritic alteration surrounding an inner Cu-dominated stockwork zone and their abrupt termination at a lithostratigraphic contact marked by a layer of

ferruginous chert (jasper) are all features found in the footwall feeder zone of a typical VMS deposit. The expected overlying massive sulfide body, however, is apparently missing from this deposit. There are three possibilities to explain the absence of a massive sulfide body here (Donzeau 1980): (1) breakup and destruction due to the unstable tectonic environment, (2) modern erosion, and (3) unsuitable depositional conditions at the seafloor. The presence of the small layer of massive sulfide fragments lying immediately under the red jasper layer suggests the first hypothesis may be the most tenable. The synsedimentary brecciation and downslope transport of massive sulfides have been documented in a number of deposits in the Japanese Kuroko ores, the Canadian Shield, and the Canadian Appalachians. The estimated ore reserves of Ash Shism mineralization are ~600,000 tons of ore, with an average grade of 2.84 wt% Cu, 1 wt% Zn, 0.14 wt% Pb, and 25 g/t Ag (Donzeau 1980).

Volcanogenic massive sulfide deposits in Jiddah terrane: The VMS deposits in the west-central part (*Jiddah terrane*) of the Arabian Shield include *Gebel Sayid*, *Umm ad Damar*, *Gebel Shayban*, and *Gebel Baydan*. They are hosted by volcanic-arc rocks of the Arj, Mahd, and Samran groups (described in Chap. 2 of this book), and situated in the northern and northwestern parts of the Jiddah terrane (Fig. 6.2), south of the Bi'r Umq suture. A similar zone of polymetallic Au-bearing VMS mineralization is present in the Ariab and Hassai districts, Sudan, representing a continuation of the Gebel Sayid–Gebel Samran–Gebel Shayban zone of mineralization along the Nakasib suture (Fig. 6.2). The Gebel Sayid deposit is a typical VMS deposit, while Umm ad Damar is a mixed epigenetic–VMS deposit (Sangster and Abdulhay 2005). The two deposits are north and south, respectively, of a set of north/west-trending Najd-related sinistral strike-slip faults (Fig. 6.3), and may be displaced parts of a single base-metal VMS-type province (Johnson and Kattan 2012). The host rocks of Gebel Sayid and Umm ad Damar deposits belong to the Arj group. They consist of several thousand meters of basaltic to andesitic lava, breccia, and tuff, laminated felsic tuff, pyroclastic rocks and volcaniclastic quartz keratophyre, chert, limestone, sandstone, and conglomerate. The Arj group is not directly dated but is older than tonalite, dated at 781 ± 8 Ma (Hargrove 2006), and older than the Mahd group, dated at ~770 Ma.

Gebel Sayid lies within a semicircular belt of volcanic rocks ascribed to the Hulayfah group, Halaban group, and Arj group (Bournat 1981; Johnson and Kattan 2012) that folded around a granite–diorite complex (Fig. 6.3). The Gebel Sayid mineralization is located at the top of a sequence of rhyolitic lavas and pyroclastic rocks, overlain by andesitic pyroclastic rocks and intercalations of flow rocks. The rhyolitic unit is intruded by diorite, granite, and granodiorite. The Gebel Sayid prospect consists of four sulfide bodies (referred to as orebodies 1–4, lodes 1–4, or deposits 1–4), three of which are overlain by an extensive chert unit, while the footwall rocks of the deposit comprise felsic tuff and breccia intensely altered to chloritite (Fig. 6.4). The orebodies spread over an area of ~1000 m extending southwest/northeast and 400 m southeast/northwest (Fig. 6.4). The hanging wall of deposits 1, 2, and 4 is a welded tuff or ignimbrite moderately altered to sericite and talc (Bournat 1981). Lenses of marble or dolomitic limestone are intercalated with

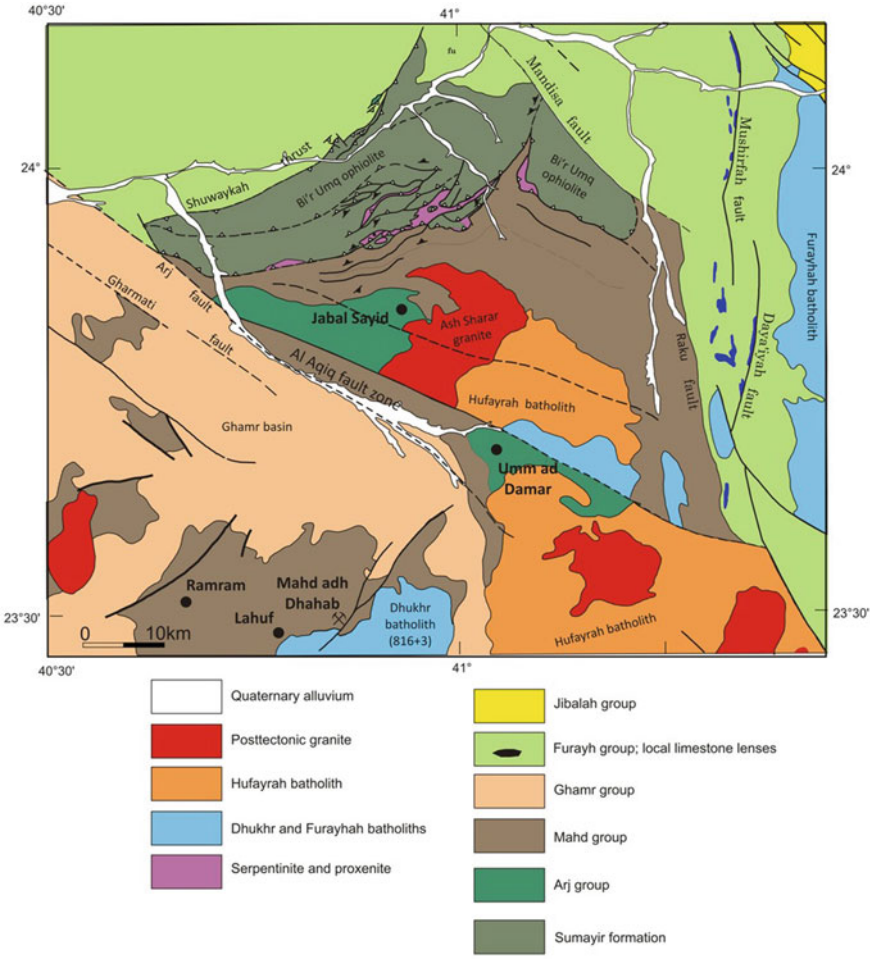

Fig. 6.3 Simplified geological map of the Mahd Adh Dhahab, Gebel Sayid, and Umm ad Damar areas (from Johnson and Kattan 2012)

the ignimbrite, and deposit 3 occurs stratigraphically higher, above the ignimbrite. The four sulfide bodies at Gebel Sayid occur at two different stratigraphic positions (Fig. 6.4). Deposits 1, 2, and 4 comprise the main massive mineralization horizon; within these bodies a massive sulfide style of mineralization was distinguished, associated with chert, and composed chiefly of pyrite and sphalerite, as well as stringer ore in veins and veinlets of pyrite and chalcopyrite. Deposit 3 comprises two massive sulfide bodies ~10 m thick composed of pyrite, pyrrhotite, chalcopyrite, and sphalerite. Lesser amounts of tellurides, native Au and Ag, electrum, and Sn-bearing minerals have also been recognized at the Gebel Sayid mineralization (Bournat 1981).

The Gebel Sayid mineralization is blind and has no surface expression; the other deposits crop out and are marked by gossans cover. Massive sulfides make up the upper part of orebody 1 and 20% of orebody 4; Cu stockwork makes up all of orebody 2 and 90% of orebody 4. Orebody 3 comprises two massive sulfide bodies ~10 m thick containing pyrite, pyrrhotite, chalcopyrite, and sphalerite. Orebody 4 is the largest at Gebel Sayid, with a total resource estimate (measured + indicated) of 20.8 Mt, with an average grade of 0.8 wt% Cu, 0.2 wt% Zn, 0.3 g/t Au, and 9 g/t Ag (Equinox Minerals Limited website, April 2011). The estimated ore reserves of deposit 1 (Bournat 1981) found to contain 8 Mt ore, with average grades of 2.2 wt% Cu, 1.4 wt% Zn, 40 g/t Ag, and 0.5 g/t Au. Deposit 2 was estimated at 1.5–2 Mt ore, with an average grade of 1.5–2 wt% Cu. The Riofinex study at 1977, reported combined reserves of deposits 1, 2, and 4 at 34.3 Mt ore, with average grades of 0.55 wt% Cu, and 6.8 Mt grading 1.12 wt% Zn. Pitre et al. (1984) calculated ore resources of deposit No. 4 to be 16.9 Mt of 2.60 wt% Cu, and those of deposit 2 at 3.02 Mt of 3.13 wt% Cu. Indicated ore resources of deposit No. 1 were 3.7 Mt ore grading at ~2.12 wt% Cu and 1.35 wt% Zn.

The Gebel Sayid deposit possesses many of the distinctive features of a proximal VMS deposit (Sangster and Abdulhay 2005). The extensive footwall Cu-rich stringer zone, surrounded by chloritic alteration, and overlain by a Zn-rich sulfide lens and a Si-rich chemical sediment all confirm the volcanogenic exhalative nature of this deposit. Recognition of these features at Gebel Sayid has resulted in a better understanding of the deposit model and constituted an important step in the exploration for other VMS deposits in the same group of rocks. The validity of this viewpoint has been confirmed with the discovery of VMS deposits in the Umm ad Damar area ~20 km southeast of Gebel Sayid.

The *Umm ad Damar* mineralization covers an area of ~6 km southeast/northwest and 3 km southwest/northeast, 20 km southeast of Gebel Sayid (Fig. 6.3). It is not as well-exposed as Gebel Sayid, but is notable for the large size of its ancient workings, slag piles, and mining village ruins and midden. The Umm ad Damar area is underlain mainly by volcanic rocks of the Arj group that the Metal Mining Agency of Japan team divided into four lithologic units, including (Sangster and Abdulhay 2005): (1) rhyodacite and rhyodacitic volcaniclastic unit, (2) dacite to dacitic volcaniclastic unit, (3) andesite flows and andesitic volcaniclastic unit, and (4) intercalations of jasper within all of the volcanic and volcaniclastic rocks. Andesite and andesitic volcaniclastic rocks of the Mahd group overlie the Arj group in the northwestern part of the Umm ad Damar area. Rocks of the Arj group have been regionally chloritized and epidotized with extensive shearing developed in the volcaniclastic rocks. Faults are dominantly northeast/southwest except for a northwest/southeast fault bounding the eastern edge of the prospect area (Fig. 6.3). The area also includes intrusive rocks of tonalite, diorite, quartz diorite, andesite, dacite, rhyodacite, and basalt.

Four mineralized zones have been identified in the area, including Gebel Sujarah, the 4/6 gossan, the Umm ad Damar north prospect, and the Umm ad Damar south prospect (Sangster and Abdulhay 2005). According to the MMAJ team, VMS-style mineralization occurs in the Gebel Sujarah and the 4/6 gossan deposits. Massive sulfides are also found at the Umm ad Damar North Prospect deposit although most

of the mineralization here is Cu-dominated vein style. Mineralization at Umm ad Damar south prospect is Cu–Zn vein style. At Gebel Sujarah, the mineralized zone is ~6 m thick and extends ~200 m along strike and at least 250 m down dip. It comprises several layers of massive and pebbly sulfides accompanied by a disseminated zone. The latter, which is mostly pyrite, extends >100 m into the dacite footwall. Thick jasper layers are developed in the hanging-wall dacitic volcaniclastic rocks. In the Umm ad Damar north prospect, eleven drill holes intersected mineralization thicknesses of 2.6–3.1 m and average grades of 1.87–2.17 wt% Cu. Mineralization occurred as a network of chalcopyrite–pyrite veins in fractured dacitic volcaniclastic rocks, intrusive dacite, and rhyodacitic volcaniclastic rocks near the western edge of a large diorite body. In the Umm ad Damar south prospect, eleven holes were also drilled and confirmed that mineralization extended ~300 m along strike (northeast/southwest) and ~300 m down dip. Mineralization occurs as chalcopyrite–pyrite–quartz veins and chalcopyrite–pyrite–sphalerite disseminations in rhyodacitic volcaniclastic rocks at the southwestern periphery of a tonalite–diorite intrusion. At the 4/6 gossan, mineralization is massive sulfide in rhyodacitic volcaniclastic rocks and consists of massive, siliceous, and pebbly ores containing chalcopyrite, sphalerite, and pyrite. Massive sulfide ranges up to 35 wt% Zn and averages 2.11 wt% Cu. Zinc grades in pebbly and siliceous mineralization range up to 9.8 wt% and Cu averages 1.24 wt% (Sangster and Abdulhay 2005). Three zones of mineralization are associated with a layer of basaltic tuff. Immediately below the tuff, a 3.7 m mineralized zone averages 2.17 wt% Zn, 0.96 wt% Cu, and 0.4 g/t Au. A second, lower, zone is 9.3 m thick, averaging 3.67 wt% Zn, 1.00 wt% Cu, and 0.4 g/t Au. Each of these two zones extends ~100 m along strike and >60 m and 120 m, respectively, down dip. Above the basaltic tuff, a 2.5 m thick mineralized zone extends ~100 m along strike and averages 3.99 wt% Zn, 0.69 wt% Cu, and 0.1 g/t Au. Precious metal contents are low in most cases (e.g., 0.4 g/t Au) but, exceptionally, reach >16 g/t Au and >440 g/t Ag.

Although there is a debate about the mineralization style at the Umm ad Damar area, whether a vein-style mineralization (intrusion-related epigenetic veins) as at the north and south prospects or, alternatively, stockworks to an undiscovered VMS deposit, there appears little doubt the massive sulfide lenses at the Gebel Sujarah and 4/6 Gossan areas are, indeed, synvolcanic massive sulfides. The coexistence of jasper (chert) and Zn–Cu sulfides strongly correlate with the Gebel Ash Shizm and Gebel Sayid VMS deposits.

The mineralization areas at *Gebel Shayban*, *Gebel Baydan*, and *Gebel Samran* are located between 150 and 200 km southwest of Gebel Sayid along the strike of the Bi'r Umq suture (Figs. 6.2 and 6.5). The country rock consists of volcanic and volcaniclastic rocks assigned to the Samran group intruded by large arc-related plutons of diorite, quartz diorite, syntectonic tonalite gneiss, and post-tectonic granite (Kamil suite) (Fig. 6.5). The Tharwah ophiolite is in the hanging wall of the suture zone. *Gebel Shayban* and *Gebel Baydan* are Cu–Zn ± Au deposits hosted by the Shayban formation (775 Ma), the middle of three formations assigned to the Samran group and correlative with the Mahd group. The Shayban formation consisting of andesitic to felsic volcaniclastic rocks, felsic lava, pyroclastic rocks, lithic arenite

and conglomerate, and phyllitic to schistose metatuff, is inferred to comprise the remains of a number of closely spaced, possibly coalescent, volcanos in an oceanic arc or rift system (Roobol 1989; Hargrove 2006). The rocks are strongly folded, faulted, and metamorphosed to the greenschist facies. The Gebel Baydan has characteristics indicating that it is a VMS deposit. The primary mineralization at Gebel Shayban consists of massive and disseminated sphalerite, lesser chalcopyrite, and finely disseminated Au. The prospect was originally examined as a Zn prospect; its Au content came into focus as a result of work by Bureau de Recherché Geologique et Miniere (BRGM) in the 1990s. It has a resource of 8.7 Mt ore grading at 1.4 g/t Au, 16.4 g/t Ag, and 0.4 wt% Cu (Equinox Minerals Limited website, http://www.equinoxminerals.com/, accessed April 2021). Drill intercepts reach depths of >200 m, but mineralization is open down dip to the west.

Gebel Baydan is also somewhat sheared but is clearly recognizable as an in-situ VMS deposit (Bellivier et al. 1999). It is preserved on the flank of a regional anticline and consists different parts of mineralization include: (1) lenses of massive sulfide, mainly sphalerite, with subordinate pyrite, tetrahedrite, chalcopyrite, galena, and possibly stannite, (2) stockworks, (3) disseminated sulfides, and (4) stratiform bodies and veins of barite–silica–carbonate containing disseminated pyrite, chalcopyrite, sphalerite, tetrahedrite, and galena. The host rocks dip moderately west and from bottom to top are a sequence of (1) andesitic lava and lapilli tuff; (2) rhyolitic lava and felsic–porphyry quartz-eye tuff; and (3) epiclastic rocks. Mineralization is in the felsic volcanic rocks. The hanging wall of the deposit is intruded by a thick granodiorite–quartz diorite sill. Gebel Baydan mineralization has a drill-indicated resource of 0.5–0.7 Mt of ore at ~16–17 wt% Zn and 1.5–2.5 g/t Au, plus Cu and Ag (Bellivier et al. 1999). The *Gebel Samran* is a small Cu-rich occurrence of enigmatic deposit type composed of quartz veins and secondary Cu-mineral fracture fillings in a quartz vein/stringer zone in volcaniclastic rocks strongly sheared by southeast-vergent thrusts. The deposit was drilled in the 1960s and has an estimated resource of 0.9 Mt ore at ~2 wt% Cu with traces of Au.

The characteristics of the Gebel Baydan and Gebel Shayban sulfide deposits with a massive, layered sulfide lens underlain by a stringer sulfide zone enveloped in a cone of Mg-metasomatized wallrock (Bellivier et al. 1999) leave little doubt that the deposits are small, vent-proximal VMS deposits. This classification is further supported by the Zn-rich nature of the massive lens ($Zn/(Zn + Cu) = 0.93$) and its position near the transition from intermediate-to-felsic volcanics, features that are typical of VMS deposits in Precambrian island arc volcanic sequences.

Volcanogenic massive sulfide deposits in the Asir terrane: In the south-central Arabian Shield of Saudi Arabia, there are two mineral districts in the northern part of the *Asir terrane*, hosted by north-trending structural belts of greenschist-facies Lower Cryogenian convergent-margin volcanic-arc rocks. They are the *Bidah* and *Shwas districts* (Fig. 6.2). The rocks in each structural district are folded about north-trending isoclinal axes and cut by numerous north-trending shears. Most mineral occurrences in the Bidah district are along or west of the Bidah fault (shear) zone, a prominent system of sinistral brittle–ductile shears along the axis of the Bidah structural belt (Johnson and Kattan 2012). The most prominent shear in the Shwas

district is the Umm Farwah shear, a serpentinite-decorated subvertical brittle–ductile strike-slip shear along the western side of the district. The shear zone has both dextral and sinistral sense-of-shear indicators and is the approximate contact between the Shwas belt and the long-lived extensional Ablah basin. The Aqiq shear zone, another serpentinite-decorated structure associated with the Aqiq Ghamid occurrences, is a sinistral strike-slip shear between the Bidah and Shwas shears on the west side of the Ablah basin.

The *Wadi Bidah mineral district* (WBMD) lies in the southwestern part of the Arabian Shield of Saudi Arabia, ~260 km southeast of Jeddah, and consists of a north-trending belt 70-km long and 20-km wide, between latitudes 20° and 21° north and longitudes 41° and 41° 30′ east (Fig. 6.6). The WBMD has been repeatedly explored, but despite the common abundant indications of mineralization, no significant deposit has yet been discovered. There are many mineralization occurrences, expressed mainly as small gossans, and extend discontinuously over the course of 120 km along strike, where there are two types of mineralization: (1) stratabound VMS-type sulfide bodies containing Cu–Zn ± Au ± Ag and (2) Au-bearing quartz veins and stringers (Volesky et al. 2003, 2017; Johnson and Kattan 2012). Sulfide bodies along the east side of the Bidah shear zone and the east side of Wadi Bidah make up the *Rabathan* mineralized area; other mineralized areas (*Shaib at Tare*, *Gehab*, and *Mulgatah*) are west of the main shear zone (Fig. 6.6). The sulfide bodies in these occurrences are folded and sheared, which indicate that the deformation event was after the mineralization process. Two of these occurrences, Shaib at Tare in the north and Rabathan in the south (Fig. 6.6), have been selected to be described here as representative examples of WBMD.

The *Rabathan* occurrence lies on the strike of the main Bidah shear zone; it is hosted by sheared calcareous quartz schist (Bidah group) and cherty-ferruginous beds at the contact with Khumrah greenstone. The Rabathan deposit is found chiefly within the carbonate-rich (now metamorphosed to calc-silicate) portions of the stratigraphy. Sulfide mineralization are found as massive-to-submassive bodies and chiefly composed of pyrite and chalcopyrite with variable minor amounts of sphalerite, pyrrhotite, rutile, and magnetite. The ore minerals occur as (Koch-Mathian et al. 1994): (1) banded sulfide layers intercalated with beds of quartz–chlorite–dolomite schist, (2) clastic sulfides comprising pyrite aggregates and fragments cemented by chalcopyrite, and (3) microbrecciated sulfides composed of fractured pyrite healed by chalcopyrite, quartz, and chlorite. Estimates of ore resources made at Rabathan, on two sulfide bodies, were, separately, ~1.5 Mt ore with average grades of 2.3 wt% Cu, 0.03 wt% Zn, 2.85 g/t Ag, and 0.16 g/t Au, and 0.6 Mt ore with average grades of 2.2 wt% Cu, 1.51 wt% Zn, 5 g/t Ag, and 4 g/t Au.

The *Shaib at Tare*, *Gehab*, and *Mulgatah* occurrences consist of stratiform lenses of massive and disseminated pyrite, sphalerite, and minor chalcopyrite, with minor barite, in chlorite–sericite–quartz schist and chlorite schist with beds of hematitic and pyritic chert and marble, west of the main Bidah shear zone (Roubichou et al. 1989; Volesky 2002). The Shaib at Tare sulfide bodies crop out as gossans, extending over a north/south strike length of ~600 m, where the Riofinex Geological Mission (1979) estimated ore resources of ~2.4 Mt with an average grade of 0.37 wt% Cu

and 0.5 wt% Zn. The Gehab mineralization was exposed as gossans over a strike length of 700 m; it has an estimated ore resource of ~1.4–1.9 Mt at 0.64–1.26 wt% Cu, 1.45 wt% Zn, 5.3 g/t Ag, and 0.09 g/t Au. The Mulgatah occurrence has a very small resource of ~140,000 tons to a depth of 100 m, with average grade of 0.28 wt% Cu, 0.87 wt% Zn, 1.5 g/t Ag, and 0.75 g/t Au (Riofinex Geological Mission 1979; Roubichou et al. 1989).

The *Shwas district* is located in the Shwas structural belt, a narrow structural domain between the An Nimas batholith on the east and the Shwas pluton and the Ediacaran Ablah group on the west. The layered rocks are similar in age to those in the Bidah belt, but the relationship between the two belts is not clear. They may be parts of a common Lower Cryogenian volcanic-arc assemblage, now separated by the younger Ablah group, or separate arcs that were juxtaposed during assembly of the composite Asir terrane. The Shwas belt contains greenschist-facies flows and pyroclastic rocks of andesitic, dacitic, and basaltic compositions; green and red, feldspathic to lithic wacke, tuff, pebble-to-boulder conglomerate; and thin grey marble. As in the WBMD, these rocks are the host for VMS-type precious- and base-metal sulfide deposits. Exploration in the district initially concentrated on base-metal targets but BRGM, in the 1980*s*, located significant Au and Ag values in gossans and supergene oxide zones. The largest Au deposit at *Al Hajar* Au mine consists of two bodies of supergene ore in a weathered zone that extends to a depth of 70 m overlying primary sulfide ore. A prefeasibility study completed by BRGM in late 1989 outlined mineable reserves of 5 Mt ore, with an average grade of 2.6 g/t Au and led to a successful trial heap leach test (Cottard et al. 1994). Open-pit mining by Ma'aden and the production of Au by heap leaching began in 2000 and ceased in 2006 on exhaustion of the supergene reserves. The open pit at the mine is now closed, but activity continues with use of the heap leach facility to reprocess previously stacked and leached materials, and to process new materials from *Jadmah*, a similar VMS/supergene deposit ~4 km west of Al Hajar Au mine (Fig. 6.2).

The primary mineralized zone (un-mined) at Al Hajar consists of low-sulfide stringers and disseminations of pyrite (3–10%, locally 40%) with subordinate chalcopyrite. The ore is hosted by porphyritic rhyolite and dacite, and the weathering produced a variety of oxidized ores referred to as siliceous facies, ferruginous facies, and bleached facies. The *Jadmah* deposit consists of Au–Ag mineralization associated with siliceous–ferruginous gossans produced by the supergene oxidation of lenses of disseminated and massive pyrite, chalcopyrite, and sphalerite. The host rocks include quartz-eye rhyolitic tuff, subordinate dacitic tuff, chloritized rhyolite ash flows, and jasper in a regional succession of felsic to intermediate volcanic flows and tuffs. The estimated in situ ore resources of oxide ore indicated the presence of ~0.52 Mt ore, with an average grade of 3.1 g/t Au and 40 g/t Ag at a cut-off grade ~0.5 g/t Au.

In the southeastern most part of the Asir terrane, there are significant convergent-margin volcanic-related sulfide mineralization, named the *Wassal Masane–Kutam mineral district* (Fig. 6.7). The belt is underlain by spreading-center and convergent-margin arc rocks in the Malahah basin (Johnson and Kattan 2012). The *Al Masane* occurrence is a classic polymetallic VMS deposit, the *Al Halahila* and *Farah Garan*

occurrences have some of the characteristics of VMS deposits, but their classification is not definitive (Sangster and Abdulhay 2005). The *Kutam* occurrence may be a VMS deposit but is highly sheared; it was described in Chap. 5 of this book under the section of shear-zone-associated mineral occurrences. The *Wadi Wassat* is a typical VMS deposit type in the possible extension-related basaltic–andesitic assemblage in the northeast of the mineral belt (Fig. 6.7).

The *Al Masane* occurrence was discovered in 1967 in a deeply incised wadi as outcroppings of gossans in a sequence of steeply west-dipping mafic tuff and lava, felsic tuff and lava, lapilli tuff, and black shale (Fig. 6.8) (Fernette 1994). The Al Masane occurrence consists of six sulfide bodies, in which four of them (the Saadah zone) hosted by felsic tuff and lava unit, one at the contact between lapilli tuff and black shale (the Moyeath zone), one in the mafic tuff and lava (the Shann zone) (Fig. 6.8) (Fernette 1994; Sangster and Abdulhay 2005). All sulfide bodies comprise stratiform lenses of massive pyrite, chalcopyrite, sphalerite, galena, and pyrrhotite, with subordinate-to-minor tellurides and sulfosalts. The Al Houra–Saadah bodies are Cu–Zn-rich, and the sulfide layers are interbedded with Mg–Mn carbonate, chert, and pyrite–talc rocks. Metal zoning is reported at Saadah with Cu toward the footwall and Zn, Au, and Ag toward the hanging wall. The Moyeath zone is Zn(Pb)-rich body. The Al Masane massive sulfide mineralization has total ore reserves (proved + probable) ~7.2 Mt, with an average grade of 1.42 wt% Cu, 5.31 wt% Zn, 1.19 g/t Au, and 40.20 g/t Ag (Al Masane Al Kobra Mining Company website: www.arabianamericandev.net, April 2011, accessed on April 2021). The Al Masane mineralized zones represent typical VMS deposits based on the following observations (Sangster and Abdulhay 2005): (1) the submarine depositional environment of the enclosing host rocks, (2) the stratiform nature of the sulfide lenses, (3) the Cu-to-Zn zoning reported in the Saadah lenses, and (4) its overall Zn-rich composition.

The *Al Halahila* occurrence is located in the eastpart of the Wassat–Al Masane–Kutam mineral district (Fig. 6.7); it is exposed as north-trending gossans on the steep slope of a deeply incised valley. It consists of three discontinuous sulfide lenses in a steeply east-dipping sequence of dolomite–sericite–chlorite schist and martitic ironstone composed of quartz and hematite pseudomorphs after magnetite, enclosed in chlorite–sericite–pyrite schist and andesitic–dacitic tuffs to the east, and andesitic metatuff to the west. The mineralization comprises veins and disseminations of pyrite and lesser sphalerite, chalcopyrite, galena, and tennantite replacing dolomite as well as subordinate banded-to-massive sulfides. The steep terrane makes drilling difficult, so the size of the deposits is not properly known, but an indicated resource has been estimated (Parker 1982) to be 1.04 Mt, with an average grade of ~2.99 wt% Zn, 0.44 wt% Cu, 25.2 g/t Ag, and 0.45 g/t Au, to a depth of 100 m.

The *Farah Garan–Kutam* belt is located in the southwest corner of the Malahah belt (Fig. 6.7); it contains two significant polymetallic mineral deposits: *Kutam* and *Farah Garan* that are situated within 10 km of each other (Fig. 6.7). The Farah Garan–Kutam belt is a part of the Malahah belt of Halaban-group rocks, which has been interpreted to be a possible back-arc rift assemblage metamorphosed to greenschist facies (Sangster and Abdulhay 2005). The local geology of Farah Garan area comprises a north trending, steeply west-dipping sequence of mafic and felsic

volcanic rocks and a varied sequence of sedimentary rocks (Fig. 6.9) (Doebrich 1989). The mafic group comprises intercalated pillow basalt, mafic agglomerate, and mafic lapilli tuff. The felsic volcanic rocks have been metamorphosed to quartz-eye sericite phyllite with quartz "eyes" (<10% of the rock) in a matrix of fine-grained quartz, sericite, feldspar, and minor chlorite, pyrite, carbonate, clinozoisite, and epidote. Sedimentary rocks are represented by a carbonatized phyllite unit, which is regarded as a clastic sedimentary unit and comprises a graphitic phyllite and quartz–chlorite–sericite phyllite unit. In addition to the volcanic and clastic sedimentary rocks, a distinct assemblage of intercalated cherty dolomite, talc, chloritite, chert, and sulfides was recognized, which are referred to as an exhalative unit. The cherty dolomite, in particular, is intimately associated with layered sulfides.

There are three layered sulfide-bearing units in the Farah Garan occurrence, and are referred to as the east, south, and west exhalative units (Fig. 6.9). The highest-grade sulfides are contained within the south unit, which has been penetrated by two drill holes (Fig. 6.9). The Farah Garan mineralization consists of banded and disseminated pyrite, sphalerite, chalcopyrite, tetrahedrite–tennantite, and galena in a sequence of exhalative cherty dolomite, talc, chloritite, and chert, that interfingers with felsic and mafic metavolcanic, volcaniclastic, and subordinate metasedimentary rocks. The rocks are steeply dipping and strongly folded, and the stratigraphy is severely disrupted, but it is believed that the felsic–metavolcanic rocks were originally below and the mafic–volcanic rocks above the sulfide mineralization. Drill holes intercepted sulfides over true thicknesses of as much as 31 m. A general upward metal zoning was reported in the area comprising an increase in Zn/(Cu ± Pb ± Zn) ratios and decrease in Cu/(Cu + Pb + Zn) ratios. The prospect has not been sufficiently drilled to yield an adequate resource estimate; however, estimated resources based on two drill holes were 0.23 Mt ore, with an average grade of 2.5 wt% Zn, 0.9 wt% Cu, 33 g/t Ag, and 2.8 g/t Au (Doebrich 1989). The lack and difficulty of drilling, inadequate sampling of fresh sulfides, and poor surface exposure make the deposit-type classification uncertain, but Sangster and Abdulhay (2005) tentatively classify the deposit as VMS type.

Volcanogenic massive sulfide deposits in Afif terrane: In the north-central shield (the *Afif terrane*), the VMS deposits occur in the *Nuqrah district* at *Nuqrah North* and *Nuqrah South* as well as in the *Shaib Lamisah* occurrence in the southwestern part of the Afif terrane (Fig. 6.2). The Nuqrah district is in the northwestern part of the Afif terrane, east of the suture between the Afif and Hijaz terranes (Fig. 6.2). The Nuqrah belt lies within the Hulayfah group of volcanic and volcano–sedimentary rocks. This group comprises two formations; the lower, or Afna formation, is mostly andesitic with basaltic flows with subordinate mafic tuff, breccia, and agglomerate. Units of rhyolitic–andesitic quartz crystal tuffs are found near the top of the formation. The upper, or Nuqrah formation, is a sequence of alternating volcanic and sedimentary rocks (Fig. 6.10). The site of the Nuqrah deposits is marked by ancient pits and trenches extending several hundred meters along strike (Sangster and Abdulhay 2005). Nuqrah south occurrence consists of sulfide ore in a steeply northwest-dipping zone of carbonaceous–graphitic tuffite and chert enclosed in dolomitic marble (Fig. 6.10). The footwall consists of rhyolitic tuff, while the hanging wall is of

andesite, basalt, and tuffite. The Nuqrah north occurrence is hosted by similar rocks, including basalt, rhyolitic tuff, graphitic tuff, dolomitic marble with graphitic intercalations, and lenses of black chert and dacite. Mineralization at both occurrences consist of Ag- and Au-rich massive, stringer, and disseminated sulfides. The sulfide lenses are layered parallel to axial plane schistosity. Primary bedding consists of millimeter-spaced alternations of sphalerite-, pyrite-, chalcopyrite-, and galena-rich laminae and graphitic laminae. Cubanite ($Cu_2Fe_4S_5$) and mackinawite ($Cu_2Fe_4S_7$) form exsolution phases in chalcopyrite. Other minerals occurring in trace amounts are boulangerite ($Pb_5Sb_4S_{11}$), bournonite ($PbCuSbS_3$), alaite (PbTe), tetradymite (Bi_2Te_2S), tetrahedrite, freibergite, native gold, electrum, hessite (Ag_2Te), empressite (AgTe) molybdenite, siegenite [$(Fe, Co, Ni)_3S_4$], melonite ($NiTe_2$), and frohbergite ($FeTe_2$).

The estimated ore resources for the Nuqrah south body range from 0.241 Mt ore (grading at 13.8 wt% Zn, 2.0 wt% Cu, 6.3 wt% Pb, 14.4 g/t Au, and 554 g/t Ag) to 1 Mt (grading at 7.6 wt% Zn, 1.2 wt% Cu, 3.44 wt% Pb, 5.86 g/t Au, and 235 g/t Ag). Resource estimates for the Nuqrah north body ranges from 0.225 Mt ore (grading at 8.2 wt% Zn, 1.0 wt% Cu, 2.2 wt% Pb, 2.3 g/t Au, and 303 g/t Ag) to 0.30 Mt ore (grading at 6 wt% Zn, 0.75 wt% Cu, 1.22 wt% Pb, 2.5 g/t Au, and 332 g/t Ag) (Delfour 1975). Although the mineralization types have been compared to VMS deposits, the association with carbonate beds and the very high Ag content differentiate the Nuqrah ore from typical Precambrian VMS deposits, and Sangster and Abdulhay (2005) suggest that the deposits may be epigenetic carbonate replacements (MVT) rather than classic VMS bodies.

The *Shaib Lamisah* occurrence is located just east of the ophiolite-bearing suture at the southwestern edge of the Afif tectonostratigraphic terrane. The Shaib Lamisah area is underlain by volcanic arc rocks of early Hulayfah age (780–730 Ma) belonging to the Hijaz orogenic cycle (Viland 1986). Early Hulayfah volcanic units comprise a varied assemblage of mafic-to-intermediate volcanic rocks with minor felsic components, some of which were deposited under subaerial conditions. The volcanic rocks are associated with fine-grained clastic sedimentary rocks dominated by calcareous and pyritic black shales and carbonate lenses. The volcanic and sedimentary rock assemblage is crosscut by intrusive bodies ranging in composition from mafic to highly evolved magmatic differentiates. The mineralized unit is composed of soapstone (tremolite and calcite), black crystalline marble (limestone or dolostone), pyritic black shale, massive or laminated gray chert, intermediate tuff, and intrusive metadiorite. Footwall black shale, normally up to 15 m thick, thins and grades northward to calcareous tuff.

Sulfide layers at Shaib Lamisah are roughly parallel to bedding in tremolite–carbonate "soapstone", as irregular patches in dolomitic marble, and as massive sulfide containing carbonate "clasts". Strong shearing has resulted in veinlets of segregated sulfides and recrystallization of chalcopyrite and pyrite. Pyrite, chalcopyrite, and sphalerite are the main components of the sulfide mineralization. Trace amounts of pyrrhotite, native bismuth, molybdenite, mackinawite, cubanite, and arsenopyrite were also observed. Gangue minerals are mainly carbonate, quartz, and tremolite. The estimated ore resources based on five diamond drill holes (Elsass

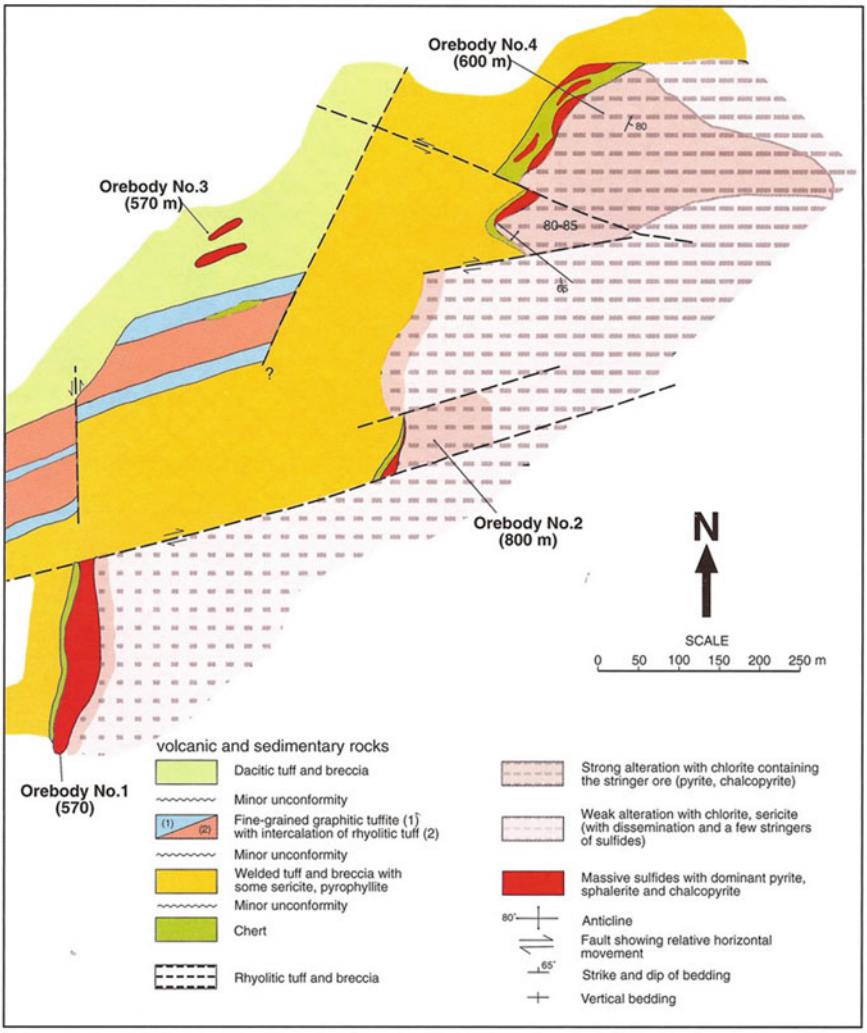

Fig. 6.4 Geologic map of the Gebel Sayid VMS deposit (after Johnson and Kattan 2012)

et al. 1983) at the Shaib Lamisah deposit found to contain ~1.4 Mt ore, with an average grade of 9 wt% Zn, 1.7 wt% Cu, and 9 g/t Ag.

6.3 Volcano–Sedimentary Mineral Deposits in Yemen

The volcano–sedimentary mineral deposits in Yemen are mainly represented by Zn–Pb–Ag ± Cu occurrences, which are mostly related to the MVT environment.

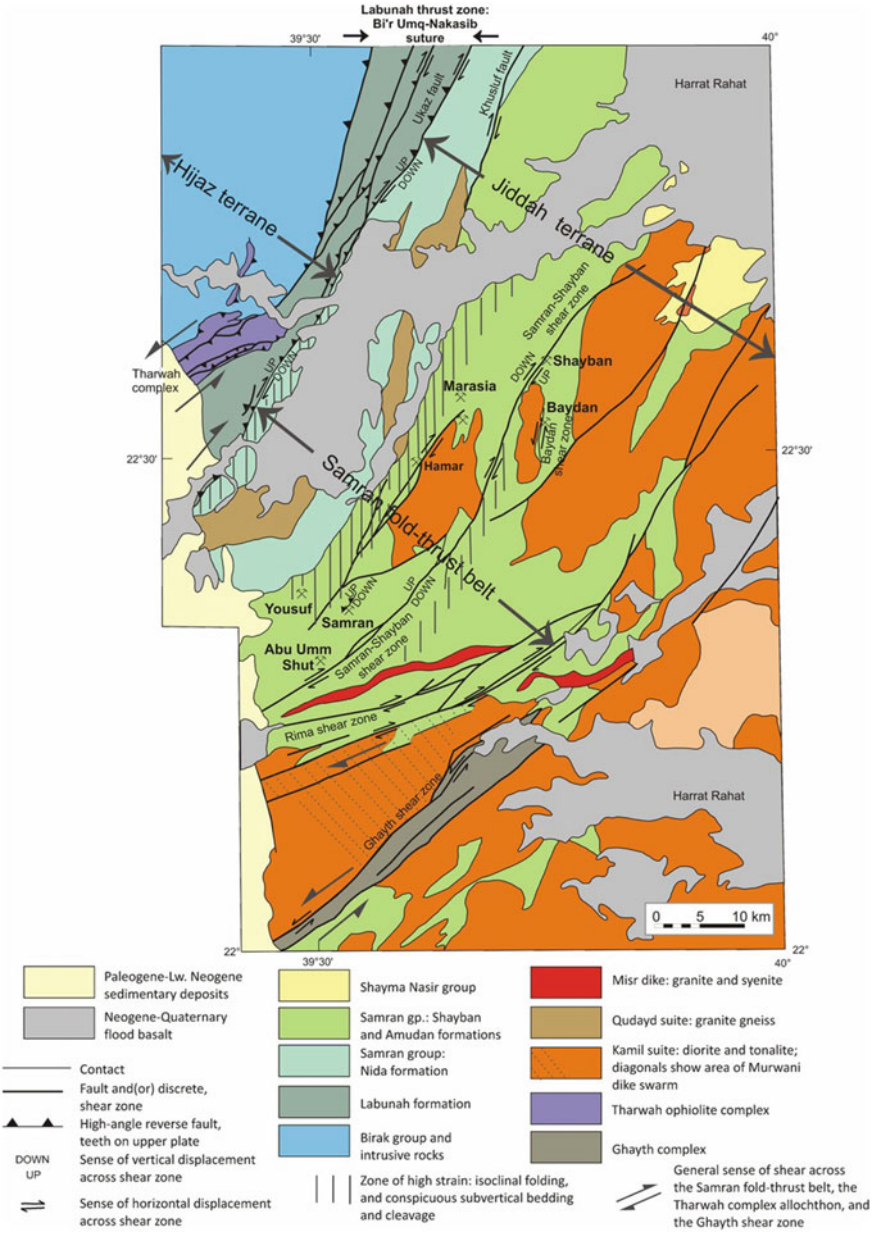

Fig. 6.5 Simplified geological map of the Gebel Samran–Gebel Shayban mineral district (after Johnson and Kattan 2012)

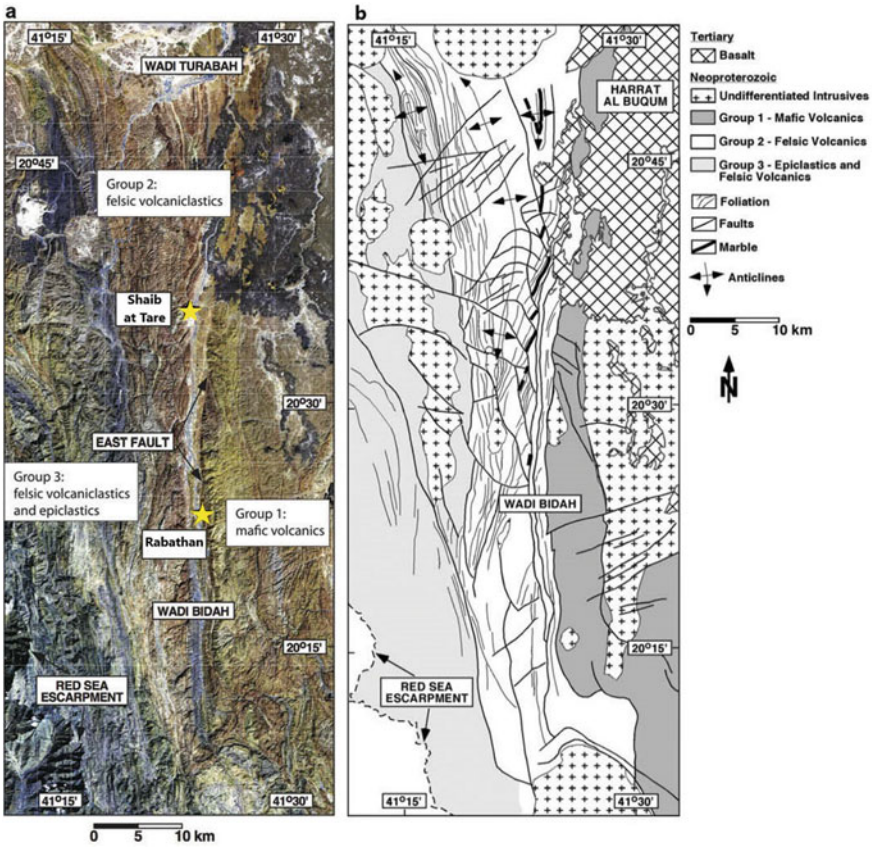

Fig. 6.6 **a** Landsat ETM^{+} (7–5–4) color composite image using the convention (R–G–B) of the WBMD indicating the locations of the Shaib al Tair and Rabathan prospects. **b** Geological map with major structures of the WBMD (after Volesky et al. 2003, 2017)

The most significant occurrences are widespread over an approximately 850 km long and up to 100 km wide rift basin of Jurassic age, which are not related to the Neoproterozoic ANS rocks. Thus, these mineral deposit types will not discussed in detail; however, it will just briefly be mentioned here for reference. Several carbonate-hosted Zn–Pb–Ag ± Cu occurrences are found along the rift, and one of the famous occurrences of these deposits is the Jabali Zn deposit.

As stated before in Chap. 2 of this book, the geology of Yemen comprises three main parts: (1) Precambrian basement rocks, (2) Jurassic pre-, syn-, and post-rift carbonate and clastic sedimentary rocks, and (3) Tertiary-to-recent sedimentary rocks and magmatic-associated rocks related to the opening of the Gulf of Aden and Red Sea rift (Menzies et al. 1994). At the end of the Proterozoic age, the southern Arabian Peninsula underwent an extensional intraplate regime, characterized by extensive volcanism and magmatism. In the late Precambrian age, this extension caused uplift

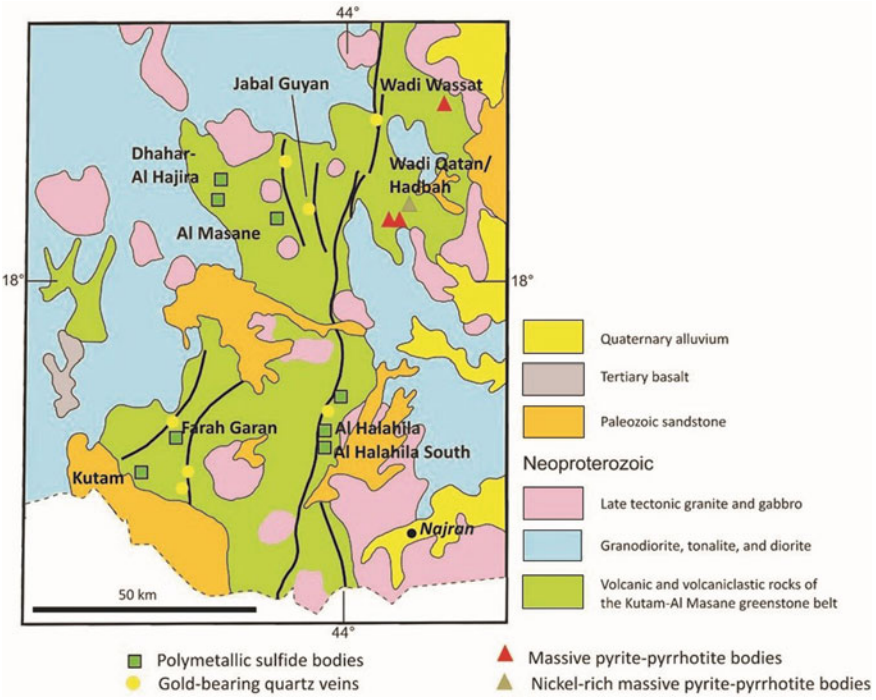

Fig. 6.7 Simplified geological map of the Wassat–Al Masane–Kutam mineral district (after Johnson and Kattan 2012)

and erosion processes of the basement rocks, followed by the formation of several basins, related to major wrench-fault systems (e.g., the Najd fault system; Ellis et al. 1996). These basins are filled by Paleozoic-to–early Mesozoic clastic sequences, deposited in marine epicontinental-to-deltaic environments, locally containing evaporites (Beydoun et al. 1998). During the Triassic to the middle Jurassic periods, Yemen was part of the Afro–Arabian plate of western Gondwanaland, where the Jurassic breakup of Gondwana caused the separation of the Arabian plate from the original supercontinent (Bosence 1997; Ahlbrandt 2002). The Mesozoic extensional tectonics of Yemen resulted in the formation of five sedimentary basins (Fig. 6.11): (1) Siham-Ad-Dali', (2) Ramlat As Sabatayn (Sabatayn), (3) Say'un-Masilah, (4) Balhaf, and (5) Jiza'-Qamar (As-Saruri et al. 2010). The Sabatayn and the Say'un-Masilah basins (Fig. 6.11) are the only hydrocarbon-producing basins in Yemen. The Jabali mineral deposit is located on the western border of the Sabatayn rift basin.

There are at least two rift-controlled basins of Jurassic age in Yemen, where most of the Zn occurrences are located at the margins of these rifts (e.g., the Sabatayn basin) or in rift-affected blocks. There are more than 100 known base-metal occurrences in Yemen, of which ~20 occurrences of them are of economic interest and considered to be prospects and/or deposits (Fig. 6.12). Much of the exploration work during the 1980s was directed to the discovery of base-metal mineralization, in particular

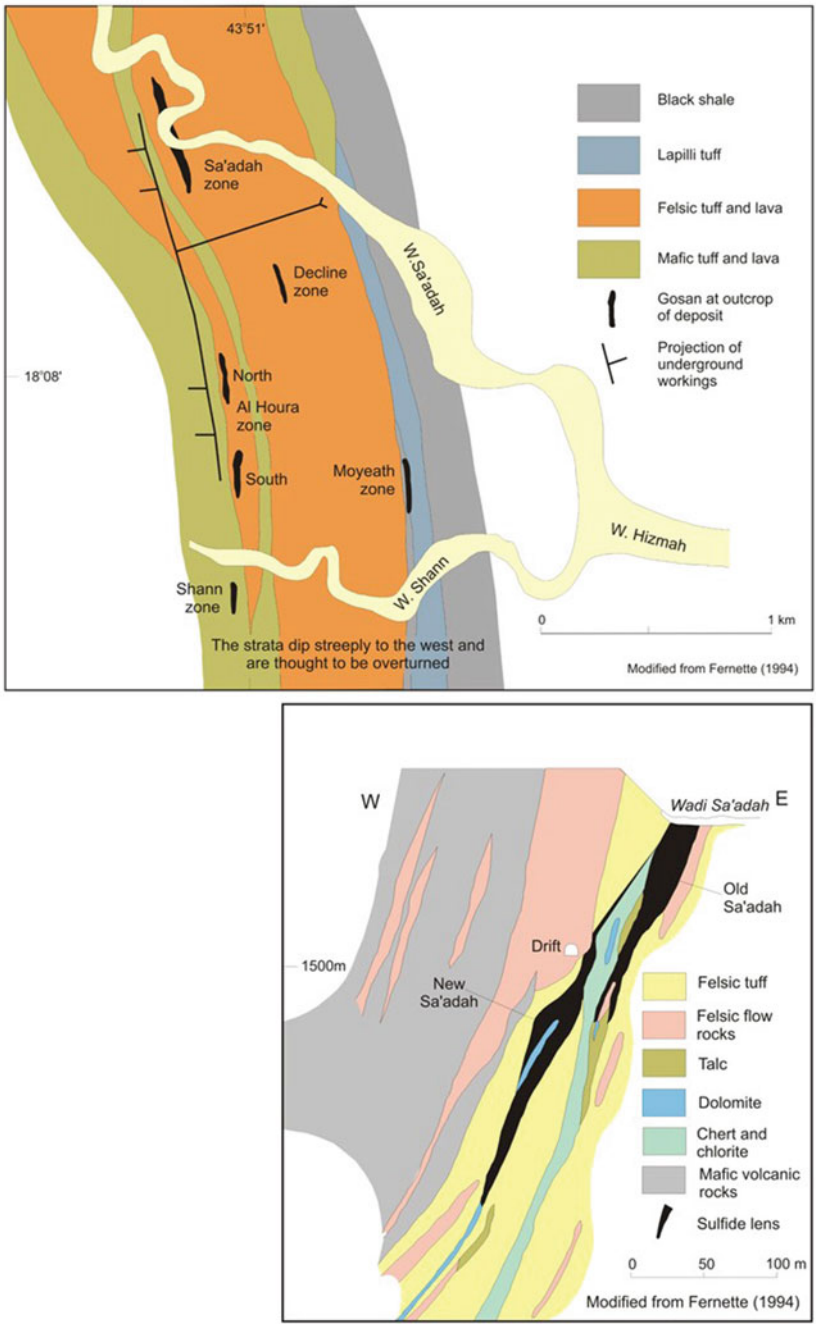

Fig. 6.8 Schematic plan (above) and cross section (below) of Al Masane VMS deposit, Asir terrane (after Johnson and Kattan 2012)

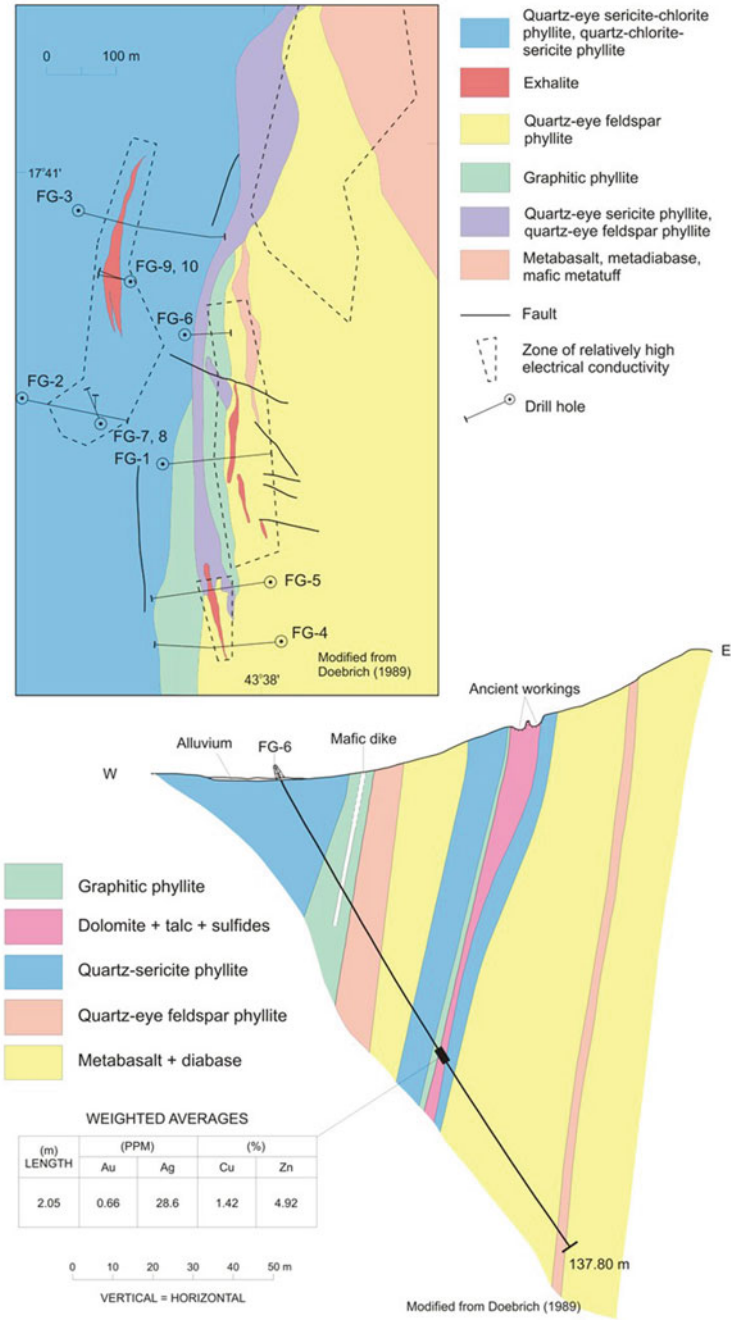

Fig. 6.9 Schematic plan (above) and cross section (below) of the Farah Garan VMS deposit, Asir terrane (after Johnson and Kattan 2012)

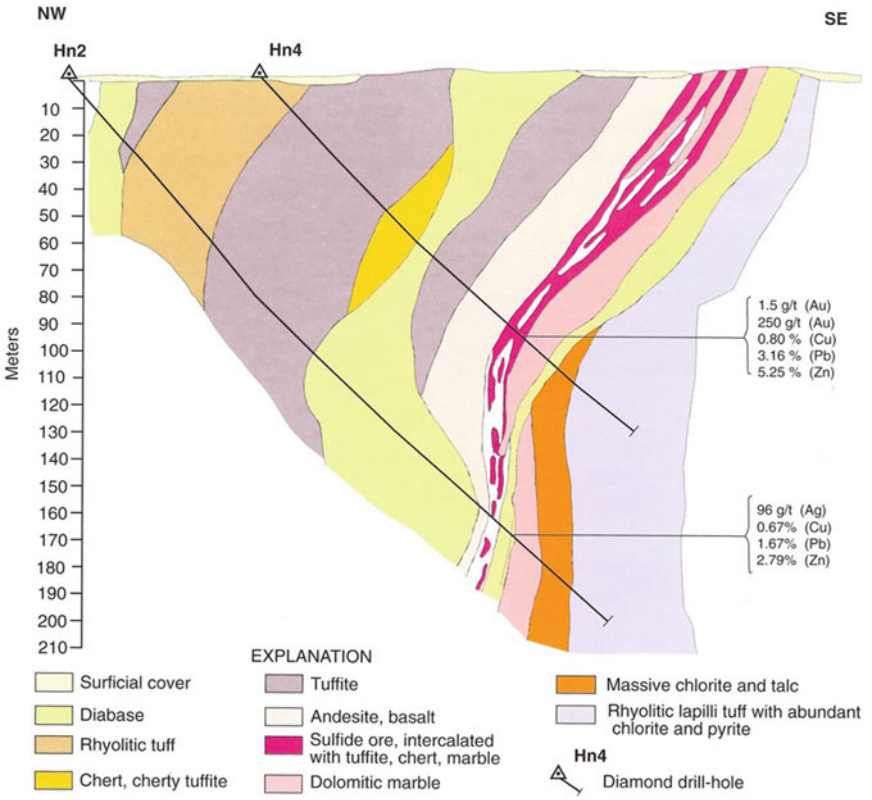

Fig. 6.10 Simplified cross section through the Nuqrah south deposit (MODS 0013) (after Johnson and Kattan 2012)

VMS deposits, which are known to occur in several localities of similar rocks in Saudi Arabia. The discovery of the Jabali Zn deposits in Jurassic carbonates led to an expansion of emphasis to include carbonate-hosted Zn–Pb deposits (known to be MVT deposits) (Christmann el al. 1989). Zinc-lead occurrences are widespread in Yemen; however, the most significant occurrences form an ~850-km-long belt in carbonate rocks within and adjacent to the Ramlat As Sabatayn rift basin. Mineralization is found in rocks ranging from Jurassic to Paleocene in age, and largely forms two sectors, located in the *Jabali* and *Tabaq* areas (Fig. 6.12).

The *Jabali* area comprises several ore mineralizations hosted by carbonate rocks of the Jurassic Amran group; it is located on the western flank of the Sabatayn basin, ~60 km northwest of the town of Marib. The Amran group directly overlies the Precambrian basement rocks, and is intruded by Tertiary igneous intrusions. Eight small-scale Zn–Pb occurrences were identified in the Jabali area, which were expressed on the surface as variously extended gossans containing limited Zn and Pb mineralization, hosted in dolomite breccias. The principal mineralization sites in

Jabali area are *Barran*, *Al-Kwal*, and *Haylan* (Fig. 6.12), which are grading at 16.5 wt% Zn and 6 wt% Pb, and by a very limited areal extension.

The *Tabaq* district is located ~360 km north/northeast of Aden, in the same rift system hosting the Jabali deposit of southern Yemen, and ~500 km east of the Jabali mining area (Fig. 6.12). In the Tabaq area, nine small-scale Pb–Zn occurrences have been identified. Similar to the Jabali area, the mineralized occurrences at the Tabaq area are hosted in the Jurassic-to-Paleocene carbonate sequence, and are associated with zones of dolomitization and strong faulting. Maximum grades of 12 wt% Zn and 3.8 wt% Pb have been measured at Tabaq along a 30-m strike section, at Wadi Rama and Jabal Al-Jubal (Fig. 6.12). The other two major occurrences of the area generally show lower grades. There is not enough mineralogical information for all of these minor occurrences. Another base-metal mineralized district is located in the southwestern part of the Say'un-Masilah basin, in the Mukalla area named Al-Masylah and Ras Sharwyn occurrences (Fig. 6.12). Mineralization of this district is fault-controlled, and consists of veins of barite and galena. A secondary nonsulfide Zn–Pb–Mn mineralization containing willemite, smithsonite, cerussite, descloizite, calcite, pyrolusite, and celestine, with anomalous grades of Ag, Cd, Ga, Ge, and Mo also occurs in this area. Following is a brief description of the Jabali Zn–Pb–Ag occurrence for reference of such MVT deposits to be compared with other volcano–sedimentary deposits in the ANS.

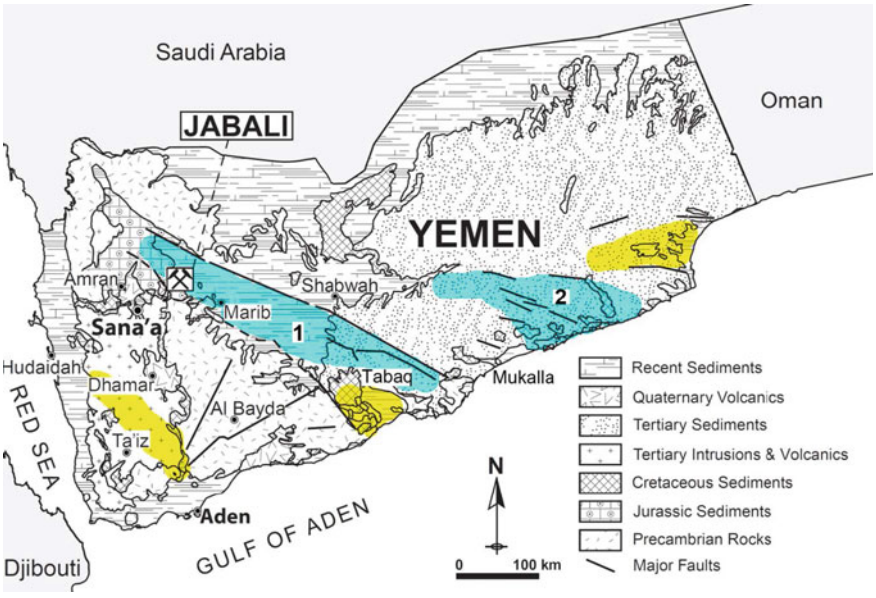

Fig. 6.11 Geological map of Yemen, showing the Jabali position (from the Yemen Geological Survey and Mineral Resources Board). 1 = Sab'atayn basin; 2 = Say'un-Masilah basin. Blue = hydrocarbon-producing Mesozoic basins; yellow = other Mesozoic basins (from Mondillo et al. 2014)

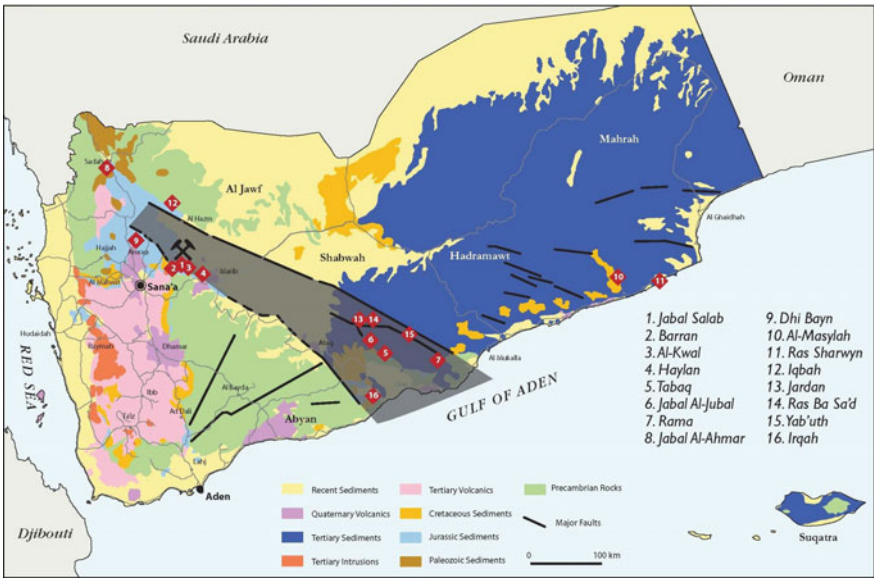

Fig. 6.12 Distribution of base-metal occurrences in Yemen (from the Yemen Geological Survey and Mineral Resources Board).

6.3.1 Jabali Mississippi Valley–Type Zn–Pb–Ag Deposit

The Jabali occurrence is the most significant base-metal mineralization in Yemen. The artisanal mine workings in the area are thought to be older than 2500 years. The Jabali MVT deposit was considered to be the greatest Ag mine in the Muslim world, with more than 400 furnaces producing "one camel load of metal" per week (Christmann et al. 1989). The old mine workings extended over an area of ~10 ha, tracing cavities filled by relatively soft oxidized ore, locally rich in Ag. The ore was processed on site, where the waste dumps contain ~120,000 tons, with average grades of 24 wt% Zn, 3.5 wt% Pb, and 160 g/t Ag. It seems that the old artisanal metallurgical processes were not effective to extract the ore, since the remaining slags still contain ~23 wt% Zn, 6.5 wt% Pb, and 40 g/t Ag (SRK Consulting 2005). The site was rediscovered by BRGM and the Yemen Geological Survey and Mineral Resources Board (YGSMRB) in 1980. Between 1981 and 1986, an exploration and evaluation program based on 57 drill holes reported an accessible open-pit resource of 3.0 Mt ore, at ~15.2 wt% Zn, and an amenable by underground mining volume of 1.24 Mt ore at ~13 wt% Zn. The BRGM and YGSMRB during and after the period of exploration at Jabali area produced several scientific papers on the characterization and genesis of the deposit (Christmann et al. 1989; Al Ganad et al. 1994) and a Ph.D. dissertation (Al Ganad 1991). No further scientific publications on the Jabali mineralization has been produced in recent years, with the exception of Mondillo et al. (2011, 2014).

The Jabali Zn–Pb–Ag deposit covers a total area of ~2 km^2, striking in a northwest direction (Fig. 6.13). The deposit is located in a small plateau on the eastern flank of a northwest/southeast-elongated mountainous area that is a segment of the western boundary of the Sabatayn basin, which extends for several square kilometers in the adjacent lowland. This mountainous area is called *Gebel Salab*. There is a small crest occurring on the northwestern part of the Jabali plateau called *Gebel Barrik* and a small valley named *Wadi Jabali* delimits this area from the southeastern part of the plateau, where the orebodies outcrop (Fig. 6.13). The plateau is dissected by another valley (Wadi Khaynar) further southeast. These valleys vertically cut the mineralized formations, which are exposed along the valley flanks. There are small igneous sills and dykes cross-cutting the Jabali orebodies and their host sedimentary rocks at the mine site.

The sedimentary rocks hosting the Jabali orebody belong to the Amran group, which directly overlie the Proterozoic basement rocks and are a maximum of 300 m in thickness (Al Ganad et al. 1994; Beydoun et al. 1998). At the mine site, the Amran group sequence subdivides into nine lithostratigraphic units (Figs. 6.13 and 6.14), starting from the base upwards as: Unit 1 is ~10-m-thick sandstone and conglomerate overlying the late Proterozoic basement. Unit 2 is ~25 m thick, comprising gypsiferous mudstone overlain by and interbedded with dolomitized calcarenite, marl, and nodular limestone. Unit 3 is ~50 m thick and composed of micritic and biomicritic limestone, containing nodular concretions and chert layers. Unit 4 of ~15 m thick from micritic limestone and finely bedded lagoonal/lacustrine dolomite. Unit 5 is ~40-m-thick partly dolomitized calcarenite, overlain by coral-bearing oolitic and oncolitic limestone. Unit 6 is ~80-m-thick grading from greenish gypsiferous mudstone to micritic ammonite-bearing limestone interbedded with marls and calcareous sandstone. Unit 7 is ~80-m-thick massive bioclastic and biomicritic limestone that is partly dolomitized. This unit outcrops at the top of the plateau where the Jabali deposit is located, which clearly are affected by strong karstic erosion. Unit 8 is up to 30-m-thick black mudstone and argillite with gypsum crystals and dolomite intercalations, grading laterally to micritic ammonite-bearing limestone. Unit 9 is ~20-m-thick biomicrite with oncolites and bio-oocalcarenite with intercalations of gypsum and lenses of arkosic sandstone. The last two units (Units 8 and 9) outcrop along the Gebel Barrik crest, which constitutes a relief over the Jabali plateau.

The Jabali Zn–Pb mineralization is mainly hosted by the dolomitized section of Unit 7 (Al Ganad et al. 1994; SRK Consulting 2005; Mondillo et al. 2011, 2014), which partly outcrops in some places of the plateau. The majority of mineralized lithologies still occur in the subsurface, below Gebel Barrik (SRK Consulting 2005). The ore is almost completely oxidized, but in some places underneath Unit 8, primary sulfides have been partly preserved from oxidation by the impervious cover of black mudstone and argillites. The Jabali mineralization seems to be structurally and lithologically controlled, which is reflected in the morphology of the orebodies that are both tabular and parallel to the stratigraphy, and aligned vertically along fractures and faults and at the intersections of these structures. At the fault intersections, the mineralization forms big vertical bodies, comparable to chimneys. The stratiform bodies, parallel to the stratigraphy, occur in three different zones: The upper

zone, which is a laterally extensive, and more sporadic lower and middle zones. These bodies are generally flat but, at the base of the Gebel Salab massif, along the northwest/southeast fault they dip towards the northeast at angles greater than 30° (Fig. 6.13). The nonsulfide ore displays massive, semimassive, and disseminated character, and is characterized by vuggy–to–highly porous, brownish-orange–to–white Zn-bearing non-sulfide minerals (Fig. 6.15) (Mondillo et al. 2011, 2014). A porous cellular boxwork structure is accompanied by numerous cavities coated with Zn minerals, dolomite, and calcite that are quite widespread.

The most common secondary Zn-bearing minerals is smithsonite, which is intimately intergrown with dolomite (Fig. 6.15a). Fine-to-granular amorphous aggregates of hydrozincite have observed in outcrops (Fig. 6.15b), but are very uncommon at depth and in drill cores. Lead is present both as cerussite and anglesite. The nonsulfide ore replaces primary sulfides (Fig. 6.15c) and the dolomite host rock (Fig. 6.15d), which is also dedolomitized and patchily replaced by calcite. Iron staining is common throughout the mining area, resulting in variable concentrations of goethite, hematite, and manganese oxyhydroxides. Silver is contained in Ag_2S and as native metal. Gypsum is very common through the entire mineralized area (Fig. 6.15e). Remnants of the primary sulfide association can be observed in outcrops and drill cores, and consist of sphalerite, galena, and pyrite/marcasite. Sphalerite occurs as two distinct generations, a first that is dark colored, and a second that is more abundant and represented by zoned euhedral-to-subhedral honey-colored or brownish-red crystals (SRK Consulting 2005). Sphalerite contains Fe, Ag, Cd, Cu, Ge, and Hg. Fluid inclusions of sphalerite have bimodal homogenization temperatures to the liquid between 60–85 °C and 85–110 °C and bimodal salinities of 10–14 eq wt% and 19–23 eq wt% NaCl, respectively (Al Ganad et al. 1994).

The Pb isotopic ratios for galena and cerussite, respectively, range between 18.85 and 18.95 $^{206}Pb/^{204}Pb$, 15.66 and 15.72 $^{207}Pb/^{204}Pb$, and 39.71 and 39.92 $^{208}Pb/^{204}Pb$ (Mondillo et al. 2011, 2014). These values are similar to the Pb isotopic composition of other Zn–Pb deposits of the Sabatayn basin and are interpreted as indicative of the contribution of an early Proterozoic crustal component (e.g., basement rocks of the basin) (Stacey and Hedge 1984; Al Ganad et al. 1994). Regarding the genesis of Jabali Zn–Pb deposits, the basic geological concepts of Al Ganad et al. (1994) have been confirmed in the reports of Allen (2000) and SRK Consulting (2005), but the genetic model for the primary and secondary mineralizations has remained an open matter and is still strongly debated. The Pb isotopic ratio of galena indicates a source of the metals from the basement (Al Ganad et al. 1994). The sphalerite fluid inclusions, on the other hand, have a basinal character and show salinities and temperatures similar to many carbonate-hosted Pb–Zn deposits. Thus, the limited research on the genesis of primary sulfide ores of the Jabali Zn–Pb deposit support the hypothesis of a MVT mineralization in the broad sense (Al Ganad et al. 1994).

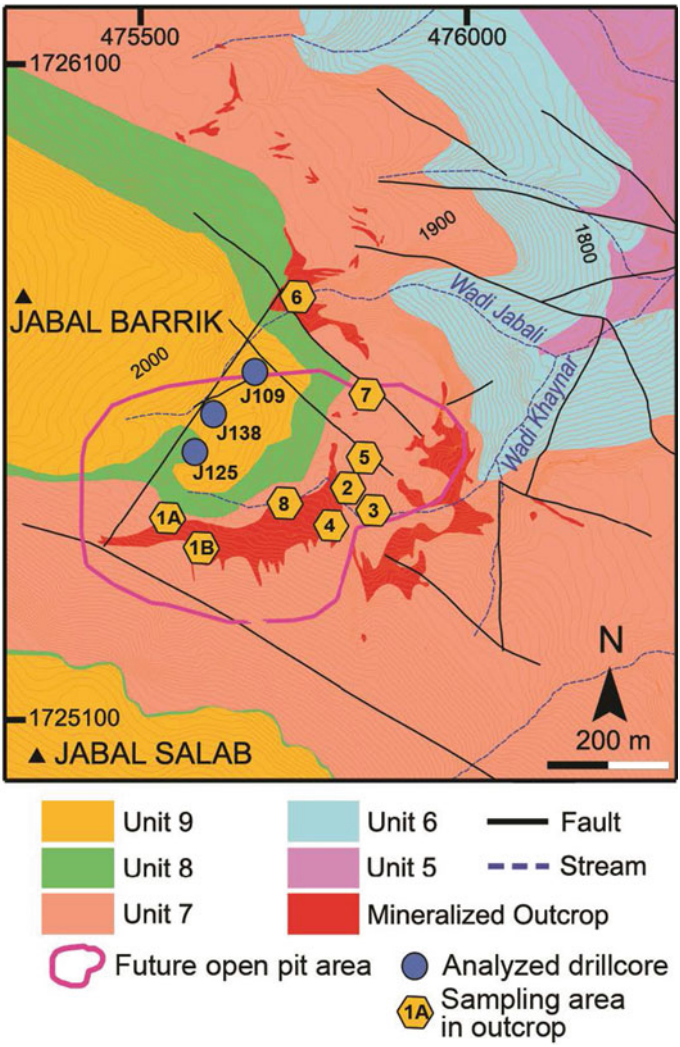

Fig. 6.13 Simplified geological map of the Jabali mining site showing the location of drill cores and an open-pit area (from SRK Consulting 2005)

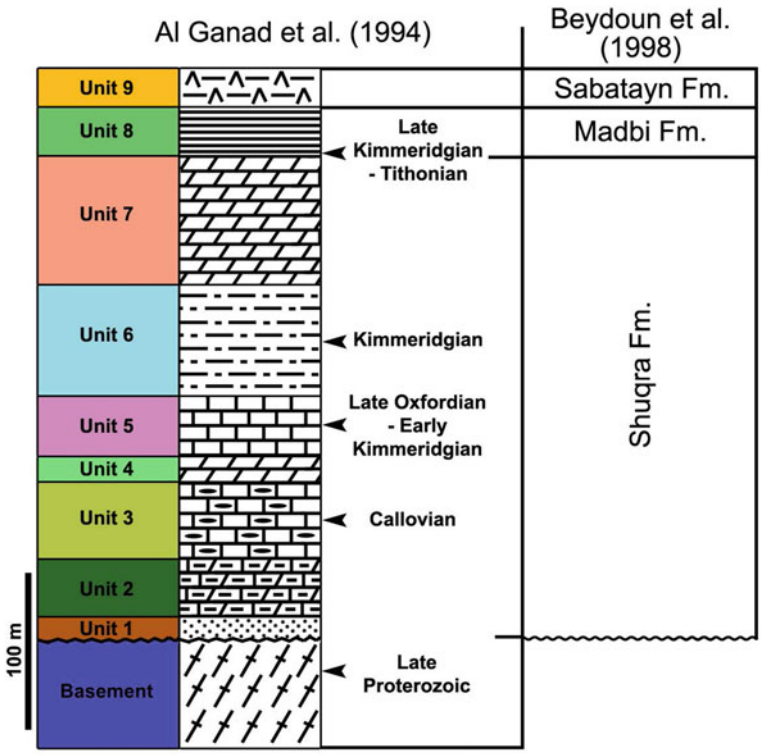

Fig. 6.14 Stratigraphic sequence of the Jabali area (Al Ganad et al. 1994)

6.4 Volcano–Sedimentary Mineral Deposits in the Eastern Desert of Egypt

6.4.1 Introduction

There are many volcano–sedimentary mineral deposits in the Central Eastern Desert (CED) and South Eastern Desert (SED) of Egypt, which are represented mainly by polymetallic VMS occurrences, including Hamama, Um Samiuki, Helgate, Maaqal, Derhib, Abu Gurdi, El Atshan, Egat, and Um Selimat. Except for the Hamama occurrence, which is located in the CED, all of other occurrences listed here are located within a small geographic area in the SED (Fig. 6.16). Despite their existence in the Neoproterozoic basement rocks of the Eastern Desert, these VMS deposits/occurrences show distinct differences in their host rocks, structural evolution, and mineralogical, textural, and bulk geochemical characteristics. Based on these differences, VMS deposits/occurrences in the Eastern Desert of Egypt can be subdivided into three main groups with different characteristics (Abd Allah 2012; Morad and Helmy 2021) including, starting from the CED and progressing to the

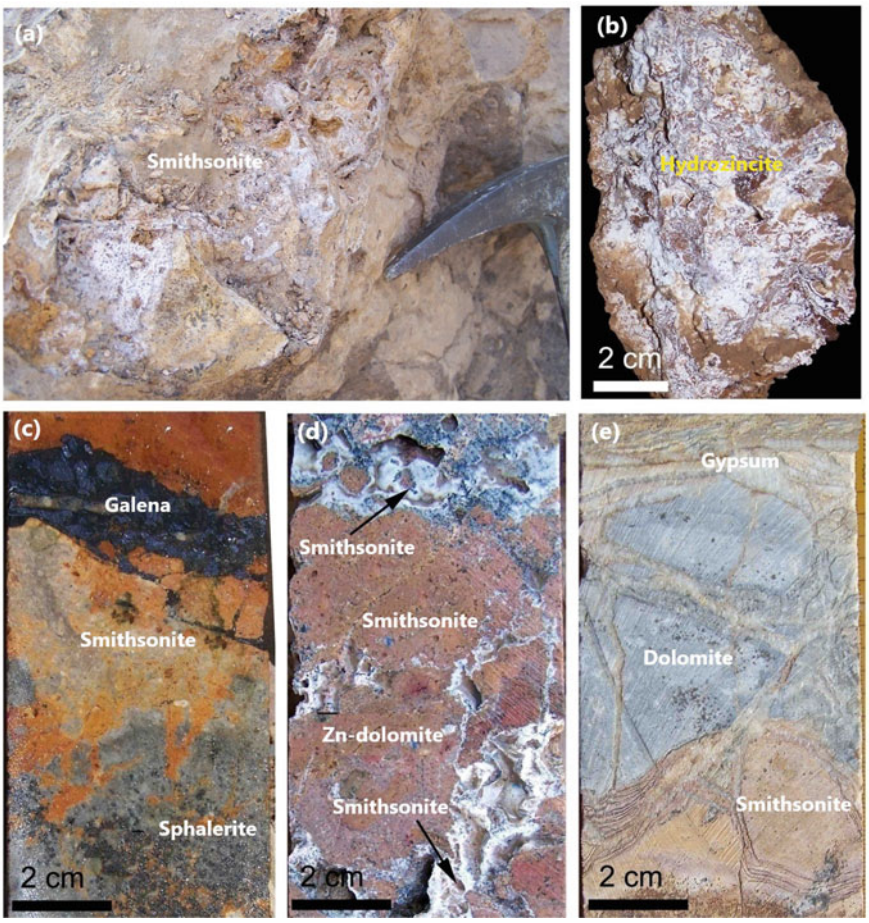

Fig. 6.15 Nonsulfide Zn–Pb mineralization of Jabali area (from Mondillo et al. 2014). **a** Smithsonite in outcrop, with a vuggy–highly porous texture. **b** Hydrozincite coating smithsonite and host rock. **c** Partly oxidized ore, with remnants of sphalerite and galena. **d** Massive smithsonite, replacing Zn-dolomite, and smithsonite crusts in cavities. **e** Gypsum veins, cutting both dolomite and smithsonite

SED: The *Hamama west*, which lies in a wider area of Aton Resources Inc.'s Abu Marawat concession of the Abu Marawat mineral district in the CED. Mineralization at the Hamama West consists of primary hypogene sulfide mineralization overlain by an oxidized zone of Au-bearing gossans. The Hamama West mineralization is interpreted as being of VMS style, although it does not have the classic massive sulfide mounds to date. The *Um Samiuki mineral district* includes Um Samiuki, Helgate, and Maaqal occurrences. The sulfide mineralization of this district occurs as massive lenses and veins that extend tens of meters, where sphalerite, chalcopyrite, pyrite, and galena are the major sulfide minerals. Ore deposits characterized

by Mn-rich sphalerite (up to 5.5 wt%) and has variable Fe content (ranging 0.5–4.5 wt%). The composition of galena is Ag- and Se-poor. Ag-rich tellurides are also recorded in these occurrences, which can be classified as Zn-dominated VMS. The *Derhib mineral district* includes occurrences at Derhib, Abu Gurdi, and Egat. The sulfide mineralization of this district is essentially located along major shear zones that intersecting ophiolitic mélange and island arc volcanic rocks. No primary structures and textures of the ores and host rocks have been preserved due to secondary deformations and metamorphism. Sulfide minerals are represented by chalcopyrite, galena, sphalerite, and pyrite. Sphalerite has high Cd content (up to 5.1 wt%) and is low in Mn content (<0.3 wt%). Galena is generally enriched in Se (up to 7.2 wt%). These occurrences are classified as Cu-dominated VMS type.

The mineralogical and geochemical differences between these three VMS groups might reflect the differences in submarine tectonic environments and host volcanic rock successions. The Zn-dominated (and Pb–Ag ± Ba-enriched) Um Samiuki and Abu Marwat mineral districts are mostly similar to those of felsic island arc environments that are comparable with the Kuroko VMS–type of Japan. The Cu-dominated Zn-rich VMS mineralization of the Derhib mineral district is mostly similar to those hosted by a mafic fore-arc or back-arc ocean-floor environment classified under the bimodal mafic Cyprus-type VMS deposits.

Following is a brief description of the VMS deposits/occurrences in the above-mentioned three mineral districts: Hamama (Abu Marawat), Um Samiuki, and Derhib, in terms of their host rocks, sulfide mineralogy, and geochemical characteristics.

6.4.2 The Hamama West Prospect (Abu Marawat Mineral District)

The majority of this section, especially the geology and mineralization, is mostly compiled from information supplied by the Aton Resources technical report (Aton Resources technical Report, March 15, 2020, accessed on April 2021). The Hamama west prospect is the only known VMS mineralization in the CED and is located ~450 km to the south/southeast of Cairo; it is located within the Aton Abu Marawat concession (Figs. 6.16 and 6.17). The Abu Marwat concession lies between latitudes 26° 18′ and 26° 34′ N, and longitudes 33° 19′ and 33° 46′ E and covers a total surface area of ~738.8 km^2. The Hamama west occurrence is located approximately between coordinates 26° 20′ 37″ N and 33° 20′ 33″ E (Fig. 6.17). Historically, the ancient workings in the Hamama area are scattered over an area of ~5 km^2. The largest ancient workings concentrated at Hamama north, which known also as the Hamama I site (Klemm and Klemm 2013) that dated back to the New Kingdom and Ptolemaic periods, consisting of a 320-m-long zone of north/south-striking trenches, from which a significant amount of vein material has been excavated. Spoil and mine

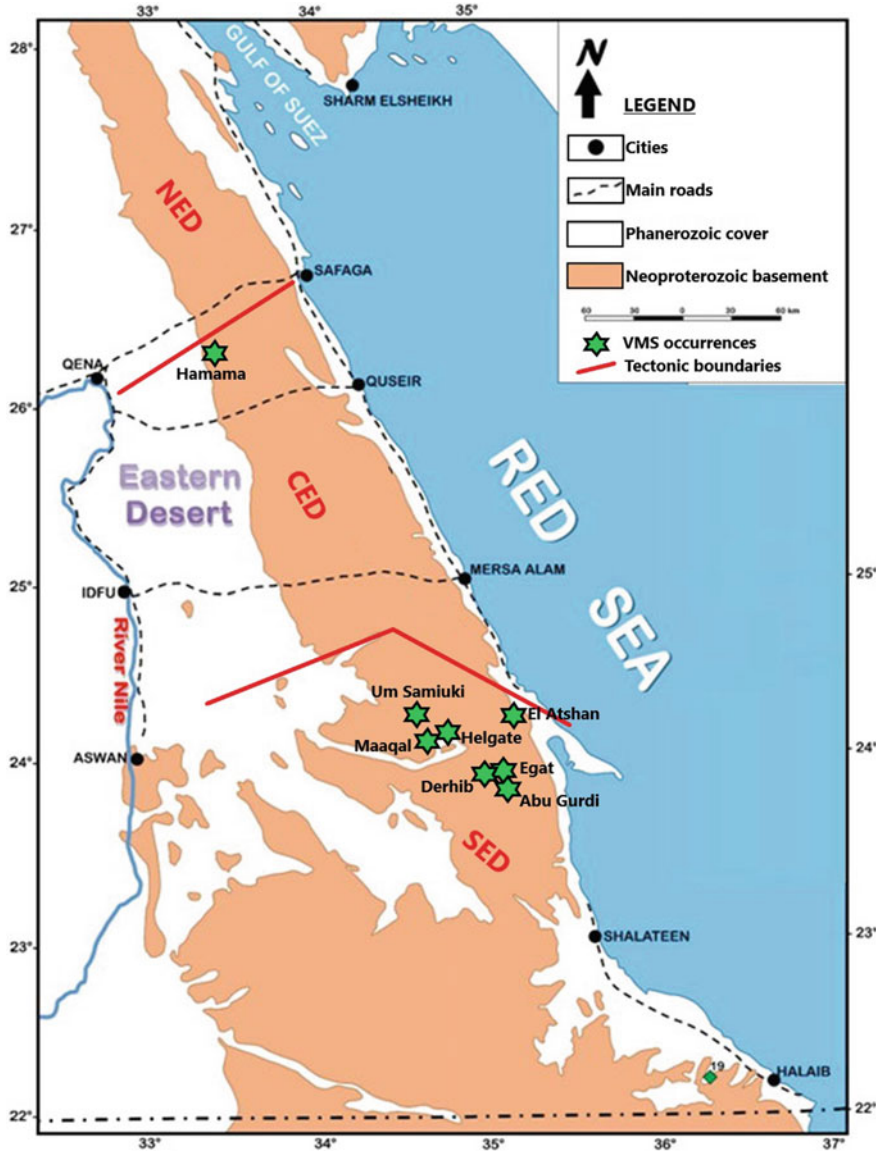

Fig. 6.16 Exposed Proterozoic ANS rocks in the Eastern Desert of Egypt showing the distribution of VMS deposits and occurrences in the SED and CED of Egypt

waste in the local area contains abundant specular hematite and red-brown gossan cover.

At the Hamama east site, there is a regionally mineralized horizon at which a small adit has been driven, a few tens of meters into the side of the hill. This area is referred to as the Hamama II site, and suggested that it was utilized in the Early Arab Period (Klemm and Klemm 2013). Zinc and Cu mineralization occurs as stockworks or thin networks of veins, along with patches of gossanous materials. Next to this adit are collections of small rectangular huts that contain numerous shards of pottery, including occasional pieces of amphoras, where a little mine waste exists in this area. At the site of Hamama west, there is relatively little evidence of ancient mining, apart from a few very small pits within a gossanous zone, over a strike length of ~70 m. Several other small workings, possibly prospecting pits, are scattered around the area. They are usually associated with very small zones of quartz veining with staining of malachite and/or chrysocolla.

In modern times, the Egyptian Geological Survey and Mining Authority (EGSMA) has carried out several exploration programs of geological traverses, trenching, and channel and lump sampling, with other national and international companies (including Minex, Centamin, Pharaoh Gold Mines NL (PGM), and, what was at the time Alexander Nubia (now Aton Resources)) from 1970 through 2007. Currently, Aton Resources has the sole right to explore and develop Au and associated mineral deposits within the concession area, where an exploration camp has been constructed at Abu Marawat and a smaller field camp at Hamama to conduct exploration activities, including detailed geological mapping over the entire Hamama area. A number of diamond drill holes were completed between 2011 and 2014 at the Hamama west, central, and east prospects. Diamond drilling was resumed again at the Hamama west site in March 2015 with an additional 70 diamond drill holes that were completed by the end of August 2016. Most exploration activities during this period were focused on the Hamama west site, although the Hamama central and Hamama east sites were also briefly drill-tested in 2015.

Geologically, the Hamama mineralization is essentially hosted by a sequence of volcano–sedimentary belts separated by narrow, sinuous belts of mafic and ultramafic rocks. These volcano–sedimentary belts are typically represented by calc-alkaline andesitic rocks with associated mafic-to-intermediate intrusive rocks (Fig. 6.17), which are all regionally metamorphosed to lower greenschist facies, before being intruded by various tectonic or post-tectonic granitoids. The local geology at the Hamama occurrence consists of a sequence of intermediate-to-felsic lavas and tuffs, overlain by tuffaceous sedimentary rocks with minor thin beds of jasper, chert, and bedded pyrite (Fig. 6.17). Numerous subvolcanic andesitic dykes and intrusives occur in the whole area, where they were subsequently folded and faulted during the Pan-African orogeny. Close to the Hamama west prospect, the entire rock package has been overturned, dipping to the north. Similarly, towards the Hamama central and Hamama east prospects, the rock units were overturned and their orientation changed to generally striking northeast dipping northwest. The main mineralized horizon and their host rocks dip from ~55° to nearly vertical.

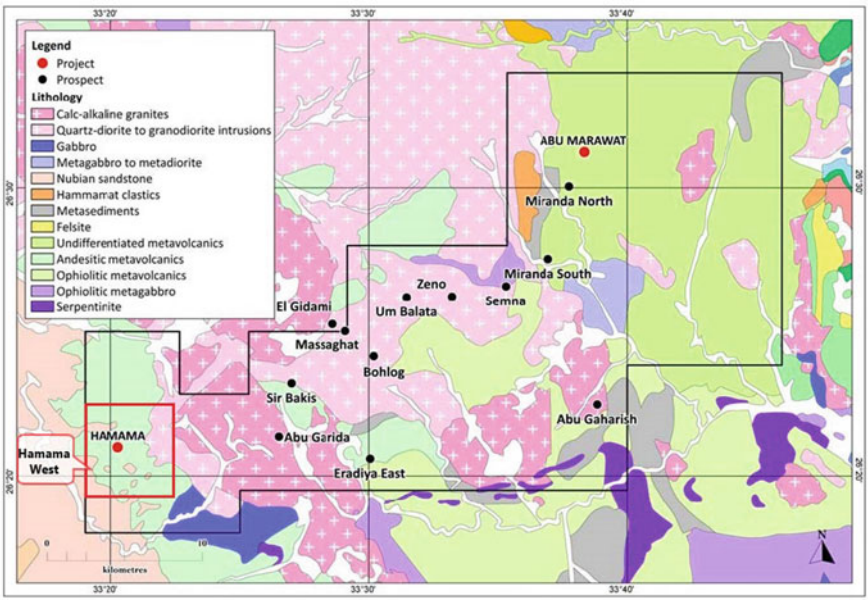

Fig. 6.17 Simplified geological map of the Abu Marwat concession of Aton Resources, showing the distribution of possible VMS deposits in Hamama west and surroundings (Aton Resources Technical Report, March 15)

Stratigraphically, the footwall rocks of the Hamama mineralization are dominated by grey-to-green andesite lavas with interbedded tuffs (Fig. 6.18). The andesite rock is mostly pillowed and is commonly porphyritic in texture and, where it is in proximity to the main mineralized zones, becomes more intensely altered to a chlorite–sericite zone and contains disseminated small pyrite crystals. The andesite unit is overlain by a sequence of felsic volcanic rocks, which represent the main mineralized horizon at Hamama west. At the Hamama west site, the basal unit is a semicoherent felsite (Fig. 6.18), exhibiting various degrees of brecciation at a local scale. A package of medium-grey tuffs, which vary from moderately poorly sorted lapilli tuffs to laminated ash tuffs, is stratigraphically overlain by the felsic volcanic rocks. This felsic tuffs are found intimately together with the brecciated felsite zones; they mostly host the primary precious and base-metal sulfide mineralization. The stratigraphy of hanging wall consists of a sequence from fine-to-medium-grained felsic to intermediate tuffaceous rocks, with argillaceous or epiclastic sedimentary rocks. Drill holes in this area intersected clasts and small blocks of massive sulfide and vein material a few meters above the contact with the main mineralized zone, which are interpreted as minor slumping or talus features related to the sea-floor topography existing at the time of the deposition of these tuffs (Aton Resources 2017). The hanging-wall unit is typically associated with thin beds of jasper and pyrite. The basal felsic tuffs or argillites grade upwards into a sequence of volcaniclastic rocks, which consist of darker grey-green tuffaceous sandstones and siltstones interbedded

with purple cherty argillites and bright-red jaspers. The jaspilitic and tuffaceous sediments grade upwards into a distinctive massive, pale-green andesitic tuff unit, which rapidly grades upwards into fine-grained, featureless, massive tuffs.

The mineralization at the Hamama occurrence consists of hypogene sulfides overlain byoxidized zone of Au-bearing gossans cover. Outcrop mapping and drilling have defined the deposit to date with ~800-m strike length and average width of ~60 m, outcropping at the surface, and an average drill-intersected depth of ~120 m below surface (Fig. 6.18). The deepest drill hole to date has intersected the mineralized zone down to a depth of 275 m below surface. The hypogene sulfide mineralization at Hamama prospect is dominated by disseminated stringer and blebby pyrite, often associated with lesser amounts of sphalerite, and, rarely, chalcopyrite and galena. In the sulfide-rich zone, Au typically occurs as native grains that are interstitial to sulfide minerals, whereas Ag is mostly associated with sulfosalts and/or galena (Payne 2013). On a broader scale, zonation of the Au and Ag mineralization is unclear at the current level of drilling, but some shallow north-plunging trends are evident (which would therefore imply a steep-to-vertical control on mineralization at the time of deposition). At a smaller scale, there is some evidence of Au enrichment near the stratigraphic hanging-wall contact. Zinc commonly occurs throughout the deposit as disseminated mineralization into the footwall andesites. The alteration associated with sulfide mineralization is dominated by silica and carbonate especially ferroan dolomite. In some places, the original textures of the host lithologies have been completely obliterated due to the intense silica–carbonate alteration. The hypogene sulfide mineralization at the Hamama deposit is capped by an approximately 30-to-40-m-thick gossan cover of weathered and oxidized materials. This zone is quite variable and consists of ruddy to reddish-brown to yellow iron oxide and clay-rich materials. Gold and silver are commonly enriched in the uppermost 3–5 m of the profile. Zinc-bearing minerals are present in the oxide zone, related to the original distribution of sphalerite prior to the weathering events, and mostly at concentrations of >10 wt%. Minerals recognized in the oxide zone include limonite, hematite, smithsonite, malachite, and chrysocolla.

Genetically, the Hamama mineralization has been variably described as a classic VMS deposit (Hall and McHugh 1989), a Au-rich VMS (Alexander Nubia Inc. 2015) and an orogenic precious/base-metals vein deposit (Voormeij 2015). The Aton Resources is interpreted the Hamama west mineralization as a *VMS–epithermal hybrid* subclass as it displays many of the characteristic features of the VMS style of mineralization. This distinct group of deposits has been variously described in the literature as "high-Au VMS" (Dubé et al. 2007), "high sulfidation VMS" (Sillitoe et al. 1996), and "hybrid VHMS–high-sulfidation epithermal deposits" (Large et al. 2001). The world-class examples of this mineralization type include the LaRonde–Penna and Bousquet deposits in Quebec, the Eskay Creek deposit in British Columbia, and the Henty and Mount Lyell deposits in Tasmania. Such types of VMS–epithermal hybrid deposits are distinguished from the more "classic" VMS ones (e.g., bimodal mafic/felsic–Noranda type) by being relatively rich in precious metals and poor in base metals, having a higher proportion of volcaniclastic rocks to flows of bimodal characters (i.e., mafic/felsic volcanics), having

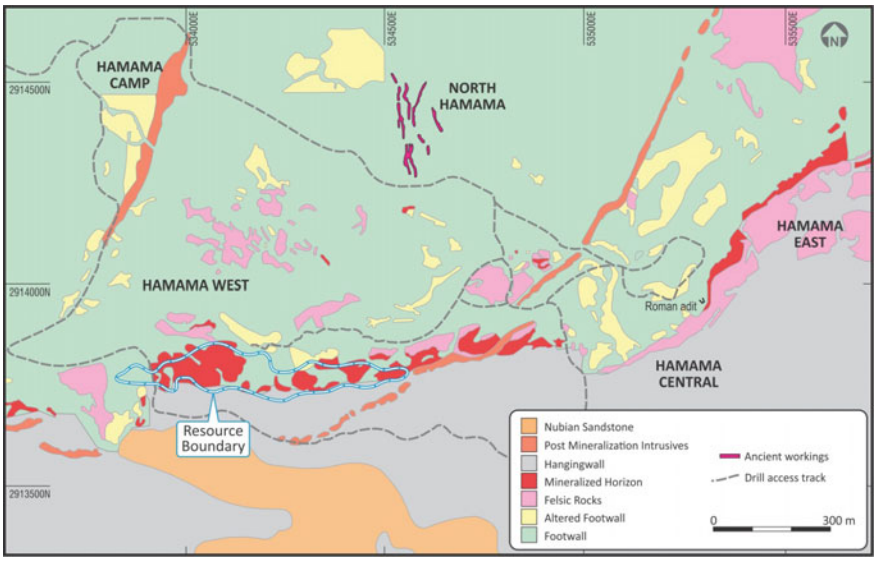

Fig. 6.18 Simplified geological map of the Hamama west VMS deposit showing the different zones of mineralization and their host rock lithology (Aton Resources Technical Report, March 15)

anomalous geochemical signatures, and exhibiting alteration assemblages indicative of low-pH fluids. They essentially represent the shallow marine equivalent to subaerial epithermal systems (Dubé et al. 2007). The hanging-wall stratigraphy, which in many places displays clear sedimentary textures, suggests a marine environment. The combination of the style of mineralization (footwall stringers), the presence of chemical sediments that occur at distinct stratigraphic breaks, and the style of volcanism are together indicators of a classic VMS environment. Alternatively, the advanced argillic alteration, colloform banded vein fragments, and vuggy silica with bladed quartz (after calcite) are suggestive of an epithermal style setting, with boiling of low-pH fluids. The anomalous geochemical signatures for As, Mo, and Sb are indicative of a magmatic volatile input. The abundance of pyroclastic rocks, especially towards the east, suggests a shallow marine setting. All of the above-mentioned features are likely indicators of a VMS–epithermal hybrid system, with fluids preferentially mineralizing a semiconsolidated pile of felsic volcaniclastic rocks with relatively high porosity.

6.4.3 The Um Samiuki Mineral District

The Um Samiuki mineral district includes several VMS occurrences, including the Um Samiuki (the largest VMS mineralization in Egypt), Helgate, and Maaqal occurrences. These mineral occurrences are hosted by a thick pile (>10 km) of volcanic

rocks named the Shadli metavolcanic belt (SMB) that comprises rhyolites, andesites, basalts, and volcaniclastic rocks. The rocks of SMB were erupted in two magmatic bimodal cycles, the lower (older) Um Samiuki group, and the overlying (younger) Hamamid group (Searle et al. 1978; Stern et al. 1991; Noweir and Abu El-Ela 1991; Takla et al. 1999). The SMB extends for >80 km in a northwest/southeast direction, an average width of ~25 km, and is flanked to the north and south by syntectonic granodiorite intrusions (Fig. 6.19a). Both mafic and felsic volcanic cycles occur as alternating belts trending mostly west-northwest/east-southeast, and separated by tectonic contacts (thrusts and strike-slip faults; Fig. 6.19b) (Faisal et al. 2020).

The lower metavolcanics group of Um Samiuki forms the main lithologic unit in the area, comprising >1000-m-thick massive, amygdaloidal, tholeiitic basalt, and andesite flows with minor intercalations of andesitic and rhyolitic volcaniclastic rocks (Fig. 6.20). They have metamorphosed and occasionally pillowed in some horizons. The lower Hamamid metavolcanics group, on the other hand, attains a maximum thickness of 2000 m. It is characterized by two distinct cycles of volcanism (cycles 1 and 2), in which each cycle commenced with the eruption of basic pillow lavas and terminated with thick beds of felsic lava and tuff (Searle et al. 1978). The mafic rocks of cycle 1 are represented by massive pillow basaltic flows and agglomerates (Faisal et al. 2020), whereas the felsic rocks of cycle 1 include dacites, rhyolites, and tuffs. The VMS sulfide orebody mainly is localized between the brecciated rhyolite and vent facies on one side and the tuffs of the felsic rocks on the other side (Fig. 6.20). These felsic lavas were previously nonconstrained by age; however, recently they were dated using in situ U–Pb zircon dating to be ~695 Ma, and are characterized by subduction-related geochemical characteristics with significant enrichments in Zr, Hf, and Sm (Faisal et al. 2020). The entire rock sequence of the SMB was later intruded by dolerites, biotite, and hornblende syntectonic granitoids, and lastly by the late- to post-tectonic muscovite granites (Figs. 6.19 and 6.20). The last phase of igneous activity in the area is represented by various dykes and sills of Phanerozoic age, some of them related to the upper Cretaceous volcanic event of Wadi Natash area (Shukri and Mansour 1980).

There are three well-known VMS occurrences in the Um Samiuki mineral district: the Um Samiuki, Helgate, and Maaqal prospects (Figs. 6.16 and 6.19b). Following are brief descriptions of these occurrences in terms of their geology and mineralogy.

The *Um Samiuki* prospect represents the largest VMS occurrence in the district; it was mined by ancient Egyptians and Romans for malachite. The Um Samiuki prospect comprises two separate occurrences of massive sulfide lenses at the top of cycle 1 rhyolitic breccia of the Hamamid group, which are known as the Um Samiuki west and Um Samiuki east mines (Fig. 6.19b). The orebody in the western mine extends for ~90 m along strike with a maximum width of 20 m and continues to a depth of ~170 m. The orebody is made up of ~6-m-thick massive and semimassive sulfide zones extending vertically and laterally. The semimassive mineralized zone extends into a disseminated sulfide halo. The massive ore contains up to 70 modal % sulfides whereas the semimassive halo contains up to 30 modal % sulfides. In the western mine, one of the drill holes intersected a zone of ~11-m-thick sulfides grading at 21.7 wt% Zn, 2.2 wt% Cu, 0.5 wt% Pb, and 0.01% Ag (Searle et al. 1978).

In the eastern mine, the ore zone extends along the surface for more than 180 m with an average outcrop width of 10 m. The ore zone diminishes with depth due to tight cross folding and faulting. Sulfide mineralization comprises two separate large lenses, 35 and 25 m in length, respectively, with an average thickness of 2 m, as well as many small bodies (<2 m long).

The massive sulfide ore of Um Samiuki prospect has variable mineralogical compositions; sometimes sphalerite-rich, bornite-rich, and pyrite-rich zones. In the sphalerite-rich ore, sphalerite forms the matrix hosting chalcopyrite and pyrite. In the bornite-rich zone, bornite constitutes ~40% modal, with lesser amounts of sphalerite, chalcopyrite, tetrahedrite–tennantite, and minor arsenopyrite and covellite. Covellite has been found to replace almost all other sulfide minerals along cracks. Pyrite is the main constituent of the pyrite-rich zone with lesser amounts of chalcopyrite and galena. Bornite, tetrahedrite–tennantite, chalcopyrite, and covellite are found to contain a high content of Ag, up to 1500 ppm (Shalaby et al. 2004). The Ag-rich character of the Um Samiuki VMS is confirmed by the presence of several Ag-bearing minerals, including (Helmy 1996, 1999; Shalaby et al. 2004): hessite (Ag_2Te), Au_Ag alloy, cervelleite (Ag_4TeS), freibergite $(Ag,Cu)_{10}(Fe,Zn)_2(Sb,As)_4S_{13}$, acanthite ($Ag_2S$), mckinstryite ($Ag_{1.2}Cu_{0.8}S$), benleonardite ($Ag_8SbAsTe_2S_3$), stephanite (AgSbS), and native Ag. These Ag minerals are commonly associated with Ag-bearing bornite, tetrahedrite, tennantite, and chalcopyrite. The common gangue minerals associated with the Um Samiuki sulfide ores are represented by barite, calcite, rhodonite, tephroite (Mn_2SiO_4), rhodochrosite, spessartine, tremolite, diopside, talc, Mn-chlorite, and quartz.

The United Nations programme (Searle et al. 1978) prospected the Um Samiuki area geologically and geochemically, where a cumulative total of 806 m were drilled in six boreholes and tens of meters of tunnels and shafts were excavated in the western and eastern mines. The estimated ore reserves from these boreholes were <300,000 t, with average grades of 11.5 wt% Zn, 1.15 wt% Cu, 1.1 wt% Pb, and 0.01% Ag.

The *Helgate* and *Maaqal* VMS mineralizations are also hosted by the SMB, which are about similar to those in the Um Samiuki prospect, which is represented by two major units: the lower and the upper metavolcanic units. The *Helgate* prospect lies on the eastward continuation of the Um Samiuki fault (Fig. 6.19b). It is characterized by a number of highly contorted lenses of manganiferous carbonate (ankerite) in complex folded rhyolite and banded tuff and chert. The mineralization zone trends northwest with ~75° dips to the south. The underground extension along strike of the Helgate mineralization zone is ~60 m although surface indications appear to be approximately twice this length (Searle et al. 1978; Abd Allah 2012). The thickness of the mineralized zone ranges 0.5–0.8 m in the form of concordant veins with the banded tuff and chert of the hanging wall. The geophysical data reveals that the orebody continues only for ~12 m farther to the southeast beneath the Wadi alluvium. To the north of Helgate prospect there is a vent area containing rhyolite breccia, mafic volcanic agglomerate, intrusive rhyolite, and a network of late basaltic dykes. Sulfide mineralization at the Helgate prospect comprises, in decreasing order of abundance, sphalerite, pyrite, chalcopyrite, and galena, without any Ag minerals identified. The common presence of micro- and cryptic layering of fine-grained thin

layers of pyrite crystals suggest primary depositional textures. Gangue minerals are dominated by chlorite, quartz, and calcite. The estimated ore reserves are ~13,000 t, with an average grade of 13.6 wt% Zn, 2.9 wt% Cu, and 11.4 wt% Pb.

The *Maaqal* prospect is located at the southern side of the meta-andesitic rocks of cycle 2 of the Hamamid group (Fig. 6.19b). This prospect is characterized by a zone of intense deformation and brecciation, which is the main host for talcose rocks and sulfide lenses. The lithologic units exposed in the Maaqal area comprise lower pillow lava overlain by rhyolite flows and lapilli tuff and capped by banded tuff and chert. The contact between the footwall pillow lava and the hanging-wall lapilli tuff is marked by a talc-rich zone, along which massive sphalerite-dominated sulfide bands are stratified. Sphalerite is the dominant sulfide mineral, forming the matrix for other sulfides; it also forms small-scale bands interlayered with chalcopyrite bands. Pyrite, chalcopyrite, and galena represent the rest of the sulfide minerals in the Maaqal prospect. Chlorite, quartz, and calcite are the most common gangue minerals associated with sulfides. The estimated average assay of the Maaqal occurrence is ~13.6 wt% Zn, 2.9 wt% Cu, and 11.4 wt% Pb (Searle et al. 1978).

6.4.4 The Derhib–Abu Gurdi Mineral District

The *Derhib* and *Abu Gurdi* prospects are located in the eastern end of the SMB, at the northern side of Baranis-Aswan Road, ~60 km from Baranis (Figs. 6.16 and 6.21). The Derhib–Abu Gurdi district is built up of late Neoproterozoic Pan-African metamorphic and magmatic rock assemblages, where the metamorphic rocks comprise gneisses/pelites and metavolcanics, which are intruded by syn- to late-tectonic magmatic granodiorite–tonalite and gabbroic rock assemblages (Ali-Bik et al. 2020). The whole sequence is dissected by post-tectonic dykes and quartz veins and plugs. The Derhib area is well known for its talc mineralization, which has been exploited since 1953, where the talc mineralization is always encountered along shear zones separating Shadli metavolcanic rocks and ophiolites from the underlying metasedimentary rocks (Fig. 6.22a). The Derhib area is covered by metasedimentary rocks, dismembered ophiolitic sequences (serpentinites, metagabbros, and metabasalts), bimodal mafic/felsic Shadli metavolcanic rocks, and younger intrusive granites and gabbros. The metasedimentary and the ophiolitic rocks are the oldest in the area and are extensively sheared and variably metamorphosed (Selim 1994). The VMS (Cu–Zn–Ag) mineralization occurs either as dissemination or as small massive sulfide lenses and veins along shear zones in talc tremolite rocks in the vicinity of ophiolitic fragments. The VMS mineralization in the whole area is commonly associated with malachite and azurite staining (Fig. 6.22b, d), where these Cu-rich hydrous carbonates and talc constitute the surface or near-surface exposures as integral parts of VMS mineralization (Ali-Bik et al. 2020).

Small-scale VMS orebodies have been recorded at the Derhib–Abu Gurdi district, where talc and talc/malachite mineralization (alteration zones) are commonly distributed mainly along the east/west-trending shear zones. The treated remote

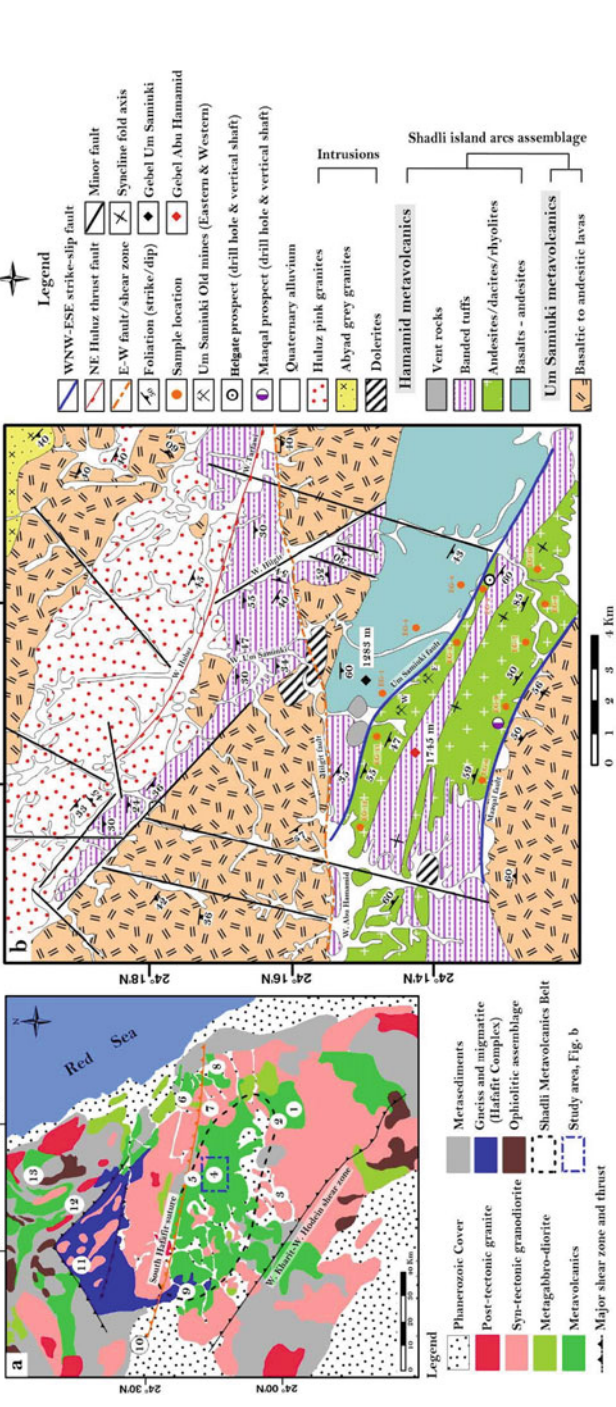

Fig. 6.19 **a** Simplified geological map of the northern part of the SED of Egypt, showing the Umm Samiuki mineral district and surroundings. 1 = Derhib, 2 = Abu Gurdi, 3 = Genina Gharbia, 4 = Um Samiuki, 5 = Abu Hamamid intrusion, 6 = Wadi Ranga, 7 = Gebel Hamata, 8 = Wadi Atshan, 9 = Wadi Kharit, 10 = Wadi Natash, 11 = Migif–Hafafit gneiss dome, 12 = Wadi El Gemal, 13 = Wadi Ghadir. **b** Geological map of the Um Samiuki mineral district (including the Um Samiuki, Helgate, and Maaqal prospects) (after Faisal et al. 2020)

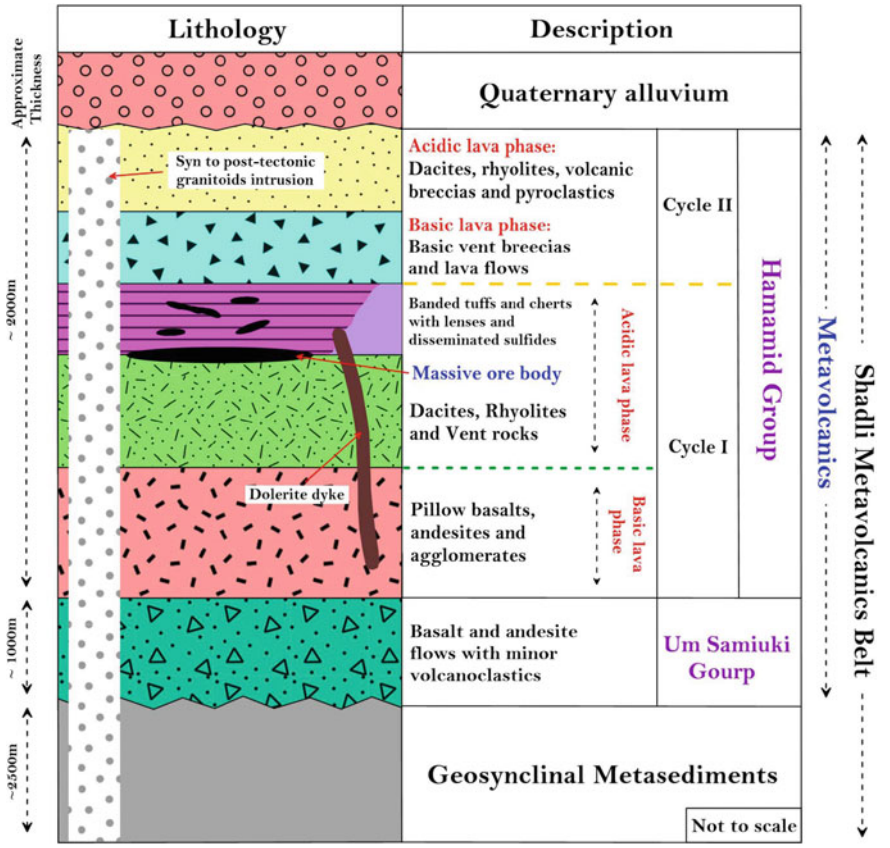

Fig. 6.20 Schematic diagram of stratigraphic column of Gebel Abu Hamamid area, South Eastern Desert, Egypt (from Faisal et al. 2020)

sensing data revealed that there are several mineralization zones scattering throughout the area, which cover an area of ~14.38 km^2, including the Derhib mine (Fig. 6.23). These scattered small-scale lenses might represent parts of a fragmented large lens or represent small successive submarine hydrothermal vents in the area. The SMB, in general, experienced an alternating ductile/brittle deformation history. The role of subsequent structures in stretching and thinning, thickening, or even fragmenting the original sulfide ore lenses or beds is thus highly expected. Hence, the original geometry and architecture of mineralization systems at the Derhib–Abu Gurdi mineral district were most probably distorted and displaced (Ali-Bik et al. 2020). However, VMS mineralizations in general tend to occur favorably within a single stratigraphic interval or a restricted number of horizons within the host volcanic sequences where ore deposition favorable horizons may represent a pause in volcanism, changes in volcanic compositions, or contacts between volcanic and sedimentary rocks (Lydon 1984; Evans 2009).

In the *Derhib* area, sulfide mineralization is hosted either by mafic dykes, which are partially talcosed and contain disseminated sulfides (mainly chalcopyrite and sphalerite), or hosted by silicified talc tremolite rocks occurring as small black zones in talcose rocks, which are hosting disseminated and massive sulfides. At the Derhib and Abu Gurdi prospects, there are two modes of occurrence of sulfide mineralization: (1) Disseminated pyrite–chalcopyrite–sphalerite ore, where sulfides occur as grains interstitial to amphiboles, talc, and chlorites in mafic dykes and talc–tremolite rocks. The sulfide proportions vary from 3 to 18 modal % of the rock volume. This type is more common at depth in the Derhib mine. (2) Massive or vein ore type, which is composed of alternating bands of chalcopyrite and sphalerite enclosed in talc. These veins or lenses follow the structural direction of the shear zone and are encountered at depths of 21–35 m. The massive and disseminated sulfide ores in the Derhib mine consist essentially of, in decreasing order of abundance: chalcopyrite, pyrite, and sphalerite, with lesser amounts of galena and pyrrhotite (Abd Allah 2012). Covellite and magnetite are the major supergene sulfide and oxide minerals, respectively.

The *Abu Gurdi* prospect is located to the southeast of the Derhib prospect (Fig. 6.21), where the sulfide–talc mineralization occurs along shear zones separating the stratigraphically lower metasedimentary rocks from the upper metagabbros. Structural control of talc and base-metal sulfide mineralization is documented by the discontinuous occurrences along the shear zone. The sulfide mineralization at Abu Gurdi is encountered in only one place, where massive sulfide lenses are hosted in a talc-rich zone. The main shear zone in the area trends east/west and is 8 km long and less than 30 m wide. The talc-sulfide mineralization zone extends for ~180 m along strike and 6 m in width area in the central part of the shear zone. The mineralization zone is expressed on the surface by light-grey brecciated rhyolite and blue gossans with green malachite staining (Fig. 6.22c, d). The sulfide minerals at Abu Gurdi prospect are represented by fine-grained pyrite, coarse-grained sphalerite, minor chalcopyrite, and galena.

The *Egat* and *Um Selimat* prospects are also talc-bearing base-metal sulfides that are located within the Derhib–Abu Gurdi mineral district (Fig. 6.16). The *Egat* occurrence is a talc mine where the sulfide mineralization occurs as pockets in the lower levels of the mine. Talc is developed after metarhyolite along a megashear zone (~300 m long and 4–10 m wide) trending east/west and dipping 70° toward the south. Malachite-rich gossans cover is well developed along the shear zone. Due to its small-scale and low-grade mineralization, no further detailed studies have been conducted on the sulfide mineralization in the Egat area. The *Um Selimat* talc mine is located ~2 km to the northwest of the Derhib mine. Like the other talc mines in the area, talc is developed along the shear zones extending >1 km intersecting sheared and brecciated metarhyolite. In this megashear, isolated lenses of talc, carbonates and tremolite are encountered (Botros 2003), where discontinuous patches of primary sulfides and malachite are hosted in talc.

Another base-metal sulfide mineralization in the area is the *El Atshan* prospect, which is also hosted in talc. It is located to the east of the Um Samiuki prospect, ~18 km west of the Red Sea coast (Fig. 6.16). This prospect is one of the most productive high-grade talc ore in Egypt (Botros 2003). The talc deposit develops in

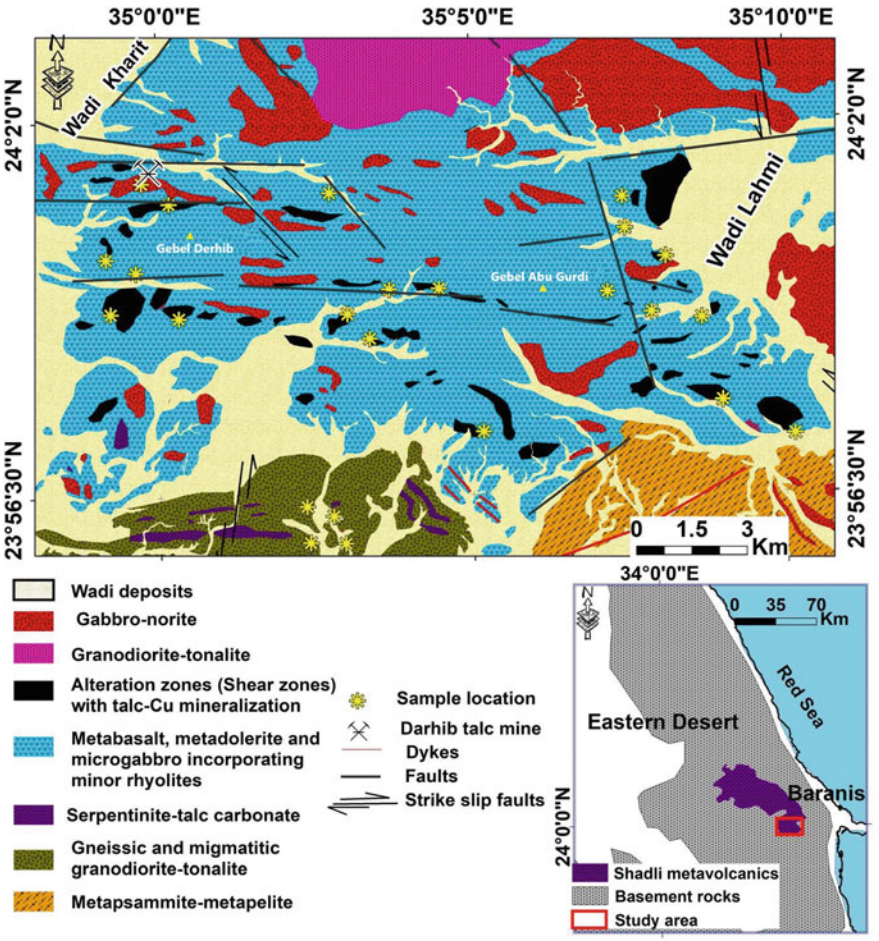

Fig. 6.21 Detailed geological map of Darhib–Abu Gurdi area, Baranis quadrangle map, scale 1:250,000. The inset shows the location area and the extent of SMB within the domain of the basement rocks of the Eastern Desert of Egypt (after Ali-Bik et al. 2020)

a sequence of volcanic and volcaniclastic rocks of basaltic to rhyolitic composition. Talc ore develops along a major alteration zone cutting through basalt and rhyolite and extends for ~500 m in an east/west orientation. Talc is commonly associated with tremolite, chlorite, and quartz. Sulfide mineralization found as massive pockets in the deeper levels of the mine and are represented by malachite in the surface, whereas the hypogene sulfide mineralogy is dominated by chalcopyrite, sphalerite, and galena, which are mostly similar to the Derhib and Abu Gurdi prospects.

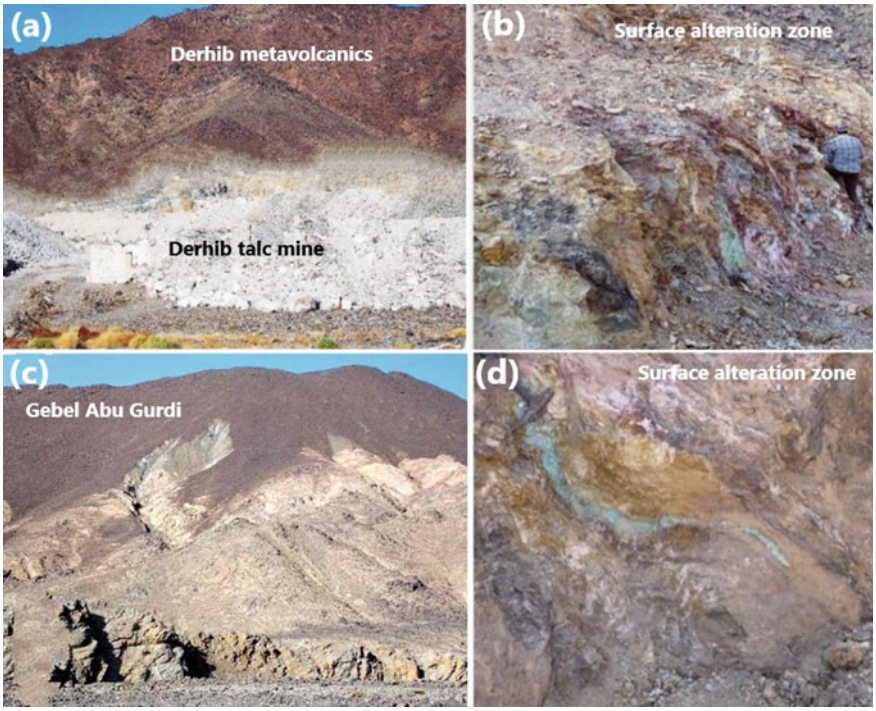

Fig. 6.22 Field photographs showing **a** the location of Derhib talc mine at the contact between Shadli metavolcanic and metasedimentary rocks. **b** Malachite (green) staining in the surface oxidized zone of Gebel Derhib. **c** Abu Gurdi talc mine along shear zones between lower metasedimentary rocks and overlying metagabbros. **d** Malachite staining in the surface oxidized sulfide-rich zone of Gebel Abu Gurdi (from Ali-Bik et al. 2020)

6.5 Volcano–Sedimentary Mineral Deposits in Sudan

Volcano–sedimentary mineral deposits in Sudan are mainly represented by VMS deposits, which are located mainly in the Ariab mineral district of northeastern Sudan. The mining operations in the Ariab district is located in a remote area within the Red Sea State of Sudan, ~450 km northeast of Khartoum and ~200 km west of Port Sudan (Fig. 6.24). The area is known variously as the *Hassai project,* the *Hassai region*, or the *Ariab mining district*. The Ariab mining district as a whole covers a surface area of ~20,000 km^2. VMS deposits containing significant amounts of Cu, Zn, and Au were discovered in the late 1970s by the joint teams of the Geological and Mineral Resources Department (GMRD) of the Ministry of Energy and Mining of Sudan (now named the Geological Research Authority of the Sudan (GRAS)) with the BRGM of France. Despite the low interest in the VMS polymetallic deposits due to low base-metal prices, some drilling of these deposits was carried out as part of the definition of the oxide deposits to adequately define the limit of the resources

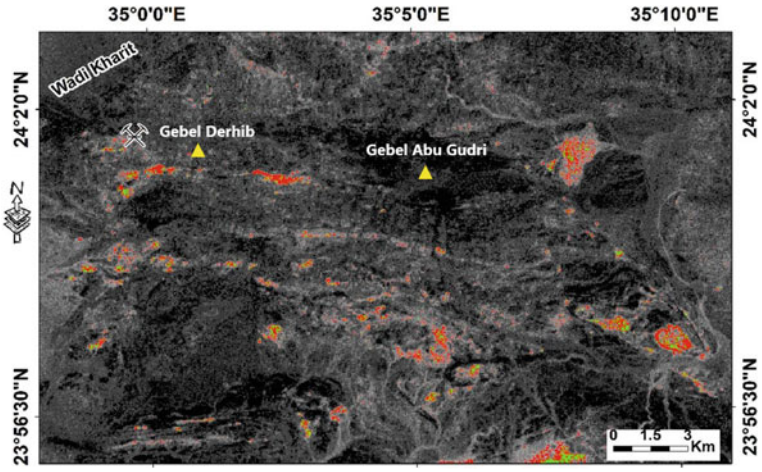

Fig. 6.23 ASTER density slice image of the Gebel Drhib and Gebel Abu Gurdi area. Red pixels represent talc-rich alteration zones, and green pixels represent the malachite-bearing alteration zones (from Ali-Bik et al. 2020)

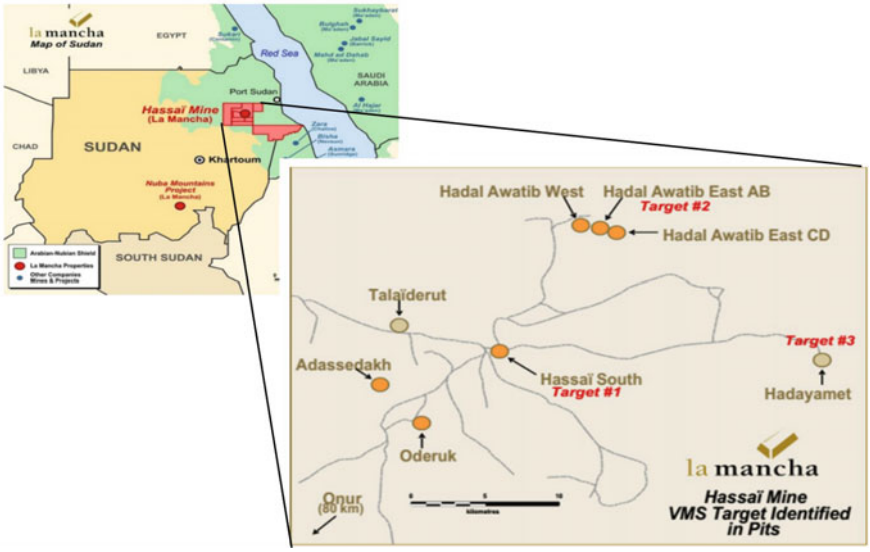

Fig. 6.24 Location map showing the distribution of VMS occurrences in the Ariab mineral district, northeastern Sudan

close to the water table. In addition, several of the pits mined for Au were not closed, in anticipation of future mining of either the gold-and-sulfide bearing oxide sulfate material, or silica/barite rocks (SBR) or the VMS exposed at the bottom of the pits. With the increase in base-metal prices, the VMS deposits are now valuable targets.

Historically, the French and Sudanese teams conducted several exploration programs during the period from 1977 through 1981 for various metals (including W, Pb, Zn, Cu, Ag, Au, and Cr, among others) over five large areas in Sudan within the framework of a cooperation agreement (La Mancha Resources Inc. Technical Report 2009). One such exploration program focused on 17 gossans areas in the central part of the Red Sea Hills (in the Ariab–Arbaat area). These gossans are the weathering products of VMS deposits found at depth. The Au in most of the Ariab mining district is associated with these gossans. Exploration work covered most of the gossans in the Ariab district from 1981 to 1984. Initial work focused on the polymetallic potential of the underlying sulfide mineralization. In 1983, however, the discovery of noteworthy Au concentrations in SBR associated with the gossans at Hassai shifted the interest towards Au. Exploration efforts were then concentrated on the Ariab district from 1984 to 1987. Major trenching work was carried out on all known gossans in the region, including Hadal Awatib southwest, Hadal Awatib east, Talaiderut, Oderuk, Baderuk, and Adassedakh (Fig. 6.24). All of these occurrences were eventually classified as Au deposits. In February 1985, sufficient data were collected at Hassai from surface trenching, percussion drilling, core logging, and pits to justify the installation of a pilot plant. In March 1987, the first Au production was started at Hassai (La Mancha Resources Inc. Technical Report 2009). In eight occurrences of these deposits (Adassedakh, Baderuk, Hadal Awatib west and east, Hassai south and north, Oderuk, and Talaiderut), Au is found to be associated with SBR and ferruginous gossans, which represent the near-surface expressions of underlying primary VMS mineralization.

The mine production of the above-mentioned deposits began in 1991 and has yielded >2.127 Moz of Au to date. Some deposits (Adassedakh, Baderuk, Baderuk north, Dim Dim 4, Dim Dim 5, Hadal Awatib east, Hadal Awatib west, Hadal Awatib north, Oderuk, and Talaiderut Oderuk west) are almost exhausted; however, the Hassai north and Umashar deposits are still being mined. At present, Au from the oxidized part of VMS deposits is nearly depleted, and the existing pits are floored by massive sulfides. The location of the oxide deposits on surface exposures is an important guide to exploration; whenever Au grades are high in oxidized horizon, it is likely that high-Au grades will also be present in the primary sulfide ores.

Geologically, the ANS rocks of the Red Sea Hills of Sudan are formed from the accretion of island arcs and back arcs onto the Nile Craton to the east. The two volcano–sedimentary series, the Ariab–Arbaat–Tokar to the south (Fig. 6.25) and the Onib–Nafardeib to the north, display the same general geological history. Both of them have (1) a lower stratigraphic section of basaltic oceanic crust overlain by arc bimodal volcanic and siliciclastic rocks, (2) transpressional deformation that occurred during arc accretion and which produced high strain zones that bound and transgress arc subterranes, (3) predominantly greenschist facies metamorphism, and (4) syn- to late-tectonic magmatism. The granitoid–greenstone terrane of the Nubian

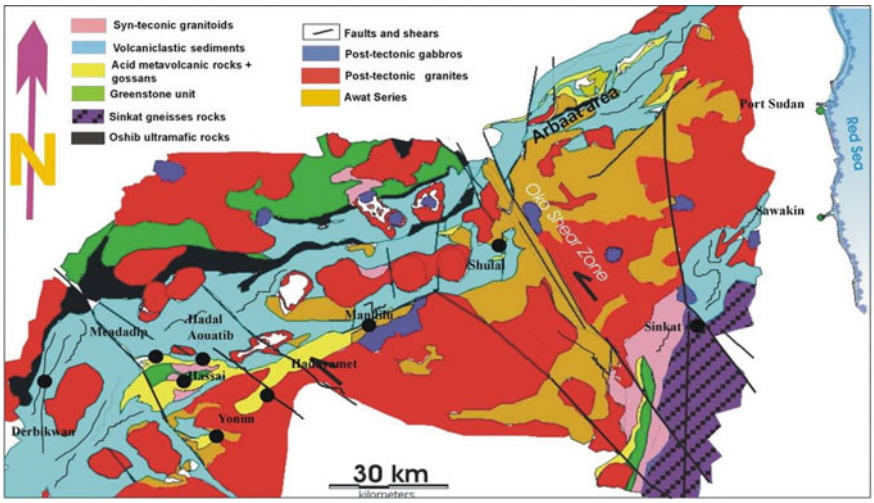

Fig. 6.25 General geological map of the Ariab–Arbaat greenstone belt. The Hassai south and Hadal Awatib deposits are also shown along with selected other deposits (La Mancha Resources Inc. Technical Report 2009)

Shield is well endowed with VMS and vein Au deposits. In addition to those of the Ariab mining district in Sudan, there are three VMS deposits in the *Eyob district*, and six VMS deposits in the *Hamissana district*, but very little information is available about these VMS localities except those of the Ariab district. In addition to the above-mentioned VMS deposits in Sudan, there are four VMS deposits in the Bisha district, western Eritrea (Bisha, Bisha NW, Harena, Hambok); and three VMS deposits in the Asmara district of eastern Eritrea (Emba Derho, Adi Nefas, and Debarwa) (Barrie et al. 2007a), which will be discussed in the next parts of this chapter.

The whole Ariab district is underlain by transitional tholeiitic to calc-alkalic volcanic rocks and fine-grained siliciclastic rocks that stratigraphically overlie and are cut by syn- to post-tectonic mafic to felsic intrusions (Abu Fatima 2006). Regarding the mineralization age, the Pb isotope data for eight mineral separates (five galena, one cerussite, one anglesite, and one altaite) from seven deposits and one stratiform barite occurrence yield a model regression age of 702 ± 15 Ma (Barrie 2008). In general, the host rocks of VMS deposits of the Ariab mining district comprise bimodal volcanic, volcaniclastic and siliciclastic rocks, and late- to post-tectonic granites. Most of the VMS deposits occur within specific stratigraphic units, commonly associated with altered felsic tuffs. Following is a more detailed description of the most common VMS deposits in the Ariab mining district including the hypogene massive sulfides at depth as well as the supergene-oxidized zones.

6.5.1 Oxidized Surface Zones (Gossans)

The oxidized surface exposures that underlain by the hypogene VMS deposits are rich in Fe and Mn oxides, oxyhydroxides, and quartz–kaolinite–barite Au deposits, which represent the main type of Au mineralization in the Ariab mining district. The area as a whole is characterized by Au enrichment in gossans and SBR, both of which are the weathering products of underlying polymetallic VMS deposits. The massive sulfide ores are volcanogenic in nature and represent an essential part from the Ariab Proterozoic greenstone belt. More specifically, most Au-rich VMS deposits are found within Unit D, the upper member of the differentiated felsic volcanic sequence of the Ariab volcanic series (Abu Fatima 2006). The typical surficial oxide–sulfate Au-bearing deposit in the Ariab area is shown in the diagrammatic representation (Fig. 6.26), where >2 Moz of Au have been exploited since the beginning of mining activities in 1992. The hypogene VMS mineralization is described in more detail in the next section. The surface oxide–sulfate Au-bearing deposit represents the main source of ore at the Hassai deposit since mining commenced. However, only small resources of this deposit type remain and some of these are currently being mined. Other lesser important oxide–sulfate Au-bearing deposits require additional exploration.

6.5.2 Hypogene Cu–Zn–Au–Ag Volcanogenic Massive Sulfide Deposits

In general, as berifly mentiond earlier in this chapter, VMS deposits can be classified into five categories based on the host rock composition, from the most primitive to the most evolved in a chemical sense, they are (Barrie and Hannington 1999): mafic, bimodal mafic, mafic siliciclastic, bimodal felsic, and bimodal siliciclastic. The VMS deposits of the Ariab mining district are classified as bimodal-siliciclastic, similar to many of the large deposits in the Iberian pyrite belt, and to the nearby Bisha VMS deposit in western Eritrea. It is important to notice that the Ariab VMS deposits are mostly comparable with other large VMS deposits globally, in terms of their large size, commonly Cu-rich deposits, and their layered, relatively Zn-rich upward zoning. Furthermore, these large VMS deposits are relatively barren in pyritic zone in the central-middle mineralized zone.

Most of the VMS mineralization in the Ariab mining district occurs as tabular bodies that vary from 0.3 to >25 m thick. In the case of Hadal Awatib, the VMS mineralization has been traced >2500 m along strike. Sulfides are typically massive, fine-grained, layered, and locally brecciated, containing mainly pyrite, sphalerite, and chalcopyrite, with lesser amounts of pyrrohotite, galena, tetrahedrite–freibergite, and arsenopyrite. The identified hydrothermal alteration in the host rocks include proximal silicification and more distal chloritization, sericitization, and, in places, carbonitization (Abu Fatima 2006). The hypogene massive sulfides of the Ariab

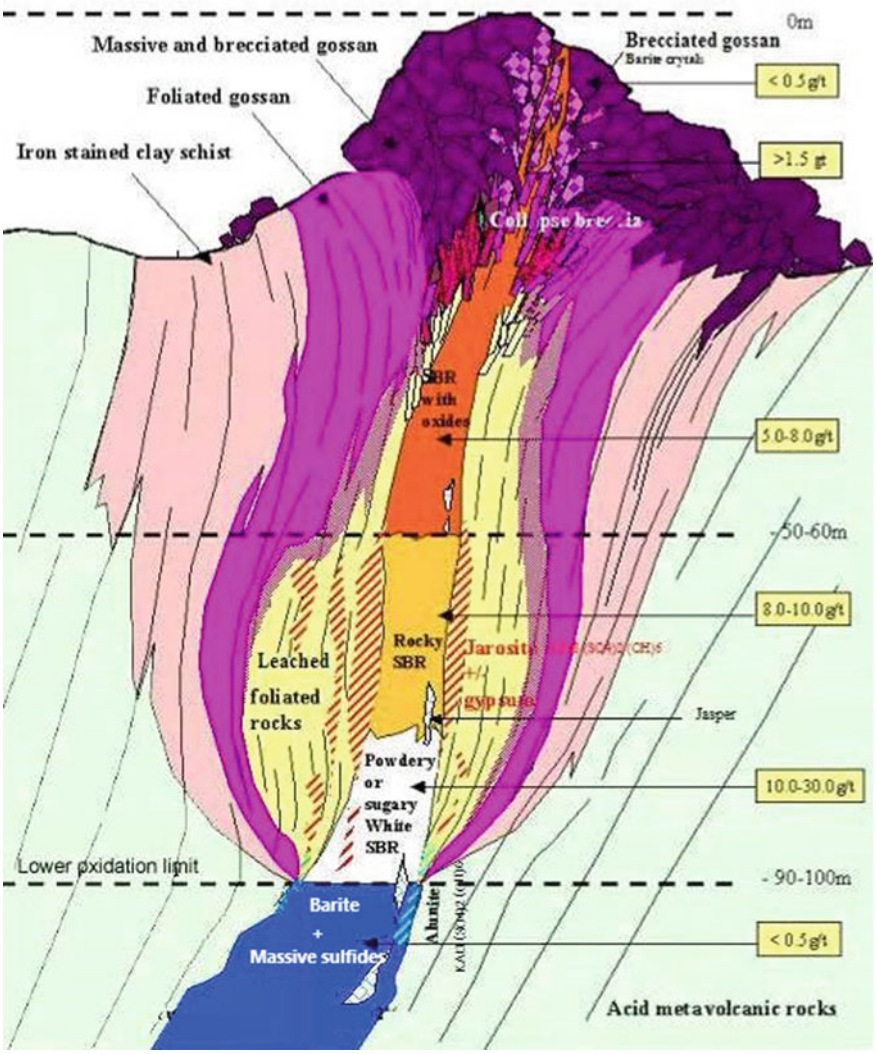

Fig. 6.26 Schematic section showing the relationship between the surface iron oxide gossans Au ore, silica barite rock "SBR" Au ore, and the beneath Cu–Zn–Au VMS mineralization (from La Mancha Resources Inc. Technical Report 2009)

mining district are mainly pyrite-rich and are locally enrichin Cu and Zn in the form of chalcopyrite and sphalerite. The Pb content is characteristically very low; the Au content ranges 0.3–1.5 g/t. In addition, the high Zn values recently obtained (La Mancha Resources Inc. 2009) at the deposit of Onur is of particular significance in the Ariab district, where the ore grade reached up to 15.2 and 1.3 wt% for Zn and Cu, respectively, and 0.3 and 20 g/t for Au and Ag, respectively. In the following

section, the exposed and easily accessible well-known Au-rich VMS occurrences of the Ariab mineral district will be summarized.

Hassai South: The Hassai south VMS deposit is located near the center of the Ariab mining district (Figs. 6.24 and 6.25). It is a single large lens that has an extension of ~1000 m along strike, mining extended to a vertical depth of ~100 m, and the oxide zone ranging 4–35 m in thickness. Beneath the oxide-Au zone, ~42.1 Mt of Cu–Zn–Au (+Ag) massive sulfide has been estimated to a depth of 500 m (La Mancha Resources Inc. 2009). The geophysical signature, however, shows an up to 800 m in depth extension trending 60° toward the south. Although the Hassai VMS deposit is not thebiggest lens in the area, it is considered to be one of the main targets in the Ariab mining district. The Hassai VMS deposit is hosted by chloritic volcaniclastic and siliciclastic rocks (chlorite–quartz ± sericite ± carbonate ± iron oxide ± pyrite ± epidote ± incipient garnet) that have foliated and are transformed into phyllite and schist (Fig. 6.27a). Minor lapilli tuffs are also present, as well as offsets of thin diorite dykes exposed in the pit walls mark minor cross-faults oriented north/south with small displacements of 10 cm–1 m (Barrie et al. 2016). The primary sulfide ore lies at a depth below the open-pit mine of the oxidized surface zone (Fig. 6.28a) and contains significant Cu and Au grade, but mostly low Zn and Ag content.

The mineralogy of the Hassai south VMS–oxide–Au system has been previously well-studied (Barrie and Kjarsgaard 2010), and numerous ore and gangue minerals have been identified. The ore minerals in the oxide-Au zone and in the SBR zone have native Au, electrum, anglesite, cerrusite, smithsonite, calaverite, petzite, tellurides of Pb, Ag, Bi, chalcocite, tenorite, malachite, azurite chrysocolla, and native Cu. Gangue minerals in the oxide-Au zone include kaolinite, gypsum, anhydrite, barite, jarosite, chalcedony, Fe–Ti oxides, epidote, chlorite, and sericite. In the hypogene and supergene massive sulfide ores, there are many ore minerals, including pyrite, chalcopyrite, sphalerite, marcasite, galena, clausthalite, tetrahedrite, tennantite, friebergite, arsenopyrite, polybasite, anglesite, altaite, tetradymite, tellurobismuthite, hessite, petzite, calaverite, electrum, cobaltite, magnetite, pyrrhotite, molybdenite, bismuthinite, mackinawite, bornite, covellite, digenite, cubanite, enargite, and several others (Barrie et al. 2016). Furthermore, there are numerous significant stockpiles and Au-bearing tailings in the mining area. As of 2012, the total resources (measured, indicated, and inferred for oxide-Au and tailings in the Ariab district) were 1.80 Moz Au at an average grade of 2.58 g/t Au (Bosc et al. 2012).

Hadal Awatib: The Hadal Awatib deposits are the largest VMS deposits in the Ariab Mining District. The Hadal Awatib area is located only 13 km east/northeast of the Hassai camp (Figs. 6.24 and 6.25). The Hadal Awatib VMS deposit has an extension ~3.1 km along strike, folded and faulted where the important part remains unexplored. The width of mineralization zone is more than 100 m, and at least 500 m depth extension (La Mancha Resources Inc. 2009). The geophysical signature, however, shows that the deposit is up to 800 m depth extension trending mostly vertical or 80° southward. The Hadal Awatib deposit can be divided into 3 sectors (Fig. 6.27b): (1) Hadal Awatib East, comprises the AB, CD open-pits and the Link. The outline of outcropping SBR and/or massive sulfide ore of the Hadal Awatib East is shown in red-dotted line (Fig. 6.28b, c). (2) Hadal Awatib West with a single

open-pit (Fig. 6.28d). The Hadal Awatib West is one of the richest exploited (13.7 g/t Au) and suggests that the sulfides below may be equally Au rich. (3) Hadal Awatib North, with the north open-pit, the Pipe and the Junction Au deposit (Fig. 6.27b). About 1 Moz of Au have been exploited since the commencement of mining of the oxidized part of Hadal Awatib, with the highest grades recorded in the whole area (1305 kt grading 13.7 g/t Au for 574 koz produced) so far (La Mancha Resources Inc. 2009; Barrie et al. 2016). Based on assays from historical drill holes on the Hadal Awatib East VMS lens, Au may have a lower average grade of about 1.1 g/t Au in comparison to that of Hassai deposits at 1.5 g/t Au. The average Cu content is about 0.9 wt%, and the average Zn and Ag contents are higher than that of the Hassai deposit.

In terms of the host rocks and size of the deposit, the Hadal Awatib VMS–oxide–Au system is classified as a bimodal-siliciclastic subtype of VMS deposit (Barrie et al. 2016). It is considered to be among the most extensive VMS deposits in the world, similar to the Kidd Creek, Ontario deposit, with a total length of 3.1 and ~1 km depth, and Neves Corvo, being 3.45 km along strike (Rosa et al. 2008). The Hadal Awatib VMS–oxide-Au deposits comprise a series of seven open-pit mines developed on a single, giant VMS system (Fig. 6.27b). The host rocks include footwall-silicified and -sericitized, massive rhyolite and rhyolite breccia (C2 rhyolite); chloritized basalt–andesite flows, tuffs, and agglomerates; and hanging-wall felsic tuff, intermediate-to-felsic volcaniclastic rocks, and fine-grained siliciclastic rocks (Fig. 6.27b). The whole package of VMS deposit and its host rocks have been folded along west-northwest/east-southeast-trending with the hanging-wall rocks extending to the north. The chloritic footwall rocks form the core of the principal west-northwest/east-southeast anticline; massive sulfide zones generally dip 65°–90° to the north. The Hadal Awatib VMS deposit comprises three horizontally stratified zones (Barrie et al. 2016): (1) surface oxide-Au zone ranging 80–120 m in depth, (2) supergene Cu-rich zone ranging 100–130 m in depth, and (3) a hypogene (unoxidized) massive-sulfide zone underneath. The massive and semimassive sulfides range in thickness from 10 to 100 m and are mainly associated with chloritic tuffaceous rocks that commonly have stringer pyrite–chalcopyrite mineralization. The hypogene sulfide minerals are, arranged in decreasing order of abundance, pyrite, chalcopyrite, and Fe-poor sphalerite, with minor galena, tennantite, hessite, cobaltite, and electrum. The supergene sulfides comprise covellite and chalcocite, with lesser amounts of pyrite and chalcopyrite. The subhorizontal contacts between the ore types are transitional on a scale of meters to tens of meters, with the oxidized ore commonly occurring along fractures and fault planes that cut the supergene sulfide. In addition, the primary massive sulfide ore shows a stratified Zn–Cu zonation.

The *Hadayamet* deposit is located ~25 km toe east of Hassai camp (Figs. 6.24 and 6.25). The Hadayamet VMS deposit has a horizontal extension of about ~300–400 m along strike, is at least 30–40 m in width, with a deep rooting of almost vertical dipping (La Mancha Resources Inc. 2009). This target was drilled in 2006, where two drill holes were carried out: (1) the ADAM 212 drill hole intersected 71 m of sulfide, dominantly pyrite, containing 1.4 wt% Cu, 2.4 wt% Zn, and 0.4 g/t Au; it includes 20 m, grading at 1.67 wt% Cu. The apparent thickness is ~71 m, since the drill hole

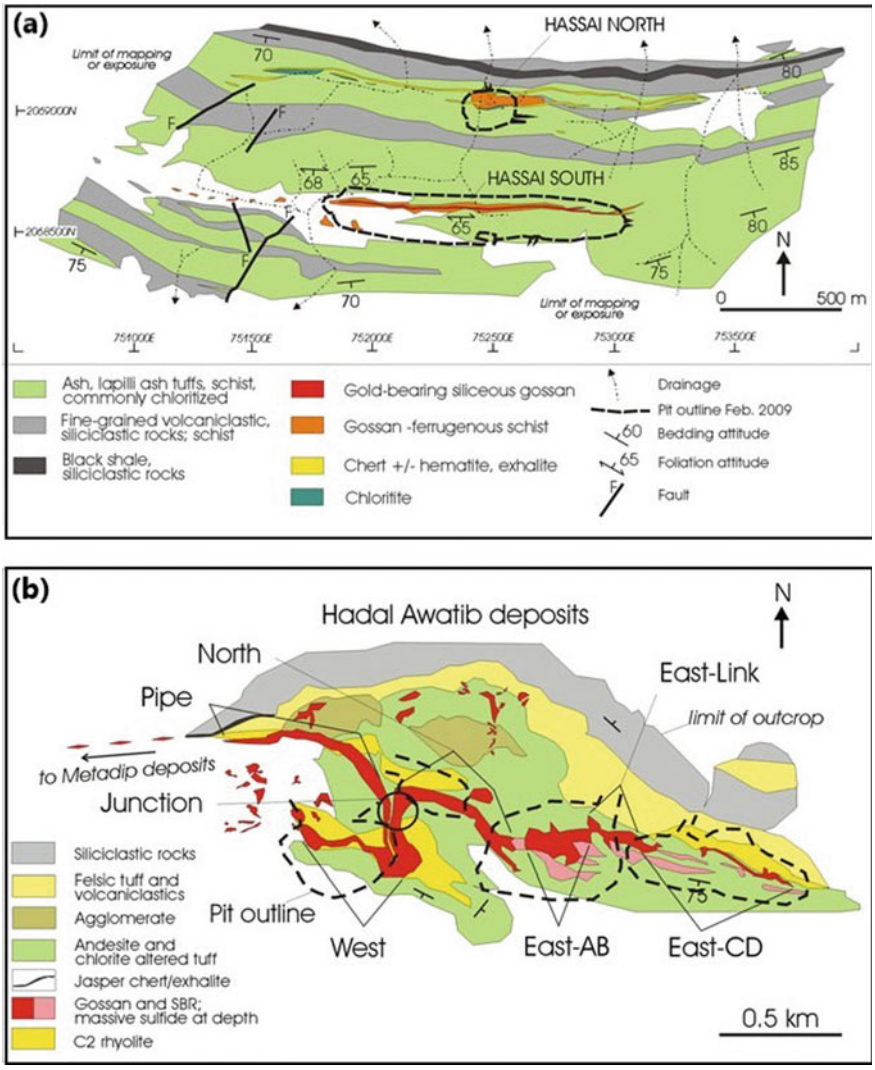

Fig. 6.27 Simplified geology of the Ariab VMS–oxide gold district, northeastern Sudan, and representative deposits. **a** Geology of the Hassai south and Hassai north area. **b** Geology of the Hadal Awatib area. Note the continuous strike length of Hadal Awatib massive sulfide lens, which is among the most extensive VMS deposits known globally (from Barrie et al. 2016)

intersects the north/south structure obliquely, and the real width may be in the range of 30–50 m. (2) The ADAM 213 drill hole, located 1 further to the east, crossing >60 m of pyrite stockwork, including 30 m of massive sulfide averaging 0.8 wt% Cu, 2.2 wt% Zn, and 0.3 g/t Au. The VMS deposit of Hadayamet is potentially of economic interest, but owing to the topography of the site, the deep part of this target

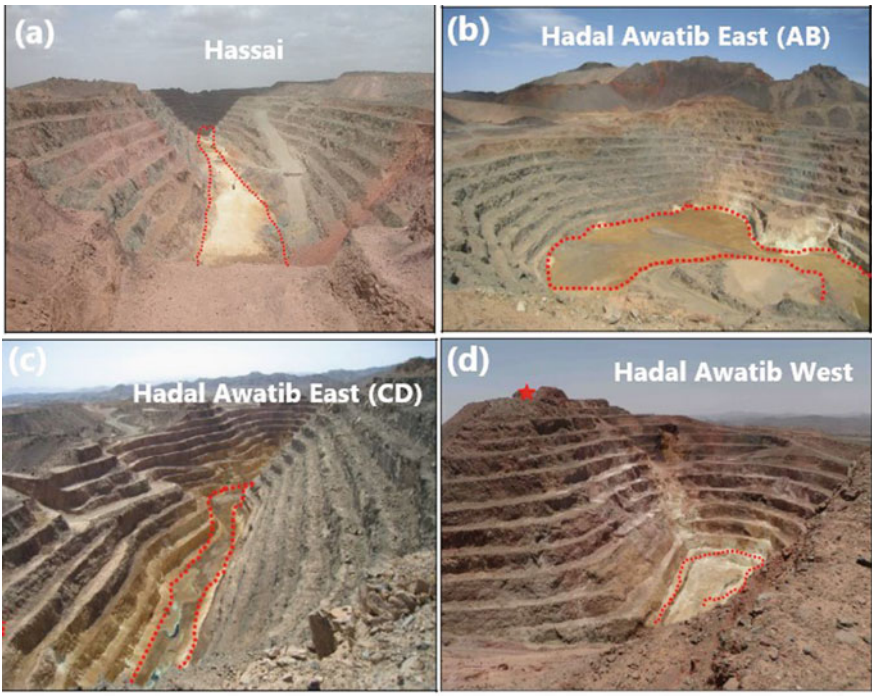

Fig. 6.28 **a** The western end of Hassai south open-pit mine, outline the outcropping silica-barite-rock (SBR) and/or massive sulfide (red dotted line). **b** Hadal Awatib east open-pit mine AB, and CD. **c** Outline the outcropping SBR and/or massive sulfide (red dotted line). **d** Hadal Awatib west open-pit mine outlining the outcropping SBR and/or massive sulfide deposit (red dotted line) (from La Mancha Resources Inc. Technical Report 2009)

is not easy to study and the structure of the deposit is not yet known in detail. The possible enriched zone is easily accessible (Fig. 6.29a) and has not been drilled so far. As at the Hadal Awatib AB pit, a small amount of enriched material may be easily recovered by deepening the open pit.

Taladeirut The Taladeirut VMS deposit is located only ~5 km northwest from the Hassai camp (Figs. 6.24 and 6.25). The Taladeirut deposit has an extension ~300–400 m along strike (Fig. 6.29b, black arrow), which is at least 15 m in width, and dipping at 80° eastward with unknown depth extension. Some historical drill holes show interesting sulfide mineralization demonstrating the potential of this target grading at 5.1 wt% Cu at 100 m. This intersection demonstrates the likelihood of supergene-enriched material in the upper part of the deposit.

Oderuk The Oderuk VMS deposit is located only ~5 km southwest from the Hassai camp (Figs. 6.24 and 6.25). The Oderuk deposit has an extension ~400–500 m along strike (Fig. 6.29c), which is at least 15 m in width, and dipping at 80° eastward with unknown depth extension, but suggesting a deep-seated primary sulfide source.

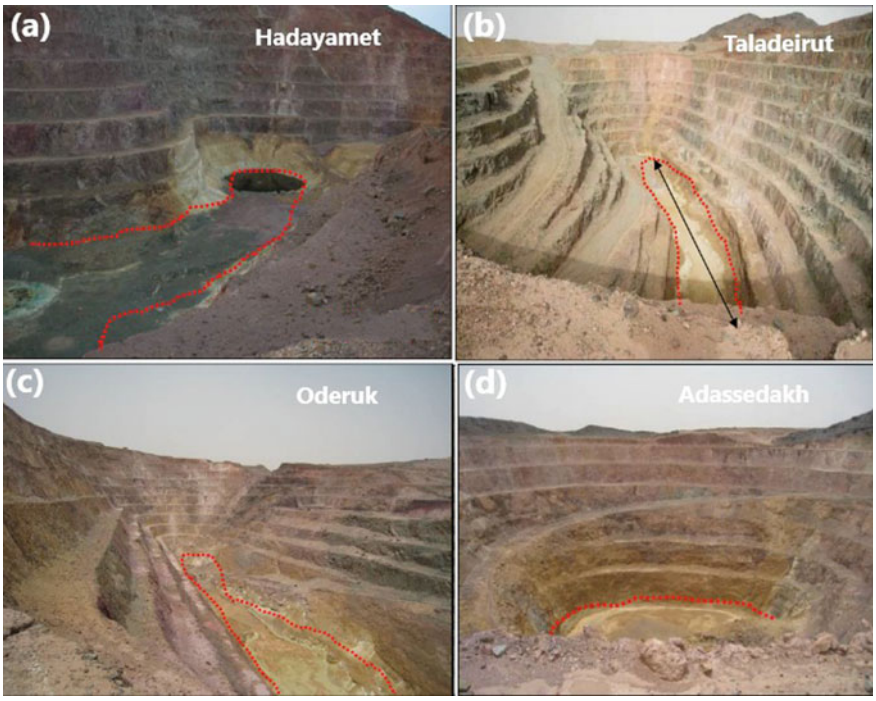

Fig. 6.29 **a** Hadayamet open-pit outline the outcropping SBR and/or massive sulfide (red dotted line). **b** Taladeirut open-pit outline the outcropping SBR and/or massive sulfide (red dotted line). **c** Oderuk open-pit outline the outcropping SBR and/or massive sulfide deposit (red dotted line). **d** Adassedakh open-pit outline the outcropping SBR and/or massive sulfide deposit (red dotted line) (from La Mancha Resources Inc. Technical Report 2009)

A drill hole intersection (ODE D058) at 6 m depth grading at 2.81 wt% Cu. This intersection demonstrates the likelihood of a supergene enrichment zone in the upper part of the deposit.

Adassedakh The Adassedakh VMS deposit is a small open-pit mine located between Taladeirut and Oderuk (Figs. 6.24 and 6.25) and was one of the richest oxides pits mined in the Ariab area. The VMS of Adassedakh site outcrops on floor of the pit (Fig. 6.29d). The estimated length of the Adassedakh deposit ranges 100–150 m along strike (Fig. 6.29d), is at least 15 m in width, and dipping at 80° eastward with unknown depth extension, but suggested a deep-seated primary sulfide source (La Mancha Resources Inc. 2009). The historical drill holes show some very interesting intersections in the upper part, where the drill hole ADS 26 at 5 m gave an average grade of 6.3 wt% Cu and 1.9 g/t Au. The drill hole ADS 24 at 15.5 m grades at 2.44 wt% Cu, 5.47 wt% Zn, and 2.27 g/t Au, and the drill hole ADS 25 at 15.2 m gaves an average grade of 3.25 wt% Cu, and 2.66 g/t Au. These three drill holes are interesting not only for their volumes of primary sulfide ore but mainly for the

high likelihood of further enriched resources in the upper part immediately below the floor of the pit encountered locally in some drill holes.

Onur Unlike other VMS deposits outlined above, the Onur deposit has not yet been exploited. However, a resource estimate was completed based on recent two drill holes that intercepted massive sulfides, which are significant because of the high Zn content. The drill hole ONU D015 at 93 m gave an average grade of 15.12 wt% Zn, 1.3 wt% Cu and 0.3 g/t Au. The drill hole ONU D 008 at 89 m gave an average grade of 3.7 wt% Zn. Such high Zn grades are not frequent in the area and it was in fact the richest intersection ever reported in the Ariab area (La Mancha Resources Inc. 2009). The oxidized part of the Onur deposit has not been exploited so far. Resources (cyanidable Au and other indicated resources per NI43-101) have been evaluated at ~310,000 t of ore grading at 3.6 g/t = 210 kg Au.

Other occurrences There are lesser or inconsistent zones of massive sulfide mineralization present below the several small SBR occurrences. Some of them contain interesting concentrations of base metals, mainly in the upper enriched supergene zone. These include *Medadip*, which is likely an extension of Hadal Awatib, *Dim-Dim*, *Abderrahman*, *Megzoub*, *Umashar*, and *Baderuk* (Figs. 6.24 and 6.25). There is no more available information about these occurrences so far.

6.6 Volcano–Sedimentary Mineral Deposits in Eritrea

The volcano–sedimentary mineral deposits in Eritrea are almost found in the western and eastern Nakfa terrane, which are represented mainly by VMS deposits that hosted by volcano–sedimentary rocks of a Neoproterozoic age. Eritrea has now emerged as having demonstrated potential to host significant VMS deposits after the discovery of Bisha, Harena, and Hambok VMS deposits in the western lowlands and the Koken deposit in the northwestern lowland. The Zara shear-hosted Au deposit and recent findings in Harab Suit and Seroa prospects also increase the potentiality of the country. Moreover, more find such as the Embaderho VMS deposit, in the VMS belt of the Asmara/Debarwa area, which includes Debarwa, Adi Nefas and Ketina and many other small prospects, has made the country to be known for this type of mineralization. Thus, nowadays there are so many exploration companies working in Eritrea having different concessions especially in the Neoproterozoic basement rocks that are concentrated in the western, northwestern, and eastern sides of the country (Fig. 6.30).

As stated in Chap. 2 of this book, Neoproterozoic basement rocks in Eritrea have been divided into four terranes on the basis of their stratigraphic and structural characteristics (Fig. 6.31), including (Barrie et al. 2007a): (1) the Barka terrane to the far west (consisting mainly of metasedimentary and mafic gneisses), (2) the Hagar terrane to the north (principally mafic metavolcanic rocks, including ophiolite-like assemblages), (3) the Nakfa terrane, the largest of the four terranes (predominantly granitoid–greenstone belts and syn- to post-tectonic granitoid rocks), and (4)

the Arig terrane to the east (composed mainly of granitoid and metasedimentary rocks). Almost all of the volcanic–sedimentary rocks of the Nakfa terrane strike in a north/south direction, and there is a significant volume of syn- to post-tectonic granite between the western and eastern halves. There are two main VMS mineralization districts in Eritrea: the *Bisha VMS district* (*Bisha*, *Bisha northwest*, *Harena*, and *Hambok*), and the *Asmara VMS district* (*Adi Nefas*, *Debarwa*, *Emba Derho*, and *Adi Rossi*) (Fig. 6.31). The two VMS districts of Eritrea are entirely hosted by the western and eastern Nakfa terrane Proterozoic rocks, respectively.

There are several indicators for the presence of massive sulfide mineralization in many areas of Eritrea including the north/northwest- to north/northeast-trending belt of gossans cover, exhalative cherts, and altered felsic rocks. The ore minerals of these VMS deposits are represented mainly by chalcocite and pyrite with minor amounts of sphalerite, chalcopyrite, and bornite. In Eritrea, there are two major belts of VMS deposit with Au and base-metal mineralization; one of them, the Asmara mineral district, passes through Asmara and includes Debarwa, Adi Nefas, Embaderho, and many other localities. It is roughly within a 50-km-wide belt over ~250 km along strike length, extending for >50 km north of Asmara and up to the Eritrean border to the south (Fig. 6.32). The second major VMS belt, the Bisha mineral district, includes the Bisha and Harena VMS deposits in the western lowlands (Fig. 6.32), has a world-class VMS deposit, and is under exploration for more deposits. There is a third belt of VMS indications farther north of Kerkebet, in Harabuit, and possibly in surrounding areas. There is a belt of Cu mineralization in Raba–Semait and sulfide-rich gossanous rock in Mt Tullului (Bedeho) in the Sahel, northern Eritrea, and in the Mt Seccar and Sheib areas in the eastern lowlands.

Following are detailed descriptions of these VMS deposits in Eritrea, starting with the Bisha VMS mineral district and followed by the Asmara VMS district.

6.6.1 Bisha Volcanogenic Massive Sulfide District

The Bisha VMS mineralization is located in the western Nakfa terrane of western Eritrea (Figs. 6.30, 6.31 and 6.32); it was discovered in 2003 after an initial drilling program intersected a substantial oxide-Au zone above massive sulfide mineralization. Further mineralization occurrences have been discovered at Bisha northwest, Harena, Hambok, and Yakob Dewar. Considering global ore resources identified at Bisha (39.0 Mt; Barrie et al. 2007b) and Hambok (40.7 Mt; Giroux and Barrie 2009), and particularly the high precious- and base-metal grades at Bisha, the economic viability of the district was found to be favorable, enabling it to be fast-tracked into production, which commenced in 2011 (Barrie et al. 2016).

Geologically, the Bisha mine area is mostly covered by Neoproterozoic volcanic and sedimentary rocks of the Augaro–Adobha belt (Fig. 6.31), which are metamorphosed at upper green schist to lower amphibolite facies. The lithology of the Bisha region is dominated by the Bisha gabbroic complex (BGC), a large (275 km^2), a partly layered mafic intrusion consisting of cumulate gabbroic rocks, with lesser

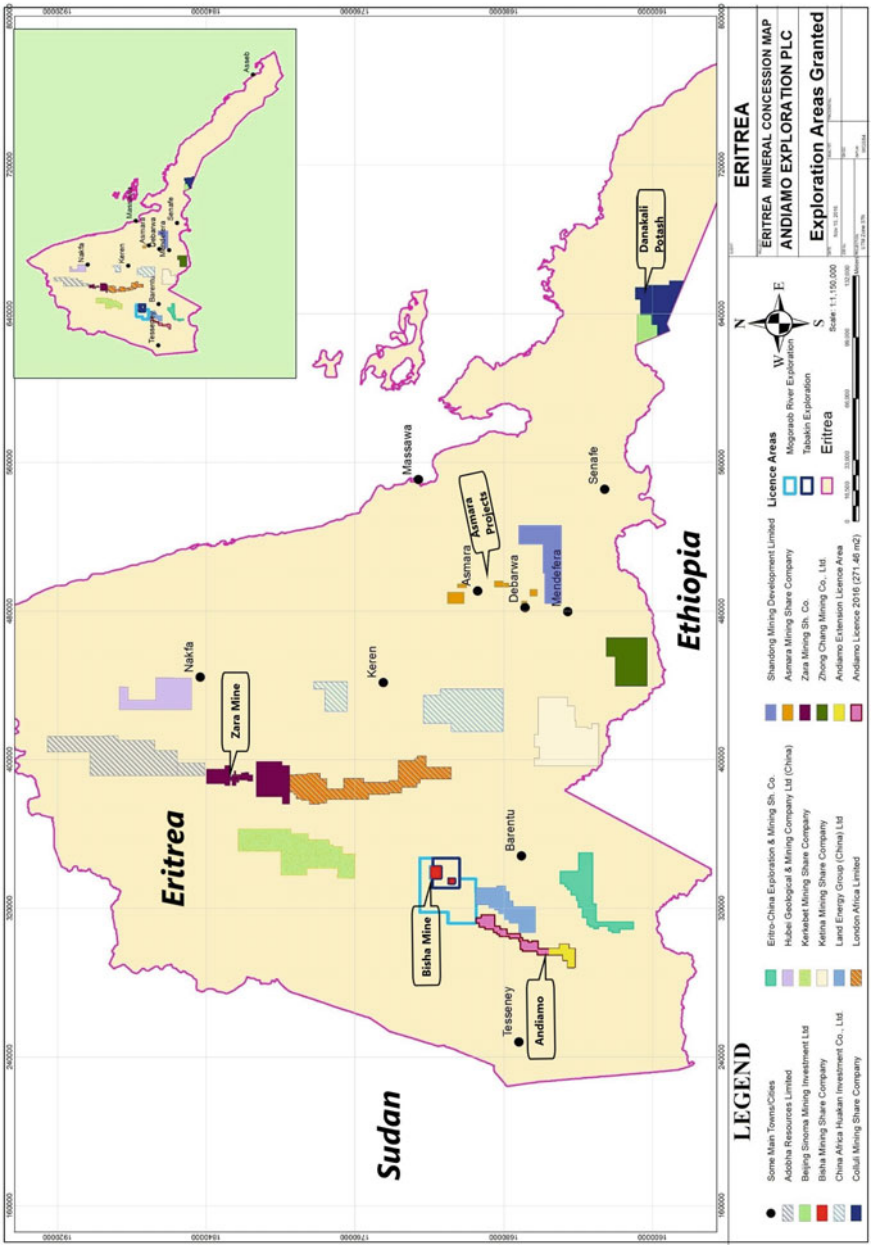

Fig. 6.30 Map of Eritrea showing the exploration licenses and companies working in base- and precious-metals exploration (Andiamo Exploration Ltd, Gold, Copper and Zinc in Eritrea 2017)

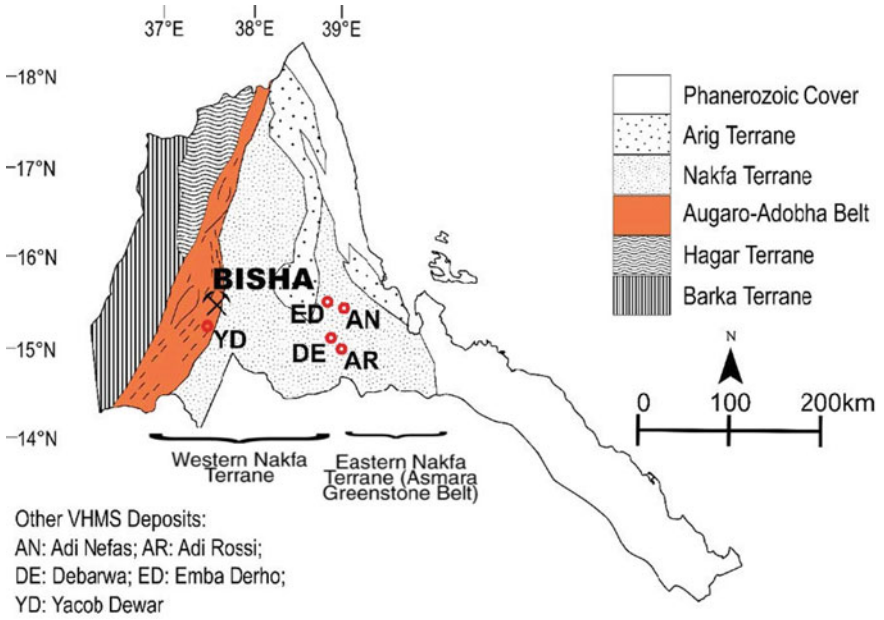

Fig. 6.31 Simplified geologic map of Neoproterozoic terranes of Eritrea with selected VMS deposits in the western and eastern Nakfa terrane (modified from Barrie et al. 2007b)

amount of gabbro–norite, pyroxenite, and ferroan gabbro containing up to 8 vol% Fe–Ti oxides (Fig. 6.33) (Giroux and Barrie 2009; Barrie et al. 2016). The BGC is overlain by a sequence of layered volcano–sedimentary units comprising, from bottom to top, a lower sedimentary sequence of carbonates and fine-grained siliciclastic rocks, including siliceous iron formation; a volcanic sequence of mafic to felsic lapilli and ash crystal lapilli tuffs with intercalated minor mafic flows and hyaloclastite; and an uppermost sequence of fine-grained volcaniclastic and siliciclastic rocks (Fig. 6.33). Rhyolite is the predominant volcanic rock type in the Bisha district, which is mostly tuffs, with minor blocky flows and agglomerates. Dacites comprise ~5% of the volcanic strata; in addition to other volcanic rocks including tholeiitic basalts. Neoproterozoic granite–syenite intrusions and minor mafic dykes/sills, and Cenozoic felsic and mafic dykes, are all cut from the older layered volcano–sedimentary rocks. Rhyolite porphyry and various types of granitic rocks are also found as quartz and feldspar phyric rhyolite/granite dykes, which is texturally and chemically distinct from the other felsic strata (NI 43-101 Technical Report Bisha Mine, SRK Consulting 2017).

The footwall of VMS deposits at Bisha mineral district (including Bisha main, Harena, Bisha northwest, Hambok, and Asheli), are all hosted by bimodal mafic and felsic volcanic rocks, whereas the hanging wall is mainly felsic rocks (Fig. 6.33). The footwall alteration is typically represented by strong quartz + chlorite alteration of tuffs, which may extend for tens of meters below massive sulfide rich zone. Below the

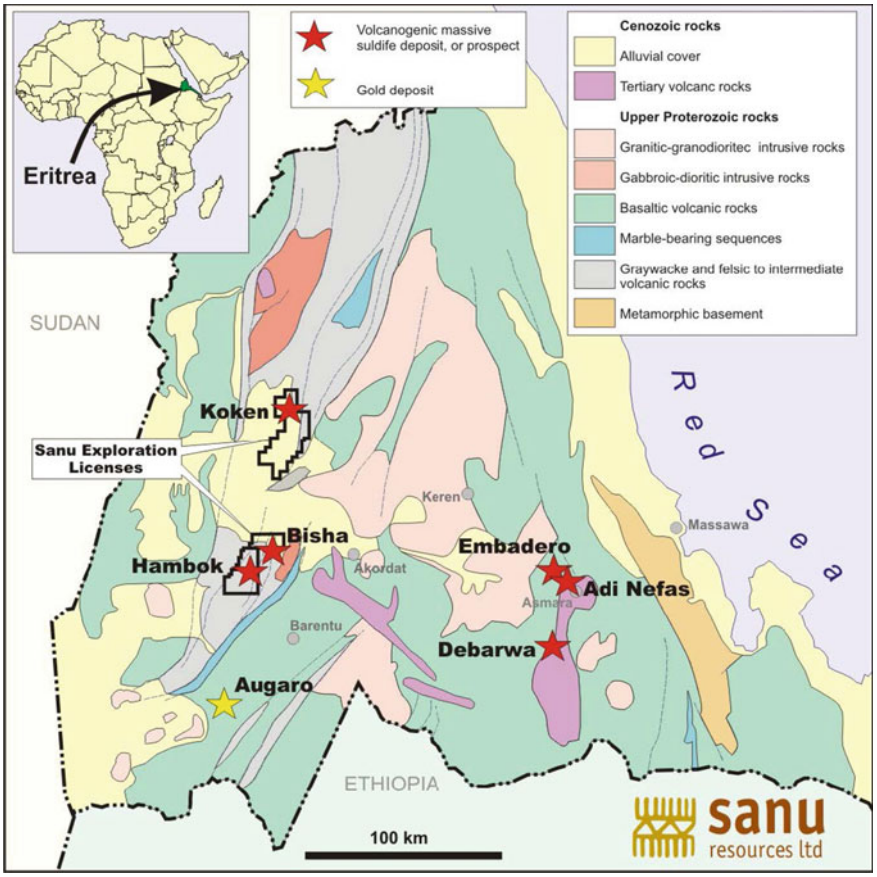

Fig. 6.32 Simplified geological map of northern Eritrea showing some selected VMS deposits in the Bisha and Asmara mineral districts (from Giroux and Barrie 2009)

footwall alteration zone, there is a thin, but variable (<3 m thick) zone of silicification and K-feldspar replacement (Chisholm et al. 2003; Nevsun 2004). This zone is more variable in alteration intensity and thickness than the chlorite alteration zone, and, in some cases, is entirely absent. Hanging-wall alteration is typically represented by strong quartz + muscovite alteration of tuffs, which may extend for tens of meters above the massive sulfide rich zone. Carbonate, epidote, and albite alteration mineral assemblages are less common; they are sometimes weak and patchy, but in some other cases are intense and pervasive.

Following are brief descriptions of geology and mineralization of the principal VMS occurrences in the Bisha mineral district. The majority of this part is summarized from the SRK Consulting Report (NI 43-101 Technical Report Bisha Mine, SRK Consulting 2017).

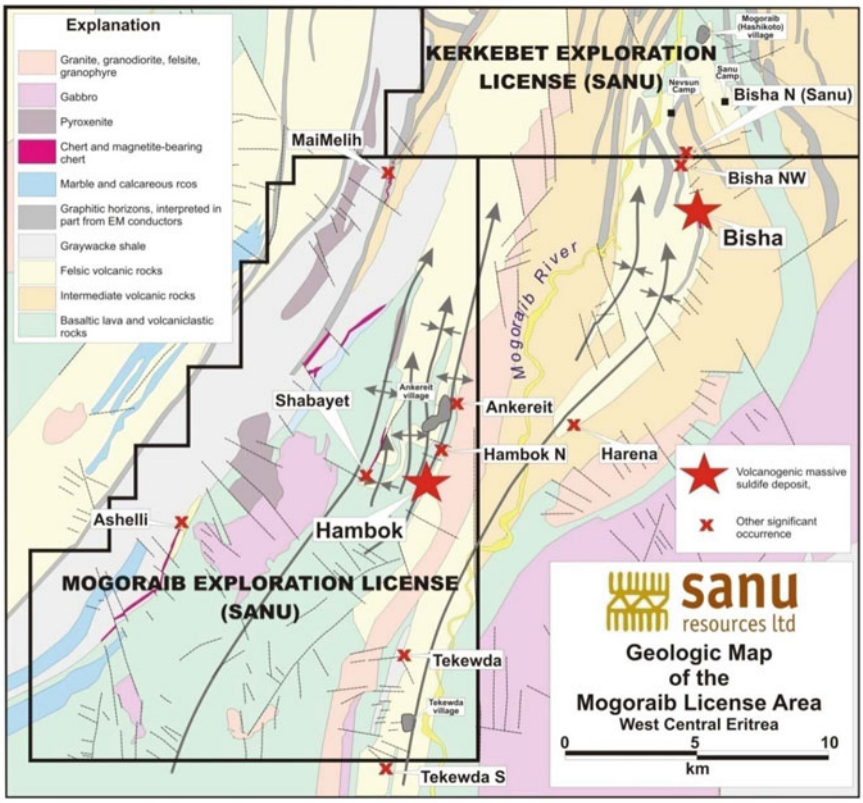

Fig. 6.33 Simplified geologic map of the Mogoraib license area, west central Eritrea, showing the VMS mineralization at Bisha (main, N, NW), Hambok and selected other occurrences in the Bisha mineral district (from Giroux and Barrie 2009)

The Bisha main deposit The Bisha main VMS deposit comprises four massive sulfide lenses that extend ~1.2 km north/south trending along strike. The sulfide-rich lenses are variable in thicknesses that reach up to 70 m and extends to a depth of ~600 m below surface. The massive sulfide bodies comprise the southern and northern zones (Fig. 6.34). The main part of mineralization in the southern zone strikes approximately north/south and dips steeply to the west, with strike and dip lengths of about ~600 m and 500 m, respectively. The main part of the mineralization in the northern zone also strikes approximately north/south and dips steeply to the west, with strike and dip lengths of ~500 m and 100 m, respectively.

The host rocks of the Bisha main deposit are strongly foliated rhyolite and rhyolite breccia interleaved with dark grey, thinly bedded mudstone and polymictic breccia. The environment of rhyolite association is typically of thick submarine domal lavas that have coherent cores and quench-fragmented margins. The footwall and hanging-wall rocks of the deposit are strongly altered. The massive sulfide intervals have

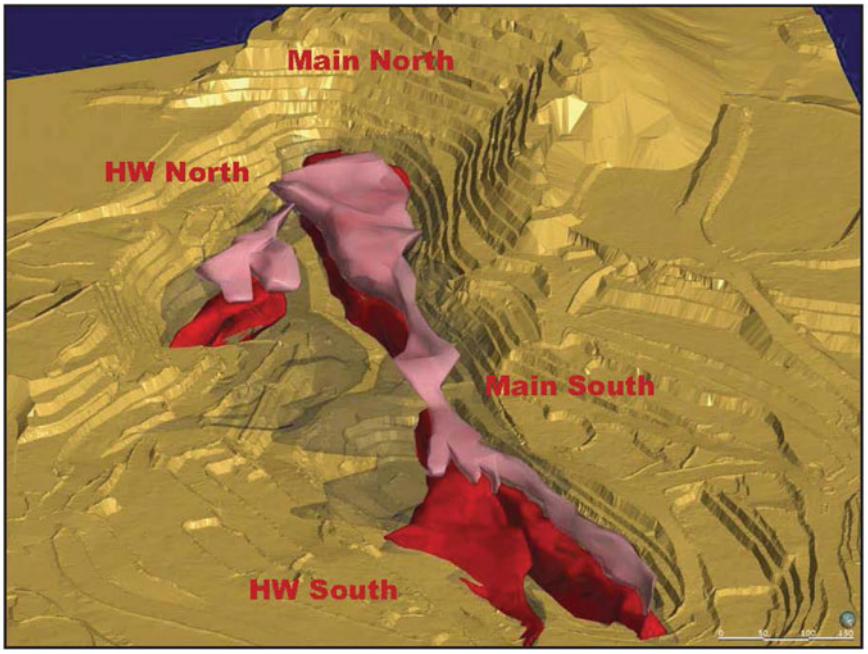

Fig. 6.34 General view of the Bisha main massive sulfide deposit below the open-pit mine below the oxide-Au surface zone (NI 43-101 Technical Report Bisha Mine, SRK Consulting 2017)

gradational contacts with sulfide stringer both above and below. The Bisha main VMS deposit has been deeply weathered, where the weathering profile is complex and locally depends on the lithology and nature of the groundwater that is generated from oxidation of the massive sulfides. Weathering zones have of the Bisha main VMS deposits can be divided into six facies (Fig. 6.35) including, from top to bottom: (1) surface gossans, (2) a near-surface oxide zone, (3) acid-leached zone (also known as an acid-soap zone), (4) a poorly consolidated pyrite-rich sand zone, (5) a supergene Cu-enriched zone, and (6) primary hypogene ore.

The zone of gossans cover is compositionally variable from highly siliceous–ferruginous to massive goethite–hematite–jarosite (Fig. 6.35). The near-surface oxide zone (saprolite) is up to 50 m deep and is composed of hematite, quartz, and clays; in places, the original rock textures are preserved. The saprolite zone is enriched in Au, Pb, Ba, and Mo, but depleted in Cu, Zn, Cd, and Co. The acid-leached (soap) zone is a white, light-yellow, or light-brown zone, and consists of clay, quartz, barite, galena, and pyrite and sometimes anglesite. Both the acid-leached and soap zones are depleted in Cu, Zn, Cd, Co, Fe, and Mn, but strongly enriched in Au, Ag, Pb, and Ba. They are poorly consolidated and their drill recoveries are generally poor (Fig. 6.35). The supergene zone is up to 20 m thick, and has elevated Cu and Ba contents, but depleted in Zn, Cd, and Mn contents. Sphalerite and chalcopyrite in the supergene zone are replaced by chalcocite, covellite, digenite, and native Cu (Ashley 2013). The

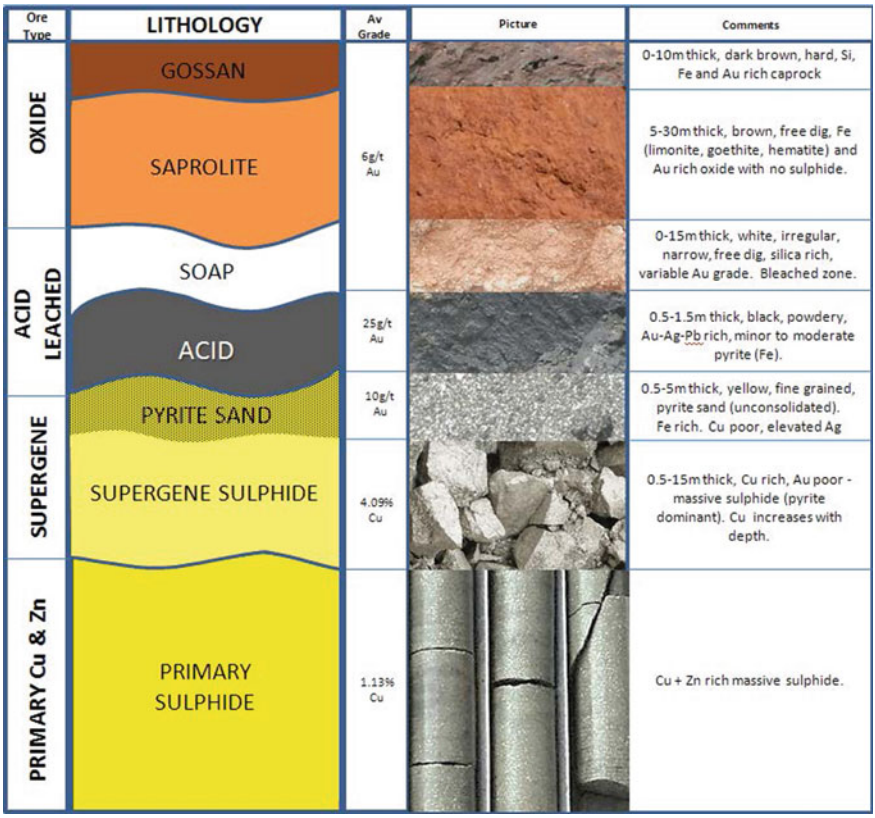

Fig. 6.35 Schematic lithological diagram showing the weathering profile of Bisha main VMS deposit (NI 43-101 Technical Report Bisha Mine, SRK Consulting 2017)

pyrite sand zone lies directly above the supergene zone and consists of unconsolidated recrystallized pyrite grains, where almost all of the Cu content has been remobilized from and redeposited in the supergene zone. In addition, some remobilization of Cu and Ba from the primary zone upwards into the supergene zone has occurred along steeply dipping basement structures. The primary (hypogene) zone represents the original massive sulfide deposit, where the mineralogy is essentially composed of pyrite and sphalerite, with minor chalcopyrite, covellite, pyrrhotite, and galena.

The estimated mineral ore resources and ore reserves at Bishmain as of 31 December 2016 follow (SRK Consulting NI 43-101 Technical Report 2017): the measured + indicated ore resources were ~34.91 Mt ore, with average grades of 0.6 g/t Au, 33 g/t Ag, 1.02 wt% Cu, and 4.18 wt% Zn. The inferred ore resources are ~33.97 Mt ore, with average grades of 0.8 g/t Au, 25 g/t Ag, 1.01 wt% Cu, and 4.74 wt% Zn. The proved + probable ore reserves of supergene sulfides were ~12 Mt ore, with average grades of 0.71 g/t Au, 17 g/t Ag, and 2.57 wt% Cu. The estimated

ore reserves of hypogene sulfides were ~7.351 Mt ore, grading at 0.74 g/t Au, 50 g/t Ag, 1.14 wt% Cu, and 6.98 wt% Zn.

The Harena volcanogenic massive sulfide deposit The Harena VMS deposit is located ~10 km to the southwest of the Bisha main deposit. The massive sulfide at Harena is a tabular body that is up to 60 m thick, extends ~900 m along strike, and dips ~60° to the northwest. The host rocks of the Harena deposit is a Neoproterozoic bimodal unit of basalts and rhyolite/dacite volcanic rocks. The stratigraphic succession at the Harena mine site comprises, from the bottom upwards: a lower footwall unit of rhyolite and dacite tuffs with an intense proximal chlorite–sericite–sillimanite alteration in the immediate footwall of the massive sulfide, and a distal silica–sericite ± biotite alteration; at least two stratigraphically distinct massive sulfide units with associated stringer mineralization on the southeastern or stratigraphically lower side; a hanging-wall unit of intercalated felsic rocks and fine- to medium-grained plagioclase–phyric mafic rocks—there is a distinctive felsic quartz breccia unit along the length of the mineralization, and the mafic rocks have a moderate silica-chlorite ± biotite alteration; and an upper sedimentary sequence of graphitic mudstone and greywacke.

The hypogene ore mainly comprises massive sulfide mineralization with subordinate semimassive sulfide within volcanic lithologies, which range in thickness from 0.4 to 100 m, averaging 19.8 m. The primary ore consists of fine- to medium-grained subhedral-to-anhedral pyrite with interstitial and/or enriched layers of sphalerite and chalcopyrite. The massive sulfide ore have a lensoidal to tabular shape, where the thicker parts of the ore elongated and plunging to the southwest. The primary massive sulfide units show typical VMS zonations from a Cu–Au–Ag rich base to a Zn–Ba rich top. The stringer or stockwork mineralization below the massive sulfide recorded in about half the drillholes; where present it is up to 58 m thick, with an average thickness of 6.6 m. The total mineralized package (massive sulfide + stringer) averages ~23 m thick. The weathering processes have produced a surface oxide layer of ~45–50 m in thickness with associated gossans cover overlaying a very thin secondary supergene zone, which grades downward into a primary massive sulfide. The oxide layerhas less Cu and Zn and greater Au and Ag than the primary mineralization. A 10-m-thick Quaternary alluvial sediment and soil almost completely covers the entire sequence at Harena site.

The estimated mineral resources at Harema as of 31 December 2016 were (SRK Consulting NI 43-101 Technical Report 2017): indicated mineral resources of the open pit are ~3.95 Mt, with average grades of 0.6 g/t Au, 28 g/t Ag, 0.87 wt% Cu, and 3.16 wt% Zn. The estimated inferred mineral resourceof open-pit oxide are ~0.12 Mt ore, with average grades of 2 g/t Au and 20 g/t Ag, while the inferred mineral resources of open-pit sulfide are ~1.92 Mt ore, with average grades 0.6 g/t Au, 28 g/t Ag, 0.87 wt% Cu, and 2.19 wt% Zn. The inferred mineral resources at underground sulfide deposits are ~23.02 Mt ore, grading at 0.8 g/t Au, 30 g/t Ag, 0.93 wt% Cu, and 4.96 wt% Zn.

Bisha Northwest The Bisha northwest deposit is located to the northwest of the Bisha main site (Fig. 6.36a), where it comprises a series of polymetallic massive sulfide

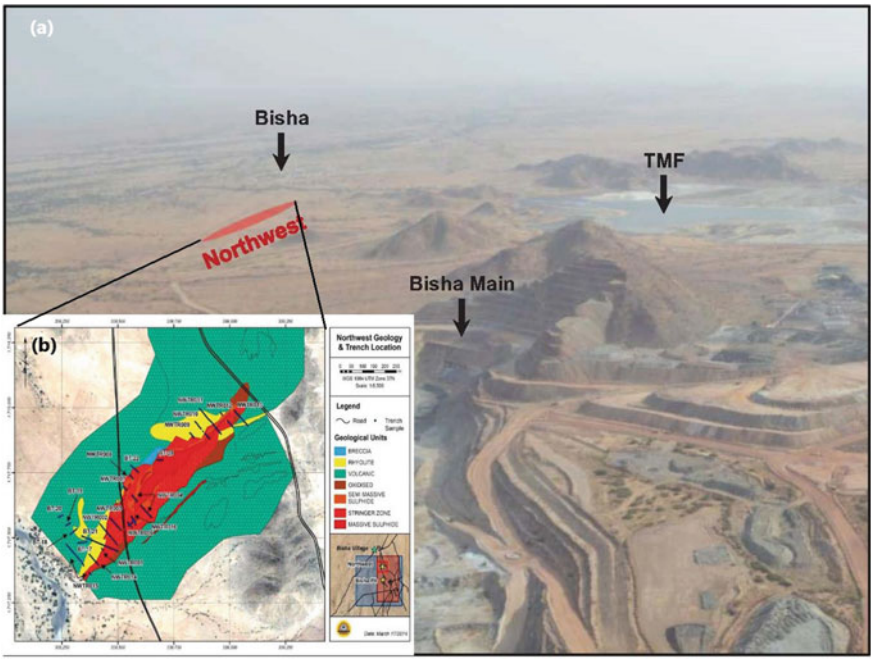

Fig. 6.36 **a** Field location of the Bisha northwest (NW) deposit project area, to the northwest of Bisha main site. **b** Simplified geologic map of the Bisha NW deposit (from NI 43-101 Technical Report Bisha Mine, SRK Consulting 2017)

lodes that have been defined over a strike length of ~800 m (Fig. 6.36b), striking northeast, and dipping from 70° northwest to an almost subvertical direction. The deposit is thickest at the center, tapering to widths of less than 8 m at its strike limits; in cross section, it has a wedge shape that narrows down-dip. The thickness of the central portion of the deposit is >85 m wide. Drilling for resource estimation has effectively defined the deposit to a maximum of 250 m below surface, but the mineralized stringer vein system still exists at depths of >350 m below the surface. The Bisha northwest deposit is subdivided into three domains. (1) The northern main lode is the largest domain, being a Cu-rich massive- and semimassive sulfide ore that increases in Zn content northwards. (2) The southern lode is a Zn-rich, discontinuous massive- and semimassive sulfide body with a pyrite-dominated mineralization. (3) The eastern lode is a separate narrow VMS lode found on the footwall side of the northwest deposit. The eastern lode is poorly drill-defined, but carries appreciable Cu and Zn base-metal grades. It is still at its earliest stages of being defined and understood.

Similar to the Bisha main deposit, the Bisha northwest deposit has a Au-oxide cap and supergene Cu-rich zone. The oxide-Au cap is not as well-endowed as those in the Bisha main deposit in terms of Au, Ag, and Cu content, reflecting the overall lower grade of the underlying northwest primary mineralization. The oxide profile

is still problematic due to core recovery problems during drilling, a problem also encountered across the Bisha main deposit. The unmined estimated mineral resources at Bisha northwest as of 31 December 2016 (SRK Consulting NI 43-101 Technical Ret 2017) follow: indicated mineral resources of the supergene zone were ~1.02 Mt ore, grading 0.2 g/t Au, 1/t and 1.47 wt% Cu. The indicated mineral resources of hypogene ore were ~2.53 Mt ore, grading at 0.3 g/t Au, 13 g/t Ag, 1.04 wt% Cu, and 1.08 wt% Zn. The inferred mineral resources of the oxide zone were ~0.50 Mt ore, with average grades of 3.7 g/t Au and 18 g/t Ag, while the inferred mineral resources of the supergene zone were ~0.10 Mt ore, grading at 3.7 g/t Au 19 g/t Ag, and 0.8 wt% Cu. The inferred mineral resources of the hypogene ore were 0.10 Mt ore, grading at 2.9 g/t Au, 15 g/t Ag, 0.9 wt% Cu, and 0.9 wt%.

Hambok volcanogenic massive sulfide deposit The Hambok deposit lies within the Bisha VMS district in the western Nakfa terrane, and part of a sequence of Late Proterozoic mafic-to-felsic volcanic and sedimentary rocks including pelites, chert, and carbonate unit (Figs. 6.32 and 6.33). One regionally extensive carbonate horizon that extends nearly the entire length of Eritrea passes east of the Hambok Bisha area through the Okreb Au mine area. This unit may correlate with a line of discontinuous carbonates on the western side of the Mogoraib River Exploration License (Fig. 6.33) between the volcanic sequence on the east and a turbidite siliciclastic sequence on the west. The Hambok deposit appears to occupy the eastern flank of a broad anticlinorium cored by basaltic rocks and ultramafic and granitic intrusions. The BGC, which as noted above is a major mafic intrusive complex, forms the core of a major regional anticline to the east of Bisha and Hambok, whereas a subordinate unnamed gabbro–diorite–pyroxenite intrusive complex forms the cores of an anticline between Hambok and Ashelli (Fig. 6.33). The Ashelli and Mai Melih massive sulfide prospects appear to occupy the western flank of this anticlinorium. The top of the bimodal volcanic sequence appears to be marked by graphitic schists, chert and carbonate horizons, and pelitic sedimentary rocks. The Hambok VMS deposit is present within a sequence of chloritic, volcaniclastic rocks with lesser amounts of massive basaltic-to-andesitic lavas and felsic tuffs. Drilling to date shows that the sulfide body is a homoclinal lenticular body dipping steeply to the east; however, some structural complications may be present in the southern part of the body, where the dips are moderate.

The Hambok VMS deposit comprises a primary Cu/Zn sulfide zone, forming the majority of the deposit, as well as a minor oxide-Au component. The primary massive sulfide mineralization is a single body with a faulted displacement at depth in the northeast of the deposit. The massive sulfide zones strike at ~15°, dipping steeply to the east, with overall strike and dip lengths of ~975 m and 400 m, respectively. The thickness of the massive sulfide ore varies from ~5.0 up to 75 m. The mineralogy of massive sulfide ore has been found to contain pyrite, sphalerite, chalcopyrite, and magnetite as the major ore mineral constituents (Barrie et al. 2007a, b, Sanu internal memorandum). Minor and accessory ore minerals (0.5–4%) are represented by galena, tennantite, digenite, and hematite. The main gangue minerals associated with the ore are quartz, sericite, Mg-chlorite, siderite, and feldspar. The Cu and Zn

have a weak zonation throughout the Hambok deposit, with Cu increasing down-dip and to the west of the massive sulfide, whereas Zn has a tendency to be enriched up-dip and to the east. The best metal grades occur at the top, bottom, and edges of the thickest accumulation of sulfides, whereas the thick pyrite core of the massive sulfide mineralization is poorly mineralized.

The preliminary estimated mineral resources at Hambok as of January 2009 were, at a 2 wt% Zn equivalent cutoff (Giroux and Barrie 2009): indicated mineral resources of ~10.7 Mt ore, with average grades of 0.2 g/t Au, 7.1 g/t Ag, 1.04 wt% Cu, and 2.21 wt% Zn. The inferred mineral resources were estimated to be ~15.9 Mt ore, grading at 0.2 g/t Au, 6.15 g/t Ag, 0.93 wt% Cu, and 1.77 wt% Zn. The estimated unmined mineral resources at Hambok as of 31 December 2016 (SRK Consulting NI 43-101 Technical Report 2017) were: indicated mineral resources of hypogene zone of ~6.86 Mt ore, grading at 0.2 g/t Au, 10 g/t Ag, 1.14 wt% Cu, and 1.86 wt% Zn. The inferred mineral resources of the oxide zone were ~20 kt ore, grading at 1.57 g/t Au and 17 g/t Ag.

Ashelli volcanogenic massive sulfide deposit The Ashelli VMS deposit is located ~10 km southwest of Hambok (Fig. 6.33), hosted within a felsic volcanic sequence that was described in the Hambok site. Various lithologies outcrop in the area, with a general north/south strike and dipping steeply to the west. The lowest unit is composed of a series of mafic flows with strong carbonate and moderate chlorite alteration. This unit thickens to the south and tapers to the north, and is cut by several felsic and mafic dykes. It is overlain by a series of felsic flows, which have undergone moderate-to-strong sericite and chlorite alteration and are locally strongly foliated. This felsic suite includes a massive sulfide mineralization unit, a magnetite-rich siliceous chemical sedimentary unit, and an intermediate lava flows unit. The Ashelli deposit is a tabular, steeply north-plunging body that is ~400 m long, 100 m wide, and up to 30 m thick, composed of pyrite, sphalerite, and chalcopyrite. The top of the deposit is 60 m below surface. The host felsic suite is overlain by a siliceous chert horizon with associated thin marble beds followed by a thick sequence of finely laminated graphitic sediments and mudstone. This unit is strongly foliated and contains a graphitic horizon with a coarse boxwork texture after the oxidized pyrite (SRK Consulting 2017).

The estimated unmined mineral resources at Ashelli as at 31 December 2016 (SRK Consulting NI 43-101 Technical Report 2017) were: the inferred mineral resources of the low-grade ore were ~1.68 Mt ore, grading at 0.36 g/t Au, 28 g/t Ag, 1.9 wt% Cu, 5.2 wt% Zn, and 0.05 wt% Pb. The inferred mineral resources of the high-grade ore were ~0.72 Mt ore, with average grades of 0.39 g/t Au, 33 g/t Ag, 1.9 wt% Cu, 16.6 wt% Zn, and 0.14 wt% Pb. The total mineral resources were ~2.40 Mt ore, grading at 0.37 g/t Au, 30 g/t Ag, 1.9 wt% Cu, 8.6 wt% Zn, and 0.08 wt% Pb.

6.6.2 *Asmara Volcanogenic Massive Sulfide District*

As mentioned earlier, the Nakfa terrain contains the Asmara greenstone belt VMS deposits (eastern Nakfa terrane) and the Bisha VMS deposit (western Nakfa terrane) (Figs. 6.30, 6.31 and 6.32). The Asmara greenstone belt comprises several tectonostratigraphic blocks, including the Adi Neared block, the central steep belt, the Asmara syncline, and other blocks to the north. That part of the granitoid–greenstone belt in the vicinity of Asmara represents a moderately evolved belt typical of the granitoid–greenstone terrains of the ANS. The sequence is dominated by mafic-to-felsic flows and tuffs with a predominant calc-alkali affinity and lesser silisiclastic rocks, typical of moderately evolved island or continental arcs.

The *Asmara VMS district* of Cu, Zn, Ag, and Au deposits is located in close proximity to Asmara, the capital of Eritrea, within 15 km to the north-northwest and 30 km to the south-southwest (Figs. 6.31 and 6.32). Individual VMS deposits and occurrences described following include *Debarwa*, *Emba Derho*, *Adi Nefas*, and *Kodatu.* The district also includes low-sulfidation epithermal gold deposits at *Gupo* and *Adi Rassi* in close proximity, accompanied by identical alteration and in the same host units, although these deposits are also described in the literature as orogenic deposits (e.g., Barrie et al. 2016). Geology of the Asmara district (Fig. 6.37) is generally east-facing, tightly folded approximately north-trending fold axes, generally dip to the east or east-southeast at 45–85° and are preserved at or below the lower greenschist facies. They consist primarily of a mafic–filsic bimodal suite of volcanic and derived volcaniclastic rocks overlain to the east by a metasedimentary sequence. The Neoproterozoic basement rocks are mostly covered by flat-lying Tertiary olivine basalts that are greater than 200 m in thickness. The basalts overlie a well-developed paleoweathering horizon along which locally thick laterite deposits have developed, and the underlying Neoproterozoic rocks are strongly saprolitized.

Three mineralized trends were described in the Asmara mineral district, all of them are trending north/northeast, these are (Barrie 2004): (1) the *Emba Derho trend* to the west of Asmara that includes the Dairo Paulos occurrence, the Woki Duba occurrence, and the Emba Derho deposit; (2) the *Debarwa–Adi Nefas trend* extends at least 25 km south and 5 km north of the capital and includes the Debarwa, Shiketi, Adi Lamza, Adi Nefas deposits, and the Adi Adieto occurrence; and (3) the *Adi Rassi–Kodato trend* to the east. The latter two trends are defined in part by a chert/exhalite unit whereas the Emba Derho trend becomes less-well delineated to the southwest where many of the metal occurrences are hosted within granitoids.

Emba Derho volcanogenic massive sulfide deposit The *Emba Derho* VMS deposit is located ~15 km north-northwest of Asmara (Fig. 6.37) within Neoproterozoic metavolcanic and metasedimentary rocks that are cut by granitoid intrusions. The VMS deposit is exposed to the surface by a prominently outcropping gossans cover developed over an area of about 800 × 220 m, which is tightly folded with northwest-oriented fold axial planes and steeply dipping limbs. The gossans have been subjected to at least two phases of folding and has a W-shape, open to the northwest. These gossans have been known since at least the 1970s. They

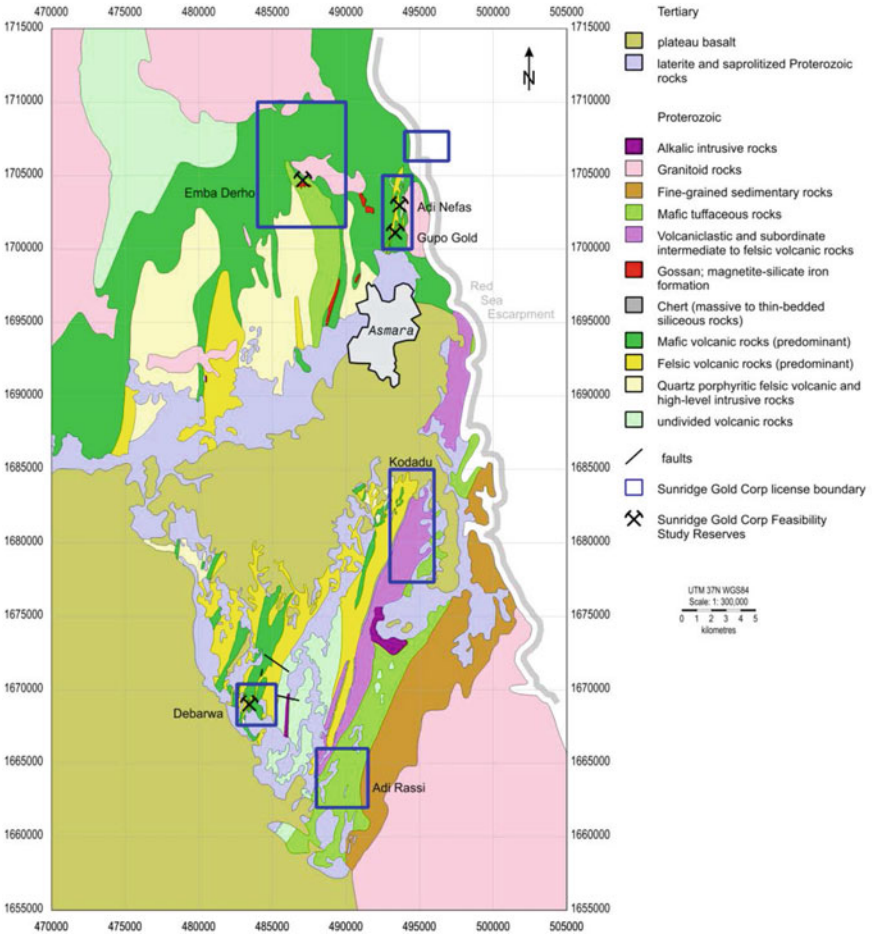

Fig. 6.37 Simplified geologic map of the Asmara mineral district showing the main VMS occurrences (from Senior et al. 2013)

comprise oxidized and supergene acid-leached felsic tuffaceous rocks and flows, weathered massive-to-semimassive sulfides, and orange-brown weathering rhyolite dykes/sills 1–2 m in thickness. The gossans are surrounded by relatively poor exposure of typically well-foliated acid-leached, predominantly fine tuffaceous rocks of both mafic and felsic composition. These lithologies are cut by strongly weathered postdeformation granitic dykes of various compositions.

The lithology of the footwall below the massive sulfide ores comprises blue quartz–phyric rhyolite flows, flow breccias, and associated felsic fragmental tuffaceous rocks that are locally altered to sericite–chlorite schists. These are overlain by stacked layers of massive-to-semimassive sulfides ranging in thickness from 5 to 40 m, separated by numerous tuffaceous and volcanic flow partings and one barite

layer (e.g., Barrie 2004; Daoud and Greig 2007). All of these rock types are cut by various postdeformation felsic dykes, which are typically 1–5 m in thickness. The hanging-wall sequence is composed of pillow basalt and pillow breccia units that have been subjected to significant epidote–silica alteration. The altered mafic volcanic units just above the massive sulfides contain several manganiferous, siliceous chemical sedimentary units; a thin sill of altered and deformed coarse-grained pyroxenite occurs within the mafic volcanic flows. The entire sequence generally dips steeply to the north.

The Emba Derho VMS deposit has a typical zonation. (1) The *gossans/oxide zone* is a dense, dark red-brown gossans cover composed of hematite, limonite, goethite, and locally magnetite that was largely derived from surface weathering of massive sulfides. It occurs as discontinuous, commonly folded layers that may be up to several meters or more in thickness. Outside of the main gossans zone, there is a local centimeters–to–tens of centimeters scale of layers and veins, predominantly within acid-altered host rocks. It has also been locally remobilized to form so-called "ferricrete" caps with very delicate textures. Oxidation typically extends to the water table, which is ~20–30 m below the surface. (2) The *Cu-enriched supergene zone* occurs as fine-to-medium-grained, vuggy, locally sandy, massive pyrite with interstitial secondary Cu minerals such as covellite, digenite, and minor bornite. This zone is found at or below the water table. Zinc is depleted relative to the hypogene mineralization. (3) The *hypogene Cu-rich massive sulfide zone* is well-defined in the northern part of the deposit and comprises medium-to-coarse-grained massive pyrite and pyrrhotite with interstitial chalcopyrite and magnetite, with massive bands, stringers, and blebs of chalcopyrite. (4) The *hypogene Zn-rich massive sulfide zone* is well-developed in the southern and western parts of the deposit and comprises fine-to-medium-grained massive pyrite with sphalerite occurring as interstitial disseminations and as thin bands and laminae within the pyrite. Different types of sphalerite were recognized: Fe-rich, rusty-brown, high-temperature-phase, honey-yellow, and Fe-poor, whitish-grey, lower-temperature-phase sphalerite. (5) The *hypogene pyritic massive sulfide zone* is a massive sulfide ore that occurs immediately below the chert and silica-rich chemical sediments and mafic flows of the hanging-wall sequence, representing the stratigraphic top of the massive sulfide horizon. Sulfide minerals are mostly fine-to-medium-grained massive pyrite with fine-grained disseminated magnetite and very minor chalcopyrite and sphalerite.

The mineralization and host rocks are cut by at least five felsic intrusive phases, the most prominent of which is a suite of fine-to-medium-grained postkinematic leucocratic rocks, ranging from tonalite to granite in composition. These are interpreted to related to a high-level intrusion of similar composition exposed to the north of the deposit. Dykes generally parallel the northwest of the layered host sequence, although north-northeast trends are common in the northeastern part of the deposit. An earlier, much less voluminous suite of postkinematic diorite dykes is also mapped, generally trending to the north.

The premining feasibility study at Emba Derho as of May 2013 (Senior et al. 2013) estimated measured + indicated mineral resources of the oxide-Au zone (0.5 g/t Au cutoff grade) at ~1.74 Mt ore, with average grades of 1.06 g/t Au, 4.3 g/t Ag,

0.07 wt% Cu, and 0.04 wt% Zn. The Cu-rich supergene ore (0.5% Cu cutoff grade) is estimated to be ~1.64 Mt ore, grading at 0.17 g/t Au, 12.2 g/t Ag, 0.94 wt% Cu, and 0.38 wt% Zn. The Cu-rich hypogene zone (0.3% Cu cutoff grade) was estimated to be ~49.8 Mt ore grading at 0.17 g/t Au, 7.7 g/t Ag, 0.83 wt% Cu, and 0.93 wt% Zn. The Zn-dominated hypogene zone (<0.3% Cu; >1% Zn cutoff grade) was estimated to be 16.8 Mt ore, with average grades of 0.31 g/t Au, 9.9 g/t Ag, 0.14 wt% Cu, and 2.80 wt% Zn. The total estimated tonnage of the Emba Derho deposit is ~70 Mt ore. The estimated inferred mineral resources of the Cu-rich hypogene zone (0.3% Cu cutoff grade) were ~13.28 Mt ore, with average grades of 0.25 g/t Au, 10 g/t Ag, 0.87 wt% Cu, and 0.89 wt% Zn. The estimated inferred mineral resources of the Zn-rich hypogene zone (<0.3% Cu; >1% Zn cutoff grade) were ~1.77 Mt ore, grading at 0.39 g/t Au, 11 g/t Ag, 0.20 wt% Cu, and 1.94 wt% Zn. The total estimated inferred tonnage of the ore is ~15.05 Mt.

The Adi Nefas volcanogenic massive sulfide deposit The *Adi Nefas* VMS deposit is located ~10 km north of the center of Asmara and ~8 km southeast of the Emba Derho deposit (Fig. 6.37). Similar to the Emba Derho, the Adi Nefas VMS deposit is also hosted by a Neoproterozoic bimodal sequence of mafic and felsic volcanic rocks (Kuroko-type), intruded by later quartz porphyry sills and dykes. Basalts in the footwall, or western side of the deposit, are strongly epidotized and are locally transformed into epidosites. The sequence on the eastern, hanging-wall side of the massive-to-semimassive sulfides, mainly comprise pillow basalts and foliated equivalents, intruded by minor quartz–porphyry dykes and sills. The pillowed basalts and associated mafic metavolcanic rocks overlain by undifferentiated tuffaceous sedimentary rocks and more pillow basalts containing silicate–magnetite chemical sediment lenses. The geological sequence of the Adi Nefas area (Fig. 6.38) can be summarized as follows, from bottom to top (Barrie 2004): (1) A >300-m-thick pillowed basalt with pillow breccia and moderate-to-intense quartz–epidote alteration. (2) A 200-m-thick dacite of heterolithic tuff/fragmental and ash lapilli tuff that has been altered to sericite and chlorite schist containing 2–10% disseminated pyrite. This part of the sequence is intruded by multiple quartz porphyry dykes and sills. (3) Adi Nefas massive-to-semimassive sulfides. (4) An approximately 200-m-thick basaltic tuff with minor dacite lapilli tuff that was altered to chloritic schist with a few quartz porphyry sill/dyke intrusions. (5) A >250-m-thick pillowed basalt with pillow breccia, locally containing amygdules; it has been subjected to quartz–epidote alteration. The interval contains one or more silicate–magnetite chemical sediment lenses and a few thinner quartz porphyry sill/dykes.

The gossans cover over the Adi Nefas hypogene deposit averages ~10 m in thickness and is well-exposed over a ~700-m interval but is sporadically mapped over a strike length of ~2 km (Fig. 6.38). It comprises a silica, hematite, and goethite-rich assemblage that represent the surface expression of the massive sulfide unit and the immediate semimassive-to-dense disseminated sulfide-rich host rocks. The Adi Nefas deposit has a vertical zonation due to weathering. The underlying deposit is an elongated north-northeast-trending (Fig. 6.38), steeply east dipping, massive sulfide

lens ranging from 5 to 20 m in thickness and is mostly hosted within a hydrothermally altered felsic quartz–sericite–chlorite–pyrite schist that is, in turn, flanked stratigraphically above and below by altered metabasaltic rocks. The more heavily altered section of the felsic sequence ranges 25–60 m in thickness. The upper oxide and underlying transition zones are leached and strongly depleted in Cu and Zn relative to the hypogene sulfide mineralization and accompanied by a slight enrichment in Au. There is, however, a slight increase in the grade of base metals with depth in these zones. These upper zones are typically developed from surface to the water table, which is generally at a depth of 20–30 m below surface. Below this level, supergene zone typically 20–40 m in thickness is significantly enriched in Cu and Au and slightly enriched in Ag relative to the hypogene sulfide mineralization. Zinc is still depleted relative to the hypogene zone. The mineralization within the hypogene sulfide zone is more Zn-rich than the other deposits of the Asmara district making it a Zn–Cu–Ag–Au VMS deposit. In all other respects, the Adi Nefas deposit is very similar in style to the Debarwa deposit.

The premining feasibility study at Adi Nefas as of May 2013 showed (Senior et al. 2013) indicated mineral resources of hypogene sulfides (2 wt% Zn cutoff grade) at ~1.841 Mt ore, grading at 3.31 g/t Au, 115 g/t, 1.78 wt% Cu, and 10.05 wt% Zn.

The Debarwa volcanogenic massive sulfide deposit The Debarwa deposit is located ~30 km south-southwest of the center of Asmara (Figs. 6.30, 6.32 and 6.37). It is hosted by an overturned, moderately-to-steeply dipping sequence of variably and intensely altered, bimodal, submarine, low-K tholeiitic basaltic and rhyolitic volcanic rocks together with minor chemical sedimentary rocks. The host rocks of the Debarwa mineralization are altered felsic rocks, underlain by mafic rocks that locally mark the stratigraphic footwall. Mafic rocks predominate within the 6-km-long NNE-trending belt that hosts the Debarwa deposit and Shiketi gossan (Fig. 6.39).

The massive sulfide mineralization at Debarwa is expressed on the surface by a gossans cover with a strike length of ~1.2 km, which marks the crest of a sharp, west-facing ridge flanking the Gual Mereb river. There are two main zones of massive sulfides (Fig. 6.39): (1) The *Debarwa main lens*, ~830 m long, which comprises at least three subparallel mineralized horizons. The western part of the lens is the best developed, thickest, and most continuous. It dips at ~50–60° W, is approximately 8–30 m thick, and has been traced to a depth of ~250 m below the surface. Massive sulfides are confined to this western horizon and vary from <1 to ~22 m in thickness. The overlying supergene and oxide zones are up to 50 m thick. (2) The *Debarwa south lens* is the smaller, is approximately 285 m long, with a massive sulfide zone that steepens from 35 to 45° W in the north to around 60° W in the south. It is thinner, low in grade, but not as continuous as the Debarwa main zone, and has been traced to ~250 m below the surface.

The mineralization at Debarwa is divided into the following parts, from top to bottom (Fig. 6.39): (1) The *gossans/oxide zone*, in which the base metals have been mostly leached over a vertical interval of ~80 m below the highest points to between 35 and 50 m below the floor of the Gual Mereb river valley. The Debarwa gossans vary from deep brick-red to black, are largely composed of iron oxides and hydroxides

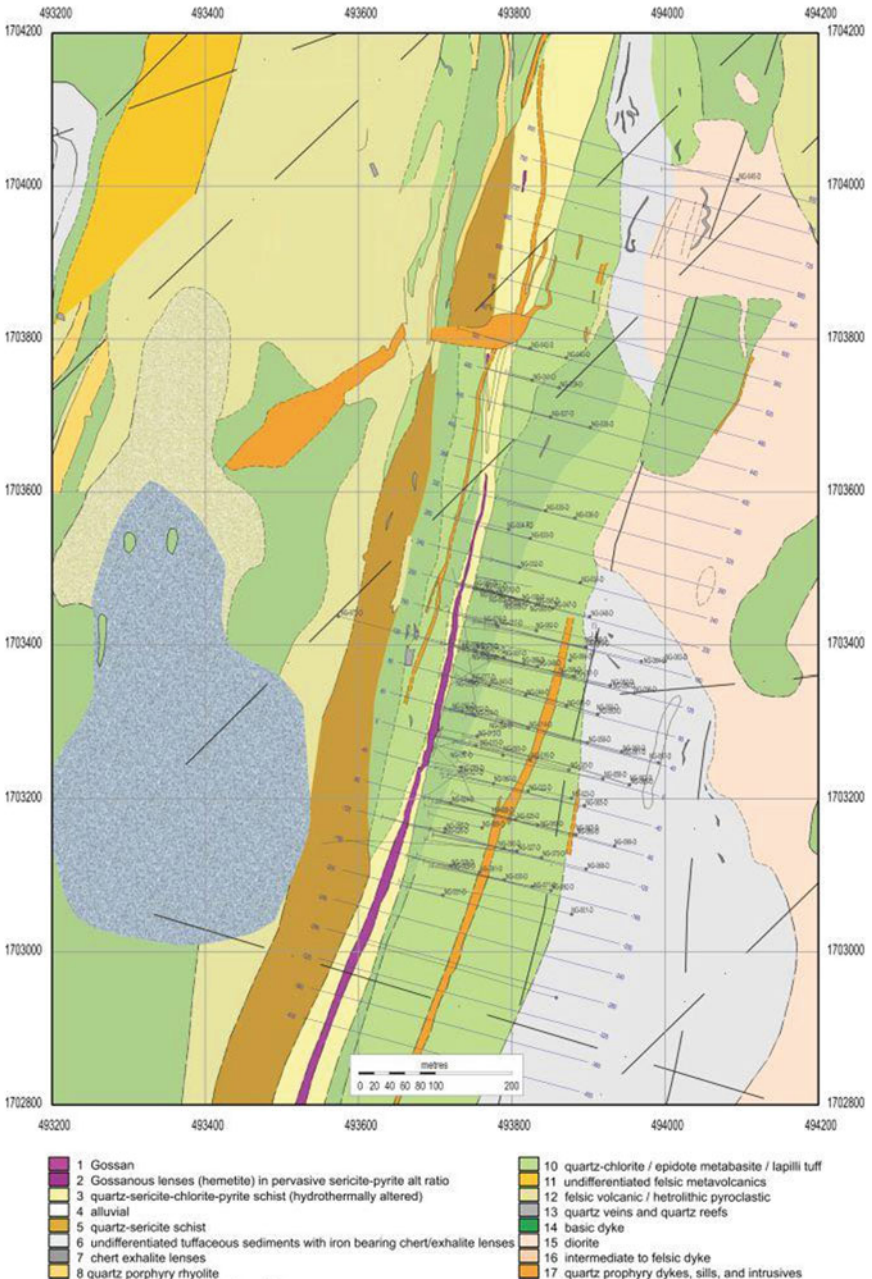

Fig. 6.38 Simplified geologic map of the Adi Nefas VMS deposit area, showing the main lithology and distribution of the gossans and hypogene mineralization (from Senior et al. 2013)

(hematite, limonite, goethite, and minor jarosite), silica, and remnant clay. They may include a variety of lithologies, including siliceous botryoidal limonite–hematite, jasperoid, and greenish impure barite layers beds. The gossans cover above the Debarwa main zone have oxides that typically contain erratic but generally high-Au grades from 0.4 to 14 g/t Au (commonly >4 g/t) over widths between 7 and 17 m. Silver values range from 0.4 and 183 g/t, typically >15 g/t, while Cu and Zn values are relatively insignificant. (2) The *transition zone* marks the gradual change from the oxide to supergene zones and is ~10–15 m thick. This transition ore zone is the most enriched in Au and Ag, but most depleted in base metals, particularly Cu and Zn. The intersection with ore zone ranges from 32 to 40 m in depth, and grades at 39.1 g/t Au, 519.5 g/t Ag, 0.07 wt% Cu, and 0.02 wt% Zn. (3) The *supergene zone*: It is the zone most enriched in Cu, derived from the acid leaching of metals from the oxide zone. Supergene mineral assemblage includes digenite, chalcocite, tenorite, covellite, and bornite. These secondary sulfides replace and form coatings around hypogene sulfides such as chalcopyrite, bornite, and pyrite, and crystallize in the voids left by sphalerite. Supergene grades are higher in the Debarwa main zone with typical supergene intersections ranging between 2 and 26 m, with grades varying from 0.9 to 32 wt% Cu. Precious metals range from 0.5 to 4 g/t Au, and 16 to 144 g/t Ag. Zinc is usually very low, having been almost completely stripped. (4) The *hypogene zone* is located just below the supergene zone, at depths of >65–90 m below the valley floor of the Mereb and Gual Mereb rivers. The sulfide assemblages in the hypogene zone are pyrite and chalcopyrite, with common bornite and sphalerite, in massive, semimassive, and stringer vein zones that range to 15 m in thickness. Typical drill intersections of the primary mineralization zone at the Debarwa main zone carry between 2.0 and 9 wt% Cu, 0.5 and 7 g/t Au, 6 and 150 g/t Ag, and 1 and 12 wt% Zn.

The premining feasibility study of mineral resources at Debarwa as of May 2013 showed (Senior et al. 2013): The measured + indicated mineral resources for the oxide-Au zone (0.5 g/t Au cutoff grade) were ~0.374 Mt ore, with average grades of 1.47 g/t Au, 6 g/t Ag, 0.06 wt% Cu, and 0.04 wt% Zn. The Cu-rich transition zone (0.5 wt% Cu cutoff grade) gave ~0.72 Mt ore, grade at 2.85 g/t Au, 27 g/t Ag, 0.08 wt% Cu, and 0.05 wt% Zn. The Cu-rich supergene zone (0.5% Cu cutoff grade) gave 1.389 Mt ore, 1.40 g/t Au, 33 g/t Ag, 5.15 wt% and 0.07 wt% Zn. The Cu-rich hypogene zone (0.5 wt% Cu cutoff grade) gave 0.774 Mt ore, grading at 1.30 g/t Au, 29 g/t Ag, 2.34 wt% Cu, and 3.92 wt% Zn. The Zn-rich hypogene zone (<0.5 wt% Cu; >2 wt% Zn cutoff grade) gave 1.24 Mt ore, grading at 0.31 g/t Au, 22 g/t Ag, 3.05 wt% Cu, and 2.80 wt% Zn. The total measured + inferred metric tonnage of Debarwa is 3.312 Mt ore. The inferred mineral resources at the oxide-Au zone (0.5 g/t Au cutoff grade) are 0.239 Mt ore, grading at 1.1 g/t Au, 5 g/t Ag, 0.10 wt% Cu, and 0.10 wt% Zn. The Cu-rich transition zone (0.5 wt% Cu cutoff grade) gave 0.138 Mt ore, at 1.4 g/t Au, 22 g/t Ag, and 0.10 wt% Cu. The Cu-rich supergene zone (0.5 wt% Cu cutoff) gave 0.144 Mt ore, with average grades of 0.6 g/t Au, 31 g/t Ag, 2.7 wt% Cu, and 0.07 wt% Zn. The Cu-rich hypogene zone (0.5 wt% Cu cutoff grade) gave 0.154 Mt ore, grading at 2.6 g/t Au, 41 g/t Ag, 1.2 wt% Cu, and 3.60 wt% Zn. The Zn-rich hypogene zone (<0.5 wt% Cu; >2 wt% Zn cutoff grade) gave 6 kt ore, at

1.1 g/t Au, 21 g/t Ag, 0.40 wt% Cu, and 3.30 wt% Zn. The total inferred tonnage was approximately 0.681 Mt ore.

6.7 Volcano–Sedimentary Mineral Deposits in Ethiopia

Base metal sulfides and gold in Ethiopia are attracting the attention of many exploration companies, including National Mining Company, Ezana Mining Development Plc (EMD), Sheba Mineral Exploration Company, Donia Mineral Exploration Company, and Harvest Mineral Exploration Company, among others. The modern extensive exploration programs in Ethiopia have resulted in delineation of many potential areas in Neoproterozoic basement in different parts of the country for base and precious metals discoveries. These efforts in the Tigray region, northern Ethiopia, have resulted in identifying many potential areas of Au and base-metal mineralization. Base-metal sulfides in the Neoproterozoic basement rocks of Ethiopia are essentially found as polymetallic VMS deposits in the northern part of the country. Exploration activities have been done and some are still running in many areas in Ethiopia, particularly in the Tigray region (including Meli, Terer, and Terakempti), where drilling is being conducted to confirm the deposit and to evaluate and estimate the mineral resources. In addition to the importance of base-metal deposits, these VMS mineralizations are also attracting attention because they are Au-bearing (Ezana 2009; Bheemalingeswara and Araya 2012). EMD is a pioneer exploration company in this regard, having identified and reported the presence of auriferous polymetallic VMS deposits near Rahwa/Meli in the Adi Ekele belt and Terer in northwestern Tigray, northern Ethiopia. The VMS deposits are mainly identified on the basis of the surface expression of gossans cap rock developed on these sulfide deposits. Among these occurrences, the focus has been made on the Meli deposit, which has ~30 m thick auriferous gossans cover (having ~2 t Au) (Bheemalingeswara and Araya 2012). Diamond drilling has confirmed the presence of a primary VMS deposit ~20–30 m in thickness beneath gossans cover in the Tigray area.

Following is detailed information on the Meli VMS occurrence, including host-rock geology, ore geology, petrography, alteration patterns, and metal content. The majority of information here is mainly based on the technical report on the geological evaluation of the Meli Property prepared by Greig and Rowe (2020) for the *Sun Peak Metals Corporation.*

The Meli volcanogenic massive sulfide deposit The Meli VMS Project is located in the northwestern part of Tigray, approximately 570 km (~1100 km by ground travel) north of the capital city of Addis Ababa, and 24 km southwest from the town of Shire (Fig. 6.40). The Meli Project concessions are located within the Asgede–Tsimbila Woreda, centered, approximately, around 13° 58′ 12″ N and 8° 2′ 26.88″ E, or in the local UTM datum WGS84, zone 37 N coordinates of 396,400 E, 1,544,620 N. The exploration license comprises a block measuring ~11 km north/south by 9 km east/west and covering a total area of ~100 km^2. The most significant with respect to

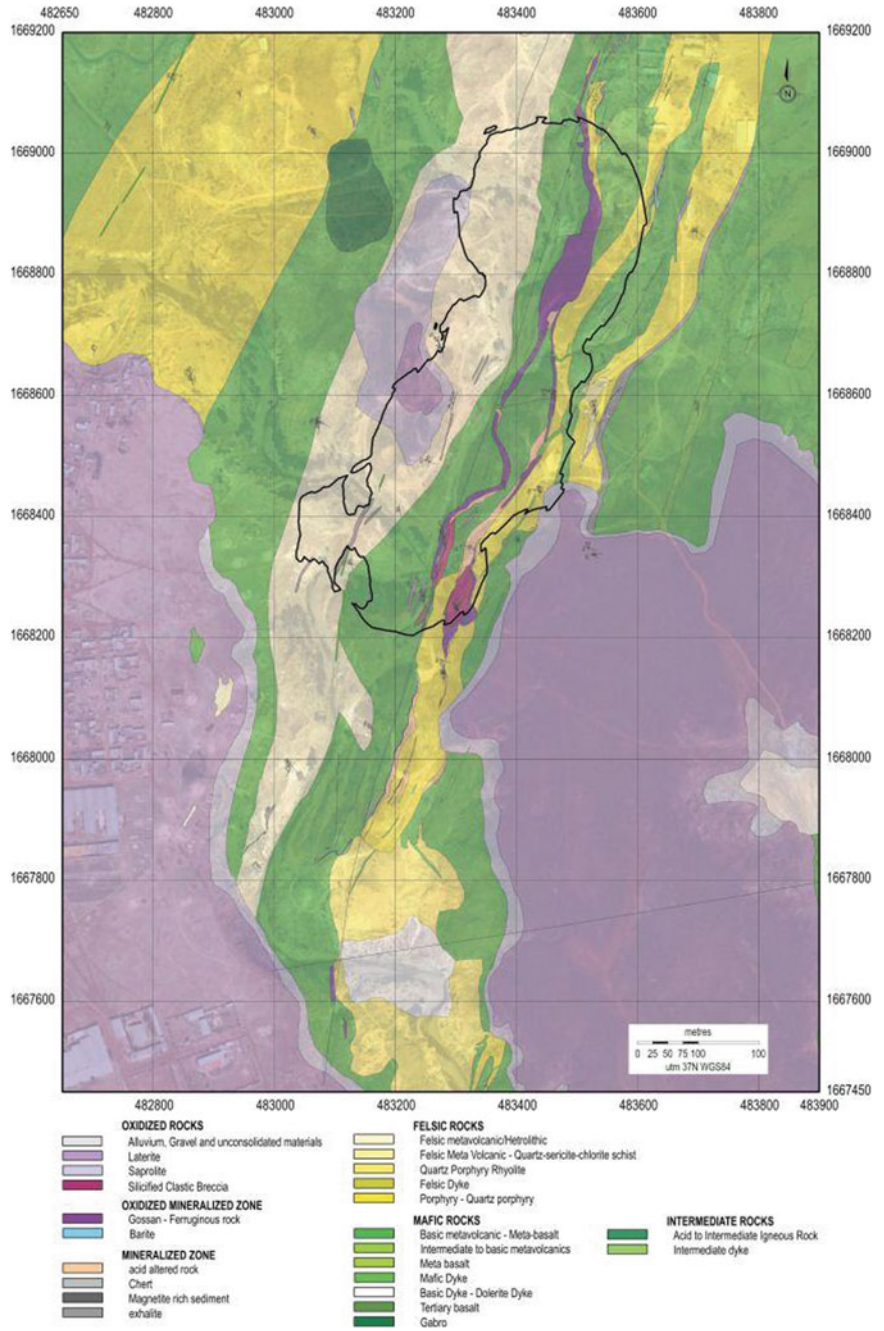

Fig. 6.39 Simplified geologic map of the Debarwa VMS deposit area, showing the main lithology and distribution of the gossans and hypogene mineralization (from Senior et al. 2013)

Fig. 6.40 Satellite image showing the location of Meli project, northern Ethiopia

the Meli project is the nearby deposits of the Asmara and Bisha mineral districts in Eritrea. The Nakfa terrane underlies much of the central part of Eritrea and is made up of mixed volcanic and metasedimentary (siliciclastic and carbonate) rocks. As described earlier, the Nakfa terrane contains the VMS deposits of the Asmara and Bisha greenstone belts. The Nakfa terrane extends southerly into the northern part of Ethiopia and comprises the area covered by the Meli property (Fig. 6.41). The Meli area is underlain by the same rock units of volcanic and volcano–sedimentary rocks as the Asmara VMS district, which is located ~160 km to the northeast. The convergence and amalgamation of the four regional belts of north-central Eritrea and northern Ethiopia of oceanic and island arc rocks resulted in deformation, metamorphism, uplift, and a late- to posttectonic granitoid intrusive events.

The Meli VMS project area is found in the southern part of the Nakfa terrane (Fig. 6.41), which has been further subdivided into a number of tectonically and stratigraphically distinct blocks, one of which, the Adi Nebrid block, host the majority of mineral occurrences. It consists of a northeasterly striking, steeply dipping, low-grade sequence of mafic-to-intermediate flows, pyroclastics, minor rhyolite, and various epiclastic sedimentary rocks of Neoproterozoic age. A number of granitoid intrusive

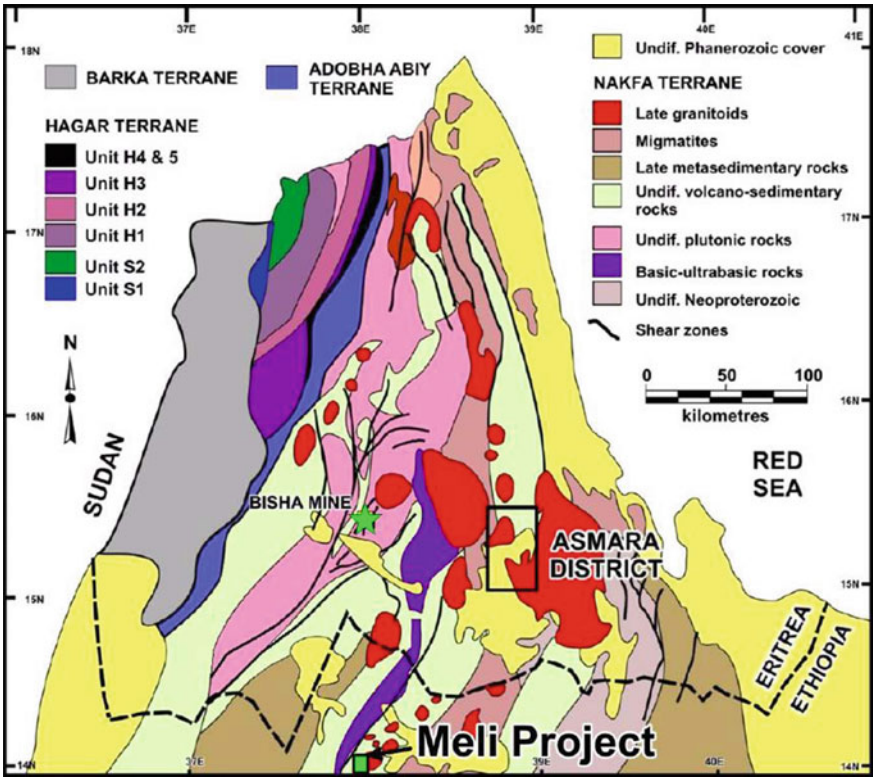

Fig. 6.41 Simplified geological map of the Meli project with relation to the Asmara mineral district and Bisha mine (from Greig and Rowe 2020)

complexes cut and locally deformed the older layered rocks. This block cuts through the area of the Meli property, which is primarily underlain by Tsaliet group metavolcanic and metavolcaniclastic rocks (Fig. 6.42). The diversity of lithologies within the Adi Nebrid block is a function of the collapsed back-arc basin of the area. This setting is postulated due to the presence of cycles of mafic and felsic volcanic and volcanoclastic rocks, synvolcanic intrusions, and the occurrence of deep and shallow water sediments (Archibald et al. 2014). The area underwent significant deformation during destruction of the back-arc basin resulting in the development of isoclinal and recumbent folds as well as thrusts and shear faults. The subsequent period of crustal thickening resulted in the emplacement of late orogenic granitic bodies (Greig and Rowe 2020).

The Meli project area is underlain by bimodal mafic-to-felsic metavolcanic rocks, quartzite, ultramafic rocks, and foliated granitoids (Fig. 6.43). Regional mapping has shown that there is a repetition in the volcanic stratigraphy from felsic to mafic dominant. Detailed mapping at prospective localities has shown that the packages are a complex sequence of interlayered extrusive and local intrusive rocks that, on some

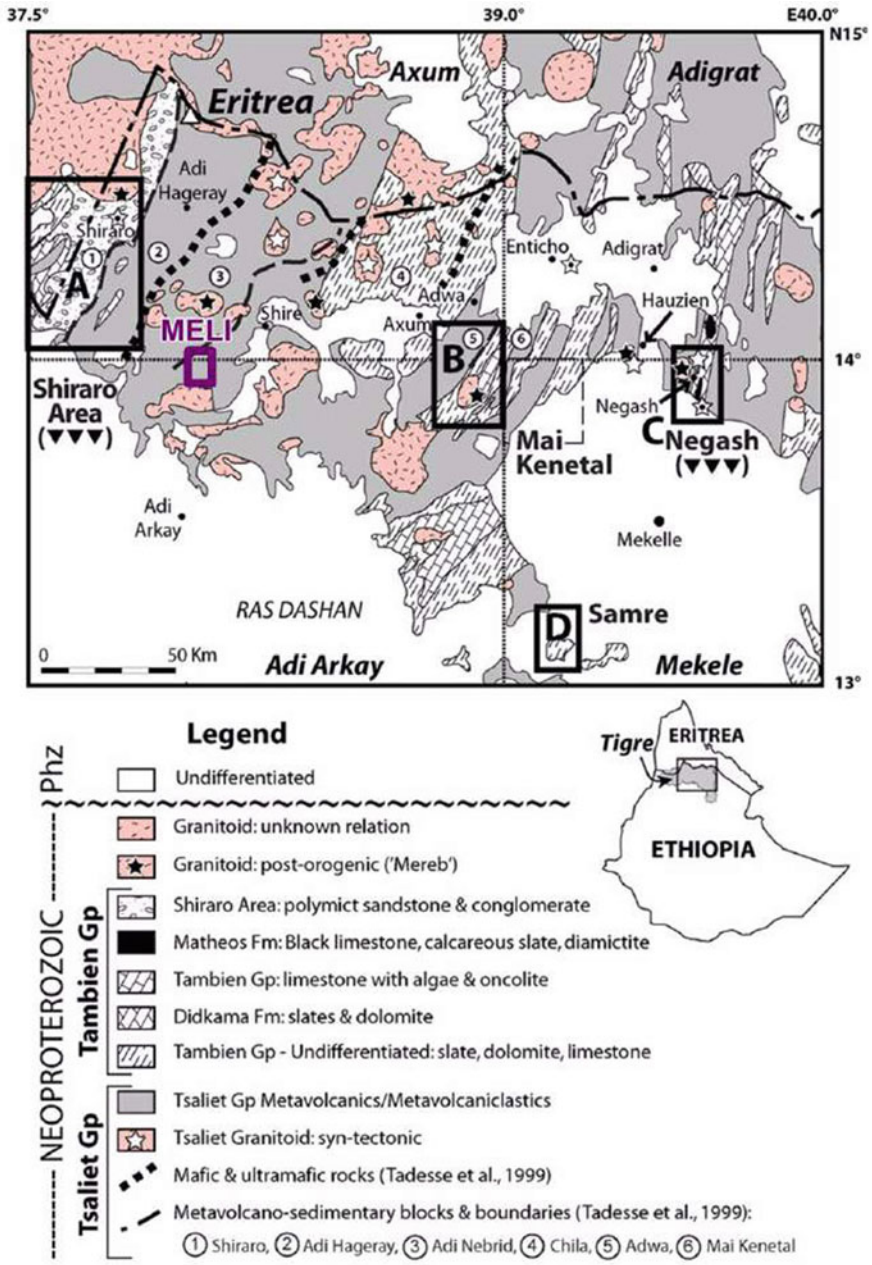

Fig. 6.42 Simplified geologic map of the Meli region, showing the Adi Nebrid block and associated VMS occurrences (from Miller et al. 2011)

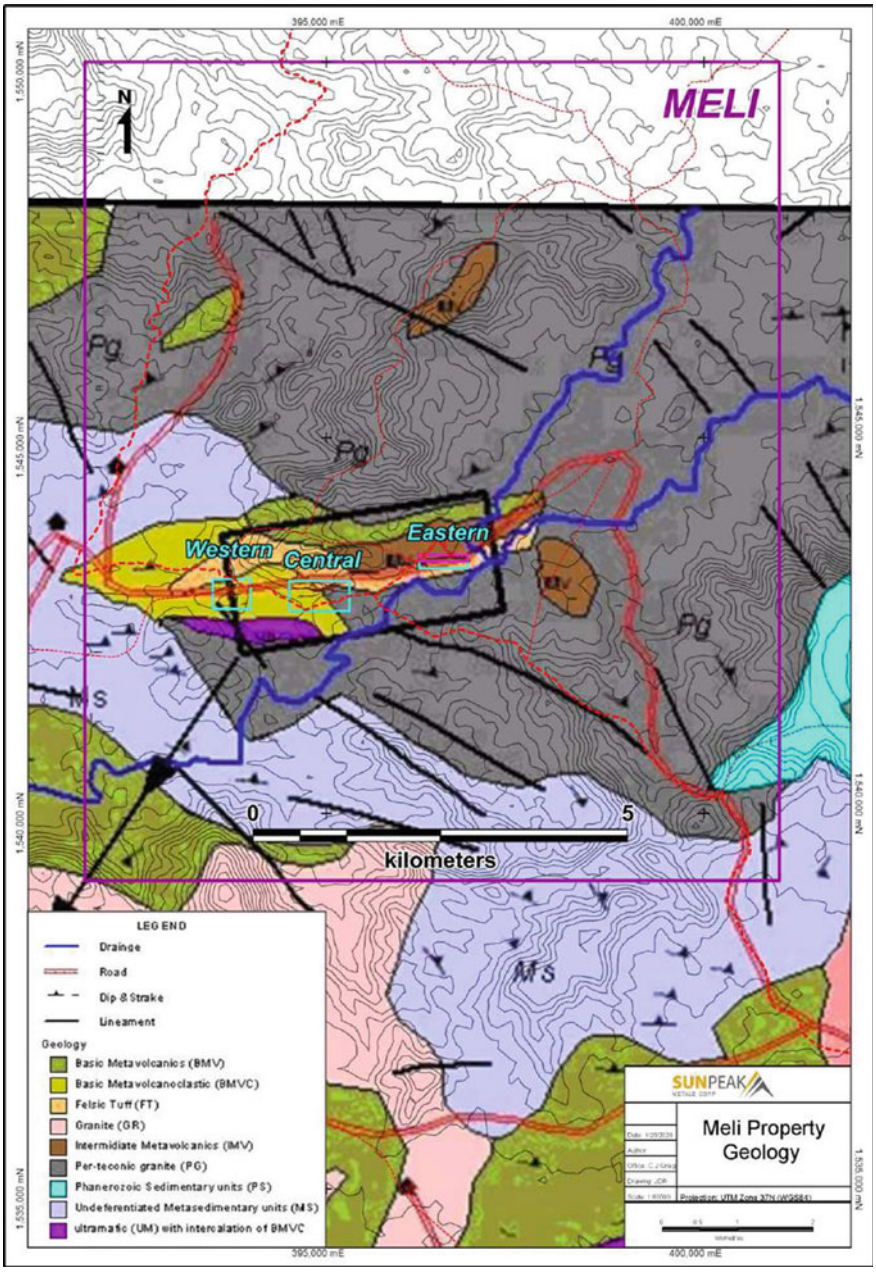

Fig. 6.43 Local geology of the Meli property (from Greig and Rowe 2020)

occasions, include minor chert horizons. The extrusive rocks can include tuffaceous and volcaniclastic sequences. The Meli VMS prospects occur more commonly within felsic or intermediate rocks, typically near their contact with mafic rocks, including at the eastern Meli gossan VMS prospect in the south-central part of the property (Fig. 6.43). Regionally, at VMS prospects, banded iron formation (BIF) and chert horizons have also been found, and jasperoid alteration is common. Detailed descriptions of the lithologies, structures, metamorphism, alteration assemblages and mineralized zones in the Meli project area can be found in the Technical Report of Meli Prospect, northern Ethiopia (Greig and Rowe 2020).

The oxidized sulfidic-rich gossans cover is localized mainly in felsic crystal tuff or flow that occur mainly as a long narrow belt adjacent to mafic and intermediate metavolcanic units in the central part of the project area. The central and western Meli gossans (Fig. 6.44) are closely associated with this rock type, with the most conspicuous feature being that it has unevenly and variably distributed grains of quartz "eyes" that vary from fine to medium and even locally coarse-grained, constituting ~10% of the rock. The rocks typically weathered to an orange-brown color, and are buff, white, or pale grey on fresh surfaces (Fig. 6.45). In places, particularly close to the gossans, the felsic tuff is more chloritic and the rock may take on a green hue. The typically strongly foliated parts may locally display a crenulation cleavage and commonly display variegated colors, ranging from reddish brown, to white–grey and locally, dark brown (Fig. 6.45). Toward the gossans, the content and size of the quartz eyes appears to decrease, possibly due to intense shearing and comminution of individual crystals. Kaolinization of these rocks may locally be prominent, and the felsic rocks are also commonly cut by abundant quartz veins. The petrographic examination of the felsic tuff revealed the following modal abundances (Greig and Rowe 2020): quartz (65%), calcite (15%), chlorite (10%), and pyrite (10%). The rocks showed well-developed schistosity outlined by fine-grained quartz, calcite, and chlorite in anastomosing bands, which wrapped around the euhedral to subhedral quartz phenocryts (Fig. 6.45), which showed wavy extinction, likely resulting from deformation.

Mineralization of the Meli property is primarily observed as Au- and minor base-metal-bearing surficial iron oxide minerals (goethite, limonite). Precious and base-metal-rich massive and semimassive sulfide VMS mineralization has been intersected in a number of deeper diamond drill holes beneath the better-developed massive gossans (Greig and Rowe 2020). The surficial gossans material is generally deep brown to red in color, locally varying to yellow. Vuggy and boxwork textures are locally created by leaching of sulfide minerals; disseminated, layered or laminated, wavy, and grooved hydrated silica (chert/jasper) have also been observed within the gossans area. Milky, glassy, iron-stained and brecciated quartz veins and veinlets occur, and are commonly concordant with the gossans. Ghosts of weathered sulfide minerals may also be observed as disseminations and fine stringers in the typically strongly foliated, sericitized, and kaolinized felsic metavolcanic rocks, which commonly occur adjacent to the gossans. Borehole drilling and geophysical surveys have defined the zones of strong oxidation beneath the gossans as occurring up to

an average depth of 30 m from the surface in the eastern gossans and, to a depth of possibly up to 75 m in the central and western gossans (Fig. 6.44).

The sizes and character of the Meli gossans vary considerably. The better-known eastern gossans zone extends for ~650 m along strike; it is ~80 m across in its eastern part, and ~1 m wide near its western end (Fig. 6.44). The trend of the mineralization is concordant with the east/west trends in the host rocks; the gossans and underlying sulfide mineralization dip steeply to the south. The central gossans has a strike length of ~100 m and the surface width varies from 1 to 5 m. The trend varies from east/west to north/east along strike and the mineralized zone appears to dip steeply to the south. Layering, quartz, and primary or secondary sulfide minerals are not observed in the central gossans. The western gossans zone has a strike length of ~100 m and the surface width varies from 1 to 6 m. The trend varies from east/west to north/east along strike and like, the other mineralized zones, the western gossans zone appears to dip steeply to the south. Brecciated quartz and banded white chert with concretion-like zones of yellowish and deep-brown hydrated silica/jasper are found within the gossans, but as with the central gossans, primary or secondary sulfide minerals and bedding are not observed.

Malachite and azurite occur very rarely in the surface gossans, which suggests that most of the primary Cu (and Zn) has been leached out from the surficial oxide zones. The Cu and Zn may have been redeposited within the supergene zones at depth. Similar to the nearby Eritrean deposits, where the supergene enrichment zone forms

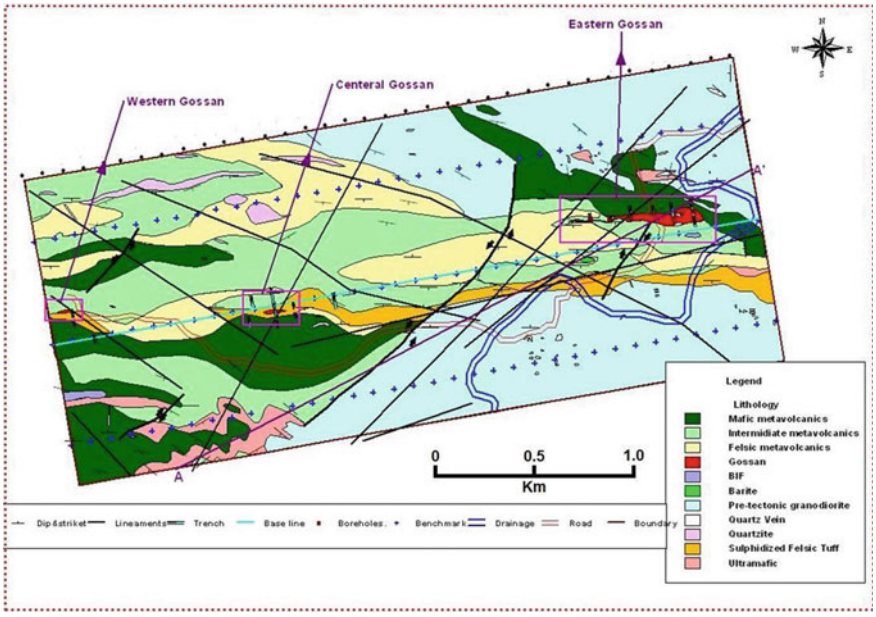

Fig. 6.44 Simplified geologic map of the Meli gossans area showing the different mineralization zones in Meli prospect (from Ezana private company Technical Report 2009)

Fig. 6.45 Foliated oxidized sulfide-rich felsic tuff cut by quartz veins (boudinaged quartz eyes) (from Greig and Rowe 2020)

significant grade concentrations, the supergene zones also represents attractive and little-tested targets in the Meli region. The eastern Meli gossans zone has long been known by its presence of Au; the majority of Au-bearing mineralized intercepts of the property come from there. The mining activities have been ongoing at the eastern Meli gossans since 2017, where drilling of the gossans has yielded some excellent intercepts in the gossanous material, such as in drill hole RVH-07, which returned 39.51 g/t Au over 12 m. Most of the drill holes were drilled only in the oxide cap; however, a number of the few deeper holes have intersected primary massive sulfide mineralization, returning very encouraging values, such as 4.2 wt% Cu, 0.7 wt% Zn, 1.5 g/t Au, and 37.1 g/t Ag over 17.4 m (hole RH-DH-01, 28.65–46.05 m) (Greig and Rowe 2020).

The identified hypogene sulfide mineral assemblage includes, in decreasing order of abundance, pyrite, chalcopyrite, sphalerite, and galena, in varying proportions. Pyrite is the most abundant sulfide mineral, where it has well-developed along fractures with other sulfides, particularly chalcopyrite and galena. Chalcopyrite, sphalerite, and gangue minerals are also found intergrown with pyrite crystals and locally as inclusions within pyrite. Chalcopyrite was the only copper mineral observed; bornite, covellite, and chalcocite, which may expected to be found in a supergene-enriched zone, were not found in the samples examined by Samuel et al. Sphalerite was locally found to be replaced by chalcopyrite and later pyrite. Galena occurs as

a minor phase, and is found as inclusions within pyrite and chalcopyrite as well as in the fractures within early pyrite. Base metal abundances and types are somewhat similar to those in the primary massive sulfide mineralization at the Bisha VMS deposit in Eritrea, which can be classified here as Cu–Zn (+Au)-rich deposit. The host rocks of the sulfide mineralization at the Meli prospect are also bimodal mafic–felsic volcanic rocks, which are comparable to that of the metavolcanic rocks of the Adi Nebrid block that host Eritrean VMS deposits in the region to the north, which has been interpreted to have been deposited in an island arc setting.

To date, with very limited drilling at the Meli project, only a single VMS lens has yielded intersections suggestive of truly significant thicknesses and, so far, that lens appears to be approximately 20 m thick with a minimum strike length of 200 m. This larger body appears to lie along stratigraphic contacts, between either mafic metavolcanic rocks and intermediate metavolcanic or meta-volcaniclastic rocks, or between flows of these metavolcaniclastic rocks. It is clear that the sulfide body follows the trend of the host rocks, where the contact is quite sharp, and the alteration is quite conspicuous in the host rocks close to the contact. In contrast to the eastern Meli gossans zone, gossanous surface exposures of the central and western zones suggest that those zones are relatively thin and discontinuous, at least close to the surface.

References

Abd Allah AG (2012) Two genetic types of volcanic-hosted massive sulfide mineralizations from the Eastern Desert of Egypt. Arab J Geosci 5:217–231

Abu Fatima M (2006) Metallogenic genesis and geotectonic evolution of the polymetallic massive sulphides and the associated gold deposits at Ariab–Arbaat Belt, Red Sea Hills, Sudan. Dissertation, Université Henri Poincaré

Ahlbrandt TS (2002) Madbi Amran/Qishn total petroleum system of the Ma'Rib-Al Jawf-Shabwah, and Masila-Jeza Basins, Yemen. USGS Bull 2202-G:1–28

Al Ganad I (1991) Etude géologique du gisement Zn-Pb-Ag de Jabali (Bordure sud du bassin du Wadi al Jawf). Unpublished dissertation, Université Orleans, France

Al Ganad I, Lagny P, Lescuyer JL, Rambo C, Touray JC (1994) Jabali, a Zn-Pb-(Ag) carbonate-hosted deposit associated with Late Jurassic rifting in Yemen. Miner Deposita 29:44–56

Alexander Nubia Inc (2015) Felsic dome at Hamama gold-rich VMS. Unpublished internal report

Ali-Bik MW, Hassan SM, Sadek MF (2020) Volcanogenic talc-copper deposits of Darhib-Abu Jurdi area, Egypt: petrogenesis and remote sensing characterization. Geol J 55:5330–5354

Allen CR (2000) Jabali ZnOx deposit, Yemen. Unpublished report, Cominco American

Archibald SM, Martin C, Thomas DG (2014) NI 43-101 technical report on a mineral resource estimate at the Terakimti Prospect, harvest property (centred at 38°21′E, 14°19′N), Tigray national region, Ethiopia. Prepared for Tigray Resources Inc

Ashley PM (2013) Petrographic report on thirty-six drill core samples from the Bisha mine, Eritrea. Unpublished technical report (#846) for Bisha Mining Share Company by Paul Ashely Petrographic and Geological Services

As-Saruri MA, Sorkhabi R, Baraba R (2010) Sedimentary basins of Yemen: their tectonic development and lithostratigraphic cover. Arab J Geosci 3:515–527

Aton Resources Ltd (2017) Hamama west deposit, Abu Marawat concession. Arab Republic of Egypt. https://www.atonresources.com/site/assets/files/1215/june152016-1.pdf. Accessed Apr 2021

Barrie CT (2004) Report on the geology and geochemistry of the Bisha VMS deposit and property, western Eritrea. Internal report, Nevsun Resources, Aug 2004

Barrie CT (2008) Lead isotope analysis of the Ariab and Nuba mountains areas, Sudan. Internal report for La Mancha Resources

Barrie CT, Hannington MD (1999) Volcanic-associated massive sulphide deposits: processes and examples in modern and ancient settings: introduction. In: Barrie CT, Hannington MD (eds) Volcanic-associated massive sulphide deposits: processes and examples in modern and ancient settings. Rev Econ Geol 8:1–11

Barrie CT, Kjarsgaard I (2010) Hadal Awatib east petrography and mineral chemistry report—internal report for La Mancha Resources Inc

Barrie CT, Nielsen FW, Aussant C (2007a) The Bisha volcanic-associated massive sulphide deposit, western Eritrea. Econ Geol 102:717–738

Barrie CT, Nielsen FW, Aussant CH (2007b) The Bisha volcanic-associated massive sulfide deposit, western Nakfa Terrane, Eritrea. Econ Geol 102:717–738

Barrie CT, Abdalla MAF, Hamer D (2016) Volcanogenic massive sulphide–oxide gold deposits of the Nubian Shield in Northeast Africa. In: Bouabdellah M, Slack J (eds) Mineral deposits of North Africa, mineral resource reviews. Springer Nature, Berlin, pp 417–435. https://doi.org/10.1007/978-3-319-31733-5_17

Bellivier F, Abu Safiyah M, Peyrol L (with the collaboration of Abdulhay G, Al Jadhali N, Artignan D, Felenc J, Genna A, Itard Y, Khali I, Miehé JM, Siddiqui AA) (1999) Mineral exploration in the Baydan area. Technical report BRGM-TR-97-6. Saudi Arabian Deputy Ministry for Mineral Resources

Beydoun ZR, As-Saruri MAL, El-Nakhal H, Al-Ganad IN, Baraba RS, Nani ASO, Al-Aawah MH (1998) International lexicon of stratigraphy, 2nd edn, vol 3. International Union of Geological Sciences and Ministry of Oil and Mineral Resources, Republic of Yemen Publication, Republic of Yemen, p 34

Bheemalingeswara K, Araya A (2012) Rahwa auriferous gossan, northern Ethiopia: a strong indicator of subsurface massive sulfide mineralization. Int J Earth Sci Eng 5:402–408

Bosc R, Tamlyn N, Kachrillo JJ (2012) The Hassai mine project—VMS resources update. Red Sea State, Sudan. NI 43-101 technical report prepared for La Mancha Resources Inc

Bosence DWJ (1997) Mesozoic rift basins of Yemen. In: Bosence DWJ (ed) Special issue on Mesozoic rift basins of Yemen. Mar Petrol Geol 14:611–730

Botros NS (2003) On the relationship between auriferous talc deposits hosted in volcanic rocks and massive sulfide deposits in Egypt. Ore Geol Rev 23:223–257

Bournat G (1981) Jabal Sayid copper-zinc deposit; synthesis of work and results of 1971–1974. Saudi Arabian Deputy Ministry for Mineral Resources open-file report BRGM-OF-01-7

Chisholm R, Delisle PC, Nielsen FW, Daoud D, Ansell S, Davis G (2003) Exploration and drilling program on the Bisha property for Nevsun Resources (Eritrea) Ltd, Bisha exploration permit 2003. Work program: internal company report. Nevsun Resources, Aug 2003

Christmann, P, Lagny, P, Lescuyer JL, Sharaf Ad Din A (1989) Discovery of the Jabali deposit (Zn-Pb-Ag) in the Jurassic cover of the Yemen Arab Republic. Chron Rech Min 43–52

Cottard F, Abdulhay GJ, Artignan D, Géïot JL, Roubichou P, Trinquard R, Vadala P (1994) The Al Hajar gold deposit (Kingdom of Saudi Arabia): a newly discovered example of supergène enrichment from a massive sulfide deposit of late Proterozoic age. Chron Rech Min/Chron Miner Res Explor 510:13–24

Daoud DK, Greig CJ (2007) Geology and mineralization of the Emba Derho deposit. Internal Sunridge report

Delfour J (1975) Geology and mineral exploration of the Nuqrah quadrangle (25/41A). Bureau de Recherches Geologiques et Minieres Saudi Arabian mission technical record 75-JED-28, 96 pp

Doebrich JL (1989) Evaluation and geochemical survey of the Farah Garan prospect, Kingdom of Saudi Arabia. Saudi Arabian Directorate General of Mineral Resources. Technical record USGS-TR-09-5

Donzeau M (1980) Geologic study of the Jabal ash Shizm prospect: Bureau de Recherches Géologiques et Minières. Technical record 80 JED 5

Dubé B, Gosselin P, Mercier-Langevin P, Hannington M, Galley A (2007) Gold rich volcanogenic massive sulphide deposits. In: Goodfellow WD (2007) Mineral deposits of Canada: a synthesis of major deposit-types, district metallogeny, the evolution of geological provinces and exploration methods. Geological Association of Canada, Mineral Deposits Division, Special Publication No. 5, pp 75–94

Ellis AC, Kerr HM, Cornwell CP, Williams DO (1996) A tectono stratigraphic framework for Yemen and its implications for hydrocarbon potential. Pet Geosci 2:29–42

Elsass P, Breton JP, Labbe JF, Sabir H, Vaillant FX (1983) The Sha'ib Lamisah prospect fieldwork 1400–1402 A.H. (1980–1982 A.D.). Saudi Arabian Deputy Ministry for Mineral Resources open-file report BRGM-OF-03-11

Evans AM (2009) Ore geology and industrial minerals: an introduction, 3rd edn. Wiley-Blackwell, Hoboken

Ezana Mining Development PLC (2009) Geological report of Meli area, private company report

Faisal M, Yang X, Khalifa IH, Amuda AK, Sun C (2020) Geochronology and geochemistry of Neoproterozoic Hamamid metavolcanics hosting largest volcanogenic massive sulfide deposits in Eastern Desert of Egypt: implications for petrogenesis and tectonic evolution. Precambrian Res 344:105751

Fernette GL (1994) Al Masane polymetallic deposit. In: Collenette P, Grainger DJ (eds) Mineral resources of Saudi Arabia. Saudi Arabian Directorate General of Mineral Resources Special Publication SP-2, pp 294–297

Gibson HL, Allen RL, Riverin G, Lane TE (2007) The VMS model: advances and application to exploration targeting. In: Milkereit B (ed) Proceedings of exploration 07: fifth decennial international conference on mineral exploration, pp 713–730

Giroux GH, Barrie CT (2009) Hambok deposit, Mogoraib exploration license, Gash-Barka District, western Eritrea, 43-101. Technical report and preliminary resource assessment

Greig CJ, Rowe JD (2020) A geological evaluation of the Meli property, Tigray national regional state, northern Ethiopia. Unpublished NI 43-101 technical report. Prepared for Sun Peak Metals Corp

Hall D, McHugh JJ (1989) Gold exploration in the eastern desert, Egypt: a case history. In: Mineral exploration programmes 89, paper 18, 25 pp

Hannington M, Jamieson J, Monecke T, Petersen S, Beaulieu S (2011) The abundance of seafloor massive sulfide deposits. Geology 39:1155–1158

Hargrove US (2006) Crustal evolution of the Neoproterozoic Bi'r Umq suture zones, Kingdom of Saudi Arabia: geochronological, isotopic, and geochemical constraints: Richardson, Texas. Dissertation, University of Texas at Dallas

Helmy HM (1996) Precious metal and base metal sulfide mineralization at Abu Swayel and Um Samiuki, Eastern Desert, Egypt. Dissertation, Minia University, Egypt

Helmy HM (1999) Um Samiuki Precambrian volcanogenic Zn-Cu-Pb deposit, South Eastern Desert, Egypt: a possible new occurrence of cervelleite. Can Mineral 37:143–154

Johnson PR, Kattan FH (2012) The geology of the Arabian Shield. Saudi Geol Surv 466

Klemm R, Klemm D (2013) Gold and gold mining in ancient Egypt and Nubia. In: Natural science in archaeology. Springer Nature, Berlin, p 341

Koch-Mathian JY, Tayeb S, Siddiqui AA (1994) Results of copper-gold exploration in the Rabathan prospect (Wadi Bidah Belt). Technical report BRGM-TR-14-2. Ministry of Petroleum and Mineral Resources, Directorate General of Mineral Resources, Jiddah, Kingdom of Saudi Arabia

La Mancha Resources Inc (2009) Hadal Awatib east Cu-Au VMS deposit, Sudan, resource estimates. NI 43-101 technical report, 106 pp

Large RR, McPhie J, Gemmell JB, Hermann W, Davidson GJ (2001) The spectrum of ore deposit types, volcanic environments, alteration halos and related exploration vectors in submarine volcanic successions: some examples from Australia. Econ Geol 96:913–938

Lydon JW (1984) Ore deposits models—8. Volcanogenic massive sulfide deposits. Part I: a descriptive model. Geosci Can 11:195–202

Lydon JW (1988) Volcanogenic massive sulphide deposits; part 2, genetic models. Geosci Can 15:43–65

Lydon JW (2007) An overview of the economic and geological contexts of Canada's major mineral deposit types. In: Goodfellow WD (ed) Mineral resources of Canada: a synthesis of major deposit-types, district metallogeny, the evolution of geological provinces, and exploration methods. St. John's, Geological Association of Canada, Mineral Deposits Division, Special Publication No. 5, pp 3–48

Menzies M, Al Kadasi M et al (1994) Geology of the Republic of Yemen. In: McCombe DA, Fernette GL, Alawi AJ (eds) Geology and mineral resources of Yemen. Geological survey and mineral exploration board, Yemen mineral sector project technical report, pp 21–48

Miller NR, Avigad D, Stern RJ, Beyth M (2011) The Tambien group, northern Ethiopia (Tigre). Geol Soc Mem 36(1):263–276

Mondillo N, Boni M, Balassone G, Grist B (2011) In search of the lost zinc: a lesson from the Jabali (Yemen) nonsulfide zinc deposit. J Geochem Explor 108:209–219

Mondillo N, Boni M, Balassone G, Joachimski M, Mormone A (2014) The Jabali nonsulfide Zn–Pb–Ag deposit, western Yemen. Ore Geol Rev 61:248–267

Morad AE, Helmy HM (2021) Convergent-margin polymetallic volcanic-hosted massive sulfide deposits. In: Hamimi Z, Arai S, Fowler AR, El-Bialy MZ (eds) The geology of Egyptian Nubian Shield. Regional geology reviews, Ch 16, pp 409–423. https://doi.org/10.1007/978-3-030-49771-2

Nevsun (2004) Exploration program on the Bisha property, Gash-Barka District, Eritrea 2004. Internal company report, Nevsun Resources (Eritrea) Ltd, Sept 2004

Noweir AM, Abu El-Ela AM (1991) The Shadli volcanic province a remnant of a Late Proterozoic island arc. Egypt J Geol 35:167–183

Parker TWH (1982) Assessment of the mineral potential of the Kutam-Al Halahila district southeast Asir: Saudi Arabian Deputy Ministry for Mineral Resources open-file report RF-OF-02-22, 149 pp

Payne JG (2013) Report 130086: petrographic report on samples from holes AHA-015, AHA-019, AHA-020, AHA-021 and AHA-026. Internal Alexander Nubia Inc. internal report, Feb 2013, 33 pp

Pitre CB, Siddiqui AA, Fauvelet E (1984) Jabal Sayid copper deposit: results of underground exploration, phase 2 (1983–1984). Saudi Arabian Deputy Ministry for Mineral Resources open-file report BRGM-OF-05-7

Ridley J (2013) Ore deposit geology. Cambridge University Press, Cambridge

Riofinex (1979) An assessment of the mineral potential of part of the Wadi Bidah district

Roobol MJ (1989) Stratigraphic control of exhalative mineralization in the Shayban paleovolcanoes (22/39A). Saudi Arabian Directorate General of Mineral Resources open-file report DGMR-OF-10-7

Rosa CJP, McPhie J, Relvas JMRS, Pereira Z, Oliveira T, Pacheco N (2008) Facies analyses and volcanic setting of the giant Neves Corvo massive sulfide deposit, Iberian Pyrite Belt, Portugal. Miner Deposita 43:449–466

Roubichou P, Artignan D, Beurrier M, Cottard F, Lescuyer JL (1989) Results of gold exploration in the Wadi Bidah district: Gihab and Mulhah gold prospects. Saudi Arabian Directorate General of Mineral Resources open-file report BRGM-OF-09-8, 50 pp

Sangster DF, Abdulhay GJS (2005) Base metal (Cu-Pb-Zn) mineralization in the Kingdom of Saudi Arabia: Jeddah. Saudi Geol Sur 128 pp

Searle DL, Carter GS, Shalaby IM (1978) Mineral exploration at Um Samiuki. U.N. technical report, 72–008/3, Egypt

Selim AQ (1994) Mineralization and wall rock alteration in Al-Derhib mine, South Eastern Desert, Egypt. M.Sc. thesis, Cairo University, Cairo, p 218
Senior N, Finch A, Ross AF, Rees SD, Martin CJ (2013) Asmara project feasibility study, an NI 43-101 technical report prepared by SENET Pty Ltd. for Sunridge Gold Corp, 264 pp
Shalaby IM, Stumpfl EF, Helmy HM, El Mahallawi OA, Kamel OA (2004) Silver and silver-bearing minerals at the Um Samiuki volcanogenic massive sulfide deposit, Eastern Desert, Egypt. Miner Deposita 39:608–629
Shukri NM, Mansour MS (1980) Lithostratigraphy of Sheikh Shadli metavolcanics and the older metasediments in Um Samiuki district, eastern desert, Egypt. Precambrian Res 6:A36–A37
Sillitoe RH, Hannington MD, Thompson JFH (1996) High Sulfidation deposits in the volcanogenic massive sulphide environment. Econ Geol 91:204–212
SRK (2017) Structural study and geotechnical review of Bisha mine, Eritrea, Mar 2017
SRK Consulting (2005) Jabali feasibility study, geology and resources. Unpublished report, ZincOx Resources plc, 45 pp
Stacey JS, Hedge CE (1984) Geochronologic and isotopic evidence for Early Proterozoic crust in the East Arabian Shield. Geology 12:310–313
Stern RJ, Kröner A, Rashwan AA (1991) A late Precambrian (710 Ma) high volcanicity rift in the southern Eastern Desert of Egypt. Geol Rundsch 80:155–170
Takla MA, Sakran ShM, Awad NT, Abd El Rahim AH (1999) Geological and structural evolution of Um Samiuki area, southeastern desert, Egypt. In: Proceeding of 4th international conference of geology of the Arab world, Cairo University, pp 168–184
Tornos F, Peter JM, Allen R, Conde C (2015) Controls on the siting and style of volcanogenic massive sulphide deposits. Ore Geol Rev 68:142–163
Viland J (1986) Assessment for gold in the Zalim area, central Arabian Shield, review of BRGM work. Saudi Arabian Deputy Ministry for Mineral Resources open-file report BRGM-OF-06-11, 110 pp
Volesky JC (2002) Massive sulfide deposits of the Wadi Bidah mineral district, Saudi Arabia; geologic control of mineralization, remote sensing and mineral exploration, geochemical exploration and petrogenesis. Dissertation, University of Texas at Dallas, 129 pp
Volesky JC, Stern RJ, Johnson PR (2003) Geological control of massive sulfide mineralization in the Neoproterozoic Wadi Bidah shear zone, southwestern Saudi Arabia, inferences from orbital remote sensing and field studies. Precambrian Res 123:235–247
Volesky JC, Leybourne MI, Stern RJ, Peter JM, Layton-Matthews D, Rice S, Johnson PR (2017) Metavolcanic host rocks, mineralization, and gossans of the Shaib al Tair and Rabathan volcanogenic massive sulphide deposits of the Wadi Bidah mineral district, Saudi Arabia. Int Geol Rev 59:1975–2002
Voormeij D (2015) Geological model for Hamama. Unpublished Alexander Nubia Inc. internal report, 3 pp

Chapter 7
Sedimentary/Surficial Mineral Deposits

Contents

7.1 Introduction . . . 411
7.2 Banded-Iron Formations in Saudi Arabia . . . 415
7.3 Banded-Iron Formations in Yemen . . . 421
7.4 Banded-Iron Formation in the Eastern Desert of Egypt . . . 422
7.4.1 Um Anab Banded Iron Formation . . . 425
7.4.2 Abu Marawat Banded Iron Formation . . . 426
7.4.3 The Gebel Semna Banded Iron Formation . . . 430
7.4.4 Wadi Kareim Banded Iron Formation . . . 431
7.4.5 Wadi El Dabbah Banded Iron Formation . . . 433
7.4.6 Um Shaddad Banded Iron Formation . . . 436
7.4.7 Um Ghamis Banded Iron Formation . . . 438
7.4.8 Gebel El Hadid Banded Iron Formation . . . 439
7.4.9 The Um Nar Banded Iron Formation . . . 441
References . . . 443

7.1 Introduction

Sedimentary/surficial deposits concentrations of detrital minerals or precipitates

(a) *Deposits related to sedimentation (chemical and clastic deposits)*

- Iron ore deposits (banded iron formation-BIF, and oolitic ironstones)
- Evaporites, phosphorites, Mn deposits, etc.
- Placer deposits

(b) *Deposits related to weathering*

A. Hassan Ahmed, *Mineral Deposits and Occurrences in the Arabian–Nubian Shield*,
Earth and Environmental Sciences Library,
https://doi.org/10.1007/978-3-030-96443-6_7

- Residual deposits (Al-laterite–bauxite, Ni-laterite)
- Supergene enrichment deposits

Surficial or external ore-forming systems refer to all processes taken place on or near the Earth's surface by chemical and physical phenomena and led to the concentration of surficial mineral deposits within the regolith, lakes, and/or shallow marine environments. Two major ore-forming processes are taking place in the formation of sedimentary/surficial deposits: (1) deposition by chemical sedimentary processes in which mineral precipitation taking place most commonly from sea water or lake waters (e.g., sedimentary iron ores, phosphorites, evaporites, and Mn nodules), and (2) deposition related to weathering, either by chemical weathering (e.g., bauxite, Ni-laterite, or supergene enrichment deposits), or physical weathering (e.g., placer deposits, as a result of physical accumulation of ore minerals during processes of sediment entrainment, transport, and deposition).

There are a number of different sedimentary ore deposit types that are essentially formed by chemical processes in sedimentary environments. These are summarized below for reference; otherwise, except for the sedimentary banded iron formations (BIF), all of the other sedimentary/surficial mineral deposits (Table 2.1, see part of it above) in the Arabian–Nubian shield are of Phanerozoic age (<541 ± 10 Ma). Thus, as the target of this book is to deal with Arabian–Nubian shield rocks of Proterozoic age (from the Tonian through the Ediacaran ages, between 541 and 1000 Ma); the discussion in this chapter of the sedimentary/surficial mineral deposits in the Arabian–Nubian shield will be restricted to distribution and occurrence of Precambrian BIF deposits.

(i) *Ironstones*, by definition, are Fe-rich sedimentary rocks (>15 wt% FeO), which are also referred to as *iron formations*. Sedimentary ironstones are the major world source of Fe. Worldwide, there are two contrasting widespread types of sedimentary iron ores: oolitic (ooidal) ironstones, and cherty BIFs. These two types of iron deposits will be briefly discussed below; however, the latter type (BIFs), will be specifically discussed in detail later on in this chapter.

(ii) *Manganese deposits* are "Mn oxide" or carbonate-rich sedimentary rock units, which are the world's major source of Mn. Manganese nodules on ocean floors are composed dominantly of fine-grained Mn-rich oxide minerals with high concentrations of certain metals adsorbed onto grain surfaces, including Ni and Cu in addition to Mn.

(iii) *Phosphorites* are sedimentary rocks with between 40 and 90% modal apatite (specifically, francolite [$Ca_{10}(PO_4)5(CO_3)F_2$].

(iv) *Evaporites* are important ores of minerals of many elements that are in relatively high concentration in seawater (e.g., common salt (NaCl), potash, magnesium carbonate). Evaporites formed in lakes in some enclosed continental basins in desert climates in tectonically and volcanically active regions, which are the dominant source of boron minerals, strontium minerals, and

sodium carbonate minerals such as trona and soda (e.g., Risacher and Fritz 2009). Lithium is also dominantly extracted from brines that are interstitial to evaporite minerals in continental evaporite basins.

(v) *Black shales*. Some organic-rich black shales have metallic ore-grade concentrations (~1 wt%) of a number of metals, most importantly Mo and Ni. The metals are considered to have been sequestered from seawater onto grain surfaces (adsorbed) or into amorphous organic matter that was on or just below the sea floor.

The first stage in the formation of Fe-rich sedimentary rock is a critical process in the genesis of sedimentary rock–hosted iron ores. In the case of oolitic iron ore, the deposit predominantly contains chamosite (Fe-rich chlorite, containing ~40 wt% FeO), and goethite or limonite in a matrix of Fe-rich minerals, such as iron carbonate (siderite) (e.g., Van Houten and Bhattacharyya 1982; Ridley 2013). Most of the oolitic sedimentary ironstones are related to the Phanerozoic eon (e.g., the Jurassic through the Oligocene–Miocene), which sometimes interbedded with carbonate units as those of the historically important iron ores in France (Lorraine) and England (Northampton shire).

On the other hand, the silica-rich BIF predominantly contain Fe oxides (e.g., hematite, magnetite), more rarely Fe carbonate (siderite), and Fe silicate minerals (e.g., greenalite, stilpnomelane) in association with fine-grained quartz. The BIF deposits include intercalations of thin laminated fine-grained Fe-rich and SiO_2-rich sediments that are being deposited at present in marine environments that are mostly associated with volcanic seamounts (e.g., Hein et al. 1994). The BIF deposits are the most economically important source of iron, which can be ~100 m in thickness or more, are almost all related to Archean and Paleoproterozoic age, and occur in most of the major shield regions of the world, including the Arabian–Nubian, Brazilian, Indian, South African, and Australian shields and the Lake Superior region of the United States. Almost all of the world's iron resources are produced from cherty BIF deposits related to the early Precambrian era.

The majority of BIF ore deposits were commonly formed during the Late Archean and Paleoproterozoic (from ~3.4 to 1.8 Ga) (Fig. 7.1), with a few exceptions that formed during the Mesoproterozoic and Neoproterozoic eras (from ~0.85 to 0.70 Ga). However, BIFs mostly disappear from the geologic record when the oxygen concentrations in the atmosphere and oceans increased, which led to removal of the dissolved iron from seawater (e.g., Rouxel et al. 2005; Stern et al. 2006). Increasing the oxygen concentrations oxidized the soluble ferrous iron (Fe^{2+}), dissolved in seawater, into insoluble ferric iron (Fe^{3+}), which precipitated and accumulated on the seafloor to form the BIF deposits. The oxidation of soluble Fe^{2+} in seawater was completed in the Paleoproterozoic, so that the BIF deposits are almost missing from the Mesoproterozoic record (Stern et al. 2006). Important BIF deposits reappeared again in the Neoproterozoic times in association with Snowball Earth events, which are considered to be the second great marine oxidation episode, which has recently been termed the *Neoproterozoic Oxidation Event* (Shields-Zhou and Och 2011).

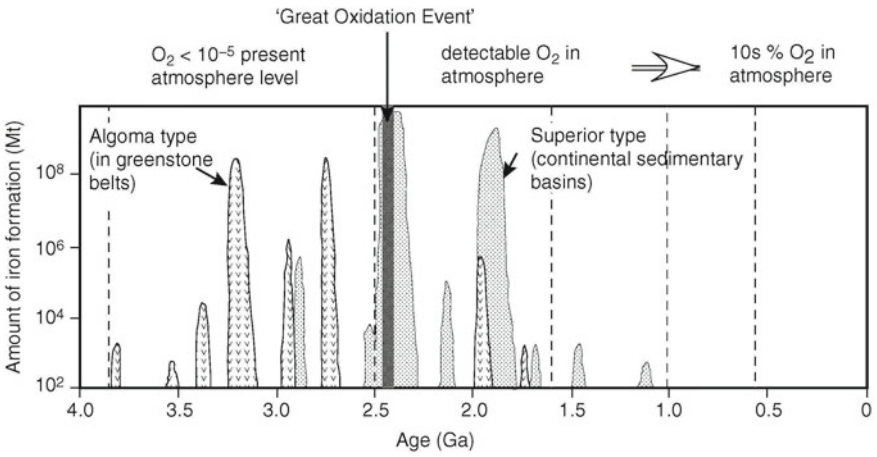

Fig. 7.1 Abundance of Algoma and superior types of BIF deposits through geological time (after Bekker et al. 2010; Ridley 2013), and major events in the evolution of oxygen in the atmosphere

Two main BIF types are distinguished worldwide based on geological setting and rock associations: (1) *Algoma-type* BIFs, which are sedimentary units in sequences of submarine volcanic rocks in greenstone belts, most commonly of Archean age. They have limited strike extent (up to tens of kilometers) and thickness (a few meters), but can be up to ~100 m thick. (2) *Superior-type* BIFs, which have high lateral extension (hundreds of kilometers) and hundreds of meters thick that typically include interbedded, thin units of Fe-rich shale. This BIF type occurs in sedimentary basins of marine strata of late Archean or Paleoproterozoic age that were deposited over igneous and metamorphic basement. The sequence of sedimentary basin typically include intercalations of carbonates, shales, sandstones, and some volcanic rocks. Multiple superior-type BIFs are present in many of these sedimentary basins. These BIF deposits, in general, are characteristically banded on multiple scales, ranging from meter (*macrobanding*) to centimeter (*mesobanding*) to millimeter (*microbanding*) scale. The meso- and microbanding BIF types are composed of alternations of Fe-rich minerals (hematite and/or magnetite) and silica-rich or cherty quartz. Macrobanding can be traced over many kilometers horizontally and is marked by Fe-rich shale bands. BIFs with granular texture constitutes a sedimentary facies, which sometimes lacks the finer-scale banding indicating deposition from marine water currents. This facies is most probably formed from transported and reworked sand- and conglomerate-sized clasts of iron-rich materials.

In the Arabian–Nubian shield, BIF deposits are well-represented in the Arabian Shield of Saudi Arabia and in the Nubian Shield of the Egyptian Eastern Desert, with very limited occurrences in the other regions covered by the Arabian–Nubian Shield. Therefore, following are detailed descriptions of the Precambrian BIF in the Arabian Shield of Saudi Arabia and, to a lesser extent in Yemen, as well as those in the Nubian Shield of the Eastern Desert of Egypt. There is not enough available

information about the BIF deposits in other countries of the Nubian Shield (i.e., Sudan, Eritrea, and Ethiopia). This chapter thus only focuses on the BIF occurrences and deposits in Saudi Arabia, Yemen, and Egypt as parts of the Neoproterozoic basement complex.

7.2 Banded-Iron Formations in Saudi Arabia

In general, three major iron deposits have been extensively described in the Arabian Shield of Saudi Arabia (Fig. 7.2): (1) An Oligocene–Miocene oolitic hematite–goethite deposit at the Wadi Fatima–Ashumaysi area (Al-Hazzaa 1973; Galmed et al. 2021), (2) a Precambrian magnetite and hematite BIF deposit at Wadi Sawawin (Stern et al. 2006, 2013), and (3) an iron oxides (±Cu-Au) magnetite deposit at Gebel Idsas (Doebrich et al. 2007). The Wadi Sawawin BIF deposit (Fig. 7.2) is the only iron deposit focused on here as it is the only Precambrian sedimentary Fe-rich deposit.

In the Arabian Shield of Saudi Arabia, BIFs are confined mainly to Wadi Sawawin in the Midyan terrane (the northwestern part of the shield) and its counterpart in the Nubian Shield of the Eastern Desert of Egypt, as well as some other areas in the Kingdom such as those in the Al Aqiq quadrangle of the southwestern part of the Asir terrane. Known outcrops in the Arabian Shield are spread over a strike length of ~25 km in the Wadi Sawawin area (Fig. 7.3) and as lenses in large roof pendants of metamorphosed volcanic and volcaniclastic rocks in granite to the northwest. The existence of BIF boulders (floats) in Wadi alluvium suggests that BIFs may also be found as much as 75 km southeast of Wadi Sawawin. The Wadi Sawawin area includes nine sites of BIF mineralization (Al Shanti 2009), in which the most important is Wadi Sawawin, and then Al Sharmah near the Red Sea shore (Fig. 7.2). The main areas hosting the BIF mineralization are bounded between latitudes 26°50′–28°20′ N and longitudes 35°15′–35°50′ E.

The Wadi Sawawin BIF deposits are located in the north-western part of the Al Hijaz mountains, some 700 km north of Jeddah and ~60 km east of the Red Sea coast (Fig. 7.2). The area is very rugged and steep, where the highest elevation, Gebel Al Dubbagh, reaches up to 2350 m above sea level. The Wadi Sawawin BIF deposits are hosting within a thick succession of Precambrian rocks composed mainly of andesitic to felsic pyroclastic and sedimentary rocks assigned to the Silasia formation (Fig. 7.3), which overlies the Ghawjah formation metavolcanic rocks. Both the Silasia and Ghawjah formations are part of the Za'am group (Davies and Grainger 1985; Johnson 2004), in which all rock types are folded and metamorphosed in the greenschist facies. The basal Ghawjah metavolcanic rocks are mostly basalts and andesites with tholeiitic to calc-alkaline affinities (Stern et al. 2013), which were erupted in an arc or back-arc basin and yield a U–Pb zircon age of ~763 ± 25 Ma (Ali et al. 2010).

The BIF-bearing Silasia formation is an approximately 1 km-thick sequence of immature clastic metasedimentary rocks that locally contains tuffs, felsic flows, and

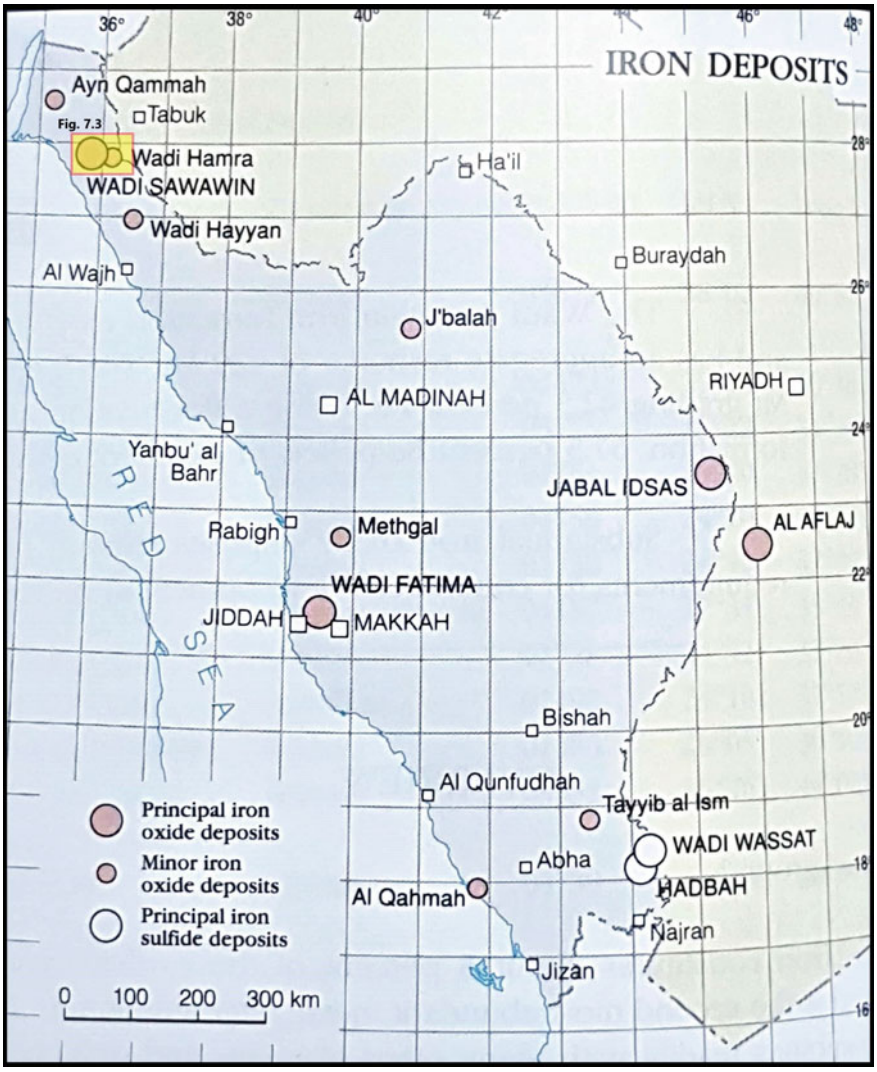

Fig. 7.2 A location map of iron distribution, with special reference to the Wadi Sawawin area (yellow rectangle), Arabian shield of Saudi Arabia (from Collenette and Grainger 1994)

dolerite sills (Fig. 7.4) that have a gradational and conformable contact with the underlying Ghawjah formation (Stern et al. 2013). The Silasia formation is divided into a lower thick unit (~1000 m thick) composed of tuffaceous sedimentary rocks and tuffs, overlain by a 5–90 m-thick middle unit of BIF and associated ferruginous tuffs (Fig. 7.4). The upper part of the Silasia formation is ~120–200 m in thickness and is composed of metatuffs and tuffaceous metasedimentary rocks, with some thin,

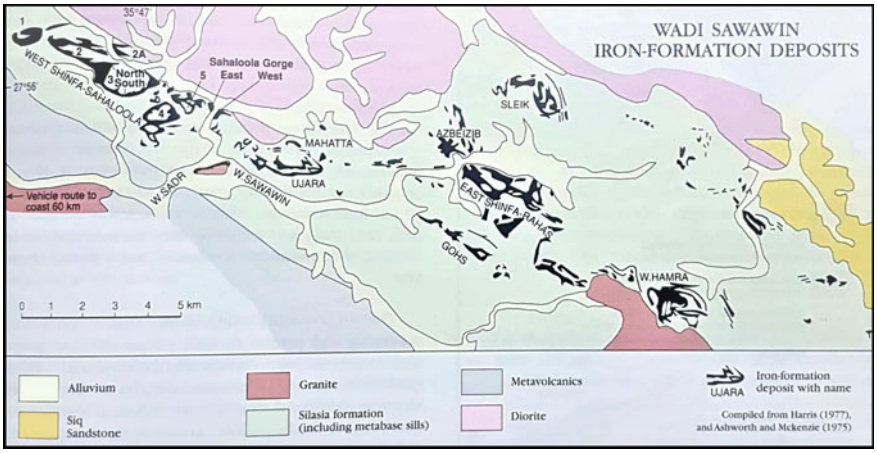

Fig. 7.3 Simplified geological map showing the outcrops of BIF in the Wadi Sawawin district, North-western part of the Arabian shield (from Collenette and Grainger 1994)

discontinuous iron-rich bands (Fig. 7.4). In the Silasia formation, BIF occurs near the top of the sequence and crops out over a strike length of ~15 km (Fig. 7.4).

The Wadi Sawawin BIF was discovered in 1953 where it was examined, mapped, and tested to be of a low-grade blast-furnace feed at that time. In 1974, the Saudi Arabia Directorate General of Mineral Resources (DGMR) undertook a review of iron deposits in the Kingdom as possible sources of feedstock, where the Wadi Sawawin BIF was selected for investigation as being the most promising iron deposit. The Wadi Sawawin iron formation is of an oxide-facies Algoma type, in which ten areas have been identified as having total resources of ~429 Mt ore; the west Shinfa–Sahaloola area is the biggest of the areas (Fig. 7.3). The second-largest and most prospective BIF deposit at Wadi Sawawin is Deposit 3 (south), which is a sheet-like body approximately 25–58 m in thickness (Fig. 7.5). Deposit 3 south is partly exposed on the dip slope, which dips northward at ~40° and covered by hanging-wall rocks (Fig. 7.5). The Wadi Sawawin BIF sequence is essentially composed of hard, finely laminated hematite and magnetite alternating with dark-red jasper (quartz and minor hematite) on a scale of millimeters to centimeters (Mukherjee et al. 2005) (Figs. 7.5 and 7.6). The individual bands can be traced for tens of meters. In addition, carbonate lenses have also been mapped in places that reach up to 40 cm thick and several meters long.

The Wadi Sawawin BIF is complexly folded (Fig. 7.6a, b), which reflects soft-sediment deformation as a result of dense, unconsolidated BIF on top of unconsolidated sediments in a tectonically unstable region. The sandstones beneath the Sawawin BIF also show evidence of soft-sediment deformation and slumping, as well as containing abundant grading, channeling, and fluid-escape structures. The whole sequence of the Silasia formation is intruded by the Sawawin diorite complex, which yields a U–Pb zircon age of 662 ± 2 Ma as well as by A-type granites (~600 Ma)

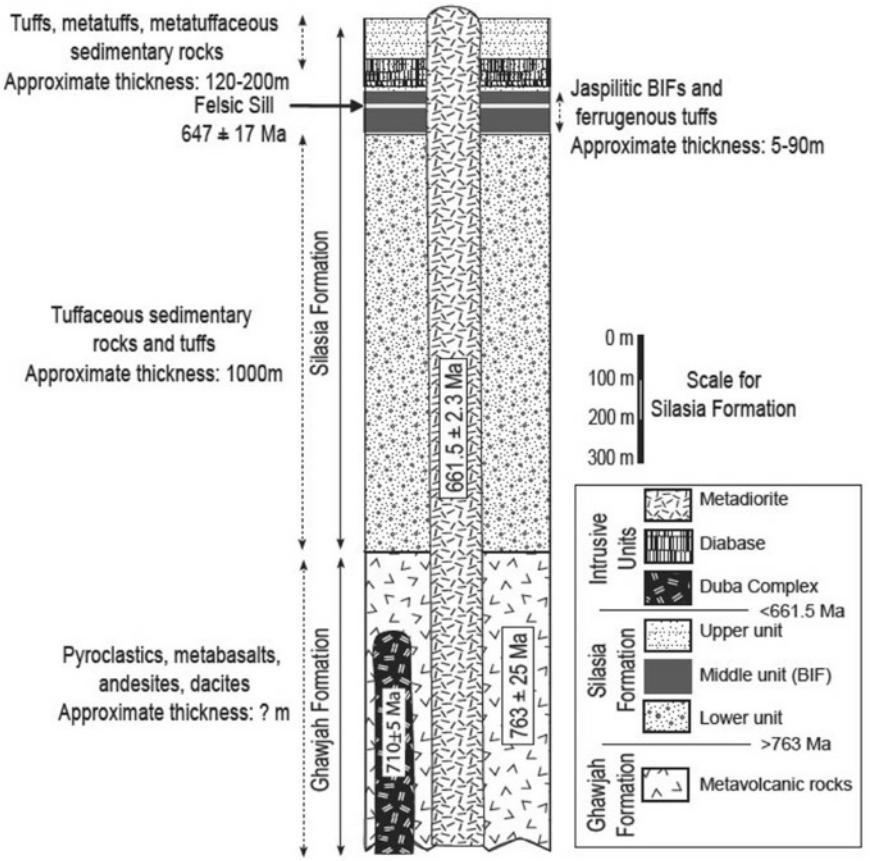

Fig. 7.4 Simplified stratigraphic column of the Wadi Sawawin BIF-bearing unit, Arabian Shield, Saudi Arabia (from Johnson and Kattan 2012)

and by undated diabase sills (Ali et al. 2010; Stern et al. 2013) (Fig. 7.4). Beds of fine-grained tuffaceous argillite as much as 1-m thick are interlayered with BIF layers (Fig. 7.6a, b). The large number of individual deposits in the Wadi Sawawin district is most probably the result of fold repetition of a limited number of Fe-rich horizons (Stern et al. 2013). The folding, local brecciation, greenschist-facies metamorphism, and intrusion by late- to post-tectonic granites are all features favorable for the capture of mobilized Au in the BIF (Johnson and Kattan 2012). Such features are clearly observed in the BIF deposits in the Eastern Desert of Egypt, where they contain 0.41–1.124 g/t Au (Dardir and El Chimi 1992). The Sawawin BIF ore is formed from microscopic interlocking grains of hematite, magnetite, and quartz that are arranged in belts or as very small lenses (Fig. 7.6c, d). Accessory gangue minerals associated with the BIF ore minerals represented by calcite, Fe-rich chlorite, sericite, apatite, and pyrite.

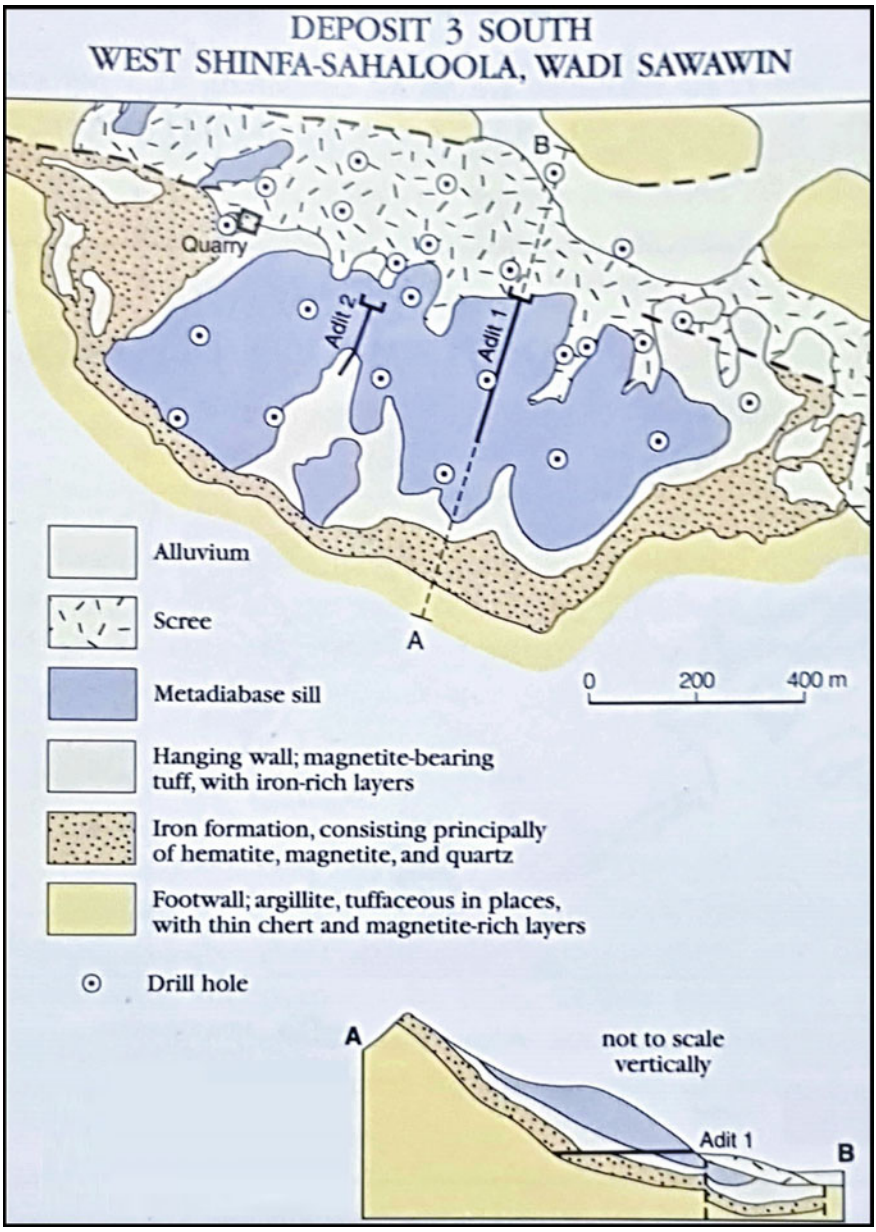

Fig. 7.5 A simplified geological map of the BIF Deposit 3 (south) of Wadi Sawawin, with a stratographic section for the Silasia formation showing its sequence and thickness of each unit (from Collenette and Grainger 1994)

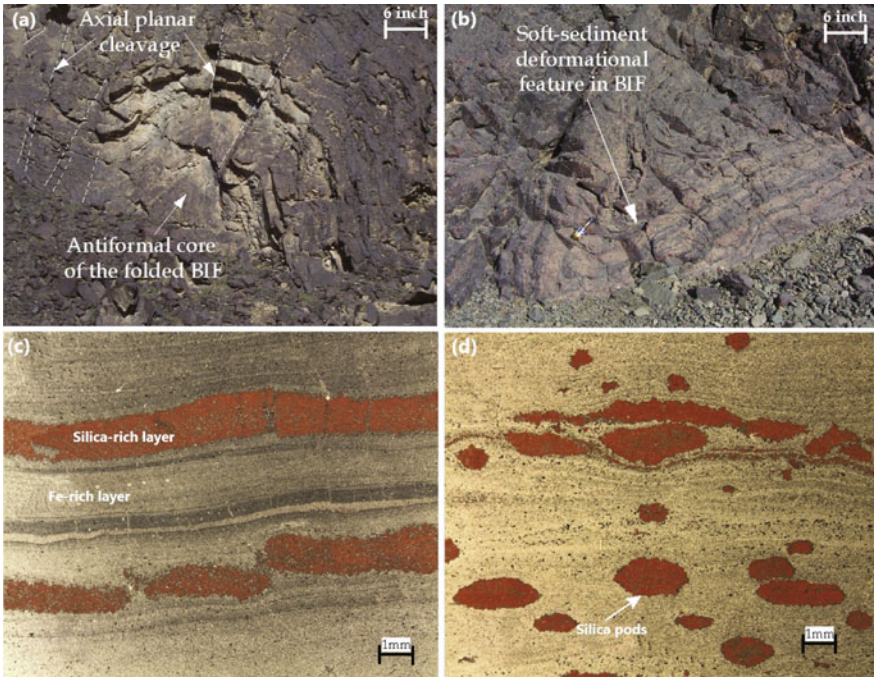

Fig. 7.6 Wadi Sawawin BIF deposit. **a**, **b** Field photographs show folding of the deposit, where **a** shows an open fold with faulted hinges and **b** shows tightly folded BIF lacking axial-planar cleavage. **c**, **d** Photomicrographs of samples from the deposit, where **c** shows typical banding where the silica-rich bands are red (jasper) and the iron-rich bands are light colored and **d** shows typical silica-rich pods (red jasper) developed due to the differential compaction and release of silica from the iron-rich layers of Wadi Sawawin BIF (from Stern et al. 2013)

The estimated ore resource of the Wadi Sawawin BIF is ~96 Mt, containing 42.5 wt% total Fe_2O_3, 28.3 wt% SiO_2, 0.31 wt% P, and 0.11 wt% S for the largest BIF body (Deposit 3). A total resource estimate for the seventeen deposits listed by Dixon and Ashworth (1994) is ~428.9 Mt. Hematite is the main iron mineral in the Wadi Sawawin BIF deposits, which is essentially concentrated in thin layers containing up to 60 wt% Fe. The hematite-rich thin layers are separated by quartz-rich layers generally containing less than 15 wt% Fe (Collenette and Grainger 1994). The ore crushing into 2 mm size containing about 55–60 wt% Fe, but liberation of hematite-rich particles requires very find grinding. Several beneficiation methods have been used to upgrade the Wadi Sawawin BIF deposits; however, gravity concentration and flocculation flotation are the only methods that gave satisfactory separation and recovery results.

Deposition of the BIF is assumed to have occurred between 760 and 650 Ma in a convergent margin setting prior to the collision of the Midyan and Hijaz terranes. The particular controls on the Wadi Sawawin BIF deposit are a matter of debate. Some authors argue that the resumption of BIF deposition during the Neoproterozoic age

was linked to the special oceanic and atmospheric conditions produced by Snowball Earth (Stern et al. 2006); others emphasize the normal emanation of iron into sea water at a convergent-margin tectonic setting with no relationship to glaciation (Basta et al. 2011; Freitas et al. 2011).

7.3 Banded-Iron Formations in Yemen

The BIF in Precambrian metamorphosed volcano–sedimentary rocks of Yemen were recorded in several localities, such as those in the Al Thanyyah (Ma'rib), Al-Bayda, Sa'dah, and Abyan (Al Majil-Ataq) areas (Al-Khirbash et al. 2021). The *Al Thanyyah* BIF occurrence is located in the Ma'rib governorate within Precambrian metavolcanic rocks in the northeastern extension of the Abas continental terrane. The BIF occurs to the northeast of the Al-Sabatayn basin as thin laminations of magnetite, hematite, and chert in several zones range in thickness from a few centimeters to several meters. The BIF mineralization is strongly deformed to various extents. It is a high-grade ore with Fe_2O_3 content reaching up to 96.3% (Yemen Iron Steel Co. 2010).

There are several BIF occurrences in the *Al Bayda* area that are distributed within a wide belt of island arc metavolcano–sedimentary associations extending ~21 km in length and ~2 km in width. The Al Bayda BIF is mostly similar to the Algoma-type BIF, as demonstrated by its small thickness, limited extent, and geological setting (Sakran 1993). A nearby area from the Al Bayda is the *Sabah* BIF locality, which is ~21 km northwest of the city of Al Bayda. The Sabah area comprises nine discontinuous, irregular, thin lenses and pockets within a limited metamorphosed volcano–sedimentary succession extending ~900 m in length and 200 m in width. The mineralized area is cross-cut by northeast and east-northeast-trending faults and shear zones (Al-Khirbash et al. 2021). Magnetite, hematite, titanomagnetite, and pyrrhotite are the main iron minerals of the ore, with estimated reserves of ~800,000 t, at an average grade of 74% Fe (Lescuyer 1981; Letalenet 1981; Al-Khirbash et al. 2021). However, the Sabah BIF occurrence, although it has a high content of iron, is economically insignificant due to its limited thickness and discontinuous nature along strike.

The *Al Masna* iron prospect at the *Sa'dah* area, mined during prehistoric times, is considered to be one of the most important iron occurrences in Yemen (Meinhold 1982). The proven ore reserve at this prospect is ~940,000 t of hematite–pyrrhotite–siderite, at an average grade of 34% Fe and 11% Mn. The Al Masna iron prospect is hosted mainly by graphite schist intercalated with marble and mafic metavolcanic rocks. At the *Abyan* area, the *Al-Majil–Ataq* BIF occurrence is located ~116 km northwest of the town of Ataq. The BIF mineralization of Abyan area is composed of several lenses of magnetite–hematite minerals; the largest lens reaches up to 150 m in length and 7.5 m in thickness. The estimated ore reserves are ~46,000 t, at an average grade of 56–76% Fe content (Isakin et al. 1990).

7.4 Banded-Iron Formation in the Eastern Desert of Egypt

The BIF of the Eastern Desert of Egypt is generally found to be intercalated with volcano–sedimentary units within the Precambrian basement. These units were amalgamated during the Neoproterozoic Pan-African orogeny, and can be simply classified into five distinct tectonic stages (Table 7.1) (see, e.g., El-Gaby et al. 1990;

Table 7.1 Tectonostratigraphic basement units of the Egyptian Eastern Desert

Eon/ Era	Tectonic Stage		Age [Ma]	Rock Types/Associations		Granitoid intrusion (age [Ma])
Phanerozoic	Post-Orogenic		<570	Younger granites (post-tectonic, alkalic): Granite, granodiorite, monzonite		Gattarian (570–475)
Neoproterozoic	Pan-African	Accretion/ Collision	650–570	Dokhan metavolcanics (andesite, rhyolite, rhyodacite, pyroclastics) intercalated with Hamamat metasediments (breccias, conglomerates, greywackes, arenites, and siltstones)		
		Subduction	750–650	Island Arc	Shadhli metavolcanics (rhyolite, dacite, tuff); volcaniclastic metasediments; diamictites (Strutian: 680–715 Ma). **Banded iron ores**	Meatiq (710–610) Hafafit (760–710)
		Spreading	850–750	Ophiolite	Tholeiitic basalt, sheeted dykes, gabbros, serpentinites, all weakly metamorphosed	Shaitian granite (850–800)
Archean?/ Paleoproterozoic	Pre-Pan-African		<1.8 Ga	Metasedimentary schists and gneisses (Hb-, Bt-, and Chl- schists), metagreywackes, slates, phyllites, and metaconglomerates **Some BIF? Um Nar?**		
				Migiff–Hafafit gneiss (Hb and Bt gneiss) and migmatite		

Stern et al. 2006): (1) rifting and breakup of Rodinia (900–850 Ma); (2) seafloor spreading (870–750 Ma); (3) subduction and development of arc–back-arc basins (750–650 Ma), contemporaneous with the older granitoid intrusions; (4) accretion/collision and shortening, coupled with escape tectonics and continental collapse, marking the culmination of the Pan-African orogeny; and (5) intrusion of the alkalic, postorogenic younger granitoids.

In the Eastern Desert of Egypt, the BIF deposits/occurrences occur in some thirteen localities in an area of ~30,000 km^2, mainly within the Central Eastern Desert (CED), almost all of them are related to the Neoproterozoic era (Fig. 7.7; Table 7.1). These iron ores occur as rhythmically layered bands, groups of bands, or separate lenses that reach a maximum thickness of 100 m; they are found intercalated with volcanic arc assemblages dominated by andesitic lava flows, tuffs and lapilli tuffs, and basaltic pyroclastics. In most cases, the BIF deposits contain synsedimentary structures such as bedding and lamination. The entire sequence of BIF and host rocks is strongly deformed and regionally metamorphosed under greenschist-to-amphibolite facies conditions.

In the Eastern Desert of Egypt, the Fe- and SiO_2-rich lithologies, which are assigned as BIF deposits, are classified into two main types (El Habaak 2021): (1) proper BIF deposits, including the occurrences of *Um Anab*, *Abu Marawat*, *Gebel Semna*, *Wadi Kareim*, *El Dabbah*, *Um Ghamis El Zarqa*, *Gebel El Hadid*, *Um Shaddad*, and *Um Nar* (Fig. 7.7). (2) Ferruginous volcanogenic chert deposits/occurrences including the *Abu Rakib*, *El Hundusi*, *Um Lassaf*, *Fatira*, *Um Ghamis El Hamra*, *Sitra*, and *Abu Diwan*, as well as other scattered areas belonging to the Shadli metavolcanics (El Habaak 1986, 2021; Khudier et al. 1989). The latter type (ferruginous cherts/jasper) have low values (<10 wt% total Fe_2O_3), and are generally related to submarine volcanic successions that are hosted mainly by weakly metamorphosed rhyolite tuffs and rhyolite instead of metamorphosed andesitic and basaltic tuffs. They form very-thin parallel layers ranging from a few centimeters to a few meters, and which are of subeconomic value. They crop out as ridges within the host tuffs and volcanic rocks, and are rather more restricted in lateral distribution (i.e., lensoidal in shape) with discontinuous extension coinciding with the main trend of their layering and schistosity. The banded nature of these ferruginous chert bodies with iron oxide composition (reddish hematite with scarce magnetite) alternate with light microcrystalline chert and jasper layers has led some researchers to consider them to be of the BIF mineralization type. However, they are not consistent with the features of a proper BIF, but instead have been attributed to low-temperature hydrothermal deposits related to underlying volcanic rocks (El Habaak 2021).

There are three genetic models for the Egyptian BIF: (1) Sedimentary origin, where the BIF was formed on a Precambrian continental shelf (e.g., El Aref et al. 1993; El Habaak and Soliman 1999). (2) Volcanogenic origin, where the BIF was formed via submarine volcanism and hydrothermal activity, which led to deposition of the oxides on the floor of an inter-arc or back-arc environments (Sims and James 1984; El Gaby et al. 1988; Takla et al. 1999; El Habaak 2005; El-Shazly and Khalil 2014). (3) Glaciogenic origin, where the BIF was formed by melting of glacial ice during interglacial periods of the Snowball Earth period (Ali et al. 2010; Stern et al.

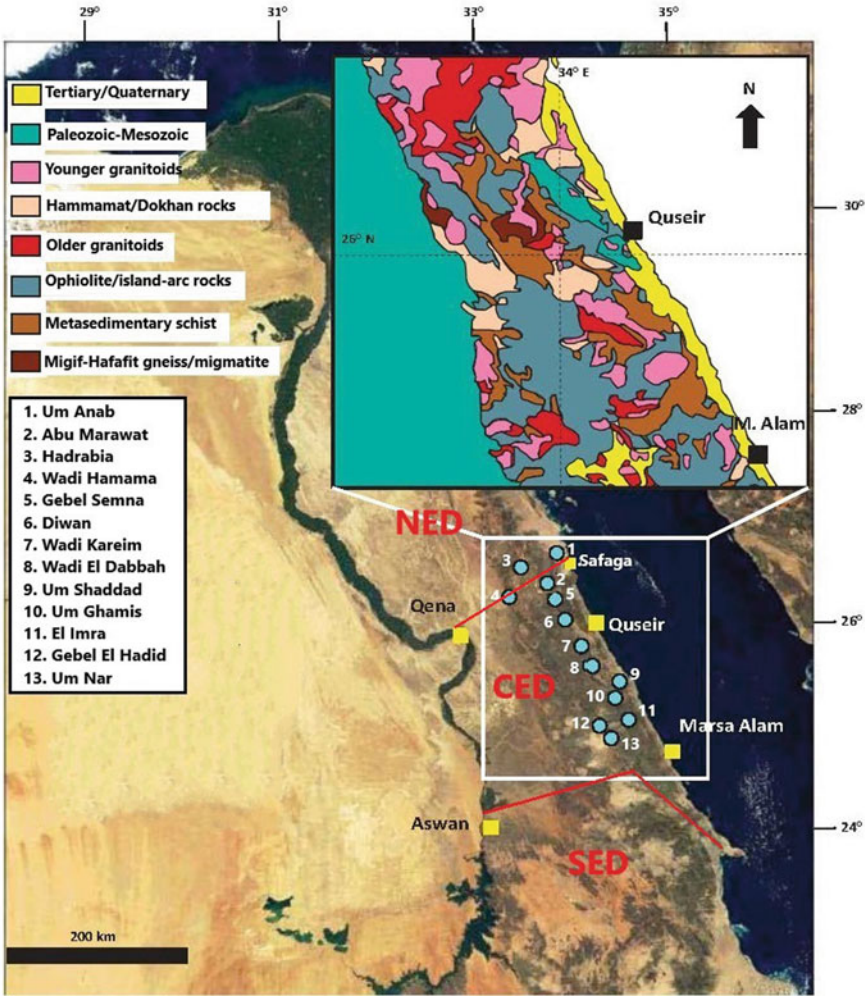

Fig. 7.7 Landsat image of Egypt showing the main locations of most important BIF occurrences (blue circles). Inset is a simplified geological map of the area outlined in the white rectangle (after Khalil et al. 2015)

2013). Furthermore, the BIF deposits of the El-Imra and Um Nar occurrences have been suggested to have been formed by a contact metamorphic/metasomatic effect (El Habaak 2004). Almost all the BIF localities in the Eastern Desert of Egypt share several geological features, including (El Habaak 2021) (1) regional deformation and metamorphism up to the greenschist facies, (2) contacts between BIF and surrounding rocks are generally sharp and easily recognized in the field, and (3) a common presence of fine lamination and slaty cleavages with preferred orientation.

Following is a brief description for the geology and mineralogy of the most important BIF localities in the Eastern Desert, starting from the north southward.

7.4.1 Um Anab Banded Iron Formation

The *Um Anab* area is located in the southern part of the North Eastern Desert (NED) of Egypt (Fig. 7.7); it is an exposure of the Neoproterozoic basement where various metavolcanic and plutonic rocks are abundant. The Um Anab metavolcanic rocks are mainly metapyroclastics, meta-andesites and metadoleritic basalts, intercalated with iron-rich bands (BIFs) and metasedimentary layers. The Um Anab area is considered to be a part of the Pan-African ophiolitic mélange, delimited by latitudes 26° 50′–26° 55′ N and longitudes 33° 30′–33° 40′ E. It is composed of a mixture of lenticular ophiolitic and volcano–sedimentary thrust sheets and blocks unconformably overlain by Dokhan volcanic and Hammamat sedimentary rocks (Fig. 7.8). Ophiolite stratigraphy in this area is largely dismembered and incorporated into tectonic mélange. The supracrustal belt consists of five major lithostructural domains with wide hiatus duration between them. They are autochthonous metasediments, island-arc association, syn-orogenic granitoids and magmatic arc Dokhan volcanics, foreland Hammamat clastic sedimentary rocks, and late- to postorogenic granites and related magmatism (Fig. 7.8). Metasedimentary rocks consist of fine-grained gneiss, migmatite, and a variety of quartzofeldspathic schist that represents the oldest rock unit in the area and probably represents a part of the Pre-Pan-African continental crust. Tectonic ophiolite mélange includes serpentinized ultramafic rocks located along the Wadi El Ghozah and Gebel Um Disi localities.

The Um Anab metavolcanic rocks represent a part of a large metavolcanic belt exposed along the Wadi Um Anab–Wadi Fatira El Zarqa site and the Wadi El Ghozah–Wadi Hammad site. The metavolcanic rocks have a thick sequence (~1500 m) of

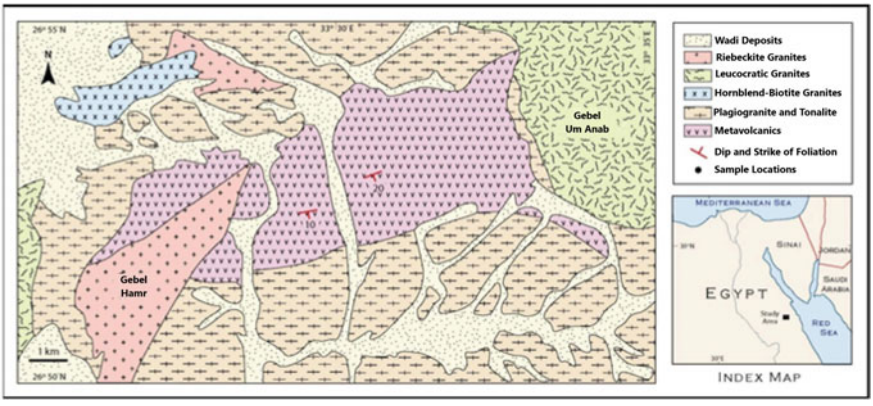

Fig. 7.8 Simplified geological map of the Um Anab area, NED of Egypt (after El-Tokhi et al. 2010)

lava flows of mafic-to-acidic composition with minor amounts of pyroclastic intercalations. They form an north-northeast-striking belt of ~13 km length and 3 km width extending from the Gebel Um Anab granite pluton westwards towards Gebel Hamr (Fig. 7.8). Metavolcanic rocks at Um Anab are intruded along sharp intrusive contacts by foliated quartz–diorite of the older granitoids. The metavolcanic rocks are also intruded by the younger granitoids of Gebel Um Anab, where there are numerous granitic dykes and offshoots intruded through the metavolcanic rocks. The Um Anab metavolcanic rocks are subdivided into three different rock units: (1) mafic rocks (amphibolites), (2) intermediate rocks (meta-andesites), and (3) acidic rocks (metafelsites and metarhyolites). All rock units in the area were subjected to regional metamorphism of the greenschist and amphibolite facies conditions.

The Um Anab BIF is the most distinctive occurrence in the NED; it is hosted by submarine island-arc volcaniclastic (pyroclastic and epiclastic) succession associated with restricted igneous activity. The BIF and host volcaniclastic horizon form a small belt, ~12 × 3 km, extending east-northeast, where the BIF is best developed in the upper (where it is ~13 m thick) and middle (where it is 6 m thick) parts of this horizon. The Um Anab BIF forms narrow discontinuous macrobands and lenses, up to 2 m thick, of limited lateral and vertical extension, where the BIF bands tend to thin and/or pinch out over long distances most probably due to ductile deformation. The BIF bands are fine grained, well-stratified and dominantly conformable with the enclosing tuff beds. It can be traceable laterally for a few tens of meters and is composed of greyish magnetite-rich or blood-red hematite-rich thin bands alternating with silica-rich bands (El Habaak 2021). Rhythmic layering of BIF and volcaniclastic packages are regionally folded, where the axes of the minor folds generally strike 105° N and plunge 70° E in the western part, and 30° E in the eastern part (Zalata 1972). Some of the BIF layers contain small irregular millimeter-sized veinlets composed of secondary quartz, chlorite, calcite, and several green epidote-rich laminae.

7.4.2 Abu Marawat Banded Iron Formation

The *Abu Marawat* BIF is part of the late Proterozoic metavolcanic rocks exposed in the southern part of the NED (Fig. 7.7). The BIF mineralization and associated metavolcanic rocks of Abu Marawat occurrence is mostly similar to the nearby Gebel Semna BIF; however, the Abu Marawat BIF is more metamorphosed and deformed than is the Gebel Semna BIF (see, e.g., Taman 2005). Metavolcanic rocks in both localities are calc-alkaline of intermediate-to-acidic compositions. The common presence of pillow lavas in the basalts of Abu Marawat area might indicate the presence of remnants of an ophiolitic association. This also can be supported by the presence of talc carbonate rocks in the area. The sedimentary structures described in the area indicate submarine deposition; however, the common synsedimentary deformations of BIF and associated metavolcanic rocks, along with slumping and microfaulting indicate deposition in unstable areas. The presence of ooidal texture in some parts of the Abu Marawat BIF is probably due to agitated water current.

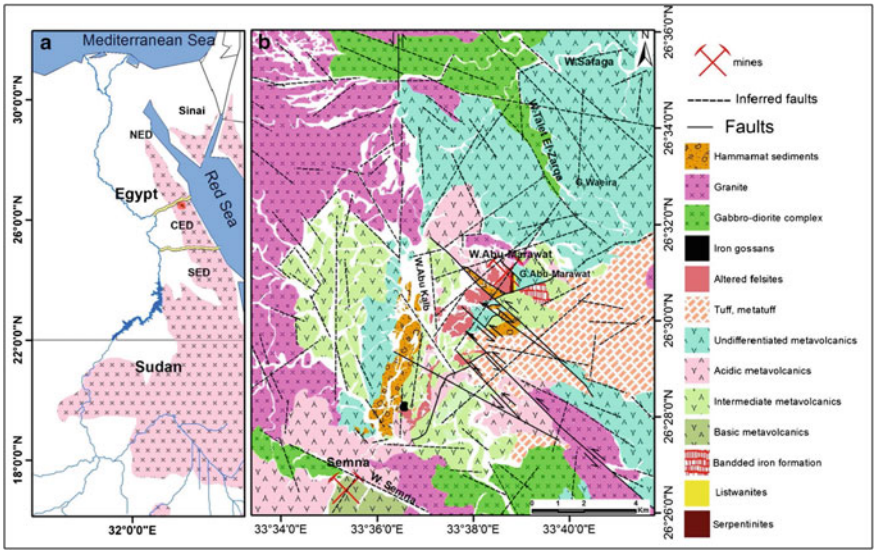

Fig. 7.9 **a** Regional geologic setting of the Arabian–Nubian shield in Egypt, Sudan, and part of Saudi Arabia. **b** Simplified geological map of Abu Marawat area (after Luo et al. 2020)

The Abu Marawat area covers an area of ~62 km^2, bounded by latitudes 26° 30′ 10″ and 26° 30″ 55 N and longitudes 33° 39′ 7″ and 33° 39′ 25″ E. The basement rocks exposed in the Abu Marawat area are, from older to younger, serpentinite, talc carbonate, and metavolcanic rocks with BIF and later intruded by arc granitoids (Figs. 7.9). Talc carbonate rocks and serpentinite are the oldest rock units, forming a curvilinear belt on the northern slope of Gebel Abu Marawat (Figs. 7.10a). Metavolcanic rocks are the most dominant rock type in the Abu Marawat area and form intercalating, moderately elevated layers ranging in thickness from 0.5 to 3 m. These rocks are highly folded and intercalated with BIF (Fig. 7.10b). The Abu Marawat metavolcanic rocks are intruded by granitoids as well as by mafic and felsic dykes in its west, northwest, and middle (Fig. 7.9b) (Luo et al. 2020). In the northern part, the metavolcanic rocks are intruded by metagabbro–diorite complex and granites (Fig. 7.9b). Metavolcanic rocks are unconformably overlain by a sequence of Hamamat sediments that trend NNE/SSW, particularly along Wadi Abu Kalb (Asran et al. 2013).

The BIF outcrops at Abu Marawat area are located mainly on the northern and southern parts of Gebel Abu Marawat, covering an area of 850 × 55 m^2. The sequence of the iron-bearing formation at Abu Marawat reaches a thickness of ~76 m, where the BIF is mainly present in the middle and upper parts of this sequence (El-Shafei 2011). It is similar to most of the world's BIF deposits where the bands are strongly persistent and show remarkable isoclinal, tight, and open-fold styles (Fig. 7.10b). The BIF bands are interlayered with slate, phyllite, and metavolcanic layers of variable thickness and repeated in a set of synclines and anticlines; this might be responsible for the

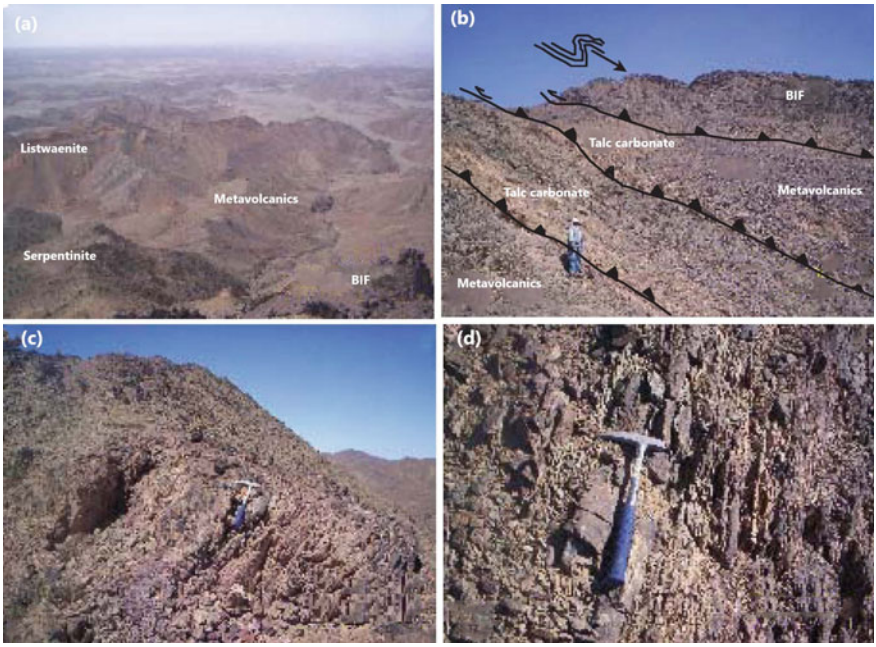

Fig. 7.10 Field photographs of **a** the northeastern side of Abu Marawat area showing BIF, serpentinite, and listwaenite rocks in contact with metavolcanic rocks, **b** imbricate thrust stacks along talc carbonate layers and metavolcanic rocks (note thrust-propagation folds in BIF), **c** highly altered and sheared felsic metavolcanic rocks, and **d** swarm of mineralized quartz veins developed along predefined shear fractures in altered rhyolite (after El-Shafei 2011)

increasing BIF thickness as well as the shortening of the bands' lateral extension (e.g., El-Shafei 2011). The BIF mineralization is present in three main intervals terminating three large depositional cycles (Fig. 7.11), each of which begins with a relatively thick tuffaceous mudstone of dark-green color and fine-grained texture at its lower part (Fig. 7.11a) that becomes yellowish-green and coarse-grained toward the middle of these cycles (Fig. 7.11b). The mudstone layers are terminated upward with the BIF-bearing intervals. The lower parts of these cycles show evidence supporting the deposition during shallow marine environment, which are confirmed by the appearance of yellowish-green and red tuffaceous mudstones, indicating deposition in a slightly oxidizing environment. The upper part of the three cycles was deposited in a more oxidized environment, where it contains red tuffaceous mudstones intercalated with red hematitic iron formation bands as the common setting of the Algoma-type BIF. The existence of the Abu Marawat BIF adjacent to and intercalated with metavolcanic rocks can be interpreted as the source of iron and silica, which were derived from hydrothermal sources associated with volcanic centers at the time of formation (e.g., El-Shafei 2011).

The Abu Marawat BIF bands strike roughly north/south with a dip angle of ~60° or more to the east direction. The individual BIF mesoband is 0.3–2 m in thickness and

Fig. 7.11 Field photographs of **a** large-scale stratigraphic cycles of BIF in the lower tuffaceous mudstone and sheeted BIF bands of the first cycle and **b** red tuffaceous mudstone and red thick hematitic BIF zone of the uppermost part of the depositional cycles (from El-Shafei 2011)

extends for ~5–800 m, comprising centimeter-scale alternating bands of iron oxides, jasper, and iron carbonates, where the Fe-rich bands are deep-brown to grey in color, ranging in thickness from 0.2 to 1.8 cm, and predominantly comprise hematite with subordinate magnetite. In some places, the BIF bands pinched out to form lensoidal bodies. On the other hand, the jasper and SiO_2-rich bands (0.5–2.8 cm thick) and lenses (up to 3 × 6 cm in extent) are brown to red. Iron carbonate bands (1–3 cm thick) display ooidal textures and slump structures in several places. In most cases, sedimentary structures are obliterated by metamorphism and deformation. The BIF layers are locally cut by milky-white quartz veins and veinlets rich in carbonate and nearly devoid of sulfides. Three folding generations (F1, F2, and F3) were defined in

the Abu Marawat area based on the recognized interference patterns, where the BIF shows the effect of superimposed folds and their sequence clearly at the summit of Gebel Abu Marawat, where early isoclinal northeast-trending F1 folds are refolded by F2 tight folds (El-Shafei 2011). The F1 folds are associated with boudin lines parallel to the foliation, whereas crenulation foliation is associated with F3 open folds, and the S-plunging F2 folds are refolded by F3 closed folds.

7.4.3 The Gebel Semna Banded Iron Formation

The *Gebel Semna* area is located ~15 km to the southwest of Abu Marawat; it is bounded by latitudes 26° 26′ 30″ and 26° 30′ N, and longitudes 33° 31′ 55″ and 33° 35′ 41″ E (Fig. 7.7). Similar to the Abu Marawat area, the essential rock units in the Semna area comprise serpentinite and related rocks, metavolcanic rocks, BIF, arc granitoids, and Hammamat sediments (Fig. 7.9). Serpentinite forms two small outcrops; a narrow belt ~1 km long on the eastern border of the map trending NW/SE between the Hammamat sediments and the granitoids. The second is a small circular body in its northwestern part. Metavolcanic rocks are the predominant rock units forming the conspicuous mass of Gebel Semna and its environs. Metavolcanic rocks form a thick-layered sequence, up to 10 m thick, of weakly metamorphosed volcaniclastic rocks with some volcanic intercalations and are divided into three horizons with unobvious contacts (Bishara and Habib 1973). The lower part of the Gebel Semna metavolcanic rocks is mostly formed of weakly metamorphosed volcaniclastic rocks comprising andesitic-to-dacitic tuffs, volcanic breccia, lapilli tuffs, and dust tuffs (Taman 2005). The middle part is represented by porphyritic and amygdaloidal tholeiitic basalt sheet trending NW/SE, forming the massive hills of Gebel Semna. The upper part is the BIF–hosting horizon, and consists of alternating bimodal metamorphosed volcaniclastic rocks and lavas of basaltic to dacitic compositions. Agglomerates are common in the lower part showing an upward decrease in grain size followed upward by an alternation of basalt-andesite and basaltic tuffs and the BIF. The lavas and volcaniclastic rocks are the essential host rocks for the BIF mineralization in Gebel Semna area.

The Gebel Semna BIF layers intercalated with volcaniclastic rocks and lavas and outcrop out in the northern foothills of Gebel Semna. Three macrobands reaching up to 3 m in thickness and extending for 1.4–5 km were recognized in the Gebel Semna area (Bishara and Habib 1973). They pinch out to the south and north; strike west-northwest/east-southeast to northwest/southeast and dip 25°–40° northward. Every macroband contains a variety of mesobands (3–7 bands, 10–60 cm thick). Each macroband and mesoband alternate with metatuffs. The mesobands are made up of alternating centimeter- to millimeter-scale bands of jasper and iron oxides.

7.4.4 Wadi Kareim Banded Iron Formation

The *Wadi Kareim* BIF represents the biggest well-known BIF occurrence in the CED. The Wadi Kareim area is located to the south of the Qift-to-Quseir road in the CED, and is bounded by latitudes 25° 59′–26° 04′ 54″ N and longitudes 33° 54′ 04″–34° 08′ 39″ E (Fig. 7.7). The area comprises the following rock units, from older to the younger (El Habaak 1992; Basta et al. 2011; Ghoneim et al. 2015): schists, ophiolitic serpentinite, metavolcanic rocks intercalated with BIF, intrusive metagabbros, older granites, younger granites, Dokhan volcanics, and alkaline volcanic rocks (Fig. 7.12). The Wadi Kareim area is largely occupied by metavolcanic rocks, which consists of tholeiitic and calc-alkaline lava flows intercalated with subordinate amounts of andesitic to dacitic pyroclastic and epiclastic rocks.

The metavolcanic and metavolcaniclastic belt of the Wadi Kareim area is locally intercalated with BIF in its middle part, where the BIF occurs as conformable bands and lenses at the top of metavolcanic ridges down to the Wadi Kareim level. The BIF here forms thick stratified bands, up to 10 m thick, and lenticular beds interbedded with andesitic–dacitic tuffs, fine-grained tuffs, and greywackes (Fig. 7.13a). The BIF bands comprise different facies, as follows: oxides, carbonates, silicates, and sulfides (which are laminated, massive, or granular) (Basta et al. 2011). Due to their resistance to weathering, the BIF bands commonly stand as ridges within their host rocks and are commonly faulted and folded, exhibiting major and minor folds (Fig. 7.13b). The thicknesses of the BIF bands vary from < 1 m up to about 12 m, and which

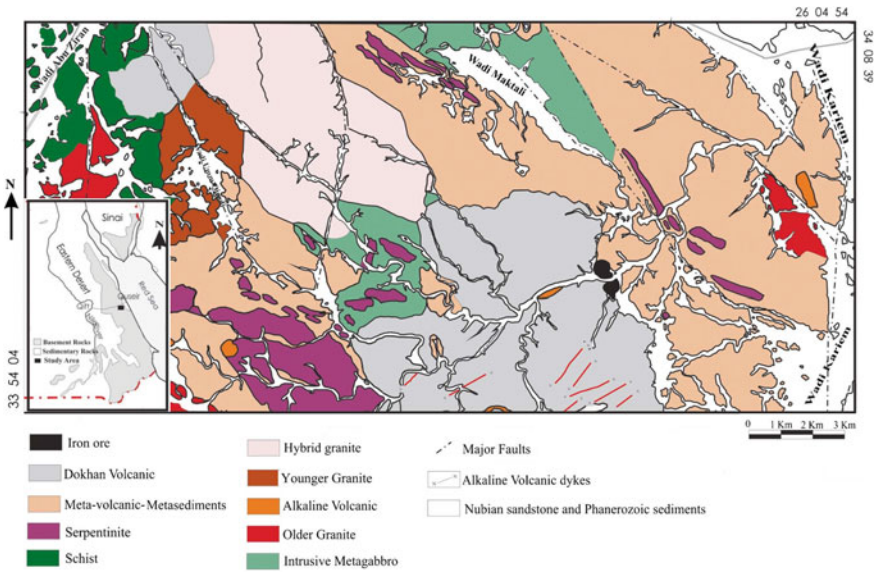

Fig. 7.12 Simplified geological map of the Wadi Kareim area and surroundings (from Ghoneim et al. 2015)

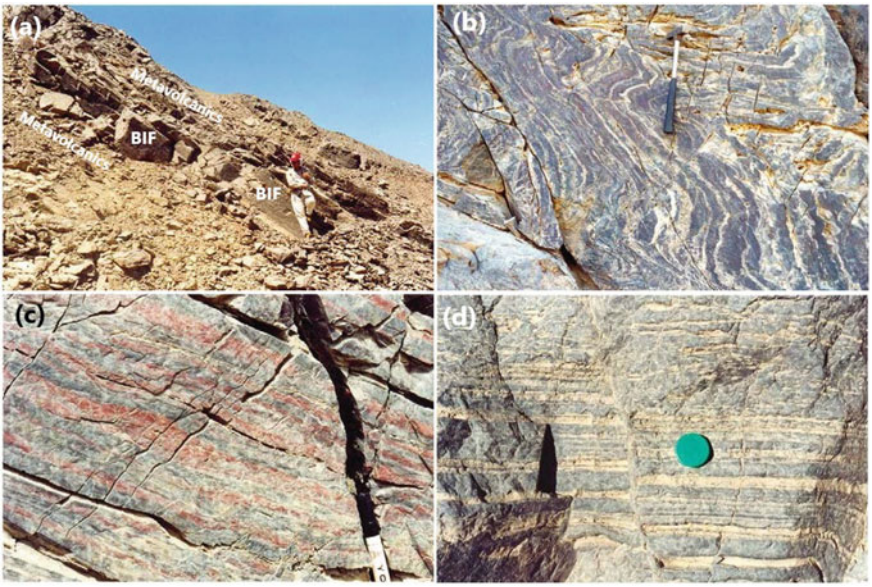

Fig. 7.13 Field photographs of the Wadi Kareim BIF, showing **a** BIF bands dip at high angle due *N*, **b** highly folded BIF bands with intercalated metavolcanic rocks, **c** BIF bands composed of jasper and iron mesobands, and **d** carbonate and Fe-oxide BIF mesobands, Wadi Karim BIF. Note the displacement of the BIF mesobands (from Basta et al. 2011)

generally increase going from northwest to southeast. The iron-rich bands in Wadi Kareim are well-bedded where mesobanding is clear, especially when the bands of gangue have a color different from that of the iron mesobands. The color of the gangue mesobands generally varies from red or violet to brownish-yellow or brown depending on whether jasper or carbonate mesobands are present (Fig. 7.13c, d). The carbonate-bearing areas of the BIF are found in the eastern part of the ore-bearing zone, whereas jasper is common in the western and central parts of the BIF-bearing zone (Basta et al. 2011). In the carbonate-dominated BIF, the carbonate mesobands are more weathered than the iron mesobands, which consequently stand out as ridges. Sometimes the gangue materials are present as lenses within the iron mesobands. The iron mesobands have sharp, straight contacts against the gangue mesobands, but wavy contacts are also encountered, especially against the carbonate mesobands.

The iron-rich bands with intercalated gangue layers of variable thicknesses show various sedimentary structures, including primary depositional structures, synsedimentary deformational structures, and biogenic structures. Rhythmic banding and laminations are the most common primary sedimentary structure where Fe-rich and Fe-poor layers, bands, or laminas rhythmically alternate. Five scales of banding are recognized in the Wadi Kareim BIF, as follows: macrobands, calamine cyclothem, mesobands, microbands, and submicrobands (El Habaak 2021). BIF macrobands (0.5–10 m in thickness) are composed of rhythmic alternations of Fe-rich bands and

Fe-free calcareous tuffs or fine-grained tuffs. The calamine cyclothem shows cyclic sequences of metatuffs and Fe-rich macrobands. Meso- and microbands are often observed in the BIF macrobands due to variations in mineral composition, grain size, and color. Microbands show alternations of thin, less than 200-μm-thick, parallel discontinuous, or wavy submicrobands of different mineral compositions and/or grain sizes. The iron minerals of all BIF scales are represented by magnetite, hematite, goethite, siderite, greenalite, stilpnomelane, minnesotaite, while pyrite, chalcopyrite, and sphalerite are present in minor amounts. Several mineral assemblages are differentiated in the Wadi Kareim BIF, including magnetite–chert, magnetite–hematite–jasper, algal chert–magnetite, hematite–magnetite–siderite, magnetite–greenalite, pyrite–magnetite–greenalite, massive iron silicate band, and granular iron silicate band assemblages.

7.4.5 Wadi El Dabbah Banded Iron Formation

The *El Dabbah* group is an ~7500 m-thick sequence of metavolcanic rocks, volcaniclastics, and BIF (Kiyokawa et al. 2020), located to the southeast of Wadi Kareim area in the CED (Fig. 7.7). Wadi El Dabbah area is mainly occupied by calc-alkaline and tholeiitic metavolcanic and metasedimentary rocks, serpentinites, older granites, Hammamat sedimentary rocks, and younger granites (Fig. 7.14). A thick sequence of low-grade metavolcanic and volcaniclastic rocks are well-exposed in the Wadi El Dabbah area of the CED (e.g., Maurice 2000; Ali et al. 2009; Kiyokawa et al. 2020). These rocks are located between the well-studied El-Sibai complex area (e.g., Fowler et al. 2007) and the Kareim basin in the CED. The sequence of metavolcanic–volcaniclastic rocks of the El Dabbah area contains well-preserved volcano–sedimentary structures, including pillow lavas, accretionary lapilli, graded volcanic tuffs, parallel laminated tuffs, and BIF sequences, indicating that the sediments were formed in an island-arc setting (Kiyokawa et al. 2020). There are four identified geological units in the Wadi El Dabbah area (Fig. 7.14): (1) The *El Dabbah group* of island-arc-related metavolcanic and volcaniclastic rocks (Fritz and Messner 1999), (2) the Atshan formation of metamorphosed subaerial sedimentary basin, (3) less-deformed terrigenous sedimentary rocks (the southern Kareim basin) that have been interpreted to be Hammamat group sediments (Fritz and Messner 1999; Wilde and Youssef 2002), and (4) weakly deformed granite and porphyry intrusions.

The metavolcanic and volcaniclastic rocks of the El Dabbah group were subject to lower greenschist-facies metamorphism (El-Shazly and Khalil 2016). These rocks can be subdivided into four fault-bounded domains (Fig. 7.14) (Kiyokawa et al. 2020): the northeast, southeast, northwest, and southwest domains. The El Dabbah fault is a remarkable sign in the area and is located within the north/south-trending area of Wadi El Dabbah; the east/west-trending and north-dipping normal faults are subdivided into four domains. The eastern boundary of the metavolcanic–volcaniclastic sequence is a northwest/southeast-trending fault and the western boundary is a north/south-trending fault that separates the sequence from the Atshan formation. The

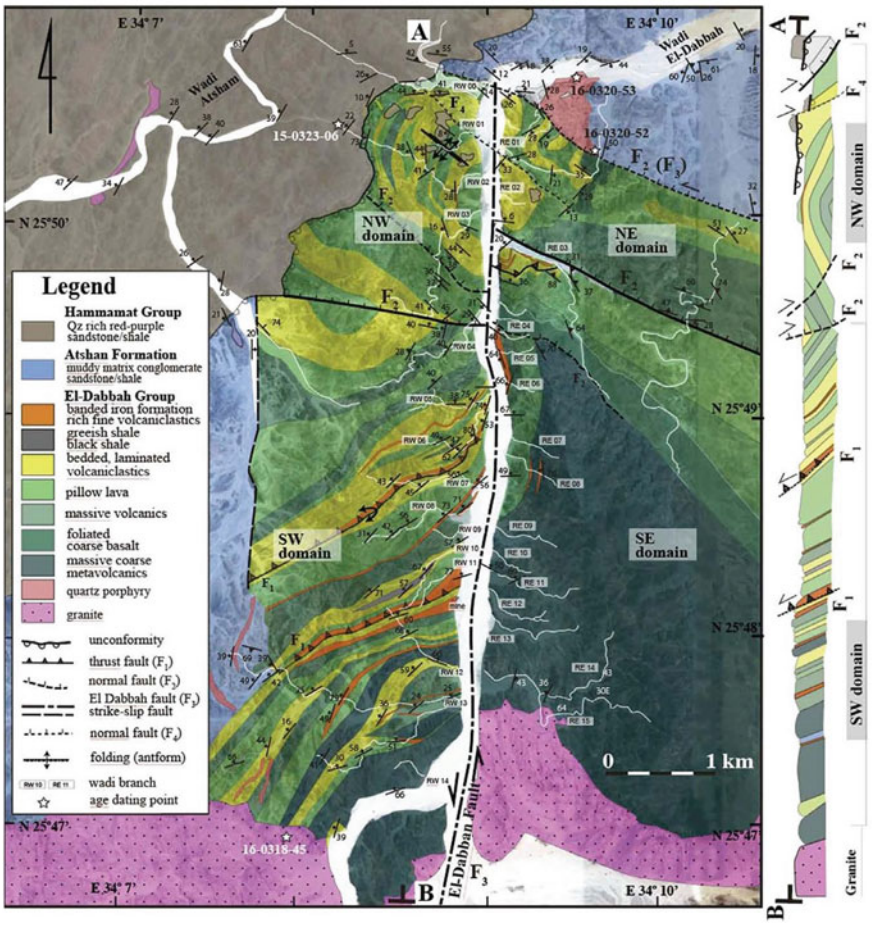

Fig. 7.14 Simplified geological map of the Wadi El-Dabbah area superimposed on an image from Google Earth map. The right image from map shows N/S cross section of the northwest and southwest domains. Scale of the cross-section is the same as map (from Kiyokawa et al. 2020)

northern boundary is an unconformable contact with the overlying Hammamat group sediments and the southern boundary is an intrusive contact with granite (Fig. 7.14).

The BIF horizon in Wadi El Dabbah area is mainly found in the southwest domain of the El Dabbah group; the total estimated thickness of this domain is ~4200 m. The El Dabbah group in the Wadi El Dabbah area is divided into three stratigraphic units (Fig. 7.15) (Kiyokawa et al. 2020): the lower El Dabbah, middle El Dabbah, and upper El Dabbah formations. The total thickness of the group is ~7500 m. The lower El Dabbah formation is represented by the massive volcanic rock unit in the southeast and southwest domains. The total thickness of this unit is ~4000 m, consisting of coarse-grained massive volcanic rocks and microgabbro interbedded with thin layers of volcaniclastic rocks and minor fine-grained dolerite. The lower boundary of this

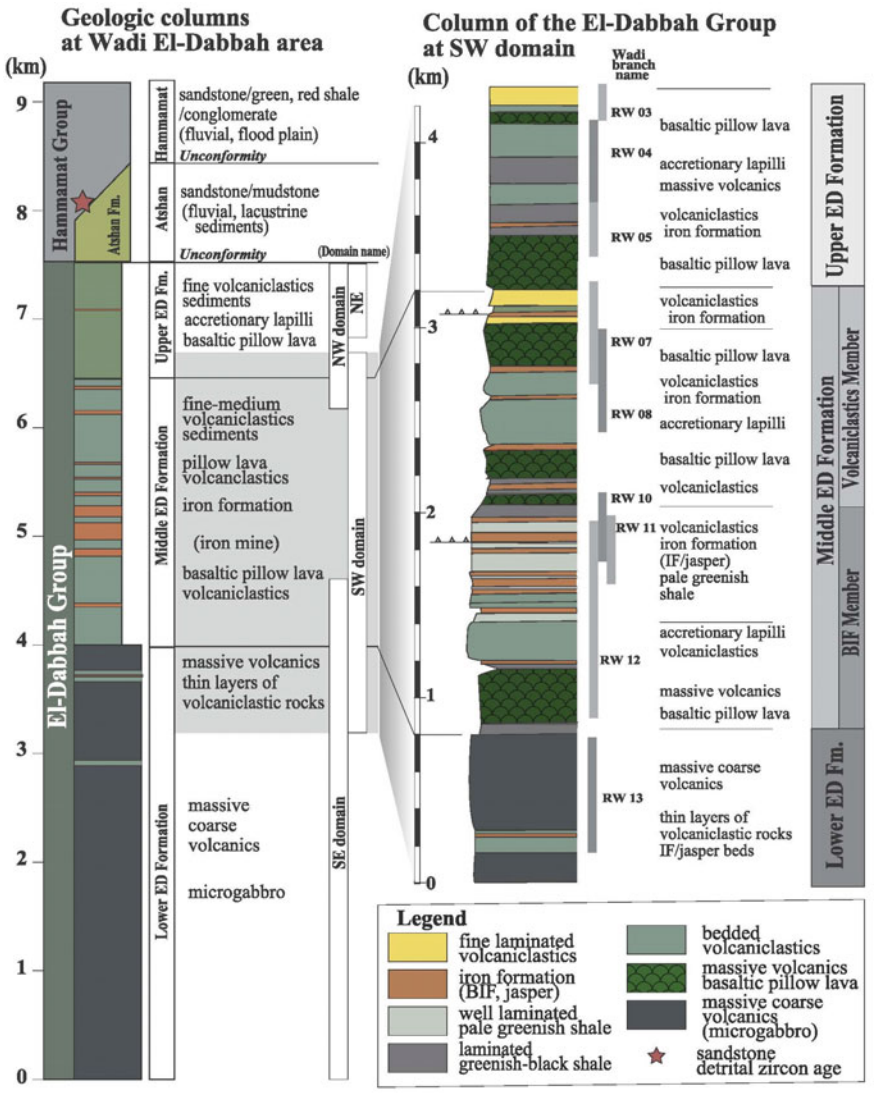

Fig. 7.15 Composite stratigraphic section of the Wadi El-Dabbah area (left) and a more detailed stratigraphic column of the southwest domain (right) (from Kiyokawa et al. 2020)

unit is poorly constrained due to the intrusion of hornblende–biotite granite into the lower part. The upper parts of the lower El Dabbah formation consist of thin layers of volcaniclastic rocks and iron-rich and jasper-bearing beds.

The middle El Dabbah formation is ~2500 m thick, including volcaniclastic sedimentary rock in the southeast domain and the volcaniclastic-BIF of the southwest domain (Fig. 7.15). It contains numerous massive basaltic lavas, pillow lavas, and

a metavolcanic–volcaniclastic sequence that is interbedded with fine-grained tuff beds, iron-rich beds, and BIF. This formation is subdivided into a BIF member and a volcaniclastic member (Fig. 7.15). The BIF memberconsists of basal massive lava flows, pillow lavas, and thick-bedded volcaniclastic rocks, with a number of fine-grained sedimentary sequences that include finely laminated volcanic rocks, black shales, iron-rich beds, and BIF. The volcaniclastic rocks and basaltic pillow lavas form beds that are a few meters thick and occur within tuffs and BIF. The BIF includes thin jasper layers, typically 2–4 m thick, that crop out on both banks of Wadi El Dabbah. The volcaniclastic member contains a thick (10–40 m) succession of volcaniclastic rocks, basaltic pillow lavas and some BIF. Some of the BIF (less than 1 m in thickness) is preserved within fine volcaniclastic sequences.

The upper El Dabbah formation is represented by a sequence of volcanic lava and volcaniclastic rocks of the southwest domain and the metavolcanic–volcaniclastic sequence of the northeast and northwest domains (Fig. 7.15). The total thickness of this formation is at least 1000 m, comprising volcaniclastic sediments, minor basaltic pillow lavas, and extensively reworked cross-stratified volcaniclastic rocks. Accretionary lapilli tuffs are partly preserved within greenish volcaniclastic sediments. Thin iron-rich beds and black shales are intercalated with greenish volcaniclastic rocks and basaltic pillow lavas. The upper boundary of the formation is defined by the unconformity below the Hammamat group. Fault contacts with the Atshan formation have also been observed.

The Wadi El Dabbah BIF bands are essentially represented by oxide and silicate facies, whereas sulfides and carbonates are found as minor constituents. Sulfide minerals are restricted to the lower parts of the sequence and silicate in the middle part. The BIF is crosscut at least by two generations of quartz veins; the early quartz veins are tightly folded and up to a few centimeters wide. The later quartz veins range in width from a few centimeters to about 40 cm and are highly controlled perpendicular to the bedding (El Habaak 2021). In addition to the lamination, the BIF displays several sedimentary structures, including graded bedding, slumping, convolute, and cross lamination, micro- to mesoscale microfaulting, and microfolding, which may be the result of soft-sediment deformation. Boulders and lenses of the laminated tuffs are encountered embedded within some BIF macrobands. Oolitic and pisolitic structures are also detected where discrete or coalesced ooides and pellets of oxide and carbonate minerals are observed. Some ooides are limonitic in composition, brown and closely packed or stratified in trains.

7.4.6 Um Shaddad Banded Iron Formation

Um Shaddad is located at the eastern flank of the CED, close to the Red Sea coast, within an area known as Um Gheig (Fig. 7.7), which is chiefly composed of highly deformed sequence of ophiolitic serpentinite, metavolcaniclastic rocks, schists, and metagabbro. These highly deformed rocks overlain by high-grade metamorphic migmatite, gneissic tonalite–granodiorite, and sheared granites (Fig. 7.16).

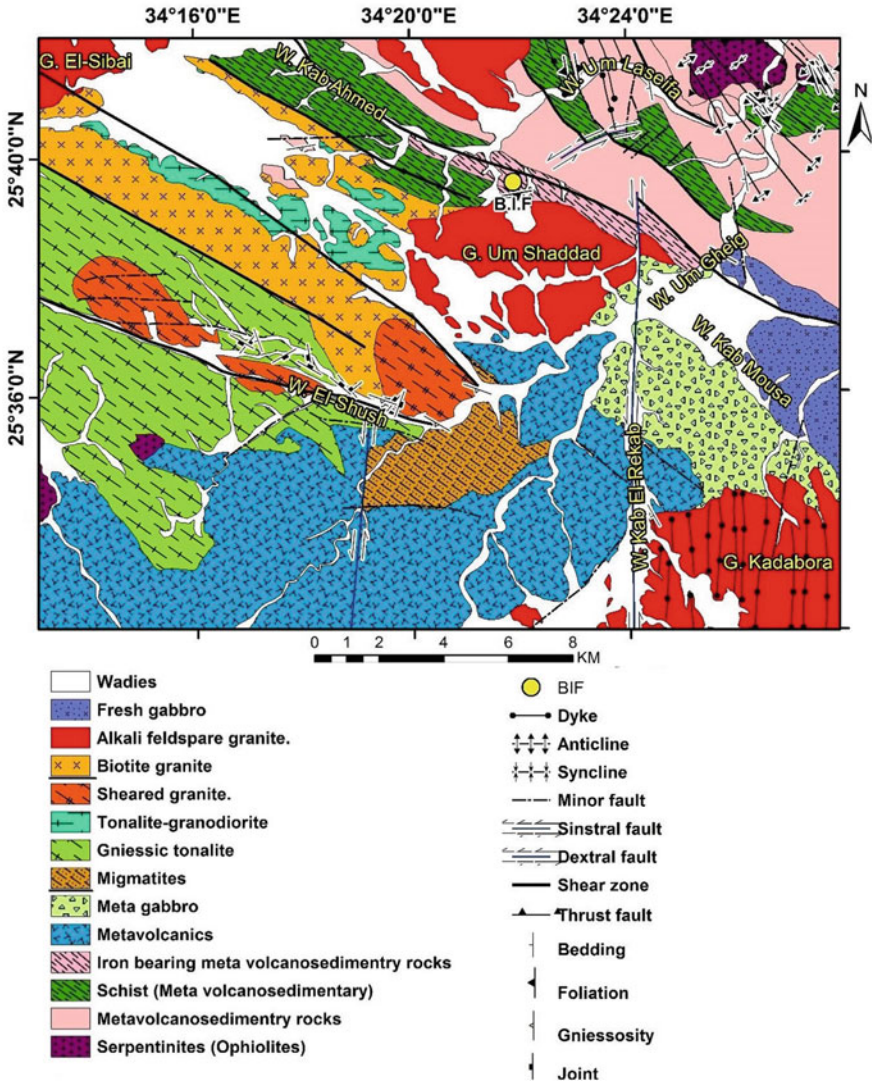

Fig. 7.16 Simplified geological map of Wadi Um Gheig area, showing the location of the Um Shaddad area (after Abu El-Leil et al. 2017)

All of these older rocks in the area had been intruded by syntectonic tonalite to granodiorite, late-to-post-tectonic granitoids, and fresh gabbro. The Um Shaddad BIF is hosted by island arc assemblage that comprises the cover nappe of low-grade metavolcano–sedimentary rocks and metavolcanic and metagabbro sequences covering the northern and the southern parts of the Um Gheig area (Fig. 7.16) (Abu El-Leil et al. 2017). The metavolcano–sedimentary rocks constitute the upper horizon of the

island-arc assemblage, which are differentiated into three sections: (1) the upper, highly folded metavolcano–sedimentary rocks that overthrusted by serpentinite rock units, (2) the high-schistose rocks intercalated with talc carbonate rocks, and (3) the metavolcano–sedimentary rocks associated with the BIF.

The Um Shaddad BIF is a limited occurrence that is exposed in the middle portion of the Um Gheig area (Fig. 7.16). No available detailed work has been carried out on this BIF occurrence in terms of its mineralogy, geochemistry, or genesis. This occurrence is best-preserved in a localized narrow area of uneconomic potential, is hosted by volcanic succession, and the equivalent volcaniclastic rocks are most probably of island-arc affinity. Any transition between BIF and host rocks was not observed, where BIF is less continuous due to the complex structure pattern affected the area. The Um Shaddad BIF is generally rust-colored iron–silicate–magnetite rock, which is considered to be weathered oxide–silicate BIF facies. The BIF is finely banded, strongly magnetic, and shows slaty or fissile appearance. The Um Shaddad BIF has thin alternating black and reddish-green or brown bands, as well as discontinuous lenses, up to 1 m thick, of limited lateral extent. The strongly magnetic black BIF layers are composed of coarse-grained magnetite, hematite, mica, goethite, and quartz, while the reddish-green layers are composed of pyroxene, epidote, and chlorite, and the brown layers are rich in garnet and magnetite (El Habaak 2021). The BIF commonly contains significant platy hematite and magnetite porphyroblasts that suffered extensive martitization.

7.4.7 Um Ghamis Banded Iron Formation

The Um Ghamis (also called *Um Ghamis El Zarqa*) area is mainly occupied by ophiolitic mélange and intrusive rocks; it is located to the southwest of the Um Shaddad occurrence in the CED (Fig. 7.7). The BIF is best exposed at the beginning of Wadi Um Ghamis, forming discontinuous lenses of limited lateral distribution. It is hosted mainly by submarine folded calcareous volcano–sedimentary successions, 2.3 × 1.6 km in extent, accompanied by limited syndepositional arc lava flows of calc-alkaline low-K andesitic-to-dacitic composition. The whole succession, including the BIF and country rocks, is affected by low-grade regional metamorphism up to greenschist facies. The layers of andesitic tuffs are characterized by conspicuous dark-grey-to-green beds intercalated with deep-brown-to-black BIF bands. They form beds of variable thickness exhibiting various synsedimentary and diagenetic structures including convolute bedding, graded bedding, and parallel lamination.

The Um Ghamis BIF mineralization is up to 5 m thick, forming a single narrow horizon within the volcaniclastic layers, which are discontinuous over a distance of ~1.5 km. Individual BIF layers of ~1–5 cm show evidence of fine-scale layering within the main bands. BIF bands are mainly composed of oxide and rarely silicate and/or carbonate facies with sharp boundaries with the host rocks. The BIF mineralization is clearly grey in appearance and fine-grained, sometimes showing a metallic

luster. The iron-rich bands alternate with voluminous bright-red jasper and silica-rich bands. The common presence of chert/jasper and pillow basalts in association with the volcaniclastic rocks is consistent with a submarine environment origin for the volcanic rock eruptions. The bedding and fine laminations indicate deposition under weakly turbulent conditions, probably resulting from the collapse of suspended sediment clouds generated by volcanic eruptions (Lowe 1988). The BIF succession thus most probably originated within hydroclastic shallow, subaqueous eruptions (El Habaak 2021).

7.4.8 Gebel El Hadid Banded Iron Formation

The Gebel El Hadid area is located very close to the southern part of the CED, between latitudes 25° 20′ through 25° 24′ N and longitudes 34° 07′ through 34° 09′ E (Fig. 7.7). The Gebel El Hadid BIF is one of the biggest in the CED; its estimated ore reserves is ~3.6 Mt with an average grade of 45.7 wt% Fe (Akaad and Abu El Ela 2002). The area is a part of the Neoproterozoic island-arc basement in the CED; it is dissected by a major east/west-striking and south-dipping thrust (Fig. 7.17) (Khalil et al. 2015). The northern part of Gebel El Hadid is mainly occupied by foliated and folded metavolcanic rocks and very small outcrops of serpentinite and metagabbro. The southern part of the area comprises metavolcaniclastic rocks associated with BIF (Fig. 7.17). These metavolcaniclastic rocks are dominated by lapilli tuffs interbedded with BIF-bearing metamudstone of tuffaceous origin. The contact between the metavolcaniclastic rocks and the BIF-bearing unit is almost gradational.

The Gebel El Hadid BIF-bearing unit is composed mainly of closely spaced tabular conformable layers of iron-rich bands within the metavolcaniclastic rocks (Fig. 7.18a, b). The whole thickness of the BIF-bearing metavolcaniclastic unit is ~900 m, while the thickness of the iron-rich bands vary from a few centimeters up to 5 m, and are extending ~1–2 km along strike. The whole sequence of the Gebel El Hadid area has been regionally metamorphosed under greenschist facies conditions during the Pan-African orogeny. Primary structures as bedding and laminations are the most common preserved sedimentary features in the iron-rich bands. The black BIF layers are sometimes locally contained, randomly dispersed microbands and pods of jasper and/or carbonate, mostly oriented parallel to the bedding of the host BIF. The colors of BIF mesobands generally vary from dull red to brownish-yellow or white depending on whether jasper or carbonate is predominant. The jasper-rich microbands and pods are composed of cherty silica with red iron oxide dust. In addition, volcaniclastic intercalations within the iron-rich bands are also common and occur either as thin bands (up to 50 cm thick) or as lenses having dimensions of up to 30 × 100 cm (Khalil et al. 2015).

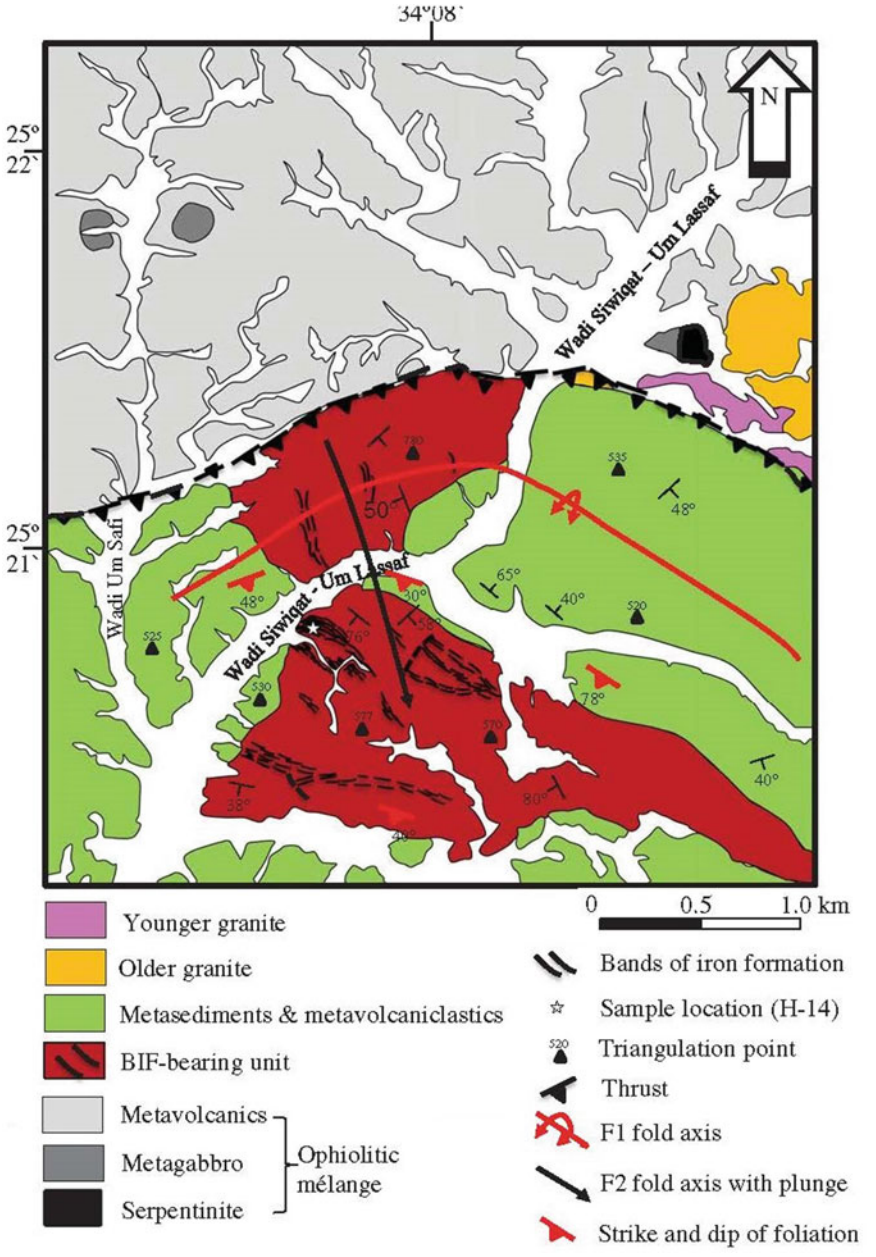

Fig. 7.17 Simplified geological map of the Gebel El Hadid area, CED, Egypt (from Khalil et al. 2015)

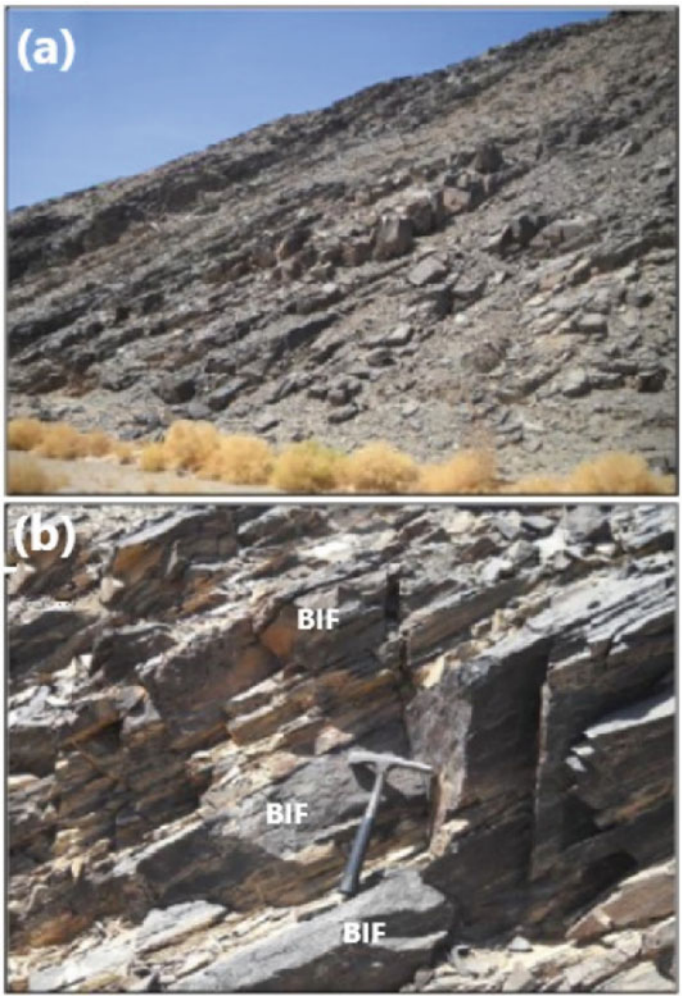

Fig. 7.18 Field photographs of **a** lineation in interlayered BIF and metavolcaniclastic rocks and **b** banding and layering structure of the BIF of Gebel El Hadid area (from Khalil et al. 2015)

7.4.9 The Um Nar Banded Iron Formation

The Um Nar area represents the southernmost exposure of BIF occurrences in the CED, and is located between latitudes 25° 14′ 32″ to 25° 16′ 7″ N and longitudes 34° 14′ 50″ to 34° 19′ E (Fig. 7.7). The Um Nar area comprises the following rock units (Fig. 7.19), arranged from older to younger (El-Shazly and Khalil 2014): (1) a large serpentinite mass, (2) two types of schists (BIF-bearing and barren schist), (3) a gabbroic intrusion (Abu Lijam diotrite–metagabbro), and (4) two granitic intrusions (Al-Mayit cataclastic mylonitic granite and Abu Karahish older granite). The schists

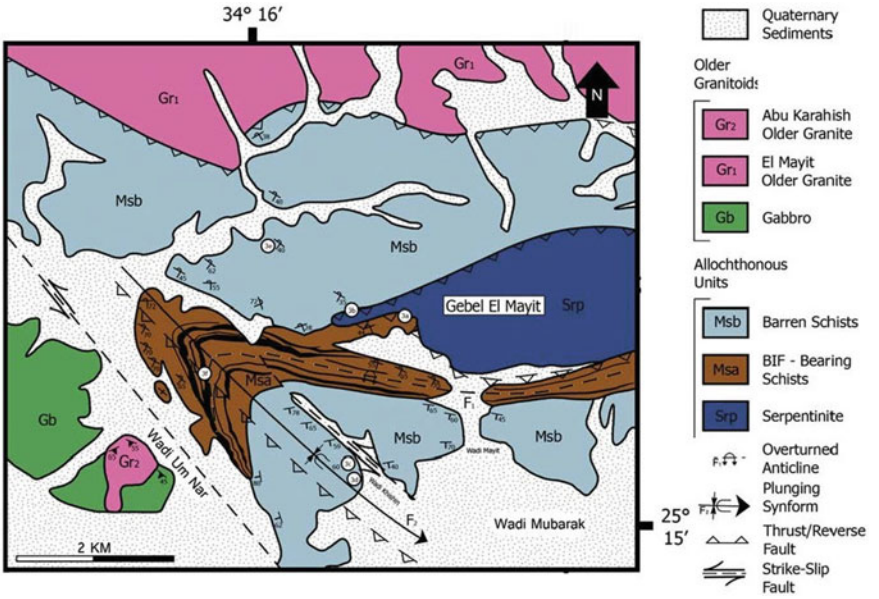

Fig. 7.19 Simplified geological map of the Um Nar area, where the BIF deposits are represented schematically in black within the metasedimentary schists (Msa) (from El-Shazly and Khalil 2014)

are metamorphosed tuffs, mudstones, and greywackes of the island-arc unit, and are known as the *El-Mayit metavolcanics*. The older schist units has prominent pebbly horizons and lacks BIF bands, while the younger unit is intercalated with up to 52 seams of BIF bands ranging in thickness from a few centimeters to 5 m (El-Shazly and Khalil 2014). Numerous rhyolitic to dacitic dikes and sills (0.5–7.5 m thick) commonly intrude both types of schist units, and are considered to be part of the older granitoids.

The Um Nar BIF occurrence is characterized by medium- to coarse-grained textures of alternating oxides and silicate bands that are parallel to the foliation of host rocks. The silicate-rich bands are dominated by quartz that commonly contains micrometer-sized hematite inclusions, giving rise to its dusty hematite or salt-and-pepper texture (El-Shazly and Khalil 2014). Millimeter-wide bands of garnet, epidote, magnetite, and small amounts of calcite are also occur in some of the silicate bands. Magnetite and hematite are the main iron minerals found in the oxide bands; their relative abundance varies from band to band, giving rise to a magnetite and hematite-dominant facies. Garnet-bearing Fe-skarn banded zones, up to 2 m thick, have been recognized (El Habaak 2004) adjacent to the BIF horizon in the Um Nar area. This might be developed during the low-pressure thermal metamorphism of a Neoproterozoic calcareous-rich BIF. This skarn is calcic, K-poor, and highly oxidized, which lies adjacent to the margin of the granodiorite intrusion and confined to the anticline. The skarn-bearing zones are well-developed as continuous or discontinuous layers and lenses in the southern part of the eastern limb of the fold.

The skarn zone has a gradational contact with the biotite schist and shows rhythmically layered ribbons of dark magnetite-rich and pale calc-silicate bands. The bands of skarn zone are unstrained and characterized by medium- to coarse-grained texture, as well as they are showing alignment of amphibole, epidote, and magnetite.

References

Abu El-Leil I, Bekiet MH, Soliman NMA, El-Hebiry MS (2017) Compressional—extensional deformation on the Neoproterozoic rocks, Eastern Desert, Egypt: a geological and structural complemental study of Um Gheig area. Al Azhar Bull Sci 9:1–24

Akaad MK, Abu El Ela AM (2002) Geology of the basement rocks in the eastern half of the belt between Latitudes 25° 30′ and 26° 30′ N Central Eastern Desert Egypt. Geol Surv Egypt 78:1–118

Al Shanti AMS (2009) Mineral deposits of the Kingdom of Saudi Arabia. Scientific Publishing Center, King Abdulaziz University, Jeddah, Saudi Arabia

Al-Hazzaa AF (1973) Evaluation of iron deposits on the Arabian Shield, Saudi Arabia. MSc thesis, University of Arizona

Al-Khirbash S, Heikal MTS, Whitehouse MJ, Windley BF, Al Selw K (2021) Evolution and mineralization of the Precambrian basement of Yemen. In: Z Hamimi et al (eds) The geology of the Arabian-Nubian shield, regional geology reviews, pp 633–657

Ali KA, Stern RJ, Manton WI, Kimura J-I, Khamees HA (2009) Geochemistry, Nd isotopes and U-Pb SHRIMP zircon dating of Neoproterozoic volcanic rocks from the Central Eastern Desert of Egypt: new insights into the ~750 Ma crust-forming event. Precambr Res 171:1–22

Ali KA, Stern RJ, Manton WI, Kimura J-I, Whitehouse M, Mukherjee SK, Johnson PR, Griffin WR (2010) Geochemical, U-Pb zircon and Nd isotopic investigations of the Ghawjah Metavolcanic rocks, Northwestern Saudi Arabia. Lithos 120:379–392

Asran AM, Bekir RK, Abdel Rahman E, Abdel El-Rashed A (2013) Petrography, geochemistry and remote sensing data of island arc assemblage along Wadi Abu Marawat, Central Eastern Desert, Egypt. Arab J Geosci 6:2285–2298

Basta FF, Maurice AE, Fontboté L, Favarger P-Y (2011) Petrology and geochemistry of the banded iron formation (BIF) of Wadi Karim and Um Anab, eastern desert, Egypt: implications for the origin of Neoproterozoic BIF. Precambr Res 187:277–292

Bekker A, Slack JF, Planavsky N et al (2010) Iron formations: the sedimentary product of a complex interplay among mantle, tectonic, oceanic, and biospheric process. Econ Geol 105:467–508

Bishara WW, Habib ME (1973) The Precambrian banded iron ore of Semna, eastern desert Egypt. Ann Geol Surv Egypt 12:29–45

Collenette P, Grainger D (1994) Mineral resources of Saudi Arabia. DGMR special publication, Ministry of Petroleum and Mineral Resources, Jeddah, KSA

Dardir AA, El Chimi KAM (1992) Geology and geochemical exploration for gold in the banded iron formation of Um Nar area, central Eastern Desert, Egypt. Ann Geol Surv Egypt XVIII:103–111

Davies FB, Grainger DJ (1985) Geologic map of the Al Muwaylih quadrangle, sheet 27A, Kingdom of Saudi Arabia, with explanatory notes. Saudi Arabian Deputy Ministry for Mineral Resources, Geoscience Map GM-82, pp 32, scale 1:250,000

Dixon AJ, Ashworth KL (1994) Wadi Sawawin iron-formation deposits. In: Collenette P, Grainger DJ (compilers) Mineral resources of Saudi Arabia. Saudi Arabian Directorate General of Mineral Resources Special Publication DGMR-SP-2:133–137

Doebrich JL, Al-Jehani AM, Siddiqui AA, Hayes TS, Wooden JL, Johnson PR (2007) Geology and metallogeny of the Ar Rayn terrane, eastern Arabian shield: evolution of a Neoproterozoic continental-margin arc during assembly of Gondwana within the East African Orogen. Precambr Res 158:17–50

E1-Tokhi M, Alaabed S, Amin BEM (2010) Late Precambrian Metavolcanics of Um Anab north eastern desert, Egypt. Geochem Tectonic Environ Stud. Eur J Sci Res 42:507–524
El Aref MM, Abdel Wahed M, El Dougdoug A, Manawi A (1993) Diagenetic and metamorphic history of the Umm Nar BIF, Eastern Desert, Egypt. Miner Deposita 28:264–278
El Gaby S, List FK, Tehrani R (1988) Geology, evolution and metallogenesis of the Pan-African belt in Egypt. In: El Gaby S, Greiling RO (eds) The Pan-African belt of northeast Africa and adjacent areas. Braunschweig (Vieweg), Wiesbaden, pp 17–68
El Habaak GH (1986) Geology of Um Samiuki area, Eastern Desert, Egypt. MSc thesis, University of Assiut, Egypt, pp 188
El Habaak GH (1992) Geology of banded iron formation and associated metavolcanics at Wadi Kareim area, Eastern Desert, Egypt. Dissertation, University of Assiut, Egypt, pp 388
El Habaak GH (2004) Pan-African skarn deposits related to banded iron formation, Um Nar area, central Eastern Desert, Egypt. J Afr Earth Sci 38:199–221
El Habaak GH (2005) Petrogenesis and tectonic implications on the rock succession hosting banded iron formation at Um Anab area, north Eastern Desert of Egypt. In: 4th international conference on the geology of Africa, vol 2, pp 479–514. Assiut, Egypt
El Habaak GH (2021) Banded iron formation in the Egyptian Nubian shield. In: Hamimi Z, Arai S, Fowler AR, El-Bialy MZ (eds) The geology of Egyptian Nubian shield, regional geology reviews, pp 425–486
El Habaak GH, Soliman MF (1999) Rare earth element geochemistry of the Egyptian banded iron formations and the evolution of the Precambrian atmosphere and ocean. 4th international conference on geochemistry. Alexandria University, Egypt, pp 149–160
El-Gaby S, List FK, Tehrani R (1990) The basement complex of the Eastern Desert and Sinai. In: Said R (ed) The geology of Egypt. Balkema, Rotterdam, pp 175–184
El-Shafei MK (2011) Structural control on banded iron formation (BIF) and gold mineralization at Abu Marawat area, Central Eastern Desert, Egypt. J King Abdulaziz Univ (JKAU) Earth Sci 22(2):155–183
El-Shazly AK, Khalil KI (2016) Metamorphic and geochronologic constraints on the tectonic evolution of the Central Eastern Desert of Egypt. Precambr Res 283:144–168
El-Shazly AK, Khalil KI (2014) Banded iron formations of Um Nar, Eastern Desert of Egypt: P-T–X conditions of metamorphism and tectonic implications. Lithos 196–197:356–375
Fowler AR, Khamees H, Dowidar H (2007) El Sibai gneissic complex, Central Eastern Desert, Egypt: folded nappes and syn-kinematic gneissic granitoid sheets–not a core complex. J Afr Earth Sci 49:119–135
Freitas BT, Warren LV, Boggiani PC, Paes de Almeida R, Piacentini T (2011) Tectono-sedimentary evolution of the Neoproterozoic BIF-bearing Jacadigo Group, SW Brazil. Sed Geol 238:48–70
Fritz H, Messner M (1999) Intramontane basin formation during oblique convergence in the Eastern Desert of Egypt: magmatically versus tectonically induced subsidence. Tectonophysics 315:145–162
Galmed MA, Abuamarah BA, Ghrefat HA, Al-Zahrani AA (2021) Petrology of oolitic ironstones of Ashumaysi formation of Wadi Fatima, western Arabian Shield, Saudi Arabia. J King Saud Univ Sci 33:101266
Ghoneim MF, Noweir MA, Abu-Alam TS (2015) Magmatic evolution of the area around Wadi Kariem, Central Eastern Desert, Egypt. Arab J Geosci 8:9221–9236
Hein JR, Yen H-W, Gunn SH, Gibbs AE, Wang C-H (1994) Composition and origin of hydrothermal ironstones from central Pacific seamounts. Geochim Cosmochim Acta 58:179–189
Isakin MM, Lobunets SS, Yegorov IV (1990) Explanatory note to the map of mineral distribution of the PDRY, scale: 1:200,000. Ministry of Energy and Minerals, Department of Geology and Mineral Exploration, Aden, pp 34
Johnson PR (2004) Proterozoic geology of Western Saudi Arabia, Northwestern Sheet. Saudi Geol Surv
Johnson PR, Kattan FH (2012) The geology of the Arabian Shield. Saudi Geol Surv, p 466

Khalil KI, El-Shzly AE, Lehmann B (2015) Late Neoproterozoic banded iron formation (BIF) in the central Eastern Desert of Egypt: mineralogical and geochemical implications for the origin of the Gebel El Hadid iron ore deposit. Ore Geol Rev 69:380–399

Khudier AA, Ali MM, El Habaak GH (1989) The metavolcanics at Um Samiuki area. Egypt Bull Fac Sci Assiut Univ 17:73–101

Kiyokawa S, Suzuki T, Horie K, Takehara M, El-Dokouny HA, Dawoud MD, Abuelhasan MM (2020) Tectonic and sedimentary history of the neoproterozoic metavolcanic–volcaniclastic rocks of the El-Dabbah Group, Central Eastern Desert, Egypt. J Afr Earth Sci 165:103807

Lescuyer JL (1981) Al Bayda project, drilling Campaign Bureau De Géologiques et Minières report 81 RDM-039 PA, pp 16

Letalenet J (1981) Southeast area of Yemen Arab Republic Al Bayda-Al Fadaha detailed geological and mineral exploration (1980 campaign), Bureau De Recherches Géologiques et Minières report 82 RDM-020 PA, pp 17

Lowe DR (1988) Suspended-load fallout rate as an independent variable in the analysis of current structures. Sedimentology 35:765–776

Luo T, Kamal El-Din G, Osman I, Abdelkareem M (2020) Geochemistry and tectonic setting of the Abu-Marawat metavolcanics, Central Eastern Desert-Egypt. Arab J Geosci 13:1056

Maurice AE (2000) Petrology and mineralization of Gebel Abu Marawat area, Eastern Desert, Egypt. MSc thesis, Cairo University, pp 226

Meinhold KD (1982) Prospecting and exploration for known ore deposits in the Sadah area, Final report, Germany, Hanover, part 1, pp 61

Mukherjee SM, Stern RJ, Manton WI, Johnson PR, Miller N (2005) A neodymium perspective for the Neoproterozoic banded iron formations from the Arabian Nubian shield: a snowball earth manifestation? Geol Soc Am Abs Programs 37:358

Ridley J (2013) Ore deposit geology. Cambridge University Press

Risacher F, Fritz B (2009) Origins of salts and brine evolution of Bolivian and Chilean salars. Aquat Geochem 15:123–157

Rouxel OJ, Bekker A, Edwards KJ (2005) Iron isotope constraints on the Archean and Paleoproterozoic Ocean Redox state. Science 307:1088–1091

Sakran SM (1993) The basement rocks of As-Swadiyah area, Al-Bayda District, Yemen Republic. Dissertation, Cairo University

Shields-Zhou G, Och L (2011) The case for a Neoproterozic oxygenation event: geochemical evidence and biological consequences. GSA Today 21(3):1

Sims PK, James HL (1984) Banded iron ore formation of Late Proterozoic age in the Central Eastern Desert, Egypt: geological and tectonic setting. Econ Geol 79:1777–1784

Stern RJ, Avigad D, Miller NR, Beyth M (2006) Evidence for the snowball earth hypothesis in the Arabian-Nubian Shield and the East African Orogen. J Afr Earth Sc 44:1–20

Stern RJ, Mukherjee SK, Miller NR, Ali K, Johnson PR (2013) ~750 Ma banded iron formation from the Arabian-Nubian Shield—implications for understanding Neoproterozoic climate change. Precambr Res 239:79–94

Takla MA, Hamimi Z, Hassanein SM, Kaoud NN (1999) Characterization and genesis of the BIF associating arc metavolcanic rocks, Um Ghamis area, Central Eastern Desert, Egypt. Egypt Mineral 11:157–185

Taman ZI (2005) Mineralogical and geochemical studies on some banded iron formations from the Eastern Desert of Egypt, and their industrial uses. Dissertation, Ain Shams University, Cairo, Egypt, pp 357

Van Houten FB, Bhattacharyya DP (1982) Phanerozoic oolitic ironstones—geological record and facies model. Ann Rev Earth Planet Sci 10:441–457

Wilde S, Youssef K (2002) A re-evaluation of the origin and setting of the late Precambrian Hammamat group based on SHRIMP U-Pb dating of detrital zircons from Gebel Umm Tawat, north Eastern Desert, Egypt. J Geol Soc London 159:595–604

Zalata AA (1972) Geology of the area around Gabal El–Shayib, Eastern Desert, Egypt. Dissertation, Ain Shams University, Cairo, pp 221

Chapter 8
Mining History of the Arabian–Nubian Shield

Contents

8.1 Introduction . . . 448
8.2 Mining History in the Shield Rocks of Saudi Arabia . . . 449
8.2.1 Introduction . . . 449
8.2.2 Mahd Adh Dhahab Old and New Gold Mines . . . 452
8.3 Mining History in the Shield Rocks of Yemen . . . 462
8.4 Mining History in the Shield Rocks of Egypt . . . 467
8.4.1 Introduction . . . 467
8.4.2 Mining During the Pharaonic Civilizations (3100–332 BCE) . . . 468
8.4.3 Mining During the Hellenic and Roman Civilizations (332 BCE–641 CE) . . . 477
8.4.4 Mining from the Arab Conquest (641 CE) Until the French Campaign (1798 CE) . . . 482
8.4.5 Gold as an Example for Mining History in Egypt . . . 482
8.5 Mining History in the Shield Rocks of Sudan . . . 493
8.5.1 Introduction . . . 493
8.5.2 Gold as an Example of Mining History in Sudan . . . 496
8.5.3 Hassaï Project as an Operating Gold-Copper Mine in Sudan . . . 498
8.6 Mining History in the Shield Rocks of Eritrea . . . 502
8.6.1 Introduction . . . 502
8.6.2 Mining Districts in Eritrea . . . 503
8.6.3 Bisha Copper-Zinc-Gold Project as an Example of Operating Mine in Eritrea . . . 507
8.7 Mining History in the Shield Rocks of Ethiopia . . . 511
8.7.1 Introduction . . . 511
8.7.2 Gold Mining in Ethiopia . . . 513
8.7.3 Tantalum Mining in Ethiopia . . . 517
References . . . 520

A. Hassan Ahmed, *Mineral Deposits and Occurrences in the Arabian–Nubian Shield*,
Earth and Environmental Sciences Library,
https://doi.org/10.1007/978-3-030-96443-6_8

8.1 Introduction

In the previous chapters of this book, the different types of mineral deposits and occurrences have been reviewed in the countries covered by the Arabian–Nubian Shield (ANS): Saudi Arabia, Yemen, Eastern Desert of Egypt, Sudan, Eritrea, and Ethiopia. The ANS represents one of the Earth's largest blocks of juvenile Neoproterozoic crust, which is also one of the largest repositories of Neoproterozoic metallic minerals. The ANS is comparable in size with the other major Precambrian shield areas in the world, such as the West African, Western Australian, and Canadian shields. The ANS is a highly prospective target but underexplored, where the relative lack of exploration in some parts of the ANS is in part due to political and legislative issues. The ANS has a wide variation of rock types, including well-preserved oceanic crust, island arcs, volcano–sedimentary basins, and a variety of igneous intrusions. Numerous ancient workings, countless smelting sites, and the innumerable ruins of mine camps, show that the ANS has been (and indeed is still) a source of gold, copper, and many other metals including base metals, for more than 7000 years.

Several mining projects are currently active in the region, producing (1) gold from orogenic and epithermal deposits, (2) base metals and gold from volcanogenic massive sulfide (VMS) deposits, (3) gold from oxidized weathered caps above VMS deposits, and (4) strategic metals (e.g., Ta, Nb, U, Th, rare-earth elements) from pegmatites in different locations in the ANS. Exploration is currently underway in many parts of the ANS, where thousands of artisanal workings are producing high yields of gold, responsible for up to 80% of the income of some of those countries (e.g., ~62 t in Sudan; ~8 t in Ethiopia). Other types of mineral occurrences that are subeconomic are merely at the exploration stage, or are hypothetical targets, including banded iron formations, Nb–Th–U, Sn–W, platinum-group elements (PGEs), chromite, porphyry copper, Fe(oxide)–(Cu–Au), and sedimentary-hosted copper and lead deposits. This range of deposit types and the value of current metal production are the direct results of the versatile rock types in and tectonic evolution of the ANS.

As described in previous chapters, the ANS rocks host different styles of mineral deposits including magmatic, magmatic–hydrothermal, hydrothermal, and sedimentary/surficial mineral deposits. In many cases, the formation and distribution of these mineral deposits are structurally controlled, and some of these mineralizations were overprinted and/or reworked by younger structural or mineralizing events. The countries covered by the ANS have long mining histories, starting from prehistoric times in the Egyptian and Saudi Arabian desert until the present in all of the ANS countries. For example, both gold and copper were mined by the ancient Egyptians from 3000 BCE, and mining took place sporadically over time in both Egypt and Nubia as well as on the Arabian Peninsula. The world's oldest known geological map, the Turin papyrus map (dated to about 1150 BCE), depicts a 15-km stretch of the Wadi Hammamat dry riverbed (*wadi* is an Arabic word meaning a dry riverbed/tributary or a valley) showing different rock types, a stone quarry, and a gold mine in the Fawakhir area of the Central Eastern Desert of Egypt. There have been numerous

mining projects in the ANS countries, many of which are of only historical interest, while many others are actively working mines, such as those in the Mahd Adh Dhahab, Gebel Sayed, Ad Duwayhi (Saudi Arabia), Sukari (Egypt), Ariab (Sudan), Bisha, Koka (Eritrea), Lega Dembi, and Tulu Kapi (Ethiopia).

This chapter will focus mainly on the available information—the most important known historical and currently operating mining projects in the ANS countries, in terms of their history and current progress. As usual, the chapter will start with the Arabian shield (Saudi Arabia and Yemen), then followed by those in the Nubian shield (Eastern Desert of Egypt, Sudan, Eritrea, and Ethiopia).

8.2 Mining History in the Shield Rocks of Saudi Arabia

8.2.1 Introduction

There are very few ancient sources and detailed reports—the history of mining activities in Saudi Arabia, but what is well known for now is that the serious and organized mining activities first started around 3000 ya in Saudi Arabia. The Kingdom of Saudi Arabia has a long history of mining that stretches back several thousands of years. The first mining record in the Kingdom has been dated back to 2100 BCE, where ^{14}C dating has shown that the operations at Madh Adh Dhahab mine were already underway by about 1000 BCE. Archaeologists have claimed that a copper mine was generating revenue for King Solomon in the tenth century BCE. Over the last 50 years, more than 1000 ancient mine sites and workings have been reported and promising sites were studied in detail in the Kingdom. Exploration geologists have documented valuable information that includes locations and operations of historic mines. These numerous ancient mines on the Arabian Peninsula were certainly not all active at the same time, but this historical record proves the enormous efforts undertaken to extract minerals and smelt them into high-value products. The main precious metals, ferrous ores, and nonferrous ores mined and produced included gold, silver, copper, zinc, lead, iron, borax, and whetstone (to sharpen swords). In addition, semiprecious stones such as onyx, turquoise, amethyst, emerald, and quartz were mined to be used for jewelry. Many of these mine sites were located close to where the Darb Zubaydah pilgrimage route from Baghdad to Makkah was built later. These mining operations were previously owned and run by clans and tribes, which in Islamic times became the first public–private partnerships with Islamic countries levying 2.5% *zakat* (charity or alms) taxes. These mining activities were very labor intensive, where the large-scale operations employing over 1000 workers. The Mahd Adh Dhahab mine was a major mining site in operation already more than 3000 ya. Its mine tailings suggest that over 1 Mt of ore were mined in medieval times, so it can be assumed that this mining operation produced 1.5 Moz of gold during its operational life—valued today at over USD 2 billion.

A real big-scale mining activity is believed to have been started in Saudi Arabia ~1500 ya, between 430 and 830 CE. At that time, the ancient Hamdah mine, which is located at the southeastern part of the Arabian shield, is believed to have produced about 1 Moz Au, which at today's values would be worth more than USD 1.5 billion. Mining at that time was essentially done by digging shallow open pits to recover the surface deposits. However, when these resources were exhausted, horizontal shafts of up to 100 m in length, or even vertical shafts of 3–8 m in depth, were dug into mountains. More than 1000 tunnels are presently known, with depths of up to 100 m, dug into the Saudi Arabian escarpments. In addition, sites of many kilns to extract metal have been discovered close to these ancient mines. Charcoal was used to fire these old kilns to achieve the necessary high temperatures of about 1063 °C, the melting point of gold. Next to the kilns, millstones used as manual crushing and grinding tools, as well as tailings and slag piles, were found at the ancient mine sites (Fig. 8.1a, b), which can give such information as the composition of extracted ore and its mineralization type.

Although the Kingdom of Saudi Arabia remains one of the world's largest petroleum producers, recent price fluctuations in the oil market has highlighted the need to diversify its economy. In addition to establishing itself in the gold market, Saudi Arabia is also setting its sights on ruling the markets for copper, zinc, and phosphate. However, despite its early growth in the development of mineral extraction,

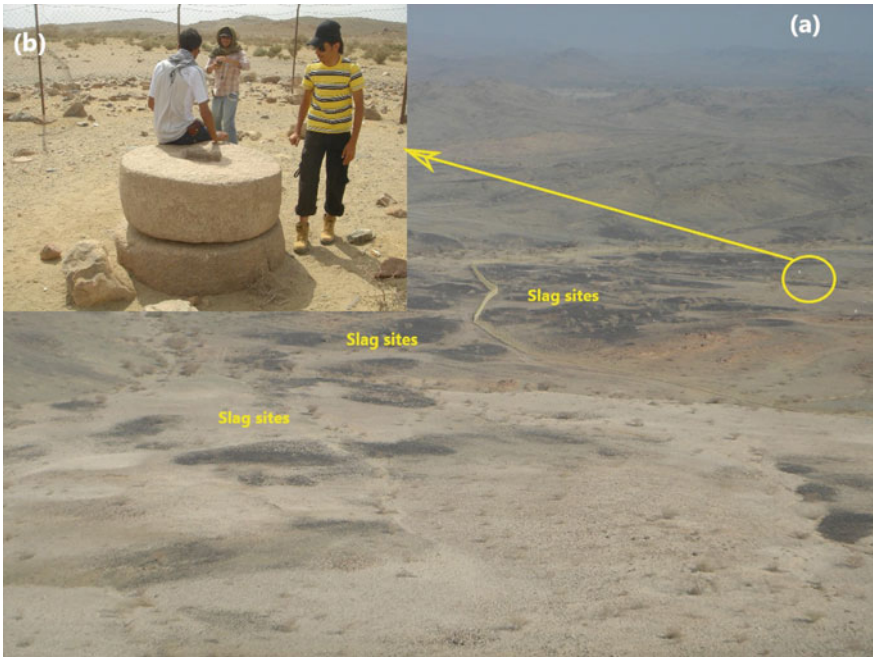

Fig. 8.1 Field photographs of **a** tailing and slag piles of ancient Cu–Au mine, and **b** manual crushing and grinding millstone at Gebel Ablah, southwestern Arabian Shield, Saudi Arabia

mineral resources in Saudi Arabia have remained relatively untapped and there is a need for further research and focus. Mining activities in the Kingdom began during the reign of King Abdul Aziz in 1934, when the Ministry of Finance concluded the initial mining agreement with an American geologist, and from which the Saudi Arabian Mining Syndicate emerged. The newly established Saudi Arabian Mining Syndicate obtained the exclusive concession for mineral exploration in the Arabian shield in Saudi Arabia to choose the mines and places that were targeted to be exploited commercially.

One of the most-prominent and well-known mines in the area is the Mahd Adh Dhahab mine, in which the mining process began in 1939, and the quantity of ore extracted from it was estimated to be ~900,000 t, producing ~770,000 Au and 1.2 Moz Ag. Due to the increase of interest from the government in the mining sector, the General Directorate of Mineral Resources was established in 1961, and the state's efforts continued in the area of mineral prospecting. Prospecting for minerals in various regions of the Kingdom resulted in the discovery of many commodities such as phosphates (with estimated resources of ~18 Mt), magnesium (~17 Mt), and iron (~4 Mt), with annual growth rate in the mining sectors reaching up to 9%. Prospecting also resulted in discoveries of other mineral resources, including tin, tungsten, aluminum, iron, chromium, molybdenum, manganese, nickel, titanium, and uranium. The building materials industry is also an important Saudi mining industry, as it has grown during recent years at a high rate; its industrial projects have reached about 400 factories, employing ~35,000 workers.

The mineral resources sector is an important support for economic development. The government of the Kingdom aims to share the Saudi private sector in mining projects to provide the local alternative for the imported mineral commodities. All the Saudi companies specialized in extracting and casting minerals appeared on the Saudi economic scene and is now one of the largest joint stock companies in the Kingdom. Recently, the Ministry of Petroleum and Mineral Resources granted the Saudi Arabian Mining Company (Ma'aden) a license to explore for copper ore and its associated mineral deposits in the Gebel Sayed area, northeast of the Mahd Adh Dhahab mine, in the Al-Madinah region, and which contains four bands of high-grade copper ore and contains important values of zinc and other metals. In this era of global economic transformation, competition between countries intensifies for better and faster economic and industrial development through the optimal exploitation of natural resources. Therefore, the Kingdom established the Saudi Arabian Mining Company, Ma'aden, in 1997 based on a generous royal decree to be a fully owned joint stock company with a capitalization of SAR 4 billion (4 billion Saudi riyals). The government has provided all means of support for Ma'aden to take the opportunity to develop the mining industry and related industries in the Kingdom through various aspects of mining activities related to all stages of the mining industry. To achieve this goal, Ma'aden has made many achievements in the exploitation of mining opportunities, enhancement of reserves of mineralized raw materials, and employment of modern technology to achieve maximum benefit through these mining industries. It is developing four productive gold projects in the Mahd Adh Dhahab, Al-Sukhybarat, Al-Hajjar, and Bulgha mines. Their gold production is ~300,000 oz per year, and

silver is ~1 Moz per year, in addition to other minerals such as copper and zinc. The Al-Amar and Al-Duwayhi mines are also gold and base-metal sulfide mines, which are came into production several years ago as a result of continuing the hard efforts in the mining sector.

Following are the historical stages of the most important mining projects in the Kingdom of Saudi Arabia.

8.2.2 Mahd Adh Dhahab Old and New Gold Mines

The *Mahd Adh Dhahab* "cradle of (the) gold," is a small gold area in the Arabian peninsula, located in the Al-Madinah province, in the Hijaz region of Saudi Arabia. It is an ancient yet also presently active mine, from which gold was first mined in Arabia in the pre-Islamic era, in 3000 BCE. A second period of mining activity was during the Islamic Abbasid period between the years 750 and 1258 CE. The latest activities at the Mahd Adh Dhahab mine by the Saudi Arabian Mining Syndicate began in 1936 using both open-pit and underground mines. Gold mining is currently done by the Saudi Arabian Mining Company (Ma'aden). The Mahd Adh Dhahab mine is intended to be closed in 2023 as now only low-grade gold is being mined due to being depleted.

Historically, the Mahd Adh Dhahab site has been identified as King Solomon's gold mine, where the archaeological sources indicate ancient exploitation of gold from the mine, as large gold quantities were extracted in the first century BCE (~3000 ya). It is also known that the mine was exploited during the period of the Prophet Mohammed, may God bless him, and it was exploited by the Banu Salim tribes, where the mine was known as the "Mineral of Bani Saleem." It is also mentioned in the history that the gold of Mahd Adh Dhahab mine was brought to the second calipha ʿOmar ibn Al-Khaṭṭāb. During the period of the Bani Umayyad caliphate, the Mahd Adh Dhahab mine received special attention and the demand for gold increased in order to satisfy the Umayyad state's need to mint its own gold coinage. This is what actually happened during the period of the calipha Abd al-Malik ibn Marwan, who was in the year 74 AH of the Islamic calendar (694 CE). Since that time, Arab coins no longer circulated in the orbit of Byzantine or Persian coins or were linked to their prices or weights. Both the Levant and Egypt carried the torch of monetary reform that was lit by the Umayyad caliphate capital during the period of the Umayyad Calipha 'Abd Al-Malik bin Marwan. This is evidenced by the appointment of a private worker, Abdullah bin Kathir, who is responsible for the affairs of the Mahd Adh Dhahab mine in the year 128 AH (750 CE). The Mahd Adh Dhahab mine has been exploited during the Abbasid state, as the historical sources confirmed that the quantity of gold that was produced from the mine reached about 40 t.

As soon as the King Abdulaziz laid the foundations for this large entity, the Kingdom's government strived to take everything that would achieve the happiness of its people despite the luxury provided by the oil flowing from the eastern region.

As part of its endeavor to build a strong and solid economy, the Kingdom's government sought to diversify sources of income and paid attention to the fields of mineral resources and exploration. In the period of King Abdulaziz, the Saudi Mining Syndicate (SAMS) mined gold and silver from the Mahd Adh Dhahab mine in the period from (1939–1954), then production stopped due to the low price of gold until it resumed again in the 1970s. From the last century, the Gold Fields Limited company signed a contract with Petromin and was granted a disclosure license in 1976. For various strategic considerations, Petromin decided to fully own the project. This was done on 15 May 1987. From that time, the Mahd Adh Dhahab mine has become a governmental organization and is under 100% Saudi administration.

The Mahd Adh Dhahab mine site is a high mountain peak with many and deep fissures and gaps, where there are several ruins and old workings found in the old mine area and in the area between the mountain and the paved road (Fig. 8.2). The old-mine area is about 250 × 100 m, but the excavation work has removed many surface collections of pottery and porcelain. A group of Islamic pottery was picked up, consisting of fragments with blue and green paint, and it dates back to the Abbasid Islamic era, the third and fourth centuries AH. In addition, an order from the Caliph al-Muqtadir to his minister Issa bin Dawad was found engraved on a piece of granite, and the order stipulates the reconstruction of the Avenue of the Pilgrims that dated back to 324 AH (946 CE). The Ministry of Mineral Resources of the Kingdom put forward a program for exploration after the production in the old mine area was stopped, which led to the discovery of more reserves in an area close to that already exhausted. A new mine site was opened in 1983 in this nearby area, in which it

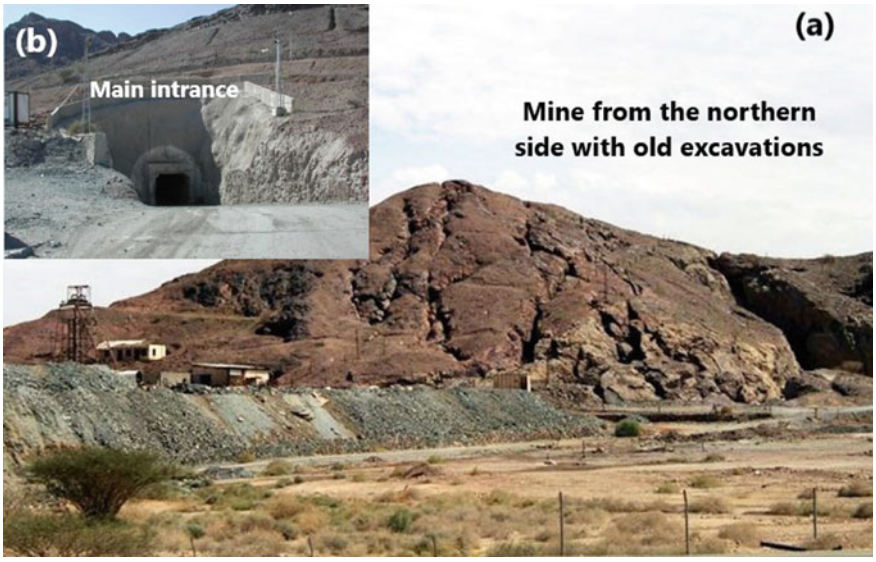

Fig. 8.2 Field photographs of **a** Gebel Al Mahd (Mahd Adh Dhahab) from its northern side showing the old excavations, and **b** the main interface of Mahd Adh Dhahab mine

was planned to handle approximately 400 t ore per day for an annual production of approximately 29 t Au and 11 t Ag.

Geologically, the Mahd Adh Dhahab mine is located within a sequence of volcanic, volcaniclastic, and sedimentary rocks that was previously known as the *Mahd Ad Dahab Series*, but now renamed the *Al Mahd group* by Kemp et al. (1982). This volcano–sedimentary sequence is overlain a granite–granodiorite batholith with some conglomeratic beds at the base of the sequence as a nonconformity surface between the batholith and the overlying volcano–sedimentary sequence. These conglomeratic beds are overlain by a set of volcaniclastic rocks interlayered with some basalt flows and andesites, which form the base of the Al Mahd group. The layered rocks of Gebel Al Mahd is classified into five lithological units, all of which dip to the north at 20–45° and extend generally from east to west. The sequence as a whole is made up of a mixture of pyroclastic and epiclastic fragments with some intercalated lava flows, tuff beds, and volcanic breccia (Fig. 8.3). The Al Mahd volcano–sedimentary sequence includes a unit of tuffs and andesitic flows overlain by the lower agglomerate unit, then the lower tuff, then the upper agglomerate, and finally the upper tuff (Fig. 8.3). Each of these units is divided into smaller units. For example, the lower agglomerate could be classified into three subunits, the lower, middle, and upper parts. The contact between the lower agglomerate and the lower tuff is graditional and covers a wide area where the agglomerate interferes with lapilli and massive tuffs. The contact between the lower tuff and the overlying upper agglomerate is a sharp contact. The upper agglomerate unite is divided into a lower agglomerate crystal lithic tuff, which grades into agglomerate and grey-colored agglomerate. The upper tuff unit is conglomeratic agglomerate that concordant with layers of argillaceous deposits and calcareous tuff,

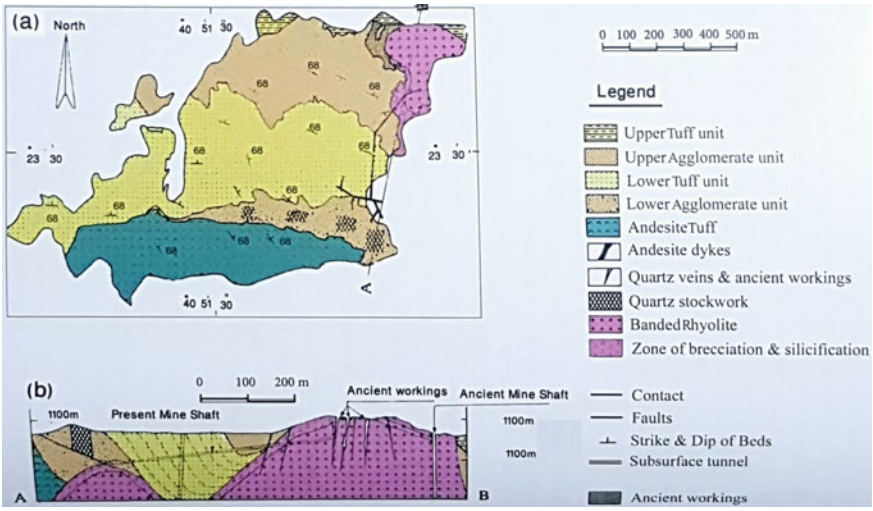

Fig 8.3 **a** Simplified geological map of Mahd Adh Dhahab mine, and **b** A-B cross section in Mahd Adh Dhahab mineralization site (from Al Shanti 2009)

especially at the base of the unit. The Al Mahd volcano–sedimentary sequence ends with a small chert cap unit that crops out at the extreme north part of the sequence (Al Shanti 2009). The Gebel Al Mahd sequence in general, and in the mine area in particular, is cut by a rhyolite porphyry intrusion. A number of andesite dykes cut all of these rock units, including the rhyolite porphyry, all of them strike from N45°E and dip at an angle of 70° to the west. In addition, few small quartz veins cut across these andesite dykes.

The Mahd Adh Dhahab mine occurs in an area of intensive faulting and folding in the northeast direction. The dominant structures in the mine area strike north followed by those oriented to the northwest or northeast. The most prominent structural feature in the mine area is the zone hosting of quartz veins, which is striking N10°E. This veining zone includes both the old and new mine areas. There is good evidence that the area has undergone a number of successive events, including faulting, veining of quartz veins, and intrusion of andesite dykes. Layering is dominant in most of the rock units with clear bedding planes in all of the tuff units and less clear in the agglomeratic ones. Folding is clear in the Al Mahd area, which lies on the hinge of an anticline plunging to the north and cut by faults to the east of the mine site. The mine area itself is in the form of a homocline with its axis striking northwest and dipping at 50° to the north. In addition, some local minor folds are also observed in the area with most of the axes striking to the north or northwest.

As mentioned in Chap. 4, the mineralization type in Mahd Adh Dhahab mine is epithermal precious metal (gold–silver) and base metal (copper–zinc) vein-type mineralization that is hosted in quartz veins. Although quartz veins are widespread all over the area, the majority of quartz veins are concentrated in a zone of ~1000 × 400 m wide and extending N10°E, as well as strongly faulted and altered containing most of the ancient workings and mining activities in the new mine site. Quartz veins range in thickness from 1 cm up to 5 m or more, but mostly are within 10–50 cm. They represent an open-space filling style of mineralization that is indicated by the common presence of vugs and comb structures. Many of the quartz veins are brecciated and cemented by a younger quartz veining generation. The ore minerals found in the Mahd Adh Dhahab mine are represented mainly by pyrite, chalcopyrite, sphalerite, and, to a lesser extent, galena, tetrahedrite, and argentite. Native gold and silver, as well as Au–Ag alloy (electrum) and tellurides are commonly associated with these sulfide minerals.

There are two mineralized bodies in the Mahd Adh Dhahab mine area, one of which was exploited in the old mine site close to the rhyolite intrusion within the upper agglomerate. The second mineralized body was discovered recently in the new mine area, also close to the rhyolite intrusion, but within the lower agglomerate. In the new mine site, it is possible to differentiate between two different mineralized zones: (1) an oxidized ore zone that extending down to a depth of 100 m from the surface, which showed some supergene minerals, including malachite, azurite, chrysocolla, covellite, and iron oxides and (2) a second mineralized zone represented by hypogene ore. In both zones, gold has been found either in native form or as telluride minerals, most of which are petzite and hessite (e.g., El-Shafei et al. 2020).

The approximate total estimated ore reserves of the Mahd Adh Dhahab mine up to 2009 is ~130 t Au and 140 t Ag. The estimated ore reserves in the new mine area is ~1.2 Mt ore, with an average grade of 26 g/t Au, 73 g/t Ag, 0.64 wt% Cu, 2.58 wt% Zn, and traces of Pb. The total tonnage of associated Zn and Cu produced up to the year 2009 is ~983 and 730 t, respectively (Al Shanti 2009).

8.2.2.1 Operating Gold and Base Metal Mining in Saudi Arabia

In addition to the Mahd Adh Dhahab mine, the Ma'aden company operates another five gold and base-metal mines, all of them are located in the western part of the Arabian peninsula, including (Fig. 8.4): the *Ad Duwayhi*, *Al Amar*, *Bulghah* and *Sukhaybarat*, and *As Suq* mines and the *Mansourah–Massarah mine project*. A subsidiary branch that is fully owned by Ma'aden is the Ma'aden Gold and Base Metal (MGBM) Company; gold accounts the majority of its business, with copper, silver, and zinc accounting for the remainder. Within the Arabian shield, gold and base-metal deposits and occurrences are abundant and widespread (Fig. 8.4), commonly taking the form of ancient mines developed on gold-bearing quartz veins and gossans and, more rarely, placer deposits. The distribution of the ancient mines provide an invaluable first-order guide of geochemical survey for further potential areas. MGBM has already produced ~415,000 oz of gold in the year of 2018, and is planning to increase this production to 1 Moz/year under Ma'aden's current strategy for the period through 2025. For base-metals mining, there is a 50/50 joint venture between

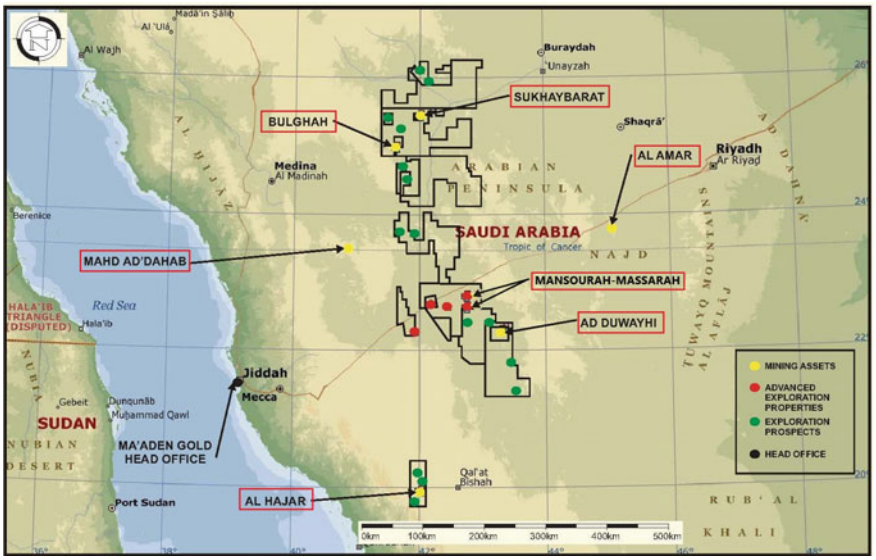

Fig. 8.4 Location map showing the operating gold mines by Ma'aden Company. (*Source* SRK Consulting, Ma'aden Gold MER—Final Report 2007)

Ma'aden and Barrick Middle East (of Toronto, Canada) to mine copper. In the year 2018, the joint venture produced ~24,950 t of copper. They expected to produce about 20,415–27,215 t of copper in 2019, with ~53,070 t of measured and indicated Cu resources, 5900 t of inferred copper resources, and 322,960 t of proven and probable copper reserves.

The *Ad Duwayhi gold mine* is the newest open-pit mine of MGBM; it started production in 2016 and is currently their largest producing mine site, with ~263,000 oz of gold produced in 2019. This mine area is located ~450 km southwest of Riyadh (Fig. 8.4), occupies ~1 km^2, and comprises an open-pit gold mine and milling operations (Fig. 8.5a, b) to produce a metal product onsite, which is then

Fig 8.5 **a** Open-pit mine and **b** milling operation unite of Ad Duwayhi gold mine, southern Arabian Shield, Saudi Arabia. (*Source* Ma'aden Company)

transported to Jeddah. The site comprises three main areas: an explosive repository, a combined process plant, and a residential area, all of which are enclosed by a common 18-km boundary fence. To facilitate these new operations, Ma'aden has commissioned a 500-km pipeline to pump treated waste water from Taif, near the Red Sea coast, to the inland mines. The 458-mm-diameter pipeline has the capacity to carry up to 13,000 m^3 of treated water to future mining operations at Ad Duwayhi, Mansourra, Massarra, As Suq, and Ar Rjum.

Geologically, the gold mineralization at the Ad Duwayhi mine was closely associated, in time and space, with emplacement of a late- to postorogenic, intracrustal, northwest-oriented granite body (659±7 Ma) and comagmatic quartz porphyry (646±11 Ma), a hypabyssal and perhaps younger phase of the granite intrusion. Mineralization is largely confined to northeast-striking, southeast-dipping fault zones. Hydrothermal alteration represented by early biotitic alteration overprinted by sericitic alteration. Gold mineralization at this site is occasionally coincident with sericitic alteration, which produced a quartz–sericite–carbonate–pyrite–rutile mineral assemblage found both as vein-filling and wallrock alteration products. Mineralization styles in the Ad Duwayhi mine are mainly arranged in the following general paragenetic sequence: (1) quartz–molybdenite veins in and near the granite stock, (2) low-grade gold-bearing quartz vein breccia in and along the margins of the granite stock, (3) gold-bearing stockwork and sheeted quartz veins, and (4) massive-to-banded gold-rich tabular quartz veins. The gold-bearing stockwork, sheeted, and tabular veins are spatially associated with quartz porphyry dikes and more distal to the granite stock. The mineralized zones at the Ad Duwayhi mine are characterized by low sulfides. low base-metal content, and gold/silver ratios of about 6:1. Gold there shows no significant correlation with other metals, except lead, and moderate correlation with silver. The estimated total mineral resources at Ad Duwayhi mine are 2.1 Moz Au contained within 17.1 Mt of ore, with an average grading of 3.9 g/t Au.

The *Al Amar Gold Mine* is an underground mine with a carbon-in-leach processing facility (Fig. 8.6a). The gold and associated base-metal production commenced in 2009. In addition to gold, the mine is producing copper and zinc concentrates for export to international markets. The Al Amar mine produced ~28,000 oz Au in 2019. The Al Amar mineralized zone is ~130 km west/southwest of the town of Al Que'eyah, at latitude 23° 47′ N and longitude 45° 4′ E in the eastern part of the Arabian shield (Fig. 8.4). It is hosted mainly in a belt of intermediate-to-felsic volcanic rocks of the Al Amar (Halaban) group, intercalated with volcanoclastic rocks and interbedded with jasperoid layers. The mineralization zone et al. Amar represented is by a series of quartz veins extending in the N-NE direction, which are made of crustified white quartz, ranging in thickness from a few millimeters up to five meters. Hypogene minerals are mainly pyrite, sphalerite, chalcopyrite, gold, and a little silver.

The Al Amar mine area is cut by two main faults extending N60°W and branching in the center and west of the area into a wide zone of cracks. These cracks are filled by cross-cutting quartz veins with pyrite, sphalerite, chalcopyrite, and silver minerals with little gold. The host rocks of these veins include fragmented rhyolite, rhyolite

Fig 8.6 **a** Stellite image (via Google Maps) of the Al Amar gold mine site showing the carbon-in-leach unit and other processing facilities in the mine site and **b** one of the exploited quartz veins in the mine area

tuff, marble, and talc beds. These quartz veins have been exploited in the past as indicated by the ruins, vertical shafts, and tunnels, as well as heaps of dumps and slag (Fig. 8.6b). The mineralized area is ~250 m in length and 130 m in width and extends to ~250 m in depth, with a dip angle of ~75° to the northwest. The mineralization is layered and zoned; it is sphalerite-rich to the south and chalcopyrite-rich to the north. The estimated ore reserves at the Al Amar mine are ~5.6 Mt ore, with an average grade of 5 wt% Zn, 0.75 wt% Cu, and 9.2 g/t Au. Later investigation showed that the mineralization extends to the northwest from the old site for the northern veins, where this extension was believed to contain ~1 Mt of ore at ~20–30 g/t Au (Al Shanti 2009).

The *Bulghah* and *Sukhaybarat mines*, about 550 km northwest of Riyadh, are some 30–50 km to the south of the Al Madinah-to-Braida highway (halfway between the two cities), about 50 km from the town of Nuqrah. This remote region is the center of historical gold and copper workings that were discovered in 1930. The two mines work cooperatively. The Bulghah mine is an open-pit mine where low-grade oxide ore is processed onsite by heap leach processing, whereas higher-grade ore is transported by trucks to the nearby Sukhaybarat plant. The Sukhaybarat mine is also an open-pit mine (Fig. 8.7) but with a carbon-in-leach processing facility. Low-grade oxide ore from the Sukhaybarat site is transported by trucks to the Bulghah site for heap leach processing. The Sukhaybarat/Bulghah district is one of more than 40 gold occurrences in this area, where the precious metal is found in both diorite

Fig. 8.7 Open-pit of the Sukhaybarat gold mine, Arabian Shield of Saudi Arabia. (*Source* Ma'aden Company)

intrusions and sedimentary formations. The modern development of the mine began in 1986 with a feasibility study by the Saudi Company for Precious Metals, a joint venture between Petromin and Boliden (a Swedish mining company). In 1991, this partnership began to operate the open-pit mining of the reserves.

The Bulghah and Sukhaybarat mines produced a total production of ~62,000 oz of gold in 2019. Mineralizations there are found in the Neoproterozoic basement, which is essentially composed of metasedimentary and metavolcanic rocks belonging to the Hulayfah/Murdamah group. Intermediate intrusive rocks (diorite and tonalite) of the Shammer group trending N/S is interlayered between the supracrustal volcano–sedimentary sequences. Younger dykes and sets of quartz veins cut the whole rock sequence including the intrusive rocks, and these veins are associated with gold mineralization. Gold mineralizations are found as disseminations in the tonalite and within quartz veins as fine-grained specks associated with arsenopyrite. The mineralization increases at the contact of the tonalite intrusion with the Murdamah group rocks. The mineralization concentrates mainly in the surface of the intrusion to a depth of not more than 100 m from the surface.

Modern operations at the Sukhaybarat open-pit gold mine started at 1991, but the area has ancient mining archeological sites dating to about 1000–3000 ya. Two such sites (Sukhaybarat al Gharbiyah and Sukhaybarat ash Sharqiyah) have been identified to be present in the main locality line. These two are within about 4–5 km

of each other and are on land then owned by the Saudi Precious Metals Company; the company produced ~16,681 kg of gold between 1991 and 1998. Hypogene minerals associated with gold are pyrite, pyrrhotite, arsenopyrite, and chalcopyrite. In addition to quartz veins, both pyrrhotite and arsenopyrite are also found as primary minerals disseminated in diorite and tonalite intrusions. The proved ore reserves, based on a wide exploration program in the area, were estimated at 2.5 Mt ore, with average grades of 2 g/t Au.

The *As Suq mine* is a small low-grade open-pit gold mine that commenced production in 2014, using heap leach technology. The mine produced ~19,000 oz of gold in 2019. Gold mineralization is localized in narrow shallow-dipping quartz veins of a N/S-trending zone of flat-dipping quartz veins and associated stringer zones within Al Siham formation sedimentary and volcanic rock sequence. The mineralized quartz-vein system extends over a horizontal lenghth of about 1.2 km with a vertical depth of at least 120 m. The estimated mine life has been suggested to be to 2023.

The *Mansourah–Massarah mine project* is the newest mining project currently in execution by Ma'aden in the Central Arabian Gold Region that extends from the Red Sea coast to the middle of Saudi Arabia (Fig. 8.4). The project consists of Mansourah and Massarah resources, which are being developed by MGBM as open-pit mines, as well as a greenfield mineral concentrator and gold processing plant (Fig. 8.8a, b). The plant will employ carbon-in-leach and pressure oxidation processes technology for gold production. The feasibility study of the integrated mining project was completed in 2018, while the key contracts were awarded in the first half of 2019. The Manssourah–Massarah mine project is scheduled to commence operations in the second quarter of 2022. When it is in full production, the Mansourah–Massarah project is expected to produce about 250,000 oz of gold annually over an estimated mine life of 12 years. The project will be the biggest-ever gold project to be developed by Ma'aden. The Mansourah–Massarah greenfield project will include the mine, processing plant and infrastructure. It is designed to process 4 Mt per year of blended sulfide and oxide ore feed to produce gold as the main product of the mine.

The project comprises the Mansourah and the Massarah open-pit gold resources (Fig. 8.8a) that form part of a 50-km long, N/S-trending string of gold deposits that occur parallel to the regional Ad Dafinah thrust fault zone in the Central Arabian Gold Region. The Mansourah mineralization is located about 460 km northeast of Jeddah, while the Massarah site is situated in the Makkah region, about 8 km to the north of the Mansourah open-pit mine, about 460 km to the southwest of Riyadh (Fig. 8.4). The Mansourah and Masarrah mine sites are separated by about 6.5 km across the Najd Fault System structures. The Mansourah–Massarah gold project sites can be accessed through an access road from the highway that connects Ta'if with Jeddah. The gold mineralization of both sites is mostly hosted within stylolitic sulfidic quartz veins and listwaenite (carbonatized ultramafic rocks) wall rocks. The estimated proven and probable ore reserves of the Mansourah deposit are about 27.7 Mt, with an average grade of 5.06 g/t Au, while the reserves estimates for the Massarah open-pit mine are ~17.3 Mt, grading at 1.99 g/t Au. The run of mine ore

Fig 8.8 **a** Open-pit mine and **b** processing plant of the Mansourah and Massarah gold mine, central Arabian shield, Saudi Arabia. (*Source* Ma'aden Company)

will be trucked to a common processing facility for the recovery of gold through carbon-in-leach and pressure oxidation processes.

8.3 Mining History in the Shield Rocks of Yemen

As in Egypt, Sudan, and Saudi Arabia, ancient and much recent mining activity in Yemen were and has been focused mainly on gold; gold mining was probably a major industry in ancient times. Yemen was probably a major gold supplier in antiquity. Although the ancient mining history of Yemen is not well-documented, various pre-Islamic and Islamic authors have recorded some of the early mining activities at various localities in Yemen. Particular examples of these ancient descriptions are those of gold mining in the Sadah, Al Jawf, and Marib areas, the silver and zinc mining from the Jabali area northeast of Sana'a, the iron ore mining from gossans around Sa'dah, and the copper mining from the Al Bayda area in southern Yemen. Recent studies by Cantex Mine Development and Thani Dubai Mining have identified and recorded the extensive scale of gold mining in the northwestern parts of Yemen. It is noteworthy that the style of mining and the gold recovery technology that were used in

the older mine workings in Yemen are essentially similar to those that were used in the Eastern Desert of Egypt and northern Sudan in Pharaonic and post-Pharaonic periods and in western Saudi Arabia. In addition to the older, possibly Pharaonic-age mining, which primarily targeted the eluvial enrichments in the weathered rocks and in the softer formations, some more recent mining activities that primarily exploited quartz veins in bedrock along adits and in deep excavations (shafts) were also recorded. The latter mining activities probably took place during the Islamic period.

The Bureau de Recherches Géologiques et Minières (BRGM) has also recorded a number of ancient workings in the Jabali area, which are believed to date back some 2500 years. These workings essentially exploited the soft oxidized ore, which is hosted in limestone, and the mining activity consisted essentially of the making of deep pits, trenches, and even some underground adits. The oxidized ores generally contain lead, zinc, and occasionally silver. It is not known whether the zinc was also recovered in addition to silver and lead from these mining activities. However, significant copper mining took place during roughly the same period in Yemen, Oman, and Saudi Arabia, so it is likely that zinc would have been recovered as well to produce bronze implements and artifacts. Lead sulfides, primarily used as a cosmetic to adorn women, have also been mined at a number of places in Yemen, and hence the lead at Jabali was probably also recovered. Furthermore, a number of ancient workings (pits and excavations) as well as slags that were produced during the reduction of the malachite-bearing ores to produce copper are known from the Al Bayda area in southern Yemen, and from other isolated areas elsewhere in the country.

Although Yemen is classified among the least-developed countries, it is seen as a promising country with important economic resources, as it has much potential wealth, most of which has not been optimally exploited so far, especially in mining. Recent efforts of the Yemeni government are focused on expanding the capacities of the national economy and focusing on exploiting the opportunities inherent in economic sectors other than oil, most importantly mining. Geological studies confirm that Yemen possesses promising mineral wealth as a result of the relevant geological diversity. Geological surveys have shown in a number of governorates of Yemen the spread of basement rocks (Fig. 8.9), considered to be among the most important host rocks for such metallic mineral deposits as gold, silver, zinc, lead, copper, nickel, platinum, iron, and titanium (among many others). Industrial minerals, however, are found hosted within Phanerozoic sedimentary and volcanic rocks of younger ages. Mining represents an important potential source of income for Yemen. For example, there are large ore resources and reserves from the metallic mineral deposits that are widely distributed throughout the country especially in the northern, southern, and western parts (Fig. 8.10). There are, for example, occurrences of gold in many areas, such as Wadi Madan (Hadramout) (Fig. 8.11a), Al-Hariqah (Hajjah), Dhamar, Saada, Al-Jawf, Al-Bayda, and Shabwah (Fig. 8.10). Many of these occurrences were operated in the past, but because of the current political instability in Yemen, almost all of these sites are not operating at the time of this writing. Security is one of the most important criteria for the attraction of foreign investment in any country.

Fig. 8.9 Outcrops of Precambrian basement rocks with a common gold mining site of Yemen. (*Source* Mineral Resources of Yemen)

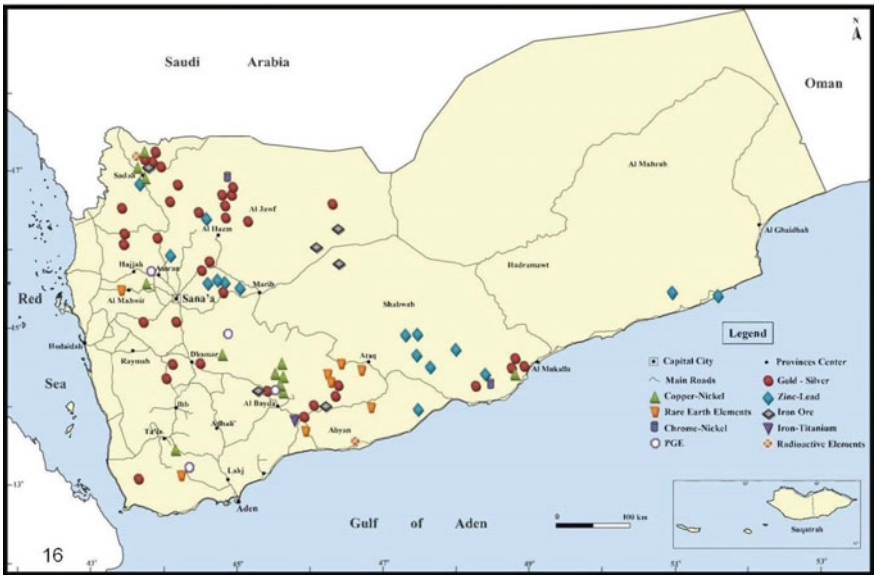

Fig. 8.10 Location distribution map of the metallic mineral deposits in Yemen. (*Source* Mineral Resources of Yemen)

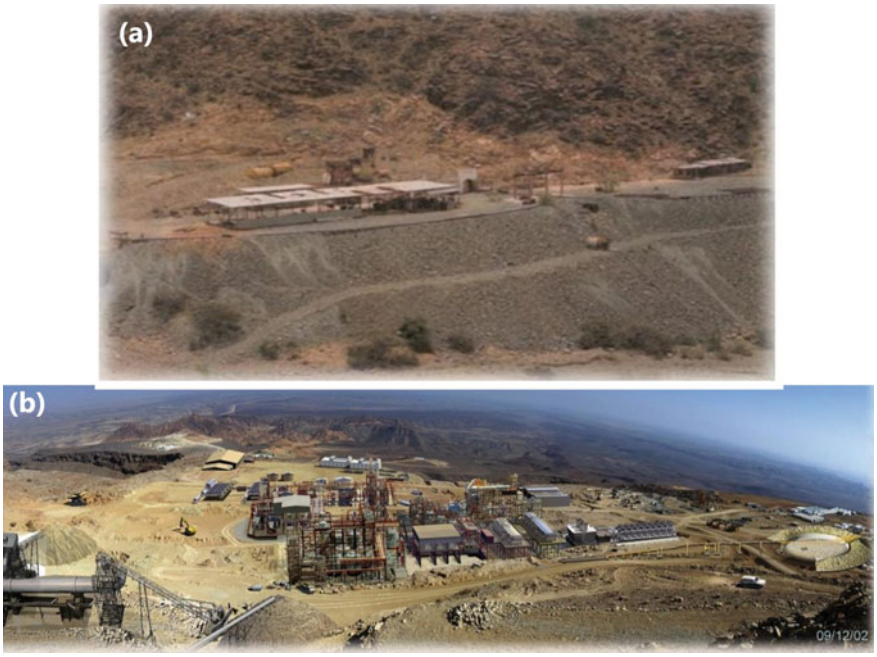

Fig 8.11 **a** Wadi Madan gold mine site, Hadramout, Yemen and **b** processing plant of the Jabali zinc–lead–silver deposits. (*Source* Mineral Resources of Yemen)

Accordingly, the field of mining, including oil and gas production, has decreased very significantly in recent times.

In addition, zinc–lead–silver mineralizations are widely distributed in Yemen, among which the most significant occurrences are associated with an approximately 650-km-long and up to 100-km-wide rift basin (Fig. 8.10) of the Jurassic period. Several carbonate-hosted zinc–lead–silver occurrences are found along this rift; the most important of these is the Jabali zinc deposit, which, after being developed, commenced production near the end of 2009 (Fig. 8.11b). In the tenth century CE, the Gebel Salab zinc–lead–silver deposit was considered to be the largest silver mine in the Muslim world. The deposit was rediscovered in 1980, in part because of a description of ancient silver mines in Al-Hamdani area and the network of old mining sites that located about 110 km northeast of Sana'a (Fig. 8.10, 8.12a). Many archaeological remains are still preserved near the new Jabali mine (Fig. 8.12b). The zinc, lead, and silver deposits at Jabali were studied in detail from 1982 to 1996 by the Geological Survey and Mineral Resources Board of Yemen in cooperation with various international organizations. The main zinc-bearing minerals were coarse- to fine-grained smithsonite (Fig. 8.12c); minor hydrozincite and hemimorphite were also representative. Lead was found to occur primarily in the form of cerussite and, to a lesser extent, galena, with silver occurring as argentite. Sulfide mineralizations were rare, found in minor occurrences in small areas or at depths below 400 m. The

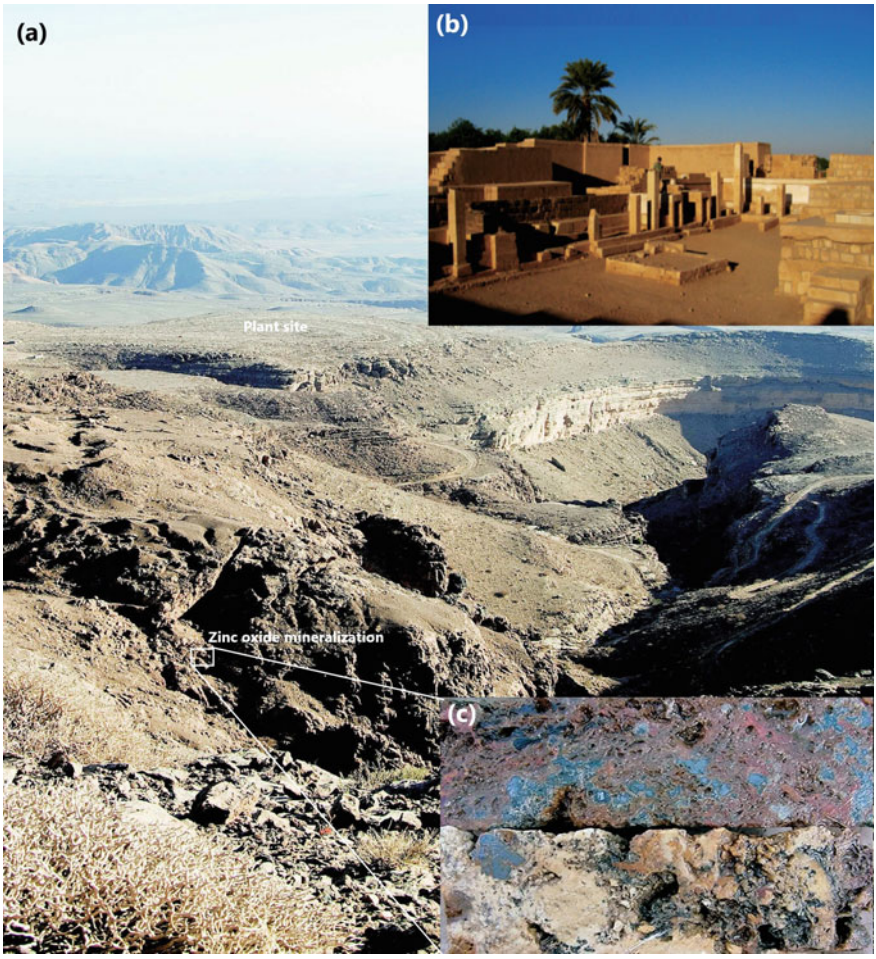

Fig 8.12 **a** Field photograph showing the open-pit mine and plant site of the Jabali zinc–lead–silver mine, **b** archaeological remains near the new Jabali mine site, and **c** coarse-grained colored smithsonite and other Zn-bearing minerals in the Jabali Zn–Pb–Ag deposits, Yemen. (*Source* Mineral Resources in Yemen)

extensive diamond drilling and geological modeling at Gebel Salab zinc–lead–silver deposits have demonstrated estimated resources of 12.6 Mt ore, with average grades of 8.86 wt% Zn, 1.17 wt% Pb, and 68.2 g/t Ag. The studies also confirmed that there is excellent potential for more resources, as the deposit is open from two sides. There are several occurrences in the immediate vicinity, including at Shabwah, Al-Jawf, and Emran, with grab samples assaying up to 16.5 wt% Zn and 6 wt% Pb.

Furthermore, mafic/ultramafic rocks are frequently distributed in the Precambrian shield rocks of Yemen, where there are many, widespread copper/nickel/PGE mineralizations (Fig. 8.10) including at Suwar (Hajjah), Al Hamurah (Ta'iz), Wadi

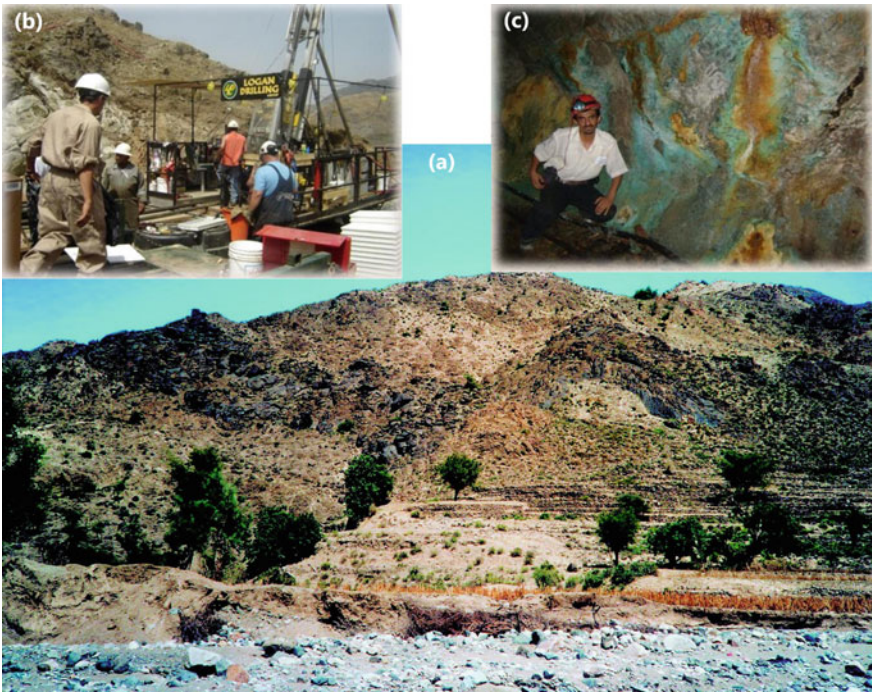

Fig 8.13 **a** Drilling sampling of the Suwar Cu–Ni–PGE occurrence, **b** malachite staining of the Cu–Ni–PGE deposits, and **c** Ni-PGE-bearing ultramafic intrusion of the Suwar area. (*Source* Mineral Resources of Yemen)

Qutabah, Byhan, Al-Qabyta, and Wadi Silbah, as well as other sites (Fig. 8.13a–c). All of these mafic/ultramafic occurrences are under consideration as copper/nickel/PGE resources but have not yet been explored. In addition to the copper/nickel/PGE occurrences, iron/titanium oxides are also widespread in the mafic/ultramafic intrusions like those in the Mikras area (Al Bayda), Al Thaniah area (Marib), and some other occurrences in Al Bayda, Lahj, and Sadah (Fig. 8.10).

8.4 Mining History in the Shield Rocks of Egypt

8.4.1 Introduction

Mining in Egypt has a long history through a succession of civilizations from ancient times. It may be divided into four main stages: (1) Pharaonic civilizations from 3100 to 332 BCE (~2800 years), (2) Hellenic and Roman civilizations from 332 BCE to 641 CE (973 years), (3) from the Arab conquest in 641 CE to the French campaign in

1798 CE (1157 years), and (4) from the French campaign to the present (223 years and counting). The history of Egypt is considered to be the history of human civilization, as the Egyptian people innovated and presented an ancient civilization that preceded any other civilizations of the world. The ancient Egyptian civilization was a good witness to the role of natural resources and their good exploitation. The Egyptian civilization was mainly based on the exploitation of stones that are available in huge quantities in Egypt, which had a great impact on its survival and continuity, from the ancient Egyptian civilization to our present time. It is not only based on the exploited types of stones but also due to the knowledge of the Egyptians and their skill in choosing the types of rocks that they used to bear their history through time. Therefore, Egypt is a home to mineral resources wealth, including gold, copper, silver, zinc, platinum, and a number of other precious and base metals. These resources are widely distributed in the Eastern Desert and the Sinai peninsula, which form an important part of that geological setting we know as the ANS. With an estimated 6.7 Moz of gold, 48 Mt of tantalite (fourth largest reserves in the world), and 50 Mt of coal, Egypt has the potential to be one of the top mining areas in the world.

Multiple civilizations proceeded in and due to Egypt, the cradle of Pharaonic civilization, an incubator for the Greek and Roman civilizations, a beacon for Coptic civilization, and a protector of Islamic civilization. All of these successive civilizations made their own contributions to Egyptian mining practices. During these various stages, the ancient Egyptian was not satisfied with obtaining basic survival needs from the raw materials found in the plateaus adjacent to the Nile, such as limestone, sandstone, alabaster, basalt, gypsum, and others, but extended to the most important and finest types of minerals and rocks in their various locations. It is interesting to know that the ancient Egyptians arrived in every place where there is a beautiful stone or a distinctive mineral, so that they reached places that people can only reach by great effort and perseverance. We are highly astonished when we try to understand what knowledge the ancient Egyptians possessed of local geology, the discovery of mineral sites, and the ability to extract the minerals in their natural form. Furthermore, what is their knowledge of the technology of metallurgy and metals, leading to the production of pure gold and the manufacture of its alloys with silver or copper in different types of rocks and minerals that are widespread in Egypt, in the Eastern Desert, Sinai, and in the Western Desert?

8.4.2 Mining During the Pharaonic Civilizations (3100–332 BCE)

The climatic conditions of the Egyptian deserts were favorable for human exploration and exploitation of the land and resources, as rainwater was available in deserts in predynastic times and continued during the first half of the ancient Pharaonic state. Afterwards, rain gradually decreased until dry desert conditions prevailed and continued to the present. Over the course of about 3000 years of exploration and

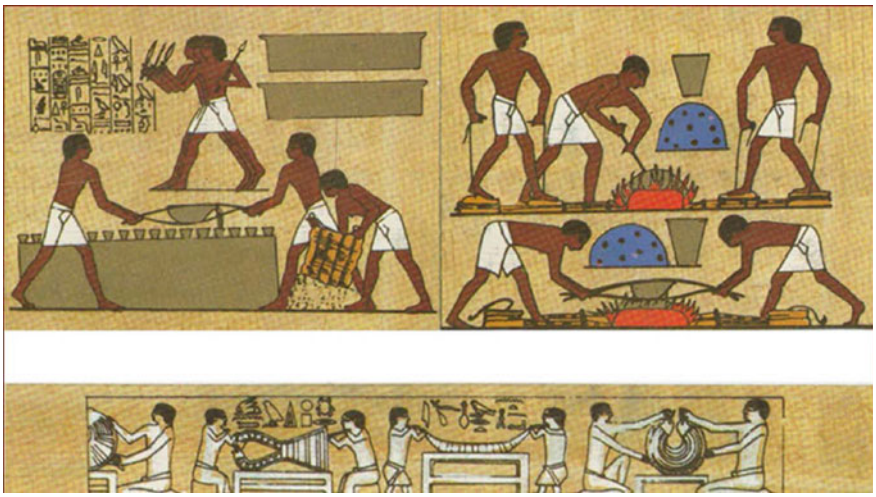

Fig. 8.14 A papyrus panel showing the ancient Egyptians' methods of smelting copper ores, casting them into molds, and forming copper products for various purposes

mining exploitation, the ancient Egyptians were able to build a civilization based on knowledge of the technology of metallic and nonmetallic mineral deposits. This knowledge was mainly on the basis of the following: (1) Knowledge of the scientific bases for exploration and the qualities of building materials and selection of the appropriate stones. (2) Knowledge of mining engineering methods for opening mines, methods of ore dressing, and metallurgical capabilities in smelting and refining metals, and of making mixtures and forming them for various purposes (Fig. 8.14), as well as the abilities to cut, transport, shape, and install suitable rocks. (3) Keep records on papyrus in libraries (or archives) of documents of mining activities, so that they can refer to and add new items to them (Fig. 8.14).

The ancient Egyptians knew copper in the predynastic period as a natural metal, and then knew how to extract this metal from its ore minerals, the most important of which were (and are) malachite and azurite. Egypt was therefore one of the first countries to enter copper-based civilization, and it expanded in the extraction of copper ores from the Sinai Peninsula, on the sides of Serabit El-Khadem and Al-Maghara. The piles of smelting waste are still there (Fig. 8.15), especially in the Al-Maghara area, which a witness to that history. In addition, copper ores were extracted from the Eastern Desert, from the Umm Samyuki and Abu Swyeil regions. Copper was used as weapons for the army, household appliances and statues, in which an exquisite example is the statue of Pharaoh Pepi I, in its natural size preserved in the Egyptian Museum.

As the need for copper increased, local resources were sometimes not enough. Egyptian influence extended to the sources of its raw materials in many places of Palestine, as Cyprus supplied it with its production of copper, especially during the Middle Pharaonic State. Then technological thought in Minor East Asia invented a

Fig. 8.15 Piles of smelting waste (slag) in the Bir Naseeb, Al-Maghara area, Sinai, Egypt

bronze alloy made of tin and copper, which had properties superior to those of copper alone. History states that, when the Hyksos army invaded northern Egypt during the seventeenth century BCE, among the reasons for its victory was that it was equipped with a weapon of bronze. At that time, the Egyptian army's weapon was still made of copper, but it then absorbed the secrets of making bronze, and its army's weapon became a match for the Hyksos army. The use of bronze was also common at the time and continued alongside the use of copper.

After that, ancient Egyptians focused their interests on the exploitation of lead, zinc, and iron. Lead- and zinc-bearing minerals are mixed in nature and could be found in Egypt on the coast of the Red Sea, including on the sides of Gebel Al-Rasas, Umm Ghaige, and Gebel Al-Zayt. Attention was focused on extracting lead metal alone, and its use was limited. The secrets of smelting and extracting iron ores were common in the Levant and Palestine about 900 BCE, but this technology did not reach Egypt until the Twenty-Fifth Dynasty (716–656 BCE). The two towns of Nokratis and Dafna in Lower Egypt were famous for their iron oxide smelting industry, starting from the Twenty-Sixth Dynasty. Perhaps iron oxides at the Bahariya Oasis and East Aswan were the sources of iron ore. Copper and gold were the two most extracted minerals through mining operations in Egypt. Tin was used with copper in making bronze, but it was not extracted in large quantities from the Egyptian mines; rather, it was imported from Syria for that purpose. King Zoser had captured the area around the Wadi Maghara site in Sinai, as the copper ore was extracted from its mines at the

beginning of the Third Dynasty. In the era of the Middle Kingdom, copper ore became available in the Eastern Desert of Egypt. By the time of the Eighteenth Dynasty, the Egyptians took control of the copper mines in Sinai, Timna, and other locations in the Wadi Araba. The finding of smelting residues around the mines indicates that mineral extraction was involved in onsite purification processes (Fig. 8.15).

The ancient Egyptians extracted gold from all over the Eastern Desert since prehistoric times, using their knowledge of copper extraction. With the regularity of state building and the unification of Egypt at the hands of King Narmer (Mina), gold became known for its importance in the state's economies. The government used to send missions on its behalf searching for gold resources, and the mission was headed by a senior statesman. The government invested in gold mines and had a monopoly on the production of gold. Starting with the Fifth Dynasty of the Old Kingdom, the state treasury system was completed by establishing the House of Gold (also known as *Barnoub*), where reserves of government gold were stored. Egypt, with its gold resources during the modern state, was considered the richest country in the region. Gold mines were extended and exploited by the ancient Egyptians in the Eastern Desert between the Nile and the Red Sea in Egypt and Sudan. Gold grains have been found in quartz veins that cross cut into the rocks, which the mines used to follow to depths up to the level of groundwater. In these ancient mines, ways of ventilation and mine supports are well known. Gold was extracted from quartz veins by fine grinding and then separating by water. There was no way to purify gold from its impurities of silver and copper except by smelting and re-smelting. In the time of the modern state, it was possible to obtain pure gold free of impurities, and it was possible to thin this pure gold by some methods until achieving a thickness of 0.001–0.0054 mm. The drafting in any place of the world could not reach what was previously reached by the formulation of the Pharaonic state in Egypt, except in the eighteenth century, when the industrial renaissance in Europe took place. Today we have a witness to the accuracy of the gold smithing in the Pharaonic period—it is the sarcophagus of Tutankhamun, weighing 133 kg of pure gold, which is preserved in the Egyptian Museum in Cairo.

Among the things we are proud of is a map drawn on papyrus of the Wadi Hammamat in the middle of the Eastern Desert. The map is known as the Turin papyrus, which was found on the western side of Luxor in 1820. It is a color map showing the location of the gold mine in the Fawakhir side of the Wadi Hammamat and is considered to be the first geological and topographical map in the world. Following is some information about the history of its discovery.

Around 1820, Bernardino Druvetti, an Italian collector of antiquities, found a papyrus scroll in a cemetery in the Deir el-Medina area on the western side of the Nile in front of Thebes (the modern city of Luxor). This was the cemetery of the family of Amenacht who was a high official (royal clerk) in the court of King Ramses IV (1151–1145 BCE). Within the scroll was a part of 2.82 m in length by an average width of 41 cm, on which a map was drawn. When this scroll was spread, it broke into 15 pieces, the largest of which was the part at its outer edge, which later turned out to be the location of one of the gold mines. This part of the roll was sold separately and the rest of the roll was sold to another party. All the parts of the scroll were later

collected and gathered at the Egyptian Museum in Turin, Italy. For a long time the link between the two parts of the scroll was not known. The focus was first on the part of the gold mine. The first person who drew attention to the importance of this part of the papyrus was Karl Richard Lepsius in 1842. This part measured 533 mm in length by 457 mm in width. It is a map of some desert landmarks, including six roads bracketed by mountains, a site for workers' homes, a temple, and a well (Fig. 8.16). Parts of the map are colored pink or red, including a mountain colored in red, on which is written "a mountain of silver and gold". In the center of the map is a pentagonal space colored in dark brown and has a white plaque with an inscription of King Seti I (1318–1304 BCE) of the Nineteenth Dynasty, thereby attributing the papyrus to him. The investigations continued regarding this map; Lepsius believed that it showed the location of the tomb of Seti I in the Valley of the Kings. In 1852, Samuel Birch suggested that the map was for the location of one of the gold mines in the Eastern Desert, suggesting that it was for the Derheib mine in Wadi Al-Allaqi. Then, in 1871, Louth published a detailed description of this part. In 1907, Ferrar proposed that it is for the area of Bir Karim (located to the west of the Umm al-Huwaitat phosphate mines), where ancient gold mines are located.

Fig. 8.16 The Turin Papyrus showing the map of an ancient gold mine during the reign of King Seti I (1350–1205 BCE)

In 1914, Gardens suggested that the mine should be linked to the Wadi Hammamat; he was the first to say that the map was a geological map. In 1942, Murray suggested that the site of the gold mine could be located next to the Umm al-Fawakhir well. On the other hand, Leblin had studied the other parts of the papyrus scroll (without knowing its relationship to the gold mine), and he published a paper in 1868 indicating that the mountains colored in black represent the quarries of the metagreywacke (*Bekhen stone,* or *Hajar Bekhen in Arabic language*) in the Wadi Hammamat. The researchers then realized that the parts of the scroll were related to each other, and they made sure of this and reconsidered the map in its entirety. This map is considered to be the first of its kind as a topographical map in the ancient history of Egypt. It was drawn on a rough scale of approximately 1:5000. This map is thought to be the first geological map in history and the first about gold sources. It distinguished a group of rocks called, in our modern scientific concept and terminology, *siliciclastic* rocks. Hammamat includes quarries for cutting limestone and greywackes and quarries of a very tenacious type of conglomerate known as *green breccia* (*Verde antico*).

Some Egyptologists attribute this map to the time of Seti I, based on the fact that the white board shown in the map is for the king Seti I. Another opinion attributes the map to the time of Rameses IV, based on the fact that the document was found in the tomb of Amenacht, who lived in the era of Ramses IV. It has been confirmed that all of the map explanations, which were written in hieratic on both sides of this papyrus, were in the handwriting of the Amenacht; the time between Seti I and Ramesses IV is about 160 years. The finding of such important documents confirms that there were libraries (or archives) of documents attached to temples or royal palaces and senior statesmen or attached to some governmental departments. We expect to include reports on the results of exploratory and extractive mining missions, and to include maps and indicative data that could be referred to before organizing new mining missions. This is what makes us to expect the existence of other papyrus documents related to desert activities, including mining activities. It is important to review the huge amount of papyri that are kept by international museums, so perhaps we can find more such as the Turin papyrus.

In addition to the metallic mineral mining, ancient Egyptians excelled in using and fabricating various types of stones. The durability of these stones preserved the history of Egypt, including the various building structures, drawings, and writings engraved on it. These stones were varied, with their own qualities and uses, as follows.

Limestones: Sedimentary rocks with chemical composition of calcium carbonate. Limestones were widespread on both sides of the Nile valley from Cairo in the north to the middle of Upper Egypt. The ancient Egyptians cut large and small blocks, built pyramids and temples (Fig. 8.17), and carved pots and vessels using limestones. The use of limestone flourished when Memphis was the capital of Egypt. The ancient Egyptians conscripted the people of the Old Kingdom in building the pyramids with all the available science and technology reached in that era. There are ten groups of pyramids built on the edge of the western plateau overlooking the Nile, extending from Abu Rawash to the Faiyum depression. In addition to the engineering creativity in building the pyramids, it was preceded by the preparation of a subsurface structure,

Fig. 8.17 Examples of using limestone by ancient Egyptians to build pyramids and temples. The Great Sphinx was carved from a rock in its place in the limestone quarry next to the pyramid of Khafre

which included digging a trench, a column well, or an inclined tunnel inside the rock, with a perfect mining study.

Sandstones: Sedimentary rocks with basic chemical composition of silica, which are widespread on both sides of the Nile from the middle of Upper Egypt to the far south of Nubia. The use of sandstone flourished while the capital of Egypt was Taibah (Luxor). The use of sandstone is evident in the ruins of the temples of Luxor, Karnak, Qurna, Ramesseum, and many other places in Upper Egypt (Fig. 8.18).

Aswan Pink Granite: A world-famous granite, where the blocks were carefully tested in the quarry before being separated from the façade. The Nile was the effective means of transportation, leaving no room for the granite to be extracted from other sources in the desert, far from the Nile. Statues, obelisks, and coffins were built from the Aswan pink granite; the walls and the roofs of many buildings were covered with it (Fig. 8.19a). The greatest obelisks were made during the modern state; few are still standing, some have been destroyed, and many have been moved abroad. Most of the obelisks, especially the large ones, were cut from granite. The genius of carving obelisks comes in choosing granite from which a single block can be cut without being damaged by breaks or cracks. The unfinished obelisk located to the east of the Aswan city is a testament to the genius of the ancient Egyptians in carving the obelisks (Fig. 8.19b). If it had been completed, it would have reached 41.75 m in height and weighed 1168 t. Many Egyptian obelisks were distributed in a number of

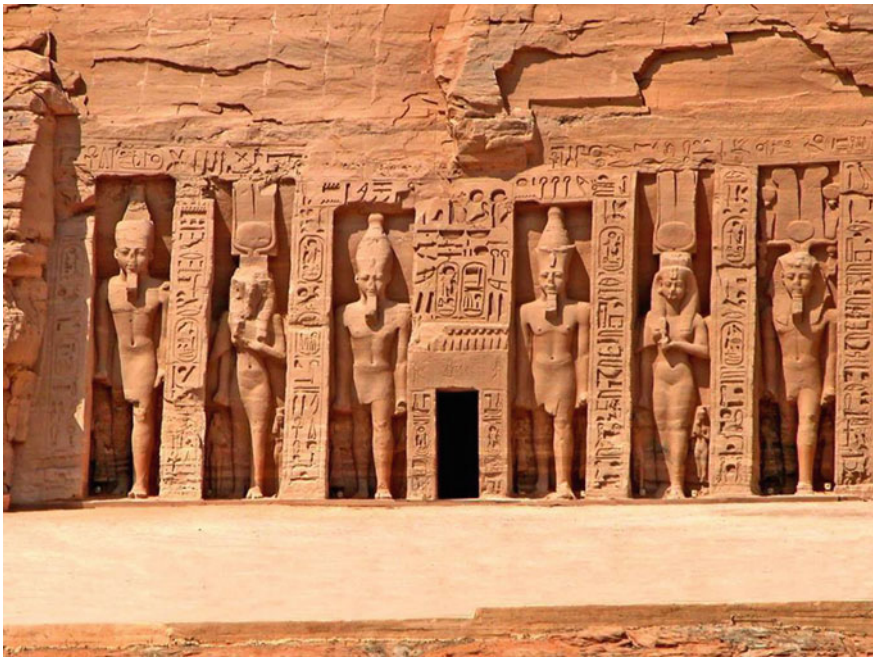

Fig. 8.18 Abu Simbel temple and its sandstone statues, Luxor, Egypt

countries, the most famous of which are in Rome, Istanbul, Paris, London, and New York. In Rome alone, there are 13 Egyptian obelisks.

Six life-size statues of King Khafre were carved out of a stone called *Khafre diorite* (Fig. 8.20a). No source for this type of stone was found except in one quarry located to the west of Toshka, in southern Upper Egypt. In the Egyptian Museum, one of the six statues is considered to be a sign of splendor (Fig. 8.20a). Alabaster is also a kind of crystalline calcium sulfate rock, which was used by ancient Egyptians to carve very nice statues like that of King Khafre (Fig. 8.20b). Statues of enormous sizes and numbers were sculpted from alabaster, of which only a limited number now remain. Small artifacts of great precision and delicacy in workmanship were also sculpted from it (Fig. 8.20b). There is a quarry of greywacke in the Wadi Hammamat between Qena and Quseir. Large numbers of statues were carved from the greywacke found there due to its ability to be polished and to give it a smooth surface that conveyed majesty and dignity.

In addition, the ancient Egyptians obtained table salt from lakes in the northern delta and from some sabkhas throughout Upper Egypt. They obtained natron, needed for medicinal formulations and embalming, from the lakes of Wadi Al-Natron and from some sabkhas in the western delta. The ancient Egyptians mastered the combination of various color pigments, the most famous of which were red ocher, yellow ocher, green malachite, and blue azurite powders. Furthermore, the ancient Egyptians knew turquoise (a blue-to-green gemstone that is a hydrated phosphate of copper and

Fig. 8.19 Obelisks fabricated from Aswan pink granite. **a** The obelisks of Luxor. **b** the obelisk of Aswan, which was not completely truncated

aluminum) from Sinai from early in history and extracted it from Sarabit Al-Khadim. They recognized blue amethyst, as well as carnelian (a brownish-red semiprecious gemstone) and agate (both of which are forms of chalcedony), and polished lobes from which they placed their jewelry.

Fig 8.20 **a** A life-size statue of Khafre fabricated from diorite called *Khafre diorite* and **b** a huge alabaster statue of King Khafre

8.4.3 Mining During the Hellenic and Roman Civilizations (332 BCE–641 CE)

Ptolemaic rule continued until 31 BCE. Rule of Egypt then moved to the Roman Empire with its capital at Rome, then moved to rule by the Byzantine (Eastern Roman) state, with its capital at Constantinople, in 395 CE. This latter stage ended with the entry of the Arab armies in 641 CE. Throughout Ptolemaic, Roman, and Byzantine rule, Alexandria was Egypt's capital, for nearly 970 continuous years. The entire civilization of Egypt had one character: Hellenic (Greek) culture mixed with the ancient Egyptian and Coptic cultures. Among the critical, defining features of this civilization were: (1) The way of writing evolved from hieroglyphs to hieratic to demotic. (2) A history of Egypt was written in Greek by Manitone, an Egyptian priest. (3) Alexandria was a beacon of knowledge led by researchers; the library of Alexandria was established to meet the needs of scholars. (4) New ports were built on the Red Sea coast, the most important of which were Baranis and Abu Shaar, and a network of roads was built in the Egyptian deserts.

The most important metallic commodity during this period was *gold*, the mining of which was the monopoly of the state and was performed by criminals and prisoners of war. Gold extraction was active from the mines of the Eastern Desert, especially in the Wadi El-Fawakhir region, so much so that Ptolemy III built a temple there, indicating the regularity and continuity of the work. In addition, the Wadi Al-Alaqi area became active for gold production. *Iron* production was limited during this period—iron ores

were smelted on a small scale and soon stopped during Byzantine rule. Among the sources of iron ore is the Wadi Abu Jarida in the northern Eastern Desert, as well as the Bahariya oases and eastern and western Aswan. Furthermore, civil life, starting from the Ptolemaic period, required quantities of *lead* to manufacture water and sewage pipes for homes. Therefore, the exploitation of lead ore resources has been active throughout the Eastern Desert, especially on the Red Sea coast between Quseir and Baranis. *Silver* was used on a large scale during the Ptolemaic period for many purposes. There were no sources of silver in Egypt, but due to the strong connection between Egypt and Greece, which had the most important sources of silver at that time, it was easy to obtain quantities of it.

The Ptolemies were the first to know the existence of *emeralds* in the Wadi Al-Gemal region in the middle of the Eastern Desert of Egypt. The Ptolemies focused on the exploitation of emeralds (a green gemstone with hexagonal crystals), and they opening mines for it at the Skait, Um Kabu, Um Debaa, and Um Harah sites. They expanded those mines so that there was permanent employment for which houses and temples were built, including a temple carved into the rock and an attic Greek writings (Fig. 8.21). Interest in emeralds continued throughout the Ptolemaic period and part of the Roman era. The Ptolemies also discovered *peridot* (greenish-color olivine crystals) on a small island in the Red Sea, Saint John's Island, off the coast of the Ras Banas peninsula. It is said that the first peridot stone extracted from it was given to Queen Pranis, mother of Ptolemy II.

Fig. 8.21 Ptolemaic temple carved into the rock at the Emerald area of Wadi Skait, Southeastern Desert, Egypt

In addition to metallic elements and gemstones, the ancient Egyptians used building and dimension stones on a large scale. Ancient Egypt, before the Ptolemies, used mortars made of a mixture of clay and roasted gypsum in building. Mortar containing quicklime did not begin to be used until the time of Ptolemy I. The Romans also introduced the use of burned bricks in buildings. Sandstone was extracted from the Al-Silsilah and Nubia quarries to build temples. Alabaster was extracted from its sources on the sides of the Nile River. Greywacke was extracted from the Wadi Hammamat, and was given the name of *ferrei coloris atque duritiae*. White marble, which was mostly imported, was popularly used for sculpting statues. In addition, the Romans were interested in cutting a type of green breccia in the Wadi Hammamat in the Eastern Desert, which they called *breccia verde antico*, that is very hard and very beautiful when polished (Fig. 8.22). It was exported in quantities throughout the Roman Empire. Despite its distance from the Nile, their choice fell on a source of grey granitic rock, granodiorite, in the west of the Safaga Mountains, to exploit it. It appears that it was dedicated to cutting and forming the huge columns. Some of these columns are still attached to the façade of the quarry. In the quarry yard, some cylindrical columns are lying around waiting to be moved; the longest of these are 18 m with a diameter of 2.6 m. The name of this historical quarry, the *Quarries of Mons Claudianus*, is attributed to the Roman Emperor Claudius.

Fig. 8.22 Cutting blocks of green breccia, called *verde antico*, in the Wadi Hammamat in the Eastern Desert of Egypt. It used to be exported in quantities throughout the Roman Empire

To the west of the city of Hurghada is a high mountain chain of volcanic rocks that have a porphyritic texture. The Romans chose a special kind of red, fine-grained, spreading rock with white granules that they called *imperial porphyry*, which, when polished, gives very beautiful surfaces (Fig. 8.23). Blocks were carved from it, from which columns and wall cladding panels were carved (Fig. 8.23). It was a material for export throughout the Roman and Byzantine empires. A number of sarcophagi remain in Egypt made from the stone of imperial porphyry in the cemetery of Kom Al-Shuqafa in Alexandria. In the Roman Museum in Alexandria, there is a huge statue of this porphyritic rock, which is believed to be for the Roman emperor Diocletian. Interest in this stone ceased with the end of the Byzantine Empire presence in Egypt. In addition, one of the most important stone engravings attributed to the Ptolemaic period is the Rosetta Stone, which was found under what is now known as the Rosetta Castle (previously, Fort Rashid or Fort Julien, among others). The stone is a block of basalt (or possibly greywacke), 113 cm × 27.5 cm (Fig. 8.24), engraved on its smooth side with a royal text celebrating the first anniversary of the coronation of

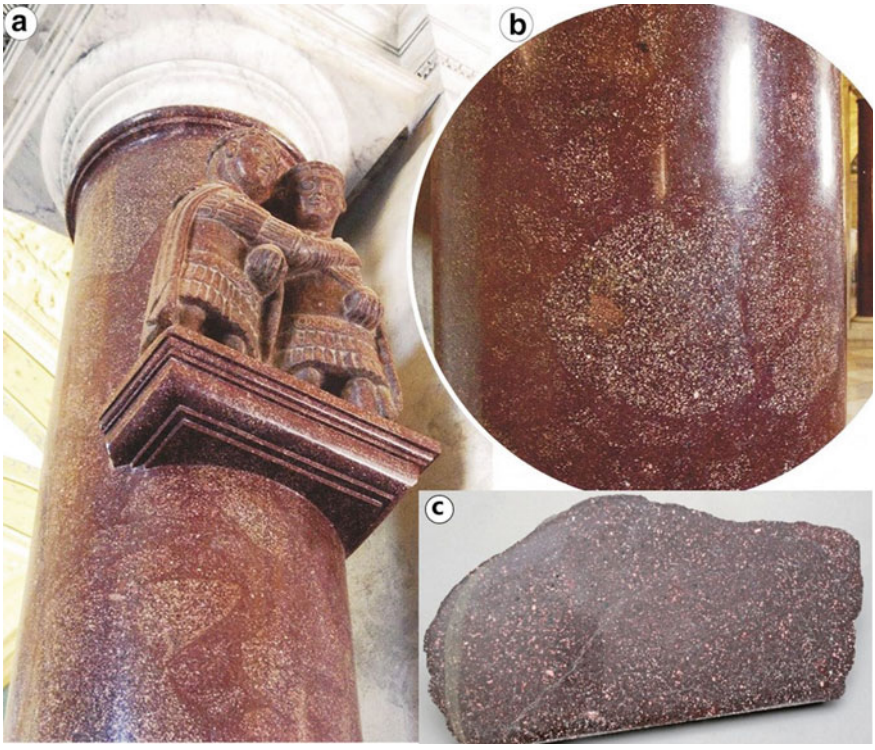

Fig 8.23 **a** Roman column of brecciated Imperial Porphyry, 3 m in length, with a sculpture of two male figures, interpreted as Roman coemperors of the tetrarchy period (293–313 CE), Vatican Library, Rome. **b** Close-up of the brecciated rock consisting of fragments with porphyritic texture, rich in white colored plagioclase phenocrysts, in a fine-grained matrix of dark purple color. **c** Hand specimen of fine-grained Imperial Porphyry rock (from Abu El-Enen et al. 2018)

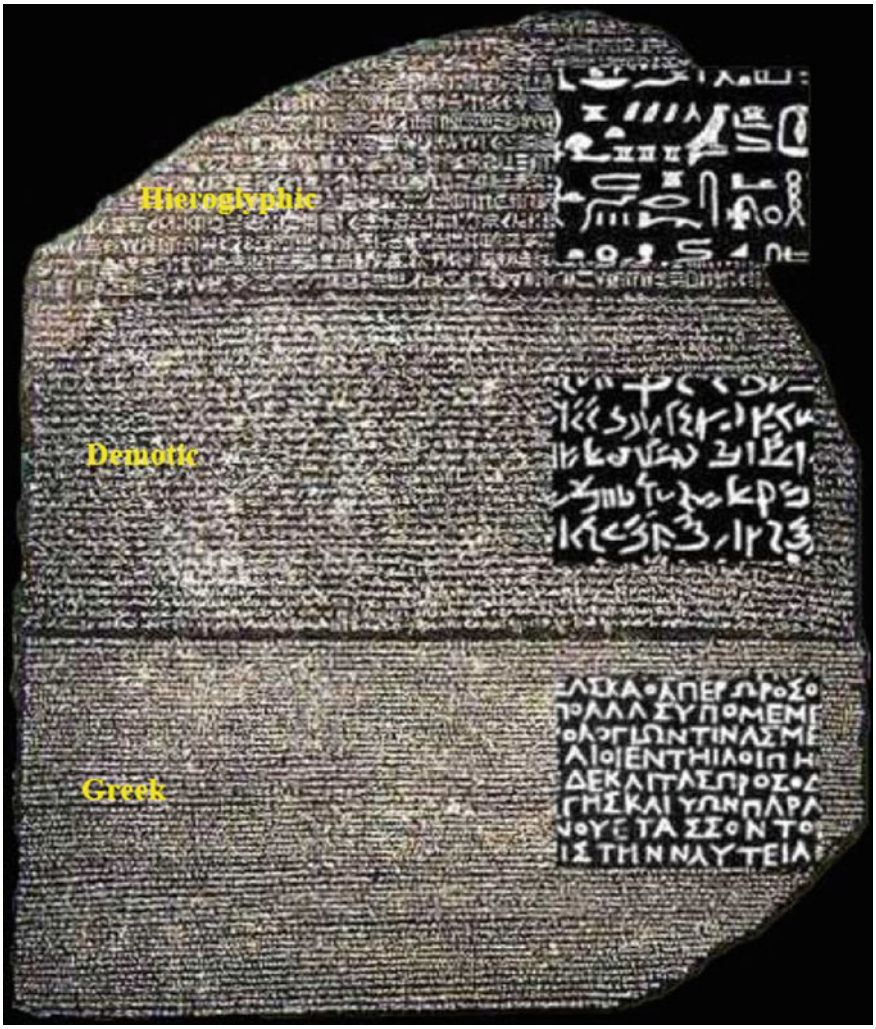

Fig. 8.24 The Rosetta Stone, discovered in Rosetta Castle, Northern Egypt, with three writing systems: hieroglyphic, demotic, and Greek. The stone is currently preserved in the British Museum in London

Ptolemy V as king. The same text is inscribed on the stone in both ancient Egyptian and Greek languages, with three writing systems (Fig. 8.24): hieroglyphics, demotic, and Greek. The stone is currently preserved at the British Museum in London.

8.4.4 Mining from the Arab Conquest (641 CE) Until the French Campaign (1798 CE)

The mining extractive activities in Egypt throughout this period did not have a significant share. Most industrial activity was concentrated in transforming metals into handicraft products of beauty and precision, the most famous of which were the copper vessels inlaid with silver and gold wires. The glass industry rose as did the ceramics industry. Despite the lack of mining activities in the Eastern Desert at that time, historians of the time mentioned the presence of ores. However, the modern mining renaissance began with the French campaign in Egypt; many scientists in various sciences accompanied the campaign, among whom, of course, were specialists in geosciences. Due, however, to the short period of the French campaign, which extended from 1798 to 1801, a long-term plan could not then be implemented. The French campaign was followed by Mohammed Ali Pasha's rule in Egypt in 1803. He succeeded in placing Egypt on the threshold of modern civilization and modernity. Mohammed Ali began sending geological expeditions to locate the raw minerals necessary for the realization and building of a modern state. He also established the school of minerals (Al-Maaden School) in Old Egypt in 1834 CE, and re-explored the sites of mining raw materials. He sought help from scientists of different nationalities, which added a spirit of competition among all, and ultimately contributed to the industrial and civilization revolution in modern Egypt.

The Authority of Egyptian Survey was established in 1896. This name was changed to the Authority of Egyptian Mines and Quarries in 1905, then to the Mining Authority, and finally, in 2005, to the Egyptian General Authority for Mineral Resources, its present-day name. Over the years of its existence, the commission has played a pioneering role in serving the national economy in the fields of geology and its applications, especially in the areas of mineral exploration and its proper exploitation and development.

8.4.5 Gold as an Example for Mining History in Egypt

Humans have appreciated gold from ancient times to the present day. Egypt was the principal gold-producing country in ancient times. Coptos (present-day Qift) on the eastern side of the River Nile was the chief politically important town in ancient Egypt. Coptos was an important harbor on the Nile (Fig. 8.25); it dates back at least to the First Dynasty, and connected with Quseir, a famous harbor on the Red Sea, via what is now known as the Qift–Quseir road. Along this road, basement igneous and metamorphic rocks outcrop from that broad, high structure, along which many ancient gold mines are located. During the Eleventh Dynasty (2133–1991 BCE), Coptos was overshadowed by Thebes (present-day Luxor), about 50 km to the south, which became the capital of the Middle Kingdom of ancient Egypt (Fig. 8.25). Coptos was the world's first gold boomtown; it was located in the Wadi Hammamat

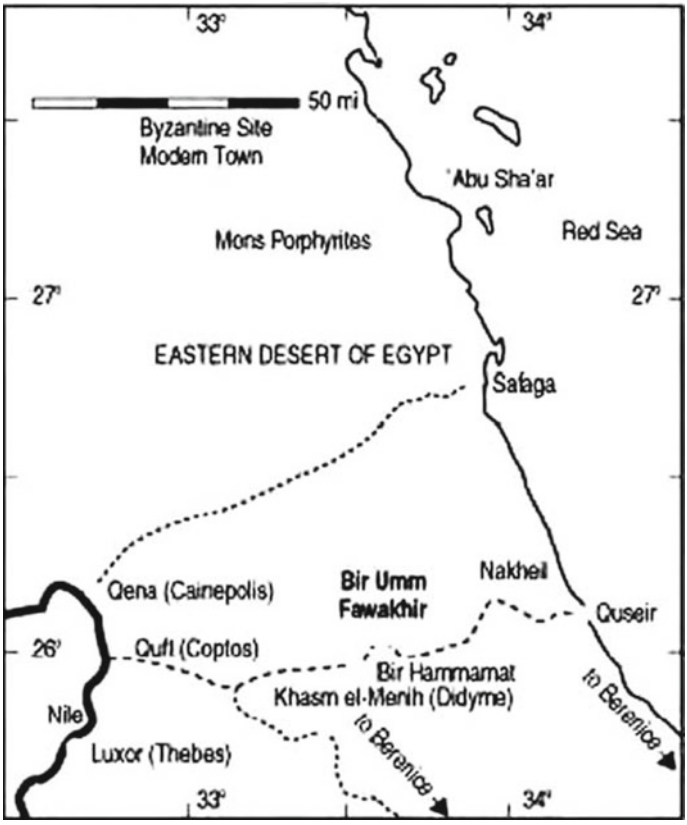

Fig. 8.25 Location map showing the city of Coptos (present-day Qift) in Upper Egypt, the most ancient gold-mining center (from Habashi 2016)

dry riverbed that alluvial gold had been washed down from the gold-bearing quartz veins found later in the surrounding granite hills. The meaning of *Nubia* in the old Egyptian language is "gold"; underground mining of gold-bearing veins was well-established, by 1300 BCE, in Nubia under Egyptian rule. There were more than 100 gold mines in the area at the time, where a series of forts were built to protect the flow of Nubian gold along the rich trade routes (Fig. 8.26). To safeguard the gold mines along the trade routes and the quarries, ancient Egyptians built forts and watchtowers along all the Coptos–Quseir route. Each fort had a water well, hosted a garrison of about 50–70 Egyptian auxiliaries, and offered rest and water to travelers, who had to pay a tax to pass through. The garrison also supplied sentinels for the watchtowers and escorts to travelers. A chain of watchtowers allowed strict control of the entire route, since towers are visible from one to another, where messages could be quickly transmitted between them by mirrors and flags. Egypt became the dominant power in the Middle East, having the greatest gold-filled treasury in the ancient world.

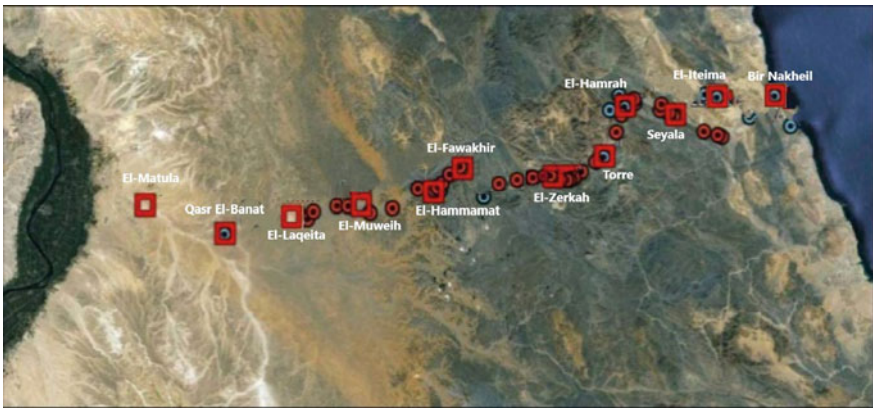

Fig. 8.26 A rich trade route along the Coptos–Quseir road (currently the Qift–Quseir road), along which a series of forts was built to protect the flow of Nubian gold transportation

The ancient Egyptians did not have an important port on the Mediterranean Sea—all their trade was through the Red Sea. The most important trade routes to the port began at Coptos (Fig. 8.25). Under the pharaohs, the whole trade of southern Egypt with the Red Sea passed over these two roads. Under the Ptolemies, in Roman and Byzantine times, merchants followed the same roads for purposes of barter with the coasts of Zanzibar, Southern Arabia, India, and the far east. This place and the surrounding area were known for the richness of its gold mines and semiprecious stones. A temple was built there by Tahutmes III, who ruled from 1503 to 1450 BCE and was coregent with Queen Hatshepsut for 21 years. The occupied area was about twice as large as Tahutmes' temple at Madinet Habu in Luxor. The ancient Egyptians were the first to treat gold-bearing rocks, which is well-documented on the wall paintings in their temples (Fig. 8.27).

Some historic gold mining sites in ancient Egypt are shown in (Fig. 8.28), where almost all ancient gold workings were confined to the rocks and wadis of the Neoproterozoic Nubian shield (Zoheir et al. 2019). Nearly all historic gold mining activities in the Eastern Desert of Egypt were located in the Proterozoic basement rocks. The ancient working sites are mostly related to the fourth century BC, from pre- and early dynastic times (Fig. 8.28), but are few in number. In the Old and Middle Kingdoms (2700–1794 BC), the ancient workings were more abundant, clustering along the western margin of the Eastern Desert in the vicinity of the major traffic routes between the River Nile and the Red Sea, as well as inland from Marsa Alam. Other clustered ancient mining sites occurred in the far northern part of the Eastern Desert (Fig. 8.28) (Zoheir et al. 2019). During this period, gold was mainly produced from gold-bearing quartz veins with minor disseminated sulfide minerals such as pyrite, chalcopyrite, and arsenopyrite. Ancient miners used secondary copper staining materials (malachite and azurite) as a key prospecting guide to recognize the mineralized sites. Fist hammers, heavy-duty two-hand hammers, and grooved stone axes, as well as stone pounders and stone grinding mills, were the main mining tools used during the Old

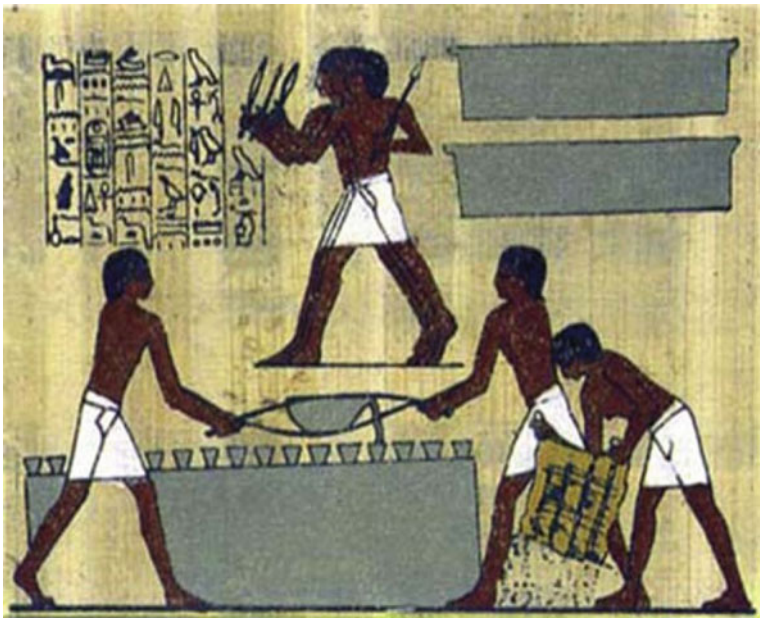

Fig. 8.27 Wall painting of Ancient Egyptians dated back to about 1450 BCE in the tomb of Rekhmire, vizier to Thothmes III at Thebes, showing metal workers casting molten gold in the molds (from Habashi 2016)

and Middle Kingdoms (Fig. 8.29a–d) and the New Kingdom (1550–1070 BC). These tools enabled grinding of the gold-bearing quartz ore down to a pea-sized fraction and a subsequent milling to flour fineness, thereby freeing micrometer-sized free gold grains.

During the Roman period, gold mining in Egypt went into a phase of decline, or even a partial standstill in the Nubian Eastern Desert. The gold mining activities were restricted in the Egyptian Eastern Desert to some known productive districts near the desert routes and water supply stations (Hydreuma) that had already been established during the Ptolemaic Period and were now being developed under the Romans. The main mining activities during the Roman Period (between the first and fourth centuries CE) are concentrated in the Eastern Desert on the well-evidenced stone quarries at Mons Claudius, Mons Porphyrites, Wadi Semna, Barud, and various smaller sites (Harrell 2002; Sidebotham 2008, Klemm and Klemm 2013). No traces of gold mining in the Roman period have been found there. However, in the earlier periods, the ore lumps had been crushed by the aid of relatively large anvil and grinding stones and even on the surfaces of runner stones; in the Ptolemaic period more specialized, but much smaller stones were used for that same purpose (Klemm and Klemm 2013).

During the conquest of Egypt by the Greek general Ptolemy, new mining expertise was brought to the region. The following period of Ptolemaic gold mining

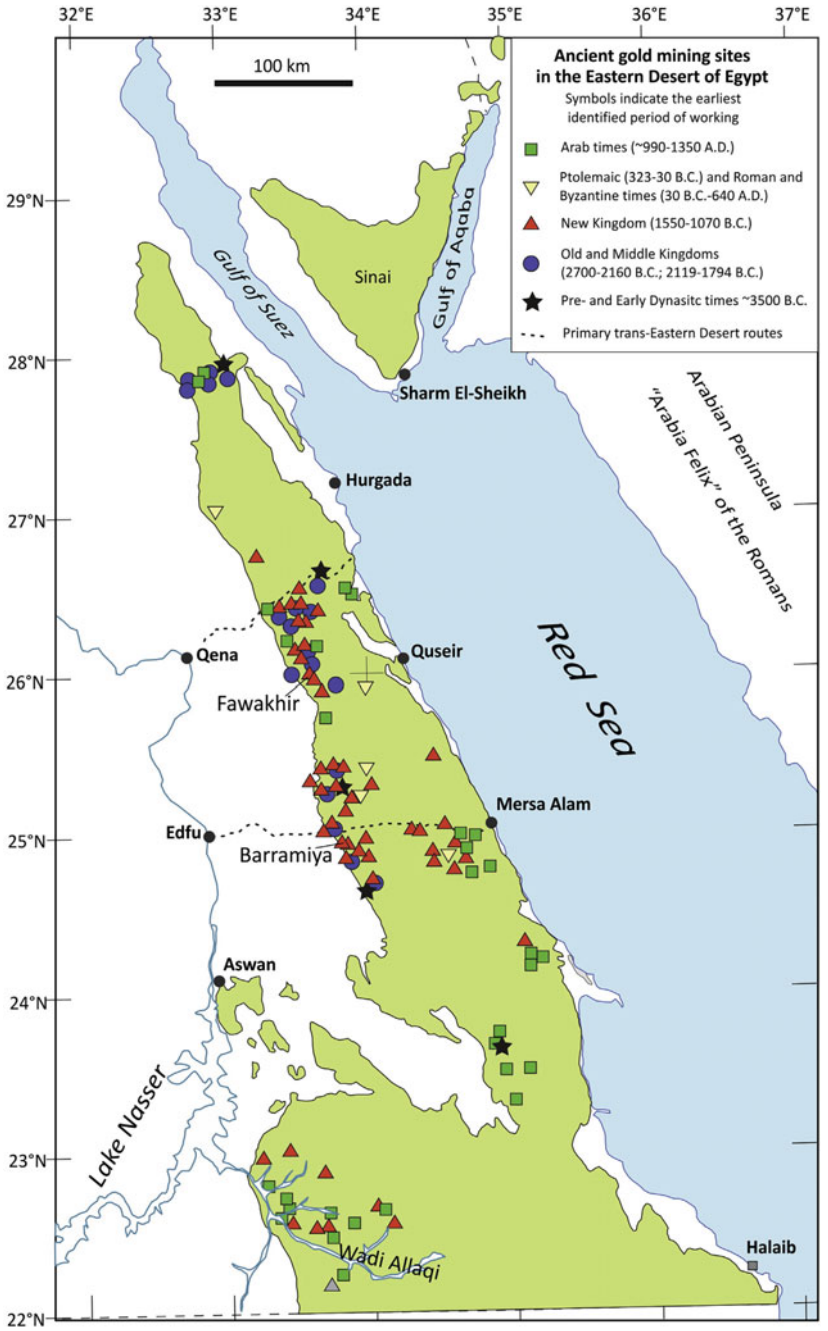

Fig. 8.28 Historical gold mines in the Eastern Desert of Egypt plotted according to the earliest known age of working (from Zoheir et al. 2019)

Fig. 8.29 Styles of ancient tools using for crushing, grinding and extraction of gold. **a** Fist hammers with originally pointed impact surfaces for chipping off ore fragments, Old Kingdom, Abu Mureiwat, Egypt. **b** Heavy duty two-hand hammers used for crushing gold-bearing quartz for extraction, Higalig mine, Egypt. **c** Mortar from red granite and pounder used for crushing gold-bearing quartz ores, Middle Kingdom, Daghbag, Egypt. **d** Flat grinding mill and fist grinder from the New Kingdom for producing quartz powder, Marahig, Wadi Allaqi, southern Egypt. (*Source* Klemm and Klemm 2013)

continued through Roman and Byzantine times (Fig. 8.28). Gold processing technology continued to improve through the introduction of the rotary mill, which remained widely in use for centuries until the Early Arabic period in both Egypt and Nubia (Fig. 8.30a, b) (Klemm and Klemm 2013). (It is still occasionally seen even in the present day in rural communities in the Nile Valley and the Eastern Desert for grinding cereals.) The rotary round mill consisted of a flat, stationary base stone with a diameter between 40 and 60 cm, and an upper rotary disc with a central fill hole and a lateral perforation for the handle (Fig. 8.30a, b). The rotor disc was slightly smaller than the stationary base stone. Beyond the Egyptian borders, it was widely used for grinding both cereals and ores in the entire Roman Empire and the British Isles until the Medieval period. The Ptolemaic gold production sites were almost exclusively in the central part of the Eastern Desert, along the Wadi Allaqi area in the south or in other areas; they mostly neglect workings in the north. The gold mining areas during the Roman times were more limited to only a few, well-defensible sites, such as Bir Fawakhir and Barramiya.

During the Arab times (c. 990–1350), gold production was focused on sites in the northern, central, and southern parts of the Eastern Desert. Arab gold mining

Fig. 8.30 Styles of advanced rotary mills of ancient tools using for crushing, grinding and extraction of gold. **a** Bottom and top different halves of rotary mills, Early Arab Period mining district at Sagia, Egypt. **b** Different shapes of globular pounders and rotary mills used for crushing gold-bearing quartz, Early Arab Period, Aradiya-East, Egypt. **c** Remains of an inclined washing table including its back flow channel and collecting basin. (*Source* Klemm and Klemm 2013)

production, in contrast to earlier periods, however, focused on alluvial gold in wadi workings compared to the hard rock operations, which were relatively scarce. The Early Arab mines often date back to older complexes from the Ptolemaic and New Kingdom periods. New mines were also opened, which tend to be located along the coastal strip of the Red Sea. The mines during Arab times were enlarged and lowered down to greater depths, and ventilation limits for breathing and lighting were driven down to depths approaching 35 m. They straightened existing mine shafts and new ones were excavated to be as straight as possible, often in large tunnels. The final separation of free gold from the milling quartz powder was done using the so-called "inclined-stone tables" or "washing tables" (Fig. 8.30c). These washing tables were used in this period as sluices to separate gold contained in the milling of gold-bearing silica ore slurries (Fig. 8.30c). Such tables were usually equipped with gutters and basins to ensure that the water used in the washing process flowed back

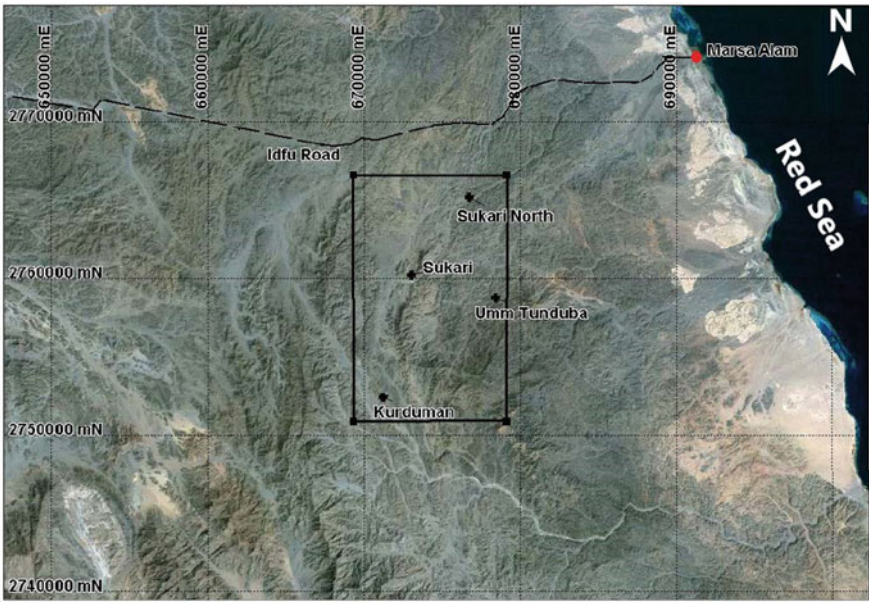

Fig. 8.31 Location map of the Sukari concession area containing the proposed Sukari mine site and surrounding prospects. (Modified from Franzmann et al. 2015)

into a collecting basin where it was retrieved before being reused in another sluicing process (Klemm and Klemm 2013) (Fig. 8.30).

Lastly, sporadic gold mining activities occurred in Egypt over the past few hundred years into modern times. Production of 6.7 t of gold from quartz veins from the El Sid gold deposit took place between 1902 and 1958 (Kochin and Basyuni 1968). The Atud gold deposit had explored by the Egyptian Geological Survey and Mining Authority (EGSMA) between 1953 and 1969 to a depth of 78 m. The Sukari gold deposit, west of Marsa Alam, is presently the only significantly producing mine in Egypt, which is operated as a joint venture between Centamin and the Egyptian government. It is worked as a large-scale open-pit and a high-grade underground mine (more detailed information is given below about the Sukari gold mine as an operating mine). The open-pit operations commenced in 2010, while underground operations began in 2011. In 2012, the Sukari Gold Mine Co. mined about 6.4 Mt of ore, processed 4.5 Mt of ore, and produced 8.175 t Au (Taib 2015). Under the Egyptian Mineral Resources Authority (EMRA) and control of the Shalatin Mineral Resources Company, licenses for small- and medium-sized mining companies are currently being issued for the southern part of the Eastern Desert. Among these, Thani Stratex Resources Ltd is exploring a system of quartz veins in granodiorite in the Anbat–Shakoosh area in the southern Eastern Desert. In the central part of the Eastern Desert, Aton Resources Inc. (formerly Alexander Nubia International Inc.) is exploring for gold associated with VMS deposits at Hamama and Abu Marawat (Zoheir et al. 2019).

8.4.5.1 The Sukari Gold Project as an Example of an Operating Mine in Egypt

The Sukari gold project is located about 25 km southwest of the Red Sea coastal town of Marsa Alam in the Eastern Desert of Egypt, at latitude 24° 56′ 50″ N and longitude 34° 42′ 27″ E. The Sukari concession (Fig. 8.31) covers an area of about 160 km^2, containing the proposed Sukari mine site and surrounding prospects. The Sukari area has a long history of mining and exploration, starting from the predynastic period (about 3200 BCE) and continuing through the Ptolemaic, Roman, Arab, and British colonial periods, and up to the present day. Gold was mined at the Sukari area in Pharaonic and Roman times, with perhaps ~1000 kg of gold produced. Small-scale mining was re-established in 1912 and continued to 1914 by British concerns, but it seems to have ceased at the outbreak of World War I. More substantial operations were undertaken in the period 1937–1951, with recorded production of 4768 kg of gold from underground workings (Franzmann et al. 2015). There are numerous small pits located over about 2 km strike on the Sukari mountain ridge. There are also small pits in riverbed (wadi) colluvium along the flanks of the ridge, most notably in Wadi Pharaoh to the east of the northern part of the ridge. The old Sukari mine was established on an outcropping quartz vein (the Sukari main lode) on the southwestern flank of Sukari Ridge. In Pharaonic times, mining of these veins extended to about 50 m from the surface, about 200 m along strike, with stopes ~1 m in width.

The Sukari gold project consists of four geographically primary zones that contain varying degrees of ore mineralization: they are, from south to north: Amun, Ra, Gazelle, and Pharaoh (Fig. 8.32). The Sukari gold project is designated as having both open-pit and underground mining systems (Fig. 8.33a, b). The open-pit mine is based on the main and Hapi ore zones, which have been extensively drilled in the various high-grade zones of the Amun and Ra/Gazelle areas. In modern times, the first gold production was commenced at Sukari in June 2009 and the commercial production began on 1 April 2010, making Sukari the first modern gold mine in Egypt. The Sukari mine produced over than 150,000 oz of gold in 2010 and more than 200,000 oz in 2011.

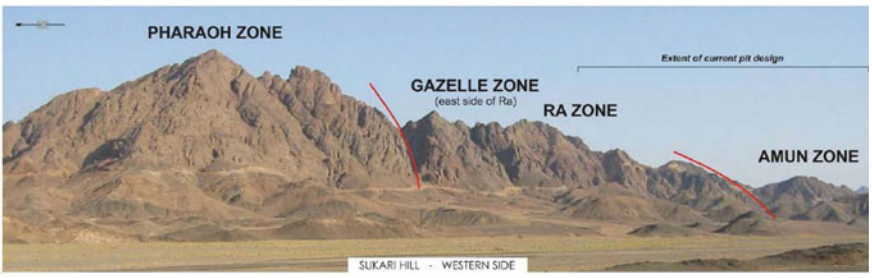

Fig. 8.32 Mining area of the Sukari Hill with different designated geographical zones (from Franzmann et al. 2015)

Fig. 8.33 Mining operations in the Sukari gold mine as open-pit **a** and underground **b** mining system

The Sukari gold-bearing vein deposit is hosted exclusively by the Late Neoproterozoic Sukari granite porphyry, which intruded within the island-arc and ophiolite rock assemblages that together occur within the Wadi Ghadir ophiolitic mélange. Porphyry granite dykes in the hanging wall of the main porphyry body show gold mineralization as do those in the main porphyry intrusion, whereas wall rocks immediately adjacent to those dykes are barren of gold. These porphyry dykes range in thickness from a few centimeters to several meters. The Sukari granite porphyry intrudes both the ophiolitic serpentinites and associated volcanoclastic sediments. The hanging-wall sequence to the east is complexly deformed and comprises a mixture of serpentinite, metaconglomerate, lesser fine-grained metasediments, minor basalt, and porphyry dykes or sills that are assumed to be genetically related to the main Sukari granite

porphyry. The footwall sequence within 50 m of the granite porphyry comprises fine-grained pelitic metasedimentary rocks with lesser basaltic rocks. Outcrops are poor, with low ridges and mounds formed by outcropping serpentinite, which suggests that this lithology dominates the footwall sequence. Gold mineralization in the Sukari mine is intimately and dominantly associated with sulfide mineralization. Pyrite is the most abundant sulfide mineral, followed by arsenopyrite. The high gold grades are mostly associated with increased arsenopyrite contents. Pyrite is found in all of the mineralized zones; it was formed continuously through the various stages of mineralization. Other sulfide minerals, including galena, chalcopyrite, sphalerite, and pyrrhotite are also found within the deposit. Silver is only present at very low levels (generally <1 ppm), with no correlation with gold content.

There are four types of mineralized quartz veins in the Sukari gold mine site: (1) Contorted and banded quartz veins, due to multiple deformation and veining episodes. These are similar in character to the low-sulfidation epithermal Au–Ag vein deposits. This type of veins is clearly shown in the Sukari Main Reef. Arsenopyrite is the main sulfide mineral in these veins. They host the highest-grade mineralization at the Sukari gold mine. (2) Brecciated veins because of brecciation of quartz vein and porphyry rock fragments. In some exposures, breccia zones can be developed at the contacts with the contorted veins and host porphyry. (3) Shear veins, which are rare centimeter-scale laminar veins with vague contact-parallel layering. They sometimes have sulfides and or hematite bands developed at the vein-wallrock contacts. (4) Spaced extensional veins, which are distinguishable by their short strike lengths and, in places, by internal structure indicating purely extensional opening with no cross vein displacement.

Gold in the Sukari mine occurs in three distinct positions within the lode system (Helmy et al. 2004): (1) anhedral grains (gold I) at the contact between As-rich zones within pyrite-arsenian pyrite; (2) randomly distributed anhedral grains (gold II) and along cracks in arsenian pyrite and arsenopyrite, and (3) large gold grains (gold III) interstitial to fine-grained pyrite and arsenopyrite in deformed and sheared smoky quartz. Gold types I and II occur as electrum and ranges 1–40 μm in diameter, followed by gold type III which has high purity and is depleted in silver (Helmy et al. 2004; Franzmann et al. 2015). Based on the fluid inclusions and stable isotope analyses, the estimated mineralization temperature is ~270–370 °C for the Sukari and other gold deposits in the district, from low-salinity carbonic fluids (Sharara 1999; Sharara and Vennemann 1999). Serpentinites in the footwall and hanging-wall rocks have been variably carbonatized and silicified to listwaenite, typically a mixture of ferroan or magnesian carbonate with cryptocrystalline silica. The listwaenite sometimes locally contains fine-grained pyrite and quartz veins, but no detectable gold has been found.

Based on the recent available information (NI 43-101 compliant Ore Reserves and Mineral Resources at 31 June 2018), the proved + probable ore reserves of the open-pit mine of the Sukari gold project are ~174.2 Mt ore, with an average grade of 1.1 g/t Au, for 192 t Au (0.4 g/t Au cut-off grade). The proved + probable ore reserves of the underground mine are ~4.4 Mt ore, with an average grade of 5.6 g/t Au, for 24.6 t Au (3.0 g/t Au cut-off grade). The estimated measured + indicated

mineral resources are ~358 Mt ore, with an average grade of 0.96 g/t Au, for 344 t Au (0.3 g/t Au cut-off grade). The estimated inferred mineral resources are ~34 Mt ore, at 0.8 g/t Au, for 27 t Au (0.3 g/t Au cut-off grade).

8.5 Mining History in the Shield Rocks of Sudan

8.5.1 Introduction

The topography and geology of Sudan vary from desert lands, hills, and scattered plutonic/volcanic mountains to valleys of different ages. The geology of the Sudan comprises four major geological units: (1) Precambrian basement complex of the Nubian shield, comprising highly folded and metamorphosed gneisses and schists that partly intruded by syn- to post-tectonic subduction-related calc-alkaline granitic rocks. (2) Anorogenic alkaline igneous ring complexes of gabbro, granites, and syenites with associated volcanic rocks. (3) Undeformed Phanerozoic sedimentary cover. (4) Cenozoic within-plate basaltic volcanic rocks. This diversified geology of the Sudan hosts a huge potential of mineral deposits, including base metals and associated gold and silver deposits in the Pan-African volcano sedimentary sequences of the Nubian shied rocks and large oolitic iron ore deposits in the Phanerozic sedimentary rocks. Orogenic and shear zone–related gold deposits are now mined extensively by artisanal and small-scale miners over wide areas of the country. Indications of strategic minerals such as rare metals, rare-earth elements, and phosphates occur both in the basement rocks and in sedimentary cover rocks. Base metals, gold, and iron ore are mined in the Precambrian shield rocks of Sudan,. Another important mineral found in the area is chromite. In addition, there are considerable reserves of zinc, lead, aluminum, cobalt, and nickel in the form of massive sulfides. Ancient historical records indicate that gold and iron mining in Sudan existed under the kingdom of Merowe and during the reign of the kingdom of Nubia, in the Pharaonic era, and during the Roman period. The name *Neb* in the Nubian language means "gold," which is attributed to the Nuba region. The British also called it as the "country of metal."

The history of mining in Sudan dates back to the era of the kingdom of old Merowe, approximately 3000 BCE, known by mining iron and gold in ancient times. The available information determined by the Sudan Ministry of Minerals show that, there are seven selected potential areas that have good potential for mining operations in Sudan, and which are summarized as follows (Fig. 8.34):

(1) The *Red Sea Hills* (Northeastern Sudan) It runs parallel with the Red Sea and separates the coastal plain of Sudan from the Eastern Desert. These hills rise to roughly 3000 *m* in elevation, and contain gold, copper, and iron ores, as well as silver, zinc, garnet, gypsum and talc deposits. Estimated amounts of major mineral resources in this area are 500,000 t Cu, 150 t Au, 4500 t Ag, and 1.9 Mt Zn. The *Hassai gold mine*, a partnership of Sudan and Canada's La

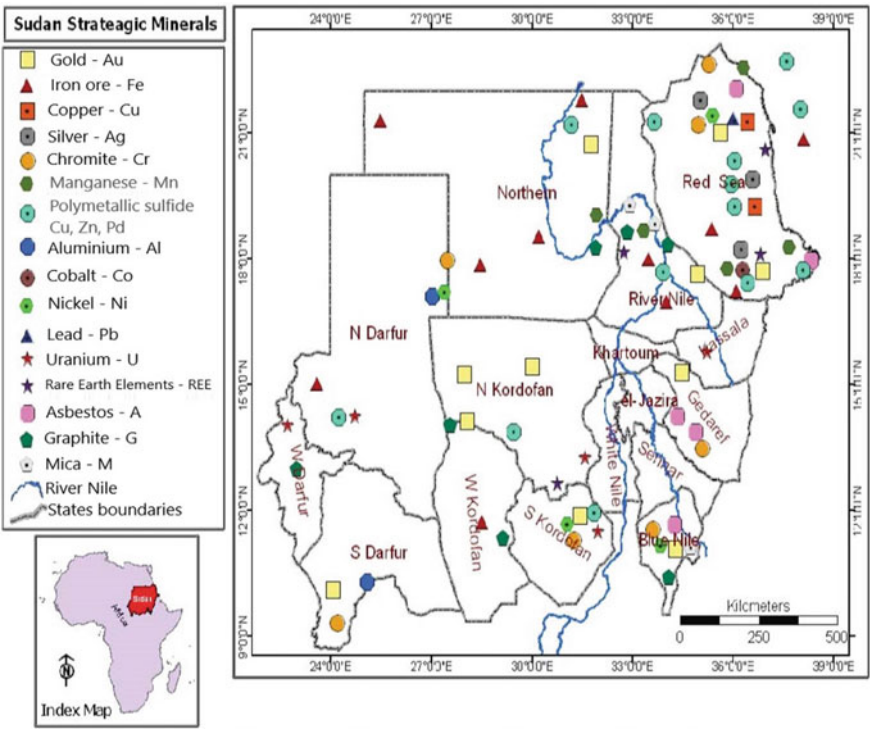

Fig. 8.34 Distribution map of the most potential metallic and some non-metallic mineral deposits in Sudan

Mancha Resources, is also located in the Red Sea Hills district. This open-pit mine, about 50 km from Khartoum, is among the largest gold mines in Sudan, with production from 1992 to 2014 documented at ~80 t Au. This was sourced predominantly from near-surface deposits in the upper oxidized cap rock.

(2) The *Bayoda Desert* (North Central Sudan): This area contains gold, iron ore, manganese, mica, silica, semi-precious metals, kyanite, feldspar, and marble deposits. Gold can be found in auriferous quartz from shallow mines and wadis.

(3) The *Gebel Maraa* (Western Sudan): This is a volcanic field located in western Sudan, with the 5 km wide Deriba caldera sitting at its summit. This area is home to deposits of garnet, salt, sulfur and various base metals.

(4) The *Gebel Wahib and Abyad areas* (Northern Wadi Hawar): Noted to have gold, chromite, bauxite, phosphate, and platinum-group metals. It is also potential for base metals, garnet, kyanite, sulfur, and Salt.

(5) The *Ingessana Complex* (Southeastern Sudan): A polymetallic complex in the Ingessana Hills in the State of Blue Nile. The mix of metamorphic and sedimentary rocks here are known to produce asbestos, chromite, gold, platinum-group metals, marble, magnesite and talc.

(6) The *Nuba Mountains*, also known as the *Nuba Hills* (South Central Sudan—Southern Kordofan): These Mountains stretch on for –48,000 km^2, but yet has a fairly undeveloped road network. These are potential for chromite, copper, gold, iron, manganese and nickel, along with other industrial minerals as well as uranium, graphite, talc, marble and phosphate.
(7) *Copper Pit*, also called *Darfur Pit* (South Darfur): potential for copper, gold, precious stones and uranium. This area produces mostly copper, another mineral the country is noted for. In fact, the Al-Qutb mine in eastern Sudan is reputed to hold ~5 Mt Cu, the largest reserve in the world. This mine also includes approximately 700,000 t Zn, 3000 t Ag, and 140 t Au.

Despite this huge mineral potential, only a small proportion is being exploited in Sudan. It now produces only approximately 70 t Au, 7 t Ag, 75,000 t of chromite, 200,000 t of iron ore, 3 Mt of clinker, 10 t of mica, and 200,000 t of salt (Final Report of GEO Services International Co. Ltd. 2015).

Gold production during the Fifteenth Dynasty was not at the hoped-for level. However, the coming of Thutmose III of the Eighteenth Dynasty (1479–1426 BCE), gave new impetus and strength to work in gold mines in the region. Gold production declined in 1300 BCE, but the advent of Seti I during the Nineteenth Dynasty (1320–1300 BCE), raised production again, where he tried unsuccessfully to develop the Darheeb mines in Wadi Al-Alaqi. In addition, he is credited with creating the oldest map in history of the Darheeb and Wadi Hammamat mines. There are more than 21 important mines in the Red Sea Mountains, specifically south of the railway line between Port Sudan and Atbara. These mines consist of long pillars reaching a height of greater than 150 ft, and were supported at the top by thick timbers to prevent any defects in the mine entrance. When the Arabs conquered Egypt, large numbers of them emigrated to the north of the country of the Beja, which was called the "country of metal," and the Arabs settled for a period of time in this region. Some geophysical research was conducted in the country for minerals exploration. Between the years 1970 and 1974 CE, the Soviet Union's Technoexport surveyed an area of 130,000 km^2 in the country of the Beja. This survey covered all of the Red Sea mountain range and its coasts. The main purpose of these surveys was to conduct research to determine the main geological structures and to explore the details of the mineralized places in the Red Sea Mountains region. These surveys helped in the identification of many places that could be exploited by mining after further geological studies and preliminary excavations. The further geological survey of the country revealed the presence of commercial quantities of iron ore, manganese, chromium, gold, marble, and gypsum.

Iron ore was discovered in several areas in the Red Sea Hills (Fig. 8.34). It is found in the Qorora area (2 Mt, 40–50 wt% Fe), and in the Safiya area (14 Mt, 43–56 wt% Fe). Iron was also found in Vodquan and Halayeb, where the Vodquan iron mine (licensed to the Central Desert Company) is strategically located on the Red Sea coast, 11 km west of the port of Ausif. Iron ore is also found in northern Sudan in the Wadi Halfa region associated with Nubian sandstone, which covers an area of 900 km^2 in the northern state; its presence extends even to near Abu Hamad in the southeast, Al-Bagrawiya and Shendi in the south, in River Nile state in the northeast,

and in western Sudan (Fig. 8.34). Iron has also been found in Darfur in the Karnoi area north of Kutum as well as in Burberry Mountains in West Darfur. The iron ore in Sudan has been divided into three types according to its color: (1) black ore covers most of the Nubian sandstone area; (2) red ore, which has the highest concentrations of iron; and (3) brown ore, which is medium in iron concentration.

Tungsten is abundant in the Gebel Abun region in the Red Sea Hills, with estimated ore reserves of ~43 Mt, with an average grade of 11 wt% W. *Copper* is found in the Ariab region in Hadal Awatib (Fig. 8.34), where it is estimated to have at ~ 40 Mt ore. In the Hassai area, it is estimated at ~13 Mt ore, and in the Oderoc area it is estimated at ~9 Mt. In Dordeb, copper is found in Abu Samar, where the ore reserves are estimated at ~2 Mt. There are also large commercial quantities of copper in Tagotepe, Emasa, and Tuhamiam. It is also found in Khor Bnqur, south of Khor Arbaat. In the regions of Gebeit and Sinkat, copper is available in commercial quantities, as well as in Safiya region. *Chromite* exploration in Sudan began commercially in the 1970s. Ore reserves there are estimated at ~2 Mt, with an average grade of 48–60 wt% Cr_2O_3 in the case of high-grade chromite ore, of which ~1 Mt are in the Ingessana Mountains in Blue Nile state (Fig. 8.34). The stock of chromite in Sudan is estimated at ~50,000 t.

8.5.2 Gold as an Example of Mining History in Sudan

The region where the Beja live (an ethnic group that lives in northeastern Sudan and southeastern Egypt on the Red Sea coast) has been known since ancient times as one of the most important mining areas in the world. The coffers of the Pharaohs were filled with gold from the Beja mines. History tells us that Pharaoh *Seneferu* (also known as Soris) was the first to be able to commercialize the mines of the Beja. He harnessed the Beja people in the mining work. Some sources claim that the discovery of gold in the mountains inhabited by the Beja tribes was between 3000 and 2500 BCE. It is also believed that the first expedition to exploit gold in the Beja Mountains was in 2745 BCE at the hands of the Fifth Pharaonic Dynasty. This period coincided with the reign of Bibi II in 2644 BCE, who sent the commander *Seibni* to the south and southeast of the area that was later called the country of the *Land of Punt*. The Beja mines witnessed increased activity during the rule of the Middle Empire (the Twelfth Dynasty through the Fourteenth Dynasty, 2000–1580 BCE). It was during the period that the Bejawin was known for the first time in the Twelfth Dynasty, when his picture appeared in a cemetery in Mir, Upper Egypt.

In addition, Sudan has been known as a source of gold since the time of the Egyptian Pharaohs in the Third Century BCE and in the ancient Nubian kingdom in the Nubian Desert and the Red Sea Hills. Thereafter, gold mining continued by some of the Sudanese tribes including the Beja, Arabs, and Nubians. In modern times, between the years 1900 and 1954, several British enterprises worked gold mines in the area of the Red Sea Hills, and extracted a considerable quantity of the metal. One mine alone reportedly produced three t of gold between 1924 and 1936. Most gold mining activities in Sudan use artisanal mining to produce gold.

Artisanal gold mining is normally referred to as small-scale gold mining, which is practiced in many countries all over the world. The southern Blue Nile region of the Sudan is famous for artisanal gold mining with gold-mining activities at the areas of Bani Shangol, which extends in the area of the southern Blue Nile close to the Sudanese/Ethiopian border. Recently, gold was extracted from Qeissan and Kurmuk (150 and 170 km south of El Damazin, respectively), which are traditional areas of alluvial gold production. Gold also has been mined along the borders between Sudan and Uganda and the Democratic Republic of the Congo, but not in such commercially profitable amounts.

During the 1970s, Sudan's Geological Survey Administration located more than fifty potential gold-producing sites in different parts of the country. A joint venture between the Sudanese Mining Corporation, a government enterprise, and foreign companies were was in the 1980s. These undertakings produced gold at Gebeit and several other mines near the Red Sea Hills beginning in 1987. In 1988, about 78,000 kg of gold were mined in Sudan. The Hassaï mine in the Red Sea Hills has been in operation since 1991 as a joint venture between the government and La Mancha Resources (Final Report of GEO Services International Co. Ltd. 2015). Gold production continues to grow by every year in Sudan. This makes the country an important gold mining investment opportunity that should be considered. With a huge potential and expected to frog jump a number of gold producers in Africa to position three in the near future, investing in the Sudan's gold sector promises better returns in the near future. For example, the total gold production of Sudan in 2020 reached up to 36.6 t, which is 9.6 t more than in 2019.

Gold mineralization in Sudan falls within distinctive groups. (1) The oxidized gossan rocks with base metals, such as copper, lead, and zinc, have been found to contain important gold deposits. These rocks are characterized by massive oxidizing sulfides, which are found in the Sequin and Ariab areas of the eastern Nuba Mountains. (2) Volcano–sedimentary sequence contains gold-rich quartz veins, which are commonly found in Blue Nile state, Obaidiya, and the North Kordofan regions. (3) Sudan also has its share of alluvial gold, which was formed as a result of the erosion of the gold-bearing quartz veins. This simply means that this kind of gold is mostly found along river valleys and creeks. Alluvial gold is commonly found along the Blue Nile and Nile rivers and in northern Sudan.

Gold deposits are widespread across Sudan, including Blue Nile state, South Kordofan, and Darfur. There are many players in the gold mining sector with international companies controlling the major gold mines. Some of the top gold mining companies include La Mancha Resources, which runs the Hassaï open-pit mines. The company started mining at the Hassaï mine in 1992 and produces about 30,000 oz of gold each year. The company also carries out gold exploration in the Nuba Mountains regions. Orca Gold Incorporated of Canada is another important player in Sudan's gold industry. The company was licensed in 2011 to explore for gold in Block 14, which is located on the northern border of Sudan and covers ~7046 km^2. Drilling results of the exploration activities show high prospects especially in the far east zone, the eastern zone, and the main zone. A Russian company in 2015 discovered some of the largest gold deposit in the country. The company's find has been

estimated at 46,000 t of gold. The gold deposits are found in two areas—one near the Red Sea and the other close to the River Nile. With the signing of the mining contract Siberian for mining is expected to start mining in the coming years. Delgo Mining Ltd. is a productive gold subsidiary of the Turkish TAHE International Metal Mining Corporation, which is active in Block 17 of northern Sudan, River Nile state, since April 2010. Additionally, on 30 April 2013, the government of the Republic of Sudan granted an exploration license for Block 30, Red Sea state, to Kush for Exploration and Production Co. Ltd. (Kush E&P). At the end of 2014, Kush E&P and its Sudanese partners established a Special Project Company named Alliance for Mining Co. Ltd. to operate the gold projects and hold a production license. Managem Mining Company is also one of the working companies in the gold sector in Sudan. It proved approximately 66 t of gold at one out of five sites in one of their three concessions.

It is not just the large mining companies that are capitalizing on Sudan's rich mineral wealth. In recent years Sudan has received attention in the metal detection community for some of the huge gold nuggets that have been found by prospectors using their own metal detectors. In some regions, prospectors are recovering several kilograms of gold per week on average, an exceptional feat especially considering the poverty that many in this country deal with. Artisanal miners are making life-changing discoveries with their metal detectors.

8.5.3 Hassaï Project as an Operating Gold-Copper Mine in Sudan

The Hassaï project area, also called the Ariab Mining District, is located within the Red Sea State of Sudan, about 450 km northeast of Khartoum and 200 km west of Port Sudan (Fig. 8.35). Ariab Mining Company (AMC) is the owner of the exploration and mining concessions in the Ariab district. It was established as a shareholding company where distributed as 51% for the Sudanese government, 44% for La Mancha (a French company), and 5% for Industrial Development Bank (of Pakistan). This ownership is governed by an original Ariab Concession Agreement, which transferred in 1991 all rights of the previous Ariab Mining Development Joint Venture to the newly established AMC. The whole Ariab Mining District has a total surface area of greater than 44,000 km^2, which includes two large concessions in the Red Sea Hills in the heart of the ANS; B11-Ariab: about 25,000 km^2, and B18-Derudeb: about 19,000 km^2 (Fig. 8.35). All of the AMC deposits in the Ariab mining district are presently covered by mining leases, each valid for gold and associated metals for a duration of 21 years (www.ariabmining.net 2021). The Hassaï or Ariab district is accessible from Khartoum by the road north to Atbara, and then the Atbara–Port Sudan road. A gravel track provides access from the Atbara–Port Sudan road to the Hassaï mine site (the western access road). From Port Sudan, Hassaï can be

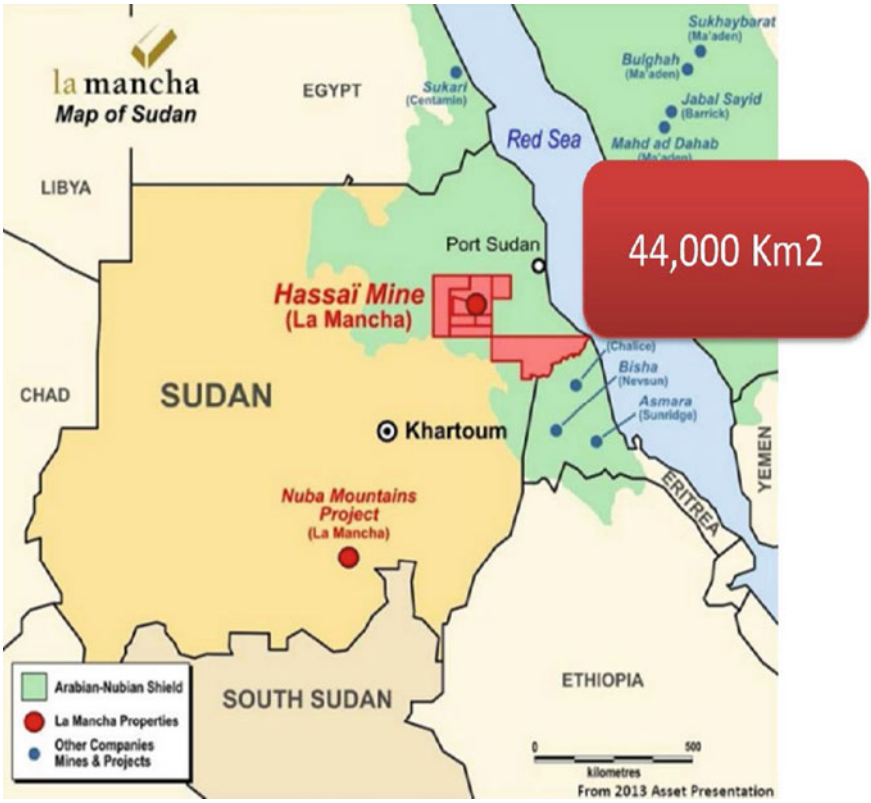

Fig. 8.35 Location map of the Hassaï gold project in the Red Sea Hills of Sudan

accessed via the Atbara–Port Sudan road to Haiya Junction and then a gravel track to the mine site (the eastern access road).

The French–Sudanese teams conducted several exploration programs over five large areas in Sudan within the framework of a cooperation agreement. This program was carried out during the period from 1977 to 1981 for various metals (including W, Pb, Zn, Cu, Ag, Au, and Cr). One such exploration program focused on 17 gossans areas (Fig. 8.36a–c) in the central part of the Red Sea Hills (Ariab–Arbaat area). These gossans covers are the weathering products of massive sulfide deposits found at depth. The gold mineralization in most of the Ariab mining district is associated with these gossans areas. A joint venture agreement was signed between BRGM and the Sudanese government in 1981 to cover the mining development of three specific areas: Eyob (50 km south of the Ariab district), Ariab, and Hamissana (~200 km north of the Ariab area). Detailed exploration work was performed over these three areas from 1981 to 1984 (NI 43-101 Technical Report, prepared by La Mancha Resources Inc 2009). Exploration work covered most of the gossans in the Ariab district. Initial work focused on the polymetallic potential of the underlying hypogene

Fig. 8.36 Examples of the mining gossans areas in the Ariab Mining District, Red Sea Hills of Sudan

sulfide deposits. In 1983, however, the discovery of noteworthy gold concentrations in silica–kaolinite–(barite) rocks associated with the gossans at Hassaï site shifted the interest towards gold mining. During the same period, the nearby occurrences of Ganaet and Kamoeb gold deposits were also explored in detail.

The exploration efforts were thus concentrated on the Ariab district during the period from 1984 to 1987. Major trench sampling was carried out on all the known gossans areas in the region including: Hadal Awatib southwest, Hadal Awatib east, Talaiderut, Oderuk, Baderuk, and Adassedakh (Fig. 8.37). All of these occurrences were eventually classified as gold deposits. In February 1985 sufficient data were collected from surface trenching, percussion drilling, core logging, and pits at Hassaï to justify the installation of a pilot plant. In March 1987 the first gold was poured at Hassaï. Gold production and exploration work was reactivated, after a short suspension, in April 1988 and the pilot operation program was satisfactorily completed in December 1989. The report of feasibility study for the Ariab gold project performed by BRGM was submitted in May 1990. The report examined ten known gold deposits in the district within a circular area measuring ~25 km in diameter. In eight of these deposits (Adassedakh, Baderuk, Hadal Awatib west and east, Hassaï south and north, Oderuk, and Talaiderut), gold is associated with silica–kaolinite–barite rock and ferruginous gossans, which are in turn the nearer-surface expressions of underlying

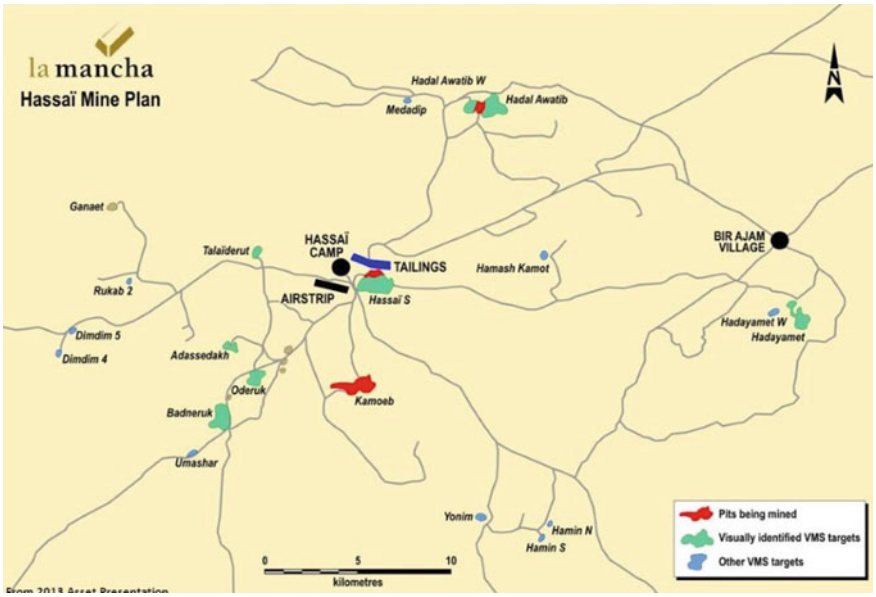

Fig. 8.37 The well-known gossans areas in the Ariab/Hassaï Mining District, Red Sea Hills of Sudan. (*Source* Ariab Mining Company)

VMS. At Kamoeb, gold is present in quartz veins, and at Ganaet, it appeared to be associated with barite lenses.

The gold production at Hassaï mine project commenced in 1991. The AMC began drilling on three of the most promising VMS targets in late 2007 with the intention of confirming and quantifying their potential. In September 2009, a NI 43-101 final report of the compliant resource estimate was released for the first target, at the bottom of the Hassaï south pit, and in November 2009, a second estimate followed for the target at the bottom of the Hadal Awatib pit. In 2011 and 2013 the drilling campaign focused in Hadal Awatib, Hassaï, and Hadayamet, filling between holes to obtain indicated and measured reserves. The results of the drilling and mining program has located VMS-style base metal mineralization at ten other deposits, indicating significant potential to expand the mineral resource base. The high gold potential associated with base-metal mineralization has been proven through greater than 25 years of gold mining yields of greater than 70 t gold from veins and essentially from the silica–barite–rocks, representing the top oxidized parts of VMS deposits. The company has developed and certified some world-class gold, copper, and zinc resources over the last decade. Two of these VMS deposits will pass to the next phase of feasibility studies as Cu–Au and Cu–Au–Zn deposits. The location of the surface oxide deposits is an important guide for exploration because when gold grades are high in oxidized horizon, it is likely that good gold grades will also exist in primary sulfide ore.

More detailed descriptions about the geology, mineralogy, and exploration of different gold-bearing hypogene VMS mineralization of the Ariab mineral district, including Hassaï mine, can be found in Chap. 7 of this book.

8.6 Mining History in the Shield Rocks of Eritrea

8.6.1 Introduction

Although Eritrea is rich in mineral resources and has highly prospective geology, it has only just recently opened up to exploration. Eritrea does not have a long history of mining activities. However, since independence in 1993 substantial investment in mineral exploration has been on going in Eritrea, resulting in the discovery of important VMS copper–zinc as well as gold deposits. More than 60% of Eritrea's land mass is covered by the Nubian shield rocks, which are the main host rocks to several gold- and base metal–rich deposits in the area. The main economic mineral deposits (Fig. 8.38) so far discovered in Eritrea can be classified into three categories concentrated in three main geologic belts: (1) Bisha (Nevsun Resources 2006–2012); (2) Zara, where mining has already started; and (3) the Asmara mining projects (the Emba Derho–Adi Nefas and the Debarwa sites) (Senior et al. 2013). The latter

Fig. 8.38 Location map of the main potential economic mineral deposits in Eritrea (from Berhe 2018)

projects are embarking into the mining phase. The Colluli potash deposit, whose feasibility study has been finalized, is in the process of raising funds for mining. In addition, Yacob Dewar gold–copper deposit is a very profitable deposit, where the indicated and inferred Australasian Code for Reporting of Exploration Results, Mineral Resources and Ore Reserves (JORC Code) has been defined for the further stage of production. Additionally, there are many earlier-stage exploration projects being operated by a variety of small to very large mining organizations from a number of countries including Australia, Canada, China, India, Russia, Sudan, and the United Kingdom.

Following is a synopsis of some of the major mining and advanced exploration project areas/belts that are potential of mining in Eritrea. The operating mining companies that operate in these regions are also highlighted.

8.6.2 Mining Districts in Eritrea

As has been previously mentioned (in Chap. 7 of this book), there are two main VMS mineralization districts in Eritrea: (1) the Bisha VMS district (Bisha, Bisha northwest, Zara, Harena, Hambok, and Yacob Dewar) and (2) the Asmara VMS district (Adi Nefas, Debarwa, Emba Derho, and Adi Rossi) (Fig. 8.39). The two mineral districts of Eritrea are entirely hosted by western and eastern Nakfa terrane, respectively, that belongs to the Proterozoic Nubian shield rocks. There are only two modern operating mines in Eritrea: (1) Bisha Mine is operating by the Bisha Mining Share Co (BMSC), 60% of which is owned by Nevsun Resources of Canada and 40% by the Eritrean state mining enterprise Eritrean National Mining Corporation (ENAMCO). (2) The second mine is operating by Zara Mining Share Co (ZMSC), 60% of which is owned by China Shanghai Foreign Economic Group Company Ltd. (China SFECO Group; a subsidiary of Shanghai Construction Group Co. Ltd (scg.com.cn)) and 40% by ENAMCO.

BMSC operates the VMS-hosted Bisha open-pit gold and base-metals mine (Fig. 8.40), which made a transition from a gold producer into a high-grade copper mine with gold and silver. BMSC has recently become a major zinc–copper producer, with gold and silver as by-products for much of the rest of its mine life until 2023, in case it does not extend its resource base in the meantime. The base-metals production was started in 2013 and was fully funded from the remaining gold production that leached out from the oxidized cap rocks.

ZMSC was at one time owned 60% by Chalice Gold from Australia and 40% by ENAMCO. However, after the project finished its feasibility study, it sold its remaining 60% stake in the Zara project in Eritrea to China SFECO Group. The high-grade gold ore, low-cost Zara project is currently being mined using open-pit mining. The ore reserves have been estimated at 760,000 oz with an average grade of 5.1 g/t Au. The average annual production has been forecast to be 104,000 oz over a 7-year mine life.

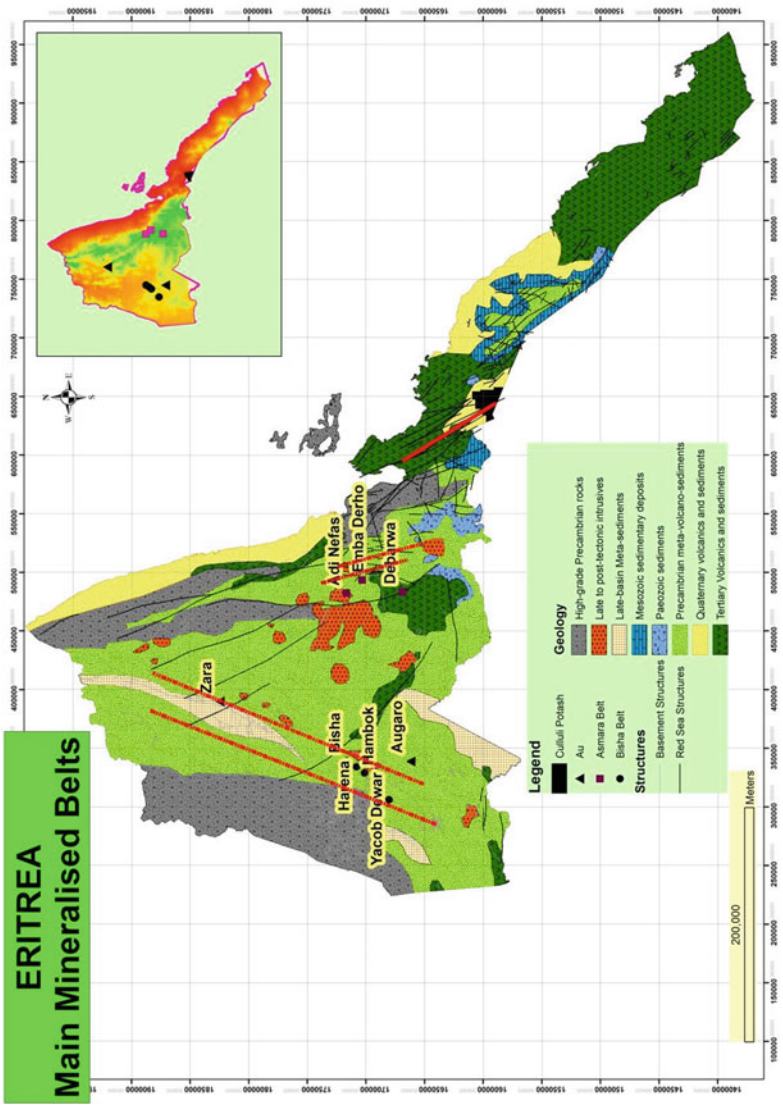

Fig. 8.39 Geologic map and distribution of the main mineralized belts with the location names of mining sites in Eritrea (from Berhe 2018)

Fig. 8.40 Open-pit and operation facilities in the Bisha gold mining site, Eritrea

The Yacob Dewar gold–copper deposit is located to the most southwestern part of the Bisha mineral district (Fig. 8.39); it was discovered by Andiamo Exploration Ltd., which is a private company incorporated in the United Kingdom. The Yacob Dewar deposit is a small, high-grade surface gold deposit extending downward to about 40 m and more than 3 km along strike (Fig. 8.41). The estimated indicated

Fig. 8.41 Field photographs showing the site of trench sampling, oxidized silica-barite exposure, and core samples of the Yacob Dewar gold mine, Eritrea. (*Source* Andiamo Exploration Ltd)

ore resources of the oxide–gold deposit in Yacob Dewar has been found to contain 80,000 oz Au, with an average grade of 2.8 g/t Au, and with a further 4.500 oz of inferred resources as well as oxide copper, which at the time of this writing is in the process of having a resource assessment finalized. Metallurgical tests have indicated that gold can be efficiently extracted by cyanide leaching with better than 90% recovery. The shallow depth, low strip ratio, relatively high grade, and simple metallurgy of the Yacob Dewar deposit give advantages to the project, which mean that it is likely to be very profitable despite its modest size. The mine life of the Yacob Dewar deposit has been estimated to be four to five years, with possible extensions depending on new discoveries during the mining stage.

Asmara Mining Share Company (AMSC) is a joint-venture company of which 60% is owned by Sunridge Gold Corp. and the remaining 40% is owned by ENAMCO. The Asmara project comprises six defined ore deposits, four of which are the subject for a feasibility study completed in May 2013 and their mining permits were granted. However, after the project finished its feasibility studies, Sunridge Gold Corp. sold its remaining 60% stake in the Asmara project in Eritrea to the to a Chinese company in Sichuan province. AMSC finished the feasibility study of the Asmara project on four of the five deposits it comprises and has outlined a mining plan that integrates the four deposits (Debarwa, Emba Derho, Adi Nefas, and Gupo Gold) being processed at a central concentrator near the large Emba Derho copper–zinc–gold–silver deposit. Furthermore, to achieve early cash flow and minimize initial capital costs, the feasibility study included a staged start-up process over the first three years of the mine life. The positive prefeasibility study for the Asmara project was completed in May 2012. It was expected that mining would start by the first quarter of 2019 and to have a life of 17 years. According to the ministry presentation provided by Alem Kibreab, Director-General of Mines for the Ministry of Energy and Mines, the mine is expected to produce an estimated amount of 381,000 t of Cu, 850,000 t of Zn, 436,000 oz of Au, and 11 Moz of Ag.

In the Asmara mineral district, the mineral resources of the Emba Derho deposit are estimated to be ~70 Mt containing more than 0.5 Mt of Cu and ~2 Mt of Zn, 506,000 oz Au, and 19.5 Moz of Ag. There are two other small deposits within 7 km of Emba Derho: Adi Nefas and Gupo Gold. Adi Nefas is a small deposit, just slightly less than 2 Mt of projected resources, but it is very high grade: greater than 10 wt% zinc and 1.8 wt% copper. It also averages 3.3 g/t Au and 115 g/t Ag. This would be the only underground mine at the project. Gupo Gold has gold resources estimated at ~952,000 t at 1.53 g/t Au and inferred resources of ~1.8 Mt at 1.85 g/t Au.

The fourth major deposit in the Asmara mineral district is Debarwa, which is located about 45 km to the south of the capital Asmara (Figs. 8.38, 8.39). It contains 3.3 Mt ore, with more than 91,000 t of Cu, about 32,000 t of Zn, and significant amounts of gold and silver. The Debarwa deposit is also highly significant because it hosts a direct shipping ore zone, which averages 16 wt% copper with gold and silver. In addition, there are two pipeline projects, namely Adi Rassi and Kodadu, which are not as advanced as the other four in the feasibility study. The Adi Rassi contains about 16 Mt ore resource, with an average grade of 0.5 wt% copper and 0.3 g/t gold.

Kodadu is estimated to be about 1 Mt ore resource, with average grades of 1.25 g/t gold and 1.6 g/t silver.

8.6.3 Bisha Copper-Zinc-Gold Project as an Example of Operating Mine in Eritrea

The Bisha mine site is located at about 150 km west of the capital, Asmara, 43 km southwest of the regional town of Akurdat, and 50 km north of Barentu, the regional or zone Administration Centre of the Gash–Barka district (Fig. 8.38). It is located on a flat-to-rolling desert-like plain, south of the Barka River, in the southwestern part of Eritrea, with an elevation varying 550–1200 m above sea level. The Bisha license is dissected by a major drainage course, the Mogoraib river that drains north into the Barka river, which is located outside the mine area. There is no record of any mining or exploration activities in the Bisha area prior to 1990, except for a single Italian colonial mine site at Okreb, 7 km south of the village of Adi Ibrahim. In late 1996, Amanuel Woldu, an Eritrean geologist working for Ophir Ventures (a private Canadian company), conducted some prospecting in the Bisha area. He carried out a traverse across gossanous outcrops, sampled them and conducted some initial mapping. This work was reported back to Ophir geologists, who upon examining the outcrop area, agreed that this was an area worth pursuing, which lately was the initial discovery of what is now known as the Bisha deposit. In late 1997 to early 1998, Ophir presented the property data to Nevsun Resources who, in turn, carried out a brief property examination. The property was recommended for acquisition, along with several others. Ultimately, a prospecting license was awarded to Nevsun in early 1998 by the Eritrean Department of Mines, where the Bisha Main deposit was discovered in November 2002 by diamond drilling of coincident geophysical and geochemical anomalies associated with a prominent gossans cover that locally had highly anomalous gold values.

Nevsun Resources carried out an intensive drilling program from 2003 to 2006 at Bisha Main to enable completion of the feasibility study. BMSC was established with Nevsun holding 60% ownership and ENAMCO holding 40% (SRK Consulting, NI 43-101 Technical Report Bisha Mine 2017). The exploration and resource development drilling continued through to 2009. As a result, the northwest and Harena deposits were discovered with 26 and 27 diamond holes drilling, respectively. About 35 geotechnical drill holes at Bisha Main and 51 holes at Harena were completed during 2009 and 2010, to better define the surface oxide zone. In addition, about 167 diamond drillholes were drilled at Bisha Main in 2011, for resource definition and metallurgical and geotechnical studies. The Bisha Main carbon-in-leach plant (stage I) was commissioned in October 2010, and commercial production commenced by February 2011. Construction of a copper flotation circuit (stage II) was completed in June 2013; where supergene copper ore processing commenced in September 2013 with the first shipment of copper concentrate in October 2013 via the port

of Massawa. The open-pit mining extracted ~620,671 t with an average grade of 0.96 g/t Au from October 2012 to June 2013 that was processed at the Bisha Main plant. The open-pit design is 340 m in length and 200 m in widthand has a maximum depth of 40 m (Fig. 8.40).

Additionally, Sanu Resources Ltd., a subsidiary of NGEx Resources of Canada, commenced a regional stream-sediment sampling and prospecting program in 1998 in which a number of gold anomalies, as well as a large siliceous gossan breccia at Hambok to the west of Harena, have been identified. Sanu applied for the Mogoraib River Exploration License in early 2003 and revisited the gossan outcrops, which resulted in the discovery of the Hambok deposit. In 2006, intensive exploration drilling program at Hambok discovered a massive sulfide deposit to the south of the siliceous breccia outcrop and from that point onward, Hambok became the main focus of exploration activities for Sanu. From 2006 to 2009, Sanu completed 27 diamond drillholes with a total length of 8962 m and 42 reverse circulation drillholes of a total length 2675 m at Hambok to define the mineral resource. The intensive exploration program in the area in 2005 and 2006 led to find a small copper–zinc anomaly at Aderat, located 4 km north of Hambok, where Sanu drilled the anomaly with four diamond holes in 2008, of which one hole returned 47 m at 1.2 wt% Zn and 27 m at 3.56 wt% Zn, 0.75 wt% Cu, and 0.87 g/t Au. Exploration results at Asheli showed anomalously high gold and base-metal values thought to represent a potential massive sulfide body. The results of four diamond holes with total length 520 m showed gold and silver mineralization in two holes, one of which had an intersection at 22 m with a grade of 1.58 g/t Au.

The Sanu Company continued its exploration work up to October 2012, when BMSC purchased the Mogoraib River license. In the first year of tenure, this license covered ~97.4 km^2, which was subsequently reduced by 25% increments annually in accordance with Eritrean policy. The area of the Mogoraib River license is currently covered by BMSC's New Mogoraib Exploration Licenses, which was granted in 2016 (SRK Consulting, NI 43-101 Technical Report Bisha Mine 2017). Additionally, a zinc flotation circuit (stage III) was commissioned by BMSC in June 2016, with the first shipment of zinc concentrate in September 2016 and commercial production achieved by October 2016.

Nevsun Resources announced that it is extending the life of its flagship copper–zinc Bisha mine in Eritrea to the end of 2022, about 18 months longer than the planned operations announced by the company. The extension of the Bisha open-pit mine would add ~3.3 Mt of high-grade ore to the mill, resulting in additional production of about 215,000 t of Zn and 25,000 t of Cu (mining.com/nevsun). The expansion also will give Nevsun the time to advance assessment of the Asheli and Harena underground deposits at Bisha, and to consider further open-pit extensions. It was estimated that the Bisha copper–zinc–gold project would contribute to 8% of the country's total gross domestic product. The copper–zinc–gold mine initially started producing small amounts of gold in February 2011. The capital from gold sales was then used to expand the mine for production of copper and zinc, which are the metals mainly produced from the mine today. Commercial production of copper began in December 2013 and zinc in October 2016. Current projections have

the Bisha Mine staying in production until 2025. The company uses conventional open-pit mining methods at the site, where there are two open pits at the site, named Bisha and Harena.

The mineralization at the Bisha deposit is divided into three major zones: oxide, supergene, and primary sulfide zones. The host rocks are felsic volcanics that have been altered to chlorite and sericite. The oxide and supergene ores were the first main processed materials at the site. Since the middle of 2016 the mine has processed supergene and hypogene (primary) VMS ores. In the surficial *oxide zone*, the deep weathering affected the primary massive sulfides producing a high-grade stratified gossanous zone that was enriched in gold. This zone varies in composition from highly siliceous and somewhat ferruginous to massive goethite–hematite–jarosite materials. The depth of this oxidation zone reaches to 35 *m* below the surface. The oxidation of the massive sulfides generated strong acid solutions that had progressively destroyed the sulfides and their host rocks. Gold remained in the oxide zone and became concentrated; this zone is now mostly mined out. The *supergene zone* was most probably formed as the acid solutions percolated downward and deposited their dissolved metals at the primary sulfide interface to produce a copper-rich supergene zone. A transitional horizon of extremely acid-leached material (or, effectively, "soap") was developed between the oxide and supergene/primary domains and the host rocks. Covellite is the principal copper mineral in the supergene zone. This zone is mostly mined out with its majority excavated by mid-2016, although remnants do remain for potential future minor campaign processing over the next few years. The *primary zone* is a typical VMS mineralization style with pyrite, chalcopyrite, and sphalerite mineralogy in the massive sulfide and chalcopyrite in the stringer zones. Mining and stockpiling of primary zinc ores commenced in March 2014 and by the end of 2016, stockpiles of 2.5 Mt of Zn ore formed part of the stockpile inventory.

The *Harena deposit* is also a typical VMS body that has been affected by weathering. The host rocks of the Harena deposit are intensely hydrothermally altered chloritized and sericitized felsic volcanic rocks. Surficial weathering processes have produced a surface gold-rich oxide/gossan zone underlain by a primary massive sulfide deposit. Supergene mineralization, however, is not well-developed at Harena compared with those in the Bisha Main deposit. The primary massive sulfide body is currently being explored and is mainly composed of pyrite, chalcopyrite, and sphalerite. Chalcopyrite-rich stringer zones occur stratigraphically beneath the massive sulfides, some of which have high precious metal contents.

The *Hambok deposit* consists of a single massive sulfide lens, where the base metal values are generally higher near the surface along the top and outer edges of the body. The deposit is hosted by variably chloritized mafic volcanic rocks and is dominantly composed of massive pyrite with zones of finely banded chalcopyrite and sphalerite. Intervals of near massive magnetite are often found associated with the massive sulfide zone. Mineralization at the *Bisha Northwest Zone* occurs in a series of predominantly pyrite-rich massive sulfide lenses hosted within altered felsic volcanic rocks. Copper- and zinc-rich stringer sulfide mineralization is sporadic within the massive sulfide lenses and in stockwork zones. Some of the massive sulfides have been exposed to weathering at the surface, creating an oxide zone that is locally

enriched in gold. Beneath these areas, some supergene copper mineralization may also be present.

The *Asheli deposit* consists of a massive sulfide body composed of pyrite, chalcopyrite, and sphalerite with minor galena underlain by pyrite and pyrrhotite stringer mineralization. A second lens of massive sulfide mineralization was intersected to the north of the main deposit in late 2016 with mineralization of a similar character but with more pyrrhotite abundance.

The most recent available technical report on the Bisha project is dated 9 August 2017 and contains mineral resources estimated as current as of 31 December 2016 (mining.com/nevsun). The recent interpretation and estimation for the Bisha project was completed on 31 December 2017 using diamond-drilled cored holes and recent reverse circulation grade control holes. The majority of the reverse circulation holes were drilled as part of a grade control program for the supergene copper phase beginning in 2013 while almost all the diamond-drilled holes were drilled prior to May 2012. Diamond drill data for the Northwest and Harena deposits include a significant proportion of drilling completed from 2012 onwards. The estimated indicated resources at Harena as of 31 December 2017 are approximately 2.5 Mt as the result of a successful near-surface infill drilling program design to convert inferred resources to indicated resources. The estimated measured and indicated resources at Bisha mine decreased from December 2016 due to mining and processing open-pit ore and from stockpiles. Bulk density values were assigned on the basis of rock type and oxidation state, as defined by the interpreted geological wireframes. The values are based on a combination of bulk densities from the previous resource estimate and in situ measurements in use at the mine derived during mining.

The original Bisha Main pit consisted of two sections one smaller section in north and the main pit in south. The north section of the ultimate pit was mostly depleted by 2017 and is now partially being used as an in-pit waste dump. The remaining Bisha Main pit is planned to be ~815 m long and 660 m wide, as well as the maximum planned slope height at the east side of the south pit of 270 m. The Harena deposit is scheduled to recommence mining at the tail end of the life of mine after the Bisha Main pit is complete. The original Bisha pit consisted of nine individual pit phases, where the first three phases targeted oxide ore production, the second three phases targeted supergene ore production, and the final three phases planned to target primary ore production. The oxide pit phases have now been exhausted, as phases 4, 5, and 6 are now operating in the supergene ore. Stripping for the primary mineralization started with phase 8 in late 2013 and continued with phase 9 in 2014. A reoptimization resulted in the suspension of phase 9 stripping in mid-2015. Phase 9 was removed from the mineral reserves in 2017; however, the Company continues to study the economics of the remaining ore resources located underneath the phase 8 pit design.

The Harena open-pit mine has two phases, one targeting the oxide production (mainly completed in mid-2013 with some remaining materials), and the final phase targeting the primary production to be mined once mining is complete at Bisha Main and the mobile equipment fleet can be redeployed. The Harena pit is currently inactive for mining, but additional exploration drilling program was completed during both 2016 and 2017 with exploration drilling continuing to highlight growing potential

at depth for underground mining. The company continues to evaluate the mineral resources below the currently planned open-pit cut back. Although the initial oxide production phase of the operation is complete, oxide ore has been mined and placed in stockpiles. The higher-grade portion of these stockpiles (~135,000 t) was directly shipped and sold during 2016 and 2017, realizing ~105,000 gold equivalent ounces. There now remain ~100,000 t of lower-grade oxide ore that will be processed at the end of the mine life.

For further information about the Bisha and surrounding deposits, their resource/reserve estimation, mining processes, and so on, the reader is invited to visit the last annual information of Nevsun Resources Ltd, dated as of 27 March 2018 at their website (www.mining.com/nevsun).

8.7 Mining History in the Shield Rocks of Ethiopia

8.7.1 Introduction

The diversity of Ethiopian geology gives rise to widespread extensive resources of several mineral commodities, including base metals, precious and rare metals, gemstones, dimension stones, and industrial construction and energy minerals. Although current mining production is still small, Ethiopia actually has a diverse and complex geological history with three major geological terranes: (1) the Proterozoic crystalline basement that underlies about 18% of the country, (2) late Palaeozoic, Mesozoic, and Tertiary continental and marine sediments that occur mostly in the East and occupy about 25% of the land area of the country, and (3) the Cenozoic volcanic and sedimentary rocks, including those of the East African Rift Valley, that transect the country in a northeasterly direction and underlie the remaining 57% of the land of the country. The oldest rock units in Ethiopia are of late Proterozoic age (900–540 Ma), which are mainly exposed in the northern, western, and southern parts of Ethiopia as greenstone terranes (Fig. 8.42). A scattering of such rocks, however, can be also found around Harrar in the eastern part of Ethiopia.

The Proterozoic basement rocks of Ethiopia include a variety of sedimentary, volcanic, and intrusive rocks. In general, gneisses are more common with metamorphic grade higher in the southern and western terranes compared to the northern terrane. These Proterozoic basement rocks are the main hosts of many metallic and nonmetallic deposits in Ethiopia, many of which are not exploited yet. Some of these mineral deposits have been, and are still, mined by artisanal and small-scale mining methods. The history of artisanal mining in Ethiopia, particularly for gold, spans three millennia, where some historians have estimated the oldest mining in the world to date back more than 6000 years. It is believed to be located in western Ethiopia near the Sudanese border, in a region called the *Asosa* area, where large quantities of gold have been produced to date, chiefly from placer deposits. The numerous

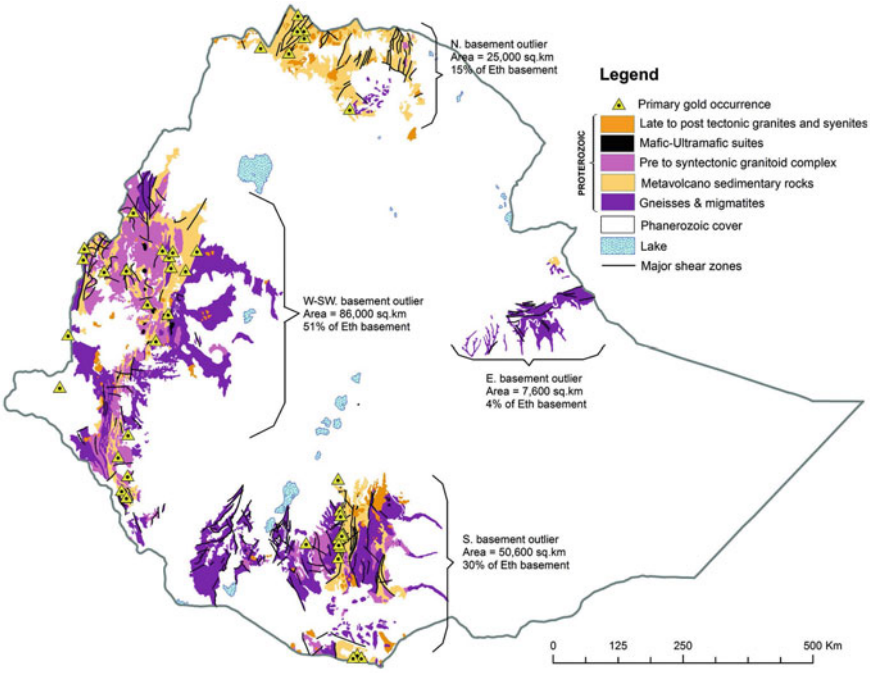

Fig. 8.42 Simplified geological map of the major Greenstone Belts and domains that are hosting the most precious and base metals in Ethiopia. Distribution of gold deposits and occurrences in these belts are shown (from the *Ministry of Mine and Petroleum, Geological Survey of Ethiopia*, updated 2020)

placer gold deposits in Ethiopia's rivers have been exploited for thousands of years by small-scale miners using rudimentary techniques from the water and river sands.

Despite of the long history of traditional mining in Ethiopia, systematic and modern mineral exploration started only recently, in the late 1960s. The exploration activities carried out in the Precambrian terranes of Ethiopia resulted in the discovery of various types of mineral deposits and occurrences in different parts of the country. Gold is by far the most important extracted mineral deposit in Ethiopia, where it has been produced from placer deposits for several thousand years, and is currently produced from a bedrock mining operation at Lega Dembi. Ethiopia is also one of the major world producers of tantalum, contributing about 10% to the world's production in 2012, according to the 2012 United States Geological Survey Minerals Yearbook. Relatively important amounts of tantalite are produced from the Kenticha mine in southern Ethiopia. Small-scale production of a wide range of industrial mineral commodities is also distributed throughout the country, and there is good potential for additional production for domestic markets, particularly in the building and construction, glass and ceramic, and fertilizer industries. Since ancient times, marble has also been quarried for a variety of architectural and artistic purposes in Ethiopia. The marble deposits existed in several regional states including Harrar, Tigray, Oromia,

and Benishangul–Gumuz. However, mineralization in the Ethiopian Nubian Shield rocks is dominated mainly by orogenic gold, tantalum, niobium, tungsten, rare earth elements, uranium, and tin.

8.7.2 Gold Mining in Ethiopia

Ethiopian mines have a long legendary history with gold mining; they provided gold to the ancient Egyptian Empire and possibly even to King Solomon's Mines and the Queen of Sheba in Yemen. Mineral exploration began in Ethiopia in the late 1890s by foreign companies; however, modern mineral exploration started in 1968 with the founding of the Geological Survey of Ethiopia (GSE) in collaboration with United Nations Development Program (UNDP). In the present day, gold occurs in schist belt of the Pan-African age and Tertiary basaltic lavas in the Asosa region of Benishangul–Gumuz, western Ethiopia, as well as in the bedrocks of the Lega Dembi gold mine, Adola district of southern Ethiopia. There is widespread artisanal gold production in the Asosa region and many other localities throughout the country, with moderate activity by small numbers of local workers producing relatively large amounts of gold. Precambrian rock occurrences are as of this writing being explored and exploited in the southern, western, and northern greenstone belts of Ethiopia. Precambrian rocks are the most important repositories for gold deposits. Most gold deposits and occurrences in Ethiopia are genetically related to the orogenic type, although skarn-related, intrusive-related, epithermal and VMS types are also currently identified. In southern Ethiopia, Lega Dembi and Sakaro are the only primary gold mines (Table 8.1). However, a number of other gold mines, including Tulu Kapi, Dish, and Jilaye (western Ethiopia), Okote (southern Ethiopia), and Meli (northern Ethiopia) have reached advanced stages of exploration and are heading towards development.

The geological belts and domains that host gold in Ethiopia can be grouped into three main Greenstone Belts (www.mom.go.et, updated 2020): (1) the southern Greenstone belt, (2) the western Greenstone belt, and (3) the northern Greenstone belt (Fig. 8.42). Following is a brief description of the main gold deposits and occurrences in these greenstone belts.

Southern Greenstone Belt

Gold mineralization in the Southern Greenstone Belt of Ethiopia includes the *Adola–Kenticha*, *Ageremariam*, *Arero*, and *Moyale* areas. The *Adola–Kenticha belt*, also known as the Adola belt, is a major Neoproterozoic shear belt within the Pan-African orogeny, which hosts major primary gold deposits confined in metavolcano–sedimentary assemblages. It comprises many primary gold deposits and occurrences including Lega–Dembi, Sakaro, Okote, Wollena, Kumudu, Megado–Serdo, Dawa–Digati, Bore, Abab River, Haranfama (northern Kenticha) and many other occurrences. The *Hageremariam and Arero greenstone region* hosts pyrite-bearing gold in metamorphosed mafic and ultramafic rocks as well as gold-bearing quartz veins in intermediate to acidic alkaline intrusive rocks. The *Moyale greenstone region*

consists of the Haramsam, Hassamte, and Chamuk gold prospect areas underlain by metagranodiorite, amphibolites, gabbro–amphibolite, and gabbro and amphibolite schist, which hosts auriferous quartz veins. At present, Ethiopia has a single operating large-scale gold mine in the southern Greenstone belt; it is the Lega Dembi mine, in the southern area of the country, owned by Midroc (98%) and the Ethiopian government (2%).

Western Greenstone Belt

The western greenstone belt extends for more than 600 km from Akobo (a district in southwest Ethiopia); its width ranges from 50 to 200 km. This belt comprises chlorite, sericitic and graphitic schists, phyllites, quartzites, and andesitic-to-rhyolitic volcanic rocks, hosting auriferous veins and alteration zones. This belt comprises major regions of gold deposits and occurrences, including *Gambela*, *Western Wollega*, and *Benishangul–Gumuz* (specifically in the *Asosa zone*), which include gold prospects at Chamo, Akobo, Guraferda, Gezana, Tumet, Godare, Baro, Ankori, Tulu Kapi, Tulu Kami, Dimma, Baruda, Oda Godare, Mengie, Ashashire, Dul, Gambella mountain, Indaka, Bekoji Motisha, Suken, Egambo, Kilaji, Wombera, Metekel (Jilaye), Guba, and many other sites.

The *Gambela* region, also known as Akobo, is a narrow greenstone sub-belt of a high-potential target for gold exploration. Akobo's geological setting comprises mafic schists, meta-ultramafic rocks, metasedimentary schists, and undifferentiated schists and gneisses. The *Western Wollega region* includes gold deposits and prospects of Tulu Kapi, Ankori, Tulu Kami, Laga Baguda, Chokorsa, Kata, Nejo, Yubdo, Oda Godere, and many others. In these areas, gold-bearing quartz veins are hosted in schists and syenite, as carbonate veins, and in auriferous zones within sheared metavolcanic rocks interbedded with chert and carbonate lenses.

The *Tulu Kapi gold mine*, one of the most promising and now is being in operation, is located at 28 km east of the town of Ayra Guliso in the state of Oromia in western Ethiopia. The mine is owned by KEFI Minerals plc, which in 2014 bought 100% of the license held by UK-based gold exploration and development company Nyota Minerals (Ethiopia). The property lies in the Tulu Kapi–Ankore license area and has a surface area of 8.44 km^2. The Tulu Kapi gold mine is a combination of open-pit and underground mining operations (Fig. 8.43), where a central processing unit with a capacity of 1.2 Mt annually is being considered. The Tulu Kapi–Ankore area consists of metasedimentary rocks of sandstone, phyllites, and quartzites at the central part, followed by metamorphosed intrusive units, including granites, syenites, and diorite–granodiorites to gabbro in the western and eastern parts of the area. There are also talc schists, chlorite schists, and mica schists. Gold mineralization in the main area of Tulu Kapi is specifically hosted in the mafic and felsic sheared syenite units. Gold mineralization occurs in veins, breccia, and crackle zones of the Proterozoic syenites along with intrusions of porphyritic syenite, diorite and dolerite. Gold mineralization is mainly associated with albitization zones, which contain quartz and sulfide-rich veins. The gold is mainly mixed with pyrite and silicate gangues. The Tulu Kapi gold mine comprises four lode structures, designated as lodes 1, 2, 3, and 4, which run parallel to each other below the surface. Mineralization lodes 1 and 2 contain a simple

Fig. 8.43 Open-pit mine of Tulu Kapi area, Western Ethiopia. (*Source* KEFI Minerals Co Ltd)

mineralogy consisting of gold along with pyrite, sphalerite, and galena, while lodes 3 and 4 are sulfide-rich and include sphalerite, galena, arsenopyrite, and chalcopyrite, as well as gold and pyrite. The gold mine is expected to produce 80,000 to 85,000 of gold a year for the ten-year initial life-of-mine. KEFI Minerals' Tulu Kapi project has reached an advanced exploration stage, where the estimated probable ore reserves are about 16.9 Mt with an average grade of 1.82 g/t Au (total, 986,000 oz Au) and indicated and inferred ore resources of 24.9 Mt at 2.34 g/t Au (total, 1.9 Moz Au). The total indicated and inferred resources in terms of gold equivalent are estimated to be greater than 2 Moz.

The *Benshangul–Gumuz* region consists of metavolcanic and metasedimentary sequences, mafic–ultramafic rocks, and minor granitic intrusions, as well as composite mafic-to-felsic plutonic complexes of bathoilithic dimensions. Gold deposits and occurrences include Galesa (Tambish, Cholo, Jilaye, Fite, and Abaydar), Ablarus, Epar, Dull, Ashashire, Dish, and other areas. The gold deposits and occurrences in Gelasa area are genetically related to the skarn-type gold deposit, amounting to greater than 40 t at an average of about 3 g/t Au. The Ablarus and Epar gold mineralizations are related to quartz mica schist and metagabbro, and the sericitized metagranite shows low-grade mineralization range from an average of 0.4–1.19 g/t gold. There is also a probability of gold occurrences related to intermediate dyke/sill swarms, skarns and brecciated, hematite quartz veins with minor occurrences in which sulfides (pyrite, pyrrhotite, chalcopyrite, arsenopyrite) are disseminated.

The *Asosa* region, as previously mentioned is located in the state of Benishangul–Gumuz, western Ethiopia, is very close to the border between the western Ethiopian highlands and south Sudan (Fig. 8.44). It is home to potentially highly profitable gold deposits. The Asosa region lies on a major suture zone in the southern ANS, which is already known to host world-class gold deposits. The Nejo district, about 100 km

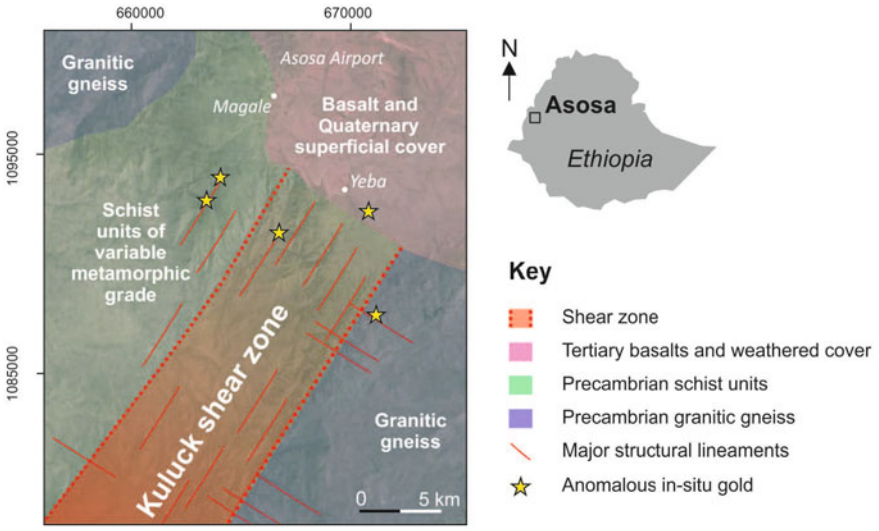

Fig. 8.44 General geology of the region hosting the well-known gold occurrence south of Asosa in the Benishangul–Gumuz region of Ethiopia (from Bullock and Morgan 2018)

southeast of Asosa, is reputed to be the site of the oldest gold mine in the world and the origin of the legend of King Solomon's Mines (Bullock and Morgan 2018). The Ethiopian Nubian shield rocks in the Asosa region have been mined for more than 6000 years and provided a principal source of gold to the Egyptian Empire. It has also been speculated that Ethiopian gold mines may even have supplied the Queen of Sheba with her riches in Biblical times. More recently, gold has been extracted by panning from alluvial deposits along the rivers and streams of the region. In the western Ethiopian basement complex region, artisanal and alluvial gold mining started in the late nineteenth and early twentieth centuries. Precious metal, base metal, and industrial mineral surveys have been conducted in western Ethiopia by many geologists and exploration companies since the beginning of the twentieth century. Placer gold mining was also recorded during the Italian occupation from 1935 to 1940 along the Kuluck and Koncha rivers and their associated alluvial plains. In addition, in the Afa valley and its tributary that crosses the northern part of the Asosa area, local inhabitants still mine gold using artisanal methods, where only minor artisanal placer gold mining and panning are evident (Bullock and Morgan 2018).

The Asosa region is characterized by the presence of the Kuluck shear zone (Fig. 8.44) as well as by syn- and postkinematic Neoproterozoic granitoid intrusions, Tertiary basalts, and a lateritic cover over basaltic lavas. Important gold mineralization zones are hosted within quartz veins, schist units (amphibolite schist, quartz graphitic schist, and quartzofeldspathic sericite schist) and granitic gneiss (Fig. 8.44). The local inhabitants in the Asosa area not only focus on the placer gold deposits within and around the streams, but also take directly from in situ bedrocks crossed

by streams (Fig. 8.45a, b). Both stream sediments samples and bedrock samples are rich in gold grains, where the small personal pan could contain up to ten gold grains. Not only the local inhabitants benefit from the Asosa placer and in situ bedrock gold deposits, but some foreign companies (Ascom Geology and Mining of Egypt being one) made a significant gold discovery in the region in 2016 (Fig. 8.46). The tentative estimated mineral resources showed that about 48 t of gold could be recovered from the area; yet this only looks like the beginning. Gold in the Asosa area is occasionally associated with some sulfides (e.g., pyrite, chalcopyrite, arsenopyrite), oxides (e.g., magnetite, ilmenite, rutile, specularite), and carbonate (ankerite) minerals (Bullock and Morgan 2018). Gold content seems to be more concentrated within schists, pegmatite, and quartz veins, which are widely abundant across the region.

Northern Greenstone Belt

The Northern Greenstone Belt is the third major Precambrian belt that located in northern Ethiopia; it comprises several metavolcano–sedimentary belts and subbelts, bounded by mafic–ultramafic rocks. It hosts gold and base-metal deposits and occurrences. The primary gold occurrences of Terakimti, Adi Zeresenay, Zager, Asgede, Mia Koka, and Niraqque as well as the base metals of Tsehafi Emba and other sites are well-identified. The gold-bearing VMS deposits, the southward extension of the Bisha VMS gold deposit being mined in Eritrea, has currently been discovered at Meli and Daro. The gold mining from the secondary enrichment of overlying gossans zones have already started at Meli by Ezana Mining Ltd. The gold deposits and occurrences of Northern Greenstone Belt are principally hosted in quartz veins of sheared intermediate metavolcanic porphyry, in a carbonatized talc–tremolite–epidote schist, as well as in sericite-chlorite and quartz sericite schists in addition to the sporadic occurrence of graphite.

8.7.3 Tantalum Mining in Ethiopia

Ethiopia is reporteded as the sixth largest producer of tantalum in the world. The Kenticha tantalum mine in the Oromia region of southern Ethiopia contain widely distributed tantalum deposits to produce as much as 9000 t of refined tantalum products over the next 15 years. The Kenticha tantalum mine is located in Guji Zone, Saba Boru district in Kenticha Kebele, southern Ethiopia. The mine has been exclusively exploited by TPLF under trade name "Ethiopian Mineral Development Share Company—EMDSC", which is currently among top 10 tantalum producers in the world. The Kenticha tantalum-bearing pegmatite is situated in the Adole area within the Precambrian basement of southern Ethiopia. The Kenticha tantalum-bearing pegmatites were first discovered during the geological mapping programme carried out by Ethiopian geologists in close cooperation with Soviet geologists in 1980. A major mapping and evaluation programme financed by the Soviet Union was

Fig. 8.45 Gold panning in the streams cross-cutting the bedrocks **a** and within streams that flow into the Kuluck River **b** in the Asosa region

Fig. 8.46 The open-pit gold mines in the Asosa region, Western Ethiopia

carried out in 1981 to 1985. The project aimed at determining the extent of the tantalum-bearing rocks and to establish whether they were of commercial interest.

Kenticha pegmatites are abundant throughout the southern part of Neoproterozoic rocks of Ethiopia, but are especially abundant in the Kenticha pegmatite field area, which covering a surface area of about 2500 km^2. The pegmatites are emplaced at or near a major NNE-SSW trending shear zone. The pegmatites range from barren feldspar-muscovite pegmatites to different types of rare-element pegmatites. The Kenticha pegmatite is a large pegmatite body exposed for 2 km in length and 400 to 700 m in width (Fig. 8.47a–c). It was emplaced in steeply dipping serpentinites and talc-tremolite schists. The thickness of the pegmatite varies; in locations where both hangingwall and footwall contacts are exposed, thickness ranges between 40 and 100 m. Kenticha pegmatites display complex zoning with a complex mineral paragenetic assemblages including columbite and a number of lithium minerals, beryls and sulfides.

The Ethiopian Mineral Development Share Company (EMDSC) is the owner and the mining company of the Kenticha tantalum deposit. The annual production is around 70 t of Ta metal (120 t of concentrate at 60 wt% Ta_2O_5). The estimated probable reserve of primary ore is about 17,000 t, with average grade of 0.017 wt% Ta_2O_5, whereas the estimated reserve of Ta_2O_5 in the weathered zone is about 2400 t at average grade of 0.015 wt% Ta_2O_5. In addition, the Kenticha pegmatites in the Adola area display additional variety of minerals of which the Li-bearing phases such as spodumene and Li-micas over time may be a valuable additional by-product.

Fig 8.47 **a** Field photograph showing the south-central part of the Kenticha pegmatite field, **b** part of the outcrop of Kenticha pegmatite, and **c** tantalite crystals (grayish black) and spodumene (greenish color) within K-feldspar pegmatite. (*Source* Mineral Resources of Ethiopia)

References

Abu El-Enen MM, Lorenz J, Ali KA et al (2018) A new look on Imperial Porphyry: a famous ancient dimension stone from the Eastern Desert of Egypt: Petrogenesis and cultural relevance. Int J Earth Sci 107:2393–2408

Al Shanti AMS (2009) Mineral deposits of the Kingdom of Saudi Arabia. Scientific Publishing Center, King Abdulaziz University, Jeddah, Saudi Arabia

Berhe M (2018) Overview of mining, mineral exploration and investment in Eritrea. Andiamo Exploration Ltd.

Bullock LA, Morgan W (2018) The Asosa region of western Ethiopia: a golden exploration opportunity. Geol Today 34(1):31–34

SRK Consulting (2007) An independent mineral experts' report on the gold mining and exploration assets of Saudi Arabian Mining Company (Ma'aden): Cardiff, SRK Consulting (UK) Ltd. https://www.maaden.com.sa/eng/SRK_Report.pdf

El-Shafei SA, Abdel-Maksoud KM, Helmy HM, Ahmed AH (2020) J Asian Earth Sci 201:104510

Franzmann D, Smith P, Johnson N, Zammit M (2015) Mineral resources and mineral reserve estimate for the Sukari gold project, Egypt. $2–101F1 report prepared for Centamin plc

GEO Services International Co Ltd (2015) Final technical report on the impact of traditional mining of gold on the social and economic life in Sudan and on the environment. A pilot study on role of mining sector to economic diversification

Habashi F (2016) Gold: an historical introduction. In: Adams MD (ed) Gold ore processing. https://doi.org/10.1016/B978-0-444-63658-4.00001-3

Harrell JA (2002) Pharaonic stone quarries in the Eastern Desert of Egypt and Nubia. In: Friedmann R (ed) Egypt and Nubia-gifts of the desert. British Museum Press, London, pp 232–244

Helmy M, Reinhard K, Fritz H, Loizenbauer J (2004) The Sukari gold mine, Eastern Desert-Egypt: structural setting, mineralogy and fluid inclusion study. Miner Deposita 39:495–511

La Mancha Resources Inc (2009) Hadal Awatib East Cu-Au VMS deposit, Sudan, resource estimates. NI 43-101 Technical Report

Kemp J, Gros Y, Prian J-P (1982) Geologic map of the Mahd adh Dhahab quadrangle, Sheet 23E, Kingdom of Saudi Arabia. Saudi Arab Deputy Ministry Mineral Resour Geol Map GM-64, scale 1:250000

Klemm R, Klemm D (2013) Gold and gold mining in ancient Egypt and Nubia. In: Natural science in archaeology. Springer, Berlin, p 341

Koshin G, Bassyuni F (1968) The mineral resources of the UAR. Part1: metallic minerals. Internal Report EGSMA-Technoexport, Contract 1247, Cairo, Egypt

Senior N, Finch A, Ros, AF, Rees SD, Martin CJ (2013) Asmara project feasibility study, an NI 43-101 Technical Report prepared by SENET Pty Ltd. for Sunridge Gold Corp

Sharara N, Vennemann TW (1999) Composition and origin of the fluid responsible for gold mineralization in some occurrences in the Eastern Desert, Egypt: evidence from fluid Inclusions and stable isotopes. In: Proceedings of the first international conference on the geology of Africa, Assiut, Egypt, vol 1, pp 421–445

Sharara NA (1999) Stable isotopes and fluid inclusions of the gold mineralization at El Sukari District, Central Eastern Desert, Egypt: genetic constraints. In: Proceeding of the fourth international conference on geochemistry. Alexandria University, Egypt, pp 317–339

Sidebotham ES (ed) (2008) The red land: the illustrated archaeology of Egypt's Eastern Desert. American University of Cairo

SRK (2017) Structural study and geotechnical review of Bisha Mine, Eritrea, Mar 2017

Taib M (2015) The mineral industry of Egypt. In: U.S. Geological survey mineral yearbook

Zoheir BA, Johnson PR, Goldfarb RJ, Klemm DD (2019) Orogenic gold in the Egyptian Eastern Desert: widespread gold mineralization in the late stages of Neoproterozoic orogeny. Gondwana Res 75:184–217